

**STUDY ON THE CORROSION INHIBITION EFFICIENCY  
OF SOME COMMON WEEDS ON MILD STEEL**

Thesis Submitted for the Award of the Degree of

**DOCTOR OF PHILOSOPHY**

in

**Chemistry**

By

**Abhinay Thakur**

**Registration Number: 11815979**

**Supervised By**

**Dr. Praveen Kumar Sharma (14155)**

Department of Chemistry (Professor)

School of Computer Science and Engineering,

Lovely Professional University,

India, 144411

**Co-Supervised by**

**Dr. Ashish Kumar**

Department of Chemistry (Professor)

NCE, Bihar Engineering University,

Department of Science and Technology,

Government of Bihar, India, 803108

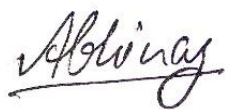


**LOVELY PROFESSIONAL UNIVERSITY, PUNJAB**

**2023**

## DECLARATION

I, hereby declared that the presented work in the thesis entitled “**STUDY ON THE CORROSION INHIBITION EFFICIENCY OF SOME COMMON WEEDS ON MILD STEEL**” in fulfilment of degree of **Doctor of Philosophy (Ph. D.)** is outcome of research work carried out by me under the supervision of Dr. Praveen Kumar Sharma, working as Professor, in the Department of Chemistry, School of Computer Science and Engineering of Lovely Professional University, Punjab, India. In keeping with general practice of reporting scientific observations, due acknowledgements have been made whenever work described here has been based on findings of other investigator. This work has not been submitted in part or full to any other University or Institute for the award of any degree.



Name of the scholar: Abhinay Thakur

Registration No.: 11815979

Department: Chemistry,

School of Chemical Engineering and Physical Sciences,

Lovely Professional University,

Punjab, India

## CERTIFICATE

This is to certify that the work reported in the Ph. D. thesis entitled “**STUDY ON THE CORROSION INHIBITION EFFICIENCY OF SOME COMMON WEEDS ON MILD STEEL**” submitted in fulfillment of the requirement for the reward of degree of **Doctor of Philosophy (Ph.D.)** in the Department of Chemistry, School of Chemical Engineering and Physical Sciences, is a research work carried out by Abhinay Thakur, 11815979, is bonafide record of his original work carried out under my supervision and that no part of thesis has been submitted for any other degree, diploma or equivalent course.

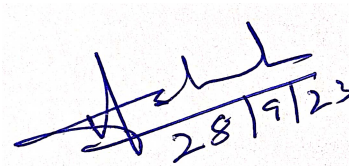


Name of supervisor: Dr. Praveen Kumar  
Sharma

Designation: Professor

Department: Chemistry

University: Lovely Professional  
University, Punjab, India, 144411



Name of co-supervisor: Dr. Ashish Kumar

Designation: Professor

Department: Chemistry

University: Bihar Engineering University,  
Department of Science and Technology,  
Government of Bihar, India, 803108

## ABSTRACT

The thesis entitled “**STUDY ON THE CORROSION INHIBITION EFFICIENCY OF SOME WEEDS ON MILD STEEL**” investigates the utilization of some common weeds as an eco-benign and cost-effective corrosion inhibitor for mild steel in 0.5 M HCL solution with the help of various techniques. Corrosion is a significant problem that affects many industries worldwide, leading to significant financial losses. Mild steel is commonly used in various industrial applications, including construction, automotive, and oil and gas industries, due to its excellent mechanical properties, low cost, and high availability. However, mild steel is susceptible to corrosion in the presence of corrosive environments, such as acids, salts, and moisture. Corrosion of mild steel can lead to material failure, which can cause accidents, downtime, and high maintenance costs. The use of corrosion inhibitors is one of the most effective ways of controlling corrosion in metallic materials. Corrosion inhibitors are chemical compounds that are added to a corrosive environment to slow down or prevent the corrosion of metal surfaces. Synthetic inhibitors have been widely used for many years, but their use is often limited due to their harmful effects on the environment and human health leading to an increase in demand for eco-friendly and cost-effective corrosion inhibitors. In recent years, there has been a growing interest in the usage of natural products as potent corrosion inhibitors owing to their eco-friendliness and minimal toxicity.

Weeds are ubiquitous plants that are often considered pests due to their ability to grow rapidly and take over fields and gardens. However, many weeds have medicinal properties and have been used for centuries in traditional medicine. Some weeds have also been shown to have antimicrobial, antioxidant, and anticancer properties. In recent years, there has been a growing interest in the use of weed extracts as corrosion inhibitors. Many weed extracts contain compounds that can inhibit corrosion, such as alkaloids, flavonoids, tannins, etc. In this work, the weeds tested for their corrosion inhibition efficiency were *Cnicus Benedictus*, *Vicia Sativa*, *Asphodelus tenuifolius*, *Polygonum Cuspidatum*, *Thysanolaena Latifolia* and *Trianthema Portulacastrum*. The study was carried out using various techniques, including weight loss analysis, surface morphology, computational analysis, adsorption and kinetics investigations and electrochemical analysis including electrochemical impedance spectroscopy, and potentiodynamic polarization. The experimental work started by preparing the weed extracts using several extraction techniques such

as Soxhlet extractor, ultrasonic-assisted extraction, Clevenger apparatus, cold maceration, etc. The mild steel samples were immersed in the weed extracts for different immersion times, and the weight loss analysis was carried out. Electrochemical impedance spectroscopy (EIS) was employed to examine the corrosion inhibition efficiency of the weed extracts. Potentiodynamic polarization was used to determine the mechanism of corrosion inhibition. With the aid of surface morphologies analyzing techniques and computational techniques, the deep insights into the adsorption of weed extract molecules and their corrosion-inhibiting characteristics were evaluated.

The hypothesis of the study on the corrosion inhibition efficiency of some common weeds on mild steel is that the eco-friendly extracts from selected weeds have the potential to act as eco-friendly and cost-effective corrosion inhibitors for mild steel in harsh environments. The study intends to evaluate the corrosion inhibition efficiency of these weeds through various methodologies including weight loss analysis, surface morphology, computational analysis, adsorption and kinetics investigations and electrochemical analysis. The hypothesis is based on previous studies that have shown the potential of natural products, such as plants, weeds and several other green extracts, as corrosion inhibitors. It is also based on the knowledge that several weeds contain compounds such as alkaloids, flavonoids, tannins, etc. that have been shown to have antioxidant and antimicrobial properties, which are desirable properties for corrosion inhibition.

The main objective of this study is to determine the potential of selected weeds extracts in preventing the corrosion of mild steel in a corrosive environment. The specific objectives of this study are:

1. To determine the inhibition efficiency of selected weeds on the corrosion of mild steel in acidic medium.
2. To study various adsorption isotherms involved in the interaction between mild steel and the selected weeds.
3. To calculate the effect of various parameters such as effect of immersion time, effect of temperature on the rate of corrosion.
4. To estimate various thermodynamic parameters like activation energy, Gibbs free energy, entropy and enthalpy.

5. To calculate quantum chemical parameters such as HOMO, LUMO etc of the selected weeds used as inhibitors for corrosion of mild steel.

After the detailed corrosion inhibition investigations of all six weeds, *Cnicus Benedictus* extract (CBE), *Vicia Sativa* extract (VSE), *Asphodelus Tenuifolius* aerial extract (ATAE), *Polygonum cuspidatum* root extract (PCRE), *Thysanolaena latifolia* leaves extract (TLLE) and *Trianthema Portulacstrum* aerial extract (TPAE) revealed as an eco-benign mild steel corrosion inhibitor in 0.5 M HCl medium, with an inhibitory efficiency of 92.45 % at 1000 ppm for CBE, 91.24% at 1000 ppm for VSE, 94.40% at 250ppm for ATAЕ, 96.71% at 1000ppm for PCRE, 93.90% at 1000ppm for TLLE and 94.33% at 1000ppm for TPAE at 298K. The development of a defensive layer over the mild steel surface in HCl solution was examined using contact angle measurement and scanning electron microscope (SEM) comprehending the electrochemical findings. Additionally, integrated computational investigations, including density functional theory (DFT), Monte Carlo (MC) and Molecular Dynamics (MD) simulations have been performed to confirm the potent inhibitory efficacy of all six weeds obtained by the experimental analysis and to support their adsorption upon the mild steel surface. In summary, our analysis revealed a sustainable, novel and effective corrosion inhibitor for mild steel in an aggressive corrosive medium.

The significance of the study on the corrosion inhibition efficacy of these six weeds on mild steel extends beyond the field of corrosion inhibition and has important implications for society and the environment. Firstly, the study highlights the importance of finding alternative and sustainable solutions to the usage of toxic corrosion inhibitors. Traditional corrosion inhibitors are often synthetic compounds that can be harmful to the environment and human health. The use of natural products such as weed extracts from weeds as corrosion inhibitors can reduce the dependence on toxic chemicals and promote environmentally sustainable practices in industry. Secondly, the use of weed extracts from weeds as corrosion inhibitors can have a positive impact on society by providing an affordable and accessible source of corrosion inhibitors. Weeds are abundant and easily available, making them a cost-effective alternative to synthetic inhibitors that can be expensive and require specialized equipment and expertise. Furthermore, the study demonstrates the potential of weeds as a valuable resource beyond their traditional use as unwanted plants. Weeds have been shown to have medicinal properties and can be used as a source of food and fiber. The use of weeds as corrosion inhibitors can provide an additional economic incentive for

their cultivation and utilization, thereby promoting sustainable agriculture practices. In addition, the study can contribute to the development of new industries and businesses that specialize in the extraction and production of natural corrosion inhibitors from weeds. This can create job opportunities and support local economies. Finally, the study can raise awareness among the general public about the environmental impact of corrosion and the importance of sustainable practices in the industry. The usage of natural products as corrosion inhibitors can promote a more eco-friendly and responsible approach to industrial processes.

## **PREFACE**

Corrosion is a natural process that occurs when metals react with their environment. It can be caused by a variety of factors, including exposure to moisture, oxygen, and chemicals. The consequences of corrosion can be severe, ranging from aesthetic damage to structural failure, which can cause significant economic losses and safety hazards. Corrosion prevention and control are critical for industries and society. One of the approaches to controlling corrosion is the usage of corrosion inhibitors. Corrosion inhibitors are substances that, when added to a metal surface or environment, reduce or prevent corrosion. Traditional corrosion inhibitors are usually synthetic compounds that are often toxic and expensive. Therefore, there is a growing interest in using natural compounds as corrosion inhibitors owing to their minimal cost, eco-friendly nature, and availability.

Several studies have explored the usage of plant extracts as corrosion inhibitors. However, most such studies have focused on agricultural crops and medicinal plants, leaving out the potential of weeds as corrosion inhibitors. Weeds are ubiquitous, easily available, and possess various biological and chemical properties that make them suitable for use as corrosion inhibitors. In this study, six common weeds were selected to evaluate their corrosion inhibition efficiency on mild steel. *Cnicus Benedictus*, *Vicia Sativa*, *Asphodelus tenuifolius*, *Polygonum Cuspidatum*, *Thysanolaena Latifolia* and *Trianthema Portulacastrum* were chosen based on their widespread availability and known biological activities. The study was conducted in two phases. The first phase involved the preparation of the extract to be used as an efficient corrosion inhibitor using several sophisticated instruments such as the Soxhlet apparatus, ultrasonic-assisted extraction, Clevenger apparatus and rotary evaporator. In the second phase, the corrosion inhibition efficiency of the extracts was examined utilizing weight loss, electrochemical techniques, surface morphologies techniques and computational analysis.

The findings of this study are significant because they provide a better understanding of the potential of weeds as corrosion inhibitors and their mechanism of action. The results could potentially lead to the development of eco-friendly and cost-effective corrosion inhibitors from natural sources. The use of weeds as corrosion inhibitors could reduce the cost and environmental impact associated with the use of synthetic inhibitors. Additionally, the identification of novel



compounds with potential applications in other fields such as medicine and agriculture could be possible. The potential applications of the findings of this study are not limited to the field of materials science and engineering. The discovery of novel compounds from natural sources could lead to advancements in various fields such as medicine, agriculture, and food science. Therefore, the findings of this study could have implications beyond corrosion prevention and control. The study of corrosion inhibition using natural compounds is an exciting and rapidly growing field. The exploration of natural compounds as corrosion inhibitors is essential for developing sustainable and eco-friendly solutions to corrosion. The findings of this study could inspire further research on the usage of weeds as corrosion inhibitors and encourage the use of natural compounds in various industries. In conclusion, this study focused on the corrosion inhibition efficiency of some common weeds on mild steel, providing insights into the potential of weeds as corrosion inhibitors. The findings of this study could contribute to the development of eco-friendly and cost-effective corrosion inhibitors from natural sources, and the discovery of novel compounds with potential applications beyond corrosion prevention and control. The study highlights the importance of exploring natural compounds as a source of novel solutions to various problems.

The thesis is structured into five chapters that cover a comprehensive study of corrosion inhibition of mild steel in acidic media using weed extracts.

### **Chapter 1: Introduction**

Chapter 1 serves as the introduction to the thesis and provides an overview of the key concepts related to corrosion. This chapter begins by defining corrosion and explaining its mechanistic approach. The factors affecting metallic corrosion are also discussed, with a particular focus on mild steel corrosion. The chapter then delves into the various techniques used for corrosion control, including the use of corrosion inhibitors. In this section, the focus is on green corrosion inhibitors, and the diverse techniques used to attain eco-friendly extracts are emphasized.

### **Chapter 2: Review of literature**

Chapter 2 provides a review of the relevant literature on corrosion inhibition, particularly in acidic media. The chapter discusses the use of green corrosion inhibitors, such as plant and weed extracts, as eco-friendly alternatives to traditional inhibitors for protecting metals, particularly mild steel, in acidic corrosive media. The purpose, scope, and objectives of the research are also

discussed in this chapter.

### **Chapter 3: Methods and Materials**

Chapter 3 is dedicated to the methods and materials used in the corrosion tests for mild steel in 0.5M HCL medium. The chapter describes the various techniques and experimental procedures employed to determine the weight loss measurements at a temperature of 298 K. Adsorption and thermodynamic parameters was also determined, which play a crucial role in corrosion inhibition. The adsorption behavior of the inhibitor molecules can be studied by analyzing the thermodynamic parameters such as the adsorption free energy ( $\Delta G^{\circ}_{\text{ads}}$ ), adsorption enthalpy ( $\Delta H^{\circ}_{\text{ads}}$ ), and adsorption entropy ( $\Delta S^{\circ}_{\text{ads}}$ ). Electrochemical impedance and potentiodynamic study of natural corrosion inhibitors on mild steel in acidic medium are also discussed in this chapter. The identification of functional groups present in selected weed extracts has been done using Fourier transform infrared spectroscopy. UV-vis spectroscopy has been also used to measure the amount of ultraviolet (UV) light absorbed by a metal surface in the presence of a corrosion inhibitor. SEM and contact angle measurement have been used for surface morphological studies and the hydrophobic character of the film produced by the weed extracts potent corrosion inhibitor. Additionally, crucial computational analyses such as DFT, MCS and MDS have been used for calculating quantum chemical parameters like energies of the highest occupied molecular orbital (HOMO), energies of lower unoccupied molecular orbital (LUMO), and the energy gap between the HOMO and LUMO. The biodegradability rate investigation has been also investigated for all the weeds extract. With the help of these parameters, the corrosion inhibition mechanism of selected weeds on mild steel surfaces in corrosive media has been effectively analyzed.

### **Chapter 4: Results and Discussion**

Chapter 4 presents the results and discussion of the research on green corrosion inhibitors. The chapter focuses on the selected weeds, including *Cnicus Benedictus*, *Vicia Sativa*, *Asphodelus tenuifolius*, *Polygonum Cuspidatum*, *Thysanolaena Latifolia*, and *Trianthema Portulacastrum*. The results of the weight loss measurements, adsorption and thermodynamic parameters, electrochemical impedance and potentiodynamic study, UV-vis spectroscopy, FT-IR analysis, SEM and contact angle measurements, and computational analyses are presented in detail. The

chapter also provides a comprehensive discussion of the mechanism of corrosion inhibition by the selected weeds.

## **Chapter 5: Summary and Conclusions**

Chapter 5 serves as the conclusion of the thesis and provides an overall summary of the research on weed extracts-based eco-benign corrosion inhibitors. The efficiency of the selected corrosion inhibitors is discussed in detail, along with a comparison of the results. The chapter also summarizes the research findings and provides a list of publications, workshops, and conferences attended. The bibliography is also included in this chapter. The future scope of work is also discussed in this chapter, which includes the development of more effective green corrosion inhibitors and the application of the inhibitors in real-world scenarios. The researcher also suggests the exploration of eco-benign weed extracts as potential corrosion inhibitors and the utilization of advanced computational tools to provide deeper insights into the inhibition mechanism.

## **ACKNOWLEDGMENT**

As a devout believer of **Lord Krishna**, I believe that starting a Ph.D. journey and undertaking a research project requires dedication, hard work, and a supportive network of individuals who believe in your abilities and encourage you to succeed. Therefore, I would like to start by expressing my heartfelt gratitude to **Lord Krishna** for his blessings and guidance throughout my academic journey.

I am deeply indebted to my esteemed supervisor, **Dr. Ashish Kumar**, for his unwavering support, guidance, and motivation throughout my Ph.D. journey. His immense knowledge, expertise, and patience were instrumental in shaping my research and refining my skills as a scholar. Without Lord Krishna's blessings and Dr. Kumar's advice and constant encouragement, this research would not have been possible. I am also grateful to **Dr. Praveen Kumar** Sharma for his contributions towards my research project. His insightful comments, suggestions, and critiques have helped me refine my research questions and methodologies. His support has been invaluable in shaping my research, and I am indebted to him for his generosity.

I would like to extend my heartfelt gratitude to my family for their unwavering support and encouragement. My mother **Smt. Shanta Thakur** and father **Sh. Ram Kumar** has always been my pillar of strength, providing me with love, care, and support throughout my academic journey. Their sacrifices and selfless devotion have been a source of inspiration to me, and I am blessed to have them in my life. I am also grateful to my elder sister **Ms. Anuja Thakur** for taking on additional responsibilities and supporting me in every circumstance. Her unwavering support and encouragement have been a source of motivation for me, and I am grateful for her contributions.

I am immensely thankful to Senior **Dr. Sumayah Bashir** and **Dr. Vivek Sharma** for providing me with invaluable support and encouragement during my research work. Their insightful feedback, suggestions, and guidance have played a crucial role in shaping my research, and I am deeply grateful for their contributions. I would like to express my gratitude to my kind-hearted senior, **Dr. Harpeet Kaur**, for her unwavering support throughout my research work. Her encouragement, guidance, and advice have been invaluable in shaping my research and helping me to navigate through the challenges that come with academic pursuits. I would also like to express my appreciation to my research mates for their invaluable support and advice throughout my research work. Their insights, feedback, and suggestions have been instrumental in shaping

my research, and I am grateful for their support.

Furthermore, I want to express my gratitude to **Lord Krishna** for giving me good health, which was essential in completing this research work. I am thankful for this gift and will continue to strive to use it to the best of my abilities to contribute positively to society. Lastly, I am deeply indebted to everyone who supported me in my research work. Their contributions have been invaluable, and I will always be grateful for their unwavering support, encouragement, and motivation. I hope to continue to make them proud in my future endeavors and to inspire others as they have inspired me.

## Table of Contents

<b>Chapter 1: Introduction</b>		
1.1.	Introduction	2
1.1.1.	The Ubiquitous Nature of Corrosion	2
1.1.2.	Mechanism of Corrosion	3
1.2.	Mild steel and its usage	6
1.2.1.	Corrosion of mild steel	7
1.3.	Corrosion mitigation techniques	8
1.3.1.	Corrosion Inhibitors	10
1.3.1.1.	Green Corrosion Inhibitors	12
1.3.2.	Corrosion inhibition mechanism	14
1.3.3.	Prominent metrics for extract preparation	19
1.3.3.1.	Extraction	19
1.3.3.2.	Plant material	20
1.3.3.3.	Pre-extraction of plant sample	21
1.3.3.4.	Fresh vs. dried sample	21
1.3.3.5.	Grinded vs. powdered samples	22
1.3.3.6.	Air-drying	22
1.3.3.7.	Microwave-drying	22
1.3.3.8.	Oven-drying	22
1.3.3.9.	Freeze-drying	23
1.3.4.	Methods of Plant extraction	23
1.3.4.1.	Hot Continuous Extraction (Soxhlet)	23
1.3.4.2.	Ultrasound-assisted extraction (UAE) or sonication extraction	24
1.3.4.3.	Supercritical fluid extraction (SFE)	25
1.3.4.4.	Maceration	26
1.3.4.5.	Decoction	27
1.3.4.6.	Counter Current Extraction	28
1.3.4.7.	Pressurized liquid extraction (PLE)	29
1.3.4.8.	Microwave assisted extraction (MAE)	30
<b>Chapter 2: Review of Literature</b>		
2.1.	Literature Survey	33
2.1.1.	Green corrosion inhibitors	33
2.1.1.1.	Plant extracts as corrosion inhibitors for metals	33
2.1.1.2.	Weed extracts as corrosion inhibitors for metals	50
2.2.	Purpose of Present Research Work	79
2.3.	Scope and intents of the present research work	79
2.4.	Objectives of the study	80
<b>Chapter 3: Methods and Materials</b>		
3.1.	Methods in brief	82
3.2.	Preparation of samples	84
3.3.	Preparation of the electrode surface	85
3.4.	Selected weeds for the investigation	85
3.5.	Test solutions	87
3.6.	Preparation of weed extracts	88

3.7.	FT-IR spectroscopy	89
3.8.	UV-vis assessment	90
3.9.	Weigh loss (WL) assessment	91
3.10.	Adsorption and thermodynamic parameters	93
3.11.	Electrochemical measurements	95
3.11.1.	Open circuit potential (OCP)	97
3.11.2.	Potentiodynamic polarization (PDP) studies	98
3.11.3.	Electrochemical impedance spectroscopy (EIS)	99
3.12.	Surface morphology assessment	101
3.12.1.	Scanning electron microscopy (SEM)	101
3.12.2.	Contact angle (CA) assessment	102
3.13.	Computational analysis	103
3.13.1.	Quantum chemical evaluation	103
3.13.2.	Molecular Dynamics (MD) and Monte Carlo (MC) Simulations	104
3.14.	Biodegradability determination	105
3.14.1.	Preparation of inoculum	105
3.14.2.	Buffer media formulation	105
3.14.3.	Dilution of H <sub>2</sub> O	106
<b>Chapter 4: Results and Discussion</b>		
4.1.	<i>Cnicus Benedictus</i>	108
4.1.1.	Preparation of <i>Cnicus Benedictus</i> extract	109
4.1.2.	FT-IR analysis	110
4.1.3.	UV-visible spectrometry	110
4.1.4.	Weight loss measurement	111
4.1.5.	Adsorption and thermodynamic parameters	113
4.1.6.	Electrochemical measurements	115
4.1.6.1.	Open circuit potential (OCP)	115
4.1.6.2.	Potentiodynamic polarization	116
4.1.6.3.	Electrochemical impedance spectroscopy (EIS)	118
4.1.7.	Surface analysis	121
4.1.7.1.	SEM	121
4.1.7.2.	Contact angle (CA) measurement	122
4.1.8.	DFT and MC simulations	123
4.1.9.	Biodegradability of CBE	129
4.2.	<i>Vicia Sativa</i>	131
4.2.1.	Preparation of <i>Vicia Sativa</i> extract	132
4.2.2.	FT-IR analysis	133
4.2.3.	UV-visible spectrometry	133
4.2.4.	Weight loss measurement	134
4.2.5.	Adsorption and thermodynamic parameters	136
4.2.6.	Electrochemical measurements	139
4.2.6.1.	Open circuit potential (OCP)	139
4.2.6.2.	Potentiodynamic polarization	140
4.2.6.3.	Electrochemical impedance spectroscopy (EIS)	142
4.2.7.	Surface analysis	145
4.2.7.1.	SEM	145

4.2.7.2.	Contact angle (CA) measurement	146
4.2.8.	DFT and MC simulations	147
4.2.9.	Biodegradability of VSE	154
4.3.	<i>Thysanolaena latifolia</i>	156
4.3.1.	Preparation of <i>Thysanolaena latifolia</i> leaves extract	157
4.3.2.	FT-IR evaluation	158
4.3.3.	UV-visible spectroscopy	159
4.3.4.	Weight loss assessment	160
4.3.5.	Adsorption and thermodynamic parameters	163
4.3.6.	Electrochemical measurements	165
4.3.6.1.	Open circuit potential (OCP)	165
4.3.6.2.	Potentiodynamic polarization	166
4.3.6.3.	Electrochemical impedance spectroscopy (EIS)	168
4.3.7.	Surface examinations	172
4.3.7.1.	SEM	172
4.3.7.2.	Contact angle (CA) assessment	173
4.3.8.	Computational analysis	174
4.3.8.1.	DFT analysis	174
4.3.8.2.	MC simulation analysis	180
4.3.9.	Biodegradability of TLLE	184
4.4.	<i>Trianthema Portulacstrum</i>	185
4.4.1.	Preparation of <i>Trianthema Portulacstrum</i> aerial extract	186
4.4.2.	FT-IR evaluation	187
4.4.3.	UV-visible spectrometry	187
4.4.4.	Weight loss analysis	188
4.4.5.	Adsorption and thermodynamic variables	191
4.4.6.	Electrochemical analysis	193
4.4.6.1.	Open circuit potential (OCP)	193
4.4.6.2.	Potentiodynamic polarization	194
4.4.6.3.	Electrochemical impedance spectroscopy (EIS)	195
4.4.7.	Surface morphology analysis	198
4.4.7.1.	SEM	198
4.4.7.2.	Contact angle (CA) assessment	199
4.4.8.	Computational analysis	200
4.4.8.1.	DFT analysis	200
4.4.8.2.	MC simulation analysis	205
4.4.9.	Biodegradability of TPAE	207
4.5.	<i>Polygonum cuspidatum</i>	209
4.5.1.	Preparation of <i>Polygonum Cuspidatum</i> root extract	210
4.5.2.	FT-IR evaluation	211
4.5.3.	UV-Vis spectrometry	212
4.5.4.	Weight loss measurement	213
4.5.4.1.	Concentration's effect on inhibition performance	214
4.5.5.	Temperature impact and activation parameters	216
4.5.6.	Adsorption studies	220
4.5.7.	Electrochemical analysis	222



4.5.7.1.	Open circuit potential (OCP)	222
4.5.7.2.	Potentiodynamic polarization	223
4.5.7.3.	Electrochemical impedance spectroscopy (EIS)	226
4.5.8.	Surface morphology analysis	230
4.5.8.1.	SEM	230
4.5.8.2.	Contact angle (CA) assessment	230
4.5.9.	Computational studies	231
4.5.9.1.	DFT	231
4.5.9.2.	MC and MD simulations	238
4.5.9.3.	RDF analysis	242
4.5.10.	Biodegradability of PCRE	244
4.6.	<i>Asphodelus Tenuifolius</i>	246
4.6.1.	Preparation of <i>Asphodelus Tenuifolius</i> extract	247
4.6.2.	FT-IR evaluation	248
4.6.3.	UV-Vis spectrometry	249
4.6.4.	Weight loss measurement	250
4.6.4.1.	Concentration's effect on inhibition performance	251
4.6.5.	Temperature impact and activation parameters	252
4.6.6.	Adsorption studies	257
4.6.7.	Electrochemical analysis	259
4.6.7.1.	Open circuit potential (OCP)	259
4.6.7.2.	Potentiodynamic polarization	260
4.6.7.3.	Electrochemical impedance spectroscopy (EIS)	263
4.6.8.	Surface morphology analysis	267
4.6.8.1.	SEM	267
4.6.8.2.	Contact angle (CA) assessment	268
4.6.9.	Computational studies	269
4.6.9.1.	DFT	269
4.6.9.2.	MC and MD simulations	275
4.6.9.3.	RDF analysis	280
4.6.10.	Biodegradability of PCRE	281
<b>Chapter 5: Summary and Conclusion</b>		
5.1.	Summary	284
5.1.1.	Experimental investigations	284
5.1.1.1.	UV-vis spectrometry	284
5.1.1.2.	FT-IR analysis	285
5.1.1.3.	Weight loss measurements	285
5.1.1.4.	Adsorption Isotherms and Thermodynamic Variables	285
5.1.1.5.	Electrochemical impedance spectroscopy	285
5.1.1.6.	Potentiodynamic polarization	286
5.1.1.7.	Surface morphology	286
5.1.1.7.1.	SEM	286
5.1.1.7.2.	Contact angle measurement	286
5.1.1.8.	Computational analysis	287
5.1.1.8.1.	Density Functional Theory	287
5.1.1.8.2.	Monte Carlo Simulation	287

5.1.1.8.3.	Molecular Dynamics Simulation	287
5.2.	Conclusion	289
5.3.	Future scope of the work	290
	References	292
	List of Publications	338
	List of Conferences/ Webinars/ Short term courses attended	343

## List of Tables

<b>Chapter 2: Review of Literature</b>		
Table 2.1	Plant extracts as corrosion inhibitors for several metals in different electrolytic media involving various plant names, techniques, nature of metal and electrolyte and nature of the adsorption of active phytoconstituents	43
Table 2.2	Weed extracts as corrosion inhibitors in hydrochloric acid solution involving various weeds names, techniques, nature of metal and electrolyte and nature of the adsorption of active phytoconstituents	73
<b>Chapter 4: Results and Discussion</b>		
Table 4.1	Effect of time on the inhibition efficiency of mild steel in 0.5M HCl in the absence and presence of 1000ppm inhibitor at 298K	112
Table 4.2	Effect of temperature on the inhibition efficiency of mild steel in 0.5M HCl in the absence and presence of 1000ppm of inhibitor	112
Table 4.3	Effect of concentration on the inhibition efficiency of mild steel in 0.5M HCl in the absence and presence of inhibitor (100-1000ppm at 298K)	112
Table 4.4	Adsorption, kinetic and thermodynamic parameters for CB (1000 ppm) as corrosion inhibitor for mild steel in 0.5 M HCl media in 298K	115
Table 4.5	Corrosion parameters for mild steel in 0.5 M HCl in the exclusion and inclusion of CBE attained through electrochemical experiments (EIS and Tafel) at 298K	118
Table 4.6	Inhibition efficiency values of CBE inhibitor for mild steel in various conc. of inhibitor	121
Table 4.7	List of quantum chemical parameters by DMol3 Accelers' 2017 Material Studio	125
Table 4.8	Representation of Molecular simulation parameters for adsorption of Chlorogenic acid (1CB) and Sinapic acid (2CB) in different H <sub>2</sub> O and H <sub>3</sub> O <sup>+</sup>	127
Table 4.9	The output energies determined by Monte Carlo simulation for Chlorogenic acid and Sinapic acid on Fe (110)	128
Table 4.10	Effect of concentration on the IE% of mild steel in 0.5M HCl without and with VSE inhibitor (50-1000ppm at 298K)	128
Table 4.11	Effect of time on the IE% of mild steel in 0.5M HCl without and with 1000ppm of VSE inhibitor at 298K	135
Table 4.12	Effect of temperature on the IE% of mild steel in 0.5M HCl without and with 1000ppm of VSE inhibitor	135
Table 4.13	Adsorption, kinetic and thermodynamic values for VSE (50-1000ppm) inhibiting mild steel corrosion in 0.5M HCl medium at 298K	135
Table 4.14	Corrosion parameters for mild steel in 0.5M HCl excluding and including VSE (50-1000ppm) obtained by the usage of electrochemical experiments at 298K	138
Table 4.15	EIS parameters obtained by the addition of several conc. (50-1000ppm) of VSE	142

Table 4.16	Data values of quantum chemical parameters using DMol3 Accelers based on Material Studio 2017	145
Table 4.17	List of Molecular simulation parameters by Montecarlo simulation (250 H <sub>2</sub> O + 5 H <sub>3</sub> O <sup>+</sup> +5CL <sup>-</sup> + Inh)	149
Table 4.18	List of Molecular simulation parameters by Montecarlo simulation in a vacuum	151
Table 4.19	The influence of time fluctuations on the IE% of TLLE on the corrosion inhibition of mild steel	153
Table 4.20	The influence of temperature fluctuations on the IE% of TLLE on the corrosion inhibition of mild steel	161
Table 4.21	The influence of concentration fluctuations on the IE% of TLLE on the corrosion inhibition of mild steel	162
Table 4.22	Adsorption, thermodynamic and kinetic variables for the corrosion inhibition of mild steel in several amounts of TLLE at 298K	164
Table 4.23	Tafel variables for the corrosion inhibition of mild steel in blank solution subjected to 50-1000ppm amounts of TLLE at 298 K	168
Table 4.24	IE% values for the corrosion mitigation of mild steel in 0.5M HCl subjected to 50-1000ppm amounts of TLLE at 298 K	172
Table 4.25	Calculated quantum chemical variables for inhibitor molecules through B3LYP/6-311G (d, p) basis sets	177
Table 4.26	E <sub>interaction</sub> and E <sub>binding</sub> (all in kJ/mol) of V(Z)-hex-3-en-1-ol, (E)-b-ionone and Phytol upon Fe (1 1 0) surface in HCl at 298K	183
Table 4.27	Influence of immersion time on the IE% of TPAE for mild steel corrosion	189
Table 4.28	Influence of temperature on the IE% of TPAE for mild steel corrosion	189
Table 4.29	Influence of conc. on the IE% of TPAE for mild steel corrosion	190
Table 4.30	Adsorption, thermodynamic and kinetic variables for the metallic corrosion mitigation in the exclusion and subjection of 1000 ppm of TPAE in 0.5 M HCl at 298K	192
Table 4.31	Tafel parameters for mild steel corrosion inhibition in 0.5M HCl with 50–1000 ppm TPAE at ambient temperature	195
Table 4.32	IE% values for the corrosion mitigation of mild steel in 0.5M HCl subjected to 50-1000ppm conc. of TPAE at 298 K	198
Table 4.33	Pertinent electronic parameters related to the extract components in the aqueous phase with the usage of the DNP 3.5 basis set and the GGA/BLYP technique	203
Table 4.34	E <sub>interaction</sub> and E <sub>binding</sub> of V(Z)-hex-3-en-1-ol, (E)-b-ionone and Phytol on Fe (1 1 0) surfaces in HCl at 298K (all in kJ/mol)	207
Table 4.35	Gravimetric outcomes for mild steel in 0.5M HCl without and with PCRE	214
Table 4.36	Corrosion rate, Inhibition performance (%) and surface coverage of mild steel in 0.5M HCl solution of PCRE	216
Table 4.37	Mild steel activation parameters (E <sub>a</sub> , ΔH <sub>a</sub> , ΔS) in the existence and non-existence of PCRE	218
Table 4.38	Various adsorption variables for PCRE in 0.5M HCl solution	221
Table 4.39	Tafel variables for the corrosion mitigation of mild steel in blank solution subjected to 50-1000ppm amounts of PCRE at 298 K	225
Table 4.40	IE% values for the corrosion mitigation of mild steel in 0.5M HCl subjected to 50-1000ppm conc. of PCRE at 298 K	229

Table 4.41	Calculated theoretical parameters (1) Piceid, (2) Resveratrol, (3) Emodin, (4) Emodin-1-O-glucoside and (5) 1-O-Methylemodin molecules	238
Table 4.42	Gravimetric outcomes for mild steel in 0.5M HCl without and with ATAE	250
Table 4.43	Corrosion rate, Inhibition performance (%) and surface coverage of mild steel in 0.5M HCl solution of ATAE	253
Table 4.44	Mild steel activation parameters ( $E_a$ , $\Delta H_a$ , $\Delta S$ ) in the existence and non-existence of ATAE	254
Table 4.45	Various adsorption variables for ATAE in 0.5M HCl solution	258
Table 4.46	Tafel variables for the corrosion mitigation of mild steel in blank solution subjected to 50-250ppm amounts of ATAE at 298 K	262
Table 4.47	IE% values for the corrosion mitigation of mild steel in 0.5M HCl subjected to 50-250ppm conc. of ATAE at 298 K	267
Table 4.48	Calculated theoretical parameters of the Trans-2-decen-1-ol, trimethylsilyl ether, 1,4-anhydro-d-glactitol and 5-hydroxymethylfurfural inhibitors	274
<b>Chapter 5: Summary and Conclusion</b>		
Table 5.1	Evaluation of inhibitory efficiency of numerous sustainable inhibitors for mild steel corrosion in the corrosive solution	288

## List of Figures

<b>Chapter 1: Introduction</b>		
Figure 1.1	Schematic representation of the mechanism of reinforcement corrosion	3
Figure 1.2	Aqueous Corrosion of iron	4
Figure 1.3	Impact of SO <sub>2</sub> and humidity on metallic corrosion (atmospheric corrosion). Reaction occurs in a very thin (invisible) aqueous layer	5
Figure 1.4	Plant ( <i>Origanum vulgare</i> ) extract being used as a corrosion inhibitor for reinforced steel which develops a layer resistant to corrosion	11
Figure 1.5	Diagram outlining the crucial factors that must be met for compounds to be considered as suitable green corrosion inhibitors for preventing metal corrosion	13
Figure 1.6	Different sources of green corrosion inhibitor	14
Figure 1.7	Corrosion inhibition impact of crude extracts (hexane, dichloromethane, methanol) from the bark of <i>Cryptocarya nigra</i> and three alkaloids identified N-methylisococlaurine N-methylaurotetanine and atherosperminine extracted from the extract of <i>Cryptocarya nigra</i> dichloromethane (CNDE) tested for mild steel corrosion in 1 M HCl solution	15
Figure 1.8	The adsorption model of OPEO on the mild steel surface	17
Figure 1.9	Adsorption mechanism of <i>Theobroma cacao</i> peel extract on the mild steel surface	18
Figure 1.10	Schematic figure of the film formation mechanism of <i>Houttuynia cordata</i> leaf extract's species for protecting steel in 0.1MHCl solution: (a) without inhibitor, (b) with low inhibitor concentration and (c) with high inhibitor concentration	19
Figure 1.11	Basic parts of a plant and their common active compounds	21
Figure 1.12	Extraction of active phytochemicals from plant dried sample by Soxhlet apparatus	24
Figure 1.13	Schematic representation of the ultrasound-assisted extraction (UAE) process used in extraction technique	25
Figure 1.14	Representation of Supercritical fluid extraction (SFE) instrument	26
Figure 1.15	Maceration procedure for extraction	27
Figure 1.16	Aqueous decoction of plant raw material	28
Figure 1.17	Counter-current Extraction apparatus	29
Figure 1.18	Pressurized liquid extraction (PLE) process	30
Figure 1.19	Microwave assisted extraction (MAE) extraction procedure	30
<b>Chapter 2: Review of Literature</b>		
Figure 2.1	Diagrammatic illustration of the adsorption of phytochemicals derived from plant extract forming a protective layer on the mild steel surface	34
<b>Chapter 3: Methods and Materials</b>		
Figure 3.1	(a) The designing of the electrode shown on a bare mild steel rod, (b) Manufacturing of the working electrode to be used in the electrochemical analysis	85

Figure 3.2	(a) <i>Cnicus Benedictus</i> , (b) <i>Vicia Sativa</i> , (c) <i>Trianthema Portulacastrum</i> , (d) <i>Thysanolaena Latifolia</i> , (e) <i>Polygonum Cuspidatum</i> and (f) <i>Asphodelus tenuifolius</i>	86
Figure 3.3	A stock solution of weed extract attained after aggregation with 0.5M HCl ( <b>left</b> ), Beaker containing 0.5M HCl solution ( <b>right</b> )	87
Figure 3.4	(a) Dried state of <i>Cnicus Benedictus</i> (b) Rota evaporator utilized to attain crude extract (c) and (d) Deep freeze extract of selected six weeds	89
Figure 3.5	Shimadzu FTIR 8400S instrument utilized in the research	90
Figure 3.6	Shimadzu UV-1900i UV/Visible Scanning Spectrophotometer utilized in the research	90
Figure 3.7	Schematic representation of weight-loss analysis of weed (PCRE= <i>Polygonum Cuspidatum</i> root extract as an example)	92
Figure 3.8	Weight loss analysis of the mild steel sample in the absence of 0.5M HCl ( <b>left</b> ) and in the presence of inhibitor+0.5M HCl ( <b>right</b> )	93
Figure 3.9	Metrohm Autolab NOVA 2.1. electrochemical workstation ( <b>left</b> ), Corrosion cell setup ( <b>right</b> )	96
Figure 3.10	Attained OCP during the electrochemical analysis (left), Graph showing OCP (Potential vs. Time) attained for weed extract illustrating the un-stabilized and stabilized OCP (right)	97
Figure 3.11	Attained Tafel plot during the experiment ( <b>left</b> ), Graph showing Tafel plot attained for weed extract illustrating the cathodic and anodic slopes ( <b>right</b> )	99
Figure 3.12	Attained Nyquist plot during the experiment ( <b>left</b> ), Graph showing Nyquist plot attained for weed extract illustrating the higher frequency and lower frequency region ( <b>right</b> )	100
Figure 3.13	Bodes graph for the corrosion mitigation of mild steel in blank media subjected to various concentrations of weed extract (inhibitor) at 298 K	101
Figure 3.14	JEOL JSM-IT100 SEM instrument	102
Figure 3.15	DSA100-E KRUSS for measuring the contact angle	103
<b>Chapter 4: Results and Discussion</b>		
Figure 4.1	Depiction of (a) <i>Cnicus Benedictus</i> , Chemical structures of (b) Chlorogenic acid, (c) Sinapic acid	109
Figure 4.2	FT-IR evaluation of the CBE	110
Figure 4.3	UV Spectra of CBE before and after the metal immersion	111
Figure 4.4	Effects of (a) time, (b) temperature and (c) concentration variation on inhibition efficiency	113
Figure 4.5	(a) Langmuir adsorption plot (b) Arrhenius plot (c) Enthalpy plot CB extract as corrosion inhibitor of mild steel in 0.5 M HCl solution	114
Figure 4.6	OCP vs time plot time plots for mild steel in 0.5 M HCl without and with various concentrations of CBE (100-1000ppm)	116
Figure 4.7	Tafel plot for mild steel corrosion inhibition in 0.5M HCl media subjected to several concentrations of inhibitor at 298 K	117
Figure 4.8	Nyquist plot for the mild steel corrosion inhibition in 0.5M HCl subjected to different inhibitor concentrations at 298 K	119

Figure 4.9	Bodes plots for the mild steel corrosion inhibition in 0.5M HCl subjected to various concentrations of inhibitor at 298 K	119
Figure 4.10	An equivalent circuit diagram was utilized to fit the data	120
Figure 4.11	SEM images of (a) plain mild steel, (b) mild steel dipped in 0.5 M HCl without inhibitor (c) mild steel in 0.5 M HCl immersed in 1000ppm of inhibitor solution	122
Figure 4.12	Contact angle measurement was done on the metal sample in (a) blank solution and (b) blank solution+inhibitor	123
Figure 4.13	HOMO and LUMO distribution of inhibitor	124
Figure 4.14	The equilibrium position of inhibitors Chlorogenic acid and Sinapic acid from Monte Carlo Simulations	127
Figure 4.15	ESP maps and isosurface of chlorogenic acid and Sinapic acid	129
Figure 4.16	Biodegradability of CBE	130
Figure 4.17	Illustrations of (a) <i>Vicia Sativa</i> and its major chemical constituents (b) (Z)-2-hexenal, (c) 1-Octen-3-ol and (d) (Z)-3-hexenol	132
Figure 4.18	FT-IR evaluation of the VSE	133
Figure 4.19	UV spectrum of VSE prior and following the immersion of metal	134
Figure 4.20	Impact of (a) concentration, (b) time (c) temperature variation on the IE% of VSE on mild steel	136
Figure 4.21	(a) Langmuir adsorption graph (b) Arrhenius graph (c) Enthalpy graph of VSE as an effective mild steel corrosion inhibitor in 0.5M HCl	138
Figure 4.22	OCP vs time graph for mild steel in 0.5M HCl excluding and including several amounts of VSE (50-1000ppm)	140
Figure 4.23	Tafel plot for the corrosion inhibition of mild steel in 0.5M HCl medium exposed to several concentrations (50-1000ppm) of VSE at 298 K	141
Figure 4.24	Nyquist plot for the corrosion inhibition of mild steel in 0.5M HCl medium exposed to several concentrations (50-1000ppm) of VSE at 298 K	143
Figure 4.25	Bodes plot for the corrosion inhibition of mild steel in 0.5M HCl medium exposed to various concentrations (50-1000ppm) of VSE at 298 K	143
Figure 4.26	An equivalent circuit diagram employed for the fitting of the EIS data	144
Figure 4.27	SEM pictures of (a) plain mild steel, (b) mild steel immersed in 0.5M HCl (c) mild steel immersed in 0.5M HCl+ VSE (1000ppm)	146
Figure 4.28	Contact angle evaluations conducted on the mild steel specimen in (a) 0.5M HCl and (b) 0.5M HCl + 1000ppm inhibitor	147
Figure 4.29	Electron density geometries of HOMO and LUMO illustrated for the optimized structure of inhibitors	148
Figure 4.30	Depiction of the insights of the electron density maps showing HOMO and LUMO positive and negative structures	149
Figure 4.31	Equilibrium positions of the most stable and persistent configuration of inhibitors on Fe (110) in a simulated HCL corrosive system	151
Figure 4.32	Equilibrium positions of most stable arrangement of inhibitors on Fe (110) in a vacuum	152



Figure 4.33	ESP mappings and isosurface of (Z)-2-hexenal, 1-Octen-3-ol and (Z)-3-hexenol	154
Figure 4.34	Biodegradability of VSE in 28 days	155
Figure 4.35	Schematic depiction of (a) <i>Thysanolaena latifolia</i> ; the main phytochemical constituents of TLLE (b) (Z)-3-hexen-1-ol, (c) (E)-b-ionone, (d) Phytol	157
Figure 4.36	FT-IR analysis of the TLLE	158
Figure 4.37	UV spectrum of pre and post of metal dipped in 0.5M HCl and with the inclusion of TLLE	159
Figure 4.38	(a) Time, (b) temperature and (c) concentration fluctuations effect on the IE% of TLLE	162
Figure 4.39	(a) Langmuir adsorption graph (b) Arrhenius graph (c) Enthalpy graph of TLLE on the corrosion inhibition of mild steel in 0.5 M HCl medium	164
Figure 4.40	OCP vs. time graph for corrosion inhibition of mild steel after exposure to 1000ppm of TLLE concentration in 0.5M HCl	166
Figure 4.41	Tafel graph for the corrosion mitigation of mild steel in blank solution subjected to 50-1000ppm amounts of TLLE at 298 K	167
Figure 4.42	Nyquist graph for the corrosion mitigation of mild steel in blank media subjected to 50-1000ppm concentrations of TLLE at 298 K	169
Figure 4.43	Bodes graph for the corrosion mitigation of mild steel in blank solution subjected to 50-1000ppm conc. of TLLE at 298 K	170
Figure 4.44	A circuit model with equivalent components employed to fit the collected data	170
Figure 4.45	SEM illustrations of (a) standard metal, (b) metal dipped in 0.5M HCl (c) metal dipped in 0.5M HCl + TLLE (1000ppm)	173
Figure 4.46	CA measurements conducted on (a) a metal specimen in 0.5M HCl and (b) a metal specimen in a solution containing 1000ppm of TLLE+blank solution	174
Figure 4.47	Optimized configuration, HOMO and LUMO distribution and total density of (a) V(Z)-hex-3-en-1-ol, (b) (E)-b-ionone, (c) Phytol using B3LYP/6-311G (d, p) basis sets	177
Figure 4.48	The positive and negative regions of HOMO and LUMO geometries of (a) V(Z)-hex-3-en-1-ol, (b) (E)-b-ionone and (c) Phytol using B3LYP/6-311G (d, p) basis sets	178
Figure 4.49	Electrostatic potential (ESP) maps and Isosurface of (a) V(Z)-hex-3-en-1-ol, (b) (E)-b-ionone and (c) Phytol using B3LYP/6-311G (d, p) basis sets	179
Figure 4.50	Balance adsorption configurations of V(Z)-hex-3-en-1-ol, (E)-b-ionone and Phytol upon Fe (1 1 0) surface in HCl at 298K	182
Figure 4.51	Biodegradability rate of TLLE	184
Figure 4.52	Schematic representation of (a) <i>Trianthema Portulacstrum</i> ; the main chemical constituents of TPAE (b) Hexahydro-farnesyl acetone, (c) Verbenene, (d) Incensole acetate	186
Figure 4.53	FT-IR analysis of the TPAE	187
Figure 4.54	UV Spectra of pre- and post-metal immersion in 0.5M HCl and with the inclusion of TPAE	188

Figure 4.55	Impact of <b>(a)</b> time (min.), <b>(b)</b> temperature and <b>(c)</b> conc. on the IE% of TPAAE for mild steel corrosion	190
Figure 4.56	Plots of <b>(a)</b> Langmuir adsorption <b>(b)</b> Arrhenius <b>(c)</b> Enthalpy on the IE% of TPAAE for mild steel corrosion in 0.5 M HCl	192
Figure 4.57	OCP vs. time plot for the mild steel in 0.5 M HCl in the exclusion and inclusion of 50-1000 ppm of TPAAE	194
Figure 4.58	Tafel graph for mild steel corrosion inhibition in 0.5M HCl with 50–1000 ppm TPAAE at 298 K	195
Figure 4.59	Nyquist graph for mild steel corrosion inhibition in 0.5M HCl with 50–1000 ppm TPAAE at ambient temperature	196
Figure 4.60	Bodes graph for the corrosion mitigation of mild steel in 0.5M HCl with 50–1000 ppm TPAAE at 298 K	197
Figure 4.61	The utilized eqv. circuit model for the data fitting	197
Figure 4.62	SEM visuals of (a) plain metal, (b) metal submerged in 0.5 M HCl (c) metal submerged in 0.5 M HCl + TPAAE (1000ppm)	199
Figure 4.63	CA assessment performed on the metallic sample in <b>(a)</b> 0.5M HCl media and <b>(b)</b> 0.5M HCl +1000ppm of TPAAE	200
Figure 4.64	Optimized geometries and FMOs (i.e., HOMO and LUMO) of the Hexahydro-farnesyl acetone, Verbenene and Incensole acetate	202
Figure 4.65	Isosurfaces of total electronic density and ESP mapping (green and red colors denote electro-positive and negative potentials, respectively) of the Hexahydro-farnesyl acetone, Verbenene and Incensole acetate	204
Figure 4.66	Side sight and top sight of the equilibrium adsorption geometry of Hexahydro-farnesyl acetone, Verbenene and Incensole acetate at the solution/Fe(1 1 0) interface	206
Figure 4.67	Biodegradability of TPAAE	208
Figure 4.68	Molecular structures of the major phytoconstituents present in the PCRE	210
Figure 4.69	FT-IR analysis of the PCRE	212
Figure 4.70	UV Spectra of pre- and post-metal dipping in 0.5M HCl and with the inclusion of PCRE	213
Figure 4.71	Corrosion rate variation at different PCRE concentrations at various temperatures	215
Figure 4.72	Effect of inhibition efficiency at different concentrations of PCRE at various temperatures	215
Figure 4.73	ln [CR] vs. 1000/T for mild steel corrosion in 0.5 M HCl solution in the exclusion and inclusion of various dosages of PCRE	218
Figure 4.74	ln [CR/T] vs. 1000/T for mild steel corrosion in 0.5 M HCl solution in the exclusion and inclusion of various dosages of PCRE	219
Figure 4.75	Langmuir isotherm for adsorption of PCRE on mild steel in 0.5 M HCl	222
Figure 4.76	OCP vs. time graph for corrosion inhibition of mild steel after exposure to various PCRE concentrations (50-1000ppm) in 0.5M HCl	223
Figure 4.77	Tafel graph for the corrosion inhibition of mild steel in blank media subjected to 50-1000ppm amounts of PCRE at 298 K	224
Figure 4.78	Nyquist graph for mild steel corrosion inhibition in 0.5M HCl with 50–1000 ppm PCRE at ambient temperature	227

Figure 4.79	Bodes graph for the corrosion mitigation of mild steel in blank media subjected to 50-1000ppm conc. of PCRE at 298 K	228
Figure 4.80	An equivalent circuit model utilized for the data fitting	228
Figure 4.81	SEM visuals of (a) plain metal, (b) metal submerged in 0.5 M HCl (c) metal submerged in 0.5 M HCl + PCRE (1000ppm) at 298K for 6hrs	230
Figure 4.82	CA assessment performed on the metallic sample in (a) 0.5M HCl media and (b) 0.5M HCl+1000ppm of PCRE	231
Figure 4.83	Charge density profiles ( $\sigma$ ) and optimized structure of the (1) Piceid, (2) Resveratrol, (3) Emodin, (4) Emodin-1-O-glucoside and (5) 1-O-Methylemodin molecules	233
Figure 4.84	Distribution of the Mulliken charges values O atoms of (1) Piceid, (2) Resveratrol, (3) Emodin, (4) Emodin-1-O-glucoside and (5) 1-O-Methylemodin molecules	234
Figure 4.85	Optimized structure, LUMO, HOMO and ESP pictures of (1) Piceid, (2) Resveratrol, (3) Emodin, (4) Emodin-1-O-glucoside and (5) 1-O-Methylemodin molecules	237
Figure 4.86	MC and MD simulations result in adsorption configurations and positions of the (1) Piceid, (2) Resveratrol, (3) Emodin, (4) Emodin-1-O-glucoside and (5) 1-O-Methylemodin molecules	240
Figure 4.87	Distribution of the $E_{ads}$ of the (1) Piceid, (2) Resveratrol, (3) Emodin, (4) Emodin-1-O-glucoside and (5) 1-O-Methylemodin inhibitors on the Fe(1 1 0) surface via MC simulation	242
Figure 4.88	Temperature fluctuation (T=298 K) and RDF of the Si and O atoms for major constituents of the extract (1) Piceid, (2) Resveratrol, (3) Emodin, (4) Emodin-1-O-glucoside and (5) 1-O-Methylemodin, obtained via MD	244
Figure 4.89	Biodegradability rate of PCRE	245
Figure 4.90	Molecular structures of the major phytoconstituents present in the ATAE	247
Figure 4.91	FT-IR analysis of the ATAE	248
Figure 4.92	UV Spectra of pre- and post-metal dipping in 0.5M HCl and with the inclusion of ATAE	249
Figure 4.93	Corrosion rate variation at different ATAE concentrations at various temperatures	251
Figure 4.94	Effect of inhibition efficiency at different concentrations of ATAE at various temperatures	252
Figure 4.95	$\ln [CR]$ vs. $1000/T$ for mild steel corrosion in 0.5 M HCl solution in the exclusion and inclusion of various dosages of ATAE	255
Figure 4.96	$\ln [CR/T]$ vs. $1000/T$ for mild steel corrosion in 0.5 M HCl solution in the exclusion and inclusion of various dosages of ATAE	256
Figure 4.97	Different isotherm for adsorption of ATAE on mild steel in 0.5 M HCl	259
Figure 4.98	OCP vs. time graph for corrosion inhibition of mild steel after exposure to various ATAE concentrations (50-250ppm) in 0.5M HCl	260
Figure 4.99	Tafel graph for the corrosion inhibition of mild steel in blank media subjected to 50-250ppm amounts of ATAE at 298 K	261
Figure 4.100	Nyquist graph for mild steel corrosion inhibition in 0.5M HCl with 50–250 ppm ATAE at ambient temperature	264

Figure 4.101	Bodes graph for the corrosion mitigation of mild steel in blank media subjected to 50-250ppm conc. of ATAE at 298 K	265
Figure 4.102	An equivalent circuit model utilized for the data fitting	265
Figure 4.103	SEM visuals of (a) plain metal, (b) metal submerged in 0.5 M HCl (c) metal submerged in 0.5 M HCl + ATAE (250ppm) at 298K for 6hrs	268
Figure 4.104	CA assessment performed on the metallic sample in (a) 0.5M HCl media and (b) metallic specimen+250ppm of ATAE	269
Figure 4.105	Graph showing the progress in the hydrophobic nature of mild steel surface after treatment with 250ppm of ATAE	269
Figure 4.106	Charge density profiles ( $\sigma$ ) and optimized structure of the (1) Trans-2-decen-1-ol, trimethylsilyl ether, (2) 1,4-anhydro-d-glactitol and (3) 5-hydroxymethylfurfural molecules	271
Figure 4.107	Distribution of the Mulliken Atomic Charges (MAC) values O and Si atoms of (1) Trans-2-decen-1-ol, trimethylsilyl ether, (2) 1,4-anhydro-d-glactitol and (3) 5-hydroxymethylfurfural molecules	272
Figure 4.108	LUMO, HOMO and ESP pictures of (1) Trans-2-decen-1-ol, trimethylsilyl ether, (2) 1,4-anhydro-d-glactitol and (3) 5-hydroxymethylfurfural molecules	274
Figure 4.109	MC and MD simulations results in adsorption configurations and positions of the (1) Trans-2-decen-1-ol, trimethylsilyl ether, (2) 1,4-anhydro-d-glactitol and (3) 5-hydroxymethylfurfural inhibitors forms	277
Figure 4.110	Distribution of the $E_{ads}$ of the (1) Trans-2-decen-1-ol, trimethylsilyl ether, (2) 1,4-anhydro-d-glactitol and (3) 5-hydroxymethylfurfural on the Fe(1 1 0) surface via MC simulation	278
Figure 4.111	Temperature fluctuation during the MD run for the (1) Trans-2-decen-1-ol, trimethylsilyl ether, (2) 1,4-anhydro-d-glactitol and (3) 5-hydroxymethylfurfural inhibitors	279
Figure 4.112	RDF of the Si and O atoms for (1) Trans-2-decen-1-ol, trimethylsilyl ether, (2) 1,4-anhydro-d-glactitol and (3) 5-hydroxymethylfurfural obtained via MD	281
Figure 4.113	Biodegradability rate of ATAE	282

## List of Abbreviations

HCl	Hydrochloric acid
H <sub>2</sub> SO <sub>4</sub>	Sulfuric acid
EIS	Electrochemical Impedance Spectroscopy
PDP	Potentiodynamic Polarization
SEM	Scanning Electron Microscope
WL	Weight loss
CBE	<i>Cnicus Benedictus</i> extract
VSE	<i>Vicia Sativa</i> extract
ATAE	<i>Asphodelus Tenuifolius</i> aerial extract
PCRE	<i>Polygonum Cuspidatum</i> root extract
TLLE	<i>Thysanolaena latifolia</i> leaves extract
TPAE	<i>Trianthema Portulacstrum</i> aerial extract
ppm	Parts per million
M	Molar
IE% or $\eta_{WL}$	Inhibition Efficiency
C <sub>R</sub>	Corrosion rate
DFT	Density functional theory
MDS	Molecular Dynamics simulations
MCS	Monte Carlo simulations
K	Kelvin
°C	Celsius
$\Delta G^{\circ}_{ads}$	Adsorption free energy
$\Delta H^{\circ}_{ads}$	Adsorption enthalpy
$\Delta S^{\circ}_{ads}$	Adsorption entropy
UV-vis	Ultraviolet-visible
FT-IR	Fourier Transform Infrared Spectroscopy
H <sub>2</sub> S	Hydrogen sulfide
CO <sub>2</sub>	Carbon dioxide

O <sub>2</sub>	Oxygen
H <sub>2</sub> O	Water
\$	Dollar
Fe <sub>2</sub> O <sub>3</sub> .H <sub>2</sub> O	Rust
Fe(OH) <sub>3</sub>	Iron hydroxide
SO <sub>2</sub>	Sulfur dioxide
FeSO <sub>4</sub>	Ferrous sulfate
SO <sub>3</sub>	Sulfur trioxide
Cl <sup>-</sup>	Chloride ion
R <sub>ct</sub>	Charge transfer resistance
R <sub>f</sub>	Retardation factor
N	Nitrogen
P	Phosphorus
H <sub>3</sub> O <sup>+</sup>	Hydronium
e.g.	Example
UAE	Ultrasound-assisted extraction
kHz	Kilohertz
SFE	Supercritical fluid extraction
SC	Supercritical
min	Minute
hr	Hour
sec	Second
CCE	Counter current extraction
PLE	Pressurized liquid extraction
MAE	Microwave assisted extraction
ECN	Electrochemical noise
EDX or EDS	Energy-dispersive X-ray spectroscopy
AC	Alternating current
CS	Carbon steel
MS	Mild steel
Fe	Iron

Zn	Zinc
Cu	Copper
Al	Aluminium
AFM	Atomic force microscopy
KE	<i>Kola nut</i> extract
mm	Millimetre
mg/L	Milligram per litre
H <sub>2</sub> C <sub>2</sub> O <sub>4</sub>	Oxalic acid
GC-MS	Gas Chromatography-Mass Spectrometry
g/L	Gram per litre
GI-XRD	Grazing incidence X-ray diffraction
CA	Contact angle
LM	<i>Lavandula mairei Humbert</i> extract
CSF	<i>Canarium schweinfurthii</i>
EN	Electrochemical noise
EFM	Electrochemical frequency modulation
LSV	Linear Sweep Voltammetry
C <sub>dl</sub>	Double layer capacitance
TFC	Total flavonoid content
AAS	Atomic Adsorption Spectroscopy
i <sub>corr</sub>	Corrosion current density
μA	Micro ampere
cm	Centimetre
π	pie
NMR	Nuclear Magnetic Resonance
XSL	<i>Xanthium strumarium</i> leaves
ICE	<i>Ixora coccinea</i> extract
<i>E. coli</i>	<i>Escherichia coli</i>
<i>Pr. Mirabilis</i>	<i>Proteus Mirabilis</i>
<i>B.subtilis</i>	<i>Bacillus subtilis</i>
<i>S. aureus</i>	<i>Staphylococcus aureus</i>

TPC	Total phenolic content
Q-TOF LC/MS	Quadrupole-Time of Flight Liquid Chromatogram/ Mass spectrometer
PQ	<i>Portulaca quadrifida</i>
E <sub>a</sub>	Activation energy
FRLE	<i>Ficus racemosa</i> leaf extract
TALE	<i>Tiliacora acuminata</i> leaf extract
LF	Low frequency
HF	High frequency
NaCl	Sodium Chloride
V/V	Volume per Volume
RT	<i>Ruellia tuberosa</i> Linn
PA	<i>Persea Americana</i>
KCl	Potassium Chloride
KBr	Potassium Bromide
KI	Potassium Iodide
E <sub>corr</sub>	Corrosion potential
OCP	Open circuit potential
Z''	Imaginary impedance
Z'	Real impedance
Z <sub>w</sub>	Warburg impedance
B3LYP	Becke, 3-Parameter, Lee-Yang-Parr
χ	Electronegativity
A or EA	Electronic affinity
η	Global hardness
σ	Softness
I or IP	Ionization potential
HOMO	Highest occupied molecular orbital
LUMO	Lowest unoccupied molecular orbital
NVT	Number volume temperature
Conc.	Concentration
ΔE	Energy gap



$\Theta$	Surface coverage
CPE	Constant phase element
$R_s$	Solution resistance
$n$	phase shift
$\chi^2$	deviation degree
$\beta_a$	Anodic Tafel slope
$\beta_c$	Cathodic Tafel slope
RDF	Radial Distribution Function
Eqv.	Equivalent
$R^2$	Regression coefficient

---

---

***Chapter 1***  
***Introduction***

---

---

## **1.1. Introduction**

### **1.1.1. The Ubiquitous Nature of Corrosion**

Corrosion is a natural process that occurs when metals react with their environment, leading to the deterioration of their physical properties. It is a major issue in several industries, including construction, manufacturing, and transportation. Corrosion not only causes damage to structures and equipment, but it also poses a significant threat to human health and the environment. Understanding corrosion mechanisms, prevention, and mitigation strategies is essential to address this global challenge <sup>1</sup>. The majority of corrosion agents are oils, liquids, chemicals, dispersed gaseous materials, humidity and elevated temperature in the environment. Several metal corrosion exhibits an inimical effect such as reducing the chemical reactivity of cathode active components, tarnishing the electrolyte, electrical resistance and intensifying self-discharge rate<sup>2-4</sup>. The oil and gas industries are seriously affected by the rupture of the corroded oil pipelines, chemical leakage and even burning. This is caused by repeated free-water extraction and highly corrosive media: including H<sub>2</sub>S and CO<sub>2</sub> flowing through oil and gas equipment, causing an approximate overall annual cost of \$1.372 billion<sup>5</sup>. Selective leaching, galvanic corrosion, crevice corrosion, intergranular corrosion, pitting corrosion, erosion-corrosion, and uniform corrosion are different types of corrosion. Uniform corrosion contributes to a uniform gradual loss in metal or material surface thickness. This is expectable effortlessly <sup>6-8</sup> and reduces the degree of material failure. In the opening or crevice on the surface of metals, crevice corrosion occurs which narrows down for either acidic or alkaline solutions to split and get stuck in. This tends to reduce the cathodic reactions in that region and give a comprehensive characteristic of the anodic phase. Due to the discrepancy of cathodic and anodic effects, the regions of the crevices become extremely corrosive and lead to the decomposition of material<sup>9,10</sup>. Pitting Corrosion occurs on the surface of a metal, creating small holes. Pitting Corrosion is rarely observed before the material collapses. This makes it the riskiest form of corrosion. It actually occurs on passivated materials and alloys in particular environments composed of iodide, chloride ions and when the electrode potential exceeds a hazardous value. Intergranular corrosion significantly improves rust or laterally destabilization of any material's grain boundaries, even though surface of the material is not corroded. Intergranular corrosion affects the material's microstructural grains, leading to decreased hardness and is unable to withstand tensile stress, and can shatter without warning<sup>11-13</sup>. Corrosion occurring either indirectly or directly between two different metals in contact with one another is galvanic

corrosion. It may also occur among other conductive materials such as graphite, metals, and alloys. Corrosion is the degradation of metals between metals and their surrounding conditions due to cathodic and anodic chemical reactions. In an acidic environment, cathodic chemical reactions are due to a decrease of oxygen or increase of hydrogen by an element. Thus, oxidation gives rise to anodic chemical reaction<sup>14-16</sup>. Oxidation is termed as the reduction of electrons, increasing oxygen, or decreasing hydrogen. This reaction is responsible for the actual degradation of the mass of any corroding material or metal as the whole corrosion mechanism on a steel bar can be observed in **Figure 1.1**.

There are two forms of corrosion: dry, and wet corrosion. Dry corrosion can be well described as; material decomposition that happens with metals interacting with oxygen in the air, resulting in oxide layer-rust formation on the metal surface. Such layer-rust oxide prevents the metal's continuous decay and is termed passivation<sup>17,18</sup>. Wet corrosion, while, is defined as material deterioration that occurs in an aqueous water, acid, or alkali solution as shown in **Figure 1.1**.

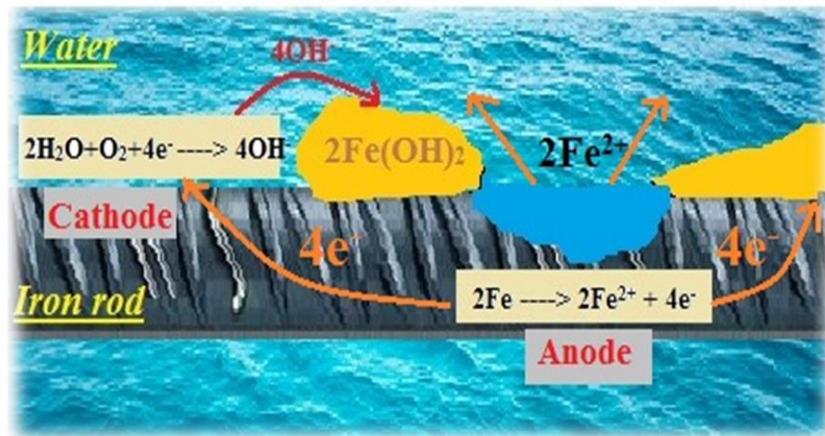


**Figure 1.1.** Schematic representation of the mechanism of reinforcement corrosion.

### 1.1.2. Mechanism of Corrosion

The corrosion process in an aqueous solution has been clearly illustrated in **Figure 1.1**. In atmospheric corrosion which illustrates uniform corrosion, a very thin layer of electrolyte is observed. It is possibly best illustrated by placing a tiny amount of seawater on a piece of steel. The following variations are found when comparing atmospheric corrosion with aqueous corrosion: Only a small amount of water and dissolved ions are found on a metal surface exposed

to the atmosphere, while access to oxygen present in the air is unrestricted. In contrast to aqueous corrosion, corrosion products form close to the metal surface and can prevent further corrosion by acting as a physical shield between the metal surface and the atmosphere, especially if they are insoluble, like in the case of steel or lead. The following is a simplified mechanism of aqueous corrosion of iron which has been shown in **Figure 1.2**.

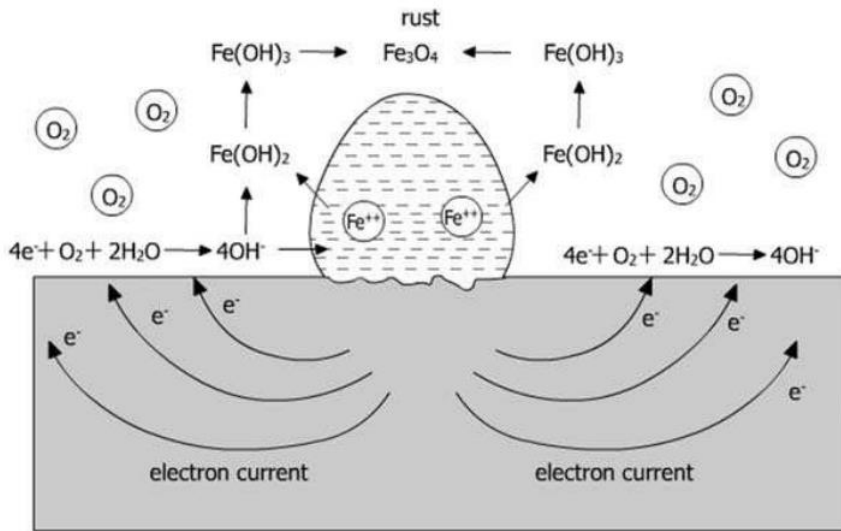
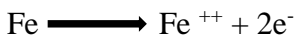
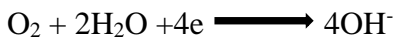


**Figure 1.2.** Aqueous Corrosion of iron. <sup>19</sup>

At the anodic areas, the anodic reaction takes place:



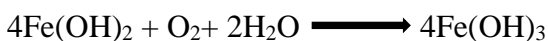
At the cathodic areas, the reduction of oxygen takes place:



The OH ions react with the Fe<sup>++</sup> ions produced at the anode:



With more access to oxygen in the air, Fe(OH)<sub>2</sub> oxidizes to Fe(OH)<sub>3</sub> and later it loses its water:



Ferrous hydroxide is converted to hydrated ferric oxide or rust by oxygen:



Rust ( $\text{Fe}_2\text{O}_3 \cdot \text{H}_2\text{O}$ ) is formed midway between the alkaline drop center and the periphery. The electrons in the metallic circuit flow from the anode (drop center) to the cathode (periphery). On the surface of iron, the ferrous ions are soluble, while those in the solution are oxidized by oxygen into insoluble ferric hydrated oxides called rust. Aside from the corroding site, rust is formed. As the ferrous ion is quickly oxidized into ferric oxide, the corrosion rate increases.  $\text{Fe}(\text{OH})_3$  is insoluble and the corrosion reaction accelerates if it forms away from a metal surface, as equilibrium is to be sustained by providing more ferrous ions ( $\text{Fe}^{++}$ ) from the surface. However if  $\text{Fe}(\text{OH})_3$  is quickly formed on the surface of a metal, corrosion (a passive film) is inhibited.

If  $\text{SO}_2$  is there as a pollutant, then  $\text{FeSO}_4$  is produced in the air. The existence of soluble sulfate ions in the media greatly affects the corrosion of iron. The sulfate ion continues to attack iron and is uneven and even pitted on the surface<sup>19</sup>. Layers of porous rust are formed in this case. Since no protection is provided to the metal by the porous rust, corrosion prevails. The effect of  $\text{SO}_2$ ,  $\text{SO}_3$ , and  $\text{Cl}^-$  ions is illustrated in **Figure 1.3**.

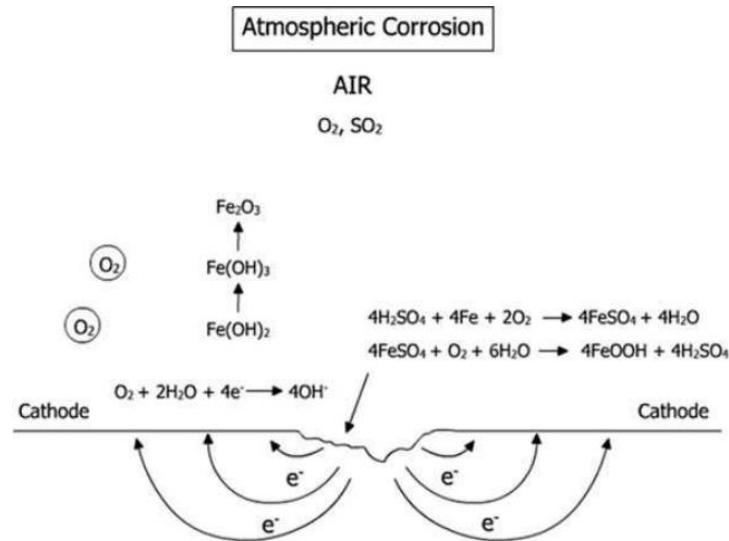


**Figure 1.3.** Impact of  $\text{SO}_2$  and humidity on metallic corrosion (atmospheric corrosion). Reaction occurs in a very thin (invisible) aqueous layer.<sup>19</sup>

## **1.2. Mild steel and its usage**

Mild steel is a type of carbon steel that is widely used in various industrial applications. It is an alloy that contains iron and carbon, with a carbon content that ranges from 0.05% to 0.25%. This low carbon content gives mild steel its unique properties, such as excellent ductility, good weldability, and high formability. Mild steel is also known for its durability, strength, and cost-effectiveness, which make it a popular choice for a wide range of applications. The properties of mild steel are influenced by its composition, which typically includes other elements such as manganese, silicon, and sulfur. These elements are added in small amounts to improve specific properties, such as strength, toughness, and corrosion resistance.

Mild steel is widely used in the construction industry due to its strength, durability, and cost-effectiveness. It is used to make various structural components such as beams, columns, and girders. It is also used to make reinforcement bars that are used in concrete structures. Mild steel is an ideal choice for these applications due to its ability to withstand heavy loads and harsh environmental conditions. In the automobile industry, mild steel is widely used to make various components such as chassis, wheels, and body panels. It is also used to make various engine components such as connecting rods and crankshafts. Mild steel is an ideal material for these applications due to its high strength and durability, which allow it to withstand the stresses and strains of automotive applications. Mild steel is also used to make pipelines for various industrial applications. It is used in the oil and gas industry to make pipelines for the transportation of crude oil and natural gas. It is also used to make pipelines for water and sewage treatment plants. Mild steel is an ideal material for these applications due to its ability to withstand high pressure and harsh environmental conditions. In addition to these applications, mild steel is used to make various machinery components due to its strength and durability. It is used to make various machine parts such as gears, shafts, and bearings. It is also used to make various industrial equipment such as boilers and pressure vessels.

One of the major advantages of mild steel is its cost-effectiveness. It is readily available and is relatively inexpensive compared to other materials. Mild steel is also easy to shape and form, making it an ideal choice for various industrial applications. It can be easily welded, bent, and twisted into various shapes without losing its strength. Mild steel is highly durable and can withstand various environmental factors such as moisture, heat, and cold. It is also resistant to

corrosion, making it an ideal material for outdoor applications. Mild steel is also easy to maintain and requires minimal maintenance. It can be easily cleaned and painted to maintain its appearance. However, mild steel is prone to corrosion, especially when exposed to moisture and air. It requires regular maintenance and painting to prevent corrosion. Mild steel also has low hardness, which makes it unsuitable for applications that require high hardness or wear resistance.

### **1.2.1. Corrosion of mild steel**

Corrosion of mild steel is a common problem in many industries, and it can lead to a wide range of incidents and accidents. While it is a popular choice for various applications due to its strength and cost-effectiveness, it is also susceptible to corrosion, especially when exposed to moisture and air. Corrosion of mild steel can occur in various forms, including uniform corrosion, pitting corrosion, and crevice corrosion. Uniform corrosion occurs when the surface of the steel corrodes evenly, resulting in a reduction in its thickness. Pitting corrosion occurs when small pits or holes form on the surface of the steel, while crevice corrosion occurs in areas where the steel is in contact with another material or in areas with stagnant fluid. One of the most significant incidents related to the deterioration of mild steel occurred in 1988 when the North Sea oil rig, Piper Alpha, suffered a catastrophic explosion and fire, resulting in the death of 167 workers<sup>20,21</sup>. The incident was caused by the corrosion of a gas pipeline that led to a leak, which ignited and caused the explosion. The incident highlighted the importance of regular inspection and maintenance of pipelines to prevent corrosion. Another incident related to the deterioration of mild steel occurred in 1997 when the Thames Barrier failed due to corrosion. The barrier was built to protect London from flooding and was designed to last for 100 years<sup>22,23</sup>. However, it suffered severe corrosion due to the harsh conditions of the Thames estuary, and several of its components failed, leading to concerns about its long-term reliability. In the aviation industry, the corrosion of mild steel can also lead to serious incidents. In 1999, a Boeing 737 crashed shortly after takeoff from Linate Airport in Milan, Italy, resulting in the death of 118 people. The incident was caused by the corrosion of a steel bracket that held the thrust reverser in place, which led to its failure during takeoff. The failure caused the thrust reverser to deploy unexpectedly, leading to the loss of control of the aircraft. The corrosion of mild steel can also cause incidents in the transportation industry<sup>24,25</sup>. In 2015, a freight train derailed in West Virginia, resulting in a massive explosion and fire. The incident was caused by



the corrosion of a rail that led to its failure, causing the train to derail. The explosion and fire resulted in the evacuation of several homes and the contamination of nearby water supplies<sup>26,27</sup>.

In the construction industry, the corrosion of mild steel can also lead to serious incidents. In 2014, a section of the roof of the Apollo Theatre in London collapsed, injuring 88 people. The incident was caused by the corrosion of a metal tie that held the ceiling in place, which failed, causing the ceiling to collapse<sup>28,29</sup>. To prevent incidents related to the deterioration of mild steel, various measures can be taken, including regular inspection and maintenance, the use of corrosion-resistant coatings, and the replacement of corroded components. Regular inspection and maintenance can help to identify corrosion before it leads to failure, while corrosion-resistant coatings can help to protect the steel from corrosion. In some cases, the use of alternative materials may also be necessary to prevent corrosion-related incidents. In conclusion, the corrosion of mild steel is a common problem in many industries, and it can lead to a wide range of incidents and accidents. The incidents related to the corrosion of mild steel can have significant consequences, resulting in the loss of life, property damage, and environmental damage. To prevent incidents related to the mild steel corrosion, regular inspection and maintenance, the use of corrosion-resistant coatings, and the replacement of corroded components are essential<sup>30-33</sup>.

### **1.3. Corrosion mitigation techniques**

Corrosion is a significant issue that can cause damage to infrastructure, equipment, and materials, leading to safety hazards, loss of functionality, and costly repairs. Corrosion mitigation techniques are critical to prevent corrosion and maintain the integrity of materials and structures. Herein, we will discuss some common techniques used to mitigate corrosion.

#### **➤ Protective Coatings**

Protective coatings are a widely used technique to mitigate corrosion. They provide a barrier between the metallic surface and the environment, preventing the metal from being exposed to corrosive agents. Protective coatings can be categorized into two types: barrier and sacrificial coatings. Barrier coatings are typically organic coatings such as paints, enamels, and epoxies that form a physical barrier between the metal surface and the environment. The coating can be applied by brushing, spraying, or dipping the material in the coating material. Barrier coatings can be used on a wide range of metals, including steel, aluminium, and copper. Sacrificial coatings are also

known as cathodic coatings. They are designed to corrode preferentially to the underlying metal, protecting it from corrosion. Common sacrificial coatings include zinc, aluminium, and magnesium coatings. These coatings are often used in marine and offshore applications, where the corrosive environment is particularly aggressive<sup>34,35</sup>.

#### ➤ **Cathodic Protection**

Cathodic protection is a technique used to prevent corrosion by making the metal surface the cathode of an electrochemical cell. The technique can be applied in two ways: sacrificial anode and impressed current. In the sacrificial anode method, a more active metal is used as an anode, and the metal to be protected becomes the cathode. The more active metal corrodes preferentially, preventing corrosion of the protected metal. Common materials used as sacrificial anodes include zinc, aluminium, and magnesium. In the impressed current method, an external current source is used to create a cathodic reaction on the metal surface, preventing corrosion. A power source such as a rectifier is used to generate an electrical current, which is then applied to the metal surface to be protected. The impressed current method is typically used in larger structures such as pipelines, storage tanks, and offshore platforms.

#### ➤ **Material Selection**

Material selection is an important consideration in preventing corrosion. Choosing materials that are resistant to the corrosive environment can significantly reduce the risk of corrosion. For example, stainless steel is resistant to corrosion in many environments due to its high chromium content. Other materials that are resistant to corrosion include titanium, nickel, and alloys such as Inconel and Monel. The selection of the appropriate material depends on the specific environment in which it will be used and the properties required of the material.

#### ➤ **Design Modification**

Design modification is another technique used to mitigate corrosion. Changes to the design can reduce the likelihood of corrosion by eliminating areas where corrosion is likely to occur or by reducing the corrosive environment's exposure to the material. For example, the use of drain holes or coatings to prevent moisture accumulation can reduce the risk of corrosion. Design modifications can be made at the initial design stage or during the operational life of the structure

or equipment. Examples of design modifications include the use of protective coatings, the use of cathodic protection, and the selection of materials that are resistant to corrosion.

### **1.3.1. Corrosion Inhibitors**

Corrosion inhibitors are chemicals that are added to the corrosive environment to reduce the corrosion rate of the metal. They work by developing a protective coating upon the metallic surface, preventing corrosive agents from reacting with the metal. Corrosion inhibitors can be added to a wide range of fluids, including water, oil, and gas. Inhibitors can be classified into three categories: anodic, cathodic, and mixed inhibitors. Anodic inhibitors function by oxidizing the metal surface, producing a passive coating that protects the metal from further oxidation. Cathodic inhibitors work by reducing the oxygen content at the metal surface, preventing the cathodic reaction from occurring. Mixed inhibitors combine both anodic and cathodic inhibition mechanisms. Most inhibitors are simple to use and give an advantage in the in-situ application without causing any major disturbance to the procedure. However, when selecting an inhibitor, there are many considerations:

- Mostly the inhibitor costs could be quite large if the material involved is expensive or the quantity required is enormous.
- The inhibitor's toxicity may cause significant harm to human beings and its surroundings.
- Inhibitors should be ecofriendly and biodegradable.

Throughout their work into the usage of corrosion inhibitors, many researchers attributed the potential of corrosion inhibition to the donation of lone electron pairs to metal atoms. As a potent factor for showing corrosion inhibition, several heterocyclic compounds and hetero atoms such as O, S, N, and P were reported respectively<sup>36-40</sup>. Although some corrosion inhibitors have exhibited remarkable anti-corrosive behavior, the majority of them are extremely toxic to humans and the environment<sup>14,41-44</sup>. The health and environmental concerns arising from corrosion inhibitors have been a worldwide issue in industries. Such inhibitors may provoke reversible (temporary) or irreversible (permanent) harm to the organ in the body, i.e., kidney or lungs, as well as could interrupt a metabolic pathway or disrupt an enzyme function at several other body sites. The toxicity can occur mostly during the synthesis of the compound, or while its implementation<sup>45,46</sup>. Because of the dangerous toxicity of certain corrosion inhibitors, green corrosion inhibitors have

been progressively being pursued. Green corrosion inhibitors ideally plant extracts are of considerable importance, as there has seen a rise in environmental concern and reform in guidelines due to their toxicity limit standard corrosion inhibitors<sup>47</sup>. Plant extracts are really an excellent resource of sustainable green corrosion inhibitors, as majority of their extracts have the requisite heteroatoms such as O, N, C and S, which are effective in organic compounds that are later adsorbed into metals or alloys to develop a thick coating that protects the metal surface and prevents corrosion as shown in **Figure 1.4**.



**Figure 1.4.** Plant (*Origanum vulgare*) extract being used as a corrosion inhibitor for reinforced steel which develops a layer resistant to corrosion. <sup>47</sup>

In addition, this area is widely summarized in several review papers, and book chapters in the recent ones (published between 2017 and 2021): Some of them are;

- a) Omnia S. Shehata, Lobna A. Korshed and Adel Attia published a book chapter “**Green Corrosion Inhibitors, Past, Present, and Future**” in which they discussed the numerous natural products and their application in different processes, especially in steel reinforcement embedded in concrete<sup>48</sup>. Also, the green inhibitors act in different media, and their protective role for different metals and alloys is discussed. Finally, industrial applications of vapor-phase inhibitors and their mechanisms are presented.
- b) Stefania Marzorati, Luisella Verotta and Stefano P. Trasatti published a review article “**Green Corrosion Inhibitors from Natural Sources and Biomass Wastes**” where they emphasize

on the green chemistry on the importance of protecting the environment and human health in an economically beneficial manner aiming at avoiding toxins and reducing wastes<sup>48</sup>. All the considerations listed are the focus of the present review and are intended as a constructive critique to highlight the shortcomings of the field of green inhibitors in re-evaluating the literature and addressing future research that still needs rationalization in the field.

- c) Lipiar K. M. O. Goni and Mohammad A. J. Mazumder deliberated their ideas about green corrosion inhibitors in a book chapter “**Green Corrosion Inhibitors**”. This chapter briefly discusses the importance and different methods of corrosion inhibitors with a particular emphasis given to the discussion on the different characteristic features of the green corrosion inhibitors reported in the literature as a comparative view of organic inhibitors.

Although the content deliberation in accordance with a better understanding of the ideology of green corrosion inhibition has been explored in an excellent manner but still some of the important aspects indulging in the field of green corrosion inhibitors are lacking as per the current trends and developments. Some important aspects that may still require further investigation in this field include:

- **Optimization of inhibitor performance:** While many green corrosion inhibitors have been identified, their performance can vary depending on the specific conditions of the system in which they are used. Therefore, there is a need for further optimization of these inhibitors to ensure their effectiveness across a wide range of conditions.
- **Compatibility with other additives:** In real-world applications, green corrosion inhibitors are often used in conjunction with other additives such as biocides, antifoulants, and scale inhibitors. Therefore, there is a need to investigate the compatibility of these inhibitors with other additives to ensure their overall effectiveness.
- **Environmental impact:** While green corrosion inhibitors are designed to be environmentally friendly, their impact on the environment is not always fully understood. Further research into the environmental impact of these inhibitors can help to ensure their safety and sustainability.

#### 1.3.1.1. Green Corrosion Inhibitors

The title “green inhibitor” or “eco-friendly inhibitor” attests to those substances which have biocompatibility in nature<sup>49</sup>. In 1930, *Celandine* (*Chelidonium majus*) plant extracts (dried leaves,

flower, root and seeds) were used in the H<sub>2</sub>SO<sub>4</sub> pickling bath. As an additive, ZH-1 consists of a finely divided oil cake and was developed to control corrosion through the use of by-product formed in phytin manufacture. Green corrosion inhibitors, derived from natural sources such as plants, weeds, shrubs, and biomass, are gaining popularity as sustainable and eco-friendly alternatives to conventional and harmful corrosion inhibitors. Extracts from these natural sources offer significant benefits, including their effectiveness, accessibility, non-toxicity, economic competitiveness, and minimal impact on the environment<sup>50,51</sup>. These extracts contain phytochemicals, such as saponin, flavonoids, alkaloids, vitamins, tannins, catechin, terpenoids, and phenolic compounds, that have electron-rich polar functional moieties and numerous bonds that allow them to bind quickly to metal substrates, forming a protective coating that inhibits the intrusion of excessive corrosion ions, thereby preventing metallic corrosion<sup>52,53</sup>. The use of green corrosion inhibitors provides a cost-reliable and environmentally benign way to combat corrosion-related issues. Unlike conventional inhibitors, these eco-friendly inhibitors are biodegradable and have minimal negative impacts on the ecosystem. Furthermore, their availability and diversity make it easy to obtain them on a large scale, making them a promising alternative for commercial and industrial applications. **Figure 1.5.** and **Figure 1.6.** summarizes the key criteria that make green corrosion inhibitors more suitable than conventional inhibitors along with the various forms of green corrosion inhibitors have been shown.



**Figure 1.5.** Diagram outlining the crucial factors that must be met for compounds to be considered as suitable green corrosion inhibitors for preventing metal corrosion.



**Figure 1.6.** Different sources of green corrosion inhibitor

According to a search on the Scopus database, there were over 3,500 publications related to green corrosion inhibitors as of 2021<sup>54,55</sup>. This indicates a growing interest in this area of research and development. Additionally, a search on the Web of Science shows that the number of publications related to green corrosion inhibitors has been increasing steadily over the past decade. In 2011, there were only around 100 publications on this topic, while in 2020, there were over 700 publications. It is important to note that these numbers are only estimates, and the actual number of publications on green corrosion inhibitors may be higher due to the availability of other databases and sources of information<sup>56,57</sup>.

### 1.3.2. Corrosion inhibition mechanism

The corrosion inhibition mechanism is the adsorption of inhibitors upon the metallic substrate. Various factors, such as the nature and charge of the metal, the chemical composition of the organic inhibitor (functional groups, aromaticity, potential steric effects, etc and the form of aggressive electrolyte, affect the adsorption process. Some decisive factors contributing to the efficacy of

corrosion inhibition are the presence of heteroatoms, the size of the organic molecule, the aromaticity and/or conjugated bonding, carbon chain length, bonding strength to the metal substrate, the type and number of bonding atoms or groups in the molecule, the ability for a layer to become compact or cross-linked, the ability to form a complex with the atom as a solid within the metal lattice, and adequate solubility in the environment. Organic compounds containing S, N, or O atoms in their configurations, functional electronegative groups, and  $\pi$  electrons in triple or conjugate double bonds are the plurality of effective inhibitors. The inhibitory activity of these organic compounds via an adsorption mechanism can be due to their interactions with the metallic surface. Mas Faiz et al.<sup>58</sup> in their study of natural products extracted three alkaloids and explained the inhibitors adsorption over mild steel surfaces as shown in **Figure 1.7** in which the inhibition effects studied alkaloids were determined by the interaction between p electrons of phenyl rings and p-electrons from the electron donor groups (N and O) with the vacant d-orbitals of metal by which they form an insoluble, stable and uniform thin defensive film on the mild steel surface.

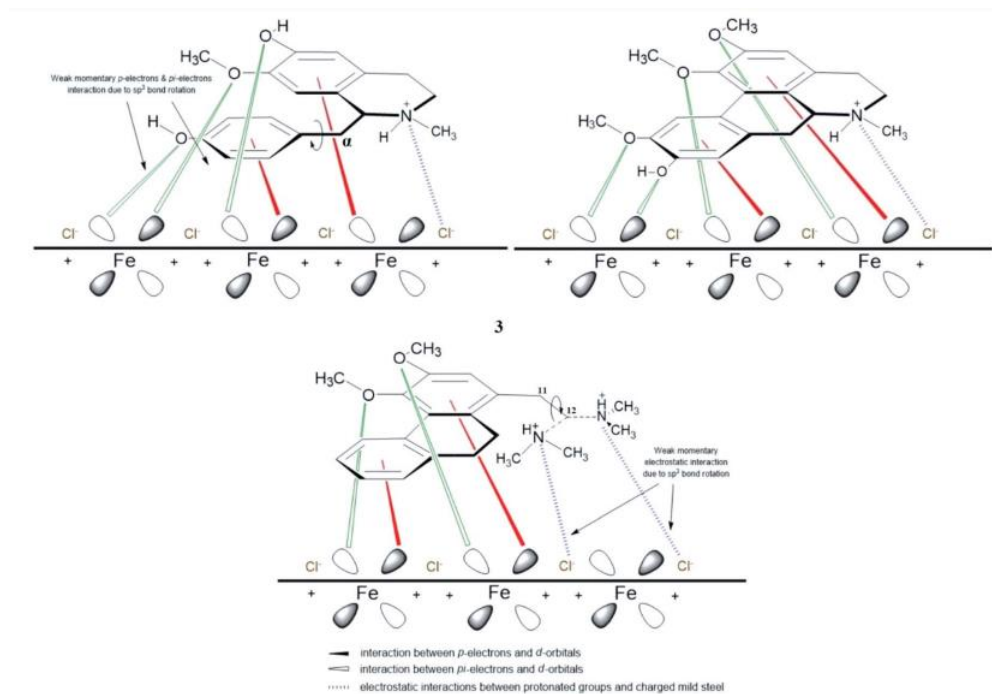


**Figure 1.7.** Corrosion inhibition impact of crude extracts (hexane, dichloromethane, methanol) from the bark of *Cryptocarya nigra* and three alkaloids identified N-methylisococlaurine N-methylaurotetanine and atherosperminine extracted from the extract of *Cryptocarya nigra* dichloromethane (CNDE) tested for mild steel corrosion in 1 M HCl solution.<sup>58</sup>



Adsorption of organic compounds on the metallic surface is most frequently induced by the electrostatic attraction of metals to charged inhibitor molecules; the interaction of heteroatomic lone pair electrons with the metal's vacant d-orbital; or a combination of either of the previous mechanisms. Subsequently, the inhibitors adsorption first on the metal's composition and surface charge. It is very clear that the inhibition mechanism should be carefully examined for all the reasons listed above because it offers a quantity of knowledge that is compulsory to take into account when working in the field of corrosion inhibition of specific metals in specific environments. Corrosion inhibitors can form either a strong coordination bond with the metal atom or a passive film on the surface. The values of inhibition efficiency depend essentially on the electron density at the active center of the inhibitor molecule. The corrosion inhibition of metal may involve either physisorption or chemisorption of the inhibitor upon the metallic surface. The physisorption process of inhibitor results from the electrostatic interactions usually van der Waals forces across electric charges of inhibitor molecules and the substrate. This process is determined from the values of standard free energy ( $\Delta G^\circ$ ) values that are over -20 kJ/mol with the application of different adsorption models with coefficients of determination near 1. Donor-acceptor interactions between free electron pairs of hetero atoms and  $\pi$  electrons of multiple bonds and vacant d-orbitals of metal result in the chemisorption of inhibitors. Strong changes have been observed in the electronic structure/electron density of the adsorbate molecule ( $> 0.5$  eV/surface site). Chemisorption has an irreversible aspect and high pressure is therefore desired. Chemisorption adsorption enthalpy is elevated to approximately 80 to 240 kJ/mol due to chemical bonding.

Huyen T.T. Bui et al.<sup>59</sup> studied the inhibition efficiency of a compound, namely Limonene, extracted from orange peel for steel corrosion in 1M HCl solutions. In Limonene's structure, C-C, C=C and C-H bonds are shown. The adsorbed film, however, contains other adsorbed moieties including C=O, O-H and C-O-C, suggesting that other compounds are present in the extract. It is therefore concluded that the presence of compounds other than limonene in HCl acid leads to the corrosion reduction of mild steel. In addition, organic compounds in acid media can be acidified or participate in the formation of by-products or intermediates in physiochemical reactions that may function as secondary steel corrosion inhibitors in acid solutions. The adsorption of the extract upon the steel surfaces can therefore be visualized by D-Limonene adsorption and several other attribute bonds in extract constituents, such as C=C and C=O, as shown in **Figure 1.8**. The figure

explains the limonene adsorption model using two C=C bonds at carbon positions 3-4 and 8-9, as well as the adsorption model of the C=C and C=O bonds in the mild steel surface OPEO constituents.

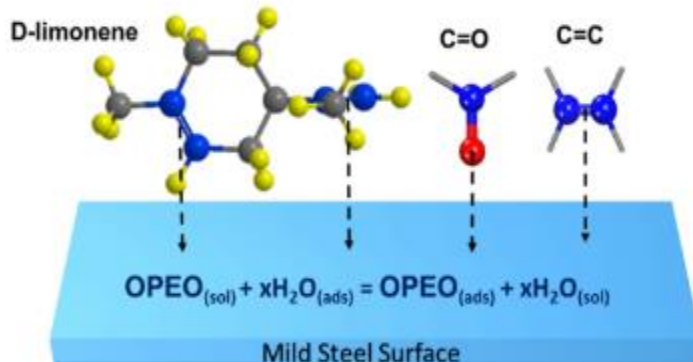


**Figure 1.8.** The adsorption model of OPEO on the mild steel surface.<sup>59</sup>

M.A. Deyab et al.<sup>60</sup> explained the inhibition of aluminum in biodiesel by the *Rosemary* extract on the basis of the adsorption of the organic compounds carnosol ( $C_{20}H_{26}O_4$ ) and carnosic acid ( $C_{20}H_{28}O_4$ ); flavonoids such as genkwanin ( $C_{16}H_{12}O_5$ ), cirsimaritin ( $C_{17}H_{14}O_6$ ) or homoplantagin ( $C_{22}H_{22}O_{11}$ ); and triterpenes such as ursolic acid ( $C_{30}H_{48}O_3$ ) present in *Rosemary* extract on the aluminium surface. By regulating both cathodic and anodic reactions, the extract inhibits corrosion. At cathodic sites on the metal surface, protonated species were frequently adsorbed and thus delayed the reaction of hydrogen evolution, which is possibly responsible for the pronounced cathodic inhibiting effect of *Rosemary* extract. The adsorption of organic compounds present in extracts on anodic sites occurs by a lone pair of electrons on oxygen atoms.

Yuli Yetri et al.<sup>61</sup> used the *Theobroma cacao* peel extract as the eco-benign inhibitor for mild steel corrosion in which he effectively revealed the inhibition mechanism. Owing to the presence of adsorption, inhibitor molecules were found upon the metallic substrate. This adsorption is due to the force of adhesion between the inhibitor and the surface of mild steel as shown in **Figure 1.9**. On the mild steel surface, inhibitor molecule, adsorption creates a thin film layer that can hinder the rate of corrosion. The bond existed on the surface of mild steel during the inhibitor adsorption process as a coordination covalent bond involving chemical adsorption.

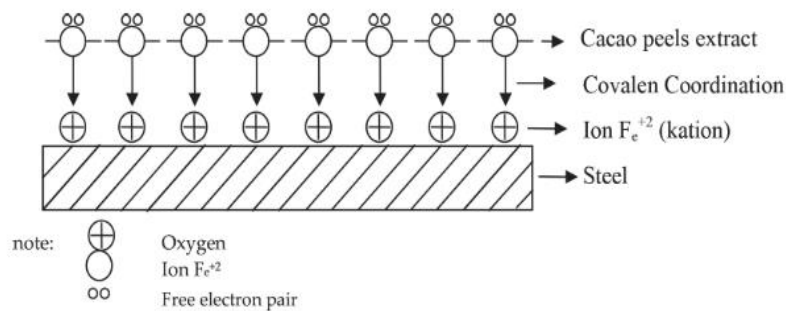


**Figure 1.9.** Adsorption mechanism of *Theobroma cacao* peel extract on the mild steel surface. <sup>61</sup>

Honarvar Nazari et al.<sup>62</sup> in their investigation of corrosion protection of steel in chloride media by an apple-based green inhibitor revealed the effect of major constituent 1-Linoleoyl-sn-glycero-3-phosphocholine ( $C_{26}H_{50}NO_7P$ ) in the inhibition properties of apple-based green inhibitor.  $C_{26}H_{50}NO_7P$ 's corrosion-inhibitory activity may be related to the functional group of its molecular structure that was also responsible for transforming  $Fe_3O_4$  into a more corrosion-resistant iron oxide product layer ( $Fe_2O_3$ ). APE molecules, via their high electron density locations, are bound to the surface of the steel. The interaction of non-bonding electrons on nitrogen and oxygen with the steel surface entails the adsorption of APE. Higher charge transfer resistance ( $R_{ct}$ ) and retardation factor ( $R_f$ ) values were correlated with more APE, demonstrating the creation of a more protective surface layer.

Le Thanh Vu et al.<sup>63</sup> studied the corrosion reduction potency of *Houttuynia cordata* leaf extract for steel in an HCl media in which it was found that *H. cordata* leaf extract has diverse organic structures containing multiple bonds and functional groups. The quantum chemical calculation showed that when the inhibitor interacts with the steel substrate and acidic solution, key positions formed by the effects of highly electronegative C, O, N, P and  $\pi$ -conjugated bonds as well as heterocycles on the organic frameworks play different roles in donating or consuming electrons as shown in **Figure 1.10**. HCLE's corrosion resistance on the steel surface is shown in two ways. First, nitrogen and oxygen from heterocyclic compounds and functional groups as well as hydrocarbon branch binding sites with functional groups tend to bind to positive  $H_3O^+$  ions to minimize their impacts on the steel surface and also serve as a bridge to  $Fe^+$  ions for the emergence of the protective layer from the solution/steel substrate interface. Secondly, functional groups comprising strongly electronegative N and O atoms and sigma bonds near them were electron-

consuming places to trap negative  $\text{Cl}^-$  ions, helping to avoid localized corrosion acceleration from the steel surface. The reduction of the interaction of the active ions  $\text{H}_3\text{O}^+$  and  $\text{Cl}^-$  to the steel substrate and the existence of protective film formation also limit the process of charge transfer at the solution/steel substratum interface.

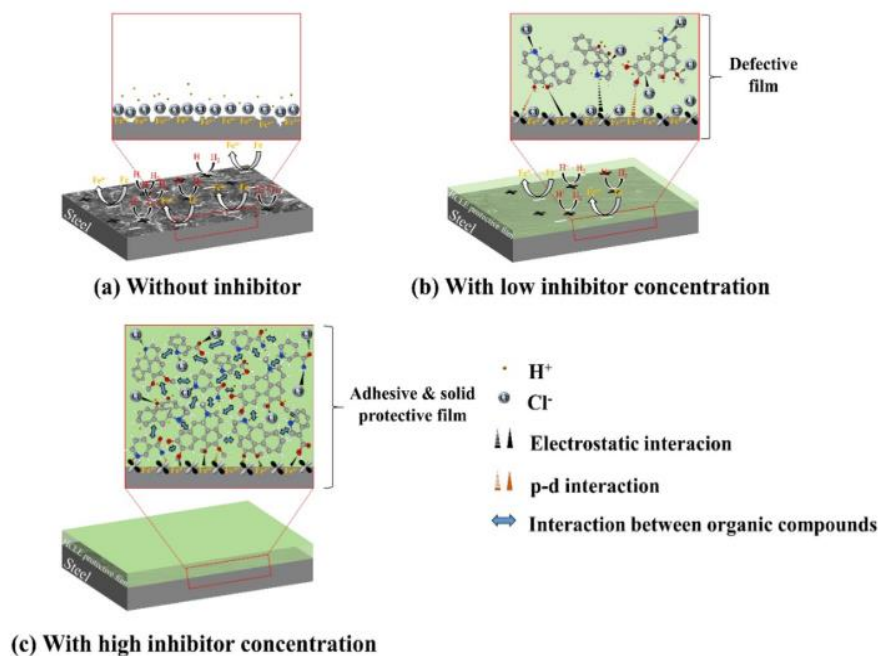


**Figure 1.10.** Schematic figure of the film formation mechanism of *Houttuynia cordata* leaf extract's species for protecting steel in 0.1M HCl solution: (a) without inhibitor, (b) with low inhibitor concentration and (c) with high inhibitor concentration. <sup>63</sup>

### 1.3.3. Prominent metrics for extract preparation

#### 1.3.3.1. Extraction

Extraction plays an important role and it is regarded as a first step towards separating the essential active phytoconstituents such as saponin, tannin, quercetin, flavonoid, etc from the plant raw materials. This method usually involves solvent extraction, sonication extraction, extraction of supercritical fluids, maceration, decoction, and counter-current extraction as per the proposition of extraction. The most frequently used process is the extraction of solvents. Generally, a natural product extraction comprises of the following steps; solvent perforates into the solid substrate > solute get dissolves in the solvent > solute gets diffused from solid substrate > Extracted solutes are finally obtained.

Any aspect which improves the solubility and diffusivity discussed in the above steps will facilitate extraction. Extraction efficiency could be influenced by the properties of the extraction solvent, solvent-to-solid ratio, the particle size of raw materials, extraction temperature and period. The basic parameters which influence an extract's quality are the plant part used for sample preparation, the solvent being used for extraction purposes and selecting the proper and efficient extraction method. The effect of active phytochemicals extracted from plants hugely affects the inhibition efficiency. These active phytochemicals can vary from the nature of the specific plant parts taken, processing degree, moisture/ humidity content and size of the extracted particles. The variations in various extraction techniques that directly impact an extract's quantity, quality and composition depend on various factors such as extraction type, extraction period, temperature, solvent nature, solvent concentration and polarity of the solvent.

### **1.3.3.2. Plant material**

Bio active phytocomponents can be attained from any part of the plant that contains active constituents such as barks, leaves, flowers, fruits, seeds, roots, etc. as shown in **Figure 1.11**<sup>64</sup>. The choice and selection of solvents also affect the effective evaluation of bio active compounds attained from plant raw material during the extraction method. The characteristics of a formidable solvent in the extraction procedure usually involve qualities such as non-hazardous nature, low heat requirement for evaporation, encouraging rapid physiological absorption of the extract, conservative action and incapable to cause complexity or dissociation of the extract. The next essential step is the factors which influence the choice of solvents for the extraction method. These factors involve the quantity of phytochemicals to be extracted, extraction rate, variability of extracted inhibitory compounds and hazardous effects from solvent.

The selection of solvent is greatly affected by what the extract is expected for. As the final product will have solvent residues, the solvent must be non - hazardous, and the bioassay should not be intervening. This selection also relies heavily on the extraction of aimed active phytoconstituents whereas the alteration in the method of extraction normally depends on the time required for the extraction period, selected solvent, solvent pH, solvent-to-sample ratio and temperature maintained during the extraction procedure.

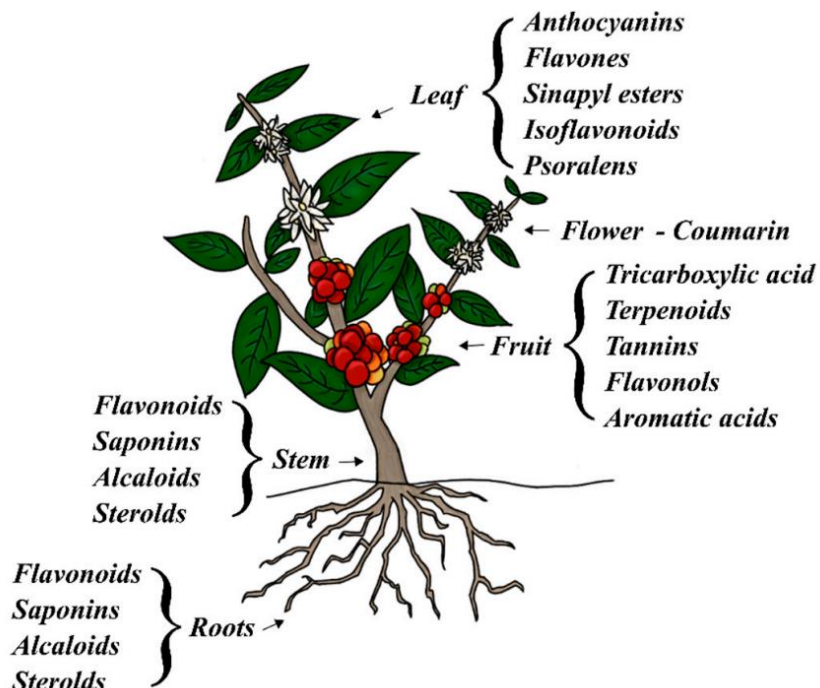


**Figure 1.11.** Basic parts of a plant and their common active compounds. <sup>65</sup>

The core premise is the refined grinding of the plant material (dry or wet) that increases surface area for extraction and therefore results in an increase in the extraction rate <sup>66-68</sup>. Various research indicated that the solvent-to-sample ratio of 10:1 (v / w) should be ideally preferred. Various solvents used for the extraction of active components are Water, Methanol, Acetone, Ethanol, Chloroform and Ethyl acetate.

### 1.3.3.3. Pre-extraction of plant sample

The beginning stage in the study of plant extracts for corrosion inhibition application is the preparation of plant samples in order to conserve the plant phytochemicals before extraction. Samples of plants such as barks, leaves, roots, flowers, and fruits could be obtained from fresh and dried plants. Some preparation techniques such as grinding and drying also have a significant effect on preserving phytochemicals in penultimate extracts.

### 1.3.3.4. Fresh vs. dried samples

Both the fresh and dried samples can be utilized in the procedure. A dried sample is favored in most situations, given the time needed for experimental design. Instead of fresh samples, several

researchers prefer the dried sample because fresh samples are frail and likely to deteriorate more rapidly than dried samples. A comparative study of various samples of plants for both fresh and dried leaves found no notable effect in total phenolic content but found higher flavonoid content in the case of the dried sample.

#### **1.3.3.5. Grinded vs. powdered samples**

Reduction in the particle size tends to increase the surface contact among the solvent and sample used for extraction. Grinding has culminated in coarser, finer samples; whereas, powdered samples provide a generally homogenized and finer material, resulting in better surface contact with the solvent. This preparation method is essential for efficient extraction where solvent should contact the targeted analytes, also particle size < 0.5 mm is advisable.

#### **1.3.3.6. Air-drying**

Air-drying generally takes 3-7 days and sometimes up to months depending upon the type of dried samples (e.g., leaves, roots, seeds). Plant samples such as stems with leaves are bound and strung together to expose the sample to air at normal room temperature. This process does not use high temperatures to drive dried plant materials; therefore, heat-labile compounds are conserved. Air drying, though, takes a longer time as compared to other drying processes, but could be vulnerable to degradation at high temperatures.

#### **1.3.3.7. Microwave-drying**

Microwave-drying utilizes electromagnetic radiation that has electrical as well as magnetic fields. The electrical field induces concurrent heating by dipolar rotation; synchronization of molecules with a dipole moment (e.g. solvent) on the electrical field, and ionic induction that creates molecular oscillation<sup>69</sup>. Oscillation induces collisions among molecules and also results in rapid heating of specimens. This method may have less drying duration but occasionally cause phytochemicals to degrade.

#### **1.3.3.8. Oven-drying**

Oven-drying is also another technique of pre-extraction that uses thermal energy to remove moisture from the sample. This method is the simplest and fastest that can conserve phytochemicals. Nevertheless, the drying effect on the sample shows no significant effect on

antioxidant activity but on bioactive phytochemicals; such the content of tannins and saponin was affected by oven and sunlight drying, proposing the temperature sensitivity of the compounds.

### **1.3.3.9. Freeze-drying**

This process is based on the sublimation principle that converts a solid into a gas without reaching the liquid state. Before lyophilization, a sample containing any fluid (e.g. solvent, moisture) is frozen at  $-80^{\circ}\text{C}$  to  $-20^{\circ}\text{C}$  to make the sample solidify. Following a freezing overnight (12-14 h), the sample is instantly lyophilized to prevent melting of frozen liquid<sup>66-68,70-73</sup>. To stop sample loss during the process, the mouth of the equipment containing the sample is covered with a parafilm. Compared with regular air drying and microwave drying, freeze-drying is a complex and costly drying process. Therefore, its use is confined to fragile, heat-sensitive materials.

## **1.3.4. Methods of Plants Extraction**

### **1.3.4.1. Hot Continuous Extraction (Soxhlet)**

In this procedure, the coarsely ground raw product is inserted in a permeable container or "thimble" formed of formidable filter paper embedded into the chamber of the Soxhlet apparatus. In the flask, the extracting solvent is heated, and its vapors condense in the condenser. The diluted extractant drips and extracts it by touch into the thimble containing the crude material<sup>74</sup>. When the liquid level in the chamber rises to the top of the siphon tube, the liquid content of the chamber siphon falls back into the flask. This method is continuous and is conducted until a drop of siphon tube solvent leaves no trace when evaporated as shown in **Figure 1.12**. Compared with previously mentioned methods, the advantage of this approach is that large amounts of extracts can be extracted with a much smaller volume of solvent. This has enormous effects on the economy in terms of time, resources and thereby financial inputs. It is only used as a batch system on a small scale, but it is much more economical and feasible when converted into a medium or large-scale continuous extraction process. The benefit of this method is that only one batch of solvent is collected, instead of several parts of warm solvent being transferred through the sample. This technique is not ideal to be used for thermolabile compounds, because excessive heat treatment will result in compound deterioration.



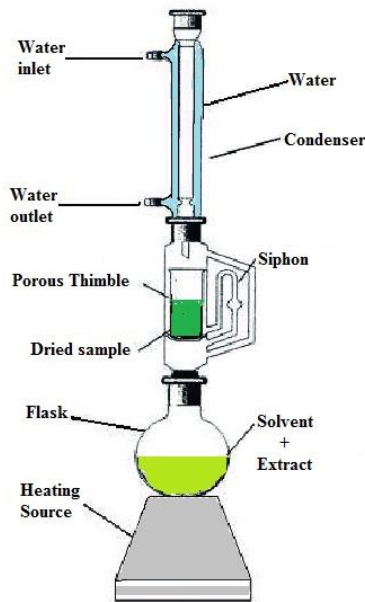


**Figure 1.12.** Extraction of active phytochemicals from plant dried sample by Soxhlet apparatus.

### 1.3.4.2. Ultrasound-assisted extraction (UAE) or sonication extraction

UAE entails the utilization of ultrasound between 20 kHz and 2000 kHz. The mechanical effect of ultrasonic acoustic cavitation improves surface contact between solvents and materials, and cell wall permeability<sup>75</sup>. The physical and chemical properties of the products subjected to ultrasound are altered and disturbed to the plant cell wall; enabling the release of compounds and improving the mass transfer of the solvents into the plant cells. The technique is versatile and fairly low-cost technology, which can be used in phytochemical extraction on both small and large scales. **Figure 1.13** shows the schematic diagram of Ultrasound-assisted extraction (UAE) having an ultrasonic generator as the main source of readings.

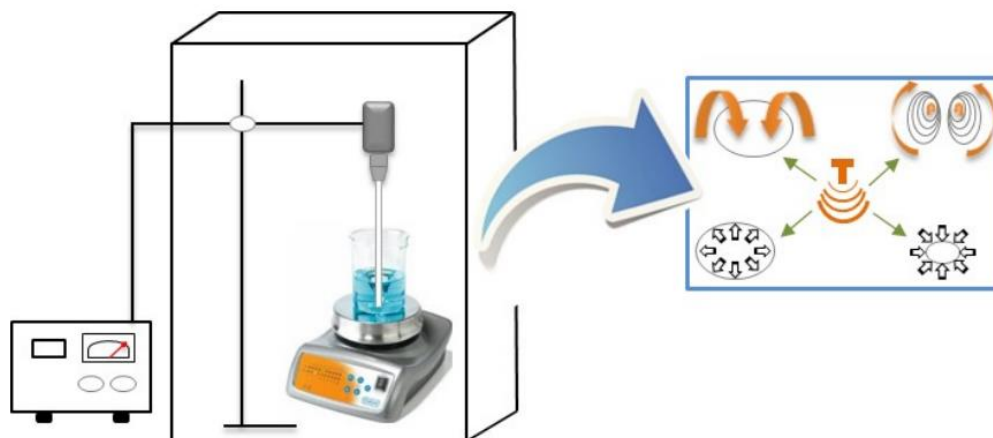


**Figure 1.13.** Schematic representation of the ultrasound-assisted extraction (UAE) process used in extraction technique. <sup>76</sup>

#### **1.3.4.3. Supercritical fluid extraction (SFE)**

Supercritical fluid or also labeled dense-gas is a substance containing both gas and liquid physical characteristics at its critical stage as shown in **Figure 1.14** summing the instrument used for supercritical fluid extraction (SFE). The determinants which move a substance into its critical region are factors like temperature and pressure. SF is more like a gas but has the solvent property of a liquid. One example of SF is CO<sub>2</sub> which becomes SF at 31.1 ° C and 7380 kPa above. Interest in Supercritical CO<sub>2</sub> (SC-CO<sub>2</sub>) extraction is widely accessible and affordable and has low toxicity due to its excellent solvent for nonpolar analytes. While SC-CO<sub>2</sub> is poorly soluble for polar compounds, amendments such as the addition of small amounts of ethanol and methanol make it possible to extract polar compounds. When CO<sub>2</sub> vaporizes at room temperature, SC-CO<sub>2</sub> also generates analytes in concentrate form. The intensity of SC-solvents can be significantly improved by altering the temperature, the pressure or by adding modifiers to reduce the extraction time.

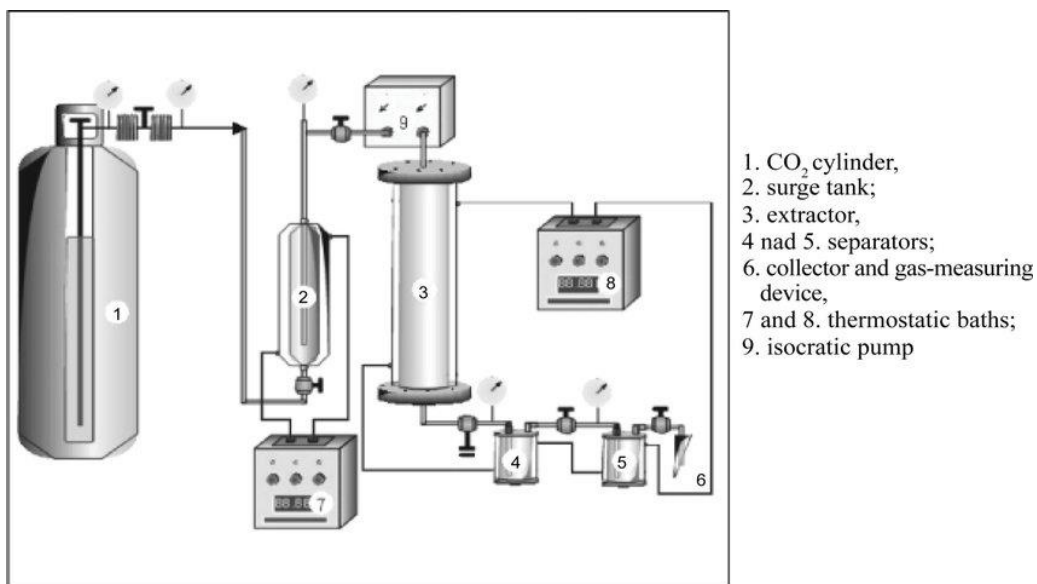


**Figure 1.14.** Representation of Supercritical fluid extraction (SFE) instrument. <sup>65</sup>

#### 1.3.4.4. Maceration

It is a very easy method of extraction with poor productivity and the downside of a long extraction duration. It is mainly recommended for thermolabile part extraction. In this method plant material or part is soaked in a halted jar filled with a solvent and permitted to stand at room temperature for a period of 2-3 days. The processed aimed at softening and breaking down the cell wall of the plant to unleash the soluble phytochemicals. The mixture is then pressed or strained by filtration after 3 days. Heat is transferred via the convection and conduction method and the quality of extracted compounds is generally influenced by the selection of relevant solvents. The diagrammatic representation can be seen in **Figure 1.15**. Where the blended peels are mixed with extraction solvent and a magnetic stirrer is used for proper mixing of the content.

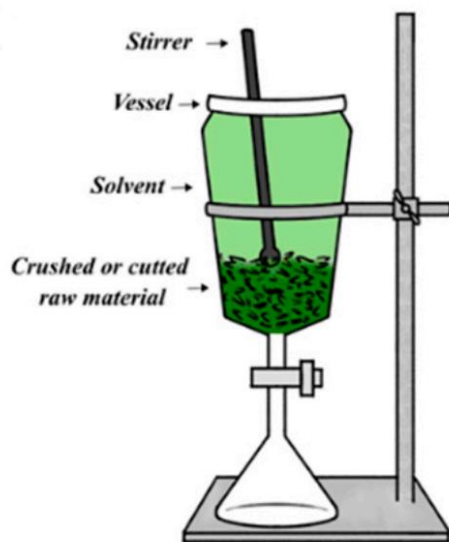


**Figure 1.15.** Maceration procedure for extraction. <sup>65</sup>

#### **1.3.4.5. Decoction**

The decoction is only effective in extracting heat-stable compounds, and raw plant parts (e.g., barks and roots), as shown in **Figure 1.16** where the aqueous decoction of plant raw material is done with the help of sparging stream and percolator metal sheet. This method is more culminated in oil-soluble compounds compared to infusion and maceration. This method uses a special instrument called a percolator in which powdered samples are placed in the percolator, and connected through boiling water for 2 hours. The percolation process typically takes place at a reasonable rate (like 7-9 drops/min) before extraction is finished to produce a concentrated extract before evaporation.

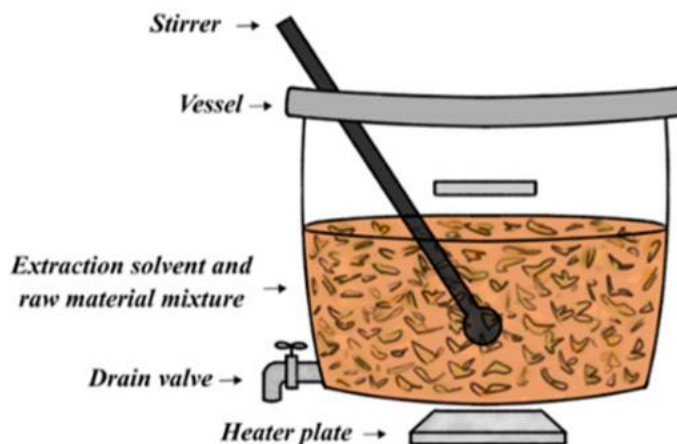


**Figure 1.16.** Aqueous decoction of plant raw material. <sup>65</sup>

#### **1.3.4.6. Counter Current Extraction**

The wet raw material is pulverized in counter current extraction (CCE) using punctured disc disintegrators to generate a fine slurry as shown in **Figure 1.17**. In this process, the material to be extracted is shifted in one direction inside a cylindrical extractor (generally in the form of fine slurry) where it comes into contact with the extraction solvent. The extract gets more condensed as the material starts to move more. Therefore, if the solvent and product concentrations and their flow velocity are adjusted, complete extraction is achievable<sup>75,77-79</sup>. The method is generally effective, requiring a limited amount of time and causing no high-temperature threat. Eventually, adequately condensed extract comes out on one end of the extractor while the marc (almost free of detectable solvent) falls off the other end.

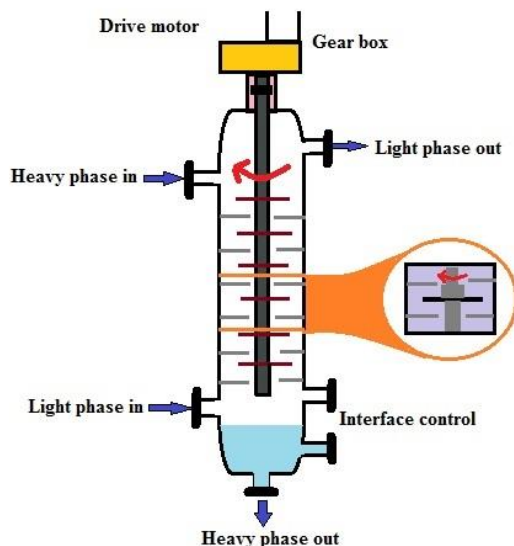


**Figure 1.17.** Counter-current Extraction apparatus

#### 1.3.4.7. Pressurized liquid extraction (PLE)

Various researchers have identified PLE as rapid solvent extraction, pressurized fluid extraction, and high-pressure solvent extraction. The PLE instrument and process have been illustrated in **Figure 1.18**. In extraction, PLE imposes high pressure. High pressure holds solvents beyond their boiling point in a liquid state, leading to high solubility and higher incidence of lipid solvent diffusion in solvent and high penetration of solvent into the matrix. PLE decreased extraction time and solvent consumption significantly and has greater reproducibility than other approaches. Scientists from various institutes have effectively implemented pressurized liquid extraction in the extraction of several forms of bio constituents including flavonoid, saponin and essential oil.

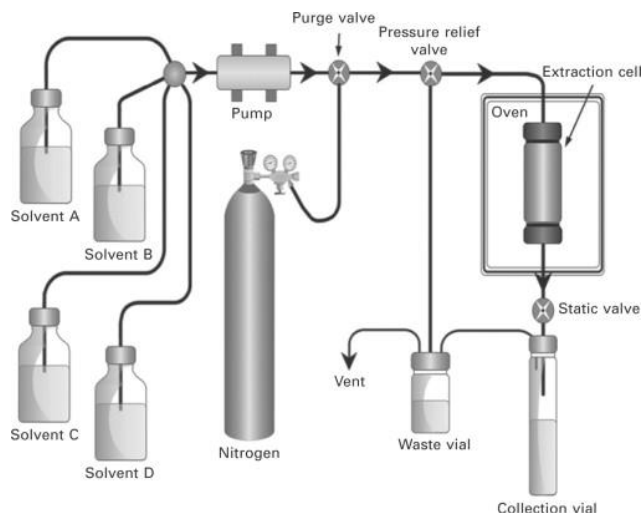


**Figure 1.18.** Pressurized liquid extraction (PLE) process. <sup>65</sup>

### 1.3.4.8. Microwave assisted extraction (MAE)

Using the ionic conduction and dipole rotation pathways, microwaves produce heat when it interacts with polar compounds like water or any other organic components present in plant matrix. In MAE, heat and mass transfer relies on the same axis, creating a synergistic impact that accelerates extraction and improves extraction yield. MAE applications deliver several advantages, including increased extract yield, reduced thermal decay and targeted material heating. MAE is often revalued as green mechanism, as it eliminates the use of organic solvent. There are two types of MAE methods: solvent-free extraction (usually for volatile compounds) and solvent extraction (usually for non-volatile compounds). An MAE extraction instrument can be easily understood in **Figure 1.19**.

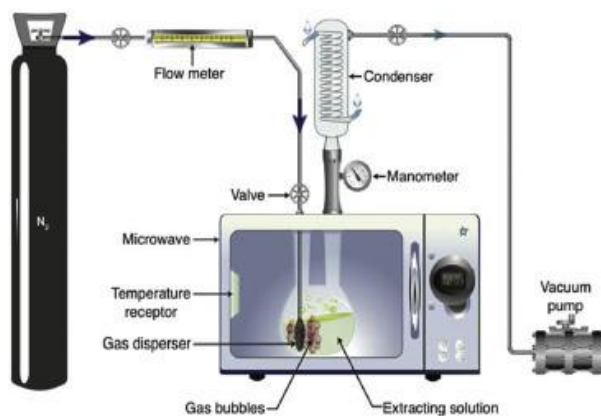


**Figure 1.19.** Microwave assisted extraction (MAE) extraction procedure. <sup>80</sup>

In a nutshell, corrosion is a pervasive and costly challenge across various industries, posing risks to infrastructure, safety, and the environment. Understanding the mechanisms and types of corrosion is essential for developing effective prevention and mitigation strategies. Green corrosion inhibitors, derived from plant extracts and natural sources, offer a promising avenue for sustainable corrosion protection. The need for green corrosion inhibitors is driven by the environmental and health concerns associated with traditional chemical inhibitors. These natural inhibitors, obtained through meticulous extraction processes, can adsorb onto metal surfaces and form protective layers, reducing corrosion rates effectively. Their eco-friendly nature aligns with the growing demand for sustainable and environmentally conscious solutions. Optimization of extraction methods, selection of appropriate plant materials, and understanding the underlying inhibition mechanisms are ongoing areas of study. These efforts aim to enhance the performance, compatibility, and long-term environmental impact of green corrosion inhibitors. The quest for green corrosion inhibitors represents a vital step towards addressing corrosion-related challenges in industries while promoting sustainability and environmental responsibility. This innovative approach holds promise for a future with reduced corrosion-related risks and a lighter ecological footprint.

In the next chapter of the literature review, the effectiveness of green corrosion inhibitors derived from weeds in various mediums for several metals, with a focus on mild steel, is explored. Weeds are a promising source of natural inhibitors as they are abundant, inexpensive, and can be easily extracted using simple methods. Several studies have investigated the use of weed extracts as green corrosion inhibitors for mild steel in numerous mediums, including acid solutions, saltwater, and alkaline solutions. These studies have found that weed extracts can significantly reduce the pace of corrosion in mild steel, with inhibition efficiencies ranging from 50-90%<sup>13,54,81-83</sup>. Additionally, the performance of weed extracts as inhibitors were found to be comparable or even superior to that of traditional inhibitors. The mechanism of action of weed extracts as corrosion inhibitors is believed to be due to the presence of various phytochemicals, such as alkaloids, flavonoids, and phenols, which can adsorb onto the metallic surface and produce a defensive film that inhibits the corrosion process. The effectiveness of weed extracts as inhibitors can also be influenced by factors such as concentration, immersion time, and temperature.



---

---

**Chapter 2**  
**Review of Literature**

---

---

## **2.1. Literature Survey**

### **2.1.1. Green corrosion inhibitors**

Metallic corrosion is a complex electrochemical process that involves the reaction of a metal with its environment. The process involves the transfer of electrons from the metal to the environment, which leads to the formation of a new compound, such as an oxide or a salt. The formation of these compounds can cause damage to the metal, leading to structural degradation, loss of performance, and even failure. One common way to mitigate metal corrosion is through the usage of corrosion inhibitors. These are chemical compounds that are added to the metal surface or the surrounding environment to slow down or prevent corrosion. Traditional corrosion inhibitors are often synthetic compounds that can have harmful environmental impacts, leading to the need for green corrosion inhibitors.

Green corrosion inhibitors are typically derived from natural sources or synthesized from renewable resources. For instance, it has been discovered that plant extracts, such as tannins, lignin, and flavonoids, are significant eco-benign corrosion inhibitors. Green corrosion inhibitors function by coating the metal's surface with a protective layer. This layer can help prevent the transfer of electrons between the metal and its environment, slowing down or preventing the formation of corrosive compounds. Additionally, the protective layer can also help prevent other environmental factors, such as humidity or moisture, from reaching the metal surface. The effectiveness of green corrosion inhibitors can depend on several factors, including the type of metal being protected, the environment in which the metal is located, and the specific inhibitor being used. Additionally, proper selection and application of green corrosion inhibitors are important to ensure effective corrosion protection.

#### **2.1.1.1. Plant extracts as corrosion inhibitors for metals**

Due to its superior mechanical properties and thermal conductivity, mild steel is universally used for the manufacturing of reactors, storage vessels, gathering pipelines, drilling equipment, and other apparatuses. Mild steel corrosion occurs commonly in acidic solution during pickling, scale-removal and rust-cleaning procedures, resulting in metal deterioration and massive economic losses<sup>84-87</sup>. The application of corrosion inhibitors is a frequently utilized convenient technique of the various methods of corrosion protection. Natural products often including plant extract, amino

acids, proteins, and natural polymers have been claimed to be effective corrosion inhibitors. Among these, plant extracts are regarded as a significant source of naturally modulated chemical compounds which can be extracted at a reasonable cost through simple procedures. These natural extracts are similar to organic synthetic inhibitors and are known to serve almost as well as their synthetic equivalents. The relevant literature as shown in table 1 states that plant extracts contain a mixture of phytochemical components, such as alkaloids, tannins, flavonoids, anthraquinones, polyphenols, saponins, glycosides, proteins, amino acids and several heterocyclic compounds which deemed to be a potent corrosion inhibitor for mild steel with a potential corrosion inhibition rate. Down below **Figure 2.1.** illustrates the adsorption of phytochemicals derived from plant extract forming a protective film on the mild steel surface.

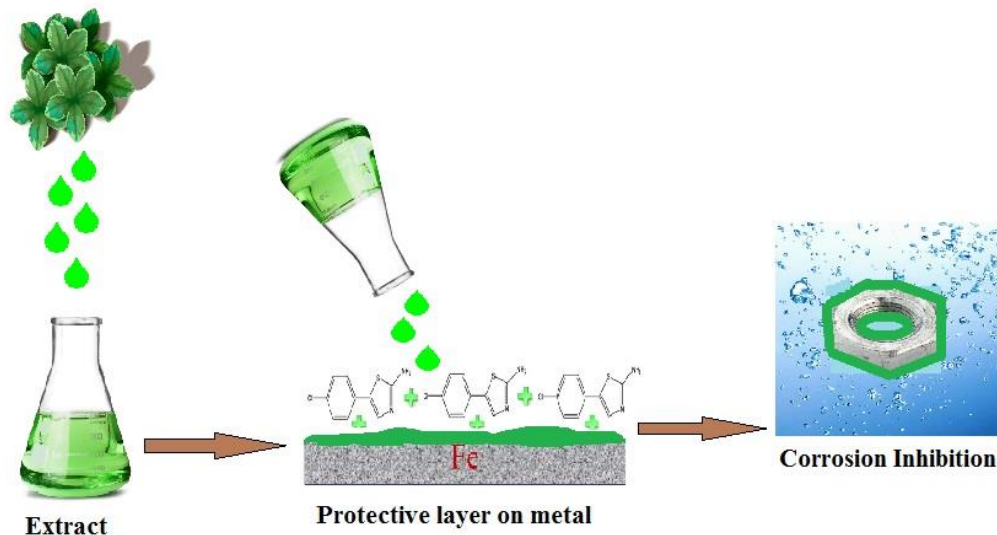


**Figure 2.1.** Diagrammatic illustration of the adsorption of phytochemicals derived from plant extract forming a protective layer on the mild steel surface.

The research study conducted by Antonio dosRde Faria Neto et al.<sup>88</sup> aimed to investigate the potential use of *Paullinia Cupana* (guarana) as a novel corrosion inhibitor for carbon steel. The study employed both gravimetric and electrochemical noise techniques to examine the potency of *Paullinia Cupana* extract in inhibiting the corrosion of carbon steel. Gravimetric measurements were carried out to determine the corrosion rate ( $C_R$ ) of carbon steel in the existence and absence of the *Paullinia Cupana* extract. The analysis showed that the corrosion rate reduced significantly in the existence of the extract, indicating its effectiveness as a corrosion inhibitor. Electrochemical

noise (ECN) measurements were also used to examine the effectiveness of the extract as a corrosion inhibitor. The technique is based on the analysis of the random fluctuations in the electrochemical potential and current caused by the corrosion process. The results showed that the extract reduced the amplitude of the electrochemical noise, indicating a reduction in the corrosion rate. The gravimetric measurements showed that *Paullinia Cupana* shell presents a strong inhibitive characteristic, showing an efficiency of about 76.8% and 57.4% for HCl and H<sub>2</sub>SO<sub>4</sub> acidic mediums, respectively, and the mechanism of action is physisorption. ECN allowed us to analyze the variation of the corrosion charge over time, and about 8.6 and 2.2 times less charge generated with the inhibitor was observed in HCl and H<sub>2</sub>SO<sub>4</sub> acidic mediums, respectively, and the type of localized corrosion also decreased. The study also investigated the mechanism of inhibition by analyzing the surface morphology of the carbon steel samples utilizing SEM and energy-dispersive X-ray spectroscopy (EDX). The results showed that the extract emerged a protective layer over the surface of the carbon steel, which effectively inhibited the corrosion process. The study concluded that *Paullinia Cupana* extract has the capability to be used as a green corrosion inhibitor for carbon steel. The extract was found to be effective in inhibiting the corrosion phenomenon, and the mechanism of inhibition was attributed to the emergence of a protective layer upon the surface of the carbon steel.

The research study conducted by I. Nadi et al.<sup>89</sup> investigated the potential use of *Sargassum muticum* extract based on alginate biopolymer as a biological corrosion inhibitor for carbon steel in the hydrochloric acid pickling environment. The study employed gravimetric, electrochemical, and surface studies to evaluate the effectiveness of *Sargassum muticum* extract in inhibiting the corrosion of carbon steel. Gravimetric measurements were carried out to determine the corrosion rate of carbon steel in the presence and absence of the *Sargassum muticum* extract. The results showed that the corrosion rate decreased significantly in the presence of the extract, indicating its effectiveness as a corrosion inhibitor. Electrochemical measurements, including potentiodynamic polarization and electrochemical impedance spectroscopy, were also used to investigate the effectiveness of the extract as a corrosion inhibitor. The results showed that the extract reduced the corrosion rate and increased the polarization resistance of the carbon steel, indicating a reduction in the corrosion process. The evaluation corrosion tests showed that this algal extract acts as a well-mixed corrosion inhibitor for carbon steel (CS) substrate in 1 M HCl since an inhibition efficiency of 97 % was reached with 1 g/L at 303 K. The alternating current (AC) impedance

findings showed that the seaweed extract added in the corrosive electrolyte increases the polarisation resistance and conversely decreases the charge capacitance at the interface. Surface studies, including SEM, EDX, and atomic force microscopy (AFM), were utilized to analyze the surface morphology and composition of the carbon steel samples in the inclusion and exclusion of the *Sargassum muticum* extract. The findings showed that the extract formed a protective layer upon the surface of the carbon steel, which effectively inhibited the corrosion process. The AFM results revealed that the surface roughness of the carbon steel was reduced in the existence of the extract. The study concluded that *Sargassum muticum* extract based on alginate biopolymer has the potential to be used as a potent corrosion inhibitor for carbon steel in the HCl pickling environment. The extract was found to be effective in inhibiting the corrosion phenomenon, and the mechanism of inhibition was attributed to the emergence of a protective layer on the surface of the carbon steel.

The research study conducted by A. A. Ayoola et al.<sup>90</sup> aimed to investigate the inhibitive corrosion performance of *Aloe vera* in acidic media on mild and stainless steel. The study employed gravimetric and linear polarization methods to evaluate the effectiveness of *Aloe vera* as a corrosion inhibitor. The results showed that the inhibition efficacy elevated with a rise in the concentration of the *Aloe vera* inhibitor (up to 10 vol/vol%) for both mild and stainless steels. Stainless steel was found to exhibit a lower corrosion rate compared to mild steel, indicating that it is more resistant to corrosion in acidic media. The study also revealed that the Langmuir adsorption isotherm was obeyed by the inhibition of mild and stainless-steel utilizing aloe vera in 0.5 M H<sub>2</sub>SO<sub>4</sub>, with the values of the regression coefficients near unity. The negative values of  $\Delta G^{\circ}_{\text{ads}}$  indicated that the inhibitor adsorption on the mild and stainless-steel surfaces was spontaneous, and a physisorption adsorption mechanism of the aloe vera inhibitor was observed. The study concluded that aloe vera is an efficient corrosion inhibitor with mixed-type inhibition properties, and its effectiveness as a corrosion inhibitor increases with an increase in its concentration. The study provides valuable insights into the usage of natural products as corrosion inhibitors, which could help to develop eco-friendly and sustainable solutions for corrosion control in various industries.

The research study conducted by Abdul-Rashid I. Mohammed et al.<sup>91</sup> evaluated the efficacy of *Kola nut* extract (KE) for reducing low-carbon steel corrosion in a simulated acid pickling

environment. The study employed weight loss, electrochemical, and surface analysis techniques to evaluate the effectiveness of KE as a corrosion inhibitor. The results showed that KE revealed novel corrosion protection properties, with the  $C_R$  deduced from 0.387 to 0.054 mm/year by 700 ppm of KE at room temperature following 24 hours of dipping, corresponding to an inhibition efficiency (IE%) of 86%. However, when the temperature increased, the IE reduced. The findings of the FTIR spectroscopy demonstrated that the phytoconstituents of KE linked with the carbon steel substrate via the O and N heteroatoms. The SEM, AFM, and EDX data gave evidence of KE adsorption upon the steel surface as the cause of the corrosion suppression, and the UV-vis investigations supplied insight into the association of KE with the carbon steel surface.

Haque et al.<sup>92</sup> investigated the potential of *Thevetia peruviana* flower extract (TPFE) as an eco-benign corrosion inhibitor for mild steel in 1M HCl medium. The inhibitory effect of TPFE was evaluated using electrochemical, surface and computational techniques. The findings of this study can help in the development of eco-friendly and cost-effective inhibitors for protecting mild steel from corrosion. The findings showed that TPFE acted as a potential corrosion inhibitor, and the highest IE% of 91.24% was observed at 200 mg/L concentration. The electrochemical studies suggested that TPFE functioned as a mixed- and interface-type of corrosion inhibitor. The results of the electrochemical measurements showed that TPFE reduced the corrosion current density and increased the polarization resistance, indicating a decrease in the  $C_R$  of mild steel. The adsorption mechanism of corrosion inhibition was further supported using AFM), Scanning Electron Microscopy-Energy Dispersive X-ray (SEM-EDX), Fourier Transform Infrared (FT-IR) and UV-visible surface studies. AFM images showed that TPFE adsorbed on the mild steel surface and emerged a defensive coating, which prevented the corrosion of the metal. SEM-EDX and FT-IR analyses provided evidence of the adsorption of TPFE on the mild steel surface. The UV-visible spectroscopy analysis showed that TPFE has an absorption peak at 285 nm, which further confirms the adsorption of TPFE upon the substrate. Furthermore, the researchers used DFT and MDS to study the anticorrosive mechanism of major phytochemicals of the TPFE. The results showed that TPFE interacts with donor-acceptor interactions, and its phytochemicals acquire flat or horizontal orientations over the metallic surface. The simulations provided insight into the molecular interactions between the TPFE and the metallic surface, which helped to understand the adsorption mechanism of TPFE upon mild steel.

Boumezzourh et al.<sup>93</sup> investigated the effectiveness of *Mentha pulegium* essential oil as a natural inhibitor of tinplate corrosion in a 0.5 M H<sub>2</sub>C<sub>2</sub>O<sub>4</sub> medium. The inhibitory effect was evaluated using weight loss, potentiodynamic polarization, and EIS measurement techniques. The chemical composition of *Mentha pulegium* essential oil was determined using gas chromatography (GC) and gas chromatography-mass spectrometry (GC-MS). The main components were found to be Pulegone and Menthone. The results of weight loss measurement and electrochemical tests showed that *Mentha pulegium* essential oil had a significant anticorrosion effect with an IE% of 80% at 4 g/L concentration. The findings were attributed to the adsorption of *Mentha pulegium* essential oil compounds on the tinplate surface. The study employed SEM spectroscopy and energy dispersive X-rays (SEM-EDX) visualization to confirm the adsorption of *Mentha pulegium* essential oil on the tinplate surface. The authors concluded that *Mentha pulegium* essential oil could be used as an alternative to synthetic inhibitors to control tinplate corrosion in 0.5 M H<sub>2</sub>C<sub>2</sub>O<sub>4</sub> medium. The study provides valuable insights into the potential of natural inhibitors derived from medicinal and aromatic plants as an effective solution to minimize the usage of synthetic inhibitors in the regulation of metal corrosion in various environments. The use of natural inhibitors may reduce the negative environmental impact of synthetic inhibitors, making them an eco-friendly and sustainable solution for corrosion control.

Sedik et al.<sup>94</sup> aimed to investigate the effectiveness of *Dardagan* Fruit (DF) extract as a green corrosion inhibitor for mild steel in 1 M HCl solution. The study used electrochemical techniques, surface morphological studies, and spectroscopic analysis to determine the corrosion inhibition mechanism and characteristics of DF extract. The results showed that DF extract has good corrosion protection ability with inhibition efficiency of 92% after 1 hour and 97% after 6 hours of immersion in a 3000 ppm inhibitor containing corrosive media. The high protection ability was attributed to the development of a homogeneously distributed protective layer over the metal. The researchers employed various techniques to investigate the corrosion inhibition properties of DF extract. They used electrochemical impedance spectroscopy (EIS) to determine the excess surface charge of mild steel and proposed an inhibition mechanism. The results showed that DF extract could form a protective film upon the surface of mild steel, which could hinder the penetration of the aggressive media into the metal. Surface morphological studies were conducted utilizing SEM and AFM to examine the surface of mild steel after exposure to test solutions. The researchers found that the surface of the mild steel was homogeneously covered with a protective film after

immersion in the DF extract containing corrosive media. The elemental composition of the surface was analyzed with the help of EDX. The researchers also performed contact angle measurements to obtain information about the surface properties of the mild steel. Spectroscopic studies were conducted to determine the major components, chemical structure, and adsorption mechanism of the extract. The findings revealed that DF extract contains natural corrosion inhibitors that could be utilized to preserve mild steel from corrosion in acidic media.

Anadebe et al.<sup>95</sup> discussed the employment of *Moringa* leaf extract as an eco-benign corrosion inhibitor for carbon steel in alkaline and acidic environments. The authors employed various electrochemical techniques, surface characterization methods, and quantum chemical studies to investigate the adsorption mechanism of the corrosion inhibitor. The findings showed that *Moringa* leaf extract had maximum inhibition efficiencies of 90%, 91.2%, and 89.8% in hydrochloric acid and 86.9%, 85.1%, and 85.9% in potassium hydroxide solution, respectively, at a quantity of 1.5 ML g/L-1. The IE% reduced with an elevation in temperature. The electrochemical study indicated that *Moringa* leaf extract behaved as a mixed-type inhibitor, and the adsorption mode for both studied environments obeyed the Langmuir model. Surface morphology analysis and the study of corrosion products indicated the presence of a dense covering upon the surface of carbon steel due to the adsorption of extract species. Additionally, the theoretical results derived from molecular dynamics confirmed that the inhibitors adsorbed upon the steel substrate via donor-acceptor interactions with a flat-lying adsorption orientation. The findings of this study suggest that *Moringa* leaf extract could be utilized as a potential corrosion inhibitor for carbon steel in both alkaline and acidic environments. The utilization of natural plant extracts as corrosion inhibitors is an important area of research as it offers an environmentally friendly alternative to traditional synthetic inhibitors. Furthermore, the study highlights the importance of combining experimental and theoretical approaches to understand the adsorption mechanism of corrosion inhibitors upon metal surfaces.

Akbarzadeh et al.<sup>96</sup> investigated the anti-corrosion effectiveness of *Papaver somniferum* plant extract as a novel corrosion inhibitor for mild steel in chloride-containing media. The study combined experimental techniques such as Fourier transform infrared spectroscopy (FT-IR), grazing incidence X-ray diffraction (GI-XRD), Raman spectroscopy, ultraviolet-visible (UV-Vis) test, AFM, field emission scanning electron microscope (FE-SEM), and contact angle (CA)



method with theoretical modeling techniques such as MDS, MCS and DFT to study the adsorption and corrosion inhibition mechanisms of the plant extract upon mild steel in saline solution. The study found that the *Papaver somniferum* plant extract, with its nitrogen-based functionalities, is an efficacious corrosion inhibitor for mild steel in simulated seawater. The EIS measurements showed that an IE% of 91% was attained with the inclusion of 1600 ppm of the plant extract to the 3.5% wt. NaCl media. The potentiodynamic polarization spectroscopy (PPS) measurements also confirmed the high inhibition efficacy of the plant extract. The investigation also found that the *Papaver somniferum* plant extract adsorbs upon the metallic surface and forms an inhibitive graphene-like film. The GI-XRD analysis indicated the formation of complexes such as p-tert-Pentyl-N, N-bis(3-phenyl propyl)aniline and iron cyanide, while FE-SEM images and Raman spectroscopy results affirmed the steel surface coverage by an inhibitive graphene-like film. The theoretical studies using MD, MC, and DFT confirmed the adsorption of the plant extract molecules on the mild steel surface. In conclusion, the study demonstrated that the *Papaver somniferum* plant extract is an effective and sustainable corrosion inhibitor for mild steel in chloride-containing media. The study also showed that a combination of experimental and theoretical techniques can provide detailed insights into the adsorption and corrosion inhibition mechanisms of plant extract-based corrosion inhibitors.

The research conducted by A. Berrissoul et al.<sup>97</sup> investigates the effectiveness of *Lavandula mairei Humbert* extract (LM) as an eco-friendly inhibitor for mild steel (MS) corrosion in 1 M HCl solution. The study utilized weight loss and electrochemical measurements, SEM, XPS, and theoretical approaches to evaluate the corrosion inhibition performance and adsorption behavior of LM on the mild steel surface. The results indicate that LM is a highly efficient inhibitor for MS corrosion in 1 M HCl solution. The corrosion inhibition efficiency increased with increasing LM concentration and reached 92% at a quantity of 0.4 g/L and a temperature of 303 K. The Langmuir adsorption isotherm model was utilized to explain the adsorption behavior of LM on the mild steel surface, and the anodic Tafel slope digression and continuous CR lessening with the LM extract concentration increase indicated the limited dissolution of mild steel. The study also employed theoretical approaches based on chemical quantum calculations and molecular dynamics simulation to explain the mode of adsorption of the majority of the molecule upon the metallic surface. The theoretical analysis provides a detailed understanding of the molecular-level interactions between LM and the mild steel surface, validating the experimental observations. The

use of LM as a green inhibitor for MS corrosion is a significant contribution to the development of environmentally friendly corrosion inhibitors. The combination of experimental and theoretical approaches provides a comprehensive understanding of the inhibition performance and adsorption behavior of LM, facilitating the development of effective corrosion inhibitors for practical applications.

Ameh et al.<sup>98</sup> examined the effectiveness of *Canarium schweinfurthii* (CSF) gum as an inhibitor for the corrosion of mild steel in a hydrochloric acid solution. The inhibition efficiency was evaluated using chemical techniques, such as weight loss, thermometric, spectrophotometric, and gasometric techniques, and electrochemical techniques, including PDP and EIS. The surface morphology of mild steel samples was investigated utilizing SEM. The study found that CSF gum was effective in inhibiting the mild steel deterioration in HCl, and the IE% increased with the quantity of the inhibitor but decreased with increasing temperature. Gas chromatography-mass spectrometer (GCMS) spectrum of CSF gum revealed the presence of various phytochemicals, including Nonacosane; 1-piperoylp; Stearic acid, 2-(hydroxymethyl)-2-nitropropane-1,3-diol, Stigmasta-5,22-dien-3-ol, dihex-5-en-2-yl phthalate, 9-octadecenoic acid, methyl ester, 1-pentadecarecarboxylic, and Oleic acid. The inhibition action of the gum showed a strong correlation with these phytochemicals in the gum, and the phenomenon of physical adsorption was proposed for the inhibition, following the Langmuir adsorption isotherm with high negative values of the free energy of adsorption ( $\Delta G^{\circ}_{ads}$ ). The CSF gum behaved as a mixed-type inhibitor, retarding both cathodic and anodic reactions with high inhibition efficiency. The results from chemical and electrochemical analysis were in excellent correlation with each other, and the surface studies demonstrated the emergence of a smooth, dense protective covering in the presence of the inhibitor. Quantum chemical computations of parameters associated with the electronic structures of specific components of the gum supported their inhibiting potentials.

Berdimurodov et al.<sup>99</sup> investigated the potential of Thioglycoluril derivative, 3a,6a-bistolylthioglycoluril (BSTGCU), as a corrosion inhibitor for low-carbon steel in a 1 M HCl medium. The research utilized various techniques, including gravimetric, thermodynamic, EIS, PDP, electrochemical noise (EN), electrochemical frequency modulation (EFM), DFT, MDS, SEM and EDX methods. The findings of the experiment revealed that BSTGCU can act as a highly effective inhibitor for the corrosion of low-carbon steel in a 1M HCl medium. At an inhibitor

quantity of 100 mg/L, the maximum IE% was found to be over 96%. Electrochemical analysis revealed that the BSTGCU acted as a mixed-type inhibitor and adsorbed spontaneously onto the metal surface by physical and chemical adsorption mechanisms following the Langmuir adsorption isotherms. The SEM-EDX analysis also confirmed that the presence of the inhibitor upon the steel surface improved its morphology. Theoretical calculations confirmed that the inhibition properties of BSTGCU depended on its molecular structure. The study showed that the inhibitory performance of BSTGCU was better in its protonated form than in its neutral form in the aqueous phase. The research demonstrated the potential of BSTGCU as a green corrosion inhibitor that could be employed in industrial applications. The study provides a comprehensive understanding of the inhibition mechanism and the role of the molecular structure of BSTGCU in corrosion inhibition. The use of both experimental and theoretical methods offers an integrated approach to understanding the inhibitory behavior of the compound. **Table 2.1** shows the efficiency of plant extracts as corrosion inhibitors for several metallic surfaces in acidic media.

**Table 2.1**

Plant extracts as corrosion inhibitors for several metals in different electrolytic media involving various plant names, techniques, nature of metal and electrolyte and nature of the adsorption of active phytoconstituents.

Plant name	Part used	Techniques	Metal and electrolyte	Nature of adsorption	Remark	Ref.
<i>Juglans regia</i>	Leaves	WL, PDP, FTIR	EIS, Stainless steel/1 M HCL	Langmuir adsorption isotherm	The maximum inhibition efficiency was found upto 88.8 %	<sup>100</sup>
<i>Chenopodium Ambrosioides</i>	Whole plant	WL, PDP	EIS, Stainless steel/0.5 M H <sub>2</sub> SO <sub>4</sub>	Langmuir adsorption isotherm	The maximum inhibition efficiency of 94% was attained at 4 g/l	<sup>101</sup>
<i>Ferula gummosa Boiss.</i>	oleo-gum-resin exudate	WL, EIS	304 Stainless steel/2 M HCL	Temkin adsorption isotherm	The main constituents, b-pinene and a-pinene are responsible for corrosion inhibition	<sup>102</sup>
<i>Gum Arabic</i>	Whole plant	WL, PDP	EIS, API 5L X42 pipeline steel/1 M H <sub>2</sub> SO <sub>4</sub>	Langmuir adsorption isotherm	The maximum IE% was found to be 92% at 2 g L <sup>-1</sup> with arabinogalactan as an active constituent	<sup>103</sup>
<i>Lavandula Stoeckas</i>	Leaves	EIS, PDP	Stainless steel/ 5.5 M H <sub>3</sub> PO <sub>4</sub>	Langmuir adsorption isotherm	The IE% increases with increased organic oil concentration attaining a maximum value of 87.3 % at 1.2 g/L	<sup>104</sup>
<i>Thymus vulgaris</i>	Leaves	WL, PDP, DFT	EIS, 304 Stainless steel/1 M HCL	Langmuir adsorption isotherm	Thymus extract acts as a green inhibitor	<sup>87</sup>

<i>Fennel</i>	Seeds	WL, PDP	EIS,	304Stainless steel/1 M HCL	Langmuir adsorption isotherm	Anethol and Fenchone are the main active constituents in the extract of fennel seed	<sup>86</sup>
<i>Coriander Seeds</i>	Seeds	WL, EFM	EIS,	304 Stainless steel/1 M HCL	Langmuir adsorption isotherm	A physical adsorption mechanism was proposed for the inhibition with Linalool and Geraniol as the main active constituents	<sup>105</sup>
<i>Calotropis procera</i>	Roots	WL, PDP, AFM, SEM	EFM, FTIR,	304 Stainless steel/2 M HCL	Langmuir adsorption isotherm	Tannins, Flavonoid acid, Saponin, and glycosides are the main phytochemicals	<sup>85</sup>
<i>Bee Wax Propolis</i>	Honeycomb waste	WL, FTIR, HPLC	EIS,	304SS /1 M H <sub>2</sub> SO <sub>4</sub>	Langmuir adsorption isotherm	Quercetin (2-(3,4- dihydroxy phenyl)- 3,5,7-trihydroxy- 4H-chromen-4-one) was observed as the active phytoconstituent revealing 97.29% inhibition efficiency at 2000 ppm	<sup>84</sup>
<i>Cassia fistula</i>	Leaves	WL, LSV	EIS,	Stainless steel/0.5 M HCL	Langmuir adsorption isotherm	10 g/L conc. of Cassia fistula leaf extract exhibited optimal inhibition efficiency of 88.46%	<sup>106</sup>

<i>Morus alba pendula</i>	Leaves	WL, SEM, FTIR, UV	EIS, AFM	Stainless steel/1 M HCl	Langmuir adsorption isotherm/mixed-type inhibitor	The maximum IE% of 93% was achieved in the existence of 0.4 g/L at a room temperature of 25 °C	<sup>107</sup>
<i>Tectona grandis</i>	Roots stem, leaves	WL, FTIR	EIS	SS304 stainless steel/2 M HCl	Langmuir adsorption isotherm/mixed-type inhibitor	anthraquinone, tannin-theaflavin, and saponin were the main phytoconstituents	<sup>108</sup>
<i>Dendrocalmus sinicus</i>	Aerial part	WL, PDP, FTIR	EIS, AFM	Stainless steel/1.0–5.0 M HCl	Langmuir adsorption isotherm	Active components are orientiuxyloside, Isoorient, vitexin-40-OCH <sub>3</sub> , luteolin-7-O-glucosioe, d-hydroxyl lysine with inhibition efficiency of 89%	<sup>109</sup>
<i>Phyllanthus amarus</i>	Leaves	WL, EIS		Aluminium/ 2 M NaOH	Langmuir adsorption isotherm	76% inhibition efficiency at the highest concentration in the alkaline environment was confirmed with phyllanthin and hypophyllathin as active constituents	<sup>110</sup>
<i>Gossipium hirsutum</i>	Leaves	WL, EIS		Aluminium/2 M NaOH	Langmuir adsorption isotherm	GE extract gave 97% inhibition efficiency with gossypo as a major constituent	<sup>111</sup>

<i>Asparagus Racemosus</i>	Stem, roots and leaves	WL, DFT	AFM,	Aluminium/1 M HCl	Langmuir adsorption isotherm	At 4000ppm concentration of inhibitor, 72.28% corrosion inhibition efficiency is observed	<sup>15</sup>
<i>Origanum Vulgare</i>	Stem and leaves	WL, DFT	SEM,	Aluminium/1 M HCl	Langmuir adsorption isotherm/mixed-type inhibitor	At 4000 ppm, maximum inhibition efficiency revealed to be 97.7% with Carvacrol and Thymol as the main components	<sup>16</sup>
<i>Sapindus</i>	Leaves and roots	WL, PDP, DFT	EIS, SEM,	Aluminium/1 M HCl	Langmuir adsorption isotherm	<i>Sapindus</i> revealed 98 % of inhibition efficiency at 2000 ppm	<sup>112</sup>
<i>Trachyspermum copticum</i>	Seed	WL, EIS		Aluminium/0.5 M NaOH	Langmuir adsorption isotherm/mixed-type inhibitor	The maximum inhibition efficiency of 94% at 500 ppm inhibitor concentration revealed	<sup>113</sup>
<i>Salvia officinalis</i>	Leaves	WL, PDP, DFT	EIS,	304 stainless steel/1 M HCl	Langmuir adsorption isotherm	Some of the active compounds reported are salvigenin, lupeol, b-sitosterol, stigmasterol, physcion, carnosol, rosmadial, rosmanol, epirosmanol, isorosmanol	<sup>114</sup>

<i>Capparis decidua</i>	Fruit, stem bark and root bark	WL, PDP		Aluminium/ 0.5N H <sub>2</sub> SO <sub>4</sub> , 1N H <sub>2</sub> SO <sub>4</sub> , 2N H <sub>2</sub> SO <sub>4</sub>	Langmuir adsorption isotherm	94.79% of inhibition efficiency was observed in 3N HCl	<sup>115</sup>
<i>Ananas sativum</i>	Leaves	WL, EIS	AFM,	Aluminium/0. 1 M HCl	Langmuir adsorption isotherm	The obtained values of $\Delta G^{\circ}_{ads}$ were low and negative, revealing the spontaneity nature of the adsorption process	<sup>116</sup>
<i>Sida acuta</i>	Roots, stem and leaves	WL, PDP		Al-Cu-Mg alloy /HCl	Langmuir adsorption isotherm	Inhibition efficiency improves from 37.42% to 93.63% over ten days with a rise in the extract percentage volume	<sup>117</sup>
<i>Citrullus Colocynthis</i>	Whole plant	WL, DFT		Aluminium/0. 5N HCl	Langmuir adsorption isotherm	87.29% inhibition efficiency observed	<sup>118</sup>
<i>Jasminum nudiflorum</i> <i>Lindl.</i>	Leaves	WL, SEM	EIS,	Aluminium/0. 1 M HCl	Langmuir adsorption isotherm	Jasmoside, jasmisnyroside, jasminin, verbascoside, and syringing are some active constituents	<sup>119</sup>
<i>Opuntia</i>	Stem, roots, leaves, fruit	WL, PDP		Aluminium/2. 0 M HCl	Langmuir adsorption isotherm	IE % increases as increasing extract conc.	<sup>120</sup>



<i>Dendrocalamus brandisii</i>	Leaves	WL, PDP, SEM	EIS,	Aluminium/1 M HCl, 1.0 M H <sub>3</sub> PO <sub>4</sub>	Langmuir adsorption isotherm	Maximum efficiency observed at 1.0 g l <sup>-1</sup> at 20 °C was 91.3% in 1.0 M HCl and 47.1% in 1.0 M H <sub>3</sub> PO <sub>4</sub>	<sup>121</sup>
<i>Aspilia africana</i>	Leaves	WL, DFT	EIS,	AA3003 Al alloy/0.5 M HCl	Langmuir adsorption isotherm	The main active compounds were Thiamine and Niacin	<sup>122</sup>
<i>Dryopteris cochleata</i>	Leaves	WL, XRD, SEM	EIS,	Aluminium/1 M H <sub>2</sub> SO <sub>4</sub>	Freundlich adsorption isotherm	The extract increases the charge transfer resistance (R <sub>ct</sub> ) and reduced the double-layer capacitance (C <sub>dl</sub> )	<sup>123</sup>
<i>Newbouldia laevis</i>	Leaves	WL		Aluminium/1.0 M HCl and 0.5 M H <sub>2</sub> SO <sub>4</sub>	Langmuir adsorption isotherm	Presence of active components such as flavonoids, tannins, terpenes, steroidal and cardiac glycosides	<sup>124</sup>
<i>Newbouldia laevis</i>	Leaves	WL		AA8011 aluminium alloy/0.5 M H <sub>2</sub> SO <sub>4</sub>	Langmuir adsorption isotherm	Spontaneous physical adsorption by the plant extract molecules	<sup>125</sup>
<i>Azadirachta indica</i>	Bark, stem, leaves	WL, SEM		Aluminium/1.85 M HCl	Langmuir adsorption isotherm	The optimum inhibition concentration observed was 50% v/v of the <i>Azadirachta indica</i> extract	<sup>126</sup>

<i>Zygophyllum coccineum L.</i>	Roots, Stem	WL, EFMT, SEM	EIS, PDP,	Copper/1 M HNO <sub>3</sub>	Langmuir adsorption isotherm	Double layer capacitances decrease with respect to blank solution confirming the adsorption of plant extract molecules on the copper surface.	<sup>127</sup>
<i>Euphorbia Heterophylla</i>	Leaves	WL, EFMT, SEM	EIS, PDP,	Copper/0.5 M HNO <sub>3</sub>	Langmuir adsorption isotherm/mixed-type inhibitor	The main active component is Saponin	<sup>128</sup>
<i>Ceratonia siliqua</i>	Aerial part	WL, EFMT, SEM	EIS, XRD,	Copper/1 M HNO <sub>3</sub>	Langmuir adsorption isotherm	The phenomenon was spontaneous and exothermic	<sup>129</sup>
<i>Thymus Vulgarise</i>	Whole plant	WL, EFMT, SEM	EIS, PDP,	Copper/1 M HNO <sub>3</sub>	Langmuir adsorption isotherm	Double layer capacitances decrease with respect to blank solution revealing adsorption of plant extract molecules on the copper surface.	<sup>130</sup>
<i>Aloe Barbadensis</i>	<i>Vera</i> Roots, leaves	WL		Copper/2M HCl	Langmuir adsorption isotherm	Folic acid, Aloe-emodin, aloetic acid, anthranol, aloin A, Pure mannan, acetylated mannan, acetylated glucomannan, glucogalactomannan are some major active phytoconstituent	<sup>131</sup>

<i>Citrullus colocynthis</i>	Leaves	WL, EIS	Copper/1 M H <sub>2</sub> SO <sub>4</sub>	Langmuir adsorption isotherm/mix ed-type inhibitor	Alkaloids, flavonoids and saponins content in Citrullus colocynthis extract was confirmed	<sup>131</sup>
<i>Morinda tinctoria</i>	Leaves	WL, EIS, EDXS, SEM, FTIR	Copper/0.5 M HCl	Langmuir adsorption isotherm	inhibition efficiency increases by further addition of halide additives	<sup>132</sup>

### 2.1.1.2. Weed extracts as corrosion inhibitors for metals

Weeds are plants that are considered unwanted or undesirable in a particular environment. They are often viewed as a nuisance and are commonly removed through manual or chemical means. However, recent studies have shown that weeds may have the potential as natural corrosion inhibitors. Weeds contain a variety of organic compounds that have been found to possess corrosion-inhibiting properties. These compounds include alkaloids, phenols, flavonoids, tannins, and saponins. Many of these compounds have been shown to have antioxidant properties, which can help to prevent corrosion by neutralizing free radicals and reactive oxygen species that contribute to the electrochemical reactions that cause corrosion. Several studies have investigated the use of weeds as corrosion inhibitors in different industries. Durodola et al.<sup>133</sup> found that the methanolic extract of *Spilanthes uliginosa* leaves had an IE% of 90% at a conc. of 500 ppm. Fouda et al.<sup>134</sup> demonstrated that an aqueous extract of *Thevetia peruviana* exhibited a maximum IE% of 90.3% at a conc. of 300 ppm. Ituen et al.<sup>135</sup> reported that *Pennisetum purpureum* extract achieved the highest IE% of 82.6% at a conc. of 5000 ppm. Akalezi et al.<sup>136</sup> showed that *Gongronemena latifolium* extract had an IE% of 91.24% at a conc. of 1000 ppm. Ramdani et al.<sup>40</sup> found that *Caulerpa prolifera* extract showed a maximum IE% of 94.33% at a conc. of 1.0 g/L. Nwosu and Muzakir<sup>137</sup> revealed that *Chromolaena odorata* extract achieved an optimum IE% of 92.39% at a conc. of 4.0 g/L. D. Li et al.<sup>138</sup> reported that *Chinese Yam Peel* extracts (CYPE) had an IE% of 96.33% using 900 ppm CYPE in artificial seawater at 298 K. Meng et al.<sup>139</sup> found that *Sugarcane purple rind* ethanolic extract (SPRE) revealed a maximum IE% of 96.2% for carbon steel with a conc. of 800 ppm at ambient temperature. These natural sources contain several polar groups like

-OH, -NH<sub>2</sub>, -SH, and -COOH or several heteroatoms including O, S, or N<sup>140-142</sup>. Additionally, the molecular mass, along with the number of polar groups and heteroatoms, plays a critical role in determining their excellent corrosion prevention characteristics<sup>143,144</sup>. There are several advantages to using weeds as corrosion inhibitors. First, weeds are abundant and easily accessible in many parts of the world. This makes them a cost-effective and sustainable alternative to traditional chemical inhibitors, which can be expensive and have negative environmental impacts. Second, weeds are natural and non-toxic. This means that they do not pose a risk to human health or the environment, unlike many chemical inhibitors that can be hazardous and require special handling and disposal. Third, weeds are versatile and can be used in a variety of industries and applications. They have been shown to be effective inhibitors for different types of metals and in different environments, making them a promising alternative to traditional inhibitors. A fourth advantage of using weeds as corrosion inhibitors is their versatility. Weeds have been shown to be effective inhibitors for different types of metals and in different environments. For example, in the oil and gas industry, weeds have been found to be effective inhibitors for mild steel in saline mediums. In the automotive industry, weeds have been effective inhibitors for aluminium in sodium chloride solutions. In the construction industry, weeds have been effective inhibitors for steel reinforcement in concrete structures. This versatility makes them a promising alternative to traditional inhibitors that may only be effective for specific applications. A fifth advantage of using weeds as corrosion inhibitors is their natural and non-toxic properties. Chemical inhibitors can be hazardous to human health and the environment, especially during handling and disposal. In contrast, weeds are non-toxic and do not pose a risk to human health or the environment. This makes them a safe and sustainable alternative to traditional inhibitors. Therefore, by utilizing the extracts of weeds to form a green corrosion inhibitor, these plants can be put to beneficial use and provide an eco-friendly solution to corrosion prevention<sup>40,145</sup>. By exploring the efficacy of weeds as a corrosion inhibitor, the authors of this study aim to contribute to the production of sustainable and cost-efficient corrosion inhibitors that are environmentally friendly and do not harm soil, marine life, and terrestrial life. The crucial aspect is that this usage will have minimal impact on both humans and the environment, and a commodity that was once considered waste can now be utilized as a potent and environmentally friendly inhibitor to mitigate metallic corrosion and combat the catastrophic global concern of corrosion.

Chung et al.<sup>146</sup> aimed to investigate the potential of *Magnolia kobus* DC. (*M. kobus*) extract as an inhibitor against mild steel corrosion in 1 M H<sub>2</sub>SO<sub>4</sub>. The researchers identified the prominent components of the extract to be myricetin and syringic acid, with a total phenolic content (TPC) of 95.26 mg/g and a total flavonoid content (TFC) of 25.38 mg/g. The researchers found that the *M. kobus* extract exhibited a high inhibition efficiency of 95.01% at 303 ± 1 K when applied at a concentration of 500 ppm. The reduction of dissolved iron content in the inhibited solution observed in Atomic Adsorption Spectroscopy (AAS) confirmed the corrosion-mitigating effect of the inhibitor on mild steel. The researchers also used SEM, AFM and EDX to analyze the protected and unprotected mild steel samples. The analysis revealed that *M. kobus* extract adsorbed onto the electrode surface, indicating its potential as an effective inhibitor. UV-vis and FT-IR studies complemented the above results, indicating that *M. kobus* extract functioned as a mixed-type inhibitor, and myricetin, along with other plant components present in the extract, contributed to the inhibition process. Overall, the findings of this study suggest that *M. kobus* extract has promising potential as an eco-benign inhibitor against mild steel corrosion. The study also provides valuable insights into the mechanism of action of the extract as an inhibitor, which can inform further research in this area.

Mohammed et al.<sup>91</sup> investigated the use of *Kola nut* extract (KE) as a corrosion inhibitor for low-carbon steel in 1 M HCl solution. The inhibiting ability of KE was evaluated using weight loss and electrochemical techniques, while the surface of the corroded carbon steel was examined using FT-IR, SEM and AFM. Additionally, UV-vis studies were conducted to ascertain the engagement of KE on the carbon steel surface and the elemental analysis of the corrosion products and/or adsorbed inhibitor coating on the carbon steel surface. The study's findings demonstrated that KE offered excellent corrosion reduction abilities. Following a 24-hour immersion using the weight loss method, the C<sub>R</sub> was decreased from 0.387 to 0.054 mm/year by 700 ppm of KE at room temperature, resulting in an IE% of 86%. However, when the temperature increased, the IE reduced. The FTIR results showed that the O and N heteroatoms of KE's phytoconstituents interacted with the carbon steel surface. The results of the spectroscopy experiments, which included FTIR, UV-vis, SEM, AFM, and EDX, demonstrated that the corrosion inhibition was caused by KE adsorption upon the steel surface. The results of this study indicate that kola nut extract could be employed as a powerful corrosion inhibitor for low-carbon steel in conditions that are acidic. Additionally, the study provides insight into the mechanism of KE adsorption on the

steel surface and the interaction between KE and the carbon steel surface. Further research could focus on exploring the usage of KE as a corrosion inhibitor in industrial settings and investigating the long-term impacts of KE on the corrosion inhibition of low-carbon steel.

Dehghani et al.<sup>147</sup> investigated the potential of *Eucalyptus* leaf extract (ELE) as a unique corrosion inhibitor for mild steel (MS) in HCl medium through a combination of experimental and computational studies. EIS and PDP tests were used to determine the degree of inhibition, while the molecular simulation was employed to study the mechanism of inhibition. The findings showed that the IE% of ELE rise with increasing quantity, reaching a maximum of 88% at 800 ppm ELE following 5 hours of immersion. Polarization test results indicated that ELE had a mixed inhibition effect with slight cathodic prevalence, and the corrosion current density ( $i_{\text{corr}}$ ) decreased from 0.93  $\mu\text{A}/\text{cm}^2$  for the uninhibited specimen to 0.25  $\mu\text{A}/\text{cm}^2$  for the specimen treated with 800 ppm ELE. The Langmuir isotherm model was found to fit the adsorption behavior of ELE molecules on the MS surface. Molecular simulation studies showed that the active compounds in ELE, including 1,8-cineole,  $\alpha$ -pinene, and  $\beta$ -pinene, interacted with the MS surface through hydrogen bonding,  $\pi$ - $\pi$  interaction, and van der Waals forces, enabling the emergence of a protective layer that prevented the corrosive species from reaching the metal surface.

Karunanithi et al.<sup>148</sup> examined the corrosion inhibition attributes of *Tephrosia Purpurea* leaf extract on mild steel in 1N H<sub>2</sub>SO<sub>4</sub> solution using electrochemical and surface morphological methods. The leaf extract was characterized using UV-Visible spectroscopy, FT-IR, NMR, and GCMS. The results showed that *Tephrosia Purpurea* leaf extract has the potential to act as a good corrosion inhibitor. The IE% increased with a rise in the mass of inhibitor molecules, and the optimum inhibitor concentration was found to be 300 ppm. The inhibition efficiency at this concentration was found to be 93%, and above this concentration, there was no significant elevation in IE%. The polarization analysis revealed that the inhibition is of a mixed type, and the EIS results confirmed that the corrosion process is controlled by a single charge transfer mechanism. The adsorption of inhibitor molecules on the mild steel electrode surface obeyed Langmuir's adsorption isotherm. The inhibition mechanism was mainly by the adsorption of inhibitor molecules on the mild steel electrode surface, which was affirmed by FT-IR, SEM, and AFM studies. The study showed that *Tephrosia Purpurea* leaf extract can be a good eco-friendly and cost-effective alternative to synthetic corrosion inhibitors for mild steel in 1N H<sub>2</sub>SO<sub>4</sub> solution. The research reveals the

potential of natural plant extracts as corrosion inhibitors and opens up new avenues for the development of eco-friendly corrosion inhibitors.

Haldhar et al.<sup>149</sup> investigated the potential of *Ficus religiosa* fruit extract as an eco-benign corrosion inhibitor for mild steel in 0.5M H<sub>2</sub>SO<sub>4</sub> medium. The study employed various techniques including EIS, PDP, SEM, AFM, UV-Vis spectroscopy, FT-IR, and quantum chemical calculations to examine the corrosion inhibition behavior and adsorption of the extract upon the mild steel surface. The results obtained from the electrochemical and gravimetric measurements revealed that *Ficus religiosa* fruit extract exhibited maximum IE% of 92.26% at a quantity of 500 mg/L. The extract constituents, namely serotonin, myricetin, and campesterol, were identified as major phytochemicals responsible for the corrosion inhibition of mild steel in acidic media. The existence of aromatic rings and heteroatoms in these components was suggested to be the reason for the effective corrosion inhibition observed. The adsorption of the extract on a mild steel surface followed the Langmuir adsorption isotherm, indicating monolayer adsorption. The EIS and PDP results indicated that the corrosion inhibition was due to the mixed-mode action of the extract. SEM and AFM images of mild steel surfaces treated with the extract revealed that the surface was covered by a protective film, indicating the adsorption of the extract upon the substrate and its role in corrosion inhibition. Theoretical studies using quantum chemical calculations showed that the extract constituents with the highest negative charges and lowest energy levels were responsible for the adsorption on the mild steel surface, which supported the experimental results.

Khadom et al.<sup>150</sup> investigated the corrosion inhibition attributes of *Xanthium strumarium* leaves (XSL) extract on low-carbon steel in 1 M HCl. The study employed the weight loss method to determine the effect of temperature and inhibitor concentration on the corrosion rate of low-carbon steel. The results showed that XSL extract acted as an efficient inhibitor for low-carbon steel in HCl, and it decreased the corrosion rate of low-carbon steel. The inhibition efficiency increased with an increase in inhibitor concentration and temperature, and the highest inhibition efficiency was found to be 94.82% at a higher level of inhibitor concentration and temperature. The adsorption behavior of XSL extract on low-carbon steel surface was found to obey the Langmuir adsorption isotherm model, indicating the formation of a monolayer coverage of the inhibitor on the surface of low-carbon steel. The values of the free energy of adsorption were more than -20 kJ/mol, which suggested a mixed mode of physical and chemical adsorption. This result indicates

that the inhibitor's adsorption on the low-carbon steel surface is a combination of both physical and chemical mechanisms. The study suggests that XSL extract has promising properties as a green inhibitor for low-carbon steel in acidic media. The inhibition efficiency of XSL extract is relatively high, and the inhibitor is eco-friendly and inexpensive. Therefore, it could be a potential alternative to synthetic inhibitors for the protection of low-carbon steel in acid environments. The study also highlights the importance of green inhibitors and their potential as corrosion inhibitors for various metals and alloys.

Perumal et al.<sup>67</sup> investigated the potential of *Bauhinia tomentosa* leaves extract (BTLE) as a green corrosion inhibitor for mild steel in a 1M HCl medium. The study utilized the weight-loss method and electrochemical techniques to evaluate the inhibition efficiency of BTLE. The effect of temperature on corrosion inhibition was also studied in the temperature range of 308-333 K. The results showed that the inhibition efficiency of BTLE increased with increasing concentration. At 700 ppm of BTLE, the maximum inhibition efficiency was found to be 93.47% at 308 K in the presence of HCl. Polarization measurements revealed that BTLE acted as a mixed-type inhibitor. Nyquist plots showed that on increasing the BTLE concentration, the charge-transfer resistance increased, and double-layer capacitance decreased. Furthermore, the adsorption of BTLE on mild steel was found to obey the Langmuir adsorption isotherm. The FT-IR, UV, SEM, and AFM techniques were used to explore the mechanism of corrosion inhibition of BTLE on mild steel. The findings indicated that BTLE could be a potential green corrosion inhibitor for mild steel in 1M HCl medium due to its ability to adsorb on the mild steel surface and form a protective layer.

Olusegun et al.<sup>151</sup> investigated the potential of using *Biden pilosa* (BP) as a natural corrosion inhibitor for mild steel in hydrochloric acid (HCl) environment. The study involved exposing prepared mild steel samples to different temperatures ranging from 303 to 333K. The researchers evaluated the inhibition efficiency and compound identification of the BP extract using gas chromatography (GC), gravimetric analysis, Tafel extrapolation techniques, and scanning electron microscopy (SEM) to establish the corrosion inhibition mechanisms. The results of the GC analysis showed the presence of four active compounds in the BP extract, namely Oleic acid, Trans-13-Octadecenoic acid, 3- hydroxypropyl ester, and cis-13-Octadecenal. The weight loss and Tafel extrapolation techniques provided consistent results of the corrosion rates. The BP extract demonstrated a high inhibition efficiency of 97% at 303 K, with a gradual decrease in inhibition



efficiency at higher temperatures, indicating physisorption as the primary adsorption mechanism. SEM analysis confirmed the protection of the mild steel substrate in the BP extract-containing environment. Overall, the study provides evidence of the potential of using natural extracts such as *Biden pilosa* as a green corrosion inhibitor for mild steel in an HCl environment. The findings also suggest the importance of considering temperature effects and adsorption mechanisms in the evaluation of the efficiency of natural extracts as corrosion inhibitors. The use of natural extracts as corrosion inhibitors offers a promising approach to reducing the use of toxic and expensive synthetic inhibitors in industrial applications.

Thomas et al.<sup>152</sup> investigated the effectiveness of *Ixora coccinea* extract (ICE) as a green corrosion inhibitor for mild steel in 1 M HCl and 0.5 M H<sub>2</sub>SO<sub>4</sub> using both physicochemical and electrochemical techniques. The research found that the corrosion inhibition capacity of ICE increased with the increase in its concentration in both acidic media. The weight loss measurement showed 89.38% and 77.96% inhibition capacity of ICE in 1 M HCl and 0.5 M H<sub>2</sub>SO<sub>4</sub> medium respectively. The electrochemical impedance parameters showed that as the concentration of ICE increased, efficiency increased, and double-layer capacitance decreased. The potentiodynamic polarization techniques also exhibited the mixed-type inhibition character of ICE, which was in good agreement with impedance studies. Additionally, the electrochemical noise spectrum strongly supported the anti-corrosive property of ICE, and the magnitude of the noise signal decreased with the increase in ICE concentration. Ixorene, one of the major constituents of *Ixora coccinea* leaves, was studied for its corrosion inhibition nature by quantum mechanical calculations and was found to match with all other results. Adsorption studies of ICE were in accordance with the Langmuir isotherm. Surface morphological studies confirmed the formation of a protective barrier on mild steel surfaces in both media, i.e., 1 M HCl and 0.5 M H<sub>2</sub>SO<sub>4</sub>. Overall, the research demonstrated that *Ixora coccinea* extract has an excellent corrosion inhibition capacity for mild steel in acidic media. The research findings provide insights into the potential of eco-friendly corrosion inhibitors in protecting metal surfaces in various corrosive environments.

Baran et al.<sup>153</sup> investigated the inhibitory effect of *Gentiana olivieri* weed extract and its fractions on the corrosion of mild steel in a 0.5 M HCl solution. The study aimed to explore the potential of weed extracts and their metabolites as environmentally friendly, low-cost, and renewable sources for corrosion inhibitors. The research utilized electrochemical techniques, including

potentiodynamic polarization and electrochemical impedance spectroscopy (EIS), to investigate the inhibitory properties of the extract and its fractions. The results of the study indicated that the methanol extract of *Gentiana olivieri* and its fractions exhibited significant inhibitory effects on the corrosion of mild steel in 0.5 M HCl solution. The maximum inhibition efficiency of 93.7% was observed at an inhibitor concentration of 800 mg/L.

Moukhles et al.<sup>154</sup> investigate the chemical composition and antibacterial activity of essential oil (EO) and hydrolat extract (HE) of aerial parts of *Thymbra capitata* (L.) Cav from Morocco. Additionally, the study evaluated the inhibitory effect of the EO and HE on the corrosion of aluminum alloy (AA6063) in 3% sodium chloride solution using potentiodynamic polarization and electrochemical impedance spectroscopy (EIS) measurements. The results of the study indicated that carvacrol was the dominant compound in the EO of *T. capitata* (L.) Cav, followed by p-cymene and  $\alpha$ -humulene. The HE of *T. capitata* (L.) Cav was found to be almost entirely composed of carvacrol with traces of other compounds. Both EO and HE showed significant antibacterial activities against Gram-negative (*E. coli*, *Pr. Mirabilis*) and Gram-positive (*B.subtilis*, *S. aureus*) bacterial strains. The inhibition efficiency of the EO was found to be 74.52% at a concentration of 2 g/L, while the HE showed an inhibition efficiency of 85.55% at the same concentration. Moreover, the EO and HE were found to be effective inhibitors for the corrosion of aluminium alloy in a 3% sodium chloride solution. The inhibition efficiency increased with an increase in the concentration of the EO and HE. The EIS results showed that the EO and HE acted as mixed-type inhibitors. The study also revealed that the inhibitory effect of the EO and HE on the corrosion of aluminium alloy was due to the adsorption of the compounds present in the EO and HE onto the aluminium alloy surface.

Shamsuzzaman et al.<sup>155</sup> evaluate the antioxidant and anticorrosive activities of *Ceriops tagal* weed extract. The authors analyzed the total phenolic content (TPC) and total flavonoid content (TFC) of the weed extract and found them to be 101.52 and 35.71 mg/g, respectively. They then tested the extract's antioxidant properties against three different free radicals and found that it exhibited 83.88%, 85%, and 87% antioxidant activity against 1,1-diphenyl-2-picrylhydrazyl (DPPH), nitric oxide, and hydrogen peroxide free radicals, respectively. The authors also investigated the anticorrosive properties of the extract by testing its inhibition efficiency against mild steel in 1 M HCl. They found that 600 ppm of the extract showed 95% inhibition, which declined over other

concentrations and temperatures. They also used atomic absorption spectroscopy (AAS) to analyze the formation of an inhibitor metal complex, which showed that the extract produced 82% inhibition at 600 ppm. Furthermore, the authors used UV-visible spectroscopy to analyze the elemental composition of the inhibited mild steel and found the presence of 84.21%, 9.01%, and 6.37% of Fe, O, and C, respectively. In comparison, uninhibited mild steel had 71.54%, 22.1%, and 4.34% of Fe, O, and C, respectively. These findings suggested the presence of a protective film on the metal surface. Scanning electron microscopy (SEM) also revealed some noteworthy changes in both uninhibited and inhibited mild steel, demonstrating that *C. tagal* plant extract is a better alternative to synthetic inhibitors. Finally, atomic force microscopy (AFM) surface topography analysis showed that 600 ppm of *C. tagal* extract significantly diminished corrosion on the surface of mild steel.

Ragul et al.<sup>156</sup> investigated the use of methanol extract from *Mitracarpus hirtus* leaves (MMH) as a corrosion inhibitor for mild steel (MS) in 1 M HCl using weight loss, colorimetric, and electrochemical methods. The study varied the concentrations of the inhibitor, acid, added halide ions, and temperature to determine the maximum efficiency of the inhibitor. The research found that the maximum efficiency of 89.06% was obtained at an inhibitor concentration of 0.6 g/L. The research results suggested that the percentage of inhibition efficiency increased with an increase in MMH concentration and decreased with temperature. This observation was supported by the thermodynamic parameters which indicated the spontaneous adsorption of MMH on the MS surface. The Langmuir adsorption process was used to confirm this observation. The chemical constituents for MMH adsorption on MS surface were confirmed by Fourier transform infrared spectroscopy, field emission scanning electron microscopy, and energy dispersive X-ray spectrometer. These analyses helped to confirm the chemical composition and physical characteristics of the MMH adsorption layer. In summary, the research findings suggest that MMH extract has significant potential as a corrosion inhibitor for mild steel in 1 M HCl. The research findings demonstrate that the MMH extract can effectively reduce the rate of corrosion, and its inhibitive properties increase with increasing concentration of the extract. The study also highlights the importance of investigating natural plant extracts as potential sources of corrosion inhibitors for use in various industries.

Sin et al.<sup>157</sup> investigated the effectiveness of *Aquilaria subintegra* leaves extracts as sustainable mild steel corrosion inhibitors in hydrochloric acid (HCl). The study tested non-inoculated and chemically inoculated leaf extracts from *Aquilaria subintegra* and found that they showed high corrosion inhibition, with up to 93% inhibition at 1500 ppm concentration. The effectiveness of the extracts was analyzed using a weight loss study, electrochemical impedance spectroscopy measurement, and potentiodynamic polarization measurement. The weight loss study showed that all the extracts had similar inhibition efficiencies, while the electrochemical measurements showed that the leaf extract from the chemically inoculated tree was the best inhibitor. The study also analyzed the adsorption behavior of the extracts on the surface of mild steel using the Langmuir adsorption isotherm model and potential zero charge analysis. The results showed that the extracts were adsorbed on the surface of mild steel by a physisorption process. Furthermore, the leaves extracts were analyzed using Quadrupole-Time of Flight Liquid Chromatogram/ Mass spectrometer (Q-TOF LC/MS), and five compounds were identified for the first time in *Aquilaria subintegra*. Adenosine was found to be an excellent inhibitor, with an inhibition efficiency of up to 62% at a very low concentration of  $1 \times 10^{-4}$  M.

Trindade et al.<sup>158</sup> investigate the use of *Gorse* extract as a green corrosion inhibitor for mild steel in an HCl aqueous solution. The research findings suggest that the gorse extract is a promising corrosion inhibitor for mild steel. The study utilizes various techniques such as weight-loss measurements, potentiodynamic polarization curves, electrochemical impedance spectroscopy, and scanning electron microscopy to investigate the effectiveness of the extract. The weight-loss measurements show that the inhibition efficiency of the extract increases with an increase in immersion time and concentration. At  $800 \text{ mg L}^{-1}$ , the extract IE ranged from 72.5% to 93.8% for 2 and 48 h, respectively. This suggests that the gorse extract could be a viable option for long-term corrosion protection. The measurements of electrochemical impedance spectroscopy show an increase in  $R_{ct}$  and a decrease in  $C_{dl}$ , reaching 96.6% of IE at  $1600 \text{ mg L}^{-1}$ . This indicates that the *Gorse* extract inhibits the corrosion process by forming a protective layer on the surface of mild steel. The potentiodynamic polarization curves show that the *Gorse* extract serves as an adsorption inhibitor, reducing both the anodic and cathodic current density. This suggests that the extract has a dual effect on the corrosion process, inhibiting both the anodic and cathodic reactions. The scanning electron microscopy results reveal that the surface morphology of the mild steel changes after exposure to the gorse extract. The extract forms a protective layer on the surface of the mild

steel, preventing the corrosive species from attacking the metal surface. The high-molecular-weight fraction isolated from the gorse extract also showed high inhibition efficiencies, suggesting that the extract contains multiple compounds that can inhibit the corrosion process.

Soltani et al.<sup>159</sup> investigated the inhibitive properties of *Gundelia tournefortii* (*G. tournefortii*) leaf extract on mild steel corrosion in HCl and H<sub>2</sub>SO<sub>4</sub> solutions. The inhibitive efficiency was determined using weight loss measurement, potentiodynamic polarization, and electrochemical impedance spectroscopy (EIS) techniques. The study found that the inhibitive efficiency of *G. tournefortii* leaf extract increased with the concentration of the inhibitor due to the adsorption of inhibitor molecules on the metal surface. The Langmuir adsorption isotherm was used to analyze the data, and it was found that the experimental data fit well with this model. The inhibition efficiency of the extract was 93% and 90% at 150 ppm in 2.0 M HCl and 1.0 M H<sub>2</sub>SO<sub>4</sub>, respectively. The polarization curves showed that *G. tournefortii* extracts acted as a mixed-type inhibitor in both acidic media, reducing both anodic and cathodic current densities. The EIS data indicated that the charge transfer controlled the corrosion process. The study also investigated the effect of temperature on the inhibition efficiency of the extract. The study concluded that *G. tournefortii* leaf extract could be used as an effective green inhibitor for mild steel corrosion in both HCl and H<sub>2</sub>SO<sub>4</sub> solutions. The inhibitive properties of the extract were attributed to the adsorption of inhibitor molecules on the metal surface, which formed a protective film, reducing the corrosion rate. The study suggested that *G. tournefortii* leaf extract could be a cost-effective and eco-friendly alternative to traditional chemical inhibitors for mild steel corrosion in acidic media. However, further studies are required to explore the long-term stability and durability of the protective film formed by *G. tournefortii* leaf extract.

Ibrahim et al.<sup>160</sup> investigated the effectiveness of *Ficus carica* leaves extract as a green corrosion inhibitor for mild steel in a practical field condition containing a 3.5% sodium chloride solution saturated with carbon dioxide. The inhibition efficiency of the extract was determined using various electrochemical techniques, and it was found to be optimum at 90% when using 50 mg/L of inhibitor within a temperature range of 25–40 °C. The polarization studies indicated that the *Ficus carica* leave extract acted as a mixed inhibitor. Moreover, the adsorption isotherm of the extract on the steel surface was found to follow the Langmuir adsorption isotherm. To determine the individual contribution of the different constituents of the extract theoretically, the researchers

modeled the adsorption of the four major organic constituents of the *Ficus carica* leaves extract on mild steel using density functional theory and quench molecular dynamic simulations. The study found that Caffeoylmalic acid made the most significant contribution to the overall inhibition action of the *Ficus carica* leaves extract. The results of this study are significant because they provide insights into the effectiveness of natural extracts as green corrosion inhibitors under practical field conditions. The use of natural extracts as green corrosion inhibitors can be a sustainable and environmentally friendly approach to reducing the impact of corrosion on various materials.

Salmasifar et al.<sup>161</sup> investigated the use of *Artichoke* extract as a green inhibitor for protecting mild steel substrates in acidic environments. The electrochemical behavior of the Artichoke extract was evaluated at different concentrations in the acidic solution using various professional measurements. The results demonstrated that *Artichoke* extract showed superior inhibition action towards mild steel in the acidic process. The charge transfer resistance of Artichoke extract with a higher concentration of 1000 ppm increased from  $\sim 9.9 \text{ ohm.cm}^2$  to  $\sim 795.2 \text{ ohm.cm}^2$  after 24 h of immersion. The maximum corrosion inhibition efficiency of about 98.7% and surface coverage of 76.3% were obtained in the presence of 1000 ppm Artichoke extract after 24 h immersion. The polarization results also revealed that the addition of Artichoke extract significantly decreased the corrosion current density of mild steel from  $6.3 \mu\text{A/cm}^2$  for the sample without inhibitor to  $0.1 \mu\text{A/cm}^2$  for the sample containing 1000 ppm inhibitor. The researchers also suggested that the Artichoke extract could effectively protect mild steel through physicochemical interaction and film formation to mitigate the serious demolition of  $\text{Cl}^-$ . In addition, the adsorption of anticorrosive chemicals on the substrate was computationally ascertained by molecular/DFT (density functional theory) modeling. The study's findings suggested that Artichoke extract could be used as a green corrosion inhibitor to address the corrosion challenges of metallic equipment in acidic processes. The use of green inhibitors such as *Artichoke* extract offers a more environmentally friendly approach to corrosion inhibition, as it eliminates the use of harmful and toxic chemicals.

Karki et al.<sup>162</sup> focused on the use of berberine isolated from the methanol extract of *Mahonia nepalensis* as a corrosion inhibitor for mild steel in an acidic medium. The study aimed to determine the efficiency and thermodynamic behavior of berberine as a corrosion inhibitor and to investigate its mechanism of action. The results of the study showed that berberine had a high

inhibition efficiency for mild steel corrosion in 1.0 M H<sub>2</sub>SO<sub>4</sub> acid medium, with an inhibition efficiency of above 91% in 0.25 h and reaching 94% in 6 h at 1000 ppm concentration. The inhibition efficiency increased with concentration and temperature, with an inhibition efficiency of 97.2% at 328 K. The results indicated that berberine behaved as a mixed type of inhibitor and effectively formed an adsorbed layer on the mild steel surface, thus suppressing corrosion. The adsorption of berberine followed a Langmuir adsorption isotherm. The thermodynamic parameters of adsorption, such as activation energy, free energy, enthalpy, and entropy, supported both physical and chemical interactions of berberine with the mild steel surface. The adsorption process was found to be endothermic and spontaneous in nature. Overall, the study concluded that berberine isolated from *Mahonia nepalensis* was a highly efficient and thermally stable corrosion inhibitor for mild steel in an acidic medium, and could be a promising candidate for industrial application. The use of natural compounds such as berberine as corrosion inhibitors offer environmental and economic benefits, making it an eco-friendly alternative to traditional corrosion inhibitors.

Khiya et al.<sup>163</sup> investigated the chemical composition, antioxidant activity, and corrosion inhibition potential of *Salvia officinalis* L. collected from the Khenifra region of Morocco. The researchers conducted a phytochemical screening and found the presence of various bioactive compounds such as polyphenols, flavonoids, saponins, and terpenoids in the methanolic extract. The methanolic extract was found to be rich in total phenols and flavonoids. The essential oil of *Salvia officinalis* L. was analyzed using GC-MS, and 105 components were identified, with Trans-Thujone, 1,8-cineol, and Camphor being the major constituents. The researchers evaluated the antioxidant activity of the extracts and found that the methanolic extract exhibited a higher inhibition efficiency than the essential oil. The methanolic extract showed an inhibition efficiency of 91.62% and 49.70% using potentiodynamic polarization and impedance spectroscopy, respectively, at a concentration of 4 g/l, whereas the essential oil exhibited an inhibition efficiency of 83.06% and 70.58% using the same methods and concentration. Moreover, the study investigated the potential of *Salvia officinalis* L. extracts as a corrosion inhibitor for iron. The results showed that both the methanolic extract and essential oil had good inhibition efficiency against iron corrosion. The methanolic extract was found to be more effective in inhibiting iron corrosion than the essential oil.

Thirupathi et al.<sup>164</sup> evaluate the corrosion inhibition behavior of an ethanolic extract of *Portulaca quadrifida* (PQ) leaves on carbon steel in well-water. The authors used weight loss studies, potentiodynamic polarization, and electrochemical impedance studies to analyze the inhibitory effect of PQ extract on carbon steel. The protective film formed on the carbon steel surface was analyzed by SEM, EDX, and AFM studies. The study also calculated the kinetic and thermodynamic parameters for different temperatures. The findings of the study showed that the ethanolic extract of PQ leaves acted as a mixed-type inhibitor and had a maximum inhibition efficiency of 92% for 500ppm of PQ and 30ppm of Zn<sup>2+</sup> ions at 303K. The study also found a synergistic effect between the PQ extract and Zn<sup>2+</sup> ions. The activation energy ( $E_a$ ) values indicated that the adsorption of PQ leaves extract on the carbon steel surface, while the enthalpy of adsorption ( $\Delta H$ ) values suggested that the reaction was endothermic. The free energy of adsorption ( $\Delta G^{\circ}_{ads}$ ) values were negative and less than  $-20\text{KJmol}^{-1}$ , indicating that the adsorption of the inhibitor on the carbon steel surface was spontaneous. The authors also found that the adsorption process of the inhibitor belonged to physisorption, and the adsorption layer had an electrostatic character. The thermodynamic parameters indicated a strong interaction between the inhibitor molecules and the carbon steel surface. The study used four adsorption isotherms, including Langmuir, El-Awady, Flory-Huggins, and Temkin models, to investigate the mode of inhibition of PQ leaf extract. The Langmuir model was found to best fit the adsorption isotherm.

Anh et al.<sup>165</sup> investigated the use of *Ficus racemosa* leaf extract (FRLE) for inhibiting the corrosion of carbon steel in a hydrochloric acid solution. The research aimed to characterize the inhibition efficiency and surface properties of carbon steel coupons with different FRLE concentrations (500, 1000, 1500, and 2000 ppm) in an aerated 0.1 M hydrochloric acid solution. The results indicate that the inhibition efficiency increases with an increase in FRLE concentration up to 1500 ppm, reaching  $93.11 \pm 1.99\%$ . However, at 2000 ppm, the inhibition efficiency decreased to  $88.86 \pm 2.15\%$ , indicating that a high concentration of FRLE could impede the formation of a solid protective film. The study suggests that the corrosion of steel is retarded via the formation of a protective film reinforced by FRLE concentration and exposure time due to the continuous adsorption of FRLE inhibitor components at suitable concentrations. The study employed various techniques to analyze the surface properties of the carbon steel coupons, including electrochemical measurements, surface analysis, and quantum chemical calculations. The quantum chemical calculations demonstrate a high binding energy between FRLE molecules and carbon steel, good



thermal stability of the adsorbent layer, and an electron abundance of the FRLE species. This could result in a more compact solid protective layer that could hinder electrochemical corrosion when carbon steel is exposed to an aerated 0.1 M hydrochloric acid solution.

Karthik et al.<sup>145</sup> investigated the anticorrosion activity of *Tiliacora acuminata* leaf extract (TALE) as a corrosion inhibitor in 1M hydrochloric acid (HCl) using various techniques such as mass loss, potentiodynamic polarization, electrochemical impedance spectroscopy (EIS), scanning electron microscopy (SEM), UV-Visible spectroscopy, and X-ray diffraction (XRD) studies. The results showed that TALE is an excellent corrosion inhibitor, and its inhibition efficiency increases with an increase in temperature from 308 to 333 K. At the highest concentration of 320 ppm and the temperature of 333 K, the inhibition efficiency reached a maximum value of 93.02%. The polarization measurements indicated that TALE acts as a mixed-type inhibitor, meaning it affects both the anodic and cathodic reactions. The Nyquist plot showed that on increasing TALE concentration, the charge transfer increased, and the double-layer capacitance decreased. This indicates that TALE is adsorbed on the mild steel surface, which reduces the corrosion rate. The Langmuir adsorption isotherm confirmed that the adsorption of TALE on mild steel obeys the Langmuir model, suggesting the formation of a monolayer of inhibitor molecules on the mild steel surface. The SEM studies confirmed the adsorption of TALE on the mild steel surface, as observed by the changes in surface morphology. The UV-Visible spectroscopy and XRD studies showed that TALE contains various phytochemicals, such as flavonoids and phenolics, which have been reported to possess excellent anticorrosion properties.

El ouariachi et al.<sup>166</sup> investigated the inhibition of corrosion of mild steel in 1 M hydrochloric acid (HCl) by the essential oil and solvent extracts of *Ptychotis verticillata*. The efficiency of inhibition was evaluated using weight loss measurements, electrochemical impedance spectroscopy, and potentiodynamic polarization curves. The results showed that the efficiency of inhibition increased with an increase in the inhibitor concentration due to the adsorption of inhibitor molecules on the metal surface. The Langmuir isotherm was used to model the adsorption of the inhibitor, and the adsorption was found to be in agreement with the Langmuir isotherm. The efficiency of inhibition was found to be 74.6% for 1.08 g/L essential oil, which was rich in phenolic compounds as major compounds (48%). The efficiency of inhibition, as determined by weight loss measurements, was 75% and 86%, respectively, for diethyl ether and ethyl acetate extracts at 0.5 g/L.

Ebdelly et al.<sup>167</sup> investigated the inhibitory effect of *Eruca sativa* aqueous extract on the corrosion of carbon steel in neutral calcareous synthetic water. The study employed various electrochemical and analytical techniques to evaluate corrosion inhibition efficiency. The results of the study showed that the *E. sativa* extract could effectively inhibit the corrosion of carbon steel, and the inhibition efficiency increased with an increase in the concentration of the extract. The electrochemical results revealed that the presence of *E. sativa* extract led to a decrease in the corrosion current and an increase in polarization resistance. Electrochemical impedance spectroscopy (EIS) results revealed two-time constants, where the first one at high-frequency range (HF) was associated with the faradic process, and the second one at low frequency (LF) was related to the redox reaction occurring in the passive film. The study found that the inhibition efficiency of *E. sativa* extract could reach up to 95% with a dose of only 30 ppm, attributed to the large fraction of phenolic compounds present in the extract. The morphology and phases of the films formed on the metallic surface under corrosion conditions were examined, and differences were detected, suggesting that the extract played a role in modifying the surface of the metal. Overall, the research findings suggest that *E. sativa* extract has significant potential as a green inhibitor for the corrosion of carbon steel in neutral calcareous synthetic water.

Okewale et al.<sup>168</sup> investigated the effectiveness of *Neem* leaf extract as a corrosion inhibitor for mild steel in an acidic solution. The weight loss method was used to determine the degree of corrosion inhibition, while FTIR, GCMS, and phytochemical tests were used to characterize the extract's composition. The results of the study showed that neem leaf extract is an effective inhibitor of mild steel corrosion in 0.1 M HCl, with an inhibition efficiency of up to 93.24%. The phytochemical analysis of the extract revealed the presence of carbonyl groups, double bonds, and aromatic rings, which are known to be viable functional groups that can serve as corrosion inhibitors. The inhibition efficiency increased with increasing inhibitor concentration, which suggests that the adsorption of inhibitor molecules on the metal surface is responsible for the observed inhibition. The adsorption isotherms were modeled using Langmuir, Freundlich, and Temkin equations, and the negative values of Gibb's free energy for the three isotherms suggested that the adsorption process is spontaneous. The study proposed a mixed type of adsorption mechanism (physisorption and chemisorption) for the *Neem* leaf extract adsorption on the surface of mild steel. The corrosion rate of mild steel decreased with increasing inhibitor concentration

and time of exposure, indicating that the mild steel surface was protected from corrosion due to the adherence of the phytochemical components on the mild steel surface.

Sathiyapriya et al.<sup>169</sup> evaluated the anti-corrosion behavior of *Araucaria heterophylla* Gum (AHG) on mild steel (MS) in 1M H<sub>2</sub>SO<sub>4</sub> medium. The researchers used various techniques like GC-MS, weight loss method, potentiodynamic polarization, electrochemical impedance spectroscopy (EIS), Density Functional Theory (DFT) studies, Scanning Electron Microscopy (SEM), and Atomic Force Microscopy (AFM) to determine the corrosion inhibition efficiency, adsorption of inhibitor molecules on mild steel, and the mechanism of corrosion inhibition. The GC-MS analysis of AHG revealed the presence of various phytoconstituents, indicating that it can act as an efficient inhibitor. The weight loss method indicated an optimum inhibition efficiency of 78.57% at 0.05% v/v on mild steel in 1M H<sub>2</sub>SO<sub>4</sub> medium at room temperature. The potentiodynamic polarization analysis revealed that the AHG acts as a mixed-type inhibitor. The change in EIS parameters in the presence of the inhibitor showed the formation of a protective layer on the mild steel surface. The adsorption of inhibitor molecules on mild steel was studied using DFT, SEM, and AFM. The results showed that the inhibitor molecules were adsorbed on the mild steel surface, forming a protective layer. The adsorption behavior was found to follow Langmuir adsorption isotherm, and the thermodynamic and activation parameters supported the physical adsorption mechanism.

Omotoyinbo et al.<sup>170</sup> investigated the inhibitive effect of pulverized *Jatropha curcas* leaves on the corrosion of medium carbon steel in 0.5 M NaCl and 0.5M H<sub>2</sub>SO<sub>4</sub> solutions using the gravimetric technique. The concentration of the extract used ranged from 0.5 – 2.5 g in 300 ml of the solutions. The results showed that the inhibition efficiency was 92.1% for the NaCl solution and 55.5% for the H<sub>2</sub>SO<sub>4</sub> solution. This indicates that *Jatropha curcas* leaf extract could be used as an inhibitor against the corrosion of medium-carbon steel in both alkaline and acidic solutions. The gravimetric technique is a commonly used method to study corrosion inhibition, where the weight loss of the metal specimen is measured over a specific period of time. The higher the inhibition efficiency, the lower the corrosion rate, which implies better corrosion resistance. In this study, the inhibition efficiency was calculated using the weight loss data, which was obtained by immersing the mild steel specimens in the solutions containing the inhibitor for a specific period of time. The results obtained from this study are promising for the use of *Jatropha curcas* leaves extract as an eco-friendly inhibitor for medium carbon steel in acidic and alkaline environments. *Jatropha curcas* is

a tropical weed that is commonly found in many parts of the world, and its leaves have been reported to possess various phytochemicals that exhibit inhibitory properties against metal corrosion. However, it should be noted that the efficiency of the inhibitor is concentration-dependent. In this study, the inhibition efficiency increased with increasing concentration of the *Jatropha curcas* leaves extract. Therefore, it is important to optimize the concentration of the extract to achieve maximum inhibition efficiency.

Olanrewaju et al.<sup>171</sup> investigated the corrosion-inhibitive properties of *Epimedium grandiflorum* weed extract on mild steel in HCl acidic media. The goal was to find a cheap, renewable, non-hazardous, and green inhibitor for environmental purposes. The gasometric, weight loss and linear polarization methods were used to determine the inhibitory properties of the extract. Adsorption isotherms were also used to validate the reaction state. The concentration of the extract was prepared by serial dilution of 10 - 50% using a stock solution of 1.75 M HCl. Mild steel coupons of known elemental compositions were immersed in test solutions of both stock solution and extract solutions. In the gasometric method, a decrease in the volume of hydrogen gas evolved was observed as the concentration of extract increased. The weight loss method also showed a similar trend of inhibitory behavior, with the weight loss experienced by the coupons reducing as the extract concentration increased. The Tafel plot for the extract indicated good inhibitive properties with inhibition efficiency increasing with extract concentration. In all three methods studied, the maximum inhibition efficiency was observed in the 50% extract concentration. The extract fits best into the Freundlich isotherm, indicating physisorption. The results suggest that *Epimedium grandiflorum* weed extract is an effective inhibitor in suppressing corrosion on the surface of the metal.

Hassan et al.<sup>73</sup> investigated the use of *Citrus aurantium* leaves extracts as a sustainable corrosion inhibitor of mild steel in sulfuric acid. The study used a weight loss technique to investigate the effect of temperature, time, and inhibitor concentration on corrosion inhibition of mild steel in 1 M H<sub>2</sub>SO<sub>4</sub>. The results obtained indicated that *Citrus aurantium* leaves extracts acted as an inhibitor for mild steel in H<sub>2</sub>SO<sub>4</sub> and reduced the corrosion rate. The inhibition efficiency increased with an increase in inhibitor concentration while the temperature showed otherwise. At 40 °C and 10 ml/l inhibitor concentration, the inhibition efficiency was found to be 89%. The study also found that the adsorption of *Citrus aurantium* leaves extracts followed the Langmuir adsorption isotherm

model. The values of the free energy of adsorption were around -20 kJ/mol, which is indicative of physical adsorption between charged molecules and a charged metal. Quantum chemical calculations were also used as theoretical support for the experimental results. Finally, the scanning electron microscope and Fourier transform infrared spectroscopy were used to examine the surface morphology and molecular structure of the inhibitor, respectively. These analyses revealed that the *Citrus aurantium* leaves extracts formed a protective film on the surface of mild steel, which reduced the rate of corrosion.

Omran et al.<sup>172</sup> investigated the use of extracts from water hyacinth and common reed as green corrosion inhibitors for mild steel in acid media. The inhibitive effect was evaluated using electrochemical impedance spectroscopy and potentiodynamic polarization techniques. The results showed that the inhibition efficiency increased with increasing concentrations of both aquatic and ethanolic extracts. The maximum inhibition efficiency was recorded as 86.8% and 89.6% for ethanolic extracts of water hyacinth and common reed, respectively. The corrosion current density decreased with the increasing concentration of the extracts. To understand the nature of adsorption behavior, the Langmuir, Florry-Huggins, and kinetic-thermodynamic models were analyzed. The results showed that the Langmuir isotherm model was the most suitable model for the adsorption behavior of both plant extracts on mild steel surface. To optimize the % IE of plant extracts for mild steel corrosion, a 2(3) full factorial experimental design was used. Three factors were studied: extraction method, pH, and extract dose. The optimum conditions were at low pH and high plant extract dose concentration, especially with ethanolic extraction. The validation models were calculated with  $R^2 \geq 0.986$ . The effectiveness of the green inhibitors was also verified using the response surface methodology. The study demonstrates the potential of using unwanted aquatic macrophytes biomasses as green corrosion inhibitors. The results suggest that the extracts from water hyacinth and common reed can effectively inhibit mild steel corrosion in acid media. The optimization of the extraction method, pH, and extract dose can further improve the inhibition efficiency. The use of green inhibitors can provide a sustainable and environmentally friendly solution for corrosion inhibition.

Divya et al.<sup>173</sup> investigated the effectiveness of *Galinsoga parviflora* (Quick Weed) leaf extract as a corrosion inhibitor of mild steel in 1 M HCl solution. The study employed weight loss, potentiodynamic polarization curves, and electrochemical impedance spectroscopy to calculate the

corrosion rate of mild steel and inhibition efficiencies. The research findings revealed that the efficiency of the inhibitor increased with an increase in its concentration, and the inhibition efficiency of above 90% was obtained at 6% V/V of the inhibitor. The optimal temperature for maximum efficiency was found to be 323 K at a 6% V/V concentration of the extract. The inhibition mechanism of the plant extract was explained based on the adsorption of a stable complex at the mild steel surface. The theoretical fitting of different isotherms was tested to clarify the nature of adsorption. The polarization curves demonstrated that GP acted as a mixed-type inhibitor. The research findings suggest that *Galinsoga parviflora* leaf extract could be an effective corrosion inhibitor for mild steel in 1 M HCl solution. The study provides insight into the inhibition mechanism of the plant extract and demonstrates the importance of optimizing the concentration and temperature of the inhibitor. The theoretical fitting of different isotherms could provide a better understanding of the adsorption behavior of the inhibitor. The use of mixed-type inhibitors could potentially enhance the effectiveness of the inhibitor and lead to the development of more sustainable and eco-friendly corrosion inhibitors for industrial applications.

Kathiravan et al.<sup>174</sup> investigated the effectiveness of *Ruellia tuberosa* Linn (RT) extract as a corrosion inhibitor for mild steel in a hydrochloric acid solution. The inhibitive ability of the RT extract was evaluated using mass loss and electrochemical studies, and the results showed that the inhibition efficiency increases with increasing concentration of the RT extract and decreases with increasing acid concentration and temperature. The extract was found to act as a mixed-type inhibitor, as revealed by the polarization studies. The impedance results indicated that the adsorption of the RT extract on the mild steel surface is through a charge transfer reaction. The adsorption process was found to be exothermic, spontaneous, and consistent with the mechanism of physical adsorption. Moreover, it was established that the adsorption process followed the Freundlich isotherm. To confirm the adsorption of the chemical constituents of the RT extract on the mild steel surface, Fourier transform infrared spectroscopy (FTIR) and field emission scanning electron microscopy (FESEM) was performed. The FTIR analysis showed that the extract contains various functional groups that could participate in the adsorption process, such as hydroxyl, carbonyl, and aromatic groups. The FESEM images revealed that the surface of the mild steel was covered with a protective film of the inhibitor. Finally, quantum chemical calculations were carried out to ascertain the possible adsorption sites of the components of the extract on to the metal surface. The results of the calculations showed that the adsorption process involves the transfer of

electrons from the inhibitor to the metal surface, and the most favorable adsorption site was found to be the carbonyl group.

Jeslina et al.<sup>175</sup> investigated the effectiveness of an alcoholic extract of *Sargassum muticum*, a seaweed, as a corrosion inhibitor for mild steel in 0.5 N HCl. Both weight loss methods and electrochemical studies were used to evaluate the inhibitory effect of the seaweed extract. The results showed that the inhibitor was highly effective, with 500 ppm of the inhibitor offering 99.25% inhibition efficiency. This suggests that seaweed extract can be a potential alternative to synthetic inhibitors, which are costly and hazardous. The polarization study revealed that the inhibitor functions as an anodic inhibitor at higher concentrations. Anodic inhibitors work by increasing the activation energy required for the anodic reaction to proceed, thereby slowing down the corrosion rate. The AC impedance spectra confirmed the formation of a protective film on the metal surface. This protective film acts as a barrier, preventing the corrosive species from reaching the metal surface, thus reducing the corrosion rate. The adsorption of inhibitor molecules on the metal surface follows the Langmuir adsorption isotherm. Langmuir adsorption isotherm is a model used to describe the adsorption of a molecule onto a surface. It assumes that there is a limited number of adsorption sites available, and once these sites are occupied, further adsorption is not possible. The adsorption process follows a monolayer formation, where the inhibitor molecules arrange themselves in a single layer on the metal surface.

Okafor et al.<sup>176</sup> investigated the inhibitory action of *Phyllanthus amarus* extracts, including leaves (LV), seeds (SD), and a combination of both (LVSD), on mild steel corrosion in HCl and H<sub>2</sub>SO<sub>4</sub> solutions using weight loss and gasometric techniques. The results revealed that the extracts functioned as good inhibitors in both acidic media, and the inhibition efficiency increased with the concentration of the extracts. Moreover, the inhibition efficiency increased with the rise in temperature, and activation energies decreased in the presence of the extract. The inhibitory mechanism of the plant extracts was attributed to the chemical adsorption of the plant components on the surface of the metal. The study proposed that the active components of the extract create a stable film on the surface of the mild steel, which reduces the corrosion rate of the metal. The adsorption of the inhibitor molecules on the metal surface followed the Temkin isotherm, which suggests that the adsorption process is due to a combination of physical and chemical adsorption mechanisms.

Odozi et al.<sup>177</sup> investigated the inhibitory effect of *Synsepalum dulcificum* leaves extract on the corrosion of mild steel in 1.0 M hydrochloric acid solution. The inhibitory properties of the extract were evaluated using electrochemical and gravimetric methods. The results showed that *S. dulcificum* has good inhibitive properties with inhibition efficiency (%I) reaching 94 at 1000 ppm inhibitor concentration. The negative value of enthalpy indicated the exothermic nature of adsorption of *S. dulcificum*, and it decreased steadily from -25.28 kJ/mol at 100 ppm to -34.41 kJ/mol at 1000 ppm *S. dulcificum* concentration. The values of Gibbs free energy were negative, suggesting the spontaneous adhesion of the *S. dulcificum* molecules on the surface of mild steel. The adsorption of *S. dulcificum* conformed to the Langmuir isotherm model, and the values of Gibbs free energy suggested that adsorption of *S. dulcificum* was physisorptive since values of  $\Delta G^{\circ}_{\text{ads}}$  up to -20 kJ/mol are consistent with physical adsorption. The activation energy increased with the increase in *S. dulcificum* concentration, indicating that the energy required for corrosion of mild steel increased in the presence of *S. dulcificum* extract. Potentiodynamic polarization studies revealed that *S. dulcificum* functions as a mixed-type inhibitor since values of corrosion potential increased on addition of *S. dulcificum* with no particular trend. Electrochemical impedance spectroscopy (EIS) analysis revealed that charge transfer resistance ( $R_{\text{ct}}$ ) increased as *S. dulcificum* concentration increased to reach 1413.3  $\Omega \text{ cm}^2$  at 1000 ppm. The results indicated that the *S. dulcificum* leaves extract could effectively inhibit the corrosion of mild steel in hydrochloric acid solution by forming a protective layer on the metal surface, which can prevent the aggressive ions from attacking the metal surface.

Iloamaeke et al.<sup>178</sup> investigated the corrosion inhibition properties of *Persea Americana* (PA) ethanol leaves extract for aluminium in 1M H<sub>2</sub>SO<sub>4</sub> medium. The study was conducted using the gravimetric method at temperatures ranging from 30°C to 60°C. The results showed that different concentrations of PA leaf extract (0.2g/l to 1.0g/l) inhibited aluminium corrosion at different temperatures. At a PA extract concentration of 1.0g/l, the percentage inhibition reached 78.90%, 58.84%, 55.3%, and 52.66% at 30°C, 40°C, 50°C, and 60°C, respectively. These results indicate that PA leaf extract is an effective inhibitor of aluminium corrosion in 1M H<sub>2</sub>SO<sub>4</sub>. The thermodynamics and kinetics parameters for the adsorption of the inhibitor on the surface of aluminium were calculated. The enthalpy was found to be negative, indicating an exothermic adsorption process. The entropy was positive, indicating that the adsorption process is spontaneous and random. The free energy of adsorption and activation energy confirmed that the mechanism is



by physical adsorption. This suggests that the adsorption of PA extract molecules on the aluminium surface is mainly due to weak van der Waals forces. The adsorption isotherms obeyed were Langmuir and Temkin isotherms. The Langmuir isotherm assumes monolayer adsorption of the inhibitor on the surface of the metal, while the Temkin isotherm assumes that the adsorption energy decreases linearly with the surface coverage. The correlation coefficient values obtained from the Langmuir isotherm were higher than those obtained from the Temkin isotherm. This suggests that the Langmuir isotherm model better describes the adsorption behavior of PA extract on the aluminium surface. **Table 2.2** shows the efficiency of weed extracts as corrosion inhibitors for several metallic surfaces in acidic media.

**Table 2.2**

Weed extracts as corrosion inhibitors in hydrochloric acid solution involving various weeds names, techniques, nature of metal and electrolyte and nature of the adsorption of active phytoconstituents

<b>Plant name</b>	<b>Part used</b>	<b>Techniques</b>	<b>Metal and electrolyte</b>	<b>Nature of adsorption</b>	<b>Remark</b>	<b>Ref.</b>
<i>Pongamia pinnata</i>	Leaves	WL, EIS, FTIR	Mild steel/1N HCl	Langmuir adsorption isotherm	6-methoxy-2-phenyl-4H-furo[2,3-h]chromen-4-one and 2-(benzo[d][1,3]dioxol-5-yl)-4H-furo[2,3-h]chromen-4-one are the main active constituents	<sup>179</sup>
<i>Urtica dioica L.</i>	Leaves and stems	EIS, PDP, EDS, AFM, SEM	Mild steel/1M HCl	Langmuir adsorption isotherm	Maximum efficiency of 92.24% was achieved at 0.3 g/l inhibitor conc. at 40 °C	<sup>180</sup>
<i>Nypa fruticans Wurmb</i>	Leaves	WL, FTIR	Mild steel/0.1 M HCl	Langmuir adsorption isotherm	The highest inhibition efficiency of 75.11% was observed with <i>N. fruticans</i> extract	<sup>181</sup>
<i>Oxandra asbeckii</i>	Leaves	EIS, PDP	Mild steel/1M HCl	Langmuir adsorption isotherm/mixed-type inhibitor	Oxoaporphinoid alkaloids such as liriodenine, azafluorenones alkaloids are the active constituent of O.A.	<sup>182</sup>
<i>Telfaria occidentalis</i>	Leaves	WL, EFMT	Mild steel/1M HCl	Langmuir adsorption isotherm	Synergistic effects increased the efficiency of the extract in the presence of halide additives in the order KCl>KBr>KI	<sup>183</sup>
<i>Murraya koenigii</i>	Leaves	WL, EIS, PDP, LP	Mild steel/0.5 M HCl	Langmuir adsorption isotherm	Main constituents of <i>Murraya koenigii</i> leaves are murrifoline-I, pyrayafoline-D and mahabinine-A.	<sup>184</sup>

<i>Andrographis paniculata</i>	Leaves	WL, PDP, EIS, FTIR	Mild steel/1M HCl	Langmuir adsorption isotherm	Andrographolide is the main phytochemical present in A.P. extract <sup>185</sup>
<i>Glycine max leaves</i>	Leaves	WL, SEM, EDS, XRD, FTIR	Mild steel/0.5 M HCl	Langmuir adsorption isotherm	Optimum inhibition efficiency reached up to 91.07 % at 2 g l <sup>-1</sup> (308 K). Genistein and daidzein were the major phytochemical components present in the extract <sup>186</sup>
<i>Mollugo cerviana</i>	Fruits	WL, EIS, SEM	Mild steel/2M HCl	Langmuir adsorption isotherm	<i>Mollugo cerviana</i> extract acts as a good inhibitor for the corrosion of mild steel in 1M HCl solution <sup>187</sup>
<i>Prosopis cineraria</i>	Leaves	WL	Mild steel/0.5 N HCl	Langmuir adsorption isotherm	A peak efficiency of 95.39% was achieved with spicigerine as the major phytochemical constituent <sup>188</sup>
<i>Euphorbia falcata</i>	Leaves	WL, SEM, EIS	Mild steel/1M HCl	Langmuir adsorption isotherm	The corrosion inhibition efficiency increases with increasing EFE concentration, and the maximum efficiency of 93% was achieved at 3.0 g L <sup>-1</sup> <sup>189</sup>
<i>Ananas sativum</i>	Leaves	WL, EIS	Mild steel/0.1 M HCl	Langmuir adsorption isotherm	Plant extracts disrupt metallic corrosion by getting adsorbed on the metal surface <sup>190</sup>
<i>Andrographis paniculata</i>	Leaves	DFT	Mild steel/1 M HCl	Langmuir adsorption isotherm	Mahabinine, Brucine are two major phytochemical constituents <sup>76</sup>
<i>Justicia gendarussa</i>	Leaves	WL, EIS	Mild steel/1 M HCl	Langmuir adsorption isotherm/mixed-type inhibitor	An inhibition efficiency of 93% was achieved with 150 ppm JGPE at 25 °C <sup>191</sup>
<i>Tiliacora acuminate</i>	Leaves	WL, XRD, EIS	Mild steel/1 M HCl	Langmuir adsorption isotherm	Maximum efficiency of 93.02 % at the highest concentration of 320 ppm at the temperature of 333 K was achieved <sup>145</sup>

<i>Adathoda vasica</i>	Stems, roots	WL, EIS	Mild steel/1 M HCl	Langmuir adsorption isotherm	Plant extract showed 99.6% inhibition efficiency at 8.0% v/v concentration	<sup>192</sup>
<i>Palicourea guianensis</i>	Leaves	EIS, PDP	C38 steel/1 M HCl	Langmuir, Temkin and Frunkin adsorption isotherms	The inhibition efficiency of 89% attained with 100 mg L <sup>-1</sup> of AEPG at 25 °C	<sup>193</sup>
<i>Glycyrrhiza glabra</i>	Leaves	WL, EIS, AFM	C38 steel/1 M HCl	Langmuir adsorption isotherm	The maximum corrosion inhibition efficiency (about 88%) and surface coverage (about 72%) were obtained in the presence of 800 ppm conc. of <i>Glycyrrhiza glabra</i> leaf extract	<sup>194</sup>
<i>Acalypha torta</i>	Aerial part	WL, EIS, PDP, SEM	Mild steel/1 M HCl	Langmuir adsorption isotherm	<i>Acalypha torta</i> corrosion efficiency increases with increasing concentration and decreases with increasing temperature	<sup>195</sup>
<i>Thevetia peruviana</i>	Whole plant	WL, EIS, EFMT	Mild steel/1 M HCl	Temkin adsorption isotherm/ mixed-type inhibitor	Peruvoside, Cannogenin, Thevetin are the major active constituents	<sup>134</sup>
<i>Cucurbitamaxima</i>	Peel	WL, FTIR	Mild steel/1 N HCl	Langmuir adsorption isotherm	Maximum efficiency of 93 % is acknowledged at the inhibitor concentration of 2 % v/v	<sup>196</sup>
<i>Strychnos Nuxvomica</i>	Seeds	WL, EIS, PDP, FTIR	Mild steel/1 M HCl	Langmuir adsorption isotherm/ mixed-type inhibitor	The main constituent of the extract of <i>Kuchla</i> ( <i>Strychnos Nuxvomica</i> ) seed is Brucine	<sup>197</sup>
<i>Isertia coccinea</i>	Whole plant	HPLC, EIS, PDP	C38 steel/1 M HCl	Langmuir adsorption isotherm	The inhibitor revealed a maximum efficiency of 91 % at 100 mg L <sup>-1</sup>	<sup>198</sup>

<i>Fig leaves</i>	Leaves	WL, EIS	Mild steel/2 M HCl	Langmuir adsorption isotherm	The inhibition efficiency of 87% attained at above 200 ppm	<sup>199</sup>
<i>Aniba rosaeodora</i>	Barks stem	XPS, WL, EIS	C38 steel/1 M HCl	Langmuir adsorption isotherm	Anibine was found to be a major phytochemical component showing good inhibition efficiency	<sup>200</sup>
<i>Zenthoxylum alatum</i>	Fruits	WL, EIS, SEM, GC-MS, FTIR	Mild steel/1 M HCl	Langmuir adsorption isotherm	Weed extract reduced steel corrosion more effectively in 5% HCl than in 15% HCl	<sup>201</sup>
<i>Pimenta dioica</i>	Leaves	WL, EIS, DFT	Mild steel/0.5 - 1 M HCl	Langmuir adsorption isotherm	Eugenol, Methyleugenol, caryophyllene, Myrcene, Limonene and 1,8-Cineole are the major phytochemicals present in <i>Pimenta di.</i> extract.	<sup>202</sup>
<i>Plectranthus amboinicus</i>	Leaves	WL, EIS	Mild steel/1 M HCl	Langmuir adsorption isotherm	Two main constituents of the leaf thymol and 1, 8-cineole were monitored for their inhibition behavior with upto 93% of maximum inhibition efficiency	<sup>203</sup>
<i>Chenopodium Ambrosioides</i>	Leaves	WL, EIS, SEM	Mild steel/0.5 M H <sub>2</sub> SO <sub>4</sub>	Langmuir adsorption isotherm	94% Inhibition efficiency attained at 4 g/l	<sup>204</sup>
<i>Chamaerops humilis</i>	Leaves and fruits	WL, PDP, EIS	Mild steel/0.5 M H <sub>2</sub> SO <sub>4</sub>	Langmuir adsorption isotherm	Inhibition efficiency reached a maximum value of 78.55% at 100 mg /L.	<sup>205</sup>
<i>Anacyclus pyrethrum L. extracts</i>	Leaves	WL, EIS, PDP	Mild steel/0.5 M H <sub>2</sub> SO <sub>4</sub>	Langmuir adsorption isotherm	Saponins, Alkaloids, Flavonoids are some active constituents	<sup>206</sup>

<i>Pongamia Pinnata</i>	Leaves	WL, FTIR, GC-MS, SEM	EIS,	Mild steel/1 N H <sub>2</sub> SO <sub>4</sub>	Temkin adsorption isotherm/ mixed - type inhibitor	<i>P. pinnata</i> leaf extract retards both anodic metal dissolution	<sup>207</sup>
<i>Strychnos nux-vomica</i>	Seeds	WL, FTIR	EIS,	Mild steel/1 M H <sub>2</sub> SO <sub>4</sub>	Temkin adsorption isotherm	Brucine observed as a major phytochemical component	<sup>208</sup>
<i>Corchorus olitorius</i>	Stems	WL, GC-MS	EIS,	Mild steel/0.5 M H <sub>2</sub> SO <sub>4</sub>	Langmuir adsorption isotherm	An inhibition efficiency of 93% attained	<sup>209</sup>
<i>Argemone mexicana</i>	Flower	WL, SEM, UV	EIS,	Mild steel/1 M H <sub>2</sub> SO <sub>4</sub>	Langmuir adsorption isotherm	Nearly 80% corrosion inhibition was observed at 200 mg L <sup>-1</sup> inhibitor concentration and a maximum of 92.5% for 500 mg L <sup>-1</sup> extract concentration in 1 M HCL	<sup>210</sup>
<i>Argemone mexicana</i>	Flowers and leaves	WL, FTIR	EIS,	Mild steel/0.5 M H <sub>2</sub> SO <sub>4</sub>	Langmuir adsorption isotherm	The maximum inhibition efficiency of 87% attained by using 600 mg L <sup>-1</sup> of inhibitor	<sup>211</sup>
<i>Tagetes erecta</i>	Flower	WL, DFT	EIS,	Mild steel/0.5 M H <sub>2</sub> SO <sub>4</sub>	Langmuir adsorption isotherm	Lutein, a major component of TEE	<sup>212</sup>
<i>Lannea coromandelica</i>	Leaves	WL, FTIR, XRD, AFM, SEM	EIS,	Mild steel/1 M H <sub>2</sub> SO <sub>4</sub>	Langmuir adsorption isotherm	Alkaloids, Flavonoids, Glucosides, Carbohydrates, Phenols, Amino acids, and Steroids are the main chemical constituents	<sup>213</sup>
<i>Telfaria occidentalis</i>	Leaves	WL, SEM		Mild steel/1 M H <sub>2</sub> SO <sub>4</sub>	Langmuir adsorption isotherm	Protonated species in the extract play a predominant role in the observed inhibitive behavior, with possible contribution by molecular constituents.	<sup>183</sup>

<i>Garcinia kola</i>	Seeds	WL, XPS	Mild steel/5 M H <sub>2</sub> SO <sub>4</sub>	Langmuir adsorption isotherm	Alkaloids, flavonoids and polyphenols marked responsible for the corrosion inhibition property of extract	<sup>214</sup>
<i>Wrightiatinctoria</i>	Leaves	WL, EIS, PDP, SEM	Mild steel/0.5 M H <sub>2</sub> SO <sub>4</sub>	Langmuir adsorption isotherm	IE% of 98% achieved	<sup>215</sup>
<i>Kleinia grandiflora</i>	Leaves	WL, FTIR, SEM, UV	EIS, Mild steel/1 M H <sub>2</sub> SO <sub>4</sub>	Langmuir adsorption isotherm	Tetradecamethylcycloheptasil oxane, 6-deoxy D-galactose, 2-ethoxycarbonyl-5-oxopyrrolidine are the major active constituents	<sup>216</sup>
<i>Aster koraiensis</i>	Leaves	WL, SEM, EDX	EIS, Mild steel/1 M H <sub>2</sub> SO <sub>4</sub>	Langmuir adsorption isotherm	90.53% maximum efficiency achieved at 2000ppm of the extract	<sup>217</sup>
<i>Murraya koenigii</i>	Leaves	WL, PDP	EIS, Mild steel/0.5 M H <sub>2</sub> SO <sub>4</sub>	Langmuir adsorption isotherm	Main constituents of <i>Murraya koenigii</i> leaves are murrayoline-I, pyrayafoline-D, mahabinine-A.	<sup>184</sup>
<i>Datura metel</i>	Leaves	WL, EIS	EIS, Mild steel/1 M H <sub>2</sub> SO <sub>4</sub>	Langmuir adsorption isotherm	The presence of alkaloids such as scopolamine and atropine in <i>D. metel</i> may be the reason for the anticorrosive activity	<sup>218</sup>
<i>Syzygium cumini</i>	Seeds	WL, PDP	EIS, Mild steel/1 M H <sub>2</sub> SO <sub>4</sub>	Langmuir adsorption isotherm	Constituents of <i>S. cumini</i> seed extracts are ellagic acid, gallic acid, quercetin and cafeic acid	<sup>219</sup>
<i>Raphia hookeri</i>	Gum	WL, FTIR	PDP, Mild steel/1 M H <sub>2</sub> SO <sub>4</sub>	Langmuir adsorption isotherm	Activation energies were higher in the presence of the exudates gum revealing the physisorption mechanism	<sup>220</sup>

## **2.2. Purpose of Present Research Work**

The purpose of the present research work is to investigate the corrosion inhibition efficiency of selected six weeds (*Cnicus Benedictus*, *Vicia Sativa*, *Asphodelus tenuifolius*, *Polygonum Cuspidatum*, *Thysanolaena Latifolia* and *Trianthema Portulacastrum*) on mild steel in the presence of 0.5M HCl. The study aims to determine the potential of these weeds as natural and eco-friendly corrosion inhibitors for mild steel. The research will involve conducting experiments such as weight loss techniques, electrochemical techniques, computational analysis, etc., to evaluate the effectiveness of different extracts of the selected weeds in inhibiting the corrosion of mild steel in different corrosive environments. The results of this research will be useful in developing new and sustainable corrosion inhibitors for mild steel, which can have significant economic and environmental benefits.

## **2.3. Scope and intents of the present research work**

The scope of the present research work is dedicated to exploring the corrosion inhibition effectiveness of various weeds on mild steel. The primary goal is to identify natural and environmentally friendly corrosion inhibitors that can be derived from common weeds commonly found in our surroundings. To achieve this, the study will involve assessing the corrosion inhibition properties of different extracts from selected weeds when applied to mild steel surfaces exposed to a 0.5M HCl corrosive environment. The intent behind this research is twofold. Firstly, it seeks to contribute to the development of sustainable corrosion inhibitors for mild steel, offering a potential alternative to the synthetic inhibitors currently in use. Secondly, the research aims to promote the adoption of natural and eco-friendly solutions for corrosion prevention, which can carry significant environmental advantages.

In essence, the research is dedicated to investigating the potential of weed extracts as natural corrosion inhibitors for mild steel when subjected to acidic corrosive conditions. The rationale for considering such natural and green inhibitors lies in their efficacy, sustainability, and their benign impact on the environment and human health. These inhibitors typically contain electronegative heteroatoms such as nitrogen (N), oxygen (O), and unsaturated bonds. Through the formation of complexes between the inhibitor molecules and the exposed ions on the metal surface, a protective barrier is created, which helps in resisting corrosion by blocking acid attacks.



Furthermore, this research endeavor also aims to shed light on the chemical and physical properties of the selected weed extracts. These insights can be invaluable for the development of novel and efficient corrosion inhibitors for mild steel. Additionally, the study contributes to the existing body of knowledge concerning the potential of natural compounds as effective corrosion inhibitors.

#### **2.4. Objectives of the study**

- 1.** To determine the inhibition efficiency of selected weeds on the corrosion of mild steel in acidic medium.
- 2.** To study various adsorption isotherms involved in the interaction between mild steel and the selected weeds.
- 3.** To calculate the effect of various parameters such as effect of immersion time, effect of temperature on the rate of corrosion.
- 4.** To estimate various thermodynamic parameters like activation energy, Gibbs free energy, entropy and enthalpy.
- 5.** To calculate quantum chemical parameters such as HOMO, LUMO etc of the selected weeds used as inhibitors for corrosion of mild steel.

---

---

***Chapter 3***  
***Methods and Materials***

---

---

### 3.1. Methods in brief

Corrosion is a natural process that occurs when metals react with their environment, leading to the deterioration of the metal. Corrosion can lead to material loss, structural weakness, and reduced durability of metals, which can have significant economic and safety implications for various industries. To address this problem, researchers have focused on developing eco-friendly and sustainable corrosion inhibitors that can reduce or prevent the corrosion of metals. In recent years, natural compounds have emerged as promising alternatives to traditional chemical inhibitors. Natural compounds are derived from plant extracts and are considered eco-friendly, sustainable, and non-toxic. The use of natural compounds as corrosion inhibitors can reduce the environmental impact of corrosion inhibitors and minimize health risks for workers in industries that use them.

In this context, the present research work was carried out to investigate the corrosion inhibition efficiency of selected weeds on mild steel in 0.5M HCl solution at various inhibitor concentrations and at a temperature of 298K. The study aimed to evaluate the potential of natural compounds as corrosion inhibitors and to develop a better understanding of the mechanisms involved in the inhibition process. The inhibitive abilities of the selected inhibitors were determined using gravimetric measurements, potentiodynamic polarization (PDP), and electrochemical impedance spectroscopy (EIS). Gravimetric estimations were used to determine the corrosion rate of mild steel in the presence of different concentrations of the selected weed extracts. This technique involves measuring the weight loss of the mild steel sample after exposure to the corrosive solution containing the inhibitor. The corrosion rate is inversely proportional to the weight loss of the mild steel sample, and hence, the inhibition efficiency of the selected weeds extract can be determined.

Adsorption isotherms and thermodynamics variables play a crucial role in understanding the mechanism of corrosion inhibition. Adsorption isotherms provide information about the amount of inhibitor adsorbed on the metal surface, while kinetic variables give insights into the rate of inhibitor adsorption and the mechanism of the adsorption process. Adsorption isotherms describe the relationship between the concentration of inhibitor in the solution and the amount of inhibitor adsorbed on the metal surface at equilibrium. The kinetic variables, including the activation energy, rate constant, and reaction order, provide information about the rate and mechanism of inhibitor adsorption on the metal surface. By combining information from adsorption isotherms and kinetic variables, it is possible to develop a complete understanding of the mechanism of

inhibitor adsorption and corrosion inhibition. For example, the Langmuir isotherm and low activation energy values suggest that the adsorption of inhibitor molecules occurs through sorption, where the inhibitor molecules form bonds with the metal surface signifying their potent corrosion inhibition efficacy.

Potentiodynamic polarization (PDP) is another technique used in this research work to study the corrosion behavior of mild steel in the presence of the selected weed extracts. PDP provides information about the electrochemical properties of the mild steel sample in the corrosive solution, including the anodic and cathodic polarization curves, corrosion potential, and corrosion current density. This technique is highly sensitive and can detect even small changes in the electrochemical behavior of the mild steel sample in the presence of the inhibitors. Electrochemical impedance spectroscopy (EIS) is another powerful technique used in this research work to study the corrosion inhibition properties of the selected weed extracts. EIS involves measuring the impedance of the mild steel sample in the presence of the inhibitor, which provides information about the resistance of the mild steel sample to corrosion. The technique is highly sensitive and can detect even small changes in the impedance of the mild steel sample, which provides insights into the mechanism of corrosion inhibition of the selected weed extracts.

Scanning electron microscopy (SEM) and contact angle measurement were used to study the surface morphology of the mild steel sample in the presence of the selected weed extracts. SEM is a powerful technique that provides high-resolution images of the surface morphology of the mild steel sample, which can reveal the extent of corrosion and the presence of any corrosion products. Contact angle measurement, on the other hand, provides information about the wettability of the mild steel surface in the presence of the selected weed extracts, which can provide insights into the mechanism of corrosion inhibition.

Spectroscopic techniques such as Fourier-transform infrared (FT-IR) spectroscopy and ultraviolet-visible (UV-Vis) spectroscopy were used to explore the mechanism of adsorption of the selected plant extracts on the surface of the mild steel sample. FT-IR spectroscopy provides information about the functional groups present in the plant extracts, which can interact with the surface of the mild steel sample and form a protective layer. UV-Vis spectroscopy, on the other hand, can provide information about the electronic transitions that occur during the adsorption process, which can provide insights into the mechanism of corrosion inhibition.

Computational analysis such as density functional theory (DFT), molecular dynamics, and Monte Carlo simulations was utilized for theoretical calculations. These techniques were used to study the interaction of the selected plant extracts with the surface of the mild steel sample at the atomic and molecular levels. DFT calculations were used to optimize the structure of the plant extracts and to study the electronic properties of the inhibitors. Molecular dynamics simulations were used to study the adsorption behavior of the plant extracts on the surface of the mild steel sample, while Monte Carlo simulations were used to study the thermodynamic properties of the adsorption process. This section provides a detailed account of the various investigative techniques employed to study the corrosion inhibition properties of the selected plant extracts. The techniques used in this research work are highly specialized and sophisticated, and they have been chosen to provide a comprehensive understanding of the mechanism of corrosion inhibition of the selected weed extracts.

### **3.2. Preparation of samples**

The investigation involved studying the corrosion behavior of mild steel under acidic conditions. The mild steel samples utilized in the investigation comprised a specific chemical composition, which was 94.2% iron (Fe), 1.8% nickel (Ni), 1.2% phosphorus (P), 1.2% silicon (Si), 0.8% manganese (Mn), and 0.8% chromium (Cr) by wt.%. The samples were sliced into 1cm<sup>2</sup> measurements to ensure consistent test conditions across all samples during their investigation in the electrochemical impedance spectroscopy (EIS), potentiodynamic polarization (PDP) and gravimetric method<sup>221</sup>. The samples were carefully prepared for testing by washing them with acetone and rinsing them with deionized water to eliminate any contaminants that could disrupt the test outcomes. The investigation adhered to the ASTM G-31 standard, which ensured that the testing was conducted following established guidelines for the preparation of test specimens, test solutions, and test conditions. Subsequently, the samples were immersed in the test medium for further analysis<sup>153,222</sup>. To create a corrosive environment that replicated real-world acidic conditions, a 0.5 M solution was generated by diluting 37% hydrochloric acid (HCl) with deionized water. The use of deionized water was essential to prevent any interference from impurities in the solution.

### 3.3. Preparation of the electrode surface

The working electrodes were specifically created for use in a variety of electrochemical tests, such as electrochemical impedance spectroscopy (EIS) and potentiodynamic polarization (PDP). To ensure consistency across all samples, the working electrodes were made of the same metal composition as the mild steel samples used in the investigation, which was described earlier. The metallic rods were initially 5 cm in length and were soldered to copper cable on one end to ensure electrical conductivity (**Figure 3.1(a)**). The working electrodes were then covered with epoxy resin, except for the lower portion, which had an exposed interfacial area of 1 cm<sup>2</sup>(**Figure 3.1(b)**). This design allowed for the metallic specimen to be partially exposed to the acidic solution during testing<sup>223,224</sup>.

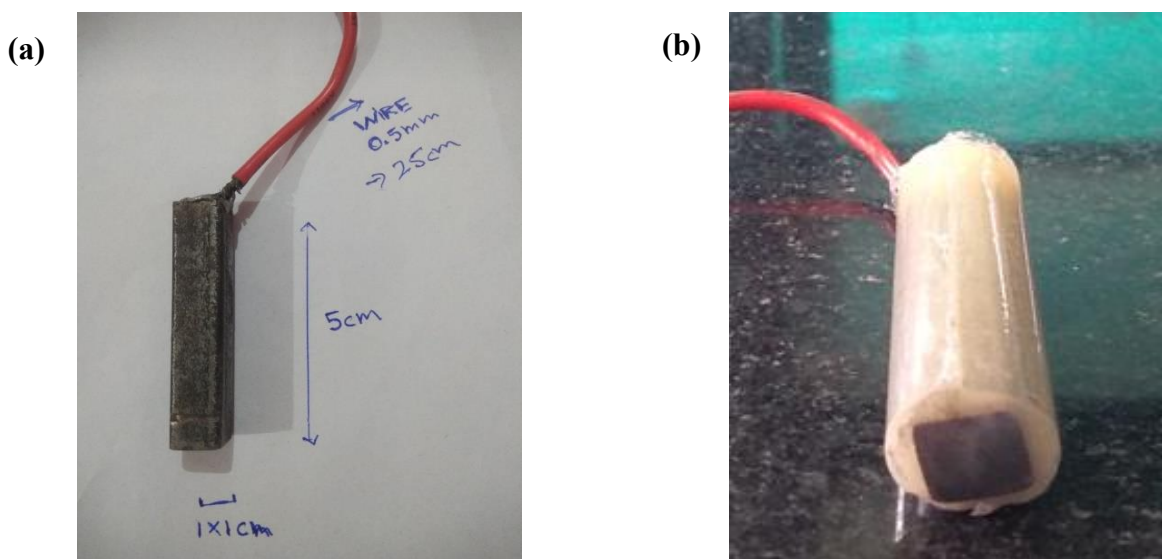


**Figure 3.1.** (a) The designing of the electrode shown on a bare mild steel rod, (b) Manufacturing of the working electrode to be used in the electrochemical analysis.

This design was crucial for the electrochemical studies as it allowed for a controlled and standardized environment for the testing. The use of identical compositional metals for both the working electrodes and mild steel samples ensured that the results obtained were consistent and reliable<sup>225–227</sup>. The epoxy resin covering of the electrodes helped to prevent any potential interference from the surrounding environment during the testing process.

### 3.4. Selected weeds for the investigation

The objective of this research is to study the potential of various weed extracts as corrosion inhibitors for mild steel in acidic media. To conduct this investigation, the researchers conducted

a literature review to select selected weeds which were *Cnicus Benedictus*, *Vicia Sativa*, *Asphodelus tenuifolius*, *Polygonum Cuspidatum*, *Thysanolaena Latifolia*, and *Trianthema Portulacastrum*. By studying the inhibitory properties of these selected weeds, the researchers aimed to contribute to the development of new, eco-friendly corrosion inhibitors that are both cost-effective and sustainable. **Figure 3.2.** showing the collected weeds for the investigation. The use of natural extracts as corrosion inhibitors has the potential to reduce the negative impact of synthetic inhibitors on the environment and human health. It may also offer an alternative approach to corrosion prevention that is more accessible and affordable to people in low-income countries.

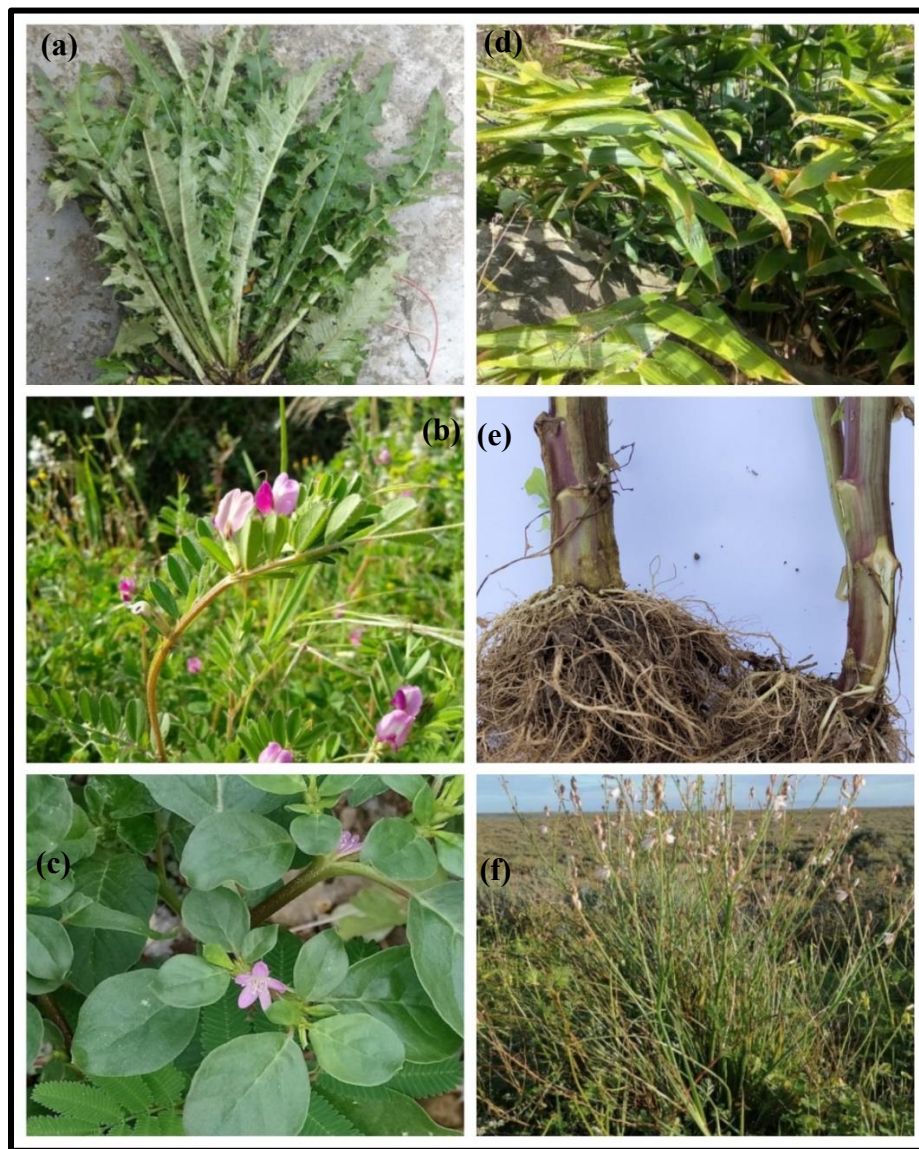


**Figure 3.2.** (a) *Cnicus Benedictus*, (b) *Vicia Sativa*, (c) *Trianthema Portulacastrum*, (d) *Thysanolaena Latifolia*, (e) *Polygonum Cuspidatum* and (f) *Asphodelus tenuifolius*.

### 3.5. Test solutions

In this investigation, the corrosion inhibition efficacy of selected weed extracts on mild steel was tested in a common corrosive environment, which is a 0.5 M HCl media. Several quantities of inhibitor concentrations ranging from (50 - 1000ppm) were aggregated with 0.5 M HCl, and the most cost-effective concentration was identified as shown in **Figure 3.3**. To create a standardized formulation with an optimum concentration of inhibitor, the inhibitor was properly dissolved in 0.5 M HCl media. Different desirable dosages were achieved by combining the required HCl media with standard solutions. Each test was conducted using newly prepared solutions to ensure consistency and accuracy of the results. These solutions were then left undisturbed in ambient conditions to ensure that external factors did not affect the outcome of the test. The investigation was performed at a constant temperature of 298 K to maintain consistency in the testing environment.



**Figure 3.3.** A stock solution of weed extract attained after aggregation with 0.5M HCl (**left**), Beaker containing 0.5M HCl solution (**right**).



### 3.6. Preparation of weed extracts

In order to prepare weed extracts, the specific parts such as aerial parts, root parts, and leaves parts of weeds were gathered from a nearby farm in Kapurthala during the summer season and later affirmed by Prof. Neera, Botany Department, HPU, India. The attained parts were first air-dried in the sun for 8-10 days to remove any moisture as shown in **Figure 3.4(a)**. After being dried, the attained parts were pounded into a minute powder and sieved to remove any large particles. The resultant powder was then combined at distinct proportions of attained parts and solvents such as ethanol for *Cnicus Benedictus*, methanol for *Vicia Sativa*, methanol for *Asphodelus tenuifolius*, methanol for *Polygonum Cuspidatum*, deionized water for *Thysanolaena Latifolia*, and deionized water for *Trianthema Portulacastrum* and further subjected to the several extraction processes such as Soxhlet extract, cold maceration process, ultrasonic assisted technique, Clevenger apparatus, etc.<sup>228</sup>. After 24-48 hrs, the mixture was filtered through a Millipore filter with a 0.45  $\mu\text{m}$  nylon membrane to remove any solid particles. The filtrate was concentrated at 40 °C using a rotary evaporator and stored in a cool place (4<sup>(b)</sup>°C) as shown in **Figure 3.4(ab-d)**. This was to prevent any degradation or degradation of the active compounds.

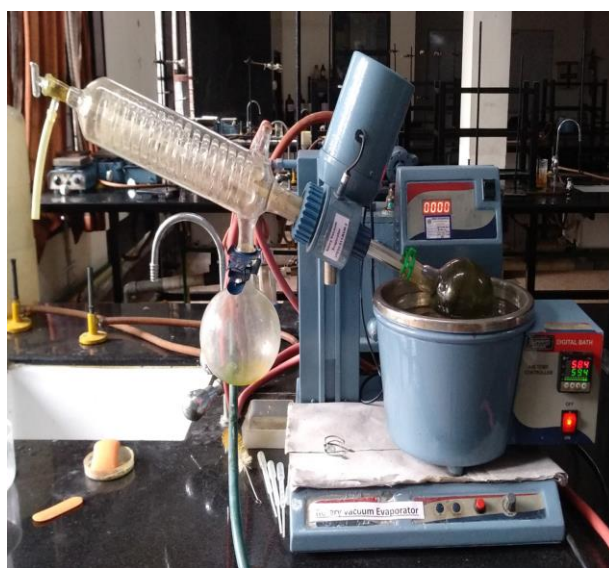




**Figure 3.4.** (a) Dried state of *Cnicus Benedictus* (b) Rota evaporator utilized to attain crude extract (c) and (d) Deep freeze extract of selected six weeds.

### 3.7. FT-IR spectroscopy

The research conducted utilized FT-IR spectroscopy as an analytical tool to identify the functional groups present in the plant extract. The analysis was conducted using a Shimadzu FTIR 8400S instrument, which recorded the FT-IR spectra in the range of 400- 4000  $\text{cm}^{-1}$  as shown in **Figure 3.5**. The FT-IR spectroscopy technique provides valuable information about the molecular structure and functional groups present in the sample, based on the absorption of infrared radiation by the sample. The resulting spectra can be used to identify specific chemical groups such as aldehydes, alcohols, amines, carboxylic acids, and esters, which can provide insight into the potential for the weed extract to act as a corrosion inhibitor. The instrument used in the study is shown in Figure, which highlights the importance of this analytical tool in the characterization of weed extracts for potential corrosion inhibition applications.



**Figure 3.5.** Shimadzu FTIR 8400S instrument utilized in the research.

### **3.8. UV–vis assessment**

In the study of corrosion inhibition, the UV measurement technique is commonly used to determine the effectiveness of a corrosion inhibitor. This method involves measuring the amount of ultraviolet (UV) light absorbed by a metal surface in the presence of a corrosion inhibitor. The measurement of UV absorbance can provide insights into the concentration of corrosion products such as metal oxides and hydroxides on the metal substrate, which can indicate the degree of ongoing corrosion and the effectiveness of the corrosion inhibitor<sup>229,230</sup>. Lower absorbance values indicate lower levels of corrosion and improved inhibition performance. In this experiment, the Shimadzu UV-1900i UV/Visible Scanning Spectrophotometer was used to record the UV-Vis spectrum of the uninhibited and inhibited medium to compare the inhibiting action of weed extracts on mild steel samples as shown in **Figure 3.6**.

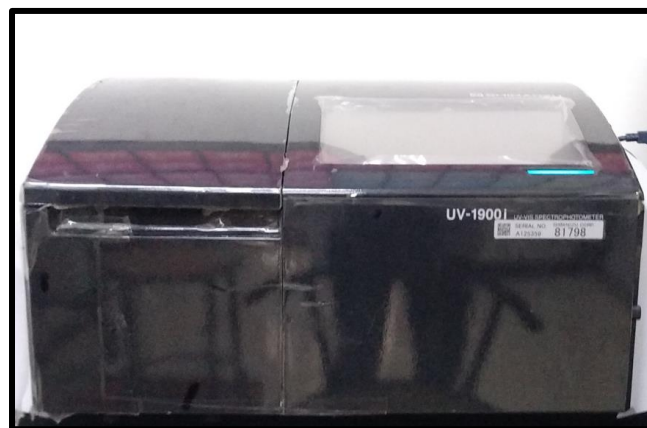


**Figure 3.6.** Shimadzu UV-1900i UV/Visible Scanning Spectrophotometer utilized in the research.

### 3.9. Weight loss (WL) assessment

Weight loss assessment is a widely used method to investigate corrosion and the effectiveness of corrosion inhibitors in materials. The method involves measuring the decrease in mass of a sample as a result of the corrosion process, which provides valuable insights into the corrosion rate and inhibitor effectiveness<sup>6,41,42,44</sup>. To perform weight loss measurements, a sample of the material being studied is weighed and then exposed to a corrosive environment. After a certain period of exposure, the sample is reweighed, and the difference in mass is used to calculate the corrosion rate. This process can be repeated with different samples to compare the effectiveness of different corrosion inhibitors. In this investigation, a conventional gravimetric approach was used to conduct a weight loss study<sup>231</sup>. Mild steel coupons of rectangular shape (2.5 cm × 2.0 cm × 0.025 cm) were immersed in 100 mL of 0.5 M HCl for 24 hours at 298K, both with and without varying concentrations of weed extracts as shown in **Figure 3.7** and **Figure 3.8** (PCRE as an example). After the immersion period, the specimens were removed and the corrosion product was cleaned mechanically, washed with ethanol, hexane, and acetone using ultrasonic cleaning and finally rinsed with double-distilled water following the ASTM G-31 standard. These samples were then processed in an oven set to 100°C, and their weight loss was calculated using an analytical balance with an accuracy of 0.1 mg. The experiment was repeated to determine the average weight loss, corrosion rate ( $C_R$ ) in  $\text{mg}/\text{cm}^2 \text{h}^{-1}$ , inhibition efficiency (IE%), and surface coverage ( $\Theta$ ). Equations (1 and 2) were used to calculate the CR and IE%.

$$C_R(\text{mm}/\text{y}) = \frac{87.6 \times w}{at D} \quad (1)$$

where  $w$  is the mild steel corrosion weight loss (mg),  $a$  is the coupon area ( $\text{cm}^2$ ),  $t$  is the exposure duration (h), and  $D$  is the mild steel density.

$$IE(\%) = \frac{W_o - W}{W_o} \times 100 \quad (2)$$

Here,  $W_o$  and  $W$  denote weight loss without and with inhibitor.

The following equation (3) can be used to correlate surface coverage ( $\Theta$ ) to weight loss and corrosion rate:

$$(\theta) = \frac{W_o - W}{W_o} \quad (3)$$

The enhancement in the inhibition efficiency of the selected inhibitors can be attributed to the formation of a protective layer on the surface of mild steel, which impedes the corrosion process. To investigate the effect of the inhibitors on the corrosion inhibition efficiencies, weight loss measurements were carried out at a temperature of 298 K under different inhibitor concentrations, as well as in the absence of any inhibitor. The weight loss measurements allowed for the determination of the corrosion rates of mild steel in the presence and absence of inhibitors. The obtained results indicated that the inhibition efficiency increased with an increase in inhibitor concentration, as the presence of higher inhibitor concentrations resulted in a thicker protective layer on the surface of mild steel, which provided better protection against the corrosive environment.

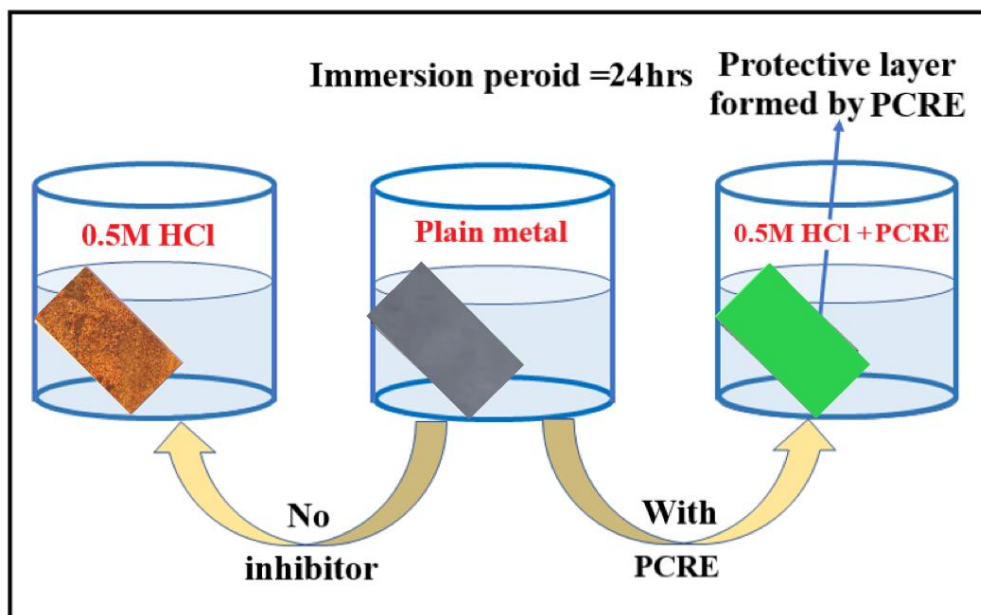


**Figure 3.7.** Schematic representation of weight-loss analysis of weed (PCRE=*Polygonum Cuspidatum* root extract as an example).

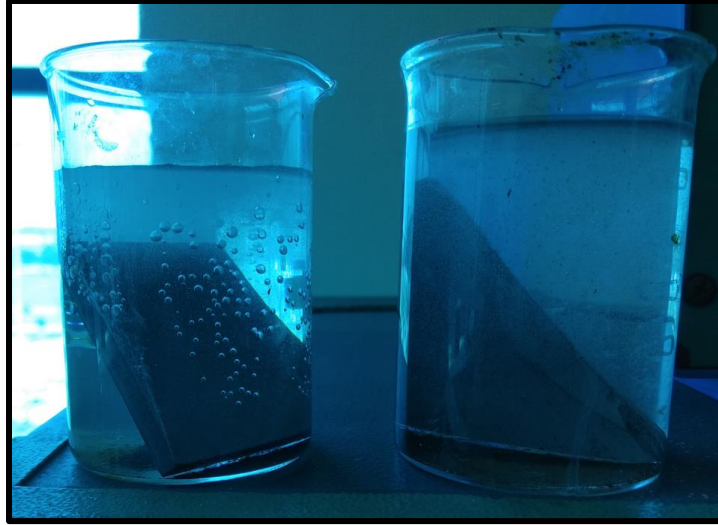


**Figure 3.8.** Weight loss analysis of the mild steel sample in the absence of 0.5M HCl (**left**) and in the presence of inhibitor+0.5M HCl (**right**).

### 3.10. Adsorption and thermodynamic parameters

Adsorption and thermodynamic parameters play a crucial role in corrosion inhibition. The adsorption of the inhibitor molecules on the metal surface reduces the corrosion rate by forming a protective layer that hinders the corrosive environment from attacking the metal surface. The adsorption behavior of the inhibitor molecules can be studied by analyzing the thermodynamic parameters such as the adsorption free energy ( $\Delta G^{\circ}_{\text{ads}}$ ), adsorption enthalpy ( $\Delta H^{\circ}_{\text{ads}}$ ), and adsorption entropy ( $\Delta S^{\circ}_{\text{ads}}$ ). The adsorption-free energy ( $\Delta G^{\circ}_{\text{ads}}$ ) provides an estimation of the spontaneity of the adsorption process. If the value of  $\Delta G^{\circ}_{\text{ads}}$  is negative, then the adsorption process is spontaneous, indicating that the inhibitor molecule has a strong affinity towards the metal surface. Conversely, if the value of  $\Delta G^{\circ}_{\text{ads}}$  is positive, the adsorption process is non-spontaneous, suggesting that the inhibitor molecule has a weak affinity towards the metal surface. The adsorption enthalpy ( $\Delta H^{\circ}_{\text{ads}}$ ) describes the energy involved in the adsorption process. A negative  $\Delta H^{\circ}_{\text{ads}}$  value indicates that the adsorption process is exothermic, meaning that the inhibitor molecule loses energy during the adsorption process. Conversely, a positive  $\Delta H^{\circ}_{\text{ads}}$  value indicates that the adsorption process is endothermic, meaning that the inhibitor molecule gains energy during the adsorption process.

The adsorption entropy ( $\Delta S^{\circ}_{ads}$ ) provides an understanding of the randomness or orderliness of the adsorption process. If the value of  $\Delta S^{\circ}_{ads}$  is positive, the adsorption process is associated with an increase in entropy, suggesting that the inhibitor molecule has more freedom to move around on the metal surface. Conversely, if the value of  $\Delta S^{\circ}_{ads}$  is negative, the adsorption process is associated with a decrease in entropy, indicating that the inhibitor molecule has limited freedom to move around on the metal surface. The adsorption isotherm is another crucial factor in studying the adsorption behavior of the inhibitor molecules. The Langmuir adsorption isotherm is often used to describe the adsorption behavior of inhibitors on metal surfaces. The Langmuir adsorption isotherm model assumes that a thin layer of inhibitor molecules forms on the metal surface, and the adsorption occurs on a homogeneous surface with a finite number of adsorption sites. The Langmuir adsorption isotherm equation (4) can be written as:

$$\frac{C_{inh}}{\theta} = \frac{1}{K_{ads}} + C_{inh} \quad (4)$$

Where  $C_{inh}$  represents the inhibitor concentration and  $K_{ads}$  is the adsorption constant. If the correlation coefficient of the straight line obtained by plotting  $C/\theta$  against  $C$  comes near unity, then it is considered that the inhibitors obey the Langmuir adsorption isotherm.

Other crucial parameters are obtained using Eqs. (5) and (6), i.e. Van't Hoff Equation

$$\log CR = -E_a/2.303RT + \log A \quad (5)$$

Here,  $CR$  = corrosion rate,  $E_a$  = activation energy,  $T$  = temperature,  $R$  = gas constant,  $A$  = Arrhenius constant

$$d \ln k_{ads} / dT = \Delta H^{\circ}_{ads} / RT^2 \quad (6)$$

Here,  $T$  = temperature,  $R$  = gas constant (suggested value 8.314 J/K/mol).

The values of Gibb's free energy and adsorption entropy were measured using Eqns. (7) and (8) correspondingly

$$\Delta G^{\circ}_{ads} = -RT \ln(55.5 K_{ads}) \quad (7)$$

$$\Delta S^{\circ}_{ads} = \Delta H^{\circ}_{ads} - \Delta H^{\circ}_{ads} / T \quad (8)$$

Here,  $\Delta S^{\circ}_{ads}$  = entropy  $\Delta H^{\circ}_{ads}$  = enthalpy

By analyzing these adsorption and thermodynamic parameters, researchers can estimate the affinity of inhibitor molecules toward metal surfaces and design better corrosion inhibitors with improved inhibition efficiency. For example, if the adsorption isotherm shows a high degree of adsorption of the inhibitor molecules on the metal surface, and the thermodynamic parameters show favorable energetics and randomness of the adsorption process, then the inhibitor is likely to be effective in preventing corrosion. In conclusion, understanding the adsorption and thermodynamic parameters of corrosion inhibitors is essential for designing effective inhibitors with improved inhibition efficiency. By characterizing these parameters, researchers can gain insight into the mechanisms by which these compounds inhibit corrosion and develop more effective and efficient inhibitors.

### **3.11. Electrochemical measurements**

Electrochemical measurements including EIS and PDP are powerful analytical techniques utilized to study corrosion and corrosion inhibition in materials<sup>232</sup>. EIS measures the impedance, or opposition to an electrical current, of a material in a corrosive media, and provides information about the corrosion rate, the corrosion mechanism, and the effectiveness of corrosion inhibitors. In EIS, a small AC voltage is applied to a material in a corrosive environment, and the impedance of the material is measured over a range of frequencies. The impedance data is then analyzed to obtain information about the corrosion mechanism, including the  $C_R$ , the resistance of the material to corrosion, and the capacitance of the material, which provides information about the thickness of the corrosion products<sup>233</sup>. In corrosion inhibition studies, EIS can be utilized to quantify the efficacy of corrosion inhibitors by measuring the change in impedance of the material in the existence of the inhibitor. Similarly, in the context of corrosion inhibition, PDP involves measuring the anodic ( $\beta_a$ ) and cathodic ( $\beta_c$ ) polarization slopes of a metallic material in the inclusion and exclusion of a corrosion inhibitor<sup>234</sup>. The  $\beta_a$  and  $\beta_c$  polarization slopes represent the relationship between the corrosion current density ( $i_{corr}$ ) and the electrode potential ( $E$ ), which allows one to determine the corrosion potential ( $E_{corr}$ ) and the  $C_R$  of the material. By analyzing the shape and position of the polarization curves, one can infer whether the inhibitor function as an anodic and cathodic inhibitor and whether it adsorbs over the metallic substrate through a chemical or physical mechanism. This information provides valuable information into the pathway of inhibition and the effectiveness of the inhibitors.<sup>235–237</sup>



In this study, the Metrohm Autolab NOVA 2.1. electrochemical workstation was utilized to conduct EIS and PDP measurements as shown in **Figure 3.9 (left)**. A single-chamber electrochemical cell was used to evaluate the electrochemical properties of various flat specimens. The electrochemical cell included three electrodes: a working electrode made of mild steel with a 1 cm<sup>2</sup> exposed region, a reference electrode consisting of a saturated calomel electrode (SCE), and a Pt rod (purity 99.9%) used as an auxiliary/counter electrode as shown in **Figure 3.9 (right)**.

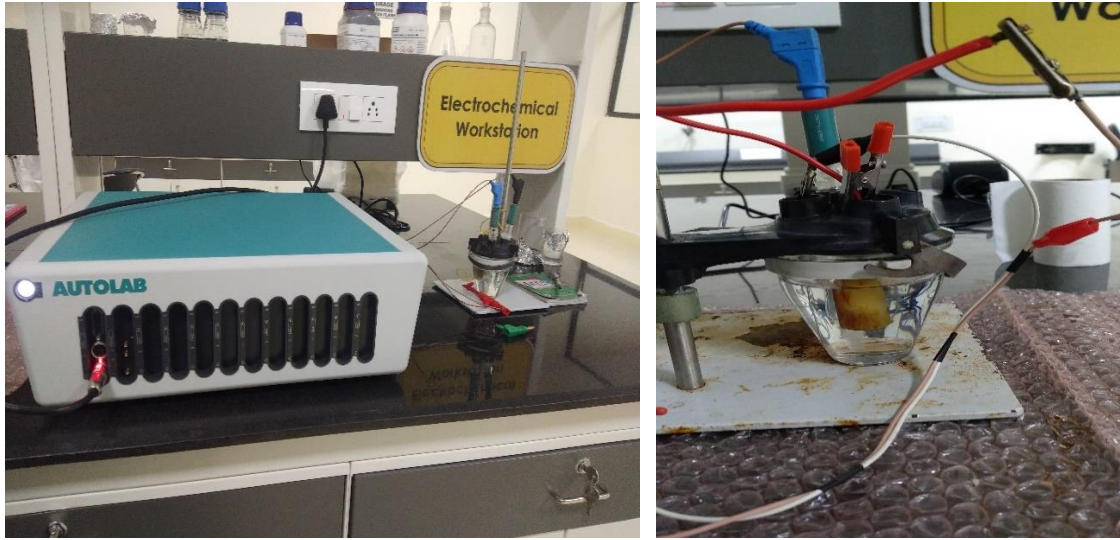


**Figure 3.9.** Metrohm Autolab NOVA 2.1. electrochemical workstation (**left**), Corrosion cell setup (**right**).

Prior to the electrochemical assessment, the working electrode was immersed in 0.5M HCl media with and without the inhibitor concentration for approximately 1 hour at the OCP (open circuit potential) to attain a steady state. The polarization slopes were then calculated at a sweep frequency of 1mV/s using varying potentials through the reported OCP following an immersion time of 1 hour. The EIS was carried out with a 0.005 V amplitude with a frequency spectrum of 100 kHz to 10 mHz. The  $i_{corr}$  was determined by interpreting the linear Tafel sections of the  $\beta_c$  and  $\beta_a$  slopes to  $E_{corr}$ . The impedance parameters and equivalent circuit were calculated by utilizing ZSimpWin freeware (version 3.6) to fit EIS data. The electrochemical assays were conducted at ambient temperature without any agitation. The following equation was employed to determine the polarization variables:

$$IE\% = \frac{i_{corr} - i_{corr}}{i_{corr}} \times 100 \quad (9)$$

Herein,  $I_{corr}$  and  $I_{icorr}$  denote the corrosion current density without and with the subjection of the inhibitor, correspondingly.

The charge transfer values were utilized to determine the IE% by employing the equation:

$$IE\% = \left[ Rct^i - \frac{Rct^0}{Rct^i} \right] \times 100 \quad (10)$$

Herein,  $Rct^0$  and  $Rct^i$  denote the charge transit resistance excluding and including the distinct concentrations of inhibitor.

### 3.11.1. Open circuit potential (OCP)

Open circuit potential (OCP) is a crucial parameter that plays a significant role in studying corrosion and corrosion inhibition of metals using electrochemical impedance spectroscopy (EIS). OCP refers to the potential of a metal when it is not connected to an external electrical circuit, and it reflects the balance between charge-transfer and mass-transport processes at the metal-solution interface<sup>238</sup>. In EIS measurements of corrosion, the OCP serves as a reference potential for the measurement. In this investigation, the mild steel rod, used as the working electrode, was submerged in the test media for 1 hour throughout each investigation involving the variation in concentrations. It is crucial to establish a consistent OCP before conducting the potentiodynamic polarization (PDP) and EIS assessments. The shifted in the potential measurements for the inhibited and uninhibited specimens indicates the nature of the inhibitor whether it acts as a cathodic inhibitor, anodic inhibitor or mixed inhibitor in the aggressive medium of 0.5 M HCl as shown in **Figure 3.10**.

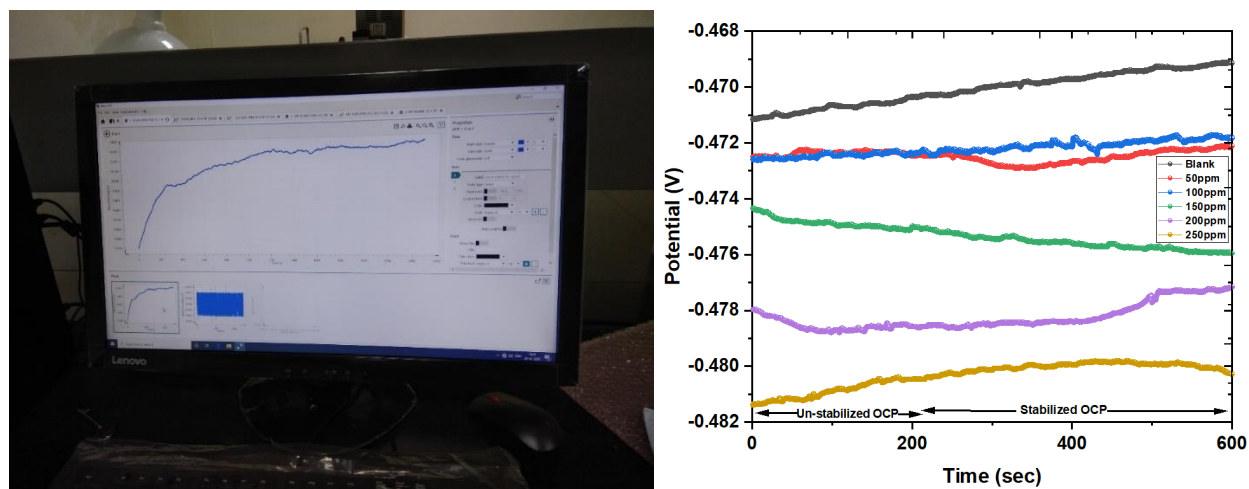


**Figure 3.10.** Attained OCP during the electrochemical analysis (**left**), Graph showing OCP

(Potential vs. Time) attained for weed extract illustrating the un-stabilized and stabilized OCP (right).

### 3.11.2. Potentiodynamic polarization (PDP) studies

Potentiodynamic polarization is a widely used electrochemical technique for studying corrosion and corrosion inhibition. It involves measuring the current response of an electrode as a function of the applied potential. The technique is particularly useful for investigating the effectiveness of corrosion inhibitors. In a typical potentiodynamic polarization experiment, the working electrode (usually a metal sample) is immersed in a solution containing the corrosion inhibitor. The potential of the electrode is then scanned over a range of values, while the current response is measured. The resulting data is plotted as a polarization curve, which typically exhibits three distinct regions: the cathodic region, the anodic region, and the passive region. The cathodic region represents the reduction of oxygen, hydrogen ions or water to hydrogen, which is usually the primary reaction that takes place in a corrosive environment. The anodic region, on the other hand, represents the oxidation of the metal, which is the primary corrosion reaction. The passive region represents the potential range where the metal surface is protected by a passive film, which is a protective layer formed on the metal surface that prevents further corrosion. The data is then plotted as a function of the potential, and the attained plot is called a Tafel plot. The Tafel plot provides information about the  $C_R$  and the corrosion potential of the metal. The Tafel plot is characterized by two linear regions, the anodic region and the cathodic region as shown in **Figure 3.11**. The anodic region is characterized by a positive slope and corresponds to the oxidation of the metal. The cathodic region is characterized by a negative slope and denotes the reduction of the corroding species. The point at which the anodic and cathodic regions intersect is the corrosion potential. The Tafel plot can be used to evaluate the impact of corrosion inhibitors on the corrosion rate and corrosion potential. For example, an inhibitor that decreases the  $C_R$  will result in a shift of the Tafel plot to more negative potentials, while an inhibitor that increases the  $C_R$  will result in a shift of the Tafel plot to more positive potentials. The IE% of the inhibitor was attained by equation (9).

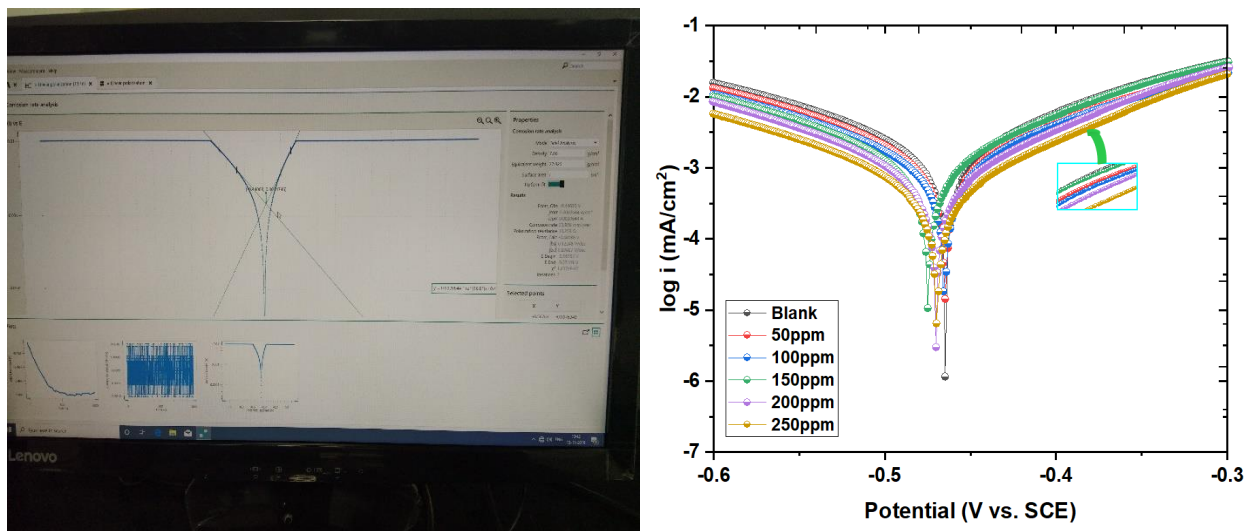


**Figure 3.11.** Attained Tafel plot during the experiment (**left**), Graph showing Tafel plot attained for weed extract illustrating the cathodic and anodic slopes (**right**).

### 3.11.3. Electrochemical impedance spectroscopy (EIS)

Electrochemical impedance spectroscopy (EIS) is a powerful electrochemical technique that is often used to study the corrosion behavior of metals and the effectiveness of corrosion inhibitors. EIS involves the application of a small amplitude sinusoidal voltage signal to an electrode and measuring the resulting current response as a function of frequency. In the case of corrosion inhibition studies, the working electrode (usually a metal sample) is immersed in a solution containing the corrosion inhibitor. The EIS measurement is then performed, and the resulting data is typically presented as a Nyquist plot, which is a graphical representation of the imaginary impedance ( $Z''$ ) versus the real impedance ( $Z'$ ) as shown in **Figure 3.12**. The Nyquist plot typically exhibits a semicircular arc at high frequencies, followed by a straight line at low frequencies. The semicircular arc corresponds to the charge transfer resistance ( $R_{ct}$ ), which is a measure of the ability of the corrosion inhibitor to inhibit the corrosion reaction. The larger the  $R_{ct}$  value, the more effective the inhibitor is at reducing the corrosion rate. The straight line at low frequencies corresponds to the Warburg impedance ( $Z_w$ ), which is related to the diffusion of ions in the solution. By analyzing the EIS data, various electrochemical parameters can be calculated, such as the corrosion rate, the corrosion potential, the double-layer capacitance, and the inhibitor efficiency. EIS can also provide information on the mechanism of corrosion inhibition, such as

whether the inhibitor acts by forming a protective film on the metal surface or by adsorbing onto the metal surface and reducing the corrosion reaction rate.

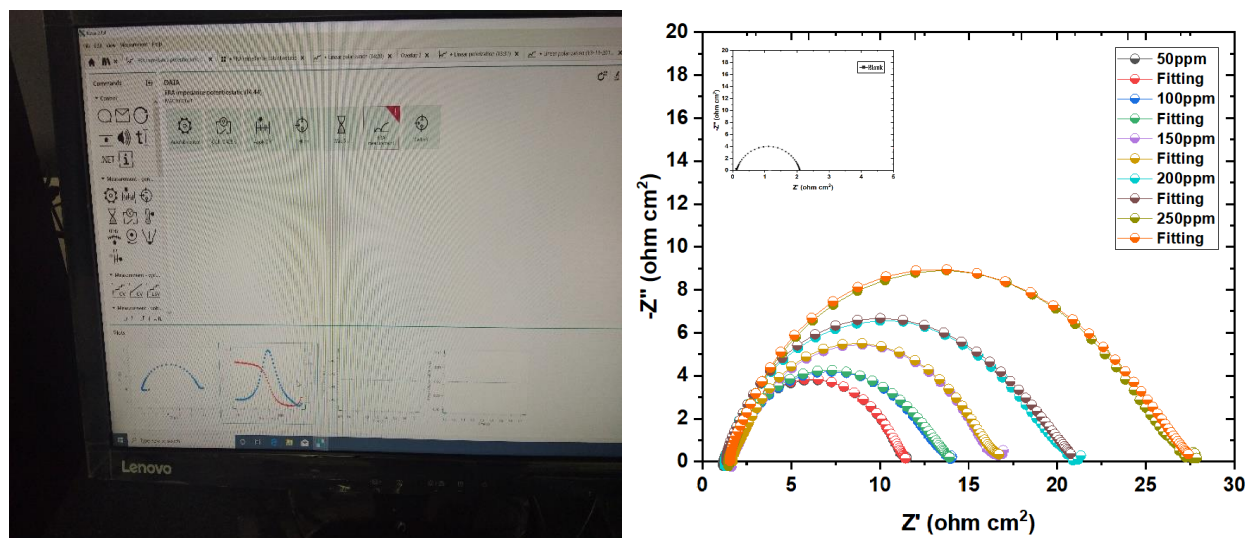


**Figure 3.12.** Attained Nyquist plot during the experiment (**left**), Graph showing Nyquist plot attained for weed extract illustrating the higher frequency and lower frequency region (**right**).

Similarly, Bode plot measurement is a commonly used methodology in the study of corrosion and corrosion inhibition of metals using electrochemical impedance spectroscopy (EIS). Bode plots are used to obtain information about the impedance and phase angle of a metal in a corrosive solution, and they provide valuable information about the  $C_R$  and the resistance of the metal to corrosion<sup>97,239</sup>. The Bode plot provides information about the impedance and phase angle of the metal in a corrosive solution as a function of frequency as shown in **Figure 3.13**. The impedance magnitude is proportional to the corrosion rate, while the phase angle is proportional to the resistance of the metal to corrosion. The impedance modulus improved with the increased quantity of inhibitor across the frequency range signifies its corrosion inhibition potential. As per the reports, the optimum capacitance at an intermediary frequency can be accepted, if the curve of the  $\log |Z|$  versus  $\log f$  with a maximum phase angle of  $90^\circ$  tends to be  $1$ <sup>229,240,241</sup>.

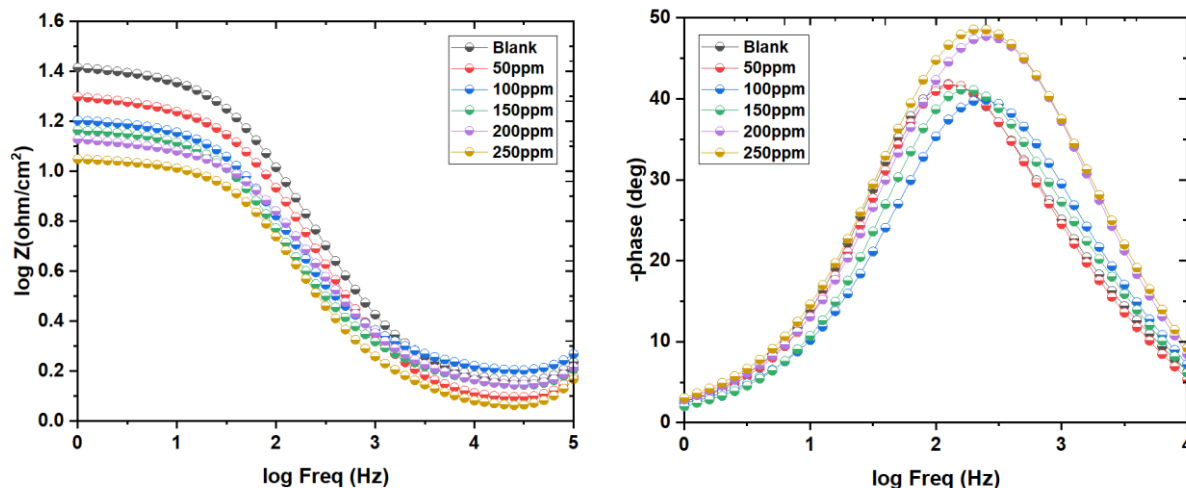


**Figure 3.13.** Bodes graph for the corrosion mitigation of mild steel in blank media subjected to various concentrations of weed extract (inhibitor) at 298 K.

### 3.12. Surface morphology assessment

#### 3.12.1. Scanning Electron Microscopy (SEM)

In order to assess the morphology of the metallic sample and the degree of the production of a defensive layer over the metallic substrate by the inhibitor molecules, the metallic samples were immersed in a corrosive solution (0.5M HCl) with the absence and presence of various concentrations of inhibitors for specific period<sup>242,243</sup>. Following the samples had been immersed for several hours, they were retrieved and dried. A scanning electron microscopy (SEM) approach was utilized to study the corrosion inhibition behavior of materials by employing a JEOL JSM-IT100 SEM as shown in **Figure 3.14**. SEM is an electron-based imaging technique that provides detailed images of the surface structure and morphology of a material. It is used to visualize the changes in surface topography and roughness due to corrosion and the presence of inhibitors. This method is frequently employed in the investigation of corrosion and corrosion inhibition and offers important insights into the progression of corrosion, the mechanics of inhibition, and the efficiency of corrosion inhibitors.

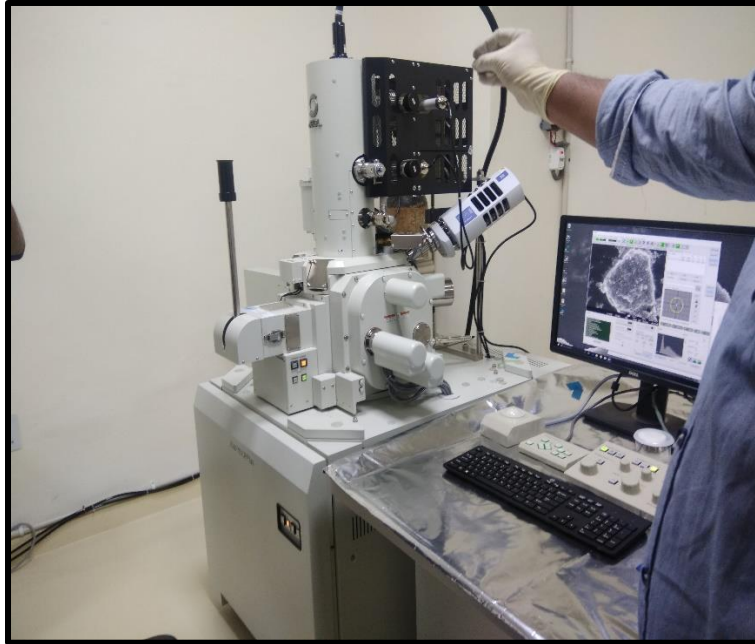


**Figure 3.14.** JEOL JSM-IT100 SEM instrument.

### **3.12.2. Contact angle (CA) assessment**

CA assessment is a technique used in corrosion inhibition investigations to evaluate the surface properties of a metal in the presence of a corrosion inhibitor<sup>91</sup>. It involves measuring the angle produced between the metal substrate and a droplet of a liquid (typically water) placed on the surface. In corrosion inhibition studies, the contact angle could offer crucial insights into the wettability of the metallic substrate, which can be an indicator of the interaction between the metallic surface and the inhibitor. A decrease in contact angle can indicate an increase in wettability and an improvement in the interaction between the metallic surface and the inhibitor, potentially leading to improved inhibition performance. In this investigation, the Drop Shape Analyzer equipment (KRUSS DSA 100) was employed to investigate the CA of untreated and treated metallic samples as shown in **Figure 3.15**<sup>244</sup>. The CA at multiple locations on the steel substrate was examined. Following spouting a water drop onto the substrate of the mild steel specimens for 120 seconds, images of both samples (unprotected and treated) were taken and their coating intensity for the hydrophobic character was analyzed.

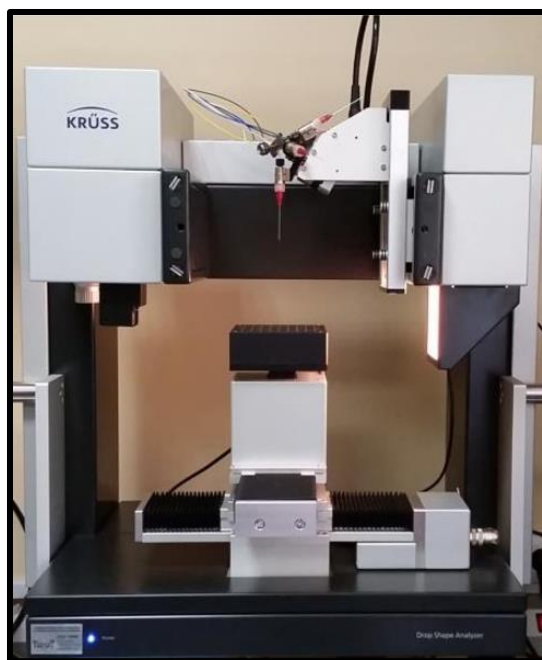


**Figure 3.15.** DSA100-E KRÜSS for measuring the contact angle.

### **3.13. Computational analysis**

#### **3.13.1. Quantum chemical evaluation**

Quantum chemical methods, and more specifically density functional theory (DFT), are increasingly used to describe molecular properties, understand the mechanism of action and predict the effectiveness of corrosion inhibitors. DFT is a widely used theoretical approach in the field of materials science, including corrosion inhibition<sup>245,246</sup>. DFT calculations can provide valuable insights into the electronic structure and reactivity of materials, which can be used to predict their function as corrosion inhibitors. In the context of corrosion inhibition, DFT can be utilized to explore the interaction across a potential inhibitor and a metal surface. By calculating the electronic properties of the inhibitor and the metallic substrate, DFT can predict the strength of the adsorption of the inhibitor onto the surface, as well as the inhibition efficiency. In this investigation, all quantum chemistry calculations and visualization of results were performed utilizing the Dmol<sup>3</sup> module incorporated into the Biovia Materials studio software. The geometric configurations of the investigated molecules were attained by global optimizations characterized by a calculation of the vibration frequencies using the DFT method (utilizing Dmol<sup>3</sup>, comprising the B3LYP/ DND / COSMO (water) model). Several quantum chemical parameters like  $E_{LUMO}$ ,  $E_{HOMO}$ ,



electronegativity ( $\chi$ ), electronic affinity (A), global hardness ( $\eta$ ), softness ( $\sigma$ ) and ionization potential (I) were computed by using the equations (11)–(17) to assess the overall reactivity of the examined extract.

$$\Delta E = E_{\text{HOMO}} - E_{\text{LUMO}} \quad (11)$$

$$I = -E_{\text{HOMO}} \quad (12)$$

$$A = -E_{\text{LUMO}} \quad (13)$$

$$\eta = \left( \frac{I - A}{2} \right) \quad (14)$$

$$\chi = \left( \frac{I + A}{2} \right) \quad (15)$$

$$\sigma = \frac{1}{\eta} \quad (16)$$

$$\Delta N = \frac{\chi_{\text{Fe}} - \chi_{\text{Inh}}}{2(\eta_{\text{Fe}} - \eta_{\text{inh}})} \quad (17)$$

Here,  $\chi_{\text{inh}}$  and  $\eta_{\text{inh}}$  denote the electronegativity and hardness of the inhibitor,  $\eta_{\text{Fe(110)}} = 0\text{eV}$  and  $\Phi_{\text{Fe(110)}} = 4.82\text{ eV}$  were applied to determine the proportion of electron transmission ( $\Delta N$ ), correspondingly.

### 3.13.2. Molecular Dynamics (MD) and Monte Carlo (MC) Simulations

MD and MC simulations are useful tools for investigating the mechanisms of corrosion inhibition and designing new corrosion inhibitors. MD simulations can be used to study the interaction across a corrosion inhibitor and the metallic substrate at the atomic or molecular level. For example, researchers can use MD simulations to study the adsorption of the inhibitor over the metallic substrate, the production of a defensive layer, and the effect of the inhibitor on the electrochemical properties of the metal<sup>94,247–249</sup>. MC simulations, on the other hand, can be used to study the thermodynamics of the inhibitor-metal system. MC simulations can calculate the free energy of

the inhibitor-metal interface, which can be used to predict the effectiveness of the inhibitor and the stability of the protective film. MC simulations can also be utilized to explore the impact of different inhibitors and their concentrations on the corrosion rate. Both MD and MC simulations can be used to design new corrosion inhibitors. Researchers can use MD simulations to screen potential inhibitors and select the most promising candidates for further investigation. MC simulations can then be used to optimize the structure and concentration of the inhibitor to maximize its effectiveness. In this investigation, we performed MC and MD simulations using the package Materials Studio 8.0. For the simulations of the adsorption modes of the molecules investigated on the Fe surface in this study, we choose the Fe(1 1 0) surface. The simulation box employed to carry out the MD simulations had the dimensions (24.823 × 24.823 × 18.241 Å). The iron slice and the number of water molecules comprising the studied compound are associated with the simulation box. Before starting the simulation, the surface of Fe(1 1 0) and the molecular geometry of the compounds studied were simulated by minimizing the energies. Using the COMPASS III (Edition 1.0) force field, MD simulations were carried out at 298 K using the NVT setup, a phase stride of 1 fs, and a simulation duration of 800 ps. This model included a Fe layer, 10 hydronium ions, 10 chloride ions, 800 H<sub>2</sub>O molecules and 1 inhibitor molecule and a 35-vacuum layer included in the simulation box. The adsorption energy ( $E_{ads}$ ) was deduced from Equation 18 to offer a quantifiable estimate of the incidence of this phenomenon.

$$E_{ads} = E_{(110)/inhibitor} - (E_{(110)} + E_{inhibitor}) \quad (18)$$

### 3.14. Biodegradability determination

A concise investigation of the biodegradability of the corrosion inhibitor is often practiced nowadays. It is well known that one of the key requirements of the excellent and green corrosion inhibitor is its biodegradability i.e., the rate at which it biodegrades up to an acceptable extent following a certain duration<sup>250</sup>.

#### 3.14.1. Preparation of inoculum

In this part, 200 g of plant field soil was dissolved in 2L of distilled H<sub>2</sub>O, stirred consistently, and allowed to rest for 2 hrs to obtain the supernatant.

#### 3.14.2. Buffer media formulation

The phosphate buffer medium was procured with dispersing 8.5g  $\text{KH}_2\text{PO}_4$ , 44.6g  $\text{Na}_2\text{HPO}_4 \cdot 12\text{H}_2\text{O}$ , 21.8g  $\text{KH}_2\text{PO}_4 \cdot 3\text{H}_2\text{O}$  and 1.7g  $\text{NH}_4\text{Cl}$  in 1L distilled  $\text{H}_2\text{O}$ . Afterward, in 1L distilled  $\text{H}_2\text{O}$ , 11.0g  $\text{MgSO}_4$ , 0.25g  $\text{FeCl}_3 \cdot 6\text{H}_2\text{O}$  and 27.6g  $\text{CaCl}_2$  were blended, correspondingly.

### 3.14.3. Dilution of $\text{H}_2\text{O}$

An oil-free air compressor was used to oxygenate 1L of distilled  $\text{H}_2\text{O}$  until the available oxygen content acquired  $8 \text{ mg L}^{-1}$ . At that point, 1mL of each of the following solutions were added:  $\text{MgSO}_4$ , phosphate buffer solution, iron chloride and  $\text{CaCl}_2$  solution.

A certain amount of the substance to be examined was added to a 500 mL serum container together with  $\text{H}_2\text{O}$  (280 mL), and inoculum (30 mL) and it was then cultured at ambient temperature. The blank assessment was conducted concurrently. The COD contents in the medium contained in the serum vessel were assessed at intervals of 1, 7, 14, 21, and 28 days. The biodegradation rate ( $\eta$ ) was calculated using the below equation (19):

$$\eta = \left( 1 - \frac{C_t - C_{it}}{C_0 - C_{i0}} + \dots \right) \times 100\% \quad (19)$$

Here,  $C_t$  resembles the assessment of COD concentration on day t,  $C_{it}$  resembles the assessment of COD concentration in the blank assessment on day t,  $C_0$  resembles the assessment of COD concentration on day 1, and  $C_{i0}$  resembles the assessment of COD concentration in the blank assessment on day 1.

---

---

**Chapter 4**  
**Results and Discussion**

---

---

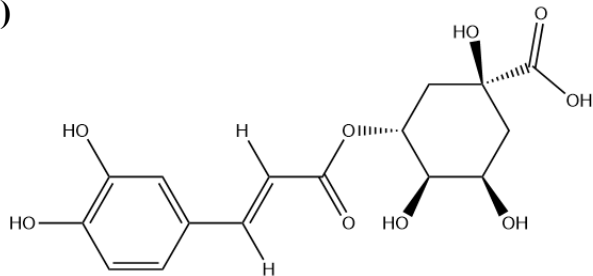
#### 4.1. *Cnicus Benedictus*

*Cnicus Benedictus* weed (Kingdom: Plantae; Subkingdom: Tracheobionta; Superdivision: Spermatophyta; Division: Magnoliophyta; Class: Magnoliopsida; Subclass: Asteridae; Order: Asterales; Family: Asteraceae/Compositae; Genus: *Cnicus*; Species: *Cnicus benedictus* L.) is a thistle-like weed in the family Asteraceae commonly known as blessed thistle. This weed could grow to a height of 30 to 50 cm. The stems are thickly branched, thistle-like, villous, and pubescent in texture. The leaves are approximately reticulate, elongated, emarginated to pinnatifid, thorny-dentated and emarginated to pinnatifid. Over the decades, it has been utilized for this purpose in both European traditional herbalism and India's Ayurvedic medicinal culture. It is primarily used as a tonic to treat dyspepsia, flatulence, and indigestion. According to the previous investigation<sup>251</sup>, *Cnicus Benedictus* extract (CBE) contains a significant proportion of phenolic acids, primarily chlorogenic acid and sinapic acid as shown in **Figure 4.1**. In this research *Cnicus Benedictus* (India), which is widely obtainable in several countries has been investigated as an eco-benign and sustainable corrosion inhibitor for mild steel in a 0.5 M HCl corrosive media. To our awareness and knowledge, none mild steel protection with CB extract (CBE) has been documented in a 0.5 M HCl media, considered among the most aggressive corrosive media. If CB aerial parts are utilized as a sustainable corrosion inhibitor for mild steel in an acidic medium, it not only recycles resources and reduces the cost of corrosion inhibitors, but also promotes CB cultivation enormously. The most essential fact is that there is very minimal harm to humans and the environment. Hence, to evaluate the inhibition performance of CBE, electrochemical, spectroscopic and microscopic techniques have been carried out in this work.

(a)



(b)



(c)

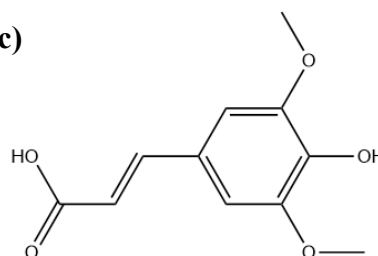


**Figure 4.1.** Depiction of (a) *Cnicus Benedictus*, Chemical structures of (b) Chlorogenic acid, (c) Sinapic acid.

#### 4.1.1. Preparation of *Cnicus Benedictus* extract

*Cnicus Benedictus* weed was gathered from the farm in Kapurthala, Punjab and was validated by Dr. Neera Rashmi, Department of Botany, Himachal Pradesh University, Himachal Pradesh, India. For the extraction technique, desiccated aerial portions were crushed (10 g), blended with 50 % (v/v) ethanol in H<sub>2</sub>O as the solvent and agitated for five minutes. After that, the extraction was carried out in a sonication water bath for 90 minutes using ultrasonic-assisted extraction (UAE) (Elma Transsonic T460, Germany). After it, the extract was filtered via filter paper microfiltered with 0.45 m poresizemicro-steps to condense essential bioactive-rich constituents containing the extract<sup>251</sup>. The acquired CB extract reached the maximum solubility in 0.5 M HCl up to 1000 mg/L. Finally, the residue obtained was stored at -20°C till further analysis was done.

### 4.1.2. FT-IR analysis

The availability of heteroatoms (O), the aromatic ring, might increase the inhibitor molecule's adsorption over the metallic substrate, hence reducing corrosion. The FTIR spectra of the CBE are shown in **Figure 4.2**. The FTIR spectra of the CBE show the  $3360\text{ cm}^{-1}$  corresponds to the O–H stretching vibration, and the broader peak width attributed that molecular association had taken place. The stretching vibration of C–H was noticed at  $2926\text{ cm}^{-1}$ . The peak at  $1062\text{ cm}^{-1}$  was attributed to the –C–O stretch. The peaks at  $2856\text{ cm}^{-1}$ ,  $1726\text{ cm}^{-1}$ ,  $1651\text{ cm}^{-1}$  and  $1456\text{ cm}^{-1}$  attributed to the –O–CH<sub>3</sub>, –C=O and –C=C stretch. Moreover, peaks at  $1259\text{ cm}^{-1}$  and  $902\text{ cm}^{-1}$  correspond to –C–O–H bend and =C–H bend. These findings suggested that CBE has oxygen in its functional groups (O–H, C=O, C–O), consistent with typical corrosion inhibitor structures. This prevalence in CBE is attributable to the superior corrosion inhibition property of CBE on mild steel in 0.5M HCl.

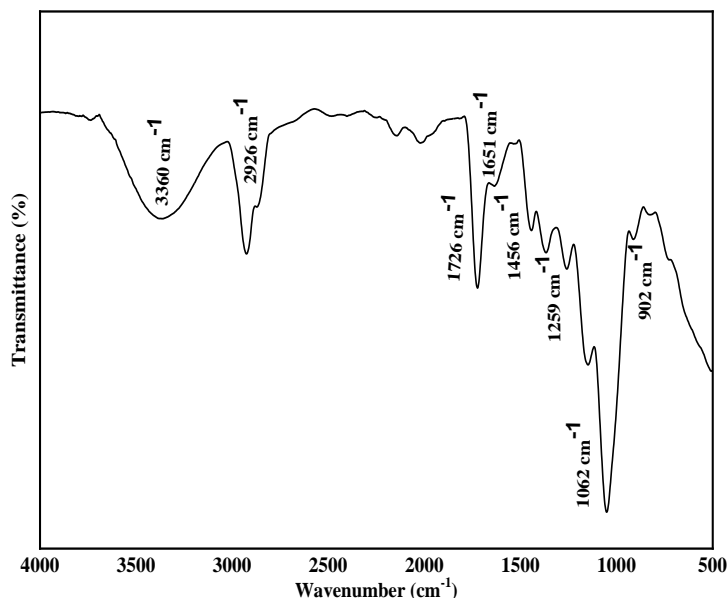


**Figure 4.2.** FTIR evaluation of the CBE.

### 4.1.3. Uv-visible spectrometry

The Uv spectra of CBE were evaluated before and after the corrosion analysis as depicted in **Figure 4.3**. The absorbance of the corrosive medium where the mild steel sample was not immersed was higher than the arrangement where the sample was dipped for 24 hours, as per the

Uv spectra. It is apparent that after immersing the metallic sample in the acidic CBE solution, a few of the solution's molecules were adsorbed upon the metal's surface, indicating that mild steel could possess a significant corrosion inhibition efficiency.

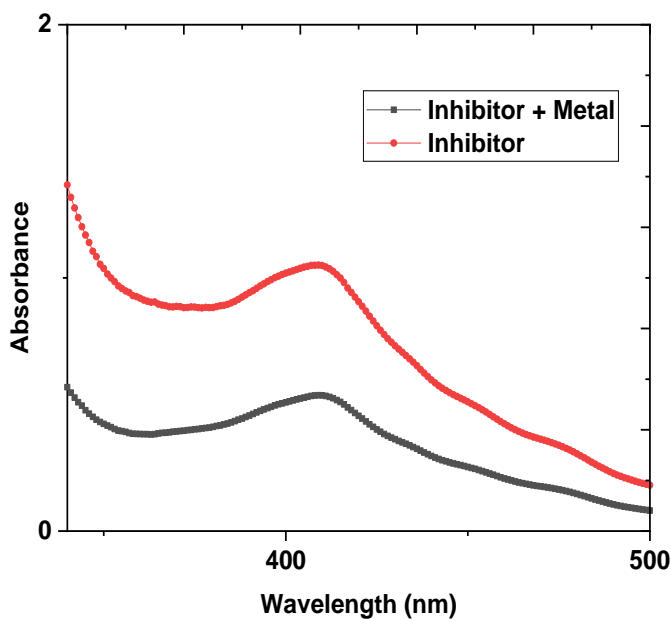


**Figure 4.3.** UV Spectra of CBE before and after the metal immersion.

#### 4.1.4. Weight loss measurements

The weight-loss technique of measuring IE and  $C_R$  is valuable owing to its ease of use and superior reliability. Herein, weight loss investigations were experimented with in the exclusion and inclusion of the inhibitor in 0.5M HCl media at 298K to examine the effect of time, temperature and inhibitor concentration on the inhibition efficacy of CBE<sup>252,253</sup>. **Tables 4.1, 4.2, 4.3,** and **Figure 4.4** shows the effect of duration, temperature and concentration on inhibitor efficacy against metallic corrosion in 0.5 M HCl. In 0.5M HCl, the extract had a maximum inhibitory efficacy of 92.45% at an optimal concentration of 1000 ppm. **Tables 4.1, 4.2, and 4.3** summarises the IE and  $C_R$  attained from the weight loss technique at various concentrations of CBE at 298K. Through **Figure 4.4**, it could be concluded that on the increasing concentration of CBE, the IE% also increases. Although, with respect to the increase in time and temperature, the IE% of CBE decreases owing to the desorption of inhibitor molecules at higher temperature and increasing time. Equations (1-3) were used to calculate  $C_R$ , IE% and  $\Theta$ .



**Table 4.1**

Effect of time on the inhibition efficiency of mild steel in 0.5M HCl in the absence and presence of 1000ppm inhibitor at 298K.

Time (min.)	W <sub>0</sub> (mg)	W <sub>i</sub> (mg)	W <sub>0</sub> -W <sub>i</sub> (mg)	IE%
15	1.433	1.324	0.109	89.034
30	1.412	1.245	0.167	82.658
45	1.478	1.181	0.297	74.766
60	1.426	1.021	0.405	64.411

**Table 4.2**

Effect of temperature on the inhibition efficiency of mild steel in 0.5M HCl in the absence and presence of 1000ppm of inhibitor.

Temp. (K)	W <sub>0</sub> (mg)	W <sub>i</sub> (mg)	W <sub>0</sub> -W <sub>i</sub> (mg)	IE%
298	1.524	1.436	0.088	90
308	1.398	1.211	0.187	81
318	1.523	1.102	0.421	61.80
328	1.543	0.923	0.62	55.49

**Table 4.3**

Effect of concentration on the inhibition efficiency of mild steel in 0.5M HCl in the absence and presence of inhibitor (100-1000ppm at 298K).

Conc. (ppm)	W <sub>0</sub> (mg)	W <sub>i</sub> (mg)	W <sub>0</sub> -W <sub>i</sub> (mg)	C <sub>R</sub>	Θ	IE%
Blank	1.934	0.834	1.1	3.06879	-	-
100	1.834	1.41	0.424	1.1828	0.6145	61.454
250	1.743	1.44	0.303	0.8453	0.7245	72.454
500	1.798	1.62	0.178	0.4965	0.8381	83.818
1000	1.793	1.71	0.083	0.2315	0.9245	92.454

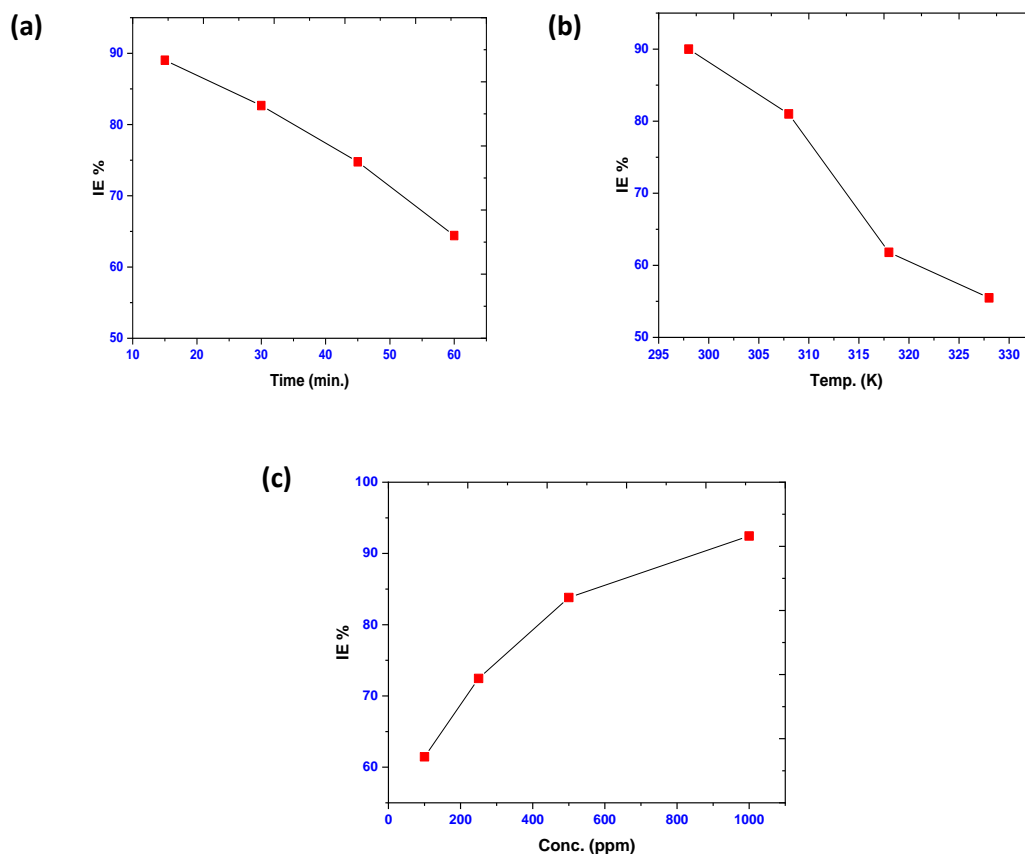


**Figure 4.4.** Effects of (a) time, (b) temperature and (c) concentration variation on inhibition efficiency.

#### 4.1.5. Adsorption and thermodynamic parameters

The potency of a corrosion inhibitor could be determined by its potential towards the reduction of the corrosion of metals by adsorption at the metal/solution interface, whereas the main characteristics of interaction among the inhibitor and the metallic surface could be determined by implying the adsorption isotherm<sup>28,33,254–256</sup>. As can be seen in the plot of  $C/\theta$  Vs.  $C$ , the value of  $R^2$  was determined to be equivalent to 1 (i.e., 0.99498) resulting in a straight curve with a regression coefficient of approximately 1, as shown in **Figure 4.5(a)**<sup>14</sup>. This behavior demonstrated that inhibitor adsorption upon the mild steel surface in a corrosive media accompanied the Langmuir adsorption isotherm implying that when the inhibitor component is

adsorbed on the metal/solution interface, it encompasses a typical adsorption region, mitigating corrosion induced by the corrosive medium<sup>257</sup>. The occurrence of Langmuir adsorption isotherm implies that a thin monolayer forms on the mild steel surface. The findings of this investigation are summarised in **Table 4.4**. The activation energy value was measured by employing slopes ( $-E_a/2.303R$ ) from the  $\log C_R$  versus  $1/T \cdot 10^{-3}K$  in **Figure 4.5(b)**. The kinetic parameters were determined by employing the Arrhenius equation<sup>6,258</sup>. As shown in **Figure 4.5(c)**, the enthalpy value was estimated using the  $\log K_{ads}$  vs.  $1/T \cdot 10^{-3}K$  plot, which provided a linear curve with a slope of  $-H/2.303R$ . These parameters have been obtained using equations (5) and (6). The values of Gibb's free energy and adsorption entropy were measured using equations (7) and (8).

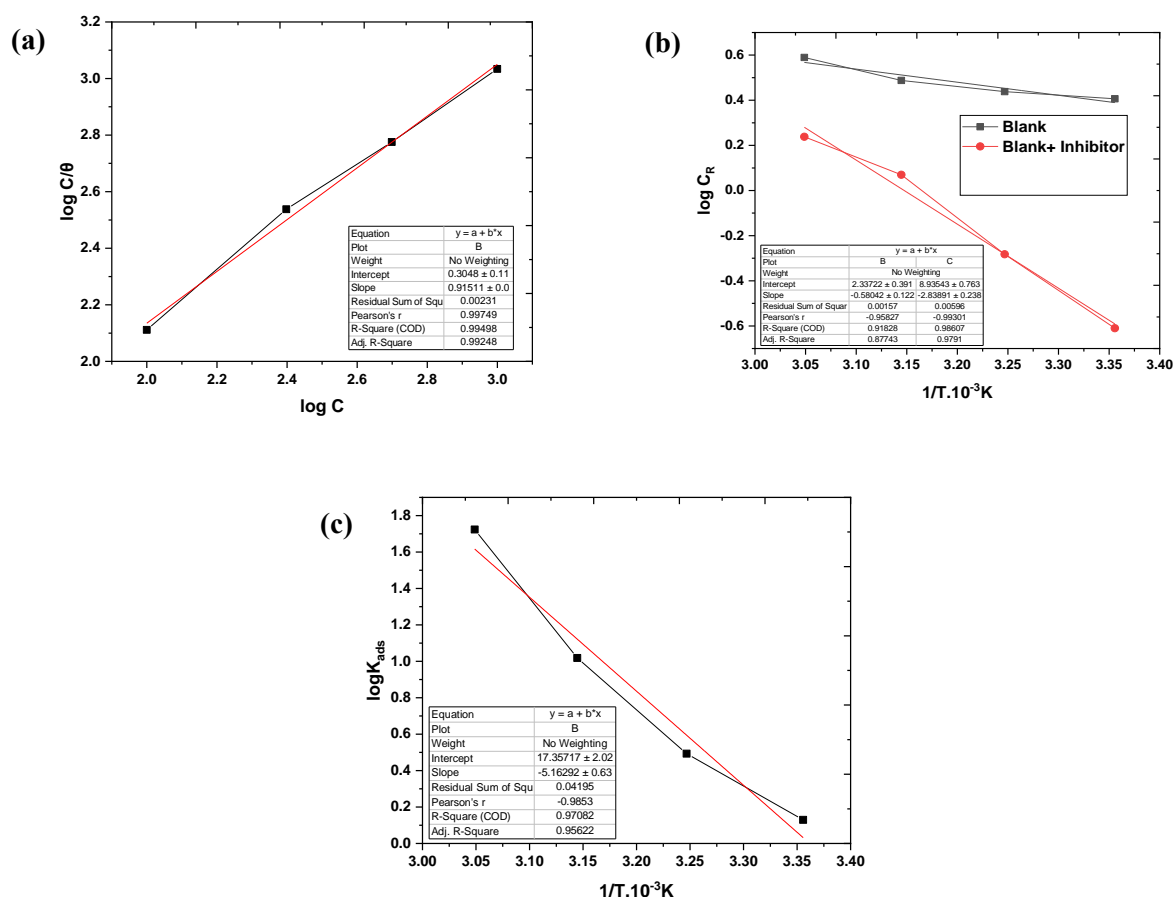


**Figure 4.5.** (a) Langmuir adsorption plot (b) Arrhenius plot (c) Enthalpy plot CB extract as corrosion inhibitor of mild steel in 0.5 M HCl solution.

**Table 4.4**

Adsorption, kinetic and thermodynamic parameters for CB (1000 ppm) as corrosion inhibitor for mild steel in 0.5 M HCl media in 298K.

Metal	Inhibitor (ppm)	log $K_{ads}$	$\Delta G^{\circ}_{ads}$ KJmol <sup>-1</sup>	$\Delta H^{\circ}_{ads}$ KJmol <sup>-1</sup>	$\Delta S^{\circ}_{ads}$ kJ.mol <sup>-1</sup> .K <sup>-1</sup>	$E_a$ KJmol <sup>-1</sup>	$R^2$
Mild steel	Blank	-	-	-	-	19.432	0.97082
	100ppm	0.129	-0.739	0.0429	0.144	32.763	
	250ppm	0.493	-2.812				
	500ppm	1.018	-5.794				
	1000ppm	1.724	-9.836				

**Table 4.4** shows that a greater  $E_a$  value than without inhibitors indicates the formation of an adsorption layer on the mild steel surface, which acts as a physical barrier to mass and charge transfer. The existence of a positive value for  $\Delta H^{\circ}_{ads}$  suggested that mild steel dissolving comprised of an endothermic process, implying that mild steel is hard to disintegrate. Furthermore, the value of  $\Delta S^{\circ}_{ads} < 0$  revealed that the adsorption process was stagnant and the development of the complex compound was linked to the rate-determining step, implying that the disorder diminishes following the creation of the complex compound, allowing H<sub>2</sub>O molecules to desorb. Furthermore, the significant  $K_{ads}$  values increment indicate that inhibitor molecules and metal surfaces have strong interactions<sup>259-261</sup>.

#### 4.1.6. Electrochemical measurements

##### 4.1.6.1. Open circuit potential (OCP)

Before proceeding with the potentiodynamic polarisation (PDP) and electrochemical impedance spectroscopy (EIS) investigations, it is critical to attain a steady OCP. During each concentration gradient experiment, the working electrode (mild steel rod) was dipped in the test solution for the duration of 1hr. **Figure 4.6** illustrates the OCP vs. time curves (sec.) in the exclusion and inclusion of several concentrations of CBE. In addition of CBE, it was evidently noticed that the OCP values propagate near the anode potential, which might be accounted by CBE adsorption on the metallic surface. After the OCPs had stabilized for a brief time, the PDP and EIS investigations were performed.

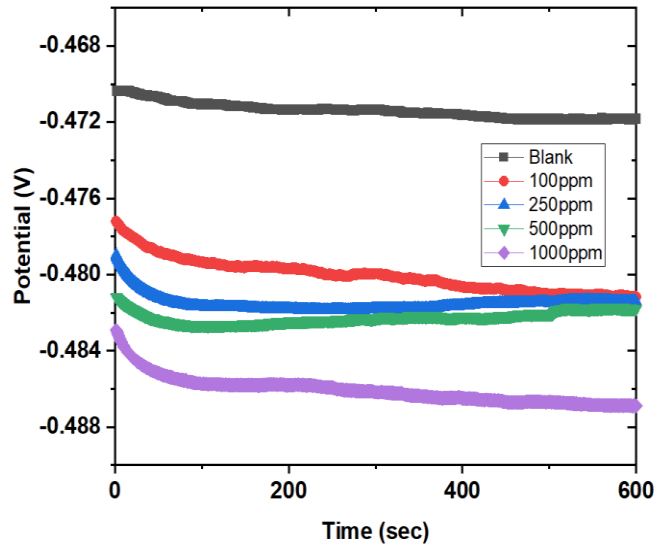


**Figure 4.6.** OCP vs time plot time plots for mild steel in 0.5 M HCl without and with various concentrations of CBE (100-1000ppm).

#### 4.1.6.2. Potentiodynamic polarization

The potentiodynamic polarization methodology was utilized to examine the influence of CBE on the anodic dissolution of mild steel and the cathodic hydrogen ions reduction process in 0.5M HCl solution<sup>262</sup>. **Figure 4.7** shows the polarization plots. The potential kinetic parameters as listed in **Table 4.5**, including corrosion potential ( $E_{\text{corr}}$ ), corrosion current densities ( $i_{\text{corr}}$ ), the cathode Tafel slope ( $\beta_c$ ) and anode Tafel slope ( $\beta_a$ ) values were attained from the evaluation of corresponding polarization curves. With increasing concentrations of CBE (100-1000ppm) and reducing values of  $C_R$  from 7.4114 to 0.97438, it is clear that the value of  $i_{\text{corr}}$  decreased significantly. This revealed that as the inhibitor concentration was increased, the protective function of inhibitors on mild steel steadily improved<sup>263-265</sup>. The polarization curves of the cathode and anode were distinct in the inclusion of inhibitor contrasted to those without inhibitor, as shown in **Figure 4.7**. These results demonstrated that inhibitors not only reduced metal dissolution but also impeded the hydrogen evolution reaction. Moreover, the polarisation curve revealed that the cathode's alteration was more noticeable than that of the anode. Furthermore, when compared to the curve acquired in the exclusion of inhibitor, the corrosion potential ( $E_{\text{corr}}$ ) migrated towards the cathode with the significant change of  $E_{\text{corr}}$  being 496.83 mV. As a result, CBE tends to be a mixed corrosion inhibitor centered on the cathode in 0.5 M HCl as a result. **Figure 4.7** further shows that

the cathode Tafel curves are nearly parallel as the inhibitor concentrations increase. **Table 4.5** also demonstrates that the cathode Tafel slope ( $\beta_c$ ) and anode Tafel slope ( $\beta_a$ ) values rarely varied, implying that the mechanism of hydrogen evolution remained unchanged when the inhibitors were applied. This could be because the inhibitor molecule covers the mild steel surface, decreasing the number of active sites for the reaction but maintaining the mechanism of hydrogen evolution by charge transfer unchanged<sup>42,76</sup>.

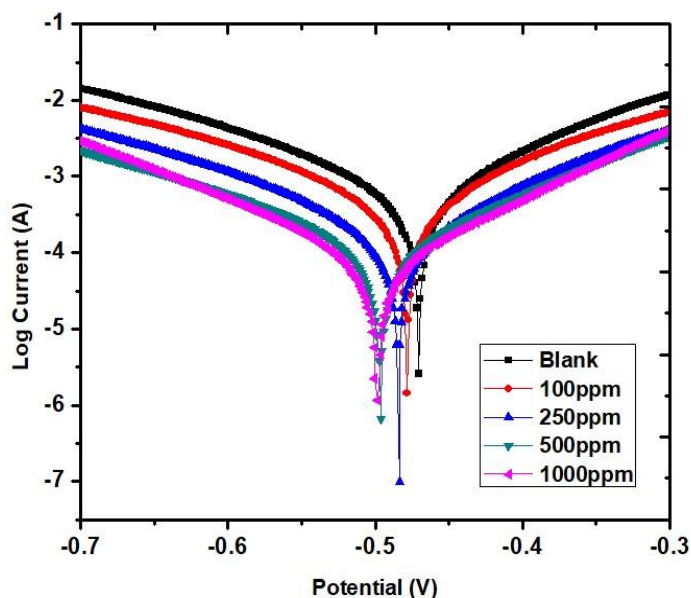


**Figure 4.7.** Tafel plot for mild steel corrosion inhibition in 0.5M HCl media subjected to several concentrations of inhibitor at 298 K.

**Table 4.5**

Corrosion parameters for mild steel in 0.5 M HCl in the exclusion and inclusion of CBE attained through electrochemical experiments (EIS and Tafel) at 298K.

Conc. (ppm)	$-E_{\text{corr}}$ (mV vs. SCE)	$i_{\text{corr}}$ ( $\mu\text{A}$ )	$j_{\text{corr}}$		$C_R(\text{mmy}^{-1})$	$\chi^2$	
			( $\mu\text{A}/\text{cm}^2$ )	$\beta_a(\text{mV}/\text{dec})$			$-\beta_c(\text{mV}/\text{dec})$
Blank	468.93	637.82	637.82	125.93	151.98	7.4114	7.4131E-08
100	476.25	481.72	481.72	141.49	163.98	5.5976	1.0223E-07
250	482.22	171.2	171.2	126.56	135.43	1.9893	2.2005E-08
500	496.68	127.79	127.79	142.79	147.1	1.4849	6.8018E-09
1000	496.3	83.854	83.85	125.42	127.15	0.97438	3.73E-09

#### 4.1.6.3. Electrochemical impedance spectroscopy (EIS)

The EIS investigations of mild steel in 0.5 M HCl with varied concentrations of CBE were conducted to confirm the findings attained from the weight loss and PDP measurements and to discover more insights about the corrosion mechanism. The significant results are reported in **Table 4.6**. **Figures 4.8** and **4.9** show Nyquist and Bode's plots, respectively. The Nyquist plot impedance spectra featured a huge capacitive loop at high frequencies and an inductive loop at low frequencies. The charge transfer reaction and surface inhomogeneity, induced the high-frequency capacitive loop, while the low-frequency inductive loop could be attributable to the relaxation phase induced by  $\text{H}_{\text{ads}}^+$ ,  $\text{Cl}^-$  and corrosion inhibitor molecules adsorption over the metal surface. The re-dissolution of the passivated surface at low frequencies could possibly be the reason. Whether there was the inclusion of inhibitor or not, the pattern of all the graphs in the Nyquist diagram remained similar, indicating that the mild steel corrosion mechanism had not changed. To look at it another way, corrosion was primarily a charge transfer process. Furthermore, due to the frequency dispersion and roughness and inhomogeneity of the electrode surface, their shapes were suboptimal. The diameters of these semicircles increased as CBE concentrations increased (100-1000ppm) indicating the higher coverage of CBE on the electrode's surface, leading to significant protection of the electrode surface.

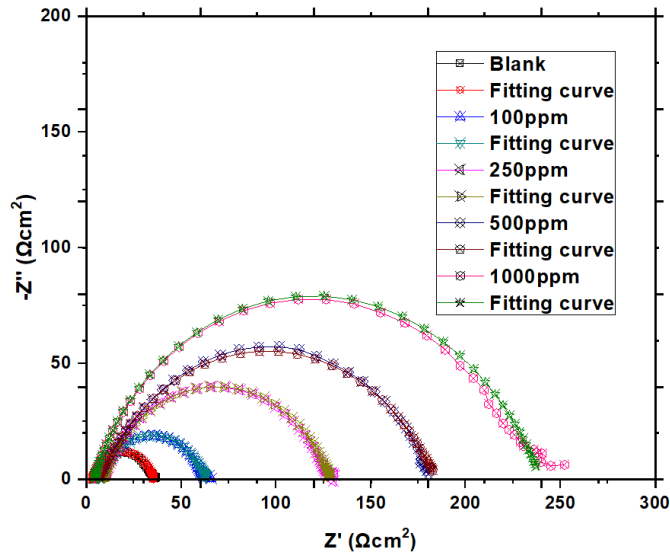


**Figure 4.8.** Nyquist plot for the mild steel corrosion inhibition in 0.5M HCl subjected to different inhibitor concentrations at 298 K.

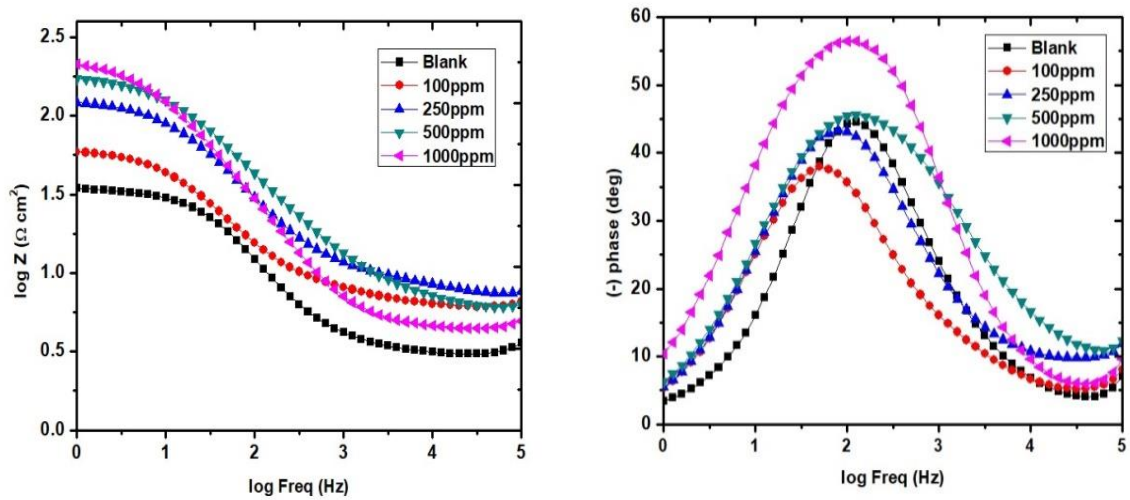


**Figure 4.9.** Bodes plots for the mild steel corrosion inhibition in 0.5M HCl subjected to various concentrations of inhibitor at 298 K.

**Figure 4.10** shows the equivalent circuit utilized to fit the EIS data.



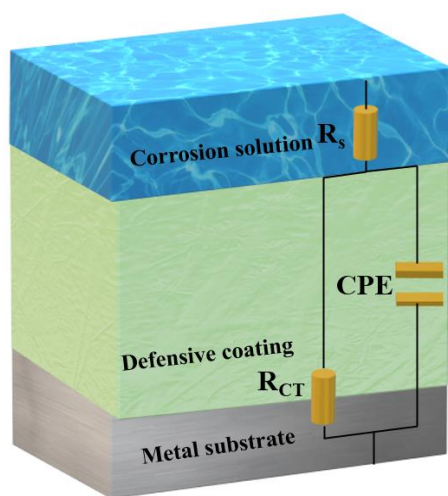


**Figure 4.10.** An equivalent circuit diagram was utilized to fit the data.

**Figure 4.9** shows the Bode plots for the mild steel in the presence and absence of various concentrations of CBE (100-1000ppm) with the inclusion of 0.5 M HCl solution at 298K. The Bode plots revealed that there was just one time constant. Moreover, throughout the frequency range used in this study, the impedance modulus increased as the CBE concentration increased. The frequency band of the maximum phase angle increased as well. All of these findings showed that CBE provided excellent corrosion protection for mild steel in the 0.5 M HCl corrosive media. As per the previous reports<sup>252,253,266,267</sup>, if the slope of  $\log |Z|$  vs.  $\log f$  tends to be  $-1$  and the highest phase angle comes out to be  $90^\circ$  then ideal capacitance at an intermediate frequency could be assured. This showed that in a 0.5 M HCl media, CBE had an excellent corrosion inhibitory effect on mild steel.

**Table 4.6** summarises the EIS parameters, where  $R_{ct}$  indicates charge transfer resistance,  $R_s$  means solution resistance (the resistance of the working electrode to the counter electrode),  $n$  denotes phase shift, CPE represents the constant phase element and  $\chi^2$  represents the deviation degree of the equivalent circuit fitting. Values of  $\chi^2$  between  $10^{-3}$  and  $10^{-5}$  have been reported to be compatible with optimal fitting, indicating that the equivalent circuit diagram is stable and reliable. According to **Table 4.6**, with the increased concentration of CBE, the charge transfer resistance ( $R_{ct}$ ) and corrosion IE% increased attaining maximum corrosion inhibition efficiency of 86% at 1000ppm, which is nearly identical to the findings of the weight loss and potentiodynamic

polarisation investigations. The  $R_s$  value did not change substantially after the inhibitor was introduced. Furthermore, the phase shift values,  $n$  (0.82358–0.75094) did not change significantly, indicating that charge transfer controlled mild steel dissolution in a 0.5 M HCl media.

**Table 4.6**

Inhibition efficiency values of CBE inhibitor for mild steel in various conc. of inhibitor.

Conc (ppm)	CPE/Yo ( $\mu\text{F}$ )	$n$	$R_s(\Omega)$	$R_p(\Omega)$	$R_{ct}$ in ( $\Omega$ )	$R_{ct}$ bl ( $\Omega$ )	$\chi^2$	IE (%)
Blank	155.4	0.82358	3.0284	31.589	-	32.763	0.084244	-
100	199.28	0.74802	5.8447	56.859	57.579	32.763	0.14203	43.090
250	87.544	0.74885	7.5247	120.23	123.343	32.763	0.2854	73.437
500	59.972	0.73967	5.4522	175.79	174.787	32.763	0.13864	81.255
1000	98.508	0.75094	4.2462	233.36	247.232	32.763	0.097033	86.748

#### 4.1.7. Surface analysis

##### 4.1.7.1. SEM

The morphology of mild steel samples following 4 hrs of immersion in 0.5M HCl solution with and without inhibitor was examined using surface electron microscopy (SEM) and the results are illustrated in **Figure 4.11**. **Figure 4.11(a)** illustrates a flat perspective of an SEM micrograph of a plain steel specimen that has not been treated. **Figure 4.11(b)** depicts a flat perspective of an SEM micrograph of the blank specimen (without inhibitor), which has a highly rough surface with corrosion products on it. This means that the blank steel surface is highly defective and depicted degradation due to corrosion. In the case of **Figure 4.11(c)**, with the introduction of inhibitor, the surface was effectively protected and the surface damage was not observed as compared with the blank specimen. In other words, SEM observations revealed a stranded inhibitive layer on the metallic surface with reduced permeability for aggressive ions.

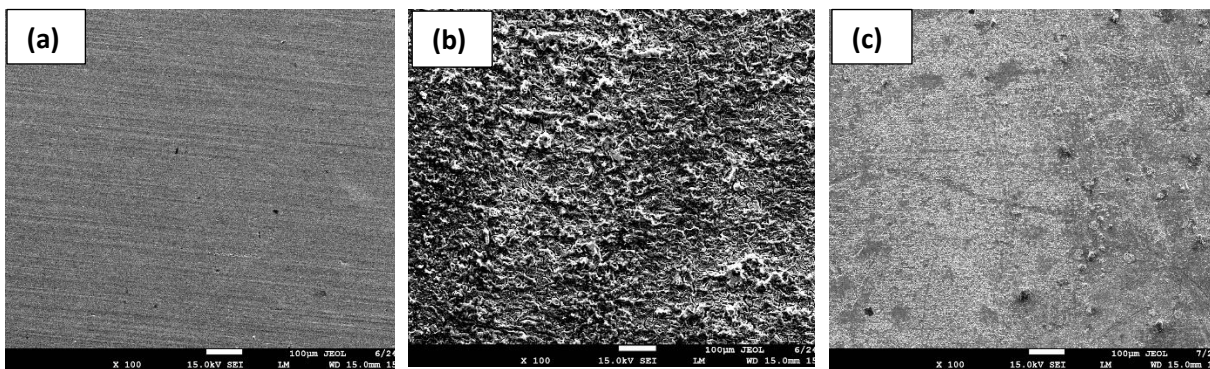


**Figure 4.11.** SEM images of (a) plain mild steel, (b) mild steel dipped in 0.5 M HCl without inhibitor (c) mild steel in 0.5 M HCl immersed in 1000ppm of inhibitor solution.

#### 4.1.7.2. Contact angle (CA) measurement

CA measurements provide additional information on phenomena such as wetting, adhesion, and absorption over the metallic surface<sup>268</sup>. In this work, the hydrophilicity/hydrophobicity of the uninhibited and inhibited metallic surfaces was determined using CA measurements. The images produced by CA observations on the metallic surface without and with 1000ppm of CB extract, respectively, are shown in **Figure 4.12 (a)** and **(b)**. According to the findings, the contact angle for mild steel specimens treated using CB extract improved ( $82.36^\circ$ ) when contrasted to mild steel samples treated with a basic acidic media ( $68.39^\circ$ ). As a result, before being exposed to CB extract, mild steel's surface was less hydrophobic (**Figure 4.12 (a)**), but it became more hydrophobic thereafter (**Figure 4.12 (b)**). Due to abrasive element's adsorption on the metallic surface in acidic environments, mild steel surfaces have a low hydrophobicity, leading to corrosion. Adsorption of inhibitor compounds may have altered surface tension, resulting in hydrophobicity and thus exhibiting the development of a protective coating over the metallic surface to protect it against corrosion.

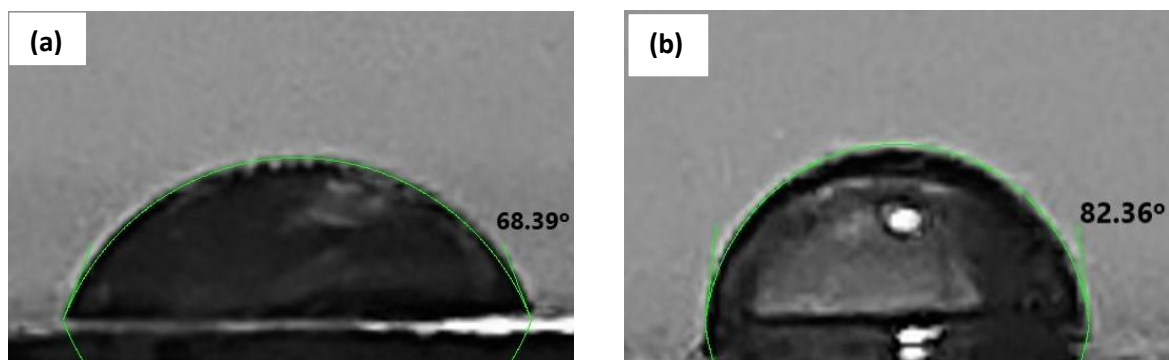


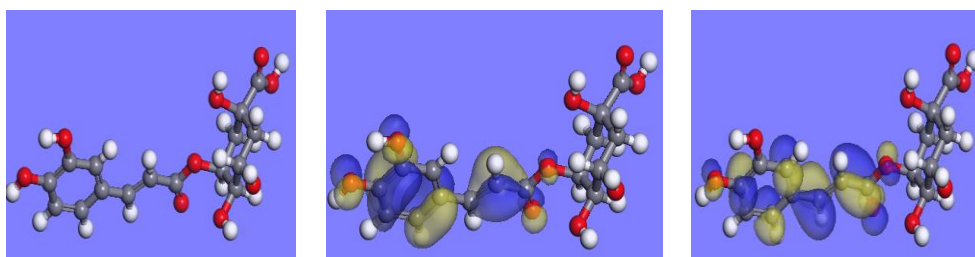
**Figure 4.12.** Contact angle measurement was done on the metal sample in (a) blank solution and (b) blank solution+inhibitor.

#### 4.1.8. DFT and MC simulations

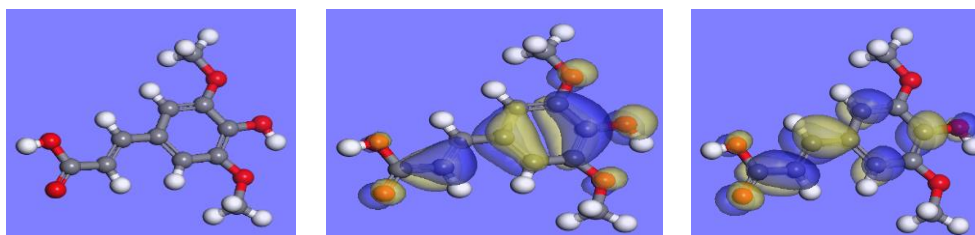
As previously discussed, this approach is a useful tool for understanding the reaction mechanism between atoms on a metal surface and an inhibiting molecule. Herein, the Forcite module (Materials Studio 2017 software) has been utilized to model the system. **Figure 4.13** and **Table 4.7** show the optimized geometries and parameters of the molecules. The maximum value of  $E_{\text{HOMO}}$  indicates a molecule's ability to transfer electrons, whereas low  $E_{\text{LUMO}}$  values indicate a molecule's ability to accept electrons. Through **Table 4.7**, it could be observed that the chlorogenic acid and Sinapic acid offered high  $E_{\text{HOMO}}$  and lower  $E_{\text{LUMO}}$  values which render to their ability to transmit and accept electrons while interacting with the metallic surface. The energy gap ( $\Delta E$ ), which is another significant metric to analyze and justify the stability index of a corrosion inhibitor, is also denoted by the fluctuation between  $E_{\text{HOMO}}$  and  $E_{\text{LUMO}}$  energies. In both cases, the lower ( $\Delta E$ ) values such as 2.995000 and 3.030265 exhibit the better mutual interaction between the inhibitor and the Fe surface, thus having a significant corrosion inhibition characteristic. The chemical hardness<sup>269</sup> is reported as the resistance towards electron cloud polarization of atomic and molecular systems. According to the Hard and Soft Acid-Base (HSAB) Principle, “Hard acids prefer the binding to hard bases and soft acids prefer the binding to soft bases. Soft molecules exhibit higher polarization and electron-donating power compared to hard ones. For that reason, an effective corrosion inhibitor should be highly soft. The maximum Hardness Principle stating that “There seems to be a rule of nature that molecules arrange themselves to be as hard as possible.” presents the close relationship between chemical hardness and chemical reactivity<sup>270</sup>. This principle implies that hard molecules are more stable compared to soft ones. According to

calculated chemical hardness values, it can be said that both molecules are effective corrosion inhibitors but the corrosion inhibition performance of sinapic acid may be higher than that of chlorogenic acid. Electronegativity is a measure of the electron withdrawal powers of chemical systems. Chemical systems with high electronegativity values are not effective against the corrosion of metal surfaces. The obtained corrosion inhibition ranking in light of the electronegativity values is sinapic acid > chlorogenic acid. Electron donating power parameter imparted to the literature by Gazquez and co-authors reflects the electron-donating ability of inhibitor systems<sup>271</sup>. The molecules having higher values of electron-donating power are effective corrosion inhibitors. According to calculated electron-donating power values, one can say that sinapic acid is a more effective corrosion inhibitor than chlorogenic acid. The theoretical conclusions established are in fair accordance with experimental findings. The fraction of electrons that a molecule transfers to the vacant orbital is represented by  $\Delta N$ . Furthermore, the  $\Delta N$  value is a well-known measure for predicting inhibitor compounds' chemical reactivity and stability. In general, a molecule that has a positive and high value of  $\Delta N$ , indicates its better inhibitory efficiency.  $\eta$  and  $\sigma$  are considerable parameters that provide data about reactivity and stability. The  $\Delta E$  value and the values of  $\sigma$  with  $\eta$ , and in addition to  $\Delta N$  are in excellent accordance with methodological observations. In general, it appears that an inhibitor molecule's strong interaction with a steel surface occurs at low values.

**Chlorogenic acid**



**Sinapic acid**



**OPTIMIZED Structure**

**HOMO**

**LUMO**

**Figure 4.13.** HOMO and LUMO distribution of inhibitor.

**Table 4.7**

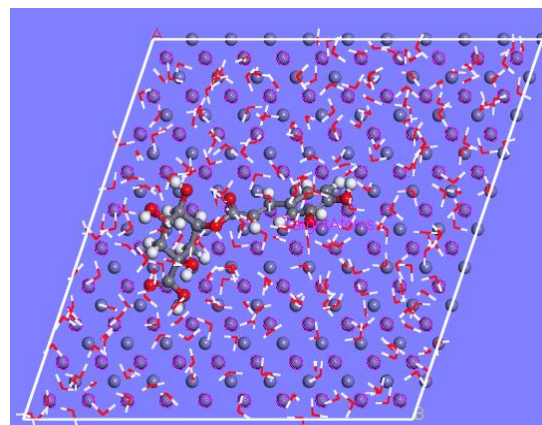
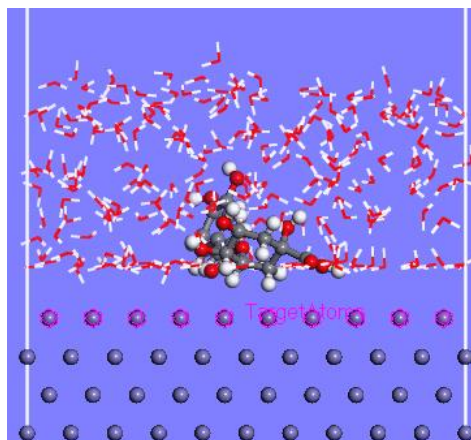
List of quantum chemical parameters by DMol3 Accelers' 2017 Material Studio.

Code	Chlorogenic acid	Sinapic acid
Program	DMol3	Dmol3
Method	DFT	DFT
Basis set	DNP	DNP
Function	GGA	GGA
$E_{\text{HOMO}}$ (eV)	-5.437895	-5.352644
$E_{\text{LUMO}}$ (eV)	-2.995000	-3.030265
$\Delta E = E_{\text{LUMO}} - E_{\text{HOMO}}$ (eV)	2.442895	2.322379
IP (eV)	5.437895	5.352644
EA (eV)	2.995000	3.030265
$\eta$ (eV)	1.221448	1.161189
$\sigma$ (eV <sup>-1</sup> )	0.818701	0.861186
$\chi$ (eV)	4.2164	4.1914
$\omega$ (eV)	7.2776	7.5647
$\omega^+$ (eV)	5.3220	5.6142
$\omega^-$ (eV)	9.5385	9.8056
$\Delta N$ max	1.726004	1.804811

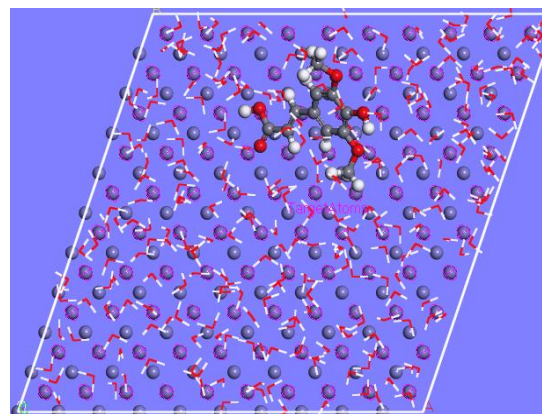
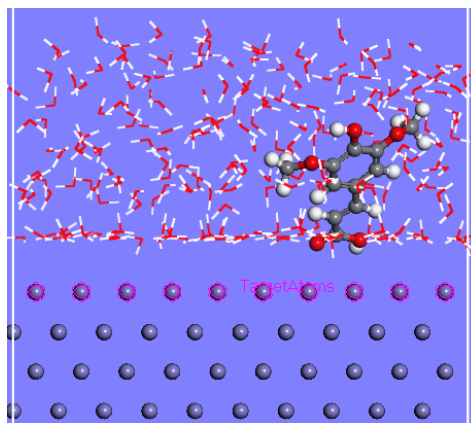
The interaction of investigated inhibitors is studied by Monte carol simulation. The most stable optimized structure of inhibitors is used in simulation studies. In order to model part of the corrosion system, the effect of water and corrosive species was considered in the Monte Carlo simulation.

From the Monte Carlo Simulations, it could be noticed that the inhibitor molecule adsorbs on the metal's surface in a semi-flat arrangement, as shown in **Figure 4.14**. The adsorbed molecule may be more stable as a result of the flat adsorption arrangement. Also, overlaying more active regions on the metallic surface offers better surface coverage.

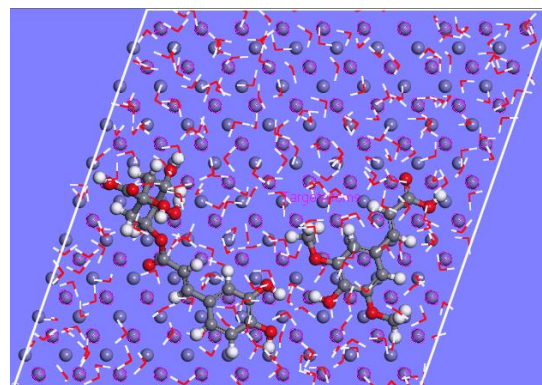
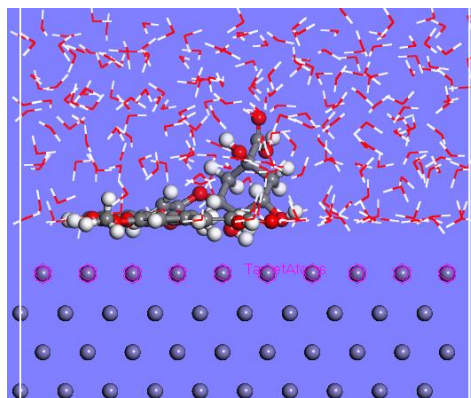
Chlorogenic acid + in H<sub>2</sub>O



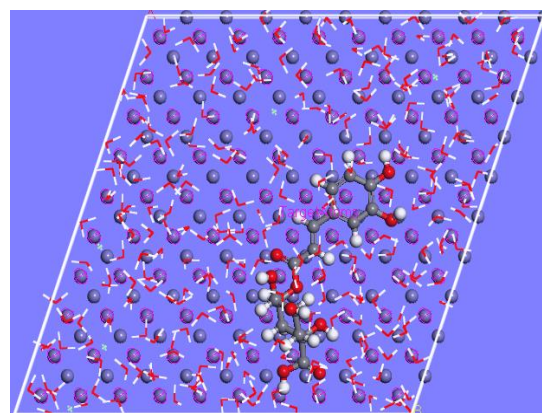
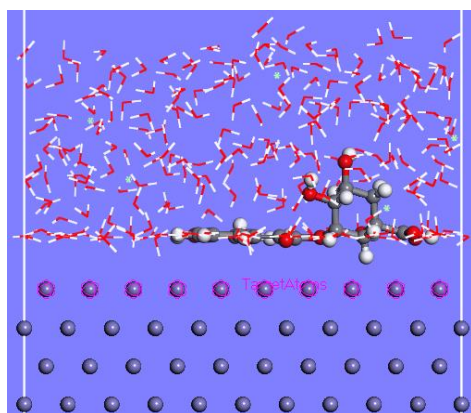
Sinapic acid + in H<sub>2</sub>O



Chlorogenic acid + Sinapic acid  
in H<sub>2</sub>O



Chlorogenic acid in HCl



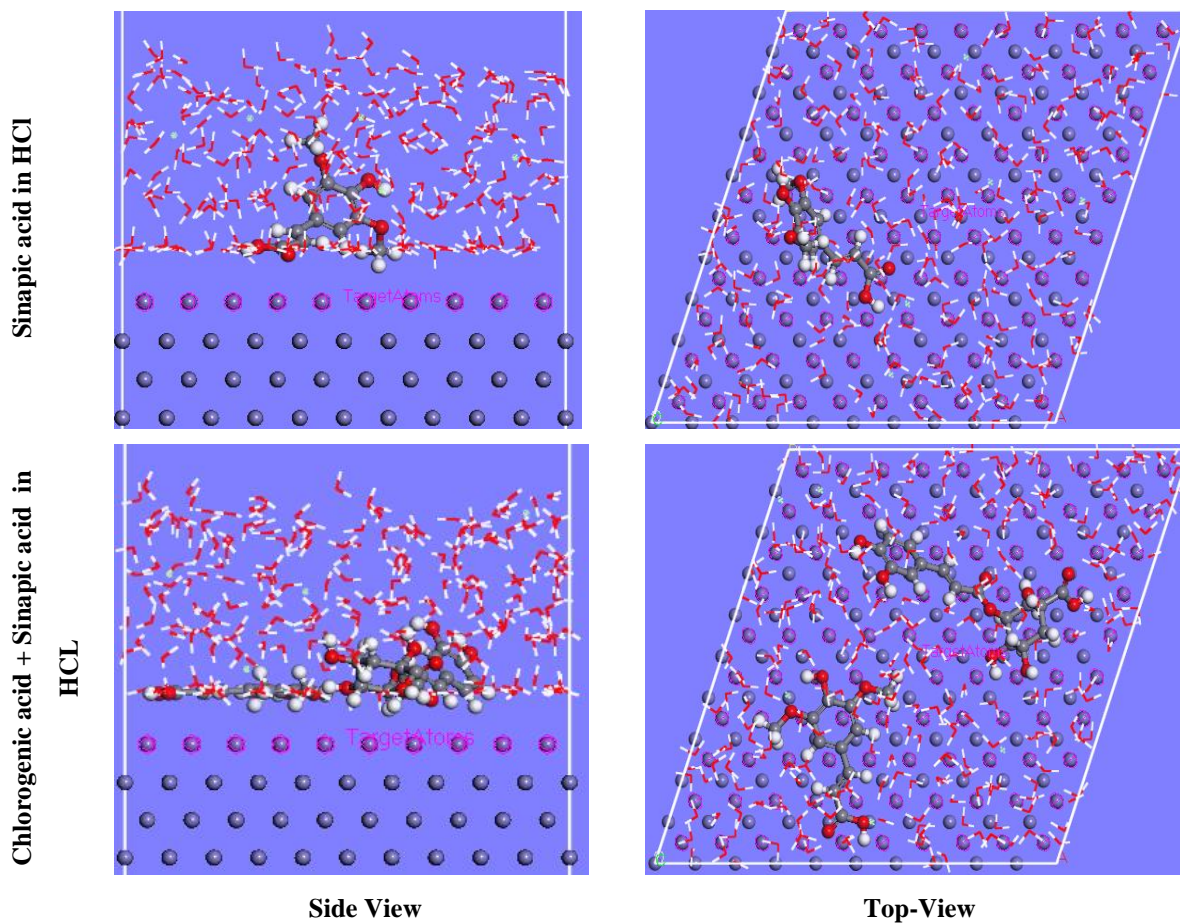
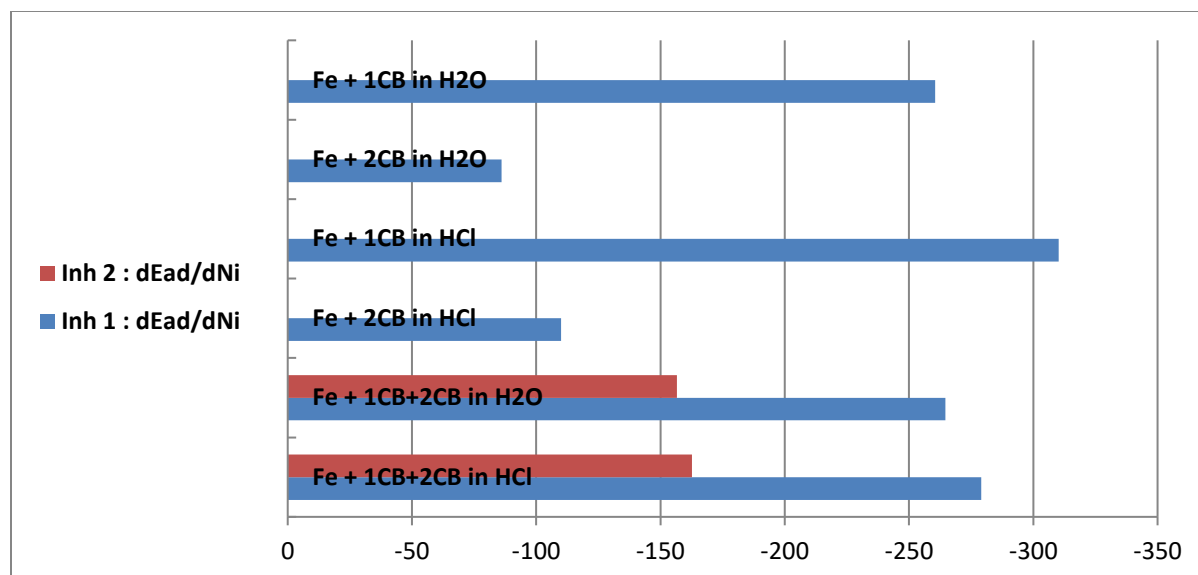


**Figure 4.14.** The equilibrium position of inhibitors Chlorogenic acid and Sinapic acid from Monte Carlo Simulations.

**Table 4.8**

Representation of Molecular simulation parameters for adsorption of Chlorogenic acid (1CB) and Sinapic acid (2CB) in different  $\text{H}_2\text{O}$  and  $\text{H}_3\text{O}^+$ .





It is worth mentioning that the adsorption energy of compounds increases while they are present together on the Fe surface (The synergistic effect could be assumed) and the adsorption of compounds is greater in HCl than in water.

**Table 4.9**

The output energies determined by Monte Carlo simulation for Chlorogenic acid and Sinapic acid on Fe (110)

Structures	Fe + Chlorogenic acid + Sinapic acid in HCl	Fe + Chlorogenic acid + Sinapic acid in H <sub>2</sub> O	Fe + Sinapic acid in HCl	Fe + Chlorogenic acid in HCl	Fe + Sinapic acid in H <sub>2</sub> O	Fe + Chlorogenic acid in H <sub>2</sub> O
<b>Total energy</b>	-4331.35	-3476.27	-4129.75	-4197.28	-3302.33	-3324.49
<b>Adsorption energy</b>	-4320.64	-3465.56	-4077.02	-4239.31	-3249.60	-3366.52
<b>Rigid adsorption energy</b>	-4436.16	-3578.45	-4260.70	-4359.01	-3426.76	-3476.23
<b>Deformation energy</b>	115.52	112.89	183.68	119.71	177.16	109.71
<b>Chlorogenic acid: dEad/dNi</b>	-279.11	-264.61	-110.01	-310.19	-86.06	-260.47
<b>H<sub>2</sub>O: dEad/dNi</b>	-13.64	-7.61	-7.25	-12.51	-12.67	-7.58

Sinapic acid:						
dEad/dNi	-162.67	-156.57	NA	NA	NA	NA
H <sub>3</sub> O <sup>+</sup> : dEad/dNi	-152.12	NA	-149.43	-150.62	NA	NA
Cl <sup>-</sup> : dEad/dNi	-128.06	NA	-154.46	-148.55	NA	NA

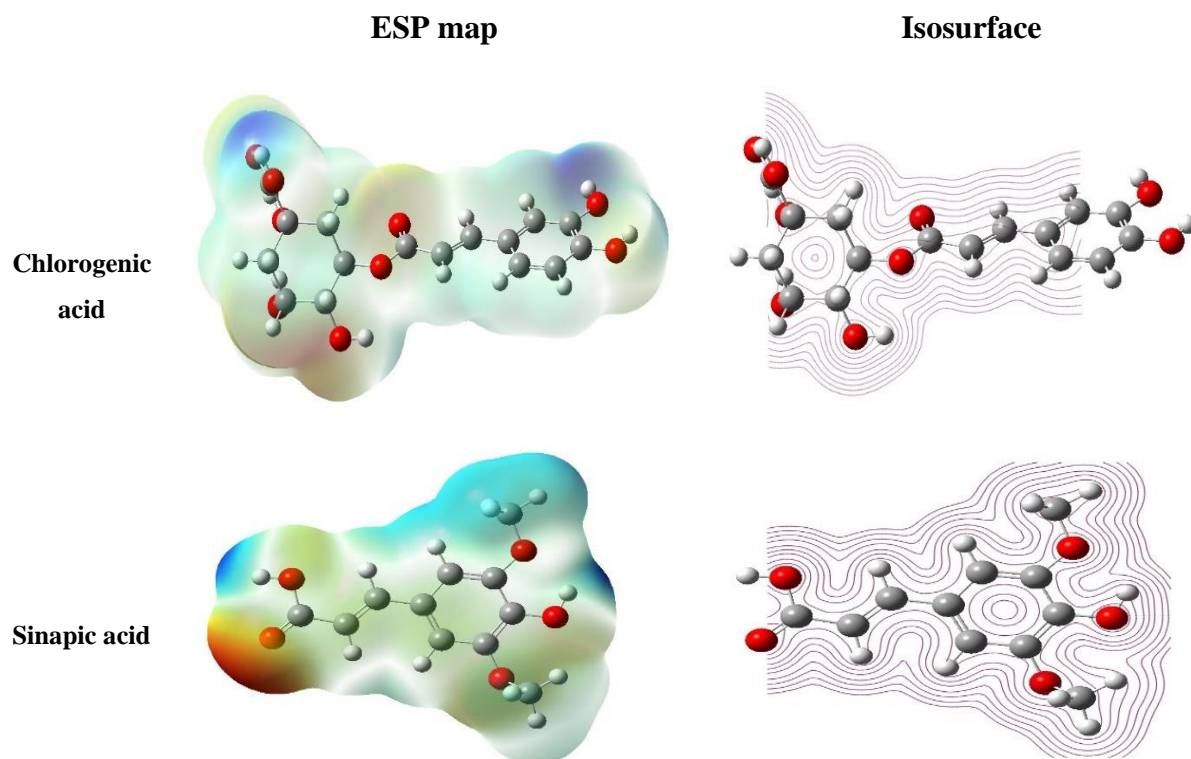


**Figure 4.15.** ESP maps and isosurface of chlorogenic acid and Sinapic acid.

Another approach that might provide insight into the electrophilic active sites existing in a chemical species is electrostatic potential mapping (ESPs). As can be observed in **Figure 4.15**, the electrophilic active site is situated in the oxygen sites, based on the ESP maps of both molecules, which exhibit a red-yellow color. As a result, these electrophilic active sites can enhance electron exchange with the Fe surface's d vacant orbital <sup>272</sup> and thus adsorb efficiently on the metallic substrate, contributing to their potent inhibition efficiency.

#### 4.1.9. Biodegradability of CBE

**Figure 4.16** depicts the biodegradation rate of CBE after 28 days computed using equation (19). The deterioration rate of CBE increased with the time interval, exceeding 84% at 28 days as shown

in **Figure 4.16**. As per the North-East Atlantic Convention for the Protection of the Environment, if the biodegradation rate is greater than 60% during 28 days, it is termed readily biodegradable<sup>273</sup>. Hence, CBE may be considered a biodegradable corrosion inhibitor.

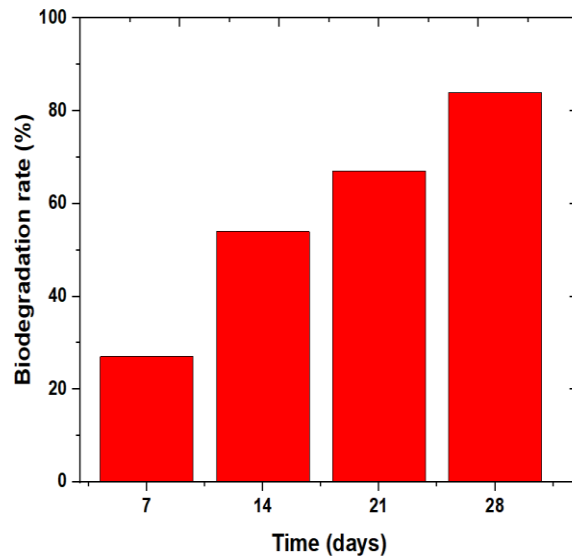


**Figure 4.16.** Biodegradability of CBE

## 4.2. *Vicia Sativa*

*Vicia Sativa* (Domain: Eukaryota, Kingdom: Plantae, Phylum: Spermatophyta, Subphylum: Angiospermae, Class: Dicotyledonae) is an annual scrambling and climbing legume. It features a long, delicate taproot that could reach lengths of 1-1.5 meters. It has slender, slanted, procumbent and branching stems that can grow up to 2 meters in length. The leaflets are complex with three to eight pairs of contrary leaflets and two to three distal tendrils that aid in ascending. *Vicia sativa* is an antimicrobial, anti-poison, amorous, anti-rheumatic and antinociceptive species that has been utilized for centuries to treat skin ailments, bronchitis, asthma and kidney disorders. According to the previous investigation<sup>274,275</sup>, *Vicia Sativa* extract (VSE) comprises a significant amount of active phytoconstituents, mainly (Z)-2-hexenal, (b) 1-Octen-3-ol, (c) (Z)-3-hexenol as illustrated in **Figure 4.17**. In this investigation, *Vicia Sativa* (India), which is extensively available in numerous nations has been evaluated as a sustainable and eco-friendly mild steel corrosion inhibitor in a 0.5 M HCl acidic medium. As per our best recollection, none of the reports has investigated the use of *Vicia Sativa* (VS) on mild steel corrosion protection in a stagnant solution of 0.5 M HCl medium to attain the most effective corrosion IE% of VSE. In stagnant 0.5M HCl solution, the presence of such suspended particles retards the corrosion due to their unique properties and their ability to deposit on metallic surfaces, hence creating a defensive layer on the metallic surface and inhibiting corrosion<sup>276</sup>. When VS aerial components are used as a green corrosion inhibitor for mild steel in a corrosive environment, it not merely reuses resources and minimizes corrosion inhibitor costs, but also substantially encourages VS cultivation. The most crucial aspect is that there are minimal repercussions to humans and the ecosystem. In this investigation, the inhibition performance of VSE has been evaluated by using weight loss, spectroscopic, electrochemical and morphological approaches.

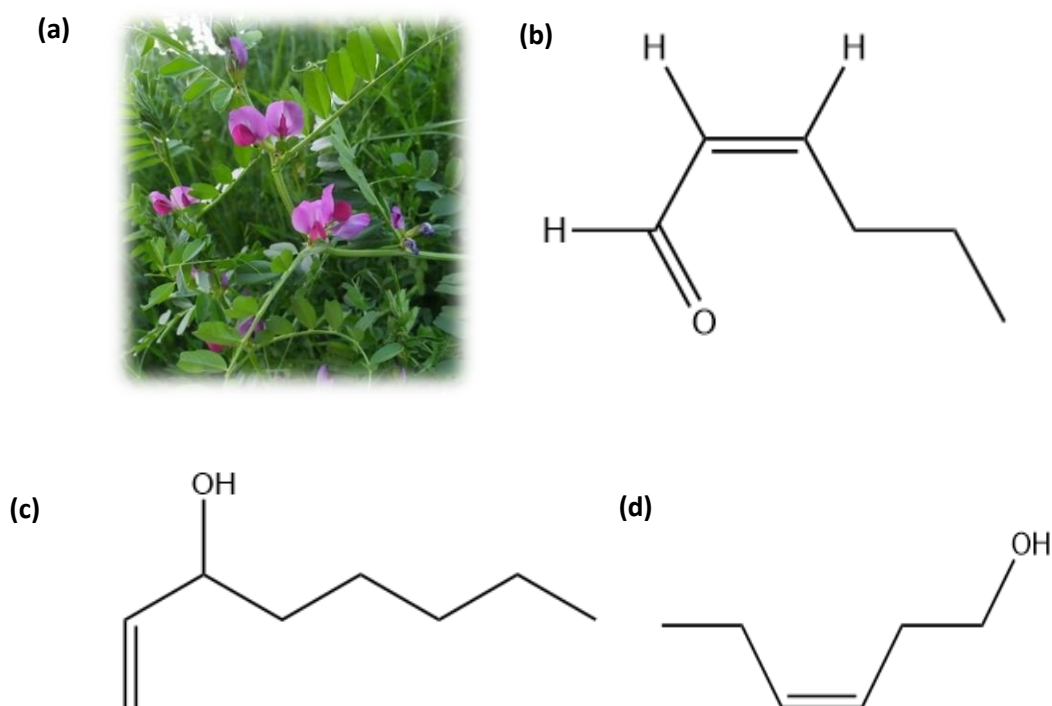


**Figure 4.17.** Illustrations of (a) *Vicia Sativa* and its major chemical constituents (b) (Z)-2-hexenal, (c) 1-Octen-3-ol and (d) (Z)-3-hexenol.

#### 4.2.1. Preparation of *Vicia Sativa* extract

*Vicia Sativa* weed was collected from the agricultural land in Hardaspur, Punjab and was verified by Dr. Neera Rashmi, Department of Botany, Himachal Pradesh University, India. The aerial portion of the weed was initially rinsed with water and sun-dried for a consecutive 6-7 days before being dried in an oven for 25–35 minutes at 40–50°C for the extraction procedure. The dried component was mechanically processed into powder<sup>275</sup>. In a standard DSE extraction, 20g of dried powder was mixed with 50% (v/v) methanol in water (H<sub>2</sub>O) as the solvent and blended for 15 minutes of duration. The extraction was then performed for 45 minutes in a sonication water bath utilizing ultrasonic-assisted extraction (Elma Transsonic T460, Germany). To concentrate the extract's primary bioactive rich components, the extract was purified using filter paper microfiltered using 0.45m pore size micro-steps after 45 minutes. The obtained VS extract had a maximal solubility of 1000mg/l in 0.5 M HCl. Subsequently, the residue was kept at -20°C until further examination could be performed.

#### 4.2.2. FT-IR analysis

The extent of corrosion can be significantly mitigated by the presence of heteroatom (O) in the aromatic ring. The heteroatom increases the adsorption of inhibitor molecules over the metallic surface which tends to reduce corrosion. The FTIR spectral studies have been carried out for VSE and the FTIR spectra obtained are given in **Figure 4.18**. A wideband was noticed at  $3339\text{ cm}^{-1}$  corresponding to O–H stretching vibration. This broad peak portion suggests the occurrence of molecular association. Further, C–H stretching vibration attained at  $2920\text{ cm}^{-1}$ . The peak obtained at  $1066\text{ cm}^{-1}$  corresponds to -C-O stretch. -C=O as well as -C=C stretching vibrations are evident at  $1730\text{ cm}^{-1}$  and  $1514\text{ cm}^{-1}$  respectively. A symmetric stretch for -CHO is spotted at  $2851\text{ cm}^{-1}$ . Also, -C-O-H bend is obtained at  $1259\text{ cm}^{-1}$  while =C-H bend is present at  $905\text{ cm}^{-1}$ . These results indicated that VSE comprises oxygen in its functional groups (-C-O-H, -C=O, -C–O), that is compatible in accordance with the configuration of conventional corrosion inhibitors. VSE's higher ubiquity is due to its greater corrosion inhibition capability on the mild steel in 0.5M HCl.

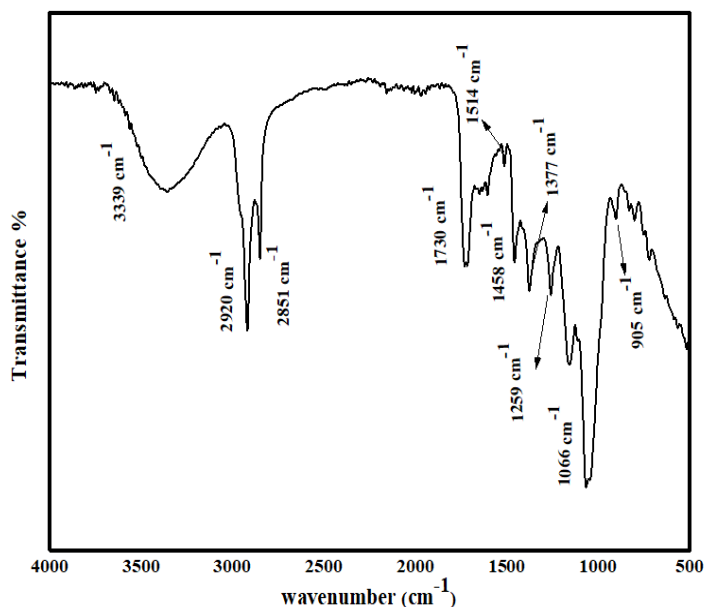


**Figure 4.18.** FT-IR evaluation of the VSE.

#### 4.2.3. Uv-visible spectrometry

As shown in **Figure 4.19**, the UV spectrum of VSE was analyzed prior and following the corrosion investigation. According to the UV spectrum, the absorption of the corrosive media in which the

mild steel specimen was not submerged was greater than the setup where the specimen was submerged for 24hrs. A fraction of the solution's components were attached to the metallic surface following submerging the metallic specimen in the acidic+VSE solution comprising 1000ppm of VSE, showing that mild steel may have a considerable corrosion IE.

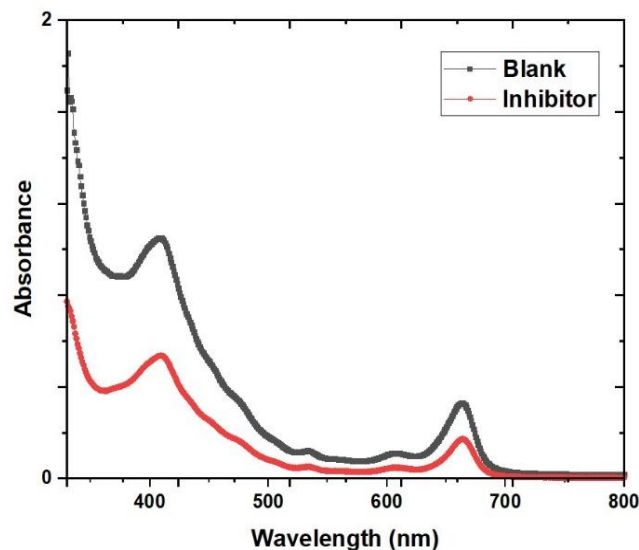


**Figure 4.19.** UV spectrum of VSE prior and following the immersion of metal.

#### 4.2.4. Weight loss (WL) measurements

The WL approach to evaluate IE% and  $C_R$  is significant due to its convenience of utilization and excellent accuracy. This experiment was carried out in the absence and presence of the inhibitor in 0.5M HCl medium at 298K to determine how the concentration, time and temperature of the inhibitor influenced the IE% of VSE<sup>277</sup>. The influence of concentration, duration and temperature on IE% towards metallic corrosion in 0.5M HCl is shown in **Table 4.10, 4.11 and 4.12** and **Figure 4.20**. At an optimum concentration of 1000ppm of VSE in 0.5M HCl, the inhibitor achieved a maximal IE% of 93.38%. The IE% and  $C_R$  acquired through the WL approach at several concentrations of VSE at 298K are summarised in **Table 4.10, 4.11 and 4.12**. It could be inferred from **Figure 4.20** that when the quantity of VSE was raised, the IE was enhanced as well. Even though, due to the desorption of the inhibitor molecules at increased temperatures and expanding duration, the IE of VSE decreases from 91.85% to 64.24% in the case of time variation and 93% to 66.28% in the case of temperature variation. Equations (1-3) were used to calculate  $C_R$ , IE% and  $\Theta$ .

**Table 4.10**

Effect of concentration on the IE% of mild steel in 0.5M HCl without and with VSE inhibitor (50-1000ppm at 298K).

Conc. (ppm)	W <sub>0</sub> (mg)	W <sub>i</sub> (mg)	W <sub>0</sub> -W <sub>i</sub> (mg)	C <sub>R</sub> (mmyr <sup>-1</sup> )	Θ	IE%
Blank	1.652	0.352	1.3	3.626	-	-
50	1.443	1.156	0.287	0.801	0.598	77.92
100	1.523	1.311	0.212	0.591	0.837	83.69
250	1.432	1.287	0.145	0.404	0.889	88.85
500	1.653	1.563	0.09	0.251	0.930	93.07
1000	1.508	1.461	0.047	0.131	0.963	93.38

**Table 4.11**

Effect of time on the IE% of mild steel in 0.5M HCl without and with 1000ppm of VSE inhibitor at 298K.

Time (min.)	W <sub>0</sub> (mg)	W <sub>i</sub> (mg)	W <sub>0</sub> -W <sub>i</sub> (mg)	IE%
15	1.512	1.431	0.081	91.85
30	1.313	1.162	0.151	84.31
45	1.825	1.494	0.331	71.89
60	1.623	1.216	0.407	64.24

**Table 4.12**

Effect of temperature on the IE% of mild steel in 0.5M HCl without and with 1000ppm of VSE inhibitor.

Temp. (K)	W <sub>0</sub> (mg)	W <sub>i</sub> (mg)	W <sub>0</sub> -W <sub>i</sub> (mg)	IE%
298	1.532	1.485	0.047	93
308	1.643	1.487	0.156	86
318	1.654	1.393	0.261	77.73
328	1.785	1.231	0.554	66.28



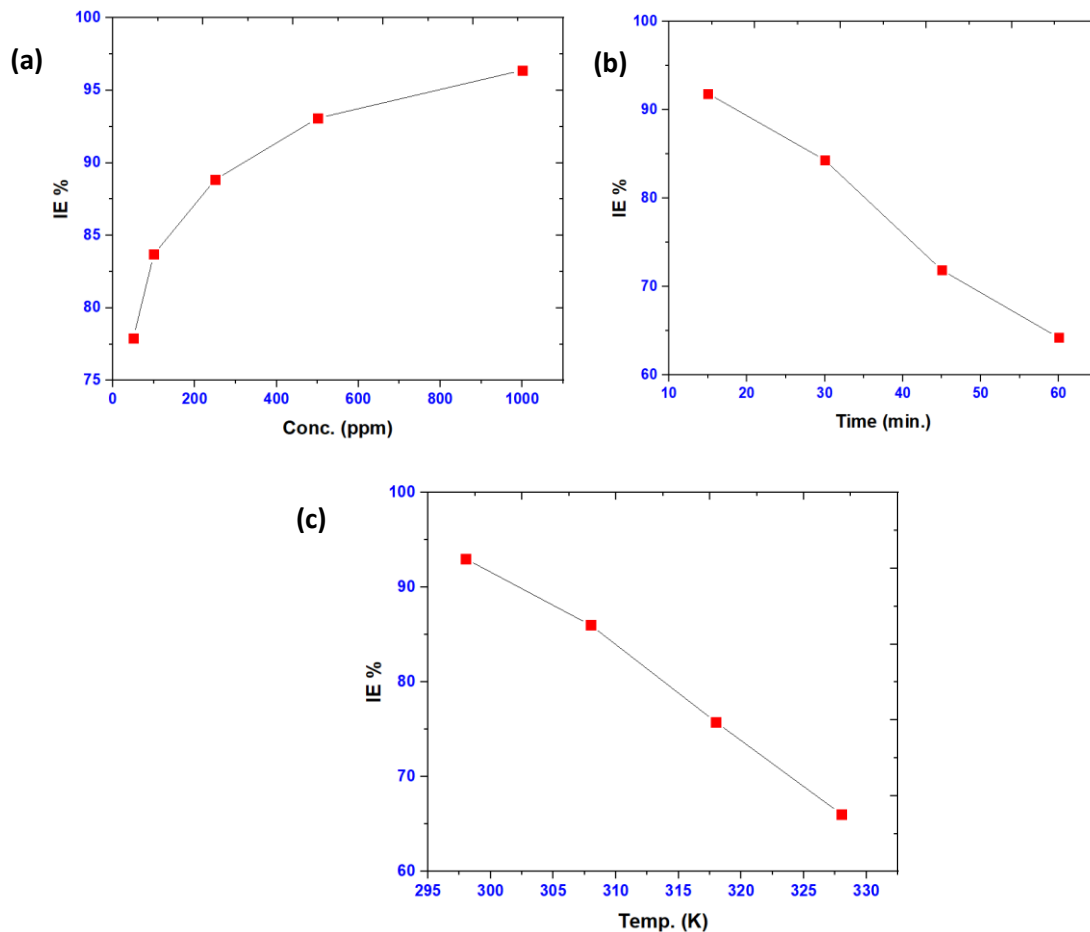
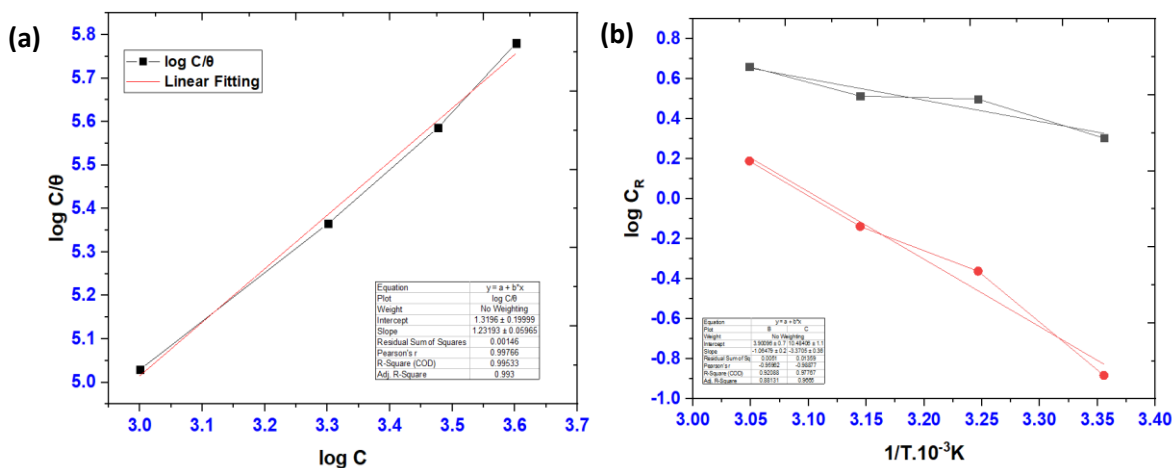


**Figure 4.20.** Impact of (a) concentration, (b) time (c) temperature variation on the IE% of VSE on mild steel.

#### 4.2.5. Adsorption and thermodynamic parameters

The efficacy of a corrosion inhibitor can be measured by its ability to reduce metal corrosion by getting adsorb at the metal/solution interface, whilst the fundamental features of the inhibitor's interaction with the metallic surface could be evaluated by extrapolating the adsorption isotherm. As illustrated in **Figure 4.21 (a)**, the coefficient of  $R^2$  which gave the degree of fit in between the empirical data and the isotherm eqn. is approximately 1 (i.e., 0.99533) as indicated in the plot of  $\log C/\theta$  Vs.  $\log C$ , wherein a linear slope has a regression coefficient of around 1, suggesting that the system obeys Langmuir adsorption isotherm at all the analyzed concentration<sup>278,279</sup>. The Langmuir adsorption isotherm was revealed to be allied with the adsorption of VSE on the metallic surface in corrosive media, indicating that while the inhibitor's molecules are deposited on the

metal/solution interface, it incorporates a classic adsorption site, preventing the corrosion caused by the corrosive solution by forming a mono-layer of the inhibitor adsorbed on the mild steel surface without interaction between the adsorbed molecules<sup>233,280</sup>. Langmuir's adsorption isotherm model relies on the premise that all the adsorption sites are analogous and the particle binding occurs independently of nearby sites being occupied or not. Additionally, the higher and positive values of  $\log K_{ads}$  signify the high adaptability of the VSE extracts on metal surfaces which correlated with its fitting with the Langmuir isotherm. At 1000 ppm of inhibitor concentration, it was observed that the value of  $\Delta G^0_{ads}$  was  $13.168 \text{ KJ mol}^{-1}$ , revealing that the inhibitor was entirely physisorbed on the metallic surface since the value of free energy was lower than  $20 \text{ K J mol}^{-1}$ . Slopes ( $-E_a/2.303R$ ) of the  $\log C_R$  vs.  $1/T \cdot 10^{-3} \text{K}$  graphs in **Figure 4.21 (b)** have been utilized to measure the activation energy value. **Table 4.13** summarises the outcomes of this analysis. The Arrhenius equation was utilized to determine the kinetic variables. The enthalpy value was calculated employing the  $\log K_{ads}$  vs.  $1/T \cdot 10^{-3} \text{K}$  plot, which yielded a straight curve having a slope of  $-H/2.303R$ , as depicted in **Figure 4.21 (c)** and further using eqns. (5) and (6). Additionally, Eqns. (7) and (8) were used to calculate Gibb's free energy and adsorption entropy.



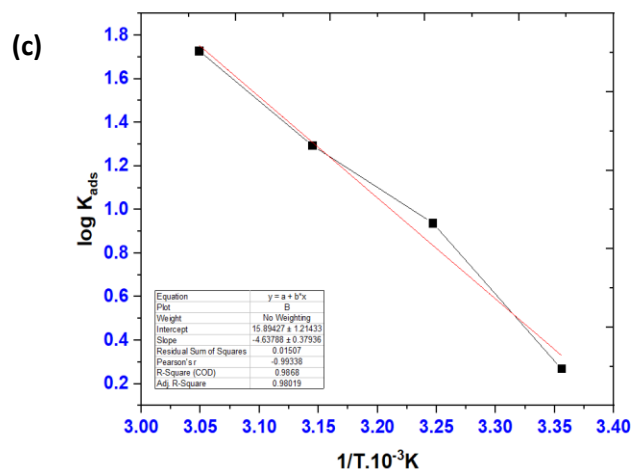


**Figure 4.21.** (a) Langmuir adsorption graph (b) Arrhenius graph (c) Enthalpy graph of VSE as an effective mild steel corrosion inhibitor in 0.5M HCl.

**Table 4.13**

Adsorption, kinetic and thermodynamic values for VSE (50-1000ppm) inhibiting mild steel corrosion in 0.5M HCl medium at 298K.

Metal	Inhibitor (ppm)	log K <sub>ads</sub>	ΔG <sup>o</sup> <sub>ads</sub> kJmol <sup>-1</sup>	ΔH <sup>o</sup> <sub>ads</sub> kJmol <sup>-1</sup>	ΔS <sup>o</sup> <sub>ads</sub> kJ.mol <sup>-1</sup> .K <sup>-1</sup>	E <sub>a</sub> kJmol <sup>-1</sup>	R <sup>2</sup>
Mild steel	Blank	-	-	-	-	1.832	
	50ppm	0.621	-1.539	0.0385	0.132	36.763	0.98019
	100ppm	2.160	-5.353				
	250ppm	2.980	-7.383				
	500ppm	3.980	-9.862				
	1000ppm	5.315	-13.168				

It is evident from **Table 4.13** that E<sub>a</sub> of the inhibited solution with the inclusion of inhibitor increased from 1.832 to 36.763 indicating adsorption of the inhibitor molecules on the metallic surface. The E<sub>a</sub> value (36.763 kJ/mol) is less as compared to the threshold value of 80 kJ/mol, essential for chemical adsorption. This indicates that the adsorption is physical adsorption, which raises the possibility that an inhibitory adsorption layer could form over the metallic substrate, physically impeding the charge and mass transfer. The positive values of ΔH<sup>o</sup><sub>ads</sub> (0.0385 kJ/mol) signify the endothermic characteristic of the metal dissolution phenomenon, indicating the

corrosion rate of mild steel in the inclusion of VSE was decreased and primarily regulated by the kinetic parameters of activation<sup>281</sup>. It is clearly evident that the values of  $E_a$  are higher than the values of  $\Delta H^{\circ}_{\text{ads}}$  revealing that the corrosion process incorporates a gaseous reaction, simply the hydrogen evolution reaction, aligned with a reduction in the total reaction volume. The negative values of  $\Delta G^{\circ}_{\text{ads}}$  indicate the stability of the adsorbed layer on the metallic surface and the spontaneity of the adsorption process.  $\Delta G^{\circ}_{\text{ads}}$  reduced (become more negative) with elevating concentration, suggesting the occurrence of an endothermic phenomenon. Also, the calculated values of  $\Delta G^{\circ}_{\text{ads}}$  are less than the threshold value (40 kJ/mol) required for chemical adsorption supporting the mechanism of physical adsorption. Furthermore, the value of  $\Delta S^{\circ}_{\text{ads}} < 0$  demonstrated that the adsorption mechanism was stationary and the formation of the complex compounds was related to the rate-determining phase, indicating that the instability decreases after the complex compound was formed, enabling  $\text{H}_2\text{O}$  molecules to desorb from the surface. Additionally, the huge enhancement in  $K_{\text{ads}}$  values from 0.621 to 5.315 also suggests that inhibitor compounds and metallic surfaces offer substantial interactions.

#### **4.2.6. Electrochemical measurements**

##### **4.2.6.1. Open circuit potential (OCP)**

It is crucial to achieve a constant OCP before progressing with the EIS and PDP experiments utilizing the Metroahm Autolab equipment coupled with the NOVA 2.1.4 software. A mild steel rod with a  $1 \text{ cm}^2$  exposed surface area utilized as a working electrode was submerged in the test solution (0.5M HCl + 50-1000ppm VSE) for 1 hour<sup>282-286</sup>. **Figure 4.22** shows the OCP vs. time (sec.) curves without and with various amounts of VSE as a corrosion inhibitor, with a reference electrode comprised of saturated calomel electrode (SCE). The presence of VSE causes the OCP values to proliferate close to the anode potential, which may be deliberate by VSE adsorption upon the mild steel surface. The PDP and EIS assessments were carried out after the OCPs had steadied for a brief duration<sup>6,44,231,287</sup>.

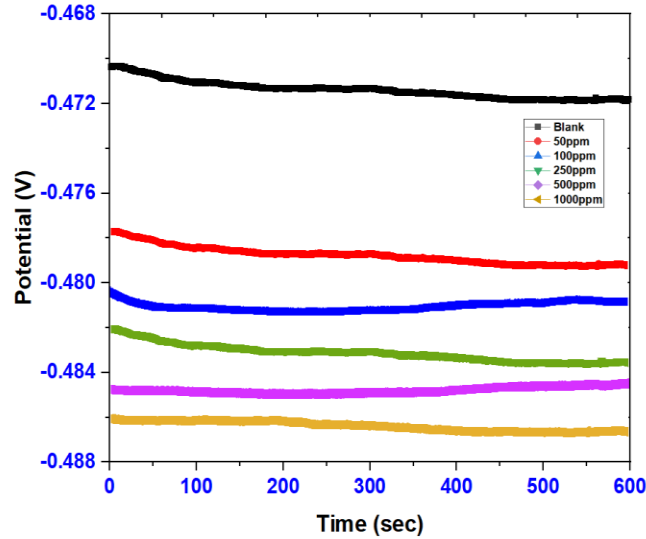


**Figure 4.22.** OCP vs time graph for mild steel in 0.5M HCl excluding and including several amounts of VSE (50-1000ppm).

#### 4.2.6.2. Potentiodynamic polarization

The corrosion inhibition efficacy of the VSE in the anodic dissolving of mild steel and the mechanism of the decrease in cathodic hydrogen ions in 0.5M HCl media were investigated utilizing the potentiodynamic polarization approach. **Figure 4.23** displays polarization graphs of mild steel corrosion inhibition in 0.5M HCl media with varying amounts of VSE inhibitor (50-1000ppm) at 298K. Several parameters such as corrosion potential ( $E_{\text{corr}}$ ), corrosion current densities ( $i_{\text{corr}}$ ) and the anode Tafel slope ( $\beta_a$ ) and cathode Tafel slope ( $\beta_c$ ) values were obtained from the examination of related polarization curves, as shown in **Table 4.14**. It could be noticed that as VSE amount increased from 50 to 1000ppm, the  $C_R$  value decreased from 8.2967 to 1.4176  $\text{mm}^{-1}$ , while the  $i_{\text{corr}}$  value declined dramatically from 749.78 to 122  $\mu\text{A}$ . This demonstrated that as the quantity of VSE was increased, the inhibition efficacy of VSE upon mild steel increased gradually. In the inclusion of various concentrations of the inhibitor, the polarization curves of the anode and cathode were distinctive from those excluding the inhibitor, as illustrated in **Figure 4.23**. As per the observations, inhibitors not only inhibited metal disintegration but also hindered hydrogen generation. Furthermore, the polarization slopes demonstrated that the cathode's shift was greatly more pronounced than the anodes<sup>288,289</sup>. The corrosion potential ( $E_{\text{corr}}$ ) shifted closer to the cathode when contrasted to the curve attained when the inhibitor was absent with a significant shift of 495.46 to 496.22mV. In conclusion, VSE evolved into a mixed corrosion

inhibitor with varying VSE concentrations focused on the cathode in a 0.5 M HCl medium. Additionally, **Figure 4.23** illustrates that when the inhibitor concentrations increased, the cathode Tafel curves become almost parallel. The anodic polarization curves were not drastically impacted by the inclusion of the inhibitor nevertheless it can be noted slight anodic current drops between 50 and 250 ppm. Additionally, it is clear that the slope of each polarization curve is different for each concentration of the VSE showing bumps in specifically 100-1000 ppm. This bump can be associated with the different  $C_R$  and inhibition properties shown by each concentration as related to the chemical composition of the mild steel. Sometimes it also relates to the inclusion of some impurities in the investigating system and heterogenous particulates on the structure of the electrode. **Table 4.14** also revealed that the cathode Tafel slope ( $\beta_c$ ) (from -142.76 to -153.24mV/dec) and anode Tafel slope ( $\beta_a$ ) (from 127.79 to 134.71mV/dec) values rarely altered when the inhibitor was introduced, showing that the process of hydrogen evolution stayed intact. That might be due to the inhibitor molecule adhesion on the metallic substrate, lessening the degree of active spots available for the reaction while sustaining the charge transfer process of hydrogen generation.

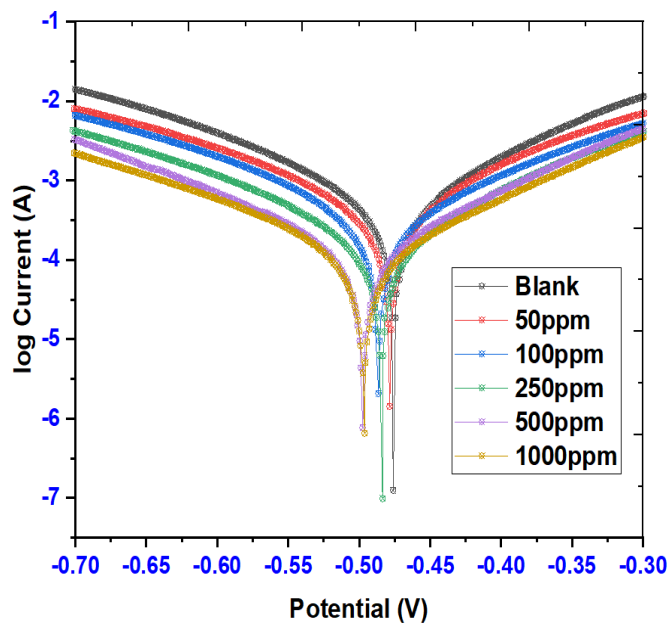


**Figure 4.23.** Tafel plot for the corrosion inhibition of mild steel in 0.5M HCl medium exposed to several concentrations (50-1000ppm) of VSE at 298 K.

**Table 4.14**

Corrosion parameters for mild steel in 0.5M HCl excluding and including VSE (50-1000ppm) obtained by the usage of electrochemical experiments at 298K.

Conc. (ppm)	-E <sub>corr</sub> (mV vs. SCE)	i <sub>corr</sub> (μA)	j <sub>corr</sub> (μA/cm <sup>2</sup> )	β <sub>a</sub> (mV/dec)	-β <sub>c</sub> (mV/dec)	C <sub>R</sub> (mmy <sup>-1</sup> )	χ <sup>2</sup>
Blank	495.46	749.78	749.78	127.79	142.76	8.29	8.2205E-07
50	478.11	554.05	554.05	154.56	178.97	6.44	5.4352E-07
100	486.11	382.28	382.28	161.21	155.01	4.44	3.0827E-07
250	484.14	171.23	171.23	126.71	135.01	1.99	1.9642E-08
500	497.45	138.92	138.92	130.44	142.26	1.61	1.4783E-08
1000	496.22	122.01	122.01	134.71	153.24	1.42	1.2858E-07

#### 4.2.6.3. Electrochemical impedance spectroscopy (EIS)

The EIS analyses of mild steel in 0.5M HCl incorporating the inclusion of various concentrations of VSE were performed to corroborate the findings of the WL and PDP assessments, as well as to acquire more about the corrosion process. **Table 4.15** summarises the most important findings<sup>233,290</sup>. The plots of Nyquist and Bode are displayed in **Figures 4.24** and **4.25**, correspondingly. At higher frequency, the Nyquist plot impedance spectrum exhibited a wide capacitive loop and at a lower frequency, an inductive loop. The high-frequency capacitive loop was induced by the charge transfer response and surface nonuniformity, whereas the low-frequency inductive loop was caused by the relaxation phase caused by Cl<sup>-</sup>, H<sub>ads</sub><sup>+</sup> and the accumulation of the corrosion inhibitor molecules upon the metallic surface. This might be due to the re-dissolution of the passivated surface of mild steel at lower frequencies. Regardless of whether an inhibitor was used or not, the arrangement of all graphs in the Nyquist plot stayed consistent, demonstrating that the mild steel corrosion pathway was not modified. To state it from another perspective, corrosion comprised a charge transfer mechanism. Moreover, their forms

were suboptimal owing to frequency dispersion, stiffness and nonuniformity of the electrode surface. The widths of these semicircles grew as VSE concentrations raised (50-1000ppm), showing that VSE was more evenly distributed on the electrode's surface, resulting in substantial electrode surface protection.

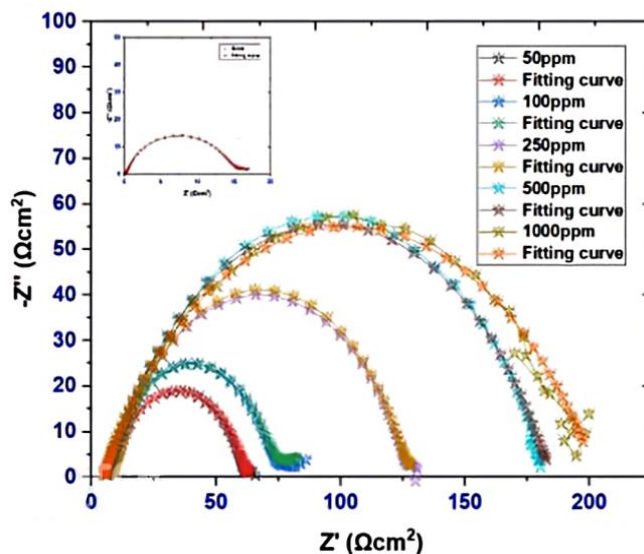


**Figure 4.24.** Nyquist plot for the corrosion inhibition of mild steel in 0.5M HCl medium exposed to several concentrations (50-1000ppm) of VSE at 298 K.

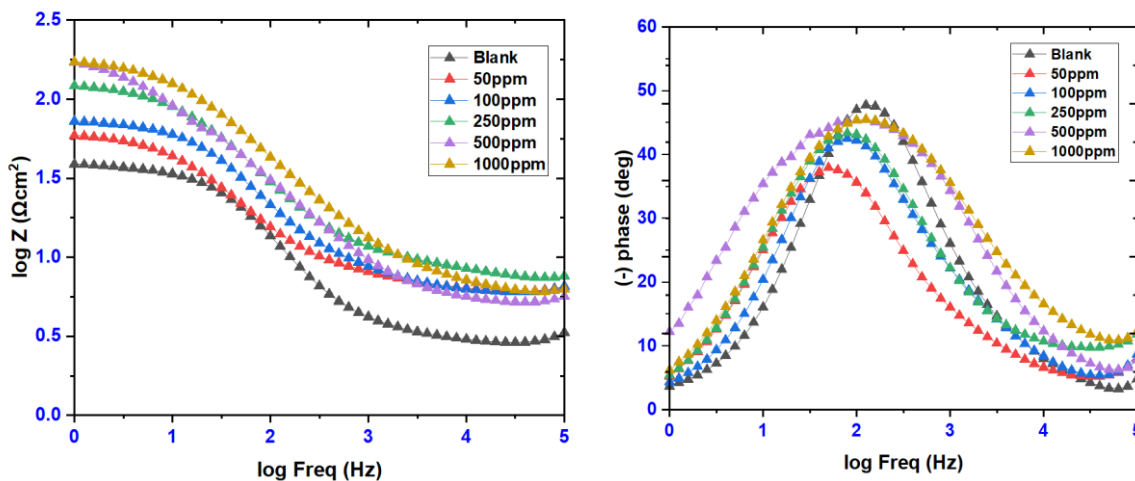


**Figure 4.25.** Bodes plot for the corrosion inhibition of mild steel in 0.5M HCl medium exposed to various concentrations (50-1000ppm) of VSE at 298 K.

**Figure 4.26** illustrates the equivalent circuit exploited for the fitting of the EIS data.



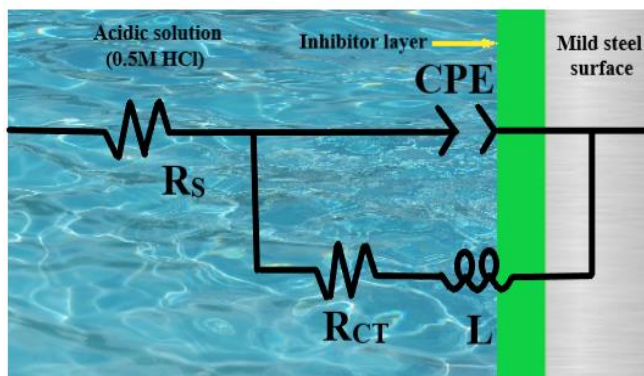


**Figure 4.26.** An equivalent circuit diagram employed for the fitting of the EIS data.

**Figure 4.25** displays Bode graphs for mild steel in the exclusion and inclusion of several amounts of VSE (500-1000ppm) in the 0.5M HCl medium at 298K. As per the Bode plots, there was merely a single time constant. Likewise, over the frequency range explored in this experiment, the impedance modulus raised as the VSE quantity raised from 50 to 1000ppm. The maximum phase angle's frequency spectrum widened as well<sup>291</sup>. All of these data demonstrated that VSE offered decent mild steel corrosion prevention in the corrosive media of 0.5M HCl. According to the previous investigations, if the curves of  $\log |Z|$  vs.  $\log f$  is often to be  $-1$  and the maximal phase angle tends to be  $90^\circ$ , then optimized and perfect capacitance at an intermediate frequency may be confirmed. This demonstrated that VSE had a superior corrosion IE on mild steel in a 0.5M HCl medium.

The EIS parameters are summarised in **Table 4.15**, where CPE for constant phase element,  $R_s$  for solution resistance (the resilience of the working electrode to the counter electrode),  $R_{ct}$  stands for charge transfer resistance,  $n$  for phase shift and  $\chi^2$  for variation extent of the equivalent circuit fitting. The parameters of  $\chi^2$  across  $10^{-3}$  and  $10^{-5}$ , indicate that the equivalent circuit arrangement is robust and consistent and has been observed to be equivalent with optimum fitting. As per **Table 4.15**, the IE% and  $R_{ct}$  elevated as the concentration of VSE expanded from 50 to 1000ppm, with a maximum corrosion IE of 91.246% at 1000ppm, which is almost similar to the observations of the WL and PDP studies. Following the inhibitor was administered in various quantities, the  $R_s$  value did not increase significantly (deviated between 5.898 and 4.823). Additionally, the phase shift values,  $n$  (0.809-0.690), did not alter considerably, showing an enhancement of the surface

inhomogeneity as a consequence of the inhibitor adsorption wherein the mild steel disintegration in a 0.5M HCl environment was regulated by charge transfer.

**Table 4.15**

EIS parameters obtained by the addition of several conc. (50-1000ppm) of VSE.

Conc (ppm)	CPE/Yo ( $\mu\text{F}$ )	$n$	$R_s(\Omega \text{ cm}^2)$	$R_p(\Omega \text{ cm}^2)$	$R_{ct \text{ in}}(\Omega \text{ cm}^2)$	$R_{ct \text{ bl}}(\Omega \text{ cm}^2)$	$\chi^2$	IE (%)
Blank	135.93	0.809	2.808	37.564	-	17.23	0.109	-
50	197.1	0.760	5.898	55.785	64.067	17.23	0.142	73.106
100	103.77	0.789	5.871	70.115	86.126	17.23	0.185	79.994
250	85.755	0.748	6.783	120.33	130.803	17.23	0.285	86.827
500	65.497	0.696	5.598	161.66	168.688	17.23	0.109	89.785
1000	148.78	0.690	4.823	191.05	196.828	17.23	0.116	91.246

#### 4.2.7. Surface analysis

##### 4.2.7.1. SEM

Surface electron microscopy (SEM) was utilized to analyze the morphological attributes of mild steel specimen after its 6hrs of exposure in 0.5M HCl media in the exclusion and inclusion of inhibitor and the findings are illustrated in **Figure 4.27**. **Figure 4.27 (a)** shows an SEM picture of a plain steel sample in an unprocessed and flat aspect before additional investigation. **Figure 4.27 (b)** depicts a highly corroded with several cavities, pits and holes showing corrosion products on the metallic specimen after the immersion of the specimen in 0.5M HCl for 6hrs<sup>292</sup>. In the context of **Figure 4.27 (c)**, the surface was sufficiently shielded by the addition of 1000ppm of VSE to the 0.5M HCl and no surface degradation was seen when contrasted to the blank sample. As a result of the lowered porosity for aggressive ions and associated corrosive impacts upon the metallic surface, SEM investigations indicated the development of a substantial inhibitive barrier of VSE on the metallic surface.

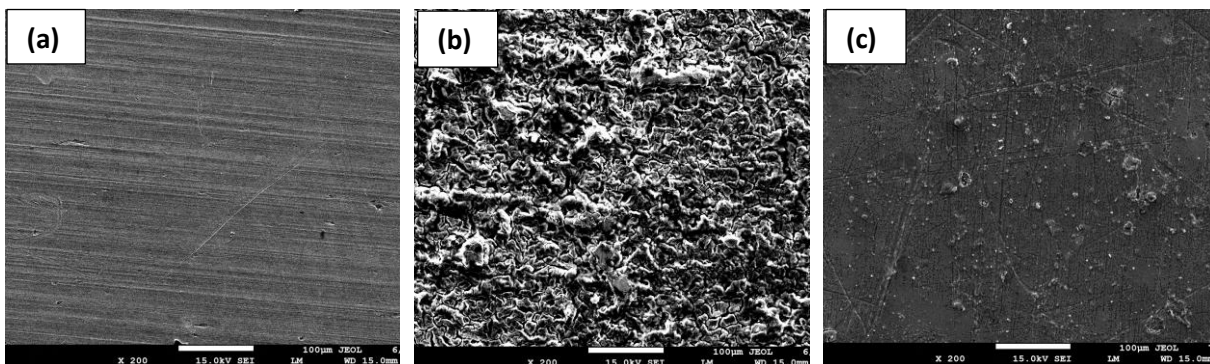


**Figure 4.27.** SEM pictures of (a) plain mild steel, (b) mild steel immersed in 0.5M HCl (c) mild steel immersed in 0.5M HCl+ VSE (1000ppm).

#### 4.2.7.2. Contact angle (CA) measurement

CA investigations were performed to understand the phenomena including wetting, adhesion and absorption on metallic surfaces<sup>293</sup>. These are commonly used to estimate the hydrophilicity/hydrophobicity of untreated and treated metal surfaces in this investigation. **Figure 4.28 (a)** and **(b)** illustrate the visuals generated by CA investigations on the mild steel surface in the lack and inclusion of 1000ppm of VSE, correspondingly. When compared to metallic samples exposed with a basic acidic solution ( $63.92^\circ$ ), the contact angle for metallic samples exposed with CB extract enhanced ( $83.39^\circ$ ), as per the observations. As a consequence, the metallic surface was reduced hydrophobic before getting subjected to VSE (**Figure 4.28 (a)**), but it acquired highly hydrophobic afterward (**Figure 4.28 (b)**). Mild steel substrate exhibits a limited hydrophobicity, which leads to corrosion, owing to harsh particle deposition over the mild steel surface in acidic conditions. Inhibitor molecule adhesion may result in a decrease in surface tension, culminating in hydrophobicity, thus leading to the production of a defensive layer across the mild steel surface to prevent corrosion.

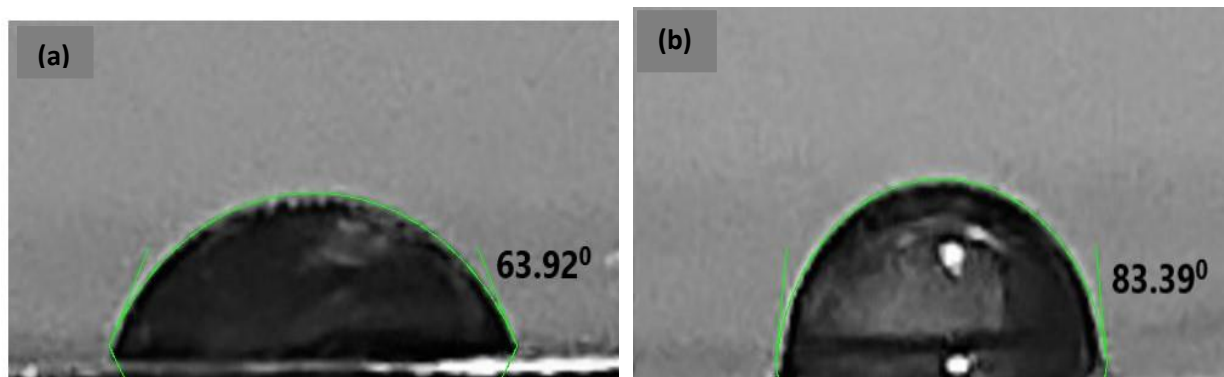


**Figure 4.28.** Contact angle evaluations conducted on the mild steel specimen in **(a)** 0.5M HCl and **(b)** 0.5M HCl + 1000ppm inhibitor.

#### 4.2.8. DFT and MC simulations

For studying the reaction pathway involving atoms on a metallic substrate and a corrosion-inhibiting molecule, computational analysis such as DFT and MC simulations is regarded as one of the most feasible and robust approaches. The Forcite module (Materials Studio 2017 application) was used to simulate the system in this analysis<sup>161</sup>. The optimized configurations and characteristics of the molecules are shown in **Figure 4.29** and **Table 4.16**. Low  $E_{LUMO}$  values show a molecule's capability to gain electrons, while high  $E_{HOMO}$  values represent a molecule's capability to transmit electrons. In **Table 4.16**, it may be validated that the (Z)-2-hexenal, 1-Octen-3-ol and (Z)-3-hexenol exhibited elevated values of  $E_{HOMO}$  and lessened values of  $E_{LUMO}$  of -6.21079, -6.27816, -5.90099 and -3.04937, -1.33563, -0.95926 which enhance their capability to emit and acquire electrons while engaging with the mild steel surface. The variation across  $E_{HOMO}$  and  $E_{LUMO}$  energies is also represented by the energy gap ( $\Delta E$ ), that is an additional crucial parameter to examine and support the resilience indices of a corrosion inhibitor. In this case, the lower ( $\Delta E$ ) values such as 3.161421, 4.942796444 and 4.917345 show an increased mutual interaction among the Fe surface and the inhibitor, resulting in substantial corrosion inhibition. The chemical hardness<sup>269</sup> of atomic or molecular structures is defined as their resilience to electron cloud polarization. "Hard acids preferred the adhering to hard bases, whereas soft acids favor the affinity to soft bases," as per the Hard and Soft Acid-Base (HSAB) Rule. When contrasted to hard molecules, soft molecules have more polarization and electron-donating ability. As a result, an excellent corrosion inhibitor must be extremely soft. The Maximum Hardness Principle, which states that "molecules

organize themselves to be as hard as feasible," demonstrates the potent correlation among chemical reactivity and chemical hardness<sup>270</sup>. According to this theory, hard molecules are much more persistent than soft molecules. Both compounds are excellent corrosion inhibitors, as per computed chemical hardness coefficients, however, corrosion IE varies of 1-Octen-3-ol may be superior to that of (Z)-2-hexenal and (Z)-3-hexenol with an excellent  $\eta$  of 2.471398 and  $\sigma$  of 0.404629. Electronegativity ( $\chi$ ) is a measurement of a chemical system's ability to remove electrons. Chemical solutions with significant electronegativity indices do not protect metal surfaces from corrosion. In view of the electronegativity parameters, the derived corrosion inhibition score<sup>271</sup>. The derived theoretical results are quite equivalent to the experimental outputs.  $\Delta N$  represents the proportion of electrons that a molecule transmits to the unoccupied orbital. Additionally, the  $\Delta N$  level is a well-known metric for estimating the chemical stability and reactivity of inhibitor molecules. A chemical with a positive and significant  $\Delta N$  value, in principle, possesses a higher IE and  $\eta$  and  $\sigma$  are important factors that offer insight into stability and reactivity. The E value, as well as the values of  $\sigma$  with  $\eta$  and  $\Delta N$ , are in great agreement with empirical findings. In particular, it reveals that the significant association of an inhibitor molecule onto a steel surface arises at minimal values.

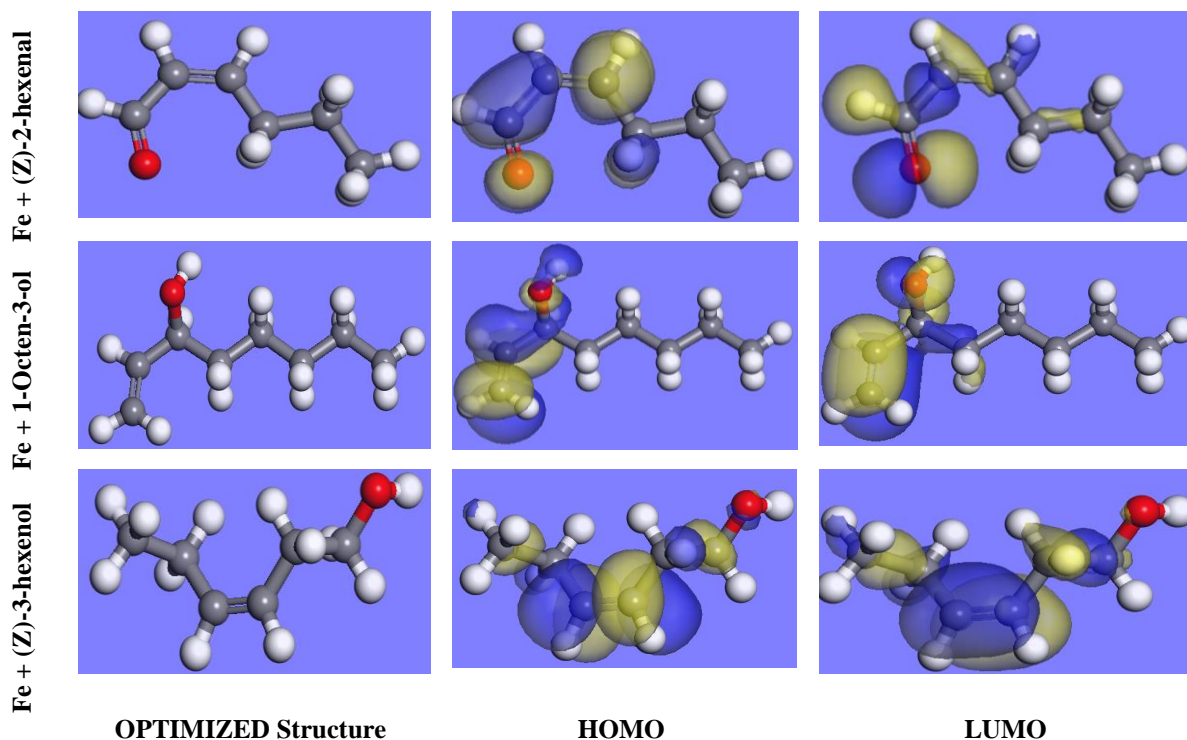


**Figure 4.29.** Electron density geometries of HOMO and LUMO illustrated for the optimized structure of inhibitors.

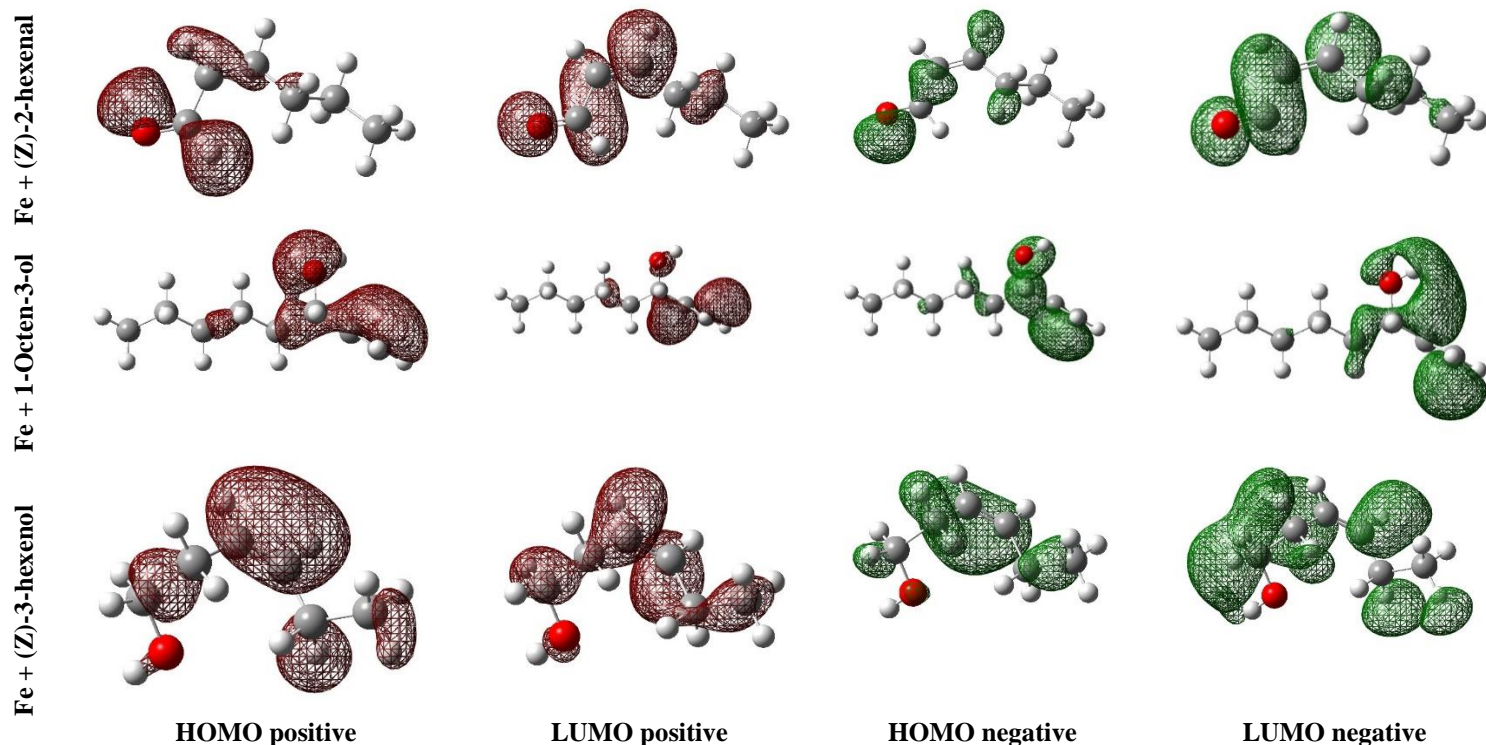


**Figure 4.30.** Depiction of the insights of the electron density maps showing HOMO and LUMO positive and negative structures.

**Table 4.16**

Data values of quantum chemical parameters using DMol3 Acceler based on Material Studio 2017.

Code	Fe + (Z)-2-hexenal	Fe + 1-Octen-3-ol	Fe + (Z)-3-hexenol
Program	Dmol3	Dmol3	Dmol3
Method	DFT	DFT	DFT
Basis set	DNP	DNP	DNP
Function	GGA	GGA	GGA
$E_{\text{HOMO}}$ (au)	-0.22825	-0.230724	-0.21686
$E_{\text{LUMO}}$ (au)	-0.11207	-0.049075	-0.03525
$E_{\text{HOMO}}$ (eV)	-6.21079	-6.278161547	-5.90099

$E_{LUMO}$ (eV)	-3.04937	-1.335365103	-0.95926
$\Delta E = E_{LUMO} - E_{HOMO}$ (eV)	3.161421	4.942796444	4.941735
$\eta = \Delta E / 2$ (eV)	1.58071	2.471398222	2.470868
$\sigma(S) = 1 / \eta$ (eV <sup>-1</sup> )	0.632627	0.404629246	0.404716
$P_i = (E_{HOMO} + E_{LUMO}) / 2$	-4.63008	-3.806763325	-3.43013
$\chi = -P_i$	4.630077	3.806763325	3.430126
$\Delta N_{max}$	1.464556	0.770163887	0.694114
$\Delta N$ (FET)	-1.46456	-0.770163887	-0.69411
$\Omega$ (eV)	6.781007	2.931831641	2.380898
$\epsilon$	0.147471	0.341083706	0.42001
$\Delta E$ Back-donation	-0.39518	-0.617849556	-0.61772

MC simulation is utilized to study the interactions of the examined inhibitors. In simulation investigations, the most stable optimal inhibitor configuration is employed<sup>31,294</sup>. Herein, the MC simulation was employed to simulate the influence of water and corrosive agents on a portion of the corrosion mechanism. The inhibitor molecule accumulates over the metallic surface specifically in a semi-flat layout, as illustrated in **Figure 4.31**, according to Monte Carlo Simulations (a similar trend in the case of **Figure 4.32**). Because of the flat adsorption configuration, the adsorbed molecule might be more persistent. In addition, adding additional active areas to the metallic surface improves surface coverage. **Table 4.17** illustrates the values of total energy and adsorption energy of the (Z)-2-hexenal, 1-Octen-3-ol and (Z)-3-hexenol with the output of total energy of -4127.104, -4.97.982, -4084.742 and -4086.084, -4077.808 and -4076.877. These values show the higher intensity of the adherence of the (Z)-2-hexenal, 1-Octen-3-ol and (Z)-3-hexenol over the mild steel in the presence of water and acidic simulated system and as well as this outcome can be further correlated with the similar findings obtained in **Table 4.18**.

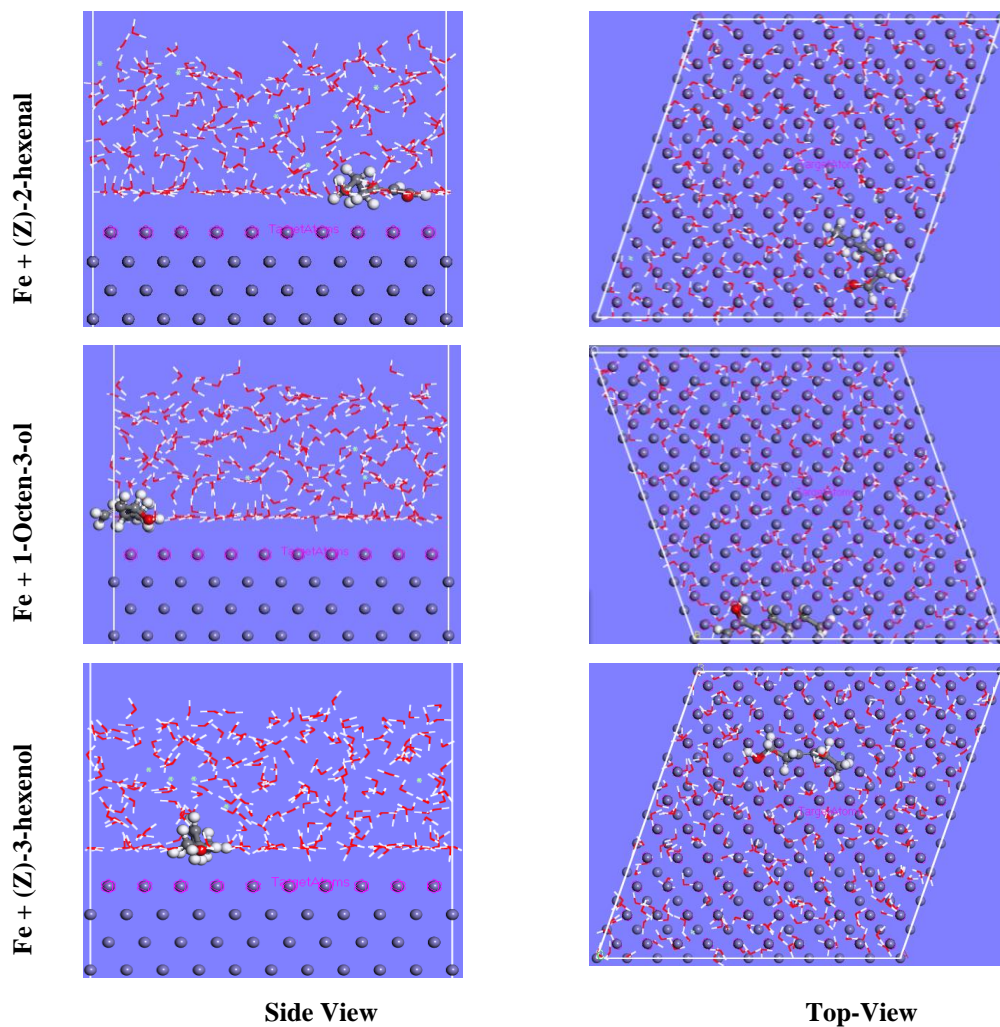


**Figure 4.31.** Equilibrium positions of the most stable and persistent configuration of inhibitors on Fe (110) in a simulated HCL corrosive system.

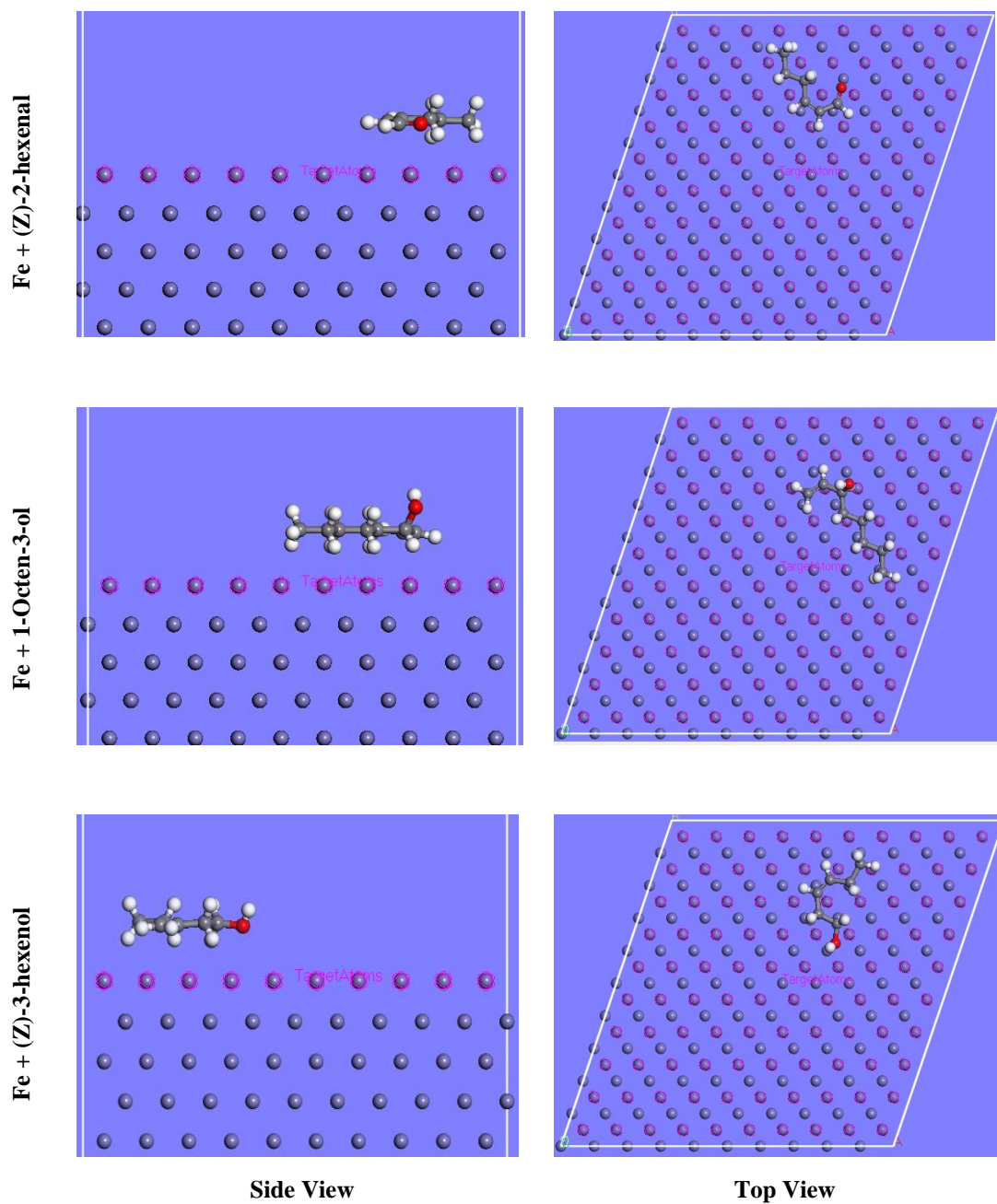
**Table 4.17**

List of Molecular simulation parameters by Montecarlo simulation (250 H<sub>2</sub>O + 5 H<sub>3</sub>O<sup>+</sup> +5CL<sup>-</sup> + Inh).

Structures	Fe + (Z)-2-hexenal	Fe + 1-Octen-3-ol	Fe + (Z)-3-hexenol
<b>Total energy</b>	-4127.104	-4097.982	-4084.742
<b>Adsorption energy</b>	-4086.084	-4077.808	-4076.877
<b>Rigid adsorption energy</b>	-4266.833	-4259.103	-4252.121
<b>Deformation energy</b>	180.7498244	181.2945097	175.2438362



<b>VS_1 : dEad/dNi</b>	-72.82928704	-103.4562364	-77.75289275
<b>H<sub>2</sub>O : dEad/dNi</b>	-12.44268269	-13.04877336	-13.17508131
<b>H<sub>3</sub>O<sup>+</sup> : dEad/dNi</b>	-151.1232305	-150.0685885	-143.5874883
<b>Cl<sup>-</sup> : dEad/dNi</b>	-150.9811659	-146.1347495	-151.2737133

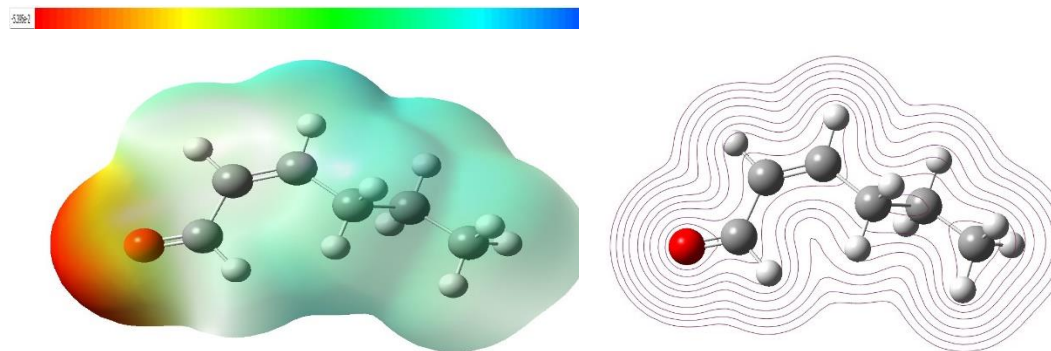
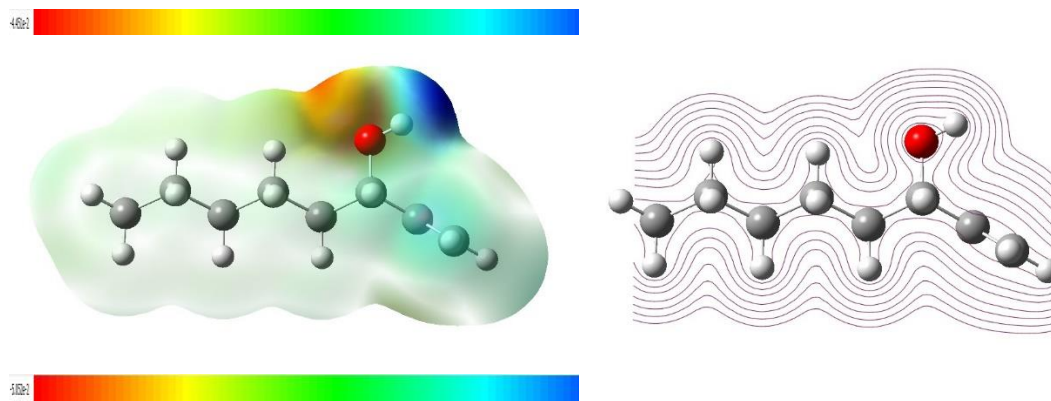


**Figure 4.32.** Equilibrium positions of most stable arrangement of inhibitors on Fe (110) in a vacuum.

**Table 4.18**

List of Molecular simulation parameters by Montecarlo simulation in a vacuum.

Structures	Fe + (Z)-2-hexenal	Fe + 1-Octen-3-ol	Fe + (Z)-3-hexenol
Total energy	-109.191	-105.793	-72.2674
Adsorption energy	-68.1698	-85.6191	-64.4025
Rigid adsorption energy	-69.8187	-85.4884	-68.9742
Deformation energy	1.64891	-0.13072	4.571699
VS Inh: dEad/dNi	-68.1698	-85.6191	-64.4025

**Fe + (Z)-2-hexenal****Fe + 1-Octen-3-ol**

Fe + (Z)-3-  
hexenol

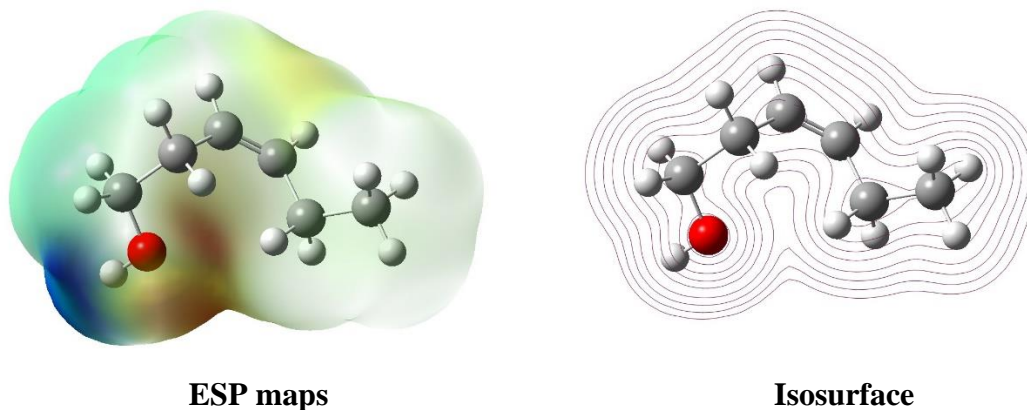


**Figure 4.33.** ESP mappings and isosurface of (Z)-2-hexenal, 1-Octen-3-ol and (Z)-3-hexenol.

Electrostatic potential mapping (ESPs) is another method for assessing the presence of electrophilic active regions in a chemical moiety. The electrophilic active region is positioned in the oxygen regions, as illustrated in **Figure 4.33** relying on the ESP mappings of all molecules, that are red-yellow in appearance<sup>295,296</sup>. As an outcome, these electrophilic active regions may increase electron transmission with the Fe surface's d unoccupied orbital and therefore bind efficiently to the metal substrate, attributing to their high inhibitory efficacy as seen in the figure above.

#### 4.2.9. Biodegradability of VSE

The biodegradation rate of VSE followed by 28 days of analysis has been depicted in **Figure 4.34**. As indicated in **Figure 4.34**, the rate of VSE deterioration expanded with time interval, reaching 82% after 28 days computed using equation (19). Referring to the North-East Atlantic Protocol for the Sustainability of the Ecosystem, readily biodegradable substances have a biodegradation rate of higher than 60% in 28 days<sup>273</sup>. As a result, VSE could be classified as a biodegradable corrosion inhibitor.

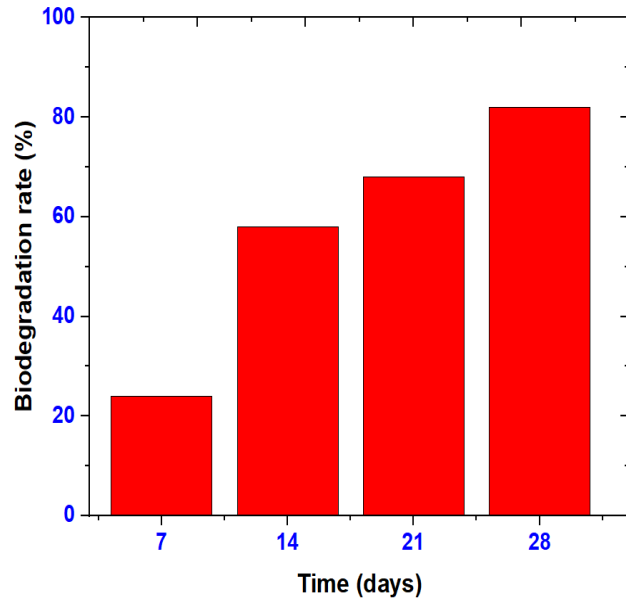


**Figure 4.34.** Biodegradability of VSE in 28 days.

### 4.3. *Thysanolaena latifolia*

*Thysanolaena latifolia* (TL) is a weed commonly referred to as Tiger Grass or Asian Broom. This species belongs to the Thysanolaeneae genus and is part of the Eukaryota domain, Plantae kingdom, Spermatophyta phylum, Angiospermae subphylum, and Monocotyledonae class. TL is a fast-growing evergreen perennial that grows to 3m (9ft). It has a circular, sturdy stem and its leaves are heart-shaped, narrow, large, leathery and taper to a fine tip. Its flowering panicles are used to manufacture long-lasting dust brooms. According to the previous investigation<sup>297</sup>, TL leaves extract (TLLE) constitutes of several major phytochemical constituents such as (Z)-3-hexen-1-ol, (E)-b-ionone and Phytol as illustrated in **Figure 4.35**. To the best of our knowledge, TLLE has not been documented as a mild steel corrosion inhibitor in an acidic environment. Through gravimetric technique, electrochemical investigations (including Tafel plots and impedance spectroscopy), and morphological evaluation utilizing scanning electron microscopy, TLLE were extracted and evaluated to mitigate the corrosion rate of mild steel in a corrosive media of 0.5M HCl. The author anticipates that using TLLE as an eco-benign corrosion inhibitor for mild steel can have several positive outcomes. Firstly, by using TLLE, there is potential to reduce the reliance on synthetic corrosion inhibitors, which can be expensive and environmentally harmful. This can lead to a lower cost of corrosion inhibitors and the reuse of TL leaves components, which can contribute to the promotion and cultivation of TL and other weeds. The use of TLLE as a corrosion inhibitor possesses only a minimal negative influence on both humans and the ecosystem. Unlike traditional corrosion inhibitors, TLLE is derived from a natural source and is non-toxic, making it a safer alternative for use in various industries. Additionally, TLLE is easily biodegradable and does not persist in the environment, which reduces the risk of long-term harm to the environment. Its use can help reduce the environmental and health risks associated with traditional corrosion inhibitors while providing an effective solution for inhibiting corrosion in various industrial applications. By using waste and useless considered weeds, such as TL leaves, as an effective corrosion inhibitor, it is possible to reduce waste; promote sustainable practices and combat the catastrophic global concern i.e., corrosion.

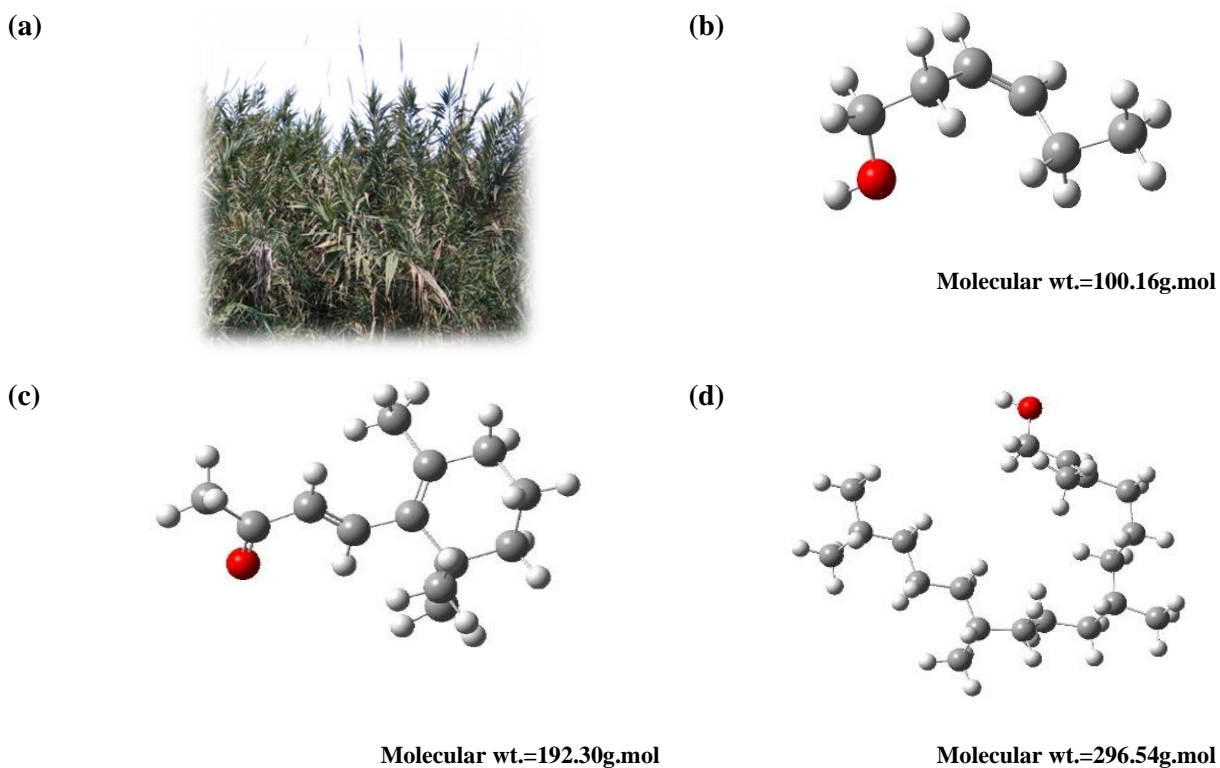


**Figure 4.35.** Schematic depiction of (a) *Thysanolaena latifolia*; the main phytochemical constituents of TLLE (b) (Z)- 3-hexen-1-ol, (c) (E)-b-ionone, (d) Phytol.

#### 4.3.1. Preparation of *Thysanolaena latifolia* leaves extract

The *Thysanolaena latifolia* (TL) leaves were collected from the agricultural region of Jalandhar and later confirmed by Prof. Neera Rashmi from the Botany department (HPU), India. The TL leaves were rinsed with circulating tap water before being treated with double distilled water to eradicate contaminants for the extraction procedure. The leaves were then air-dried at ambient conditions for 5-7 days. Utilizing the previous method documented in the literature<sup>297</sup>, the dried leaves (1000g) were crushed in a lab mill and extracted using steam distillation with 2500ml deionized water for 4 hrs. The extract was purified using a 0.45  $\mu\text{m}$  filter to concentrate its bioactive components. The best solubility of the TL extract in 0.5 M HCl was found to be 1000 mg/L, and the remaining extract was reserved at  $-20^{\circ}\text{C}$  for future use.

### 4.3.2. FT-IR evaluation

The accessibility of heteroatoms (O) and aromatic rings may facilitate the adsorption of inhibitor molecules upon the metallic surfaces, thus mitigating corrosion. **Figure 4.36** illustrates the TLLE's FTIR spectrum. The FTIR spectra of the TLLE illustrate the –OH stretching vibration at  $3379\text{ cm}^{-1}$  and the wider peak suggested that a molecular interaction had been procured. The peak at  $2924\text{ cm}^{-1}$  symbolizes the stretching vibration of –C–H. –C–O stretch was attributed to the peak attained at  $1159\text{ cm}^{-1}$ . The spikes at  $2856$ ,  $1373$ ,  $1456$ ,  $1715$  and  $1645\text{ cm}^{-1}$  correspond to the –CHO stretch, –CH<sub>3</sub> bend, –CH<sub>2</sub> bend, –C=O stretch and –C=C stretching. The spikes at  $904\text{ cm}^{-1}$  and  $1261\text{ cm}^{-1}$  are attributed to the =C–H bend and –C–O–H bend. Such outcomes demonstrated the presence of oxygen in TLLE's functional moieties (C=O, O–H, C–O), which is persistent with the structure of common corrosion inhibitors<sup>243,296,298,299</sup>. The existence of these functional moieties in TLLE may facilitate the adsorption of inhibitor molecules onto the metallic surface, which can mitigate corrosion. The availability of aromatic rings and heteroatoms including oxygen, in the extract, may also contribute to its corrosion inhibition properties. Therefore, the TLLE extract inhibited mild steel deterioration in 0.5M HCl owing to the existence of these functional moieties.

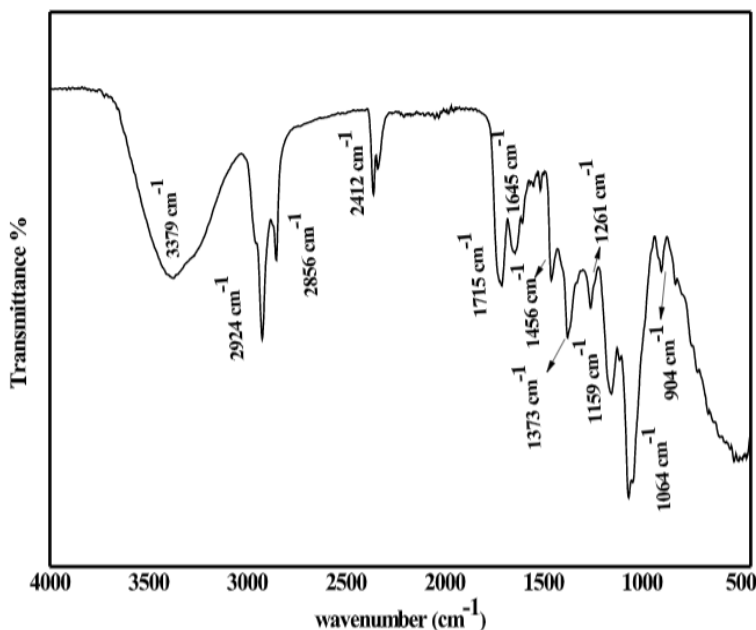


**Figure 4.36.** FT-IR analysis of the TLLE.

### 4.3.3. UV-visible spectroscopy

The UV spectrum analysis of TLLE was conducted to investigate the changes in its chemical composition after the corrosion experiments. The UV spectrum was taken pre and post of corrosion experiments, and the absorption maxima were analyzed as shown in **Figure 4.37**. The results showed that TLLE had two absorption maxima at 354.64 nm and 419.22 nm, which relates to the  $n-\pi^*$  and  $\pi-\pi^*$  transitions, respectively. The primary peak observed in the spectra was due to the  $\pi-\pi^*$  transition and was attributed to the C=C conjugation that existed in the inhibitor molecules. The absorption peak observed in the 250-350 nm range corresponded to the  $n-\pi^*$  transition and was ascribed to the various functional moieties found in inhibitor molecules, including C–O–H, C–O. After the corrosion experiments, the absorption maxima were redistributed, indicating that a complex had formed between Fe and phytochemicals present in TLLE. The hypsochromic shifting of the maximum adsorption indicated that some of the inhibitor molecules had effectively adhered to the metallic substrate while the mild steel sample was dipped in the 0.5M HCl + TLLE. The UV spectra analysis provided information on the chemical changes in TLLE after the corrosion experiments, indicating that the TLLE molecules had potentially been adsorbed onto the substrate to impede corrosion. The results suggested that the TLLE inhibitor was effective in forming a preventive covering over the mild steel surface to prevent corrosion in acidic environments.

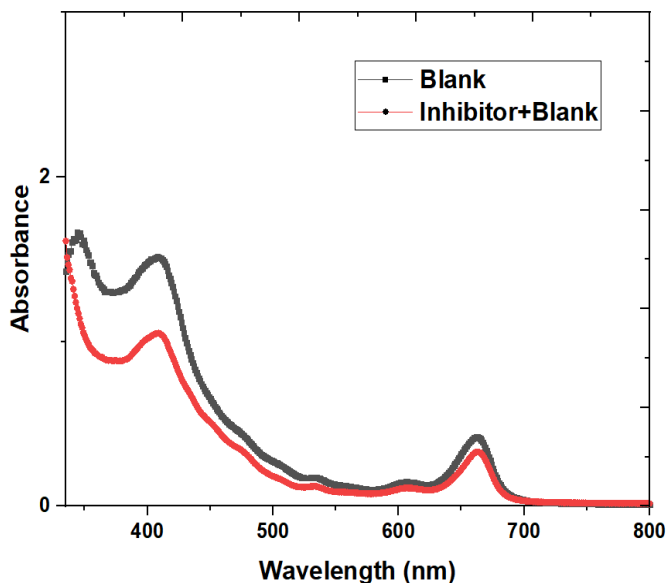


**Figure 4.37.** UV spectrum of pre and post of metal dipped in 0.5M HCl and with the inclusion of TLLE.



#### 4.3.4. Weight loss (WL) assessment

WL assessment is a common approach used to compute the corrosion rate of metallic materials. In this method, a metal specimen of known weight is exposed to corrosive surrounding for a certain duration<sup>96,300</sup>. Following exposure, the specimen is taken out, cleaned, and reweighed as shown in **Figure 4.38**. The  $C_R$  is then determined by deducting the initial weight from the weight following exposure, or weight loss. The WL assessment approach is based on the principle that the  $C_R$  is directly linked to the amount of metal loss due to corrosion. The weight loss method is straightforward, making it a commonly used technique in the field of corrosion studies. In this experiment, WL investigations were carried out to determine the influence of time (15–60 min.), temperature (298–328 K), and TLLE concentration (50–1000 ppm) on the effectiveness of TLLE on the mild steel corrosion inhibition in 0.5M HCl media at the optimal temperature for the specified time (as mentioned in **Table 4.19** and **4.20**). Following obtaining the pre- and post-weight of the mild steel specimen immersed in blank and several quantities of TLLE, the  $\Theta$ , IE%, and  $C_R$  were evaluated employing equations (1-3).

The impacts of time, temperature, and concentration upon the effectiveness of the inhibitor against mild-steel corrosion in 0.5 M HCl have been provided in **Table 4.19**, **4.20** and **4.21** and **Figure 4.38** beneath. From **Table 4.19**, it could be noticed that the IE% of TLLE toward mild steel corrosion decreases with expanding time. The IE% values range from 88.160% at 15 minutes to 62.854% at 60 minutes. This suggests that the potential of TLLE as a corrosion inhibitor decreases with expanding exposure time to the corrosive environment. However, even at 60 minutes, the IE% value of TLLE is still relatively high, indicating its potential as a corrosion inhibitor. **Table 4.20** shows the influence of temperature variation on the IE% of TLLE on mild steel corrosion in the presence and absence of the inhibitor. The experiment was conducted at distinct temperatures varying from 298 K to 328 K, and the weight loss measurements were taken to calculate the IE%. The outcomes revealed that the IE% of TLLE on mild steel corrosion decreases with an expansion in temperature. At 298 K, the IE% was found to be 88%, which decreased to 82% at 308 K, 77.16% at 318 K, and 63.59% at 328 K. The reduction in IE% with temperature increase can be associated with the fact that at higher temperatures, the corrosion rate of mild steel increases owing to the increased rate of chemical reactions involved in the corrosion process. Additionally, **Table 4.21** shows that at 0 ppm concentration (blank), the weight loss was 0.901 mg, and the corrosion rate was  $2.513 \text{ mmyr}^{-1}$ . The inhibition efficiency was not calculated since there was no inhibitor in the

blank sample. As the concentration of TLLE increased from 50 ppm to 1000 ppm, the weight loss decreased from 0.210 mg to 0.073 mg, demonstrating a decrease in  $C_R$ . The corrosion rate also decreased from  $0.585 \text{ mmyr}^{-1}$  to  $0.203 \text{ mmyr}^{-1}$  with an elevation in TLLE concentration. This demonstrates that the TLLE has an inhibiting effect on mild steel corrosion. The IE% of TLLE also enhanced with an increase in concentration, ranging from 59.843% at 50 ppm to 91.897% at 1000 ppm. This indicates that higher concentrations of TLLE are more effective in inhibiting mild steel corrosion. The concise evaluation of **Figure 4.38 (b)** and **(c)** demonstrated that the IE% enhanced with increasing TLLE amount while decreasing with increasing temperature (as shown in **Table 4.20**), suggesting that a defensive covering developed on the surface of mild steel by the inhibitor becoming less prolonged at high temperatures. Overall, the results suggest that TLLE has viability as a corrosion inhibitor for mild steel in acidic environments.

**Table 4.19**

The influence of time fluctuations on the IE% of TLLE on the corrosion inhibition of mild steel.

Time (min.)	W0 (mg)	Wi (mg)	W0-Wi (mg)	IE%
15	1.762	1.623	0.139	88.160
30	1.712	1.512	0.211	82.935
45	1.943	1.698	0.245	74.019
60	1.854	1.552	0.302	62.854

**Table 4.20**

The influence of temperature fluctuations on the IE% of TLLE on the corrosion inhibition of mild steel.

Temp. (K)	W0 (mg)	Wi (mg)	W0-Wi (mg)	IE%
298	1.917	1.794	0.123	88
308	1.982	1.769	0.213	82
318	1.974	1.792	0.182	77.16
328	1.847	1.373	0.474	63.59

**Table 4.21**

The influence of concentration fluctuations on the IE% of TLLE on the corrosion inhibition of mild steel.

Conc. (ppm)	W0 (mg)	Wi (mg)	W0-Wi (mg)	C <sub>R</sub>	Θ	IE%
Blank	1.819	0.918	0.901	2.513	-	-
50	1.682	1.472	0.210	0.585	0.598	59.843
100	1.924	1.641	0.284	0.792	0.684	68.479
250	1.735	1.521	0.215	0.599	0.761	76.137
500	1.824	1.671	0.154	0.429	0.829	82.907
1000	1.874	1.801	0.073	0.203	0.918	91.897

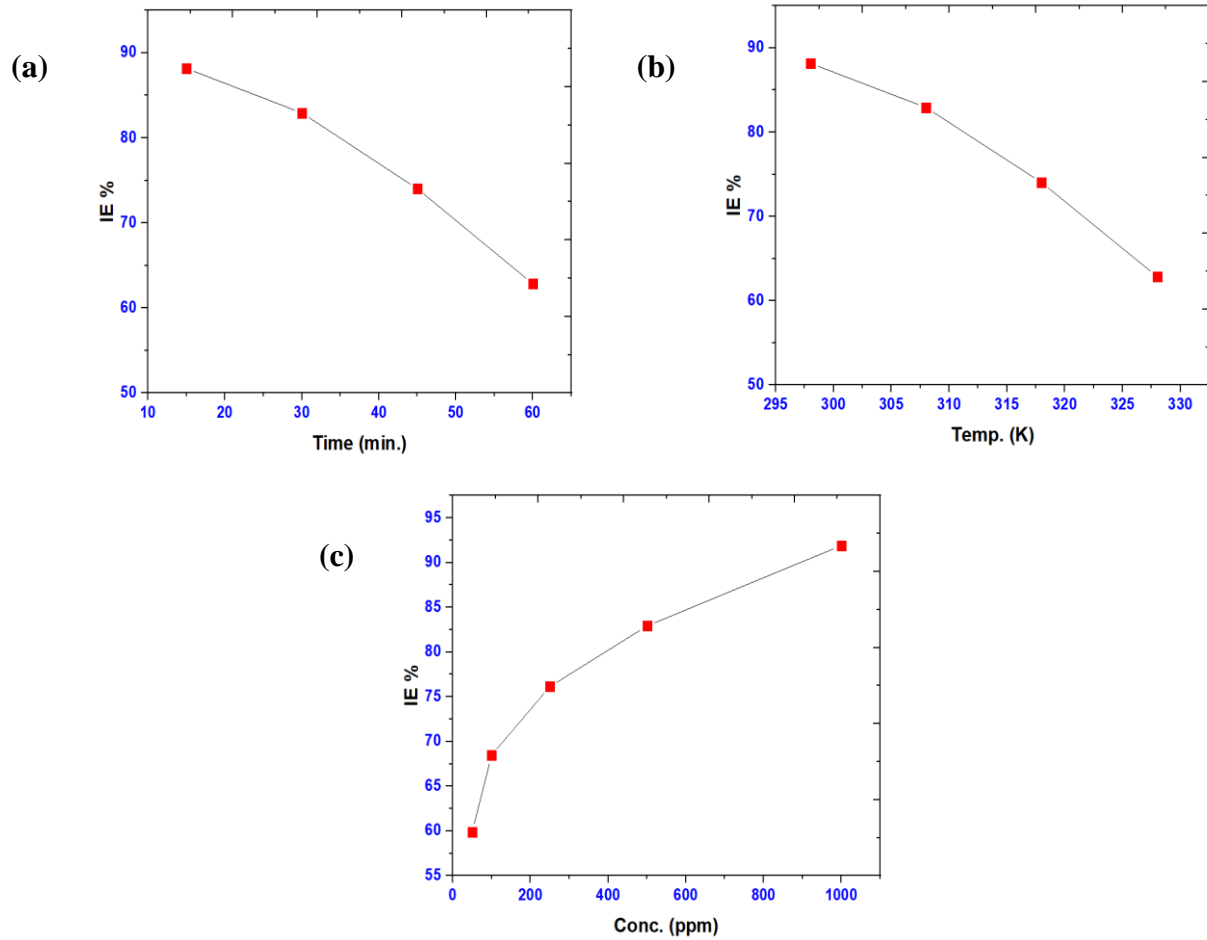


**Figure 4.38.** (a) Time, (b) temperature and (c) concentration fluctuations effect on the IE% of TLLE.

#### 4.3.5. Adsorption and thermodynamic parameters

Adsorption and thermodynamic parameters are crucial in analyzing the mechanism of corrosion inhibition. The adsorption isotherms are utilized to determine the adsorption behavior of inhibitors on the metal surface, while the thermodynamic variable including the free energy of adsorption, entropy of adsorption and enthalpy of adsorption provide crucial insights into the nature and strength of the adsorption phenomenon<sup>241,301,302</sup>. In corrosion inhibition, adsorption occurs through the emergence of a preventive covering on the metallic surface. This film prevents the corrosive environment from accessing the metal surface, thus reducing the  $C_R$ . The adsorption of inhibitors on the metallic surface can occur through numerous mechanisms such as electrostatic attraction, chemical bonding, and physical adsorption. The type of adsorption phenomenon relies on the nature of the inhibitor and the metallic surface. The free energy of adsorption ( $\Delta G^\circ_{\text{ads}}$ ) indicates whether the adsorption process is spontaneous or not. A negative  $\Delta G^\circ_{\text{ads}}$  value indicates spontaneous adsorption, while a positive value indicates non-spontaneous adsorption. The enthalpy of adsorption ( $\Delta H^\circ_{\text{ads}}$ ) provides information about the energy involved in the adsorption process. A negative  $\Delta H^\circ_{\text{ads}}$  value indicates exothermic adsorption, whereas a positive value reflects endothermic adsorption. The entropy of adsorption ( $\Delta S^\circ_{\text{ads}}$ ) indicates the degree of disorder linked with the adsorption phenomenon. The gathered experimental data showed that inhibitor adsorption occurs on mild steel substrate by following the Langmuir adsorption isotherm, demonstrating the production of a thin monolayer over the metal's substrate. The plot of  $\log C/\theta$  Vs.  $\log C$  revealed that the regression coefficient ( $R^2$ ) was nearer to unity, 0.99973, leading to a straight inclination featuring an  $R^2$  value of 1, as depicted in **Figure 4.39 (a)**. The outcomes of this examination are depicted in **Table 4.22**. In **Figure 4.39 (b)**, a graph of  $\log C_R$  vs  $1/T \cdot 10^{-3} \text{K}$  showed a linear inclination, and slopes ( $-E_a/2.303R$ ) which were employed to compute the activation energy value. The Arrhenius equation was further employed to compute the kinetic factors<sup>6,258</sup>. The  $\Delta H^\circ_{\text{ads}}$  value was computed utilizing a  $\log K_{\text{ads}}$  vs.  $1/T \cdot 10^{-3} \text{K}$  graph having a linear inclination over curve  $-H/2.303R$ , as shown in **Figure 4.39 (c)**. These parameters were calculated using equations (5) and (6). Additionally, equations (7) and (8) were employed to determine the values of  $\Delta G^\circ_{\text{ads}}$  and  $\Delta S^\circ_{\text{ads}}$ .

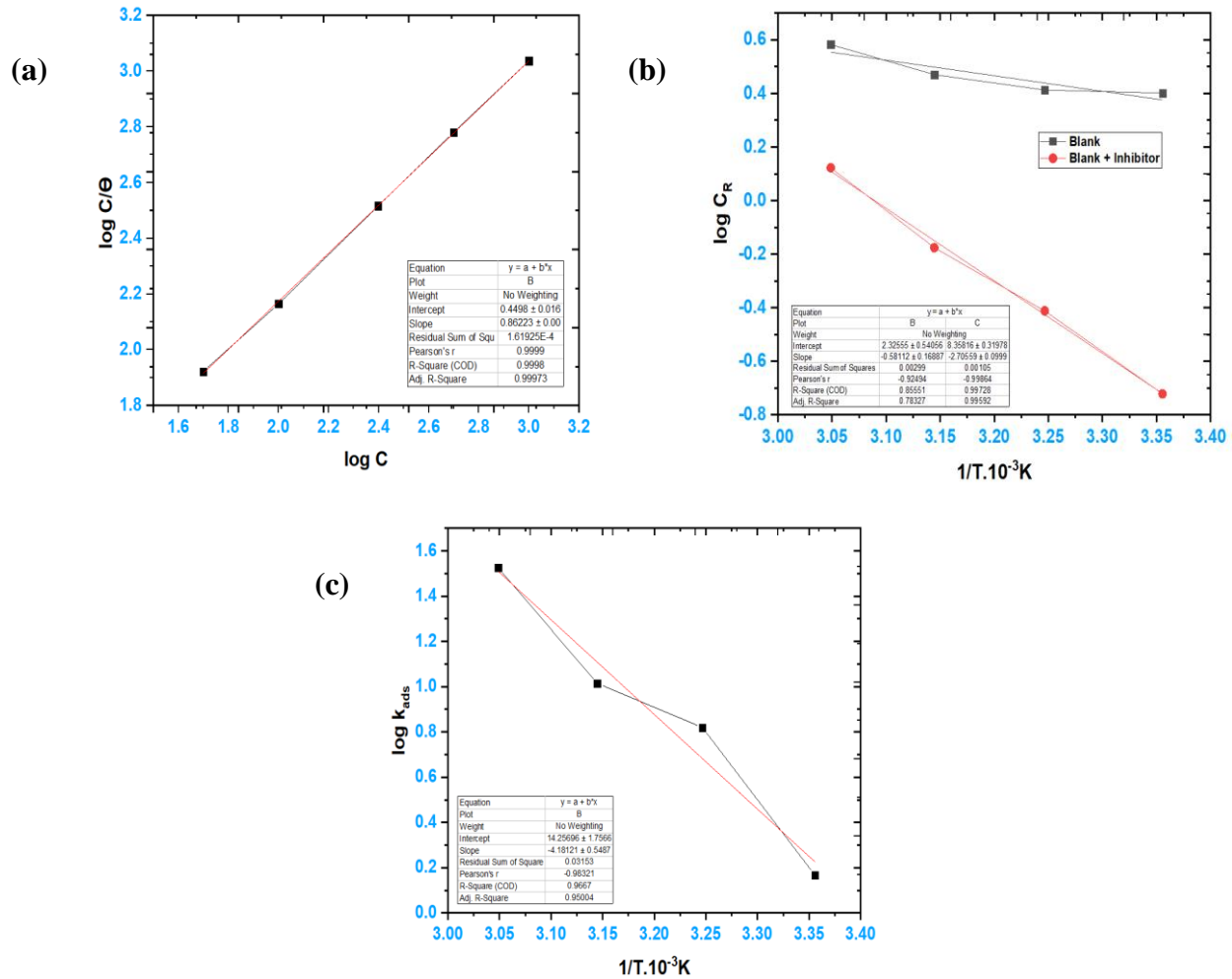


**Figure 4.39.** (a) Langmuir adsorption graph (b) Arrhenius graph (c) Enthalpy graph of TLLE on the corrosion inhibition of mild steel in 0.5 M HCl medium.

**Table 4.22**

Adsorption, thermodynamic and kinetic variables for the corrosion inhibition of mild steel in several amounts of TLLE at 298K.

Metal	Inhibitor (ppm)	$\log K_{ads}$	$\Delta G^0_{ads}$ kJmol <sup>-1</sup>	$\Delta H^0_{ads}$ kJmol <sup>-1</sup>	$\Delta S^0_{ads}$ kJmol <sup>-1</sup>	Ea kJmol <sup>-1</sup>
			1		1	
Mild steel	Blank	-	-	-	-	3.165
	50ppm	0.397	1.886	0.0348	0.118	17.864

<b>100ppm</b>	0.502	2.336
<b>250ppm</b>	1.649	3.512
<b>500ppm</b>	2.433	4.183
<b>1000ppm</b>	4.179	0.384

**Table 4.22** elaborates that with the inclusion of TLLE, a higher value of  $E_a$  suggests the development of a defensive covering upon the metallic surface by the adsorption of TLLE molecules, which physically prevents mass and charge transmission. Due to the endothermic attribution of mild steel dissolution demonstrated by the existence of positive  $\Delta H_{ads}^o$  values, mild steel corrosion was difficult to procure even in the existence of low TLLE concentrations<sup>281</sup>. Additionally, the value of  $\Delta S_{ads}^o < 0$  indicated that the adsorption phenomenon was static and the rate-determining step was associated with the emergence of the complex compounds, which means that once the intricate compound has developed, the instability declines and  $H_2O$  molecules desorbed from the substrate. Significant interactions between inhibitor molecules and metallic substrates are also suggested by the dramatic increase in  $\log K_{ads}$  values. Our investigation,  $\Delta G_{ads}^o$  confirms that the TLLE is effectively adsorbed on the mild steel via interacting  $\pi$ - $\pi$  electrons and lone pair of electrons. Consequently, the molecules are firmly adhered over the metallic surface culminating in excellent corrosion IE% of the investigated inhibitor.

#### 4.3.6. Electrochemical measurements

##### 4.3.6.1. Open circuit potential (OCP)

It is vital to attain a consistent OCP priorly to beginning with the PDP and EIS analysis. Herein, the working electrode comprised of the mild steel rod was submerged in the test media for 1hr throughout each investigation involving the concentration variation from 50ppm to 1000ppm of TLLE. **Figure 4.40** shows the OCP vs. time (sec.) trends in the exclusion and inclusion of several amounts of TLLE (50-1000ppm). By evaluating **Figure 4.40**, it could be observed that when the concentration of TLLE ascended from blank to 1000ppm, the value of  $E_{ocp}$  transmits toward a more negative value, suggesting that TLLE acts as a cathodic inhibitor<sup>303,304</sup>. This shift relied upon the TLLE molecules' interaction with the mild steel sample. Additionally, the negative shift of OCP for the bare specimen could be accounted for the iron oxide formation/dissolution over the metallic substrate

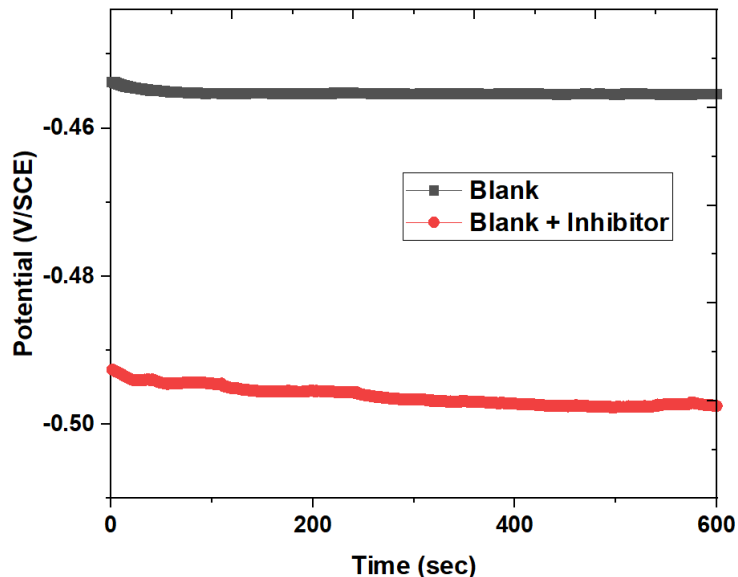


**Figure 4.40.** OCP vs. time graph for corrosion inhibition of mild steel after exposure to 1000ppm of TLLE concentration in 0.5M HCl.

#### 4.3.6.2. Potentiodynamic polarization

Potentiodynamic polarization is a technique used in corrosion studies to investigate the corrosion functionality of metals and to evaluate the effectiveness of corrosion inhibitors<sup>95,305,306</sup>. The technique involves measuring the current-potential relationship of a metal surface in a corrosive environment while subjecting it to a controlled change in potential. The impact of TLLE on the cathodic hydrogen ions reduction mechanism and anodic dissolving of mild steel in corrosive media was determined by the utilization of the PDP technique<sup>307</sup>. The anodic Tafel slope ( $\beta_a$ ) and cathodic Tafel slope ( $\beta_c$ ), corrosion current densities ( $i_{corr}$ ), and corrosion potential ( $E_{corr}$ ) values have been attained through the analysis of resultant polarization parameters, as depicted in **Table 4.23**. The value of  $i_{corr}$  and  $C_R$  declined dramatically from 498.54 to 117.91 ( $\mu A$ ) and 7.279 to 1.183 (mm/yr) with increasing TLLE concentrations (50-1000ppm) revealing significant corrosion inhibition potential of TLLE. The preventative influence of the TLLE on mild steel was continuously enhanced as the quantity of inhibitor was elevated from 50 to 1000ppm. These results demonstrated that inhibitors hindered the mechanism of hydrogen production as well as the dissolution of metal<sup>308,309</sup>. The polarization slope as shown in **Figure 4.41** also showed that the cathode shift was greater than the anode shift. Therefore, TLLE acts as a mixed-type corrosion inhibitor, mainly as a cathodic inhibitor, in a 0.5 M HCl solution. **Table 4.23** demonstrates that the

addition of the TLLE frequently resulted in the variation of the  $\beta_c$  and  $\beta_a$  values from -145.65 mV/dec to -104.38 mV/dec and 165.78 mV/dec to 102.84 mV/dec, demonstrating that the mechanism of hydrogen evolution persists to be constant. This could be due to the inhibitor molecules binding to the mild steel substrate, which creates a defensive covering and reduces the availability of active sites for the reaction, thereby controlling the charge transfer mechanism of hydrogen evolution.

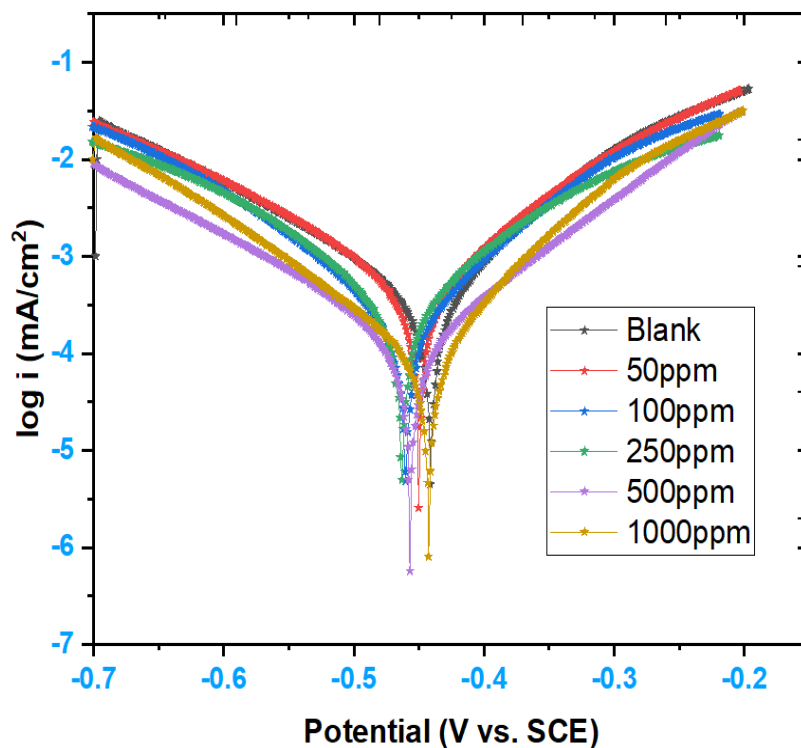


**Figure 4.41.** Tafel graph for the corrosion mitigation of mild steel in blank solution subjected to 50-1000ppm amounts of TLLE at 298 K.



**Table 4.23**

Tafel variables for the corrosion inhibition of mild steel in blank solution subjected to 50-1000ppm amounts of TLLE at 298 K.

Conc. (ppm)	-E <sub>corr</sub> (mV vs. SCE)	i <sub>corr</sub> (μA)	j <sub>corr</sub> (μA/cm <sup>2</sup> )	β <sub>a</sub> (mV/dec)	-β <sub>c</sub> (mV/dec)	C <sub>R</sub> (mm/yr)	χ <sup>2</sup>
<b>Blank</b>	472.91	498.54	498.54	165.78	145.65	7.279	4.546E-06
<b>50</b>	440.85	454.32	454.32	145.32	142.95	5.279	3.422E-06
<b>100</b>	460.07	262.58	262.58	126.45	131.34	4.351	1.1163E-06
<b>250</b>	442.51	156.29	156.29	120.32	115.78	4.051	6.0561E-07
<b>500</b>	465.8	142.48	142.48	116.14	117.75	3.191	6.8035E-08
<b>1000</b>	479.49	117.91	117.91	102.89	104.38	1.183	9.6359E-08

#### 4.3.6.3. Electrochemical impedance spectroscopy (EIS)

EIS is a powerful approach utilized in the study of corrosion inhibition. It involves the application of a minimal sinusoidal voltage to a metal surface immersed in an electrolyte and the measurement of the resulting current response. The impedance of the metal-electrolyte interface is then analyzed to obtain information about the corrosion behavior and the effectiveness of corrosion inhibitors. EIS can offer crucial insights into the corrosion inhibition mechanism, including the inhibition efficiency, film formation, and adsorption behavior of the inhibitor over the metallic surface<sup>310,311</sup>. The impedance spectra obtained from EIS typically contain several components, including the solution resistance (R<sub>s</sub>), the charge transfer resistance (R<sub>ct</sub>), and the double-layer capacitance (C<sub>dl</sub>). The PDP and WL assessments' findings were validated by the EIS evaluations of mild steel in a solution of 0.5 M HCl using a range of TLLE amounts, which were also used to gather pertinent data on the corrosion process. The data collected from the evaluations were compiled and summarized in **Table 4.24**. **Figures 4.42** and **4.43** illustrate the plots of Nyquist and Bode, correspondingly. The Nyquist graph impedance spectrum (**Figure 4.42**) demonstrated a significant inductive arc at the minimal frequency and a capacitive arc at a greater frequency. While the lessen frequency inductive loop was created by the relaxation state spurred by Hads<sup>+</sup>, Cl<sup>-</sup>, and TLLE molecule adsorption upon the mild steel substrate, the higher frequency capacitive arc was generated by the charge transmission process and substrate inhomogeneity. The re-dissolution of

the passivated substrate at a lower frequency may be feasible. The layout of all slopes in the Nyquist plot remained constant whether an inhibitor was used or not, showing that the mild-steel corrosion process was unaffected. Additionally, due to frequency diffusion, irregularities, and inhomogeneities of the surface of the working electrode, their forms were not optimum. The diameters of the illustrated semicircles enlarged as TLLE inclusion expanded from 50 to 1000 ppm, suggesting that the dispersion of TLLE upon the electrode increased and a defensive coating was formed, providing effective electrode surface protection from corrosion moieties.

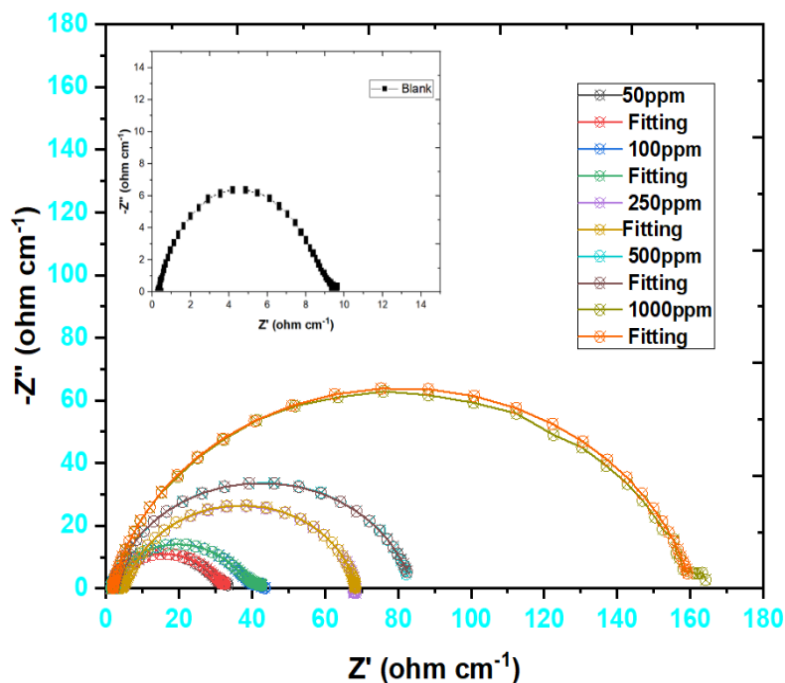


**Figure 4.42.** Nyquist graph for the corrosion mitigation of mild steel in blank media subjected to 50-1000ppm concentrations of TLLE at 298 K.

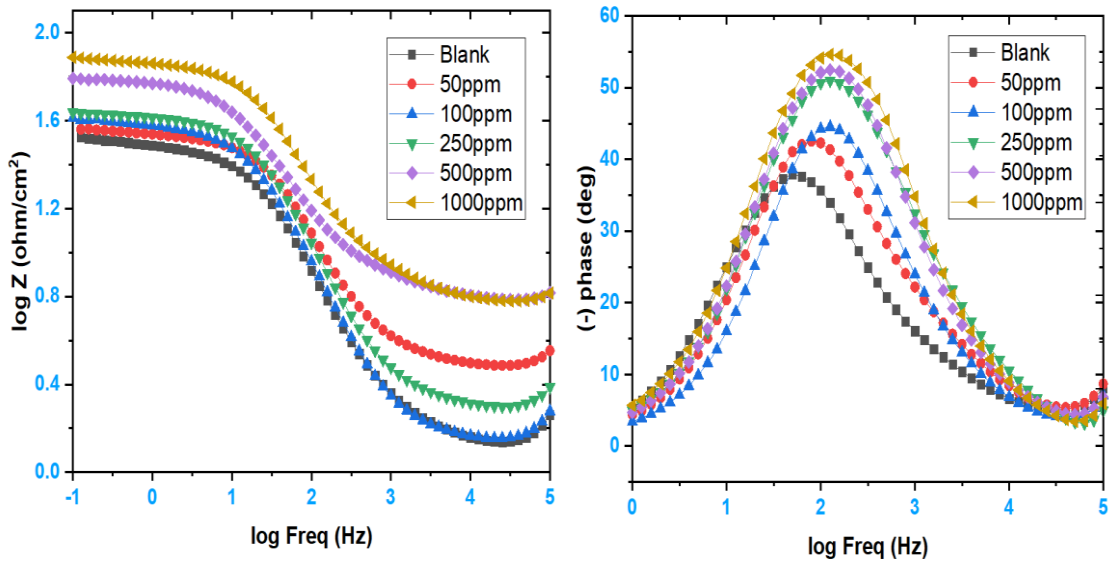


**Figure 4.43.** Bodes graph for the corrosion mitigation of mild steel in blank solution subjected to 50-1000ppm conc. of TLLE at 298 K.

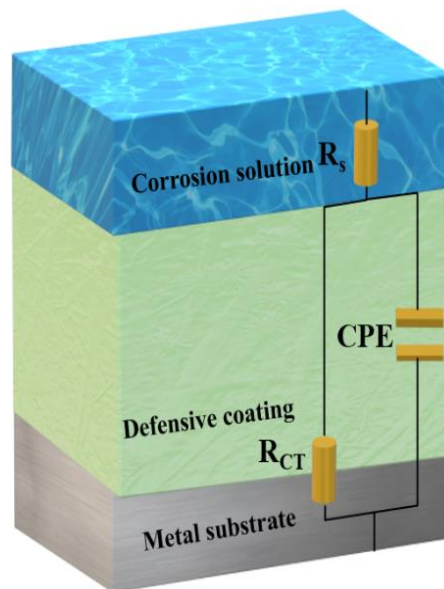


**Figure 4.44.** A circuit model with equivalent components employed to fit the collected data.

**Figure 4.43** depicts the Bode graph for mild steel in the 0.5 M HCl medium with the inclusion and exclusion of various amounts of TLLE (50–1000 ppm). During the analysis, it was observed that as the concentration of TLLE increased, the impedance modulus of the mild steel also increased

across the frequency spectrum being analyzed. Additionally, it was observed that at the highest phase angle, the frequency spectrum widened. These observations are consistent with previous research<sup>252,253,266,267</sup>, which has shown that if the slope of  $\log |Z|$  vs.  $\log f$  is approximately equal to 1 and the maximum phase angle is  $90^\circ$ , then the optimal capacitance at an intermediate frequency can be identified. These findings indicate that TLLE has a significant inhibitory effect on the corrosion of mild steel in a solution of 0.5 M hydrochloric acid. The results suggest that TLLE may be a promising candidate for corrosion inhibition applications in industrial settings.

**Table 4.24** deliberate the EIS variables including  $R_{ct}$ ,  $R_s$ ,  $CPE$  (constant phase element) and  $\chi^2$  resembles the equivalent circuit fitting's discrepancy degree. The equivalent circuit layout (as shown in **Figure 4.44**) is stable and robust and observed to be consistent with optimal fitting, according to datasets of  $\chi^2$  (chi-squared) within a small range of deviance.  $\chi^2$  is a statistical measure used to evaluate the goodness of fit of a model to a set of experimental data. In the context of EIS, it is used to evaluate the quality of fit of the experimental data to the equivalent circuit model employed to analyze the EIS data. In the given data,  $\chi^2$  values are provided for each concentration of TLLE tested. Lower values of  $\chi^2$  indicate a better fit of the empirical data to the circuit model with equivalent components used for analysis. In this case, all the values of  $\chi^2$  are relatively small, indicating a good fit of the data to the model. **Table 4.24** demonstrates how the  $R_{ct}$  and IE % improved as the amount of TLLE was raised, achieving an optimum IE of 93.90 % at 1000 ppm, which is strikingly equivalent to the results of the WL and PDP experiments. In this case, the enhancement in  $R_p$  values with increasing TLLE concentration, reveals a higher resistance to electron transfer and a more significant protective layer formation with increasing TLLE concentration. The values of  $R_s$  increase with increasing TLLE concentration, demonstrating a higher resistance of the electrolyte solution with the addition of TLLE. Additionally, the  $n$  values represent the non-ideal behavior of the electrode's double layer. The value of  $n$  is typically between 0.5 and 1, with a lower value indicating a more non-ideal behavior. In this case, the values of  $n$  are relatively constant and close to 0.8 (i.e., 0.794-0.857), revealing that the electrode's double layer behavior is relatively close to ideal, independent of the TLLE concentration.

**Table 4.24**

IE% values for the corrosion mitigation of mild steel in 0.5M HCl subjected to 50-1000ppm amounts of TLLE at 298 K.

Conc. (ppm)	CPE.Yo (μF)	<i>n</i>	Rs (Ω)	Rp(Ω)	Rct in (Ωcm <sup>2</sup> )	Rct bl (Ωcm <sup>2</sup> )	IE (%)	χ <sup>2</sup>
<b>Blank</b>	247.07	0.794	1.316	30.784	-	9.726	-	0.138
<b>50</b>	163.48	0.802	1.388	38.672	32	9.726	69.60	0.166
<b>100</b>	216.87	0.826	1.458	42.548	43.54	9.726	77.66	0.126
<b>250</b>	245.31	0.864	1.897	59.746	69.83	9.726	86.07	0.064
<b>500</b>	275.85	0.879	2.027	81.583	82.34	9.726	88.18	0.072
<b>1000</b>	289.22	0.857	1.810	157.83	159.627	9.726	93.90	0.089

#### 4.3.7. Surface examinations

##### 4.3.7.1. SEM

The SEM analysis was conducted to examine the topographical changes in mild steel samples following dipping in 0.5 M HCl with and without the existence of TLLE (1000 ppm). The first SEM micrograph (**Figure 4.45(a)**) shows the surface of an untreated standard steel sample, which appears smooth, indicating that there was no apparent degradation or damage to the metallic surface. However, the SEM micrograph of the blank sample (0.5 M HCl without TLLE) (**Figure 4.45(b)**) shows numerous pits on the metallic surface, which resemble corrosion products. This indicates that the metallic surface has undergone obvious degradation and profound corrosion due to immersion in the acidic media. The surface of the metallic sample appears unusually coarse, which indicates severe corrosion damage. In contrast, when the mild steel specimen was immersed in TLLE (1000 ppm concentration+0.5 M HCl), it emerged a defensive covering on the metallic surface. This covering acted as a shield, preventing the corrosive ions from attacking the metallic surface<sup>312-314</sup>. As a result, the SEM micrograph (**Figure 4.45(c)**) shows reduced pits and corrosion products, which indicates that the TLLE molecules developed a defensive covering to protect the metallic substrate from the attack of corrosive ions. This protective film reduced the rate of corrosion, culminating in a reduction in the number of pits and corrosion products on the surface of the metallic specimen.

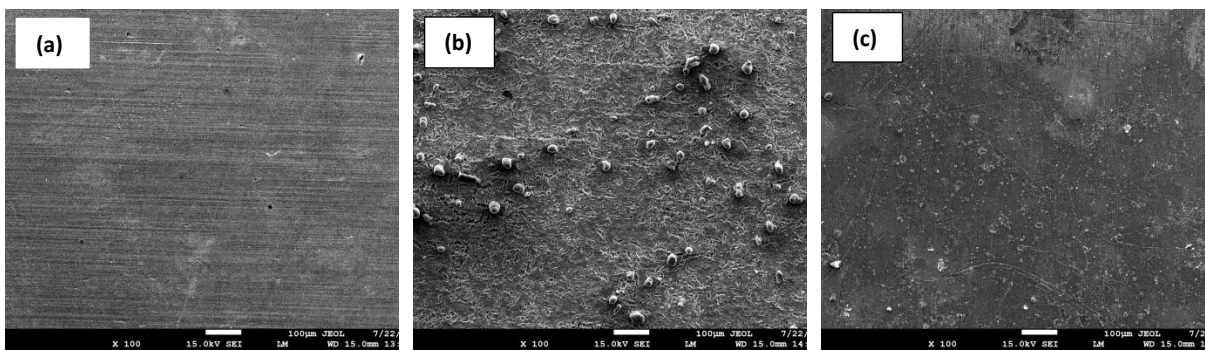


**Figure 4.45.** SEM illustrations of (a) standard metal, (b) metal dipped in 0.5M HCl (c) metal dipped in 0.5M HCl + TLLE (1000ppm).

#### 4.3.7.2. Contact angle (CA) assessment

CA assessment is a valuable tool for studying corrosion inhibition because it offers crucial insights into the wetting behavior of the metal surface. CA is the angle between the tangent to the liquid-solid interface and the solid surface, measured through the liquid phase. The CA measurement can provide information about the surface energy, surface tension, and chemical interactions between the metallic substrate and the liquid. In corrosion inhibition, the CA measurement can be used to determine the hydrophobicity or hydrophilicity of the metallic surface pre and post the application of an inhibitor. A hydrophobic surface repels water and other polar liquids, while a hydrophilic surface attracts water and other polar liquids. Inhibitors can alter the surface properties of metals and change the wetting behavior, culminating in the emergence of a defensive covering that inhibits corrosion. **Figure 4.46 (a)** and **(b)** show CA images of mild steel without and with 1000ppm of TLLE, correspondingly. The outcomes showed that the CA increased from  $46.54^\circ$  to  $79.82^\circ$  after mild steel was processed with 1000ppm of TLLE, making it more hydrophobic. Prior to the addition of the TLLE inhibitor, the metallic substrate had poor hydrophobicity, which made it more susceptible to corrosion due to abrasive particles adhering to the surface in acidic surroundings. However, the inhibitor molecules adsorbed onto the substrate may have increased surface tension and formed a hydrophobic protective film to prevent corrosion. The development of a hydrophobic protective film on the metallic surface is an essential mechanism for corrosion inhibition, as it can reduce the contact of the corrosive environment with the metal surface. The results of the CA evaluations provide further evidence that the TLLE inhibitor was effective in

forming a defensive covering on the metal surface, enhancing its hydrophobicity and reducing its susceptibility to corrosion.

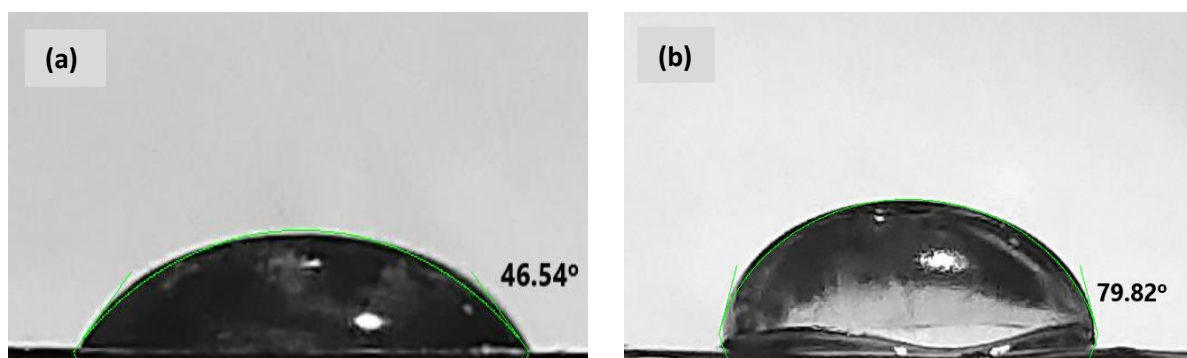


**Figure 4.46.** CA measurements conducted on (a) a metal specimen in 0.5M HCl and (b) a metal specimen in a solution containing 1000ppm of TLLE+blank solution.

### 4.3.8. Computational analysis

#### 4.3.8.1. DFT analysis

DFT has become one of the most prominent and noteworthy computational modeling approaches for assessing the effectiveness of various corrosion inhibitors<sup>315-317</sup>. One of the most important aspects of DFT and other computer modeling is the capacity to potentially examine earlier complex and perilous chemical synthesis corrosion inhibition ability as well as numerous other chemical reactivity variables of chemical molecules. Computational modeling is an eco-benign, takes less time and cost-effective approach for designing chemical species for a wide range of commercial and biotechnological applications, particularly corrosion inhibitors. An additional characteristic of DFT-based computational modeling is that by utilizing frontier molecular orbital (FMOs) representations, molecular structure influences and locations for interaction with the metallic surface may be conveniently discovered. Charge sharing or electron donation usually takes place in the confined portions of molecules. Charge donation is handled by localized HOMO (highest occupied molecular orbital) sites, while charge acceptance is handled by targeted LUMO (lowest unoccupied molecular orbital) sites. Corrosion inhibitors converse with metallic surfaces through a charge-sharing mechanism.

In this assessment, the Becke, 3-parameter, Lee-Yang Parr (B3LYP) system was employed wherein, the 6-311G (d, p) basis sets were employed to determine numerous variables and the chemical activities of molecules to achieve the investigation's objectives. It is a prudent strategy

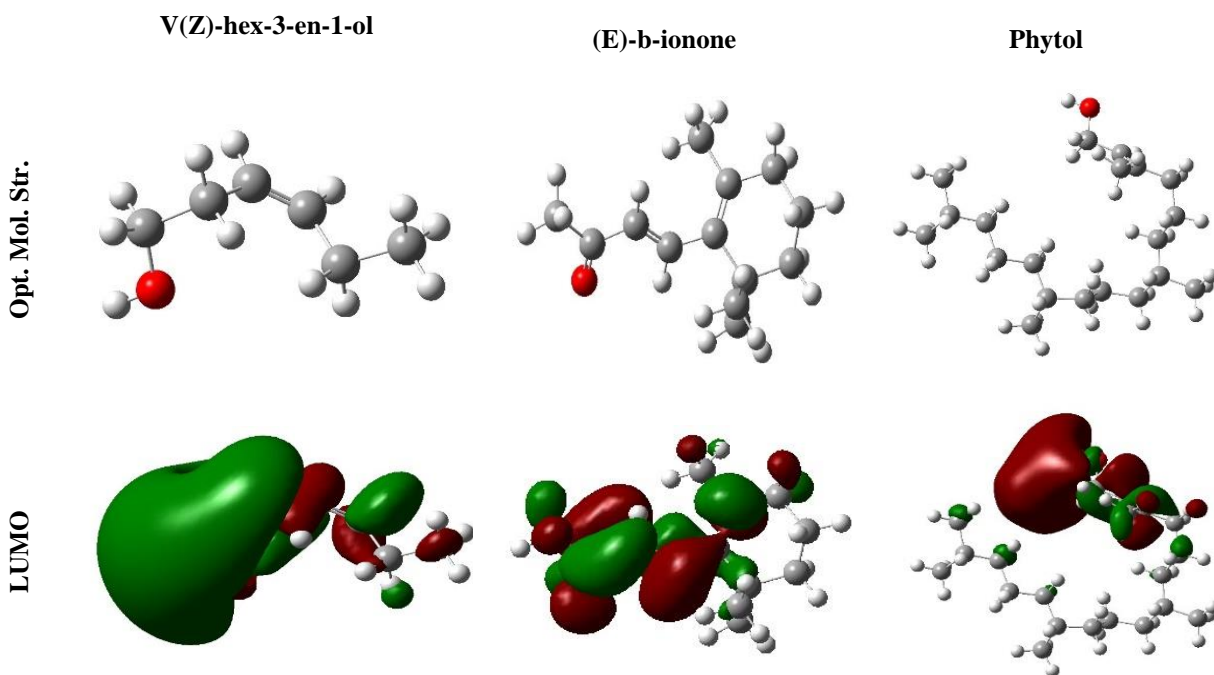
since all quantum variable computations were performed utilizing the DFT technique and Gaussian software without the usage of any laboratory equipment. Quantum chemical analyses have been used to analyze several quantum chemical variables, including  $E_{\text{HOMO}}$ ,  $E_{\text{LUMO}}$ , IP, EA,  $\eta$ ,  $\sigma$  and  $\chi$  by equations (11-17). Thus, these factors are very helpful in elucidating the adsorption pathway over the surface of the corroding moieties.

**Figure 4.47** shows the optimized,  $E_{\text{HOMO}}$  and  $E_{\text{LUMO}}$  geometries of the V(Z)-hex-3-en-1-ol, (E)-b-ionone and Phytol. Through the investigation of **Figure 4.47**, it might be noticed that HOMO and LUMO in V(Z)-hex-3-en-1-ol, (E)-b-ionone and Phytol molecules are located approximately throughout the molecular fractions. This finding suggests that all of the three molecules V(Z)-hex-3-en-1-ol, (E)-b-ionone and Phytol are involved in charge sharing. The presence of heteroatom moiety and aromatic ring configuration in their molecular compositions, correspondingly, is linked to their relatively significant involvement in charge. Following these considerations, it has been shown that the molecules V(Z)-hex-3-en-1-ol, (E)-b-ionone, and Phytol have exceptional anti-corrosive capabilities that are accountable for corrosion mitigation.

Furthermore, the obtained quantum chemical variables of the included molecules have been shown in **Table 4.25**. A molecule's tendency to acquire electrons is shown by lower  $E_{\text{LUMO}}$  values, whereas its propensity to release electrons is indicated by higher  $E_{\text{HOMO}}$  values. The difference between the  $E_{\text{HOMO}}$  and  $E_{\text{LUMO}}$  energies is an important factor in determining the energy gap ( $\Delta E$ ), a crucial parameter for evaluating the stability of a corrosion inhibitor. The greater the inhibitor's synergistic interaction with the Fe substrate, the smaller the  $\Delta E$  value<sup>318,319</sup>. As contrasted to V(Z)-hex-3-en-1-ol and phytol, the value of  $\Delta E$  of (E)-b-ionone comes out to be the lowest of all i.e., 0.164. This result could be ascribed to the availability of aromatic rings and heteroatoms in its structure. **Table 4.25** shows that all of the compounds possess significant  $E_{\text{HOMO}}$  values (V(Z)-hex-3-en-1-ol = -0.244 eV, (E)-b-ionone=-0.233 eV and Phytol= -0.244 eV) and lower  $E_{\text{LUMO}}$  values (V(Z)-hex-3-en-1-ol=-0.005 eV, (E)-b-ionone= -0.069 eV and Phytol= -0.013 eV ), which show that all of the inhibitor's molecules have a substantial potential for adhering to metallic surfaces and, as a result, have a considerable corrosion-inhibiting property. In several works of literature<sup>99,320-322</sup>, physical adsorption is also stated as being represented by the negative value of  $E_{\text{HOMO}}$ . According to the DFT outcomes, for all of the compounds,  $E_{\text{HOMO}}$  values were negative, indicating that physical adsorption has a higher probability than chemical adsorption.



Additionally,  $\Delta N$  represents electron release to the empty orbital. Moreover, a recognized criterion for predicting the chemical reactivity and persistence of inhibitor compounds is the " $\Delta N$  value,". A molecule's ability to inhibit is increased when its  $\Delta N$  value is significant and positive. In this case, all three molecules V(Z)-hex-3-en-1-ol, (E)-b-ionone and Phytol have quite positive and similar  $\Delta N$  values of 0.295, 0.202 and 0.285, which corresponds to their better chemical reactivity and stability. IE% raised with an increase in  $\sigma$  and reduced on  $\eta$  elevation as shown in **Table 4.25**.  $\eta$  and  $\sigma$  are the crucial variables that reflect information on stability and reactivity. It could be summarized that  $\eta$  having a minimal value proposes a higher IE%. Through **Table 4.25**, it can be observed that the (E)-b-ionone possesses a low value of  $\eta$  i.e., 0.082 and a high value of  $\sigma$  i.e., 12.19 followed by the Phytol ( $\eta=0.115$ ,  $\sigma=8.679$ ) and V(Z)-hex-3-en-1-ol ( $\eta=0.119$ ,  $\sigma=8.367$ ), which again corresponds to the better inhibitor efficiency of the extract. The  $\Delta E$  value, together with the  $\Delta N$ ,  $\sigma$  and  $\eta$  values, precisely complement the conclusions of the empirical investigation<sup>323</sup>. This shows that the molecules V(Z)-hex-3-en-1-ol, (E)-b-ionone and Phytol render to be the least susceptible to charge donation and acceptance. These outcomes demonstrated that the extract effectively prevents corrosion on mild steel surfaces<sup>268,324</sup>.



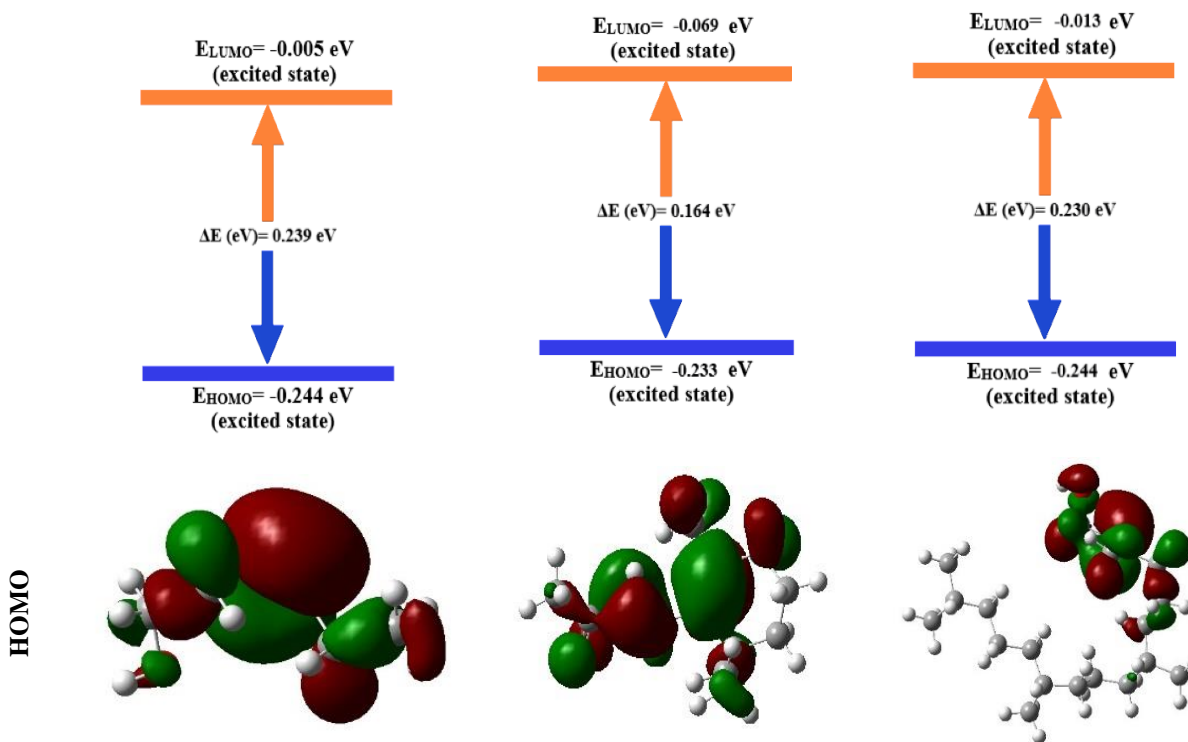


**Figure 4.47.** Optimized configuration, HOMO and LUMO distribution and total density of (a) V(Z)-hex-3-en-1-ol, (b) (E)-b-ionone, (c) Phytol using B3LYP/6-311G (d, p) basis sets.

**Table 4.25**

Calculated quantum chemical variables for inhibitor molecules through B3LYP/6-311G (d, p) basis sets.

Parameters	V(Z)-hex-3-en-1-ol	(E)-b-ionone	Phytol
Dipole moment	1.562	3.822	2.005
$E_{\text{HOMO}}$ (eV)	-0.244	-0.233	-0.244
$E_{\text{LUMO}}$ (eV)	-0.005	-0.069	-0.013
$\Delta E$ (eV)	0.239	0.164	0.230
IP (eV)	0.244	0.233	0.244
EA (eV)	0.005	0.697	0.013
$\eta = \Delta E / 2$ (eV)	0.119	0.082	0.115
$\sigma = 1/\eta$ (eV)	8.366	12.191	8.679
$\chi$ (eV)	0.125	0.151	0.128
$\Delta N$	0.295	0.201	0.284

The HOMO and LUMO geometries of the molecules could be visualized more clearly in **Figure 4.48** to better comprehend the insights of the molecules during conversion in the HOMO and LUMO phases.

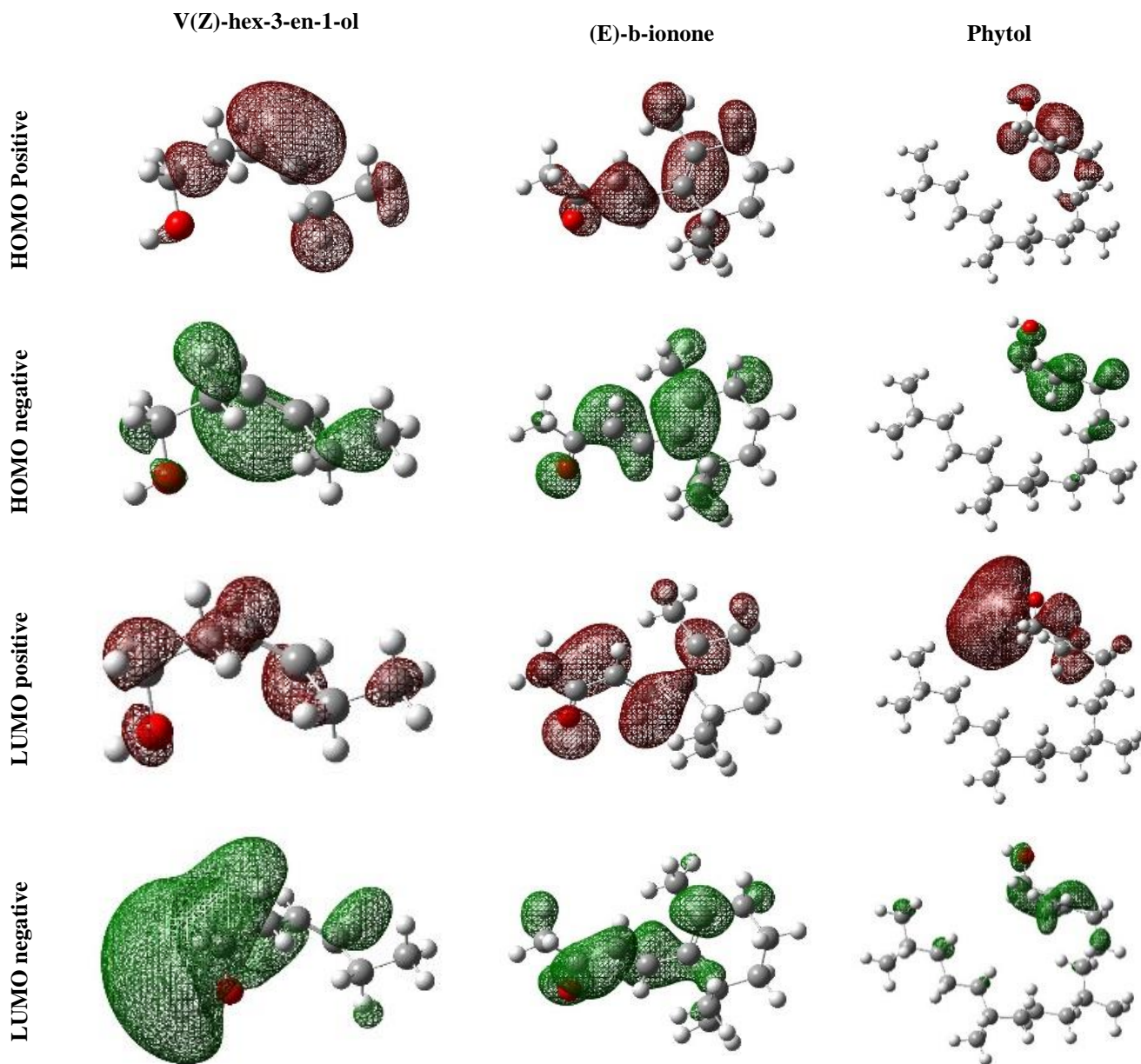


**Figure 4.48.** The positive and negative regions of HOMO and LUMO geometries of (a) V(Z)-hex-3-en-1-ol, (b) (E)-b-ionone and (c) Phytol using B3LYP/6-311G (d, p) basis sets.

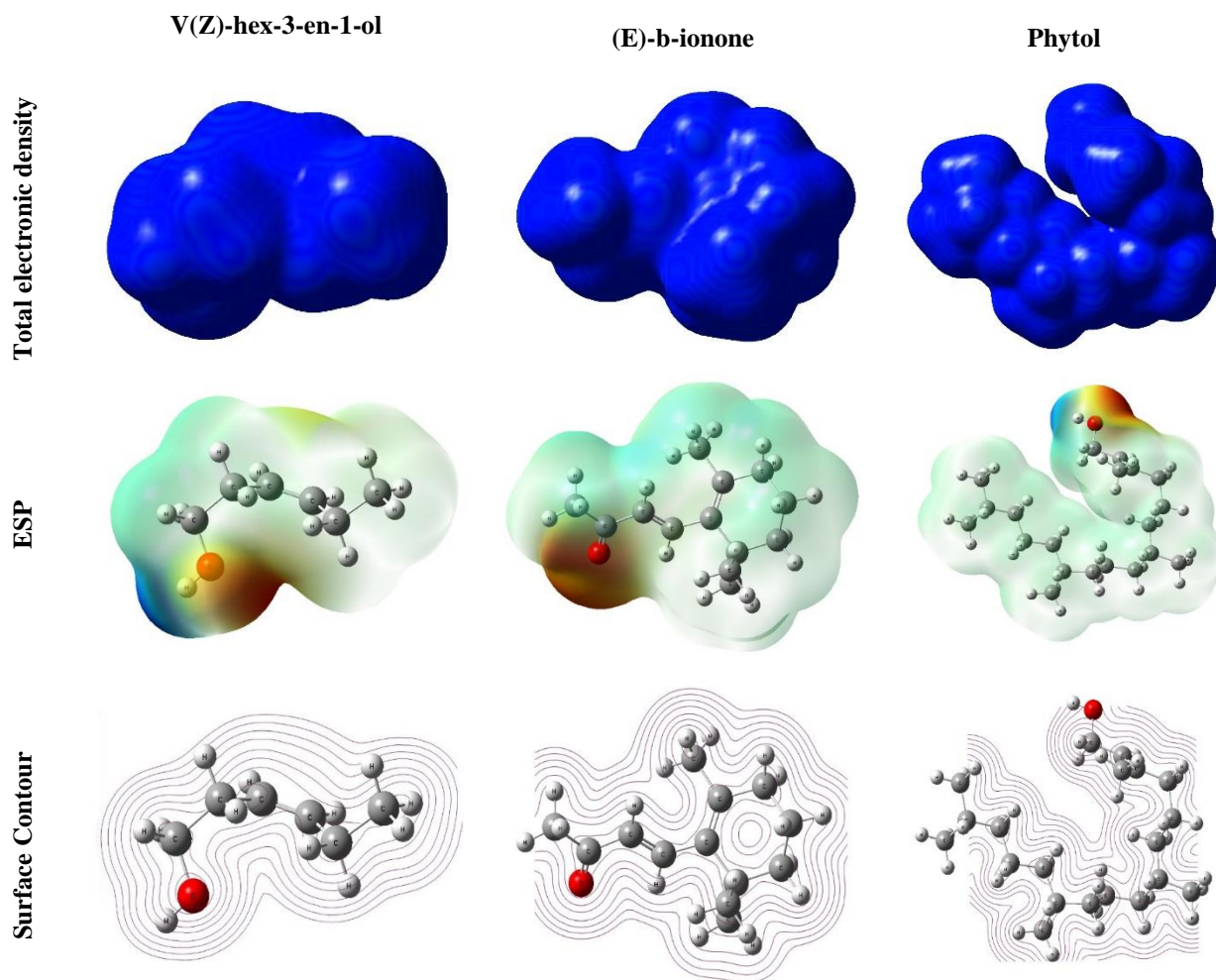


**Figure 4.49.** Electrostatic potential (ESP) maps and Isosurface of (a) V(Z)-hex-3-en-1-ol, (b) (E)-b-ionone and (c) Phytol using B3LYP/6-311G (d, p) basis sets.

Electrostatic potential (ESP) maps are a visualization tool that can help in assessing the polarity of a surface. The ESP maps depict the distribution of electrostatic potential on a surface, which can help in identifying regions that are susceptible to nucleophilic or electrophilic attacks. In the context of corrosion, ESP maps can provide insights into the susceptibility of metallic surfaces to corrosion. The ESP maps show regions of positive and negative electrostatic potentials. The positive potential regions (shaded in blue) are susceptible to electrophilic attacks, while the negative potential regions (shaded in red) are susceptible to nucleophilic attacks. As shown in **Figure 4.49**, the red regions are often located surrounding the heteroatom (oxygen) that might form a covalent link with the Fe atom. Positive potential spots have been found near carbon and

hydrogen atoms, behaving as ideal targets for electrophilic attack. The calculated quantum chemical variables, including EHOMO, ELUMO,  $\Delta E$ , IP, EA,  $\eta$ ,  $\sigma$ ,  $\chi$ , and  $\Delta N$ , provide a complementary perspective on the susceptibility of surfaces to corrosion. For example, V(Z)-hex-3-en-1-ol, (E)-b-ionone, and Phytol have a higher negative potential and lower  $\sigma$  values, indicating that they have a superior potential to gain electrons from the metallic surface. Similarly, the  $\Delta N$  values for these molecules suggest that they are more prone to nucleophilic attacks.

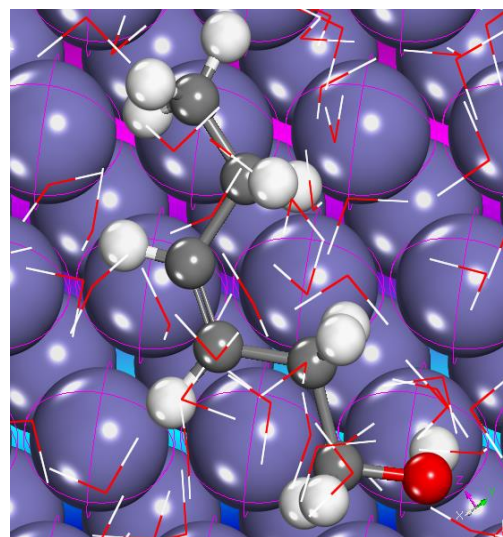
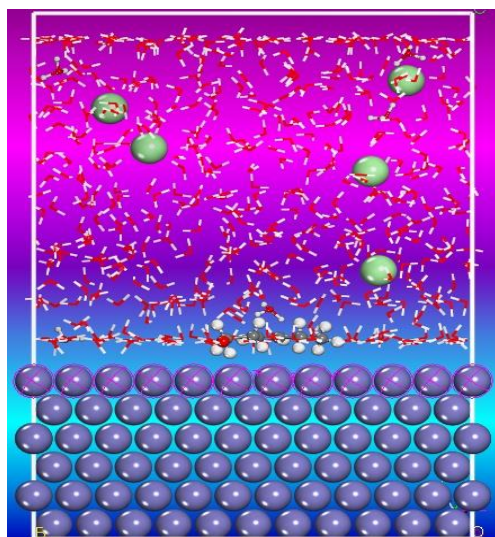
#### **4.3.8.2. MC simulation analysis**

Monte Carlo (MC) simulation is a computer-based approach utilized to model the behavior of systems under different conditions. In this particular case, MC simulation was used to comprehend the reaction pathway between the inhibitory molecule and the metallic surface. The simulation was performed using Materials Studio 8 software's Forcite module. The simulation box was set up with periodic boundary constraints and a 6-layer slab structure to simulate the Fe (1 1 0) substrate. The simulation box had a size of  $27.306 \times 27.306 \times 37.134 \text{ \AA}^3$ , and it was depleted by  $29 \text{ \AA}$ . The box contained  $500\text{H}_2\text{O}$ ,  $5\text{H}_3\text{O}^+$ ,  $5\text{Cl}^-$ , and the inhibiting molecule. The Andersen thermostat ensemble by NVT was employed to control the temperature of the simulation model at 298K. During the simulation, the interaction between the inhibitory molecule and the Fe (1 1 0) substrate was examined to understand the reaction pathway between them. By simulating the functionality of the system under distinctive conditions, the MC simulation allowed for an insightful comprehension of the reaction mechanism and the effectiveness of the inhibitory molecule in mitigating corrosion. The simulation was run for a duration phase of 1.0 fs and a simulated period of 200 ps using the COMPASS force field. The results obtained from the simulation provided valuable insights into the pathway of inhibition and the efficacy of the inhibitory molecule in mitigating corrosion.

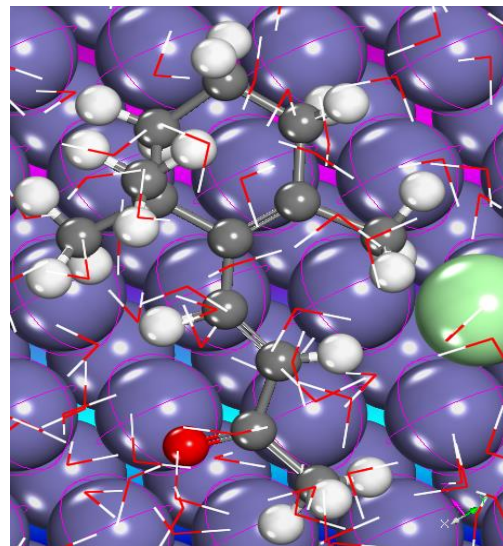
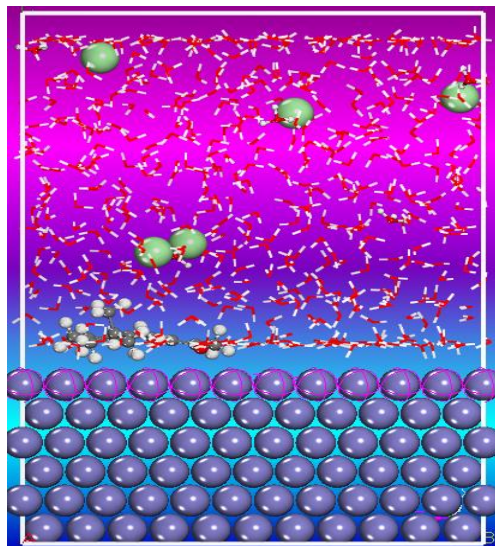
Side view

Top view

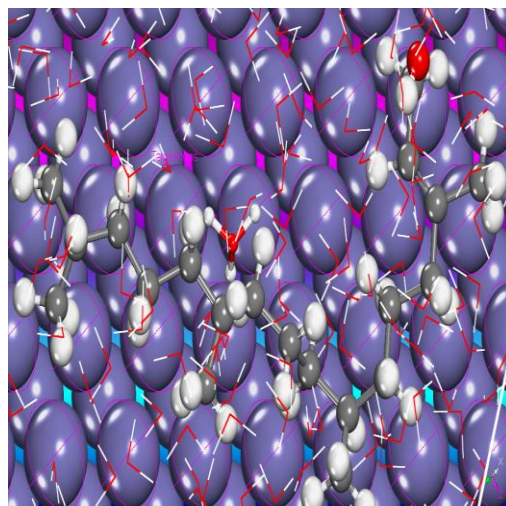
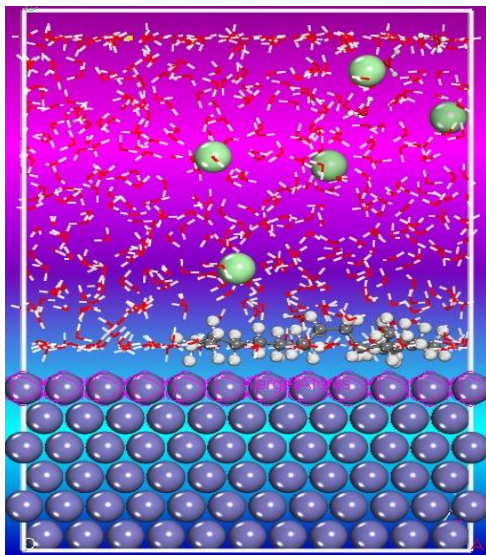
V(Z)-hex-3-en-1-ol / Fe(1 1 0)



(E)-b-ionone / Fe(1 1 0)



Phytol/Fe(1 1 0)



Three compounds  
/Fe (1 1 0)

Associative effect:

The associative effect of the V(Z)-hex-3-en-1-ol, (E)-b-ionone and Phytol improves the coverage rate of the metallic surface, culminating in the mitigation of the corrosion process rate of the mild steel.

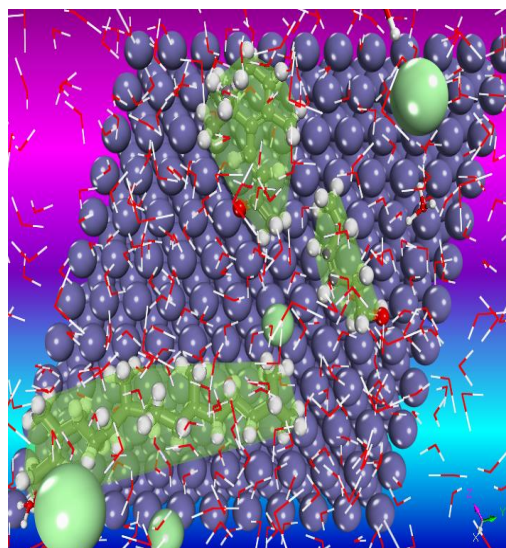
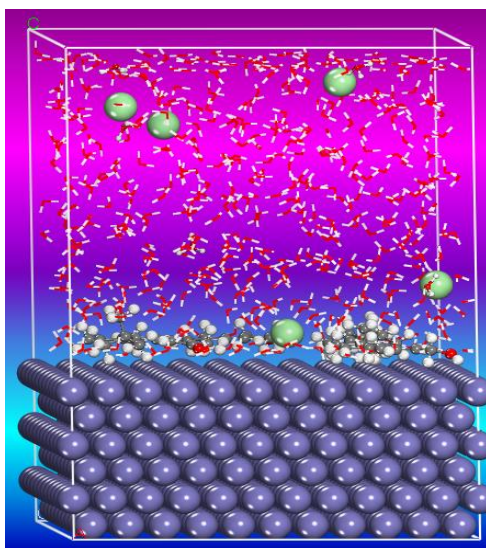


**Figure 4.50.** Balance adsorption configurations of V(Z)-hex-3-en-1-ol, (E)-b-ionone and Phytol upon Fe (1 1 0) surface in HCl at 298K.

**Table 4.26**

$E_{\text{interaction}}$  and  $E_{\text{binding}}$  (all in kJ/mol) of V(Z)-hex-3-en-1-ol, (E)-b-ionone and Phytol upon Fe (1 1 0) surface in HCl at 298K.

Systems	$E_{\text{interaction}}$	$E_{\text{binding}}$
V(Z)-hex-3-en-1-ol /Fe(1 1 0)	-345.34	345.34
Phytol/Fe(1 1 0)	-367.56	367.56
(E)-b-ionone/Fe(1 1 0)	-412.38	412.38
Three compounds/Fe(1 1 0)	-995.45	995.45

According to the findings illustrated in **Figure 4.50**, the inhibitor's molecule effectively adsorbs over the Fe (1 1 0) surface in a nearly concurrent or flat direction, showing that the active portions of the V(Z)-hex-3-en-1-ol, (E)-b-ionone, and Phytol molecules possess a significant interaction with Fe atoms. The adsorbed molecule might be reasonably steady because of the flat adsorption configuration. Additionally, increasing the metallic surface's active zones enhances surface coverage. The values of the binding energy could also be used to assess the molecules' adsorption capabilities. **Table 4.26** lists the calculated inhibitor adsorption binding energies over the Fe (1 1 0) surface. Significant adsorption on the interface of the iron was substantiated by the existence of a large amplitude of binding energies. In this case, it shows the energy change when each of the three compounds is placed near the Fe (1 1 0) surface in HCl. The negative sign demonstrates that the interaction between the compounds and the surface is attractive, meaning that they are energetically favorable to be close to each other. The binding energy is the energy discharged when a molecule is bound to a surface. In this case, it represents the energy change when each of the three compounds binds to the Fe (1 1 0) surface in HCl. The positive value indicates that the binding of the compounds to the surface is energetically favorable, and they release energy upon binding. In comparison to V(Z)-hex-3-en-1-ol (345.34 eV) and Phytol (367.56 eV), the  $E_{\text{binding}}$  of the (E)-b-ionone molecules is rather high, i.e., 412.38 eV, as reported in **Table 4.26**, which again correlates with the findings attained from quantum chemical parameters. A similar pattern can be observed in the case of  $E_{\text{interaction}}$  values in which a significant negative value of  $E_{\text{interaction}}$  has been attained indicating greater adsorption. The synergistic  $E_{\text{binding}}$  value of all three molecules, which is 995.45 eV is remarkable and significantly enhances the extent to which the examined inhibitor



molecules attach to the metallic substrate, revealing remarkable corrosion inhibition efficiency attributes<sup>325</sup>.

#### 4.3.9. Biodegradability of TLLE

The biodegradation degree refers to the extent to which a substance breaks down into simpler, harmless components in the environment through the action of living organisms such as bacteria, fungi, and other microorganisms. **Figure 4.51**, mentioned in the statement, represents a graphical representation of the biodegradation degree of TLLE over 28 days computed with the use of equation (19). The graph shows that the degradation rate of TLLE increased over time, reaching 83.87% after 28 days, indicating that TLLE undergoes rapid biodegradation. The North-East Atlantic Accords for the biodegradability of chemical compounds. According to this convention, products that biodegrade rapidly must possess a biodegradation rate of over 60% within 28 days<sup>273</sup>. Since the biodegradation rate of TLLE exceeds this limit, it could be contemplated as a biodegradable and eco-benign corrosion inhibitor.

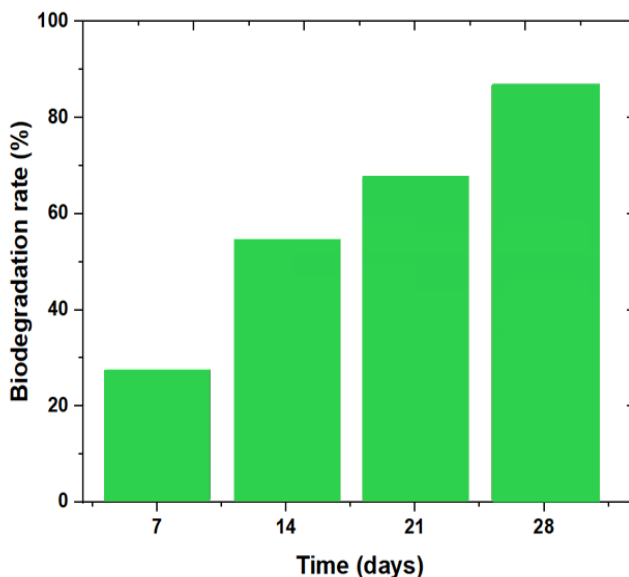


**Figure 4.51.** Biodegradability rate of TLLE

#### 4.4. *Trianthena Portulacstrum*

*Trianthena Portulacstrum* (TP) (Domain: Eukaryota, Kingdom: Plantae, Phylum: Spermatophyta, Subphylum: Angiospermae, Class: Dicotyledonae) is a perennial herb having a robust taproot that grows up to 60 cm tall, moist, flat, or ascending, and frequently has several branches. It can be found in paddy farms, grasslands, parks, farmed fields, and fallow land. It has ascending stems that are at least 50 cm long and are either silky or irregularly textured. Plain, elliptical and 1-2 cm long leaves are present. Petals are 4-5mm long and straight to broadly delate. The ovary is tubular, and the style is around 2mm long. The roots are slender, thin, sinuous, curving, and flexible, measuring 5–15 cm in length and 0.3–2.5 cm broad. It can quickly establish itself as a weed in disturbed regions and on agricultural land. It flourishes in a broad range of ecosystem types. The roots have emetic, aphrodisiac, cathartic, and emergency contraceptive qualities (in high dosages). Asthma and amenorrhea are also treated with them, along with liver clogs. In order to cure venereal discharge, an infusion of the pulverized root is consumed.

According to previous investigation <sup>326</sup>, TP aerial extract (TPAE) contains several main phytochemical components such as hexahydro-farnesyl acetone, verbenene, and incensole acetate as illustrated in **Figure 4.52**. TP which is extensively available in many countries has been examined in this study as an eco-friendly corrosion inhibitor for mild steel in a corrosive media of 0.5 M HCl. This work was essential since there is no comprehensive, research evidence on the usage of TP aerial extracts as a corrosion inhibitor for mild steel. Through gravimetric technique, electrochemical investigations (including Tafel plots and impedance spectroscopy), and morphological evaluation utilizing scanning electron microscopy, TPAE were extracted and evaluated to mitigate the corrosion rate of mild steel in 0.5M HCl media. The author anticipates that by using TPAE as a sustainable corrosion inhibitor for mild steel, TP aerial components will not only reuse assets and lower the price of corrosion inhibitors but moreover effectively advance TP and other weeds cultivation and effective usage. The key point is that both humans and the ecosystem suffer very minor harm and a waste-regarded commodity could be effectively utilized as a potent and green inhibitor to mitigate metallic corrosion and combat the catastrophic global concern i.e. corrosion <sup>272,327–329</sup>.

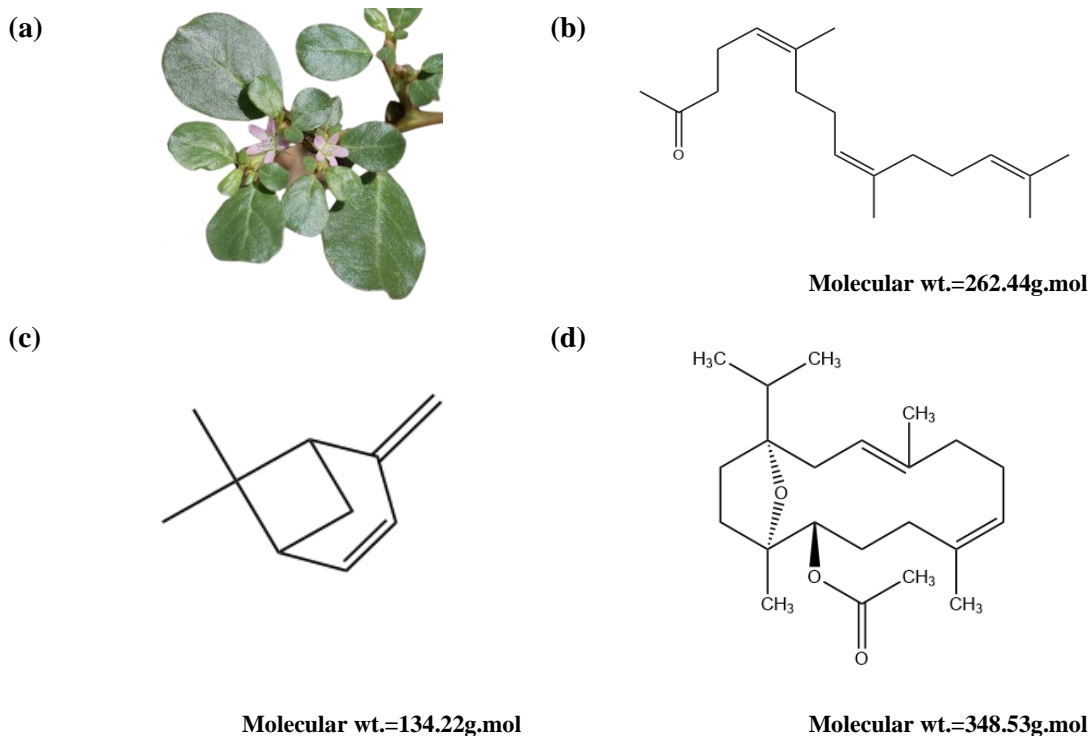


**Figure 4.52.** Schematic representation of (a) *Trianthema Portulacastrum*; the main chemical constituents of TPAE (b) Hexahydro-farnesyl acetone, (c) Verbenene, (d) Incensole acetate.

#### 4.4.1. Preparation of *Trianthema Portulacastrum* aerial extract

The aerial parts of *Trianthema Portulacastrum* (TP) were gathered from a nearby farm in Kapurthala in the flowering stage during the summer season and later affirmed by Prof. Neera, Himachal Pradesh University (HPU), India. The TP aerial parts were manually cut 1 cm above the soil surface, later cleaned with distilled water, and allowed to dry completely over multiple days at ambient temperature (25°C) in a secluded area before being processed with double distilled water to remove impurities for the extraction method. The dried leaves (800g) were grounded by a laboratory mill and subjected to steam distillation extraction using 2500ml de-ionized water for 6hrs, following the procedure mentioned in the literature<sup>326</sup>. The extract was then processed to concentrate its primary bioactive-rich components using filtrate with 0.45 µm pore size micro-phase. In 0.5 M HCl, the obtained TP extract was most soluble up to 1000 mg/L. The attained extract was preserved till subsequent examination in impermeable sample bottles that were capped with aluminium foil and refrigerated at 4°C.

#### 4.4.2. FT-IR evaluation

The adsorption of TPAE's molecules onto mild steel surfaces for corrosion reduction might be facilitated by the inclusion of aromatic ring geometries and heteroatoms (O). **Figure 4.53** illustrates the TPAE's FTIR spectrum. The FTIR spectra of the TPAE illustrate  $\text{-C-O}$  and  $\text{-C-H}$  stretching vibration at peaks  $1020$  and  $2918\text{ cm}^{-1}$ . The peaks at  $1415$  and  $1377\text{ cm}^{-1}$  correspond to the  $\text{-CH}_3$  bend. The peak intensities at  $1460$ ,  $1732$  and  $1604\text{ cm}^{-1}$  correlate to  $\text{-CH}_2$  bending,  $\text{-C=O}$  stretching and  $\text{-C=C}$  stretching. The peaks at  $2990$  and  $798\text{ cm}^{-1}$  attributed to the  $\text{=C-H}$  and  $\text{-C-H}$  stretch. These outcomes showed that TPAE included heteroatom (oxygen) in  $\text{-C-O}$ ,  $\text{-C=O}$  moieties, aromatic ring structures and linear molecules, which illustrates that TPAE has significant corrosion inhibition efficacy in  $0.5\text{M HCl}$  and the attained results are in accordant with the geometries of conventional corrosion inhibitors.

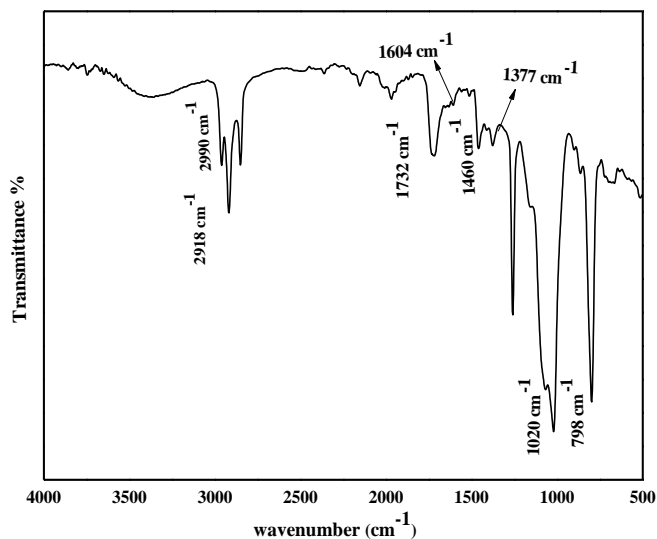


**Figure 4.53.** FT-IR analysis of the TPAE.

#### 4.4.3. UV-Vis spectrometry

The UV-Vis spectrum of TPAE was considered for the pre-and post-corrosion test, illustrated in **Figure 4.54**. The inhibitor configuration exhibits adsorption peaks at  $412\text{ nm}$  and  $546.29\text{ nm}$ , illustrating the  $n\text{-}\pi^*$  and  $\pi\text{-}\pi^*$  transitions, correspondingly, subsequent to the corrosion predictions. The  $\pi\text{-}\pi^*$  transition, which is associated with the  $\text{C=C}$  conjugation found in the inhibitor molecules, is attributed to the initial peak. The absorption spectra of TPAE shows an absorption peak in the

wavelength region of 350–550 nm, corresponding to the  $n-\pi^*$  transition ascribed to the numerous functional moieties prevalent in inhibitor molecules including  $-C=O$ ,  $-C-O$ , and so on. Afterward the corrosion study, the results show a hypsochromic shifting of the optimum adsorption. The results confirmed the possibility of a complex forming between Fe and phytochemicals, as shown in **Figure 4.54**, and that these peaks were redistributed after the corrosion analysis. It vividly illustrates that when the metallic sample was dipped in the 0.5M HCl+1000ppm of TP AE, several molecules from the media (inhibitor) were adsorbed onto the metallic substrate.

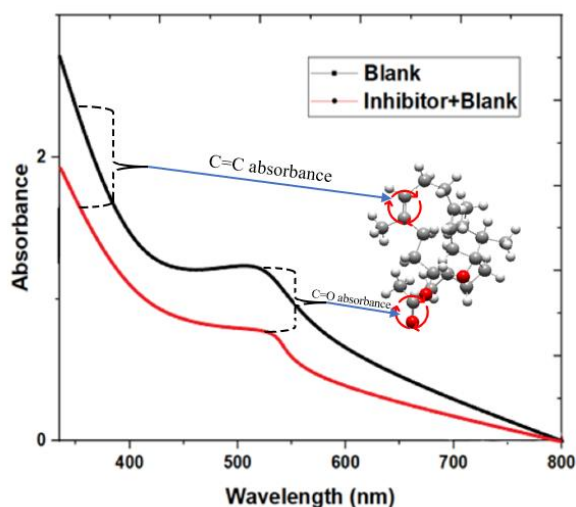


**Figure 4.54.** UV Spectra of pre- and post-metal immersion in 0.5M HCl and with the inclusion of TP AE.

#### 4.4.4. Weight Loss analysis

The WL method is a simple technique to acquire a fundamental understanding of the correlation between inhibitor concentration and IE%. In this experiment, WL studies were conducted in the inclusion and exclusion of TP AE in 0.5M HCl solution at 298K for the desired period to investigate the impact of time (15-60min.), temperature (298-328K) and inhibitor concentration (50-1000ppm) on inhibition efficacy of TP AE on the corrosion mild steel as shown in **Figure 4.55**. The  $\theta$ , IE% and  $C_R$  were estimated using eqns. (1-3), after acquiring the pre- and post-weight of the mild steel specimen submerged in blank and several concentrations (50-1000ppm) of TP AE. Beneath, **Figure 4.55** and **Table 4.27**, **4.28** and **4.29** exhibit the impact of time, conc. and

temperature over the TPAE IE% against mild steel corrosion in 0.5 M HCl media. In 0.5M HCl, at an optimized quantity of 1000ppm of TPAE, the TPAE had a maximal inhibitory efficacy of 93.18%. An elevation in extract concentration did not contribute to a substantive alteration in the extract's efficacy towards corrosion protection of metallic samples. **Table 4.29** encompasses the IE % and  $C_R$  determined using the WL method at a varying concentration of TPAE at 298K. According to the clear analysis of **Figure 4.55**, it could be revealed that on raising the inhibitor concentration, the IE increased, whereas on increasing the temperature, the IE decreased (as shown in **Table 4.28**), implying that a protective coating has been developed upon the mild steel surface by inhibitor becomes less prolonging at elevated temperatures.

**Table 4.27**

Influence of immersion time on the IE% of TPAE for mild steel corrosion.

Time (min.)	$W_0$ (mg)	$W_i$ (mg)	$W_0 - W_i$ (mg)	IE%
15	1.453	1.364	0.089	91.222
30	1.422	1.295	0.127	88.053
45	1.478	1.199	0.279	75.244
60	1.376	1.061	0.315	69.653

**Table 4.28**

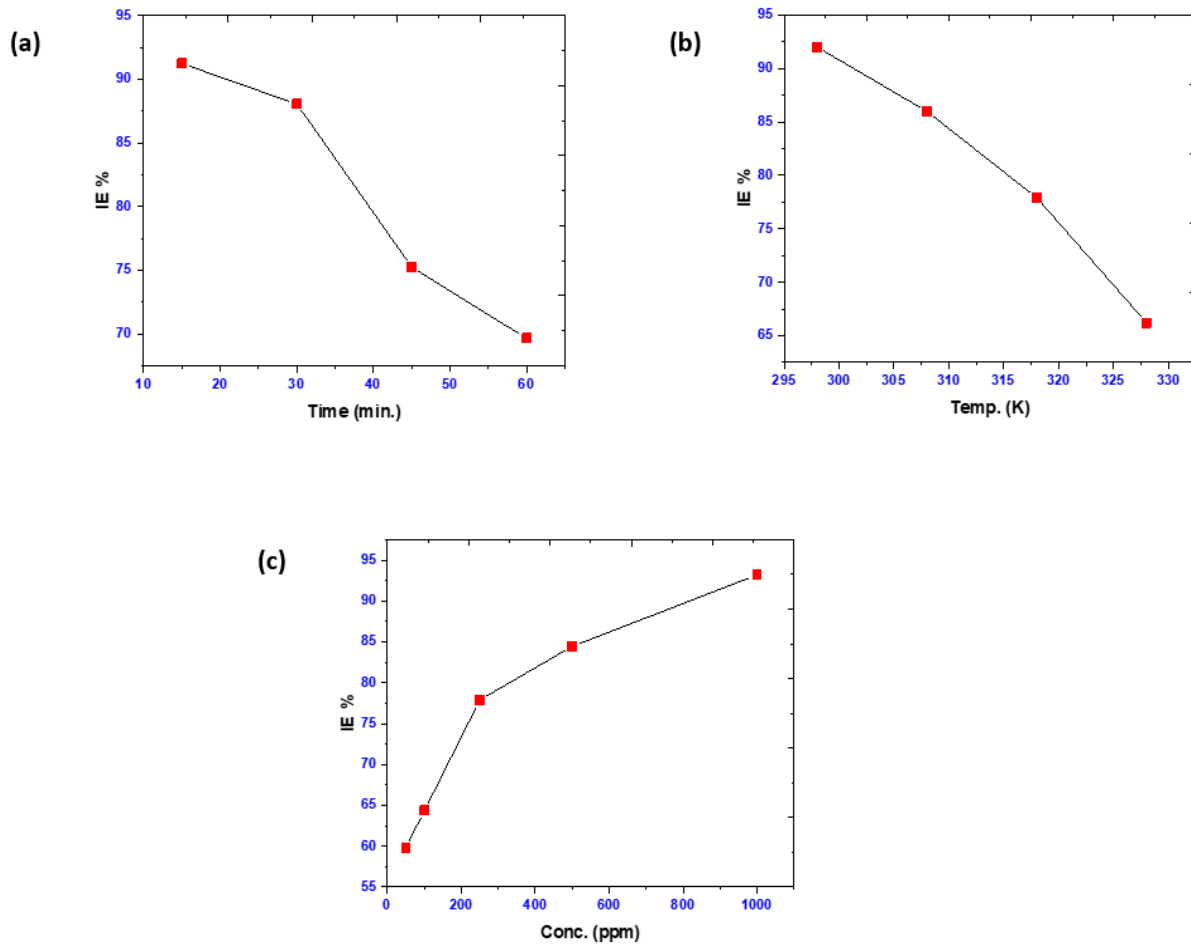
Influence of temperature on the IE% of TPAE for mild steel corrosion.

Temp. (K)	$W_0$ (mg)	$W_i$ (mg)	$W_0 - W_i$ (mg)	IE%
298	1.524	1.456	0.068	92
308	1.387	1.245	0.142	86
318	1.351	1.112	0.239	77.91
328	1.397	0.923	0.474	66.22

**Table 4.29**

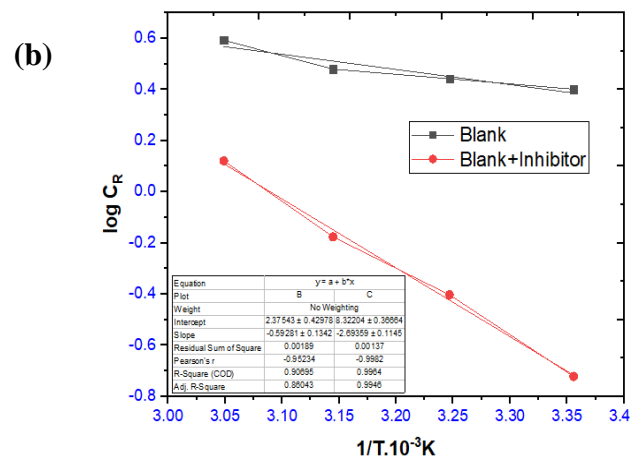
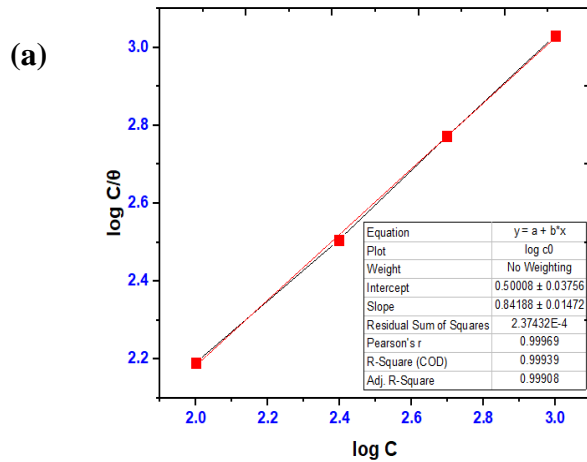
Influence of conc. on the IE% of TPAE for mild steel corrosion.

Conc. (ppm)	W <sub>0</sub> (mg)	W <sub>i</sub> (mg)	W <sub>0</sub> -W <sub>i</sub> (mg)	C <sub>R</sub>	Θ	IE%
Blank	1.934	0.834	1.1	3.068	-	-
50	1.793	0.72	1.073	2.993	0.598	59.843
100	1.822	1.43	0.392	1.093	0.643	64.363
250	1.723	1.48	0.243	0.677	0.779	77.909
500	1.791	1.62	0.171	0.477	0.844	84.454
1000	1.755	1.68	0.075	0.209	0.931	93.181

**Figure 4.55.** Impact of (a) time (min.), (b) temperature and (c) conc. on the IE% of TPAE for mild steel corrosion.

#### 4.4.5. Adsorption and thermodynamic variables

With the aid of adsorption isotherm, the capability of TPAE as a significant corrosion inhibitor for the mild steel by getting adsorbed on the metal/solution interfaces could be effectively determined. A straight gradient featuring a regression coefficient ( $R^2$ ) value of 0.99939; equivalent to 1 was attained in **Figure 4.56 (a)**,  $\log C/\theta$  versus  $\log C$  graph. Through the findings, it has been assessed that the Langmuir adsorption isotherm was followed by the inhibitor adsorption on mild steel substrate, revealing the formation of a thin monolayer on the metal's substrate while **Figure 4.56 (b)** depicts a linear incline in the plot  $\log C_R$  versus  $1/T \cdot 10^{-3}K$ . **Table 4.30** outlines the outcomes of this assessment. The kinetic variables were computed with the use of the Arrhenius equation and the  $E_a$  value was evaluated through slopes ( $-E_a/2.303R$ ).<sup>6,258</sup>. As depicted in **Figure 4.56 (c)**, the plot of  $\log K_{ads}$  vs.  $1/T \cdot 10^{-3}K$  was utilized to compute the enthalpy value with a straight arc across slope  $-H/2.303R$ . These parameters were calculated using equations (5) and (6). Additionally, equations (7) and (8) were employed to determine the values of  $\Delta G^{\circ}_{ads}$  and  $\Delta S^{\circ}_{ads}$ .





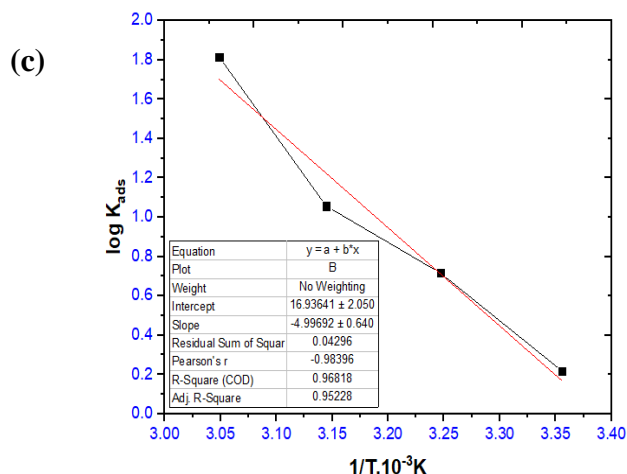


**Figure 4.56.** Plots of (a) Langmuir adsorption (b) Arrhenius (c) Enthalpy on the IE% of TP AE for mild steel corrosion in 0.5 M HCl.

**Table 4.30**

Adsorption, thermodynamic and kinetic variables for the metallic corrosion mitigation in the exclusion and subjection of 1000 ppm of TP AE in 0.5 M HCl at 298K.

Metal	TPAE (ppm)	log K <sub>ads</sub>	$\Delta G^{\circ}_{ads}$ kJmol <sup>-1</sup>	$\Delta H^{\circ}_{ads}$ kJmol <sup>-1</sup>	$\Delta S^{\circ}_{ads}$ kJmol <sup>-1</sup>	E <sub>a</sub> kJmol <sup>-1</sup>
Mild steel	Blank	-	-	-	-	2.942
	50ppm	0.397	-1.728	0.0415	0.141	19.625
	100ppm	0.502	-1.243			
	250ppm	1.649	-4.085			
	500ppm	2.433	-6.027			
	1000ppm	4.179	-10.354			

It is demonstrated from **Table 4.30** that a raised value of E<sub>a</sub> than excluding inhibitor implies the development of an inhibitor adsorption film over the metallic substrate, acting as a physical hindrance to charge and mass transmission. The presence of  $\Delta H^{\circ}_{ads}$  with a positive value revealed mild steel dissolution to be an endothermic reaction, indicating mild steel corrosion difficult even at low TP AE concentrations<sup>281</sup>. Additionally, the value of  $\Delta S^{\circ}_{ads}$  came out to be <0, demonstrating

that the adsorption process was static and that the rate-determining step was associated with the development of the intricate compounds. This indicates that once the intricate compound has developed, the destabilization declines, allowing H<sub>2</sub>O molecules to desorb from the substrate. Significant interactions between inhibitor molecules and metallic substrates are also suggested by the dramatic increase in logK<sub>ads</sub> values. Our investigation,  $\Delta G_{ads}^o$  confirms that the TPAE is effectively adsorbed on the mild steel via interacting  $\pi$ -electrons and lone pair of electrons. Consequently, the molecules are firmly adhered to the metal surface culminating in excellent corrosion inhibition efficacy of the investigated inhibitor.

#### **4.4.6. Electrochemical analysis**

##### **4.4.6.1. Open circuit potential (OCP)**

In this section, the working electrode comprised of the mild steel rod was submerged in the test media for 1hr throughout each investigation involving the concentration variation from 50ppm to 1000ppm. It is essential to create a consistent OCP priorly conducting the PDP and EIS assessments. **Figure 4.57** shows the OCP versus time (sec.) trends in the absence and presence of various TPAE amounts. By evaluating **Figure 4.57**, it could be observed that after 1hr dipping, the potential pertaining to mild steel specimens dipped in a media containing all the desired concentrations of the TPAE became stabilized. The potential measurements for the inhibited and uninhibited specimens both significantly shifted toward the negative value, indicating that TPAE behaves as a cathodic inhibitor in the aggressive medium of 0.5 M HCl. The negative shift of OCP for the bare specimen could be accounted for the iron oxide formation/dissolution over the metallic substrate.



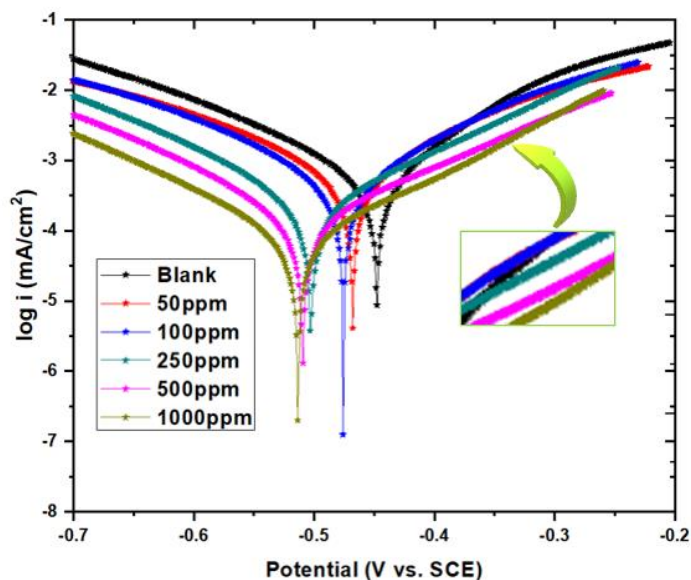


**Figure 4.58.** Tafel graph for mild steel corrosion inhibition in 0.5M HCl with 50–1000 ppm TP AE at 298 K.

**Table 4.31**

Tafel parameters for mild steel corrosion inhibition in 0.5M HCl with 50–1000 ppm TP AE at ambient temperature.

Conc. (ppm)	$-E_{corr}$ (mV vs. SCE)	$i_{corr}$ ( $\mu$ A)	$j_{corr}$ ( $\mu$ A/cm <sup>2</sup> )	$\beta_a$ (mV/dec)	$-\beta_c$ (mV/dec)	$C_R$ (mm/yr)	IE%	$\chi^2$
Blank	449.85	595.11	595.11	369.93	121.31	6.591	-	8.1321E-08
50	469.11	441.55	441.55	121.27	138.8	4.293	25.80	2.3621E-07
100	474.66	394.12	394.12	108.95	121.97	3.579	33.77	2.5723E-08
250	501.65	203.96	203.96	125.26	111.03	2.370	65.72	5.8262E-09
500	512.36	119.10	119.10	136.48	105.87	1.384	79.98	5.7321E-09
1000	516.61	64.059	64.059	124.22	103.53	0.744	89.23	4.1971E-08

#### 4.4.6.3. Electrochemical impedance spectroscopy (EIS)

In order to attain relevant information regarding the corrosion inhibition mechanism, the EIS evaluation of mild steel immersed in several amounts of TP AE in 0.5 M HCl was conducted to

corroborate the results of the PDP and WL examinations. The critical outcomes are summarized in **Table 4.32**. The graphs of Bode and Nyquist are depicted in **Figures 4.59** and **4.60**, correspondingly. A substantial capacitive curve could be observed at a higher frequency on the Nyquist graph, whereas an inductive curve is visible at a lower frequency. The adsorption of  $\text{Hads}^+$ ,  $\text{Cl}^-$ , and TP AE molecules on the surface of mild steel expedited the relaxation phase that formed the lower-frequency inductive loop. In contrast, the surface distortion and charge transfer mechanism generated the high-frequency capacitive curve. The re-disintegration of the passivated substrate at a lesser frequency may be a probability. The pattern of all slopes in the Nyquist graph remained unchanged whether an inhibitor was used or not, showing that the metallic corrosion mechanism was unaffected. Furthermore, their geometries weren't ideal due to frequency dispersal, roughness, and non-uniformity of the working electrode substrate. The radii of the curves were demonstrated to increase as TP AE levels increased from 50 to 1000 ppm, indicating that TP AE dispersion over the electrode substrate improved and a protective covering formed, thereby preventing corrosion on the electrode surface.

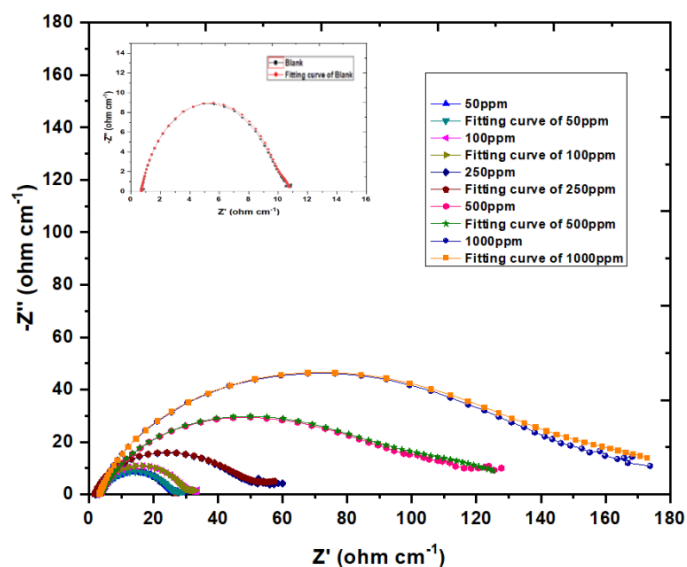


**Figure 4.59.** Nyquist graph for mild steel corrosion inhibition in 0.5M HCl with 50–1000 ppm TP AE at ambient temperature.

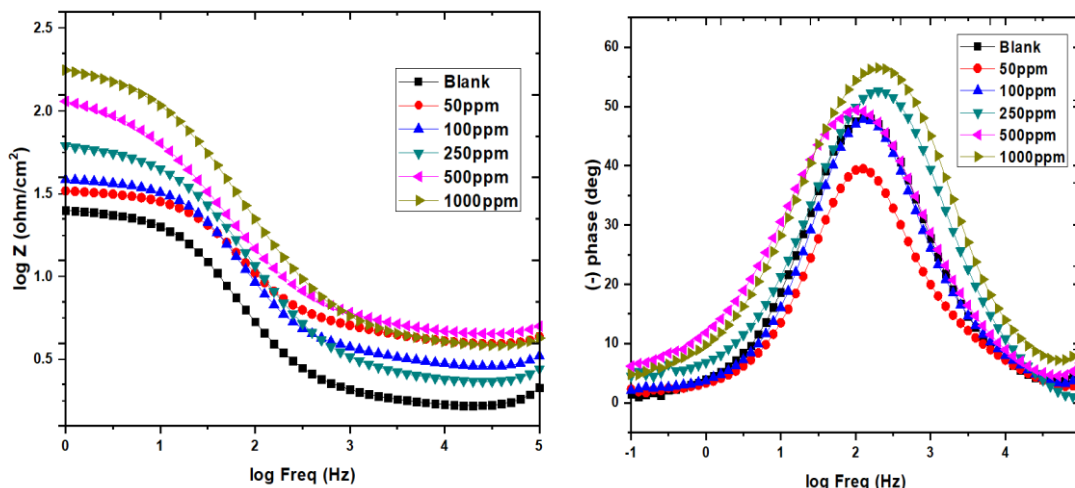


**Figure 4.60.** Bodes graph for the corrosion mitigation of mild steel in 0.5M HCl with 50–1000 ppm TPAE at 298 K.

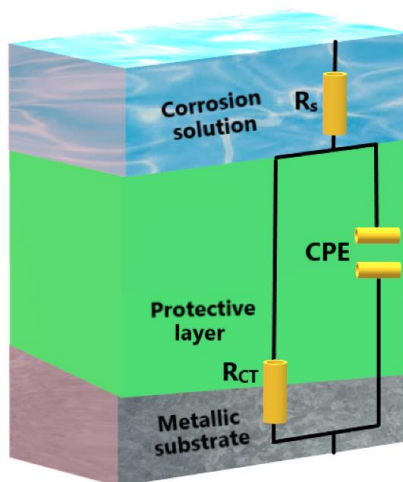


**Figure 4.61.** The utilized eqv. circuit model for the data fitting.

The Bode graphs for the metal in the addition and lack of diverse quantities of TPAE (50–1000 ppm) in the acidic solution at 298K are depicted in **Figure 4.60**. The impedance modulus improved with the increased quantity of TPAE across the frequency range investigated in this research. The frequency spectra also expanded at the highest phase angles<sup>252,253,266,267</sup>. As per the previous reports, the optimum capacitance at an intermediary frequency can be accepted, if the curve of the  $\log |Z|$  versus  $\log f$  with a maximum phase angle of  $90^\circ$  tends to be  $1$ <sup>330–332</sup>. This

demonstrated that in the 0.5 M HCl, TP AE has a remarkable inhibition efficacy on the corrosion of mild steel.

**Table 4.32** reports the EIS metrics, wherein  $R_s$  represents solution resistance,  $R_{ct}$  stands for charge transfer resistance,  $n$  denotes phase shift, CPE denotes constant phase element and the discrepancy scale of the eqv. circuit fitting denoted by  $\chi^2$ . The datasets of  $\chi^2$  within  $10^{-3}$  and  $10^{-5}$  suggest that the depicted equivalent circuit layout is reliable and stable, confirming to be consistent with the ideal fitting. **Table 4.32** illustrates that as the quantity of TP AE was expanded, the  $R_{ct}$  and IE% increased, reaching an optimum IE% of 94.33% at 1000ppm, revealing to be remarkably consistent with the analyses of the PDP and WL experimentations. When several amounts of TP AE were introduced, the  $R_s$  value did not alter drastically. Moreover, the  $n$  values (0.897–0.652) did not impact considerably, demonstrating that charge transfer regulated the mild steel dissolution in 0.5 M HCl medium.

**Table 4.32**

IE% values for the corrosion mitigation of mild steel in 0.5M HCl subjected to 50-1000ppm conc. of TP AE at 298 K.

Concentration (ppm)	CPE.Yo ( $\mu F$ )	$n$	$R_s$ ( $\Omega$ )	$R_p$ ( $\Omega$ )	$C_{dl}$ ( $\mu F cm^{-2}$ )	$R_{ct}$ in ( $\Omega cm^2$ )	$R_{ct}$ bl ( $\Omega cm^2$ )	IE (%)	$\chi^2$
Blank	242.77	0.897	1.269	30.219	114.885	-	10.089	-	0.136
50	138.34	0.850	3.851	29.298	78.121	30.245	10.089	66.64	0.137
100	132.4	0.812	3.942	35.058	39.474	34.374	10.089	70.65	0.149
250	117.84	0.761	4.226	62.767	28.347	60.68	10.089	83.37	0.234
500	103.62	0.686	4.294	128.08	22.596	130.447	10.089	92.26	0.310
1000	69.423	0.652	6.580	198.95	14.303	178.036	10.089	94.33	0.392

#### 4.4.7. Surface morphology analysis

##### 4.4.7.1. SEM

In this research, SEM was employed to evaluate the topographical state of metallic samples after the 6hrs of dipping in a solution of 0.5M HCl in the absence and presence of TP AE, and the outcomes have been shown in **Figure 4.62**. The flat view of SEM micrograph of the unprocessed

plain steel sample has been depicted in **Figure 4.62 (a)**. While **Figure 4.62 (b)** represents the flat view of the sample immersed in 0.5 M HCl which is characterized by an extremely coarse surface having several pits on it resembling corrosion products over the metallic surface. It means that there is obvious degradation and substantial degradation on the blank steel surface. The inclusion of an inhibitor (1000 ppm concentration) created a defensive film on the mild steel specimen's surfaces, preventing corrosive ions from attacking the surface and leaving fewer pits and corrosion products shown in the corresponding figure which consequently leads to corrosion reduction which is the goal of this research.

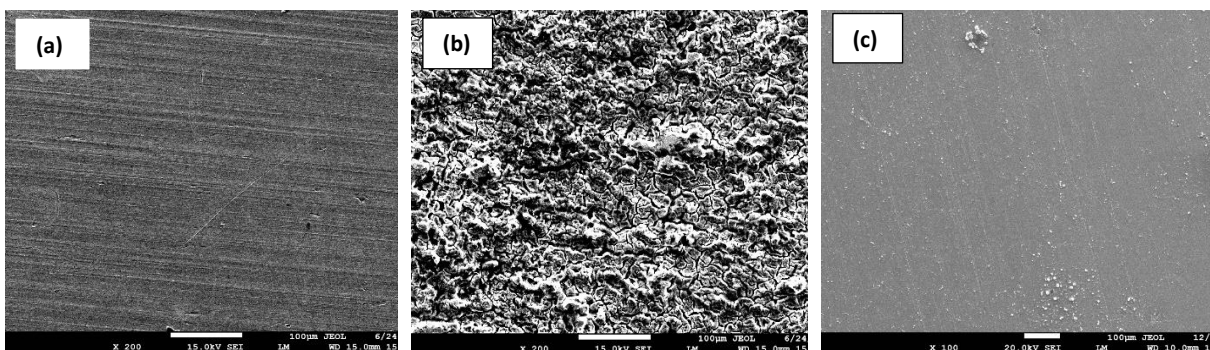


**Figure 4.62.** SEM visuals of (a) plain metal, (b) metal submerged in 0.5 M HCl (c) metal submerged in 0.5 M HCl + TPAE (1000ppm).

#### 4.4.7.2. Contact angle (CA) assessment

Through this assessment, additional details about anomalies including adhesion, wetting and absorption upon mild steel surfaces are attained <sup>268</sup>. In this approach, CA analysis was utilized to evaluate the hydrophobicity/hydrophilicity of the unprocessed and processed mild steel substrates.

**Figure 4.63 (a, b)** depicts the images acquired through the CA examinations on the metal substrate in the exclusion (a) and inclusion of 1000ppm of TPAE (b). From the figure, it could be noticed that the metallic sample processed with the inhibitor reveals an enhancement in CA (83.30°), as compared to the sample solely processed with 0.5M HCl (65.37°). As a result, the surface of mild steel had a lower hydrophobicity before being subjected to TPAE (**Figure 4.63 (a)**), but later on, the hydrophobicity increased (**Figure 4.63 (b)**). The aggressive ions can adsorb on mild steel



surfaces in an acidic environment because of their minimal hydrophobicity, which encourages corrosion. The surface tension may have been altered by the adhesion of inhibitor molecules, culminating in the creation of a defensive layer upon the metallic substrate to reduce corrosion.

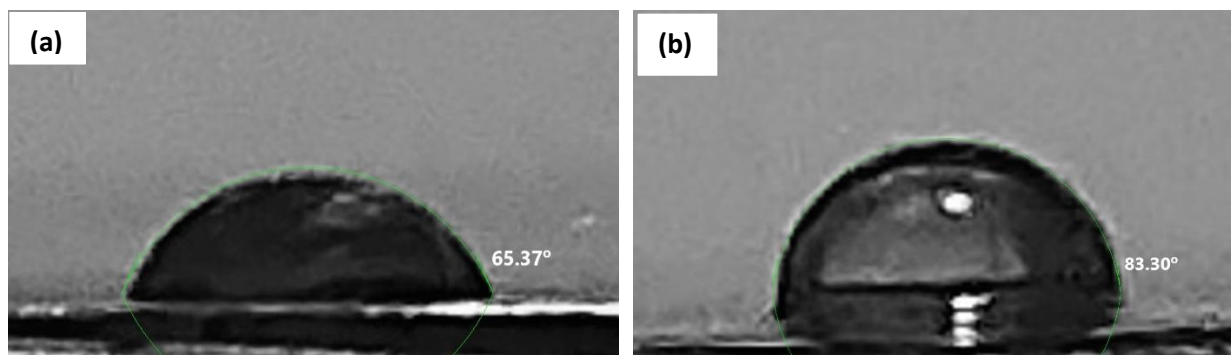


**Figure 4.63.** CA assessment performed on the metallic sample in (a) 0.5M HCl media and (b) 0.5M HCl +1000ppm of TPAC.

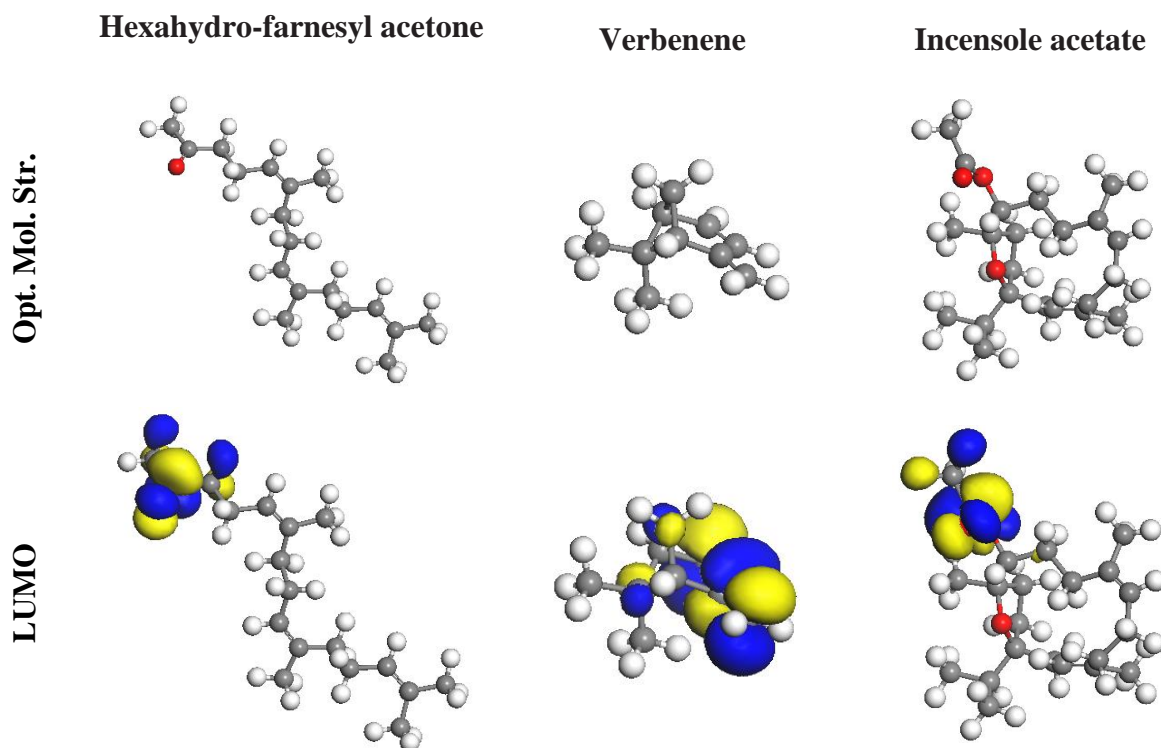
#### 4.4.8. Computational analysis

##### 4.4.8.1. DFT analysis

DFT has subsequently emerged as among the most influential and remarkable computer modeling techniques for evaluating efficient corrosion inhibitors. Among the most significant features of DFT and other computer modeling is that corrosion inhibition capability as well as many other chemical reactivity parameters of chemical entities can indeed be hypothetically analyzed earlier for complex and hazardous chemical synthesis. Owing to duration, expense, and ecological aspects, and also the insufficiency of traditional methodologies, the utilization of computational methods such as DFT for investigations of metal corrosion inhibition has increased exponentially. This technique allows one to assess an organic compound's ability to reduce metal corrosion by evaluating how chemically reactive it is. To achieve this goal, we have utilized the DFT approach, utilizing the GGA technique with BLYP functional to investigate electron-correlation encounters and a basis set comprised of DNP 3.5 to carry out theoretical calculations and calculate the  $E_{HOMO}$  and  $E_{LUMO}$  of the examining inhibitor in explaining their adsorption and inhibition efficacy. The DMol<sup>3</sup> tool in the Materials Studio version 6.0 package was used in conjunction with the COSMOS solvation model (H<sub>2</sub>O). The chemical quantum investigation was

performed using the Gaussian 09 W software. Quantum chemical parameters like  $E_{\text{HOMO}}$ ,  $E_{\text{LUMO}}$ ,  $I$ ,  $Z$ ,  $\eta$  and  $\chi$  were calculated by using the eqns. (11)–(17) to assess the overall reactivity of our examined extract.

**Figure 4.64** shows the optimized,  $E_{\text{HOMO}}$  and  $E_{\text{LUMO}}$  geometries of the hexahydro-farnesyl acetone, verbenene, incensole acetate. Through the investigation of **Figure 4.64**, it could be noticed that HOMO and LUMO in hexahydro-farnesyl acetone, verbenene and incensole acetate molecules are located approximately throughout the molecular fractions. This finding suggests that all three molecules hexahydro-farnesyl acetone, verbenene and incensole acetate are involved in charge sharing. The presence of heteroatom moiety and aromatic ring configuration in their molecular compositions, correspondingly, is linked to their relatively huge participation in charge. Following these considerations, it has been shown that the molecules hexahydro-farnesyl acetone, verbenene and incensole acetate have exceptional anti-corrosive capabilities that are accountable for corrosion mitigation.



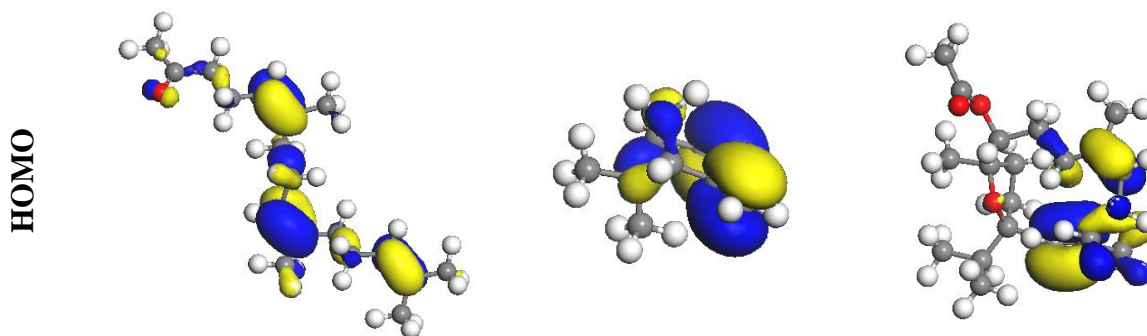


**Figure 4.64.** Optimized geometries and FMOs (i.e., HOMO and LUMO) of the Hexahydro-farnesyl acetone, Verbenene and Incensole acetate.

The acquired quantum chemical characteristics of the listed molecules are reported in **Table 4.33**. The intensity of a molecule to accept electrons could be ascribed to the low  $E_{LUMO}$  values, whereas the intensity of a molecule to transmit electrons is reflected by the maximal  $E_{HOMO}$  value. The energy gap ( $\Delta E$ ) which is the difference in energy between  $E_{HOMO}$  and  $E_{LUMO}$  also plays an important role while analyzing and supporting the corrosion inhibitor's stability indices. The lower the value of  $\Delta E$ , the stronger and more reflexive connection between the inhibitor and the Fe substrate. In this case, among all, the value of  $\Delta E$  of verbenene comes out to be the smallest i.e., 0.16405, which could be ascribed to the availability of hetero atom and aromatic ring in its structure as compared to Hexahydro-farnesyl acetone and Incensole acetate. **Table 4.33** shows that all of the molecules possess low  $E_{LUMO}$  and significant  $E_{HOMO}$  values. This means that TPAE molecules exhibit a considerable capability for adhering to metallic surfaces and, as a result, significantly inhibiting corrosion. In several articles, it is also explained that the negative value of  $E_{HOMO}$  represents physical adsorption. In the latest study, the  $E_{HOMO}$  values of all the compounds come out to be negative, therefore depicting more chances of physical adsorption than chemical adsorption.

The symbol  $\Delta N$  represents the ratio of electrons that a molecule transfers to the vacant orbital. It is a renowned indication of the chemical reactivity and stability of corrosion inhibitor molecules. In actuality, a positive and greater value of  $\Delta N$  reveals a molecule's stronger inhibitory function. In this case, all the molecules Hexahydro-farnesyl acetone, Verbenene and Incensole acetate have quite positive and similar  $\Delta N$  values of 0.445, 0.474, and 0.478, which corresponds to their better chemical reactivity and stability. It is also well mentioned that  $\eta$  with a low value proposes a higher

IE. Through **Table 4.33**, it can be observed that the Hexahydro-farnesyl acetone possesses a low value of  $\eta$  i.e., 1.784 followed by the Verbenene (1.827) and Incensole acetate (2.032), which again corresponds to the better inhibitor efficiency of the extract. In contrast to the  $\Delta N$  value, the  $\eta$  value is also in great agreement with the empirical findings. This shows that the molecules Hexahydro-farnesyl acetone, Verbenene and Incensole acetate are the least susceptible to charge donation and acceptance. As a result, they show that the extract has a strong corrosion inhibitory effect on mild steel surfaces.

**Table 4.33**

Pertinent electronic parameters related to the extract components in the aqueous phase with the usage of the DNP 3.5 basis set and the GGA/BLYP technique.

<b>Code</b>	<b>Hexahydro-farnesyl acetone</b>	<b>Verbenene</b>	<b>Incensole acetate</b>
<b>Basis set</b>	DNP	DNP	DNP
<b>Function</b>	GGA	GGA	GGA
<b>E<sub>HOMO</sub> (eV)</b>	-5.018	-4.914	-4.909
<b>E<sub>LUMO</sub> (eV)</b>	-1.449	-1.260	-0.845
<b><math>\Delta E</math> (eV)</b>	0.23904	0.16405	0.23043
<b>I (eV)</b>	5.018	4.914	4.909
<b>Z (eV)</b>	1.449	1.260	0.845
<b><math>\eta</math> (eV)</b>	1.784	1.827	2.032
<b><math>\chi</math> (eV)</b>	3.233	3.087	2.877
<b><math>\Delta N</math> (Fe) (e)</b>	0.445	0.474	0.478
<b><math>\Delta E_i</math> (Fe) (eV)</b>	-0.353	-0.411	-0.464
<b><math>\Delta E_{b-d}</math> (Fe) (eV)</b>	-0.446	-0.457	-0.508

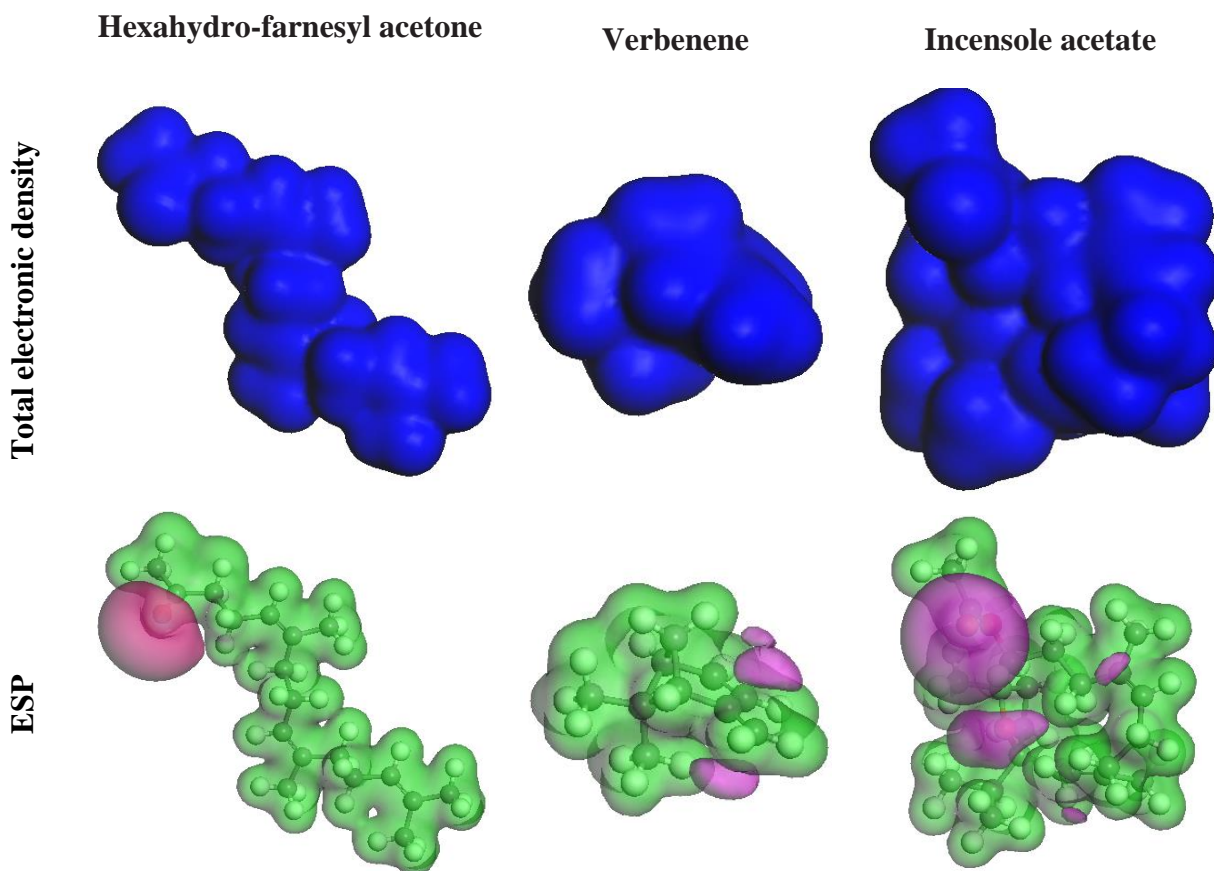
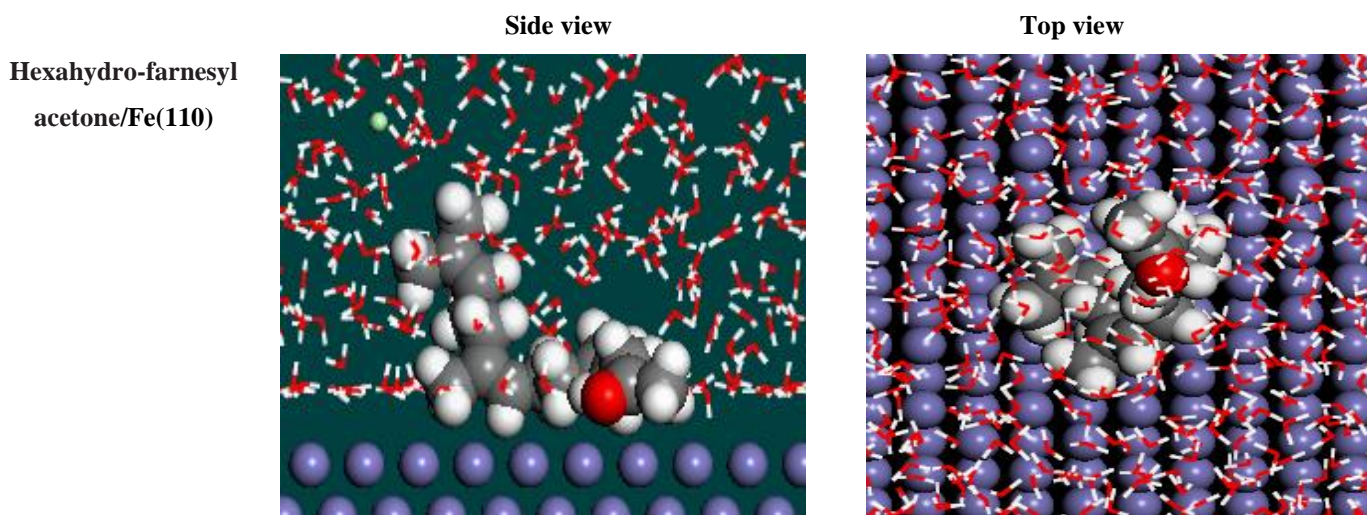


**Figure 4.65.** Isosurfaces of total electronic density and ESP mapping (green and red colors denote electro-positive and negative potentials, respectively) of the Hexahydro-farnesyl acetone, Verbenene and Incensole acetate.

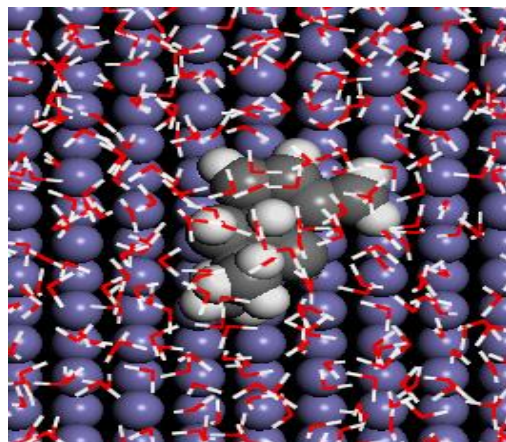
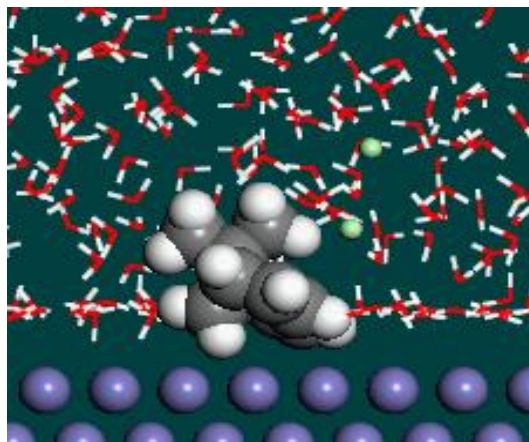
Electrostatic potential surface ESP maps could offer an instinctive approach to quantifying polarity, that facilitates the evaluation of the corrosion process. The negative electrostatic potential portion (tint of red) is susceptible to nucleophilic attacks, whereas the positive potential portion (tint of blue) is susceptible to electrophilic attacks. The red areas are typically found around the heteroatom (oxygen), which could establish a covalent bond with the Fe atom, as shown in **Figure 4.65**. Positive potential sites are found near carbon and hydrogen atoms as they are ideal targets for electrophilic attack. Hexahydro-farnesyl acetone, Verbenene, and Incensole acetate offer a superior potential to gain electrons from the metallic surface because it has a higher negative potential. Similar findings were attained from the  $\Delta N$  and frontier molecular orbitals ( $E_{HOMO}$  and  $E_{LUMO}$ ) investigation (**Table 4.33**).

#### 4.4.8.2. MC simulation analysis

The utilization of MC simulation in computational studies of metal corrosion inhibition offers meaningful insight information into the pathway and interaction between a metal surface and inhibitor molecules at a minimal price. Subsequently, the application of MC for simulating metal surface-inhibitor interaction has piqued the interest of researchers and scientists across the world, and the subject of corrosion science has advanced significantly<sup>33,304,333–337</sup>. This simulation was performed in this research with the aid of the Forcite module included in the Materials Studio 8 software. In this analysis, the Monte Carlo simulation is allied with the simulated annealing algorithm (MCS-SAA). The number of simulation cycles was three with 15 000 steps per cycle. The interactions of the molecule on the Fe (1 1 0) substrate were studied using a simulation box with periodic perimeter constraints that have dimensions of 22.34 Å × 22.34 Å × 38.11 Å. By 29 Å, the simulation box had been substantially depleted. 400 H<sub>2</sub>O + 5 H<sub>3</sub>O<sup>+</sup> + 5 Cl<sup>-</sup> and an inhibiting molecule inhabited this vacuum. The *Van der Waals* and electrostatic interactions were evaluated by *Ewald* and atom-relied summation techniques, correspondingly. The Andersen thermostat, and NVT ensembles, employing the COMPASS force field with a simulation duration of 200 ps and a time scale of 1.0 fs were utilized to regulate the temperature of the simulation model, which was 298K.



Verbenene/Fe(110)



Incensole  
acetate/Fe(110)

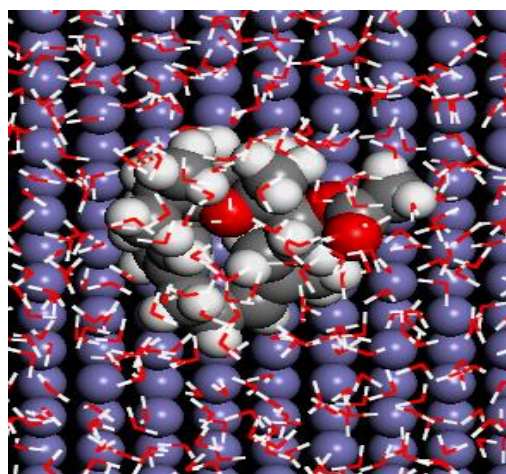
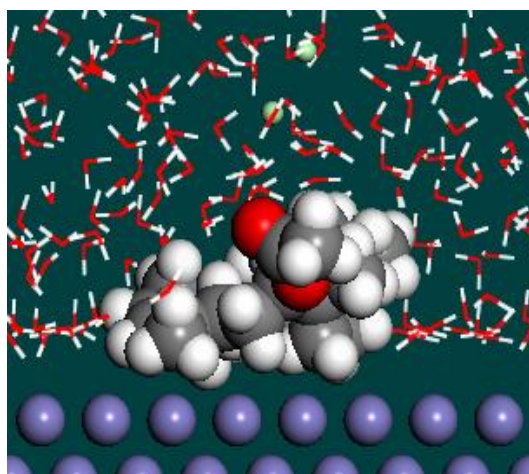


**Figure 4.66.** Side sight and top sight of the equilibrium adsorption geometry of Hexahydro-farnesyl acetone, Verbenene and Incensole acetate at the solution/Fe(1 1 0) interface.

From the outcomes in **Figure 4.66**, it can be understood that the inhibitor molecule adsorbs upon the Fe (1 1 0) substrate in a flat or parallel way, revealing that the Hexahydro-farnesyl acetone, Verbenene and Incensole acetate molecules offer a significant interaction across active regions and Fe atoms. The durability of the adsorbed molecule may be increased by the flat adsorption arrangement. Additionally, greater surface coverage is provided by covering more active spots onto the metallic surface. The values of the binding energy could also be used to assess the molecules' adsorption capabilities. **Table 4.34** lists the calculated inhibitor adsorption binding energies on the Fe (1 1 0) surface. The potent adsorption of all chemical components of TPAE, including hexahydro-farnesyl acetone (-6122.206), verbenene (-6.15E+03), and incensole acetate (-

6.11E+03), upon the Fe(1 1 0) substrate was endorsed by the existence of a high magnitude of adsorption energies, which again correlates with the results obtained from quantum chemical parameters. A similar pattern can be noticed in the case of  $\Delta E_i$  values in which an elevated negative value of  $\Delta E_i$  has been attained which indicates enhanced adsorption as listed in **Table 4.33**. It is amazing to notice the significant values of  $\Delta E_i$  and  $\Delta E_{b-d}$  of all three molecules which contribute to the adsorption and binding of the investigated TPAAE molecules upon the metallic substrate to a great extent and thereby reveal excellent corrosion inhibition efficiency characteristics.

**Table 4.34**

$E_{\text{interaction}}$  and  $E_{\text{binding}}$  of V(Z)-hex-3-en-1-ol, (E)-b-ionone and Phytol on Fe (1 1 0) surfaces in HCl at 298K (all in kJ/mol).

System	Adsorption energy	Rigid adsorption energy	Deformation energy	Inhibitor: dEad/dNi	H <sub>2</sub> O: dEad/dNi	H <sub>3</sub> O <sup>+</sup> : dEad/dNi	Cl <sup>-</sup> : dEad/dNi
Hexahydro-farnesyl acetone/Fe(110)	-6122.206	-6311.803	189.597	-134.394	-15.098	-162.153	-155.712
Verbenene/Fe(110)	-6.15E+03	-6.25E+03	101.859	-137.030	-14.346	-156.680	-152.356
Incensole acetate/Fe(110)	-6.11E+03	-6.30E+03	190.643	-146.663	-14.590	-161.236	-163.960

#### 4.4.9. Biodegradability of TPAAE

The rate of TPAAE's biodegradation after 28 days is shown in **Figure 4.67**. At 28 days, the rate of CBE degradation accelerated over the period, reaching 90.23 % as depicted in **Figure 4.67** as computed by equation (19). According to the North-East Atlantic Accords for the Ecological Prevention, anything is considered rapidly biodegradable if it degrades more than 60 % in 28 days<sup>273</sup>. TPAAE could therefore be interpreted as a biodegradable corrosion inhibitor.



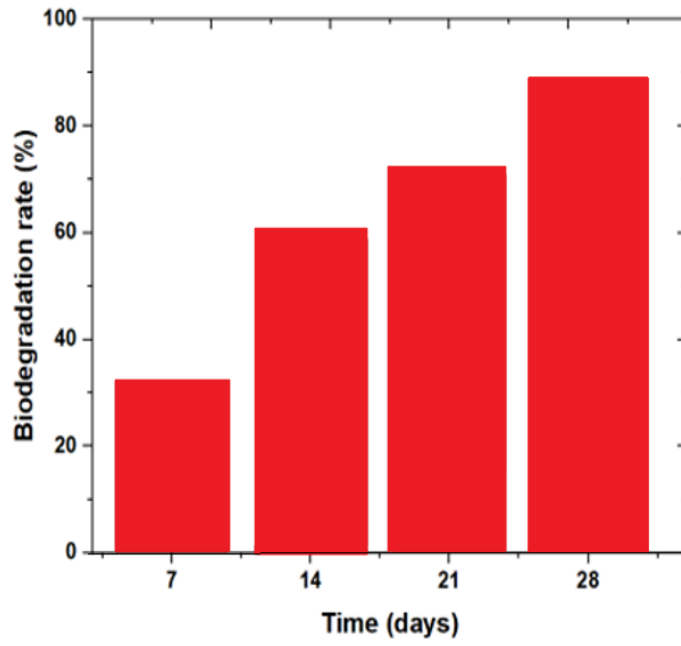


**Figure 4.67.** Biodegradability of TPPE.

#### 4.5. *Polygonum cuspidatum*

*Polygonum cuspidatum* (PC) is a perennial plant that belongs to the genus *Polygonum* and the family *Polygonaceae*. It is found in Japan, China, Korea, and North America where it is also known as Mexican bamboo. The plant has a bushy, upright structure that can grow to over 3m tall. In spring, the shoots are red to purple but turn green as they grow into canes. The ripe canes are cylindrical and mottled with purple, and they bloom in late autumn and summer with creamy white blooms. The stem base is encased in a permeable coating above each joint. The leaves are about 15cm in length and 8–10cm in width, widely oval to slightly triangular, and pointed at the tip. The triangular, glossy, and 2.5 mm long seeds are present. Huzhang, a traditional Chinese medicine, is made from the dried root of the PC plant and is listed in the Chinese Pharmacopoeia<sup>69,338,339</sup>. It is also used in folk medicine in Japan and Korea, where it is known as Japanese knotweed. The plant can be used as an antipyretic, aesthetic, diuretic, anti-inflammatory agent, and expectorant, among other therapeutic purposes. Also, it is employed in the treatment of cancer, hypotension, hypercholesterolemia, leucorrhoea, atherosclerotic, dysmenorrhea, trauma involving blood stagnation, wounds, snake stings, bronchiolitis, contagious hepatitis, diarrhea, allergic inflammatory disorders, and dysmenorrhea. According to the previous investigation<sup>340</sup>, PCRE contains several key phytochemical components such as Piceid, Resveratrol, Emodin, Emodin-1-O-glucoside and 1-O-Methylemodin, as illustrated in **Figure 4.68**. In this study, PCRE, which is broadly available in several nations, has been evaluated as an eco-friendly corrosion inhibitor for mild steel in an aggressive medium of 0.5 M HCl. The research was crucial because there is currently no comprehensive evidence on the effectiveness of PCRE as a corrosion inhibitor for mild steel in corrosive media. The researchers used gravimetric techniques, electrochemical investigations (including EIS and PDP), and morphological evaluation utilizing SEM to extract and evaluate PCRE's ability to reduce the intensity of mild steel corrosion in 0.5M HCl media. By using PCRE as an eco-friendly corrosion inhibitor for mild steel, PCRE will not only reduce the price of corrosion inhibitors but significantly promote PC and other weed cultivation and effective usage. The crucial aspect is that this usage will have minimal impact on both humans and the environment, and a commodity that was once considered waste can now be utilized as a potent and environmentally friendly inhibitor to mitigate metallic corrosion and combat the catastrophic global concern of corrosion.

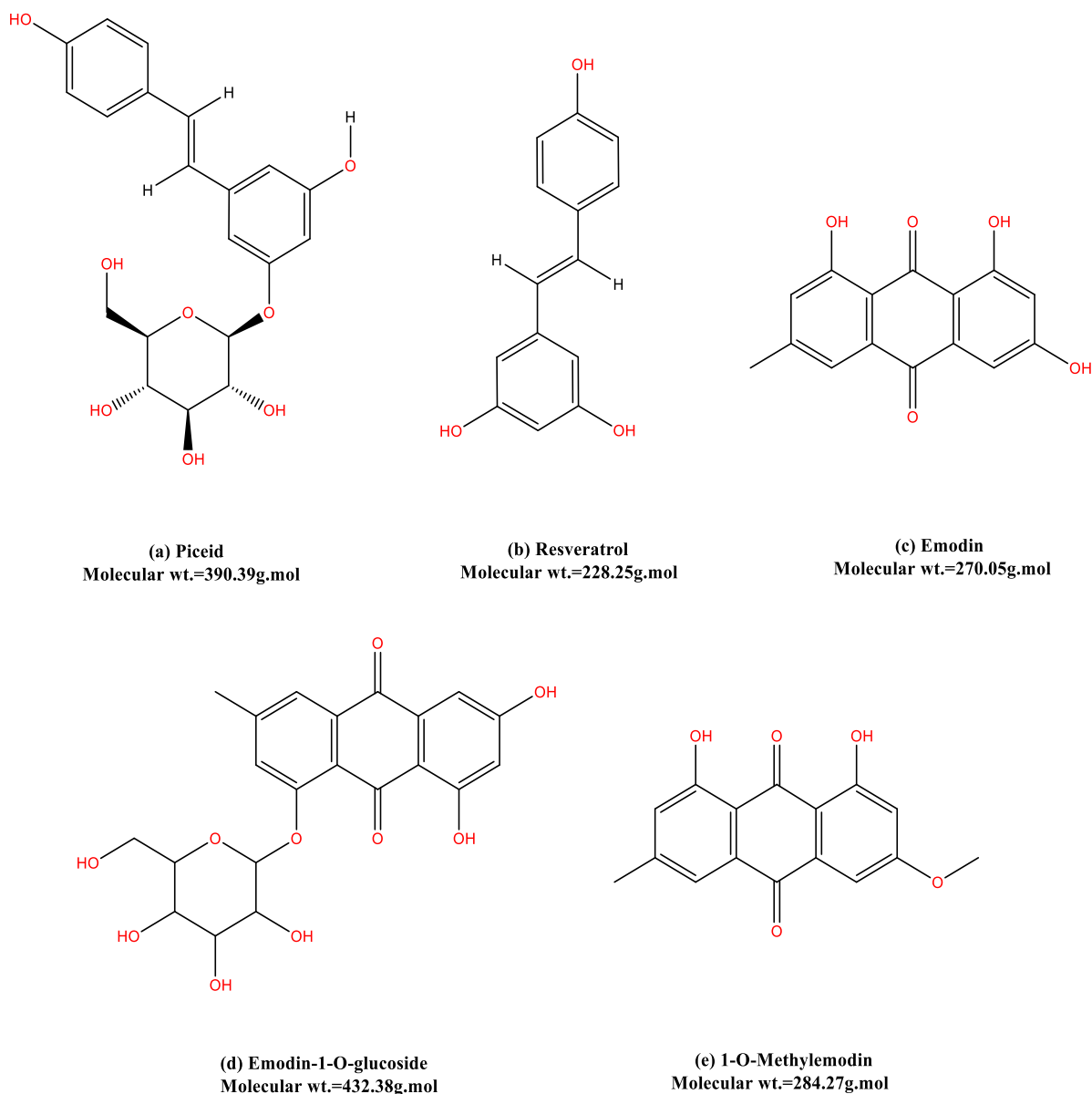


**Figure 4.68.** Molecular structures of the major phytoconstituents present in the PCRE.

#### 4.5.1. Preparation of *Polygonum cuspidatum* root extract

The root parts of *Polygonum cuspidatum* (PC) were gathered from a nearby farm in Kapurthala in the flowering stage during the summer season and later affirmed by Prof. Neera, Botany Department, HPU, India. The roots were first air-dried in the sun for 8 days to remove any moisture. After being dried, the roots are pounded into a minute powder and sieved to remove any large particles. The resultant powder was then combined at a proportion of 1:2 (w/v) with 80%

methanol. After that, this mixture was poured into a water bath that was shaken and left to soak for 24 hrs at ambient temperature. The purpose of using a shaking water bath was to ensure that the extract was thoroughly mixed with the methanol and to aid in the extraction of the active compounds. After 24 hrs, the mixture was filtered through a Millipore filter with a 0.45  $\mu\text{m}$  nylon membrane to remove any solid particles<sup>340</sup>. The filtrate was then concentrated to increase the concentration of the active compounds. This was typically done by evaporating the methanol, either through heating or by using a rotary evaporator. After that, the crude extract was refrigerated at 4°C until use<sup>142</sup>. This was to prevent any degradation or degradation of the active compounds. In 0.5 M HCl, the obtained PC root extract was most soluble up to 1000 mg/L.

#### 4.5.2. FT-IR evaluation

The adsorption of PCRE molecules onto mild steel surfaces for corrosion reduction might be facilitated by the inclusion of aromatic ring geometries and heteroatoms (O). **Figure 4.69** illustrates the PCRE's FTIR spectrum. The FTIR spectra of the PCRE illustrate  $\text{-C-H}$  stretch at 2851  $\text{cm}^{-1}$  as indicative of the presence of aliphatic hydrocarbon groups in the sample.  $\text{-O-H}$  stretch at 3359  $\text{cm}^{-1}$  as indicative of the existence of hydroxyl groups in the sample.  $\text{-C-O}$  stretch at 1019  $\text{cm}^{-1}$  as an indicative of the existence of carbonyl groups in the sample.  $\text{-CH}_3$  bend at 1457  $\text{cm}^{-1}$  and 1380  $\text{cm}^{-1}$  are indicative of the existence of methyl groups in the sample.  $\text{-C=O}$  stretch at 1637  $\text{cm}^{-1}$  as indicative of the presence of carbonyl groups in the sample.  $\text{-C=C}$  stretch obscured with  $\text{C=O}$  stretch is indicative of the presence of aliphatic hydrocarbon moieties in the sample.  $\text{=C-H}$  stretch at 2922  $\text{cm}^{-1}$  is indicative of the existence of aliphatic hydrocarbon groups in the sample.  $\text{-C-H}$  bend at 614  $\text{cm}^{-1}$  is indicative of the existence of aliphatic hydrocarbon groups in the sample. Based on the FTIR outcomes, it can be documented that the sample contains aliphatic hydrocarbon groups, hydroxyl groups, carbonyl groups, and methyl groups. Additionally, these outcomes showed that PCRE included heteroatom (oxygen) in  $\text{-C-O}$ ,  $\text{-C=O}$  moieties, aromatic ring structures and linear molecules, which illustrates that PCRE has significant corrosion inhibition efficacy in 0.5M HCl and the attained results are in accordant with the geometries of conventional corrosion inhibitors.

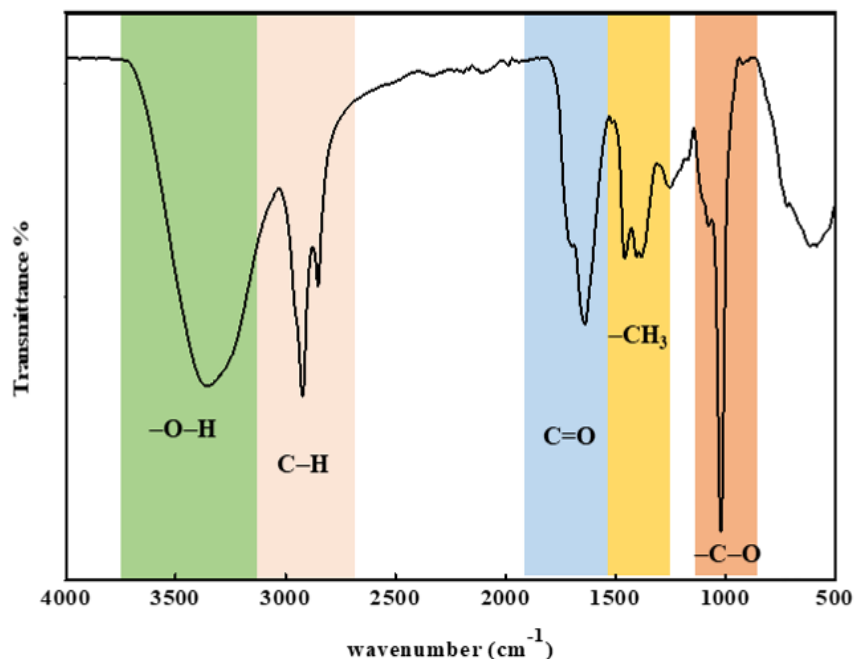


**Figure 4.69.** FT-IR analysis of the PCRE.

### 4.5.3. UV-Vis spectrometry

The UV-Vis spectrum of PCRE was considered for the pre-and post-corrosion test, illustrated in **Figure 4.70**. The inhibitor configuration exhibits adsorption peaks at 624 nm and 452.97 nm, illustrating the  $n-\pi^*$  and  $\pi-\pi^*$  transitions, correspondingly, subsequent to the corrosion predictions. The  $\pi-\pi^*$  transition, which is associated with the  $C=C$  conjugation found in the inhibitor molecules, is attributed to the initial peak. The absorption spectra of PCRE shows an absorption peak in the wavelength region of 550-650 nm, corresponding to the  $n-\pi^*$  transition ascribed to the numerous functional moieties prevalent in inhibitor molecules including  $-C=O$ ,  $-C-O$ , and so on. Afterward the corrosion study, the results show a hypsochromic shifting of the optimum adsorption. The results confirmed the possibility of a complex forming between Fe and phytochemicals, as shown in **Figure 4.70**, and that these peaks were redistributed after the corrosion analysis. It vividly illustrates that when the metallic sample was dipped in the 0.5M HCl+1000ppm of PCRE, several molecules from the media (inhibitor) were adsorbed onto the metallic substrate.

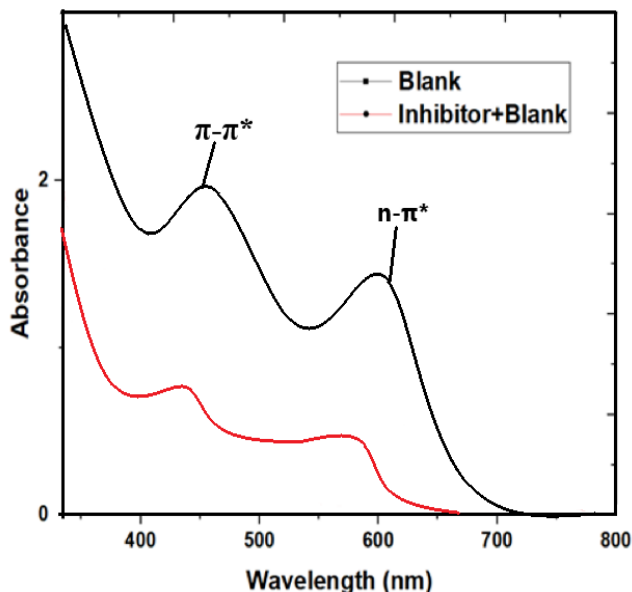


**Figure 4.70.** UV Spectra of pre- and post-metal dipping in 0.5M HCl and with the inclusion of PCRE.

#### 4.5.4. Weight loss measurement

Weight loss measurement is a common method used to study corrosion and corrosion inhibition in materials. It involves measuring the decrease in the mass of a sample due to the corrosion process and offers crucial insights into the  $C_R$  and the effectiveness of corrosion inhibitors. In this experiment, WL assessment was done after the stipulated 24-hrs immersion period in 0.5M HCl solution. **Table 4.35** summarizes the  $C_R$  and  $IE\%$  evaluated by gravimetric analysis. It was evident from the measurements that PCRE had outstanding  $IE\%$  properties against MS corrosion in 0.5M HCl medium. In fact, as the concentration of the inhibitors increased from 50ppm to 1000ppm, the corrosion rate did indeed decrease effectively from  $3.380$  to  $0.110 \text{ mg.cm}^{-2}.\text{h}^{-1}$  and the inhibition performance increased from 91.94 to 96.71% at 298K. Additionally, the surface coverage also increased from 0.919 to 0.967 suggesting the strong adsorption capabilities of PCRE by establishing a protective barrier on the metallic substrate and retarding the  $C_R$  in an aggressive corrosive medium which is responsible for the excellent efficacy displayed by PCRE<sup>341</sup>.

**Table 4.35**

Gravimetric outcomes for mild steel in 0.5M HCl without and with PCRE.

Inhibitor	Conc. (ppm)	$C_R$ (mg.cm <sup>-2</sup> .h <sup>-1</sup> )	$\eta_{WL}(\%)$	$\theta$
<b>Blank</b>	0	3.380	-	-
	50	0.270	91.94	0.919
	100	0.223	93.33	0.933
<b>PCRE</b>	250	0.187	94.41	0.944
	500	0.150	95.52	0.955
	1000	0.110	96.71	0.967

#### 4.5.4.1. Concentration's effect on inhibition performance

The effect of concentration on the inhibition performance of a corrosion inhibitor relied on various parameters, including the type of inhibitor, the type of metal being protected, the corrosive environment, and the method of evaluation. In general, an increment in the concentration of a corrosion inhibitor leads to an enhancement in its IE% up to a certain point. This is because a higher concentration of the inhibitor provides more active sites for adsorption on the metal surface, leading to a greater reduction in the  $C_R$ . In this experiment, utilizing a weight loss plot, the  $C_R$  of mild steel in 0.5M HCl vs. varied dosages of the PCRE (50ppm to 1000ppm) were examined during the immersion time of 24 hrs at a temperature range of 298-313K (**Figure 4.71**). Evidently, as inhibitor concentrations were raised, the  $C_R$  was decreased and the effectiveness of inhibition was increased (**Figure 4.72**). This is as a result of the inhibitor being firmly adsorbed on the mild steel surface and reducing the metal dissolving process. In the current study, the highest IE% of the examined inhibitor has been attained to be 96.71% with a rate of corrosion 0.110 (mg.cm<sup>-2</sup>.h<sup>-1</sup>) at 1000ppm.

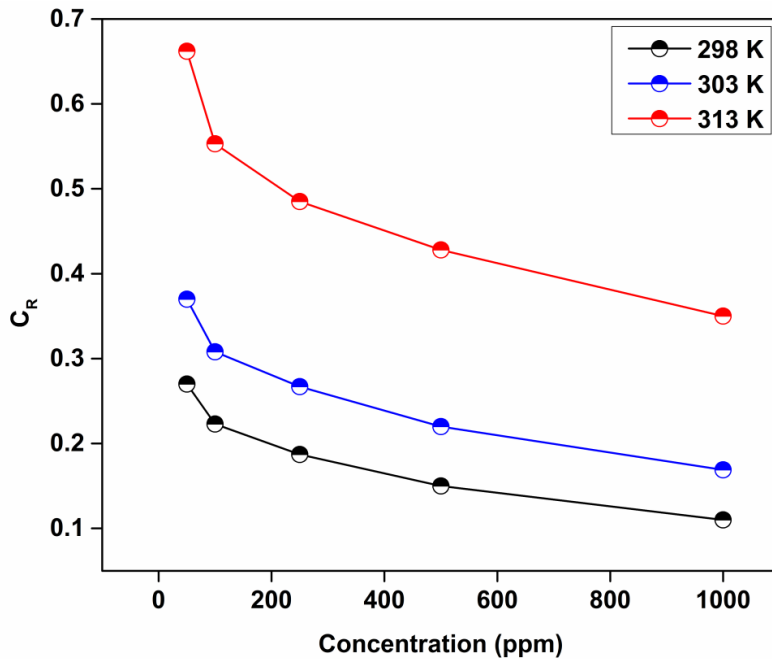


**Figure 4.71.** Corrosion rate variation at different PCRE concentrations at various temperatures.

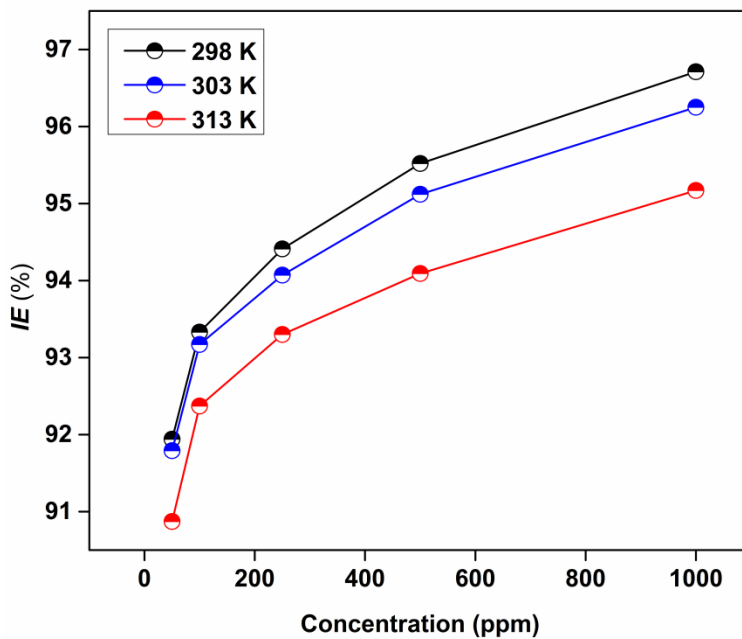


**Figure 4.72.** Effect of inhibition efficiency at different concentrations of PCRE at various temperatures.



#### 4.5.5. Temperature impact and activation parameters

Temperature is the next significant factor that influences the activity of inhibitors and substrates in hostile media. At higher temperatures, the PCRE molecules become more soluble and desorb from the metallic substrate, as a result, mild steel's corrosion resistance declines as the temperature rises. In this experiment, three different temperatures (298K, 303K, and 313K) were taken to conduct gravimetric analysis with varying concentrations of PCRE (50-1000ppm) to ascertain the impact of temperature on the IE% of the PCRE. **Table 4.36** illustrates the impact of various inhibitor concentrations on corrosion rates under different temperatures. The results of the experiment conducted at 298K indicate that an increase in the inhibitor efficiency percentage (IE%) from 91.935 to 96.714 led to a decrease in the  $C_R$  from 3.348 to 0.110, along with an increase in surface coverage from 0.919 to 0.967. At 303K, the  $C_R$  decreased from 4.510 to 0.169 with an increase in IE% from 91.796 to 96.252, and the surface coverage increased from 0.917 to 0.962. However, at 313K, the  $C_R$  increased from 7.247 to 0.350, and the surface coverage decreased from 0.908 to 0.951 with an increase in IE% from 90.865 to 95.170. These findings significantly suggested that with an increase in temperature from 298K to 313K, the  $C_R$  increased with a reduction in the IE% and  $\Theta$  as compared to the findings in 298K and 303K revealing the desorption of adhered molecules of PCRE on the mild steel surface and increase in the active spots for the attack of corrosive ions which ultimately led to the corrosion of mild steel.

**Table 4.36**

Corrosion rate, Inhibition performance (%) and surface coverage of mild steel in 0.5M HCl solution of PCRE.

Temperature (K)	Concentration (ppm)	$C_R$ (mg.cm <sup>-2</sup> .h <sup>-1</sup> )	$\eta_{WL}$ (%)	$\Theta$
298	0	3.348	-	-
	50	0.270	91.935	0.919
	100	0.223	93.339	0.933
	250	0.187	94.414	0.944
	500	0.150	95.519	0.955
	1000	0.110	96.714	0.967
303	0	4.510	-	-

303	50	0.370	91.796	0.917
	100	0.308	93.170	0.931
	250	0.267	94.079	0.940
	500	0.220	95.122	0.951
	1000	0.169	96.252	0.962
313	0	7.247	-	-
	50	0.662	90.865	0.908
	100	0.553	92.369	0.923
	250	0.485	93.307	0.933
	500	0.428	94.094	0.940
	1000	0.350	95.170	0.951

It is clear that the  $C_R$  increased as the temperature rose from 298K to 313K, which illustrates that the protective inhibitors' ability to reduce corrosion at various concentrations decreased, suggesting that the protective layer was eroding as the temperature rose. Additionally, to deliberate more, an Arrhenius-type behavior has been exhibited between temperature and  $C_R$ . By using equation (20) the activation energy ( $E_a$ ) of the corrosion mechanism at different temperature ranges was evaluated in both the presence and absence of PCRE.

$$\ln C_R = A - \frac{E_a}{RT} \quad (20)$$

Following transition state theory, the thermodynamic parameters enthalpy ( $\Delta H_a$ ) and entropy ( $\Delta S$ ) for the corrosion process were computed. The slope of the equation ( $-E_a/RT$ ) in the inclusion and exclusion of the investigated inhibitor was used to compute the activation energy of the metal-dissolving process (**Figure 4.73**)

$$C_R = \frac{RT}{Nh} \exp\left(\frac{\Delta S}{R}\right) \exp\left(\frac{-\Delta H_a}{RT}\right) \quad (21)$$

Herein,  $R$ ,  $T$ ,  $N$ ,  $h$ ,  $\Delta H_a$ , and  $\Delta S$  stand for the system's gas constant, Temperature, Avogadro number, Planck's constant, enthalpy and entropy, respectively. **Table 4.37** shows the several activation parameters in the existence and non-existence of PCRE.

**Table 4.37**

Mild steel activation parameters ( $E_a$ ,  $\Delta H_a$ ,  $\Delta S$ ) in the existence and non-existence of PCRE.

Medium	Conc. (ppm)	$E_a$ (KJ/mol)	$\Delta H_a$ (KJ/mol)	$\Delta S$ (J mol <sup>-1</sup> K <sup>-1</sup> )	$E_a - \Delta H_a$ (KJ/mol)
Blank	0	39.435	36.801	-73.869	2.6
	50	46.339	43.786	-71.446	2.6
	100	46.949	44.425	-70.918	2.5
PCRE	250	48.956	46.296	-65.958	2.6
	500	53.930	51.249	-51.079	2.6
	1000	59.494	56.931	-34.505	2.6

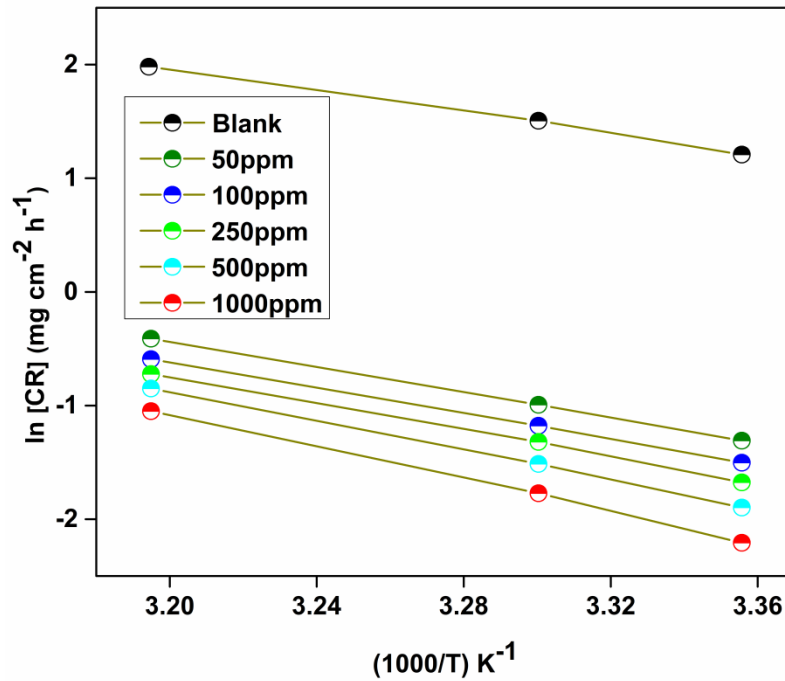


**Figure 4.73.**  $\ln [CR]$  vs.  $1000/T$  for mild steel corrosion in 0.5 M HCl solution in the exclusion and inclusion of various dosages of PCRE.

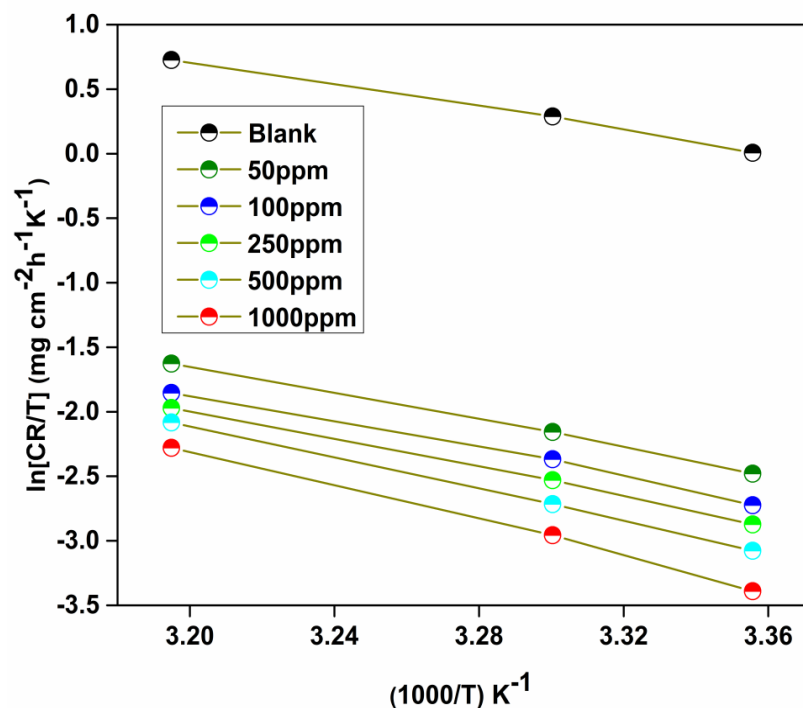


**Figure 4.74.**  $\ln [CR/T]$  vs.  $1000/T$  for mild steel corrosion in 0.5 M HCl solution in the exclusion and inclusion of various dosages of PCRE.

The values of  $\Delta H_a$  and  $\Delta S$  are shown in **Table 4.37** and were computed from the plot of  $\ln(C_R/T)$  v/s  $1/T$  (**Figure 4.74**). This table provides information on the activation energy ( $E_a$ ), enthalpy of adsorption ( $\Delta H_a$ ), the entropy of adsorption ( $\Delta S$ ), and the difference between  $E_a$  and  $\Delta H_a$  for PCRE adsorbed onto a medium at different concentrations (50-1000 ppm). The  $E_a$  represents the energy needed for a chemical reaction to occur. In the context of adsorption,  $E_a$  indicates the energy required for the adsorbate (PCRE) to overcome the barrier to adsorption and become adsorbed onto the adsorbent surface. The enthalpy of adsorption ( $\Delta H_a$ ) represents the variation in enthalpy interlinked with the adsorption mechanism, and the entropy of adsorption ( $\Delta S$ ) represents the variation in entropy interlinked with the adsorption mechanism.

The difference between  $E_a$  and  $\Delta H_a$  can provide insight into the nature of the adsorption process. If  $E_a - \Delta H_a$  is positive, it suggests that the adsorption process is primarily driven by enthalpy changes (e.g. attractive forces between the adsorbate and the adsorbent surface). If  $E_a - \Delta H_a$  is negative, it suggests that the adsorption process is primarily driven by entropy changes (e.g. an

elevation in the disorder of the system). In this case, the blank medium (0 ppm) had an  $E_a$  of 39.435 kJ/mol,  $\Delta H_a$  of 36.801 kJ/mol, and  $\Delta S$  of  $-73.869 \text{ J mol}^{-1}\text{K}^{-1}$ . Whereas, the 1000ppm concentration had an  $E_a$  of 59.494 kJ/mol,  $\Delta H_a$  of 56.931 kJ/mol, and  $\Delta S$  of  $-34.505 \text{ J mol}^{-1}\text{K}^{-1}$ . The average difference in  $E_a - \Delta H$  ( $\sim 2.6 \text{ kJ/mol}$ ) resembles the average  $RT$  ( $2.64 \text{ kJ/mol}$ ), inferring the corrosion mechanism via a unimolecular gaseous reaction<sup>342</sup>. It is evident that as the dosage of PCRE increased from 50 to 1000 ppm, both the  $E_a$  and  $\Delta H_a$  increased, while the  $\Delta S$  decreased. Overall, these findings revealed that the adsorption of PCRE onto the medium is primarily driven by enthalpy changes (as  $E_a - \Delta H_a$  is positive), and that the adsorption process becomes stronger at higher concentrations of PCRE. The reduction in entropy of adsorption with elevating PCRE concentration suggests that the system becomes more ordered as more PCRE is adsorbed onto the medium.

#### 4.5.6. Adsorption studies

Adsorption isotherms and kinetics are crucial parameters in the study of corrosion inhibition. They offer crucial insights into the adsorption behavior of corrosion inhibitors on the surface of the corroded material and the rate of adsorption<sup>343,344</sup>. Adsorption isotherms describe the relationship between the dosage of a corrosion inhibitor in solution and its amount adsorbed on the surface of the corroded material. Different kinds of adsorption isotherms, including Langmuir, Freundlich, Temkin, etc., could be utilized to describe the adsorption behavior of different inhibitors. The shape of the adsorption isotherm can provide information about the type of adsorption and the function of the interaction between the inhibitor and the substrate of the corroded material. Adsorption kinetics variables describe the rate of adsorption of a corrosion inhibitor on the surface of the corroded material. In this investigation, in order to correlate the surface coverage ( $\Theta$ ) vs. conc. of the inhibitors ( $C_{inh}$ ), Langmuir adsorption isotherm by using equation (4) (**Figure 4.75**) has been used to provide basic knowledge about the adsorption behavior.  $\Theta$  values have been collected from **Table 4.40**.

After data evaluation, it is determined that the linear curve fitting produced by the Langmuir adsorption isotherm has a regression coefficient of 0.9999, near to the unity. The Langmuir adsorption isotherm is a model utilized to describe the behavior of the adsorption of molecules onto a solid surface. It assumes that adsorption occurs at specific sites over the surface and that each site can only adsorb one molecule. The experimental results revealed that the experimental

results obtained with the PCRE are highly reliable and compatible with the Langmuir adsorption isotherm. It indicates that the Langmuir model is a good fit for exploring the adsorption behavior of the PCRE onto the adsorbent surface and that the assumptions made by the Langmuir model are likely valid for this system. Equation (4), which is the reciprocal of the intercept of a linear line, was used to compute  $K_{ads}$ , and equation (8), which correlates  $K_{ads}$  to  $\Delta G^{\circ}_{ads}$  (standard free energy of the adsorption isotherm), was also used.

**Table 4.38**

Various adsorption variables for PCRE in 0.5M HCl solution.

<b>Isotherm</b>	<b>Inhibitor</b>	<b><math>R^2</math></b>	<b>Parameter</b>		<b><math>K_{ads}</math></b>	<b><math>\Delta G^{\circ}_{ads}</math>(kJ/mol)</b>
<b>Langmuir</b>	PCRE	0.9999	Slope	1.0135	806.452	-26.53

**Table 4.38** provides information on the Langmuir adsorption isotherm for an inhibitor compound (PCRE) and its adsorption onto an adsorbent surface. The table includes the regression coefficient ( $R^2$ ) obtained from the data evaluation, as well as the Langmuir model parameters  $K_{ads}$  and  $\Delta G^{\circ}_{ads}$ . In this case, the Langmuir adsorption isotherm for the inhibitor compound PCRE produced an  $R^2$  of 0.9999, indicating a high degree of correlation between the experimental data and the Langmuir model. The Langmuir parameter  $K_{ads}$  was determined to be 1.0135, indicating a strong affinity of the adsorbent surface for the PCRE inhibitor. Finally, the value of  $\Delta G^{\circ}_{ads}$  (-26.53 kJ/mol) indicates the free energy change associated with the PCRE adsorption over the adsorbent substrate. A negative value for  $\Delta G^{\circ}_{ads}$  indicates that the adsorption process is exothermic and spontaneous, meaning that the adsorbate is energetically favorable to adsorb onto the adsorbent surface. Overall, this information suggests that the Langmuir adsorption isotherm is an appropriate model for describing the adsorption behavior of the PCRE inhibitor over the adsorbent surface and that the adsorption mechanism is energetically favorable and driven by the strong affinity between the adsorbate and the adsorbent surface.

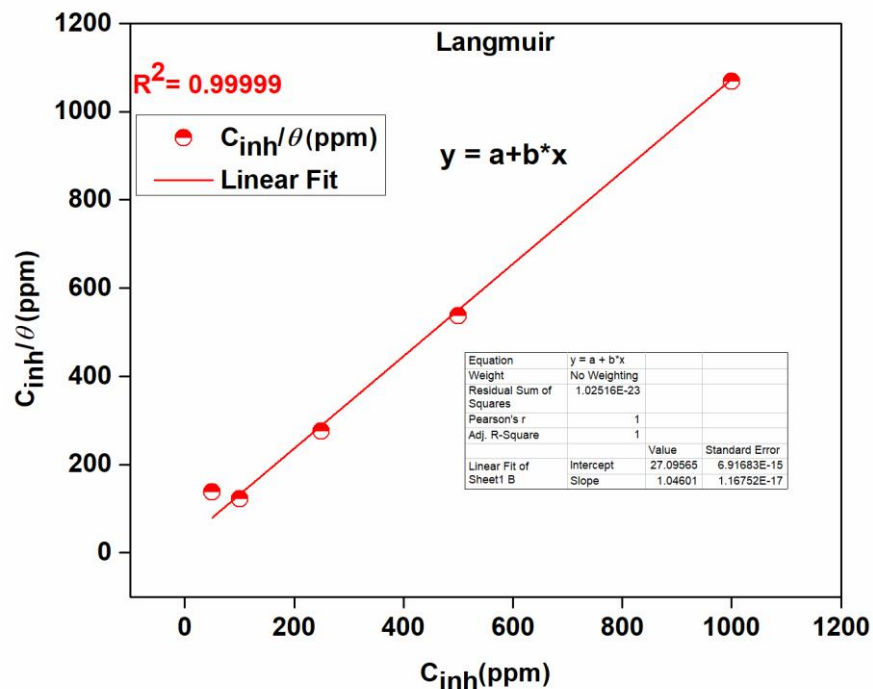


**Figure 4.75.** Langmuir isotherm for adsorption of PCRE on mild steel in 0.5 M HCl.

#### 4.5.7. Electrochemical analysis

##### 4.5.7.1. Open circuit potential (OCP)

Open-circuit potential (OCP) is a crucial parameter in the study of corrosion and corrosion inhibition of metals using EIS<sup>96</sup>. The OCP is the potential of a metal when it is not connected to an external electrical circuit, and it reflects the balance of charge-transfer and mass-transport processes at the metal-solution interface. In EIS measurements of corrosion, the OCP is used as a reference potential for the measurement<sup>345</sup>. In this investigation, the working electrode comprised of the mild steel rod was submerged in the test media for 1hr throughout each investigation involving the concentration variation from 50ppm to 1000ppm. It is essential to create a consistent OCP priorly to conducting the PDP and EIS assessments. **Figure 4.76** shows the OCP versus time (sec.) trends in the exclusion and inclusion of various PCRE dosages. By evaluating **Figure 4.76**, it could be observed that after 1hr dipping, the potential pertaining to mild steel specimens dipped in a media containing all the desired concentrations of the PCRE became stabilized. The potential measurements for the inhibited and uninhibited specimens both significantly shifted toward the negative value, indicating that PCRE behaves as a cathodic inhibitor in the aggressive medium of

0.5 M HCl. The negative tilt of OCP for the pristine specimen could be accounted for the iron oxide production/dissolution over the metallic substrate.

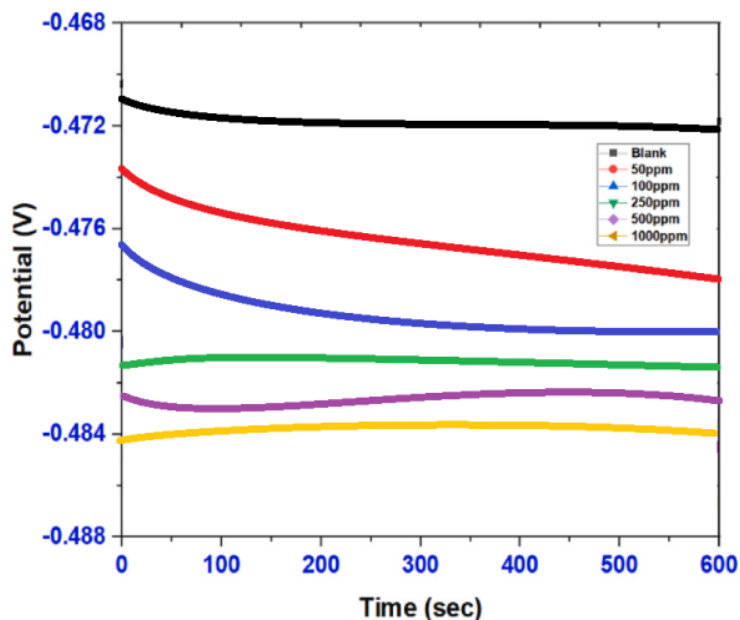


**Figure 4.76.** OCP vs. time graph for corrosion inhibition of mild steel after exposure to various PCRE concentrations (50-1000ppm) in 0.5M HCl.

#### 4.5.7.2. Potentiodynamic polarization (PDP)

PDP measurement is a commonly used approach in the study of corrosion and corrosion inhibition of metals. PDP is used to evaluate the  $C_R$  and the corrosion potential of metal in a corrosive solution. The corrosion potential is the potential at which the metal begins to corrode, and it is an important parameter for the evaluation of corrosion inhibitors. In PDP measurement, a metal is subjected to a series of increasing potentials in a corrosive solution, and the current density at each potential is measured<sup>346</sup>. The data is then plotted as a function of the potential, and the attained plot is called a Tafel plot. The Tafel plot provides information about the  $C_R$  and the corrosion potential of the metal. The Tafel plot is characterized by two linear regions, the anodic region and the cathodic region. The anodic region is characterized by a positive slope and corresponds to the oxidation of the metal. The cathodic region is characterized by a negative slope and denotes the reduction of the corroding species. The point at which the anodic and cathodic regions intersect is the corrosion potential. The Tafel plot can be used to evaluate the impact of corrosion inhibitors on the corrosion rate and corrosion potential. For example, an inhibitor that decreases the  $C_R$  will



result in a shift of the Tafel plot to more negative potentials, while an inhibitor that increases the  $C_R$  will result in a shift of the Tafel plot to more positive potentials. In this investigation, by using the PDP technique, the impact of PCRE over the cathodic hydrogen ions reduction and anodic dissolving of mild steel was determined. Additionally, the kinetics of cathodic and anodic reactions was evaluated using PDP analysis. The polarization plots are depicted in **Figure 4.77**. The corrosion potential ( $E_{\text{corr}}$ ), corrosion current densities ( $i_{\text{corr}}$ ), anodic ( $\beta_a$ ) and cathodic ( $\beta_c$ ) Tafel slope values were attained through the analysis of associated polarization parameters, as reported in **Table 4.39**. The IE% of PCRE was attained by equation (9).

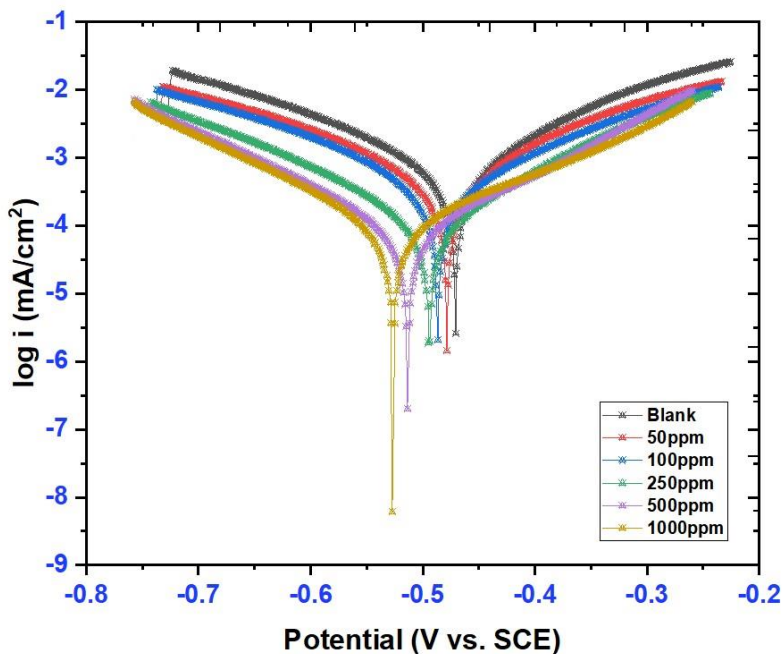


**Figure 4.77.** Tafel graph for the corrosion inhibition of mild steel in blank media subjected to 50-1000ppm amounts of PCRE at 298 K.

**Table 4.39**

Tafel variables for the corrosion mitigation of mild steel in blank solution subjected to 50-1000ppm amounts of PCRE at 298 K.

<b>Conc. (ppm)</b>	<b>-E<sub>corr</sub>(mV vs. SCE)</b>	<b>i<sub>corr</sub> (μA)</b>	<b>j<sub>corr</sub> (μA/cm<sup>2</sup>)</b>	<b>β<sub>a</sub> (mV/dec)</b>	<b>-β<sub>c</sub> (mV/dec)</b>	<b>C<sub>R</sub> (mm/yr)</b>	<b>IE%</b>
<b>Blank</b>	477.78	522.28	522.28	114.96	131.32	3.745	-
<b>50</b>	483.55	250.48	250.48	127.19	125.49	2.911	52.041
<b>100</b>	491.89	177.255	177.255	101.66	107.14	0.898	66.061
<b>250</b>	494.43	125.275	125.275	106.6	118.65	0.758	76.013
<b>500</b>	515.24	96.814	96.814	124.83	108.54	0.765	81.463
<b>1000</b>	527.93	46.692	46.692	127.48	104.49	0.775	91.059

Through the investigation of **Figure 4.77** and **Table 4.39**, it could be noted that the value of  $i_{\text{corr}}$  and  $C_R$  declined dramatically from 522.28 to 46.692 and 3.7449 to 0.7449 with increasing PCRE concentrations (50-1000 ppm). The preventative impact of the PCRE on mild steel was continuously enhanced as the inhibitor amount was elevated from 50 to 1000 ppm. These results demonstrated that PCRE delayed the mechanism of hydrogen generation as well as the dissolution of metal. Furthermore, the cathode shift was significantly prominent as compared to the anode shift, as shown by the polarization slope affirming the mixed-type nature of the PCRE inhibitor action, as the displacement in the  $E_{\text{corr}}$  is <85mV. **Table 4.39** further depicts that when the inhibitor was added, the  $\beta_c$  and  $\beta_a$  values often altered, illustrating that the utilization of the PCRE inhibitor does not alter the corrosion process nature. Furthermore, the anodic Tafel slope is generally higher than the cathodic Tafel slope, indicating that the anodic reaction may be more rate-limiting in the corrosion process. Additionally, the values for both the  $\beta_c$  and  $\beta_a$  Tafel slopes seem to decrease as the concentration of the PCRE increased, which suggests that the existence of the PCRE reduced the rate at which the current density changes with potential, resulting in lower corrosion rates. This may be own to the inhibitor molecule's adsorption upon the mild steel surface, obscuring it and

restricting the extent of active spots for the interaction despite retaining the charge transmission pathway of hydrogen evolution.

#### 4.5.7.3. Electrochemical impedance spectroscopy (EIS)

EIS measurement is a frequently utilized approach in the study of corrosion and corrosion inhibition of metals<sup>95</sup>. Nyquist plots attained from this study are used to obtain information about the impedance and conductivity of a metal in a corrosive solution, and they provide valuable information about the  $C_R$  and the resistance of the metal to corrosion. In EIS measurements of corrosion, a metal is subjected to an alternating current in a corrosive solution, and the resulting potential and current responses are measured. The data is then plotted as a Nyquist plot, with the imaginary component of the impedance on the y-axis and the real component of the impedance on the x-axis. The Nyquist plot is characterized by a semi-circle in the low-frequency region and a straight line in the high-frequency region. The semi-circle represents the impedance of the metal and its corroded surface, while the linear line represents the impedance of the metal. The shape and position of the semi-circle provide crucial insights into the  $C_R$  and the resistance of the metal to corrosion, while the shape and position of the straight line provide information about the resistance of the metal. In this investigation, in order to attain relevant information regarding the corrosion mitigation process, the EIS evaluation of mild steel dipped in several amounts of PCRE in 0.5 M HCl was conducted to corroborate the findings of the PDP and WL examinations. The critical outcomes are summarized in **Table 4.40**. The Nyquist plot is depicted in **Figure 4.78**. A substantial capacitive curve could be observed at a higher frequency on the Nyquist graph, whereas an inductive curve is visible at a lower frequency. The adsorption of  $Hads^+$ ,  $Cl^-$ , and PCRE molecules over the surface of mild steel expedited the relaxation phase that formed the lower-frequency inductive loop. In contrast, the surface distortion and charge transfer mechanism generated the high-frequency capacitive curve. The re-disintegration of the passivated substrate at a lesser frequency may be a probability. The pattern of all slopes in the Nyquist graph remained unchanged whether an inhibitor was used or not, showing that the metallic corrosion mechanism was unaffected. Furthermore, their geometries weren't ideal due to frequency dispersal, roughness, and non-uniformity of the working electrode substrate. The radii of the curves were demonstrated to increase as PCRE levels increased from 50 to 1000 ppm, indicating that PCRE dispersion over

the electrode substrate improved and a protective covering formed, thereby preventing corrosion on the electrode surface.

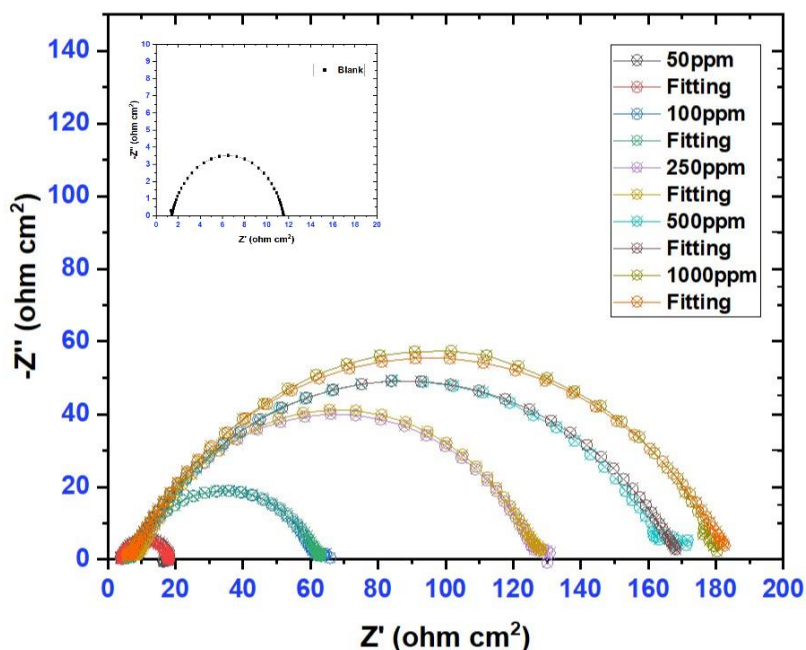


**Figure 4.78.** Nyquist graph for mild steel corrosion inhibition in 0.5M HCl with 50–1000 ppm PCRE at ambient temperature.

Similarly, Bode plot measurement is a commonly used methodology in the study of corrosion and corrosion inhibition of metals using electrochemical impedance spectroscopy (EIS). Bode plots are used to obtain information about the impedance and phase angle of a metal in a corrosive solution, and they provide valuable information about the  $C_R$  and the resistance of the metal to corrosion<sup>97,239</sup>. The Bode plot provides information about the impedance and phase angle of the metal in a corrosive solution as a function of frequency. The impedance magnitude is proportional to the corrosion rate, while the phase angle is proportional to the resistance of the metal to corrosion. The Bode graphs for the metal in the addition and lack of diverse quantities of PCRE (50-1000ppm) in the acidic solution at 298K are depicted in **Figure 4.79**. The impedance modulus improved with the increased quantity of PCRE across the frequency range investigated in this research. The frequency spectra also expanded at the highest phase angles. As per the previous reports, the optimum capacitance at an intermediary frequency can be accepted, if the curve of the  $\log |Z|$  versus  $\log f$  with a maximum phase angle of  $90^\circ$  tends to be  $1$ <sup>229,240,241</sup>. This demonstrated

that in the 0.5 M HCl, PCRE has a significant inhibition efficacy toward the corrosion of mild steel.

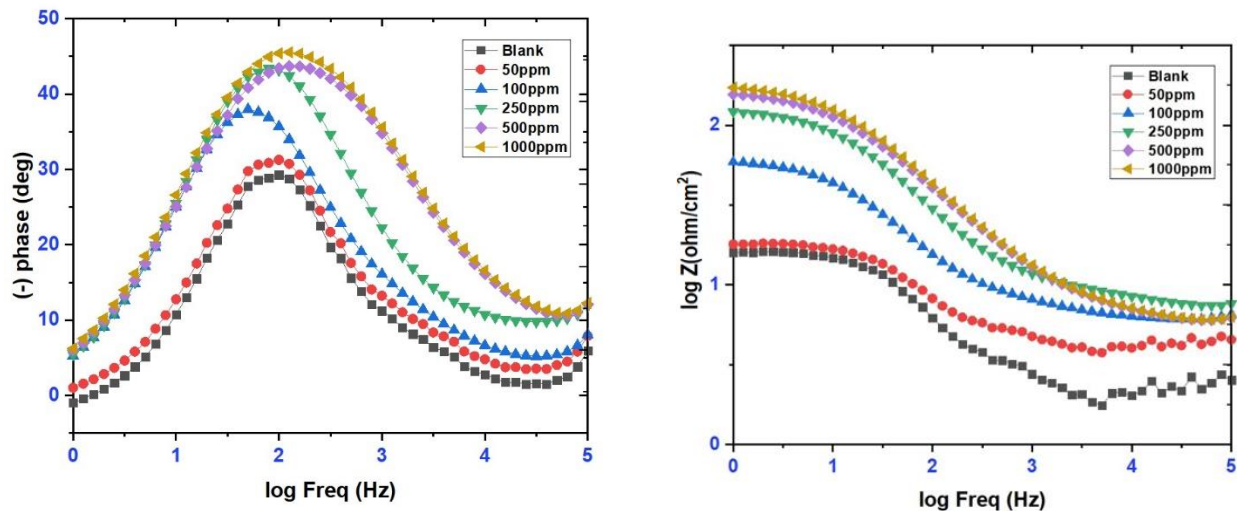


**Figure 4.79.** Bodes graph for the corrosion mitigation of mild steel in blank media subjected to 50-1000ppm conc. of PCRE at 298 K.

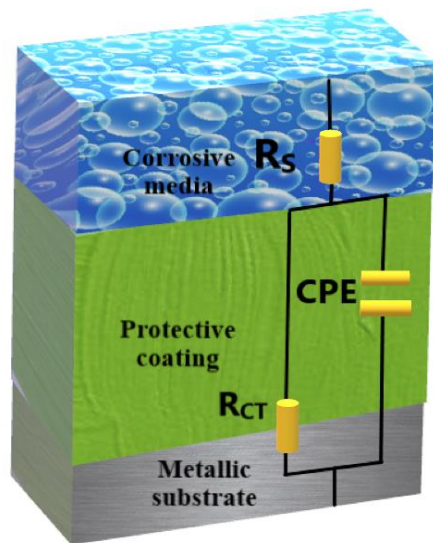


**Figure 4.80.** An equivalent circuit model utilized for the data fitting.

**Table 4.40** reports the EIS metrics, wherein  $R_s$  represents solution resistance,  $R_{ct}$  denotes charge transfer resistance,  $n$  represents phase shift, CPE denotes constant phase element and the discrepancy scale of the eqv. circuit fitting denoted by  $\chi^2$ . The datasets of  $\chi^2$  within  $10^{-3}$  and  $10^{-5}$

suggest that the depicted equivalent circuit layout is reliable and stable, confirming to be consistent with the ideal fitting. It could be observed that at increasing concentrations of the inhibitor, there is a decrease in CPE.Yo and n values, indicating a decrease in the double-layer capacitance and a change in the surface characteristics of the metal. There is also an increase in  $R_s$ ,  $R_p$ , and  $R_{ct\ in}$ , indicating a decrease in the ion conductivity and an elevation in the charge transit resistance at the metal-inhibitor interface. At 1000 ppm, the inhibitor has the lowest CPE.Yo and n values, the highest  $R_p$  and  $R_{ct\ in}$  values, and the lowest Cdl value, indicating the highest inhibition efficiency. **Table 4.40** illustrates that as the quantity of PCRE was expanded, the  $R_{ct}$  and IE% increased, reaching an optimum IE% of 93.61% at 1000ppm, revealing to be remarkably consistent with the analyses of the PDP and WL experimentations. When several amounts of PCRE were introduced, the  $R_s$  value did not alter drastically. Moreover, the  $n$  values (0.923–0.624) did not impact considerably, demonstrating that charge transfer regulated the mild steel dissolution in a corrosive medium. Overall, the results suggest that the inhibitor has a valuable impact on the impedance parameters of the metal-inhibitor system, with higher concentrations providing greater protection against corrosion.

**Table 4.40**

IE% values for the corrosion mitigation of mild steel in 0.5M HCl subjected to 50-1000ppm conc. of PCRE at 298 K.

Conc. (ppm)	CPE.Yo ( $\mu F$ )	$n$	$R_s$ ( $\Omega$ )	$R_p$ ( $\Omega$ )	$R_{ct\ in}$ ( $\Omega cm^2$ )	$R_{ct\ bl}$ ( $\Omega cm^2$ )	Cdl ( $\mu F/cm^2$ )	IE (%)	$\theta$	$\chi^2$
<b>Blank</b>	312.87	0.923	2.584	28.648	-	11.86	732.896	-	-	0.197
<b>50</b>	294.54	0.865	4.251	49.548	18.57	11.86	75.055	46.134	0.361	0.175
<b>100</b>	198.39	0.762	6.034	55.643	64.98	11.86	17.743	81.748	0.817	0.142
<b>250</b>	86.854	0.752	7.395	119.53	129.84	11.86	11.409	90.865	0.909	0.285
<b>500</b>	65.222	0.696	5.363	161.89	170.95	11.86	8.051	93.062	0.931	0.109
<b>1000</b>	61.685	0.624	5.621	174.01	185.74	11.86	2.896	93.615	0.936	0.131

#### 4.5.8. Surface morphology analysis

##### 4.5.8.1. SEM

In this research, SEM was employed to evaluate the topographical state of metallic samples after the 6hrs of dipping in a solution of 0.5M HCl at 298K in the exclusion and inclusion of PCRE, and the outcomes have been shown in **Figure 4.81**. The flat view of the SEM micrograph of the unprocessed plain steel sample has been depicted in **Figure 4.81 (a)**. While **Figure 4.81 (b)** represents the flat view of the sample immersed in 0.5 M HCl which is characterized by an extremely coarse surface having several pits and an incredibly high degree of roughness on it resembling corrosion products over the metallic surface. It means that there is obvious degradation and substantial degradation on the blank steel substrate. With the introduction of PCRE (1000 ppm concentration), the surface's roughness was substantially reduced compared to the uninhibited environment by creating a defensive film on the mild steel specimen's surfaces, preventing corrosive ions from attacking the surface and leaving fewer pits and corrosion products shown in the corresponding **Figure 4.81 (c)** which consequently leads to corrosion reduction which is the goal of this research. These findings imply that the PCRE molecules were adsorbed onto the mild steel surface, creating a defensive covering composed of CI mono-layers leading to a smoother outer layer.

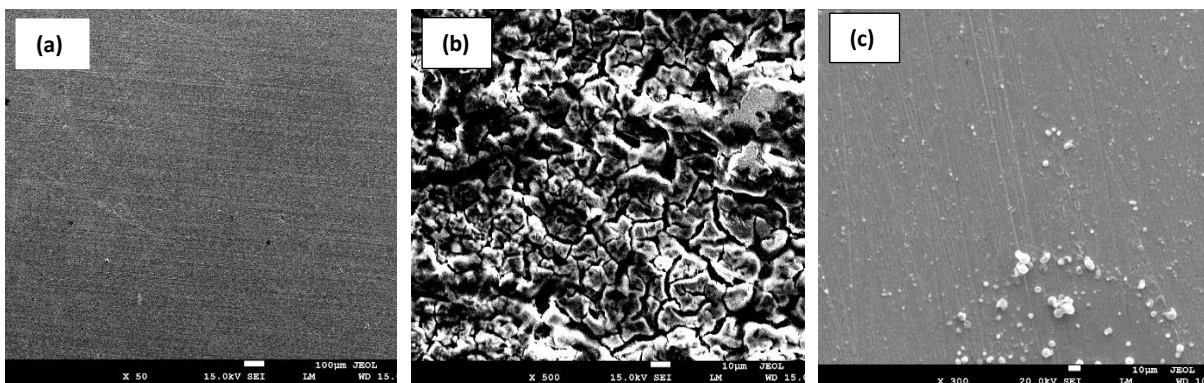


**Figure 4.81.** SEM visuals of (a) plain metal, (b) metal submerged in 0.5 M HCl (c) metal submerged in 0.5 M HCl + PCRE (1000ppm) at 298K for 6hrs.

##### 4.5.8.2. Contact angle (CA) assessment

This assessment provides additional information about adhesion, wetting, and absorption anomalies on mild steel surfaces. The researchers used CA analysis to evaluate the

hydrophobicity/hydrophilicity of unprocessed and processed mild steel substrates. **Figure 4.82 (a, b)** shows images obtained from the CA examinations of the metal substrate with and without the inclusion of 1000ppm of PCRE<sup>302,347</sup>. The figure indicates that the metallic sample processed with the inhibitor had a higher CA value (79.54°) compared to the sample processed solely with 0.5M HCl (60.11°). This suggests that the surface of mild steel had lower hydrophobicity before being treated with PCRE (**Figure 4.82 (a)**), but the hydrophobicity increased after treatment (**Figure 4.82 (b)**). It has been observed that the aggressive ions can adhere to mild steel surfaces in an acidic environment due to their minimal hydrophobicity, which promotes corrosion. However, the adhesion of inhibitor molecules may alter the surface tension and result in the creation of a defensive covering over the metal substrate, ultimately reducing corrosion.

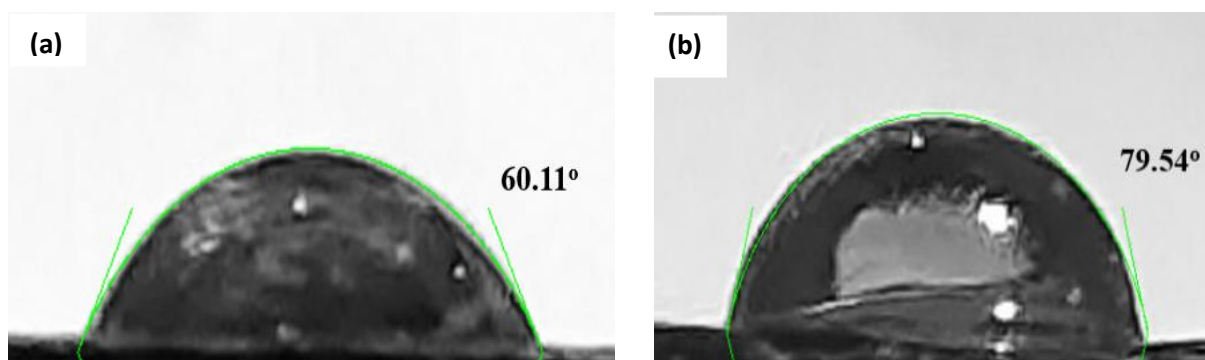


**Figure 4.82.** CA assessment performed on the metallic sample in **(a)** 0.5M HCl media and **(b)** 0.5M HCl+1000ppm of PCRE.

#### 4.5.9. Computational studies

##### 4.5.9.1. DFT

Quantum chemical methods, and more specifically density functional theory (DFT), are increasingly used to describe molecular properties, understand the mechanism of action and predict the effectiveness of corrosion inhibitors. DFT is a widely used theoretical approach in the field of materials science, including corrosion inhibition. DFT calculations can provide valuable insights into the electronic structure and reactivity of materials, which can be used to predict their efficacy as corrosion inhibitors<sup>24,332</sup>. In the context of corrosion inhibition, DFT can be utilized to explore the interaction between a potential inhibitor and a metallic surface. By calculating the electronic properties of the inhibitor and the metallic surface, DFT can predict the strength of the adsorption



of the inhibitor onto the surface, as well as the IE%. In this analysis, the geometric structures of the studied molecules were obtained by global optimizations characterized by a calculation of the vibration frequencies using the DFT method (utilizing Dmol<sup>3</sup>, which comprised the B3LYP/ DND / COSMO (water) model). We have used the Materials Studio 8.0 software to perform MC and MD simulations. For the simulations of the adsorption modes of the molecules investigated on the Fe surface in this study, we choose the Fe(1 1 0) surface. The simulation box employed to carry out the MD simulations had the dimensions (24.823 × 24.823 × 18.241 Å). The iron slice and the number of water molecules comprising the studied compound are associated with the simulation box. Before starting the simulation, the surface of Fe(1 1 0) and the molecular geometry of the compounds studied were simulated by minimizing the energies. Using the COMPASS III (Edition 1.0) force field, MD simulations were carried out at 298 K using the NVT setup, a phase stride of 1 fs, and a simulation duration of 800 ps. This model included a Fe layer, 10 hydronium ions, 10 chloride ions, 800 H<sub>2</sub>O molecules and 1 inhibitor molecule and a 35-vacuum layer included in the simulation box.

The charge density profiles indicate how electrons are dispersed on a surface and elaborate on the solubility of the inhibitor molecules. Employing the COSMO model's computations enables the production of a charge density curve accompanied using a  $\sigma$ -profile. Partial atomic charges represent the electrostatic potential. As shown in **Figure 4.83**, the major phytoconstituents of PCRE i.e., Piceid, Resveratrol, Emodin, Emodin-1-O-glucoside and 1-O-Methylemodin are proficient in functioning the dual role of H-bond donors and acceptors. The formation of H-bond acceptor/donor interactions between water molecules during inhibitor dissolution determines the inhibitors' solubility, which is governed by their ability to create H-bonds. The geometry optimizations were performed on all molecules. The stable structures of the molecules are presented in **Figure 4.84**.

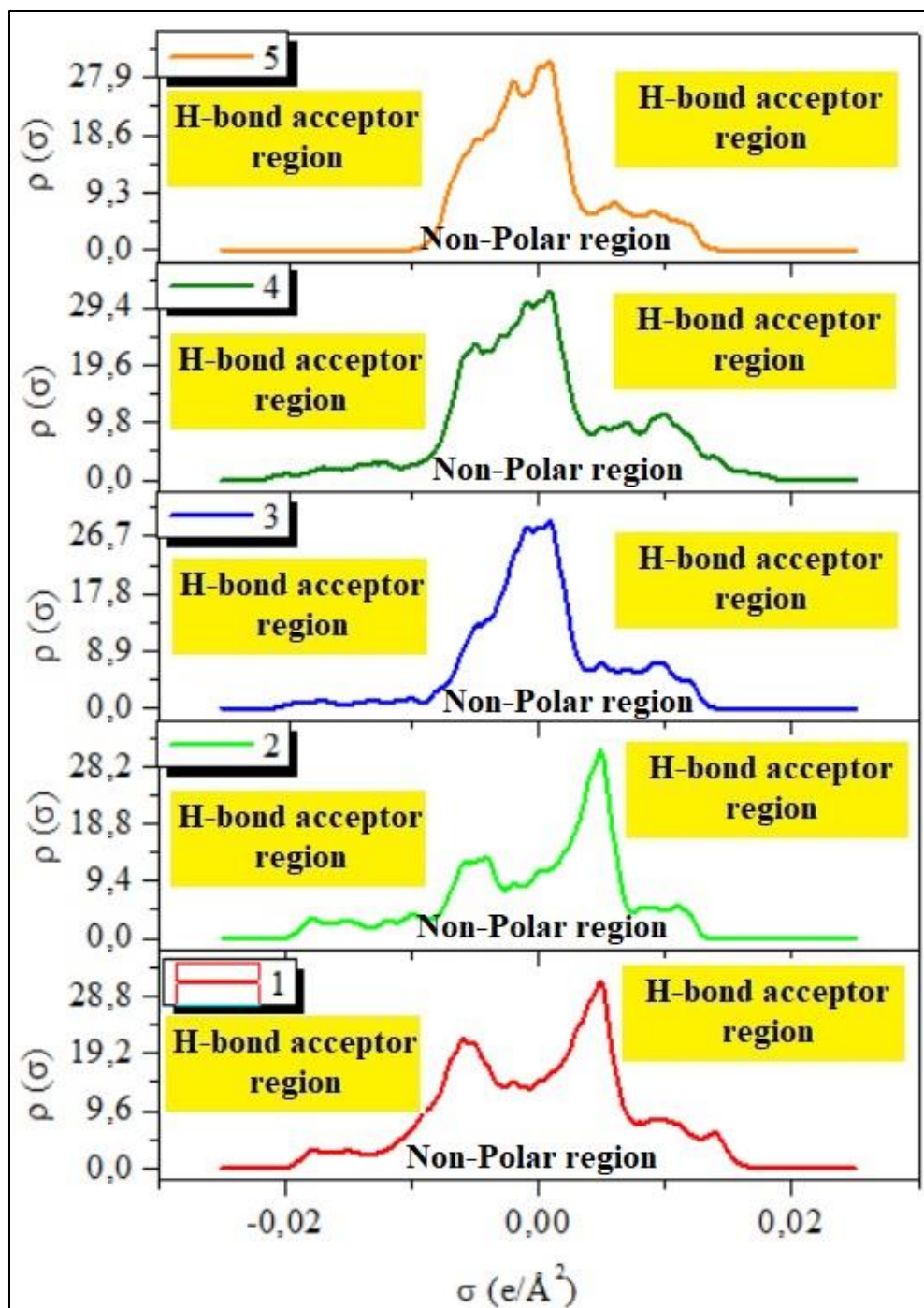


**Figure 4.83.** Charge density profiles ( $\sigma$ ) and optimized structure of the (1) Piceid, (2) Resveratrol, (3) Emodin, (4) Emodin-1-O-glucoside and (5) 1-O-Methylemodin molecules.

**Figure 4.84** illustrates the optimized geometric configurations of the investigated molecules, procured by global optimization of the vibration frequencies. The electronic charge dispersion on each atom in a molecule or other molecule is quantified by the Mulliken Atomic Charges (MAC).

They offer a reliable and compelling marker of the atoms that are engaged in the mechanism of metal adsorption, in which metal ions bond to the surface of a substance. In the case of inhibitors, these are molecules that are added to the surface of a metal to prevent or reduce the rate of corrosion. The MAC values are calculated using quantum mechanical methods that take into account the electron density and the molecular configuration of the atoms. In the context of metal adsorption, the MAC values of the metal atoms over the surface and the inhibitor molecules can be compared to identify which atoms are most likely to interact.

The Mulliken charges of the atoms, determined for molecule 1 (Piceid) (**Figure 4.84**), indicate that the most negative atom is O in red (-0.779) the latter constitutes the active adsorbent center. The Mulliken charges of the atoms, deliberated for molecule 3 (Resveratrol) (**Figure 4.84**), indicate that the most negative atom is oxygen in red O (-0.757), for molecule 4 (Emodin) the most negative atom is oxygen in red O (-0.774), for molecule 4 (Emodin-1-O-glucoside) the most negative atom is oxygen in red O (-0.750) and for molecule 5 (1-O-Methylemodin) the most negative atom is oxygen in red O (-0.742). This atom constitutes the adsorption center of these compounds on the metallic substrate.

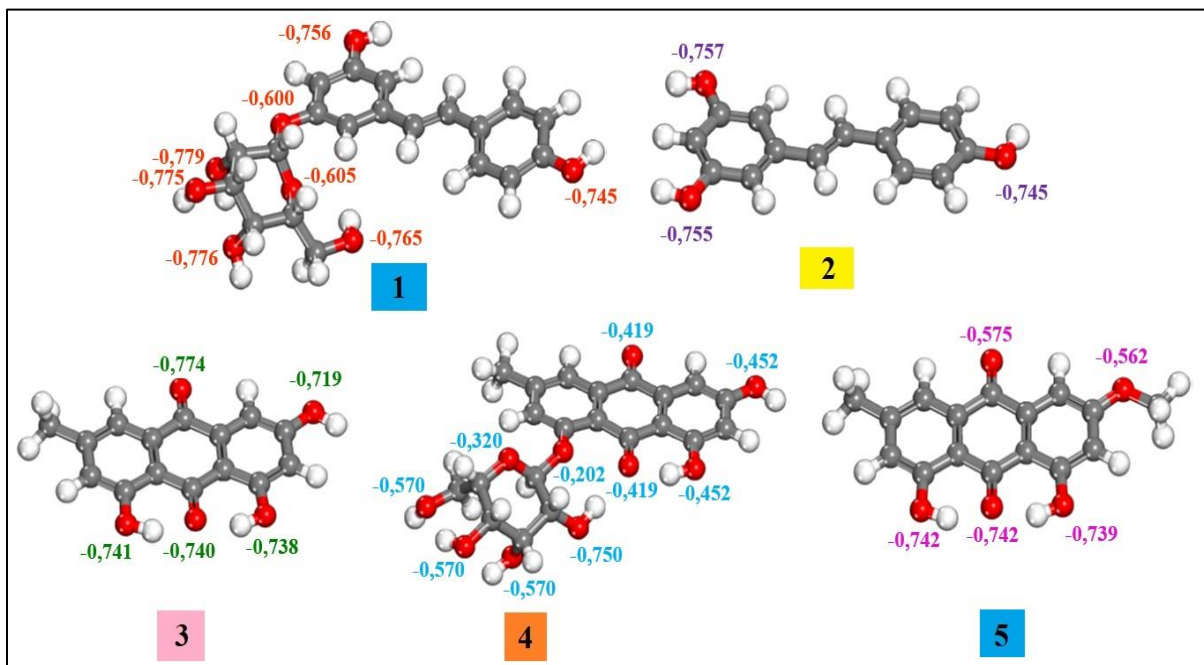


**Figure 4.84.** Distribution of the Mulliken charges values O atoms of (1) Piceid, (2) Resveratrol, (3) Emodin, (4) Emodin-1-O-glucoside and (5) 1-O-Methylemodin molecules.

Furthermore, HOMO is the capability of an orbital to donate an electron to the vacant metal d orbital and form a coordination bond. HOMO indicates the electron-donating (nucleophilic) capability of the molecule. Higher levels of  $E_{\text{HOMO}}$  thereby influence the electronic transmission through the adsorbed layer, facilitating the adsorption of the inhibitor molecule on the metal substrate and subsequently the IE%. An inhibitor orbital's capacity to accept an electron from the metal surface is known as LUMO. With reduced  $E_{\text{LUMO}}$  values, one can anticipate a higher adsorption capability (the chance of absorbing electrons by the molecule is significant) and greater corrosion inhibition since LUMO shows the capability of molecules to receive electrons (electrophilic).

Several quantum chemical variables were computed and detailed in **Table 4.41**. The differences between the inhibition efficiency of the Piceid, Resveratrol, Emodin, Emodin-1-O-glucoside and 1-O-Methylemodin cannot be explained in terms of their geometry, it could be partly explained in terms of the energies of the frontier orbitals LUMO and HOMO and other quantum parameters of the inhibitors computed and presented in **Table 4.41**. It is noted that the  $E_{\text{HOMO}}$  values of the inhibitor are different, and the electron transfer capacity of compound 2 (Resveratrol) is the best by comparing it with the four other remaining inhibitors. The band gap ( $\Delta E = E_{\text{LUMO}} - E_{\text{HOMO}}$ ) (the gap), presenting the difference between the HOMO and LUMO energy levels of the molecule, is also a crucial parameter that can be taken into consideration in the process of corrosion by inhibition in using organic compounds. Consequently, the lower the energy difference ( $\Delta E$ ) between the frontier orbitals of the donor and the acceptor, the more easily the electrons of the inhibitors pass over the surface of the metal and the greater the IE% will be, for example. against larger values will provide low chemical reactivity. It is noted that the compound 5 (1-O-Methylemodin) has the smallest energy difference (2.267 eV), therefore it is the least stable and the most chemically reactive compared to the others (1(Piceid), 2 (Resveratrol), 3 (Emodin) and 4 (Emodin-1-O-glucoside)).

The values of  $\Delta E$  can be classified according to the following decreasing order: compound 5 (1-O-Methylemodin) (2.267 eV) < compound 3 (Emodin) (2.288 eV) < compound 4 (Emodin-1-O-glucoside) (2.343 eV) < compound 1 (Piceid) (2.931 eV) < compound 2 (Resveratrol) (2.952 eV), which means that the molecule of 5 is easy to adsorb to the metal surface than others.

A value of number of electrons transferred ( $\Delta N$ )  $< 3.6$  indicates that the molecule tends to donate electrons to the metal substrate. In general, inhibitory efficacy increases with increasing electron fraction. The outcomes presented in **Table 4.41** that all the calculated values are positive and less than 3.6. These results clearly indicate that all our inhibitor molecules have a good capacity to transfer their electrons to the free metal orbitals.

In order to evaluate the active zones of the inhibitor molecule, the optimal molecular structures, and orbital density distributions (HOMO and LUMO orbitals) of inhibitors and ESPs were determined and shown in **Figure 4.85**. The configurations obtained confirm that all the molecules are rich in electrons and are able of donating electrons to the metal or oxide surface, which greatly improves their ability to inhibit the corrosion of metals, forming a very stable protective barrier. It is observed that the HOMO and LUMO distribution on all molecules 2 (Resveratrol), 3 (Emodin) and 5 (1-O-Methylemodin) is located on the entire molecule except for the two molecules 1 (Piceid) and 4 (Emodin-1-O-glucoside).

Molecular electrostatic potential (ESP) maps indicate the active electrophilic and nucleophilic zones are depicted by different colors. The potential values can be classified according to the following increasing sequence: red (negative electrostatic potential) \ yellow \ orange \ green (region of zero potential) \ blue (positive electrostatic potential). In all cases, the most electron-rich regions are generally presented around heteroatoms and conjugated double bonds.

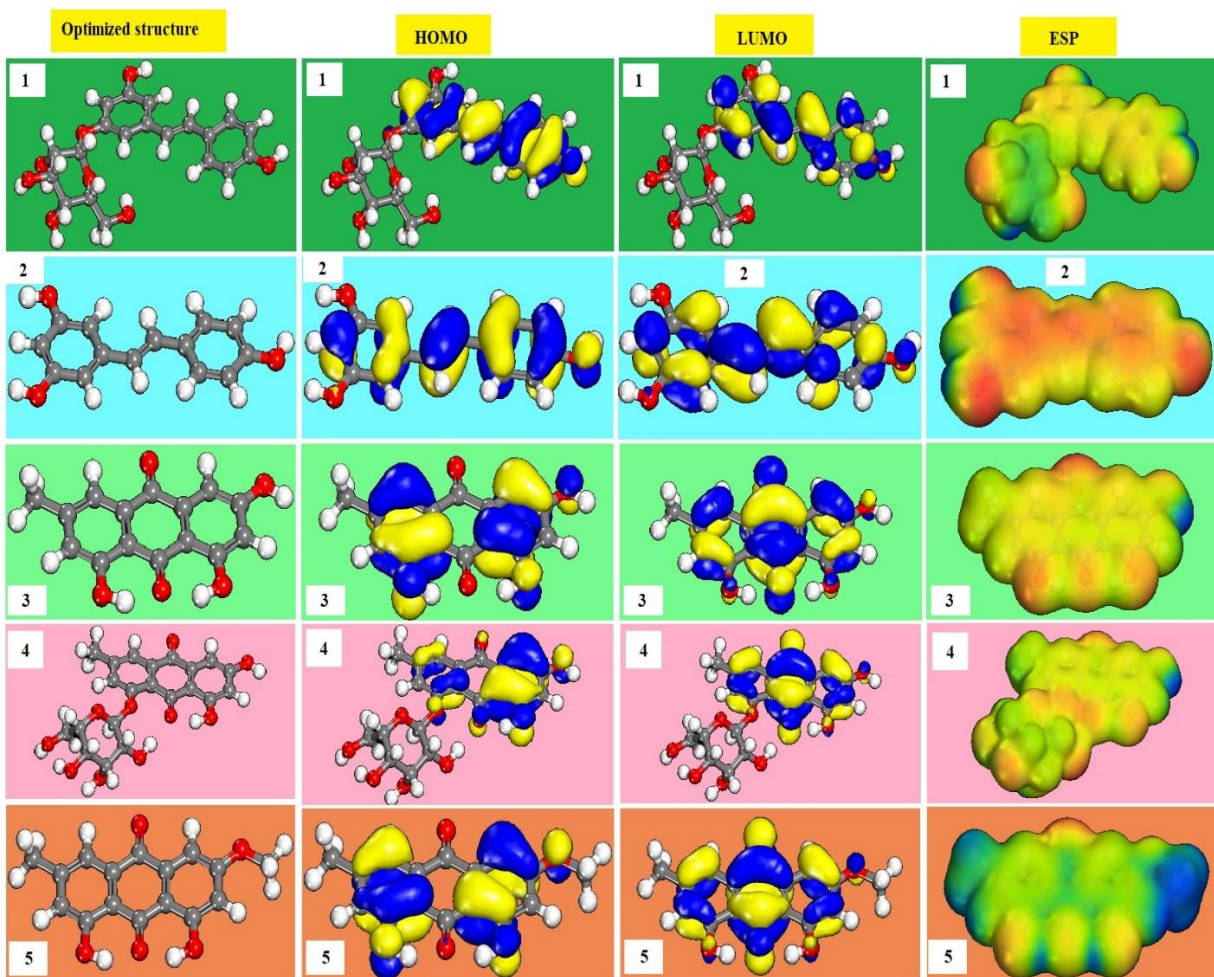


**Figure 4.85.** Optimized structure, LUMO, HOMO and ESP pictures of (1) Piceid, (2) Resveratrol, (3) Emodin, (4) Emodin-1-O-glucoside and (5) 1-O-Methylemodin molecules.

**Table 4.41**

Calculated theoretical parameters (1) Piceid, (2) Resveratrol, (3) Emodin, (4) Emodin-1-O-glucoside and (5) 1-O-Methylemodin molecules.

Theoretical parameters	Piceid	Resveratrol	Emodin	Emodin-1-O-glucoside	1-O-Methylemodin
$E_{\text{HOMO}}$ (eV)	-4.868	-4.843	-5.881	-5.927	-5.835
$E_{\text{LUMO}}$ (eV)	-1.937	-1.891	-3.593	-3.584	-3.568
$\Delta E$ (eV)	2.931	2.952	2.288	2.343	2.267
$I$ (eV)	4.868	4.843	5.881	5.927	5.835
$A$ (eV)	1.937	1.891	3.593	3.584	3.568
$\chi$ (eV)	3.402	3.367	4.737	4.755	4.701
$\eta$ (eV)	1.465	1.476	1.144	1.171	1.133
$\sigma$ (eV <sup>-1</sup> )	0.682	0.677	0.874	0.854	0.882
$\Delta N$	1.228	1.230	0.989	0.958	1.014
$\Delta E_{\text{back-donation}}$	-0.366	-0.369	-0.286	-0.292	-0.283

#### 4.5.9.2. MC and MD simulations

The last few years have seen a rapid increase in the use of MC and MD simulations to understand the interaction across the corrosion inhibitor and the metal surface. MC and MD simulations are powerful computational techniques used to explore the function of molecules and materials at the atomic level. These simulations are increasingly being used in the field of corrosion inhibition to comprehend the mechanisms of corrosion inhibition and design new corrosion inhibitors. MD simulations involve the integration of the equations of motion for a system of atoms or molecules to simulate the behavior of the system over time. This allows researchers to investigate the behavior of corrosion inhibitors at the molecular level, such as their interactions with metal surfaces and the formation of protective films. MD simulations can also be used to study the impact of different environmental factors, including temperature and pH, on the potency of corrosion inhibitors. MC simulations, on the other hand, use random sampling to simulate the behavior of a

system. In the context of corrosion inhibition, MC simulations can be used to explore the adsorption of corrosion inhibitors onto metal surfaces. This involves randomly placing inhibitor molecules over the substrate and calculating the free energy of adsorption. MC simulations can also be used to study the impact of various factors, including inhibitor concentration and temperature, on the adsorption behavior. The adsorption energy ( $E_{\text{ads}}$ ) may be deduced from Equation 18 to offer a quantifiable estimate of the incidence of this phenomenon. The adsorption equilibrium configurations of the studied inhibitory molecules (1) Piceid, (2) Resveratrol, (3) Emodin, (4) Emodin-1-O-glucoside and (5) 1-O-Methylemodin inhibitors on the Fe(1 1 0) substrate are presented in **Figure 4.86**.

In **Figure 4.86**, it has been observed that the inhibitor molecules have been adsorbed on the substrate of Fe (1 1 0) in a specific position. As the inhibitor molecules are almost exactly in line with the plane of the metallic surface, it is likely that they have a close affinity for the substrate. Chemisorption interactions involving the iron and oxygen atoms of the inhibitor molecules are the main interactions between the inhibitor molecules and the substrate. The distance between the iron atoms and the oxygen atoms of the inhibitors is less than 3.5 Å for the (1) Piceid, (2) Resveratrol, (3) Emodin, (4) Emodin-1-O-glucoside and (5) 1-O-Methylemodin inhibitors. This distance is important because it indicates that the inhibitor molecules are closely bonded to the Fe atoms through strong chemical bonds. In addition to chemisorption interactions, physical interactions also occur across the inhibitor molecules and the iron atoms. These physical interactions are induced by Van der Waals dispersion forces, which are weak attractive forces between molecules. These forces contribute to the attraction of the net molecule surface to the substrate.



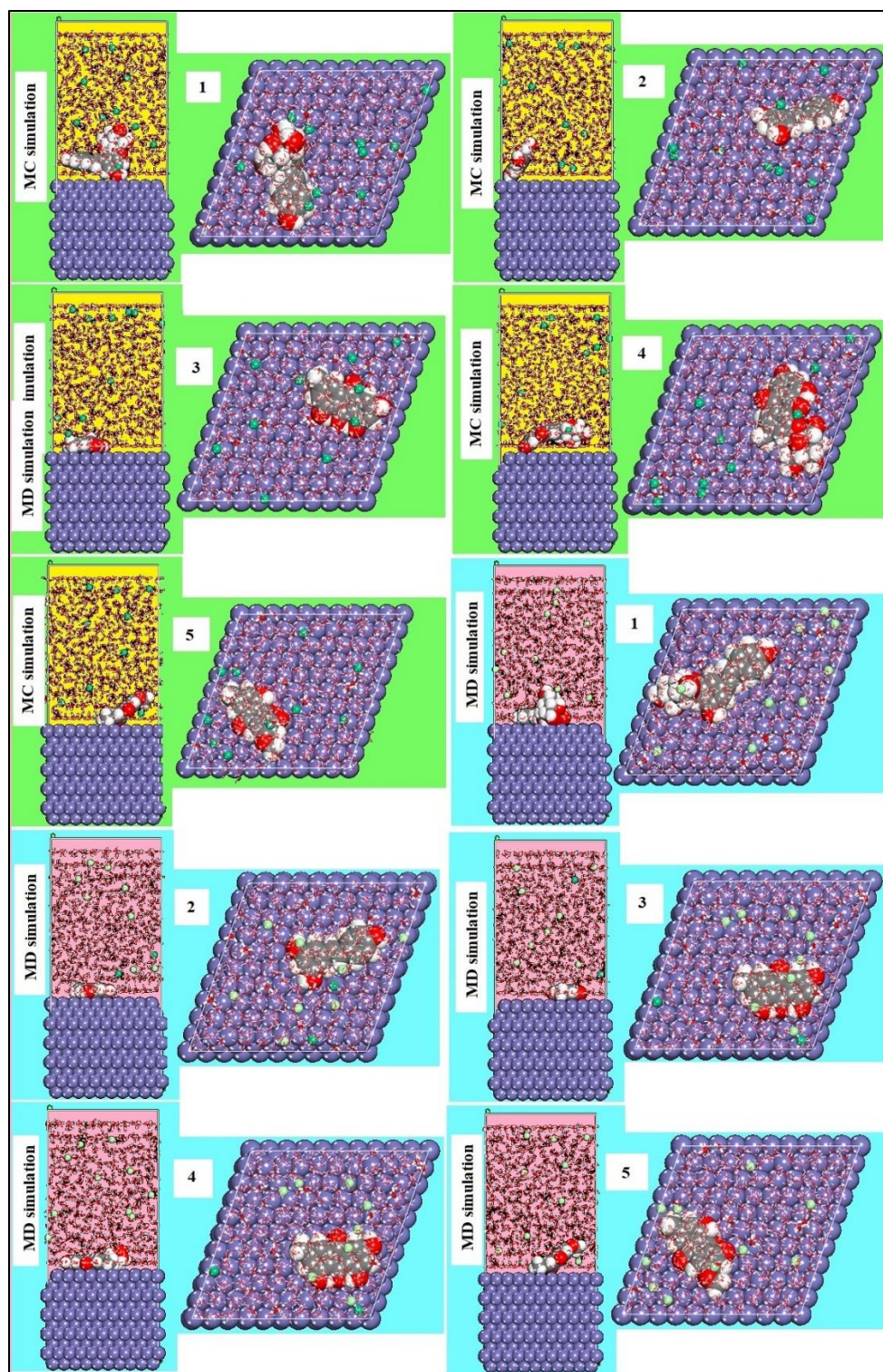


**Figure 4.86.** MC and MD simulations result in adsorption configurations and positions of the (1) Piceid, (2) Resveratrol, (3) Emodin, (4) Emodin-1-O-glucoside and (5) 1-O-Methylemodin molecules.

**Figure 4.87** indicated the distribution of the  $E_{\text{ads}}$  for the (1) Piceid, (2) Resveratrol, (3) Emodin, (4) Emodin-1-O-glucoside and (5) 1-O-Methylemodin inhibitors form onto the Fe(1 1 0) substrate by MC simulations. According to these results, the values of  $E_{\text{ads}}$  can be classified according to the following order: 3 (Emodin) (-170,75 kcal/mole) > 1 (Piceid)=5 (1-O-Methylemodin) (-125,65 kcal/mole) > 4 (Emodin-1-O-glucoside) (-119,15 kcal/mole) > 2 (Resveratrol) (-101,65 kcal/mole) (**Figure 4.87**). The elevated values of binding energies are contrasted to the stiffness of the interaction of molecules over the steel substrate. It is found that compound 3 (Emodin) is the most effective inhibitor due to its molecular structure. The lone pair electrons of the -OH groups, the C=O groups, the  $\pi$ -electrons of the aromatic rings, and the double bonds may donate electrons to the empty d-orbitals of the Fe atoms present in the compound 3 (Emodin) is mainly accountable for the adsorption of corrosion inhibitor.

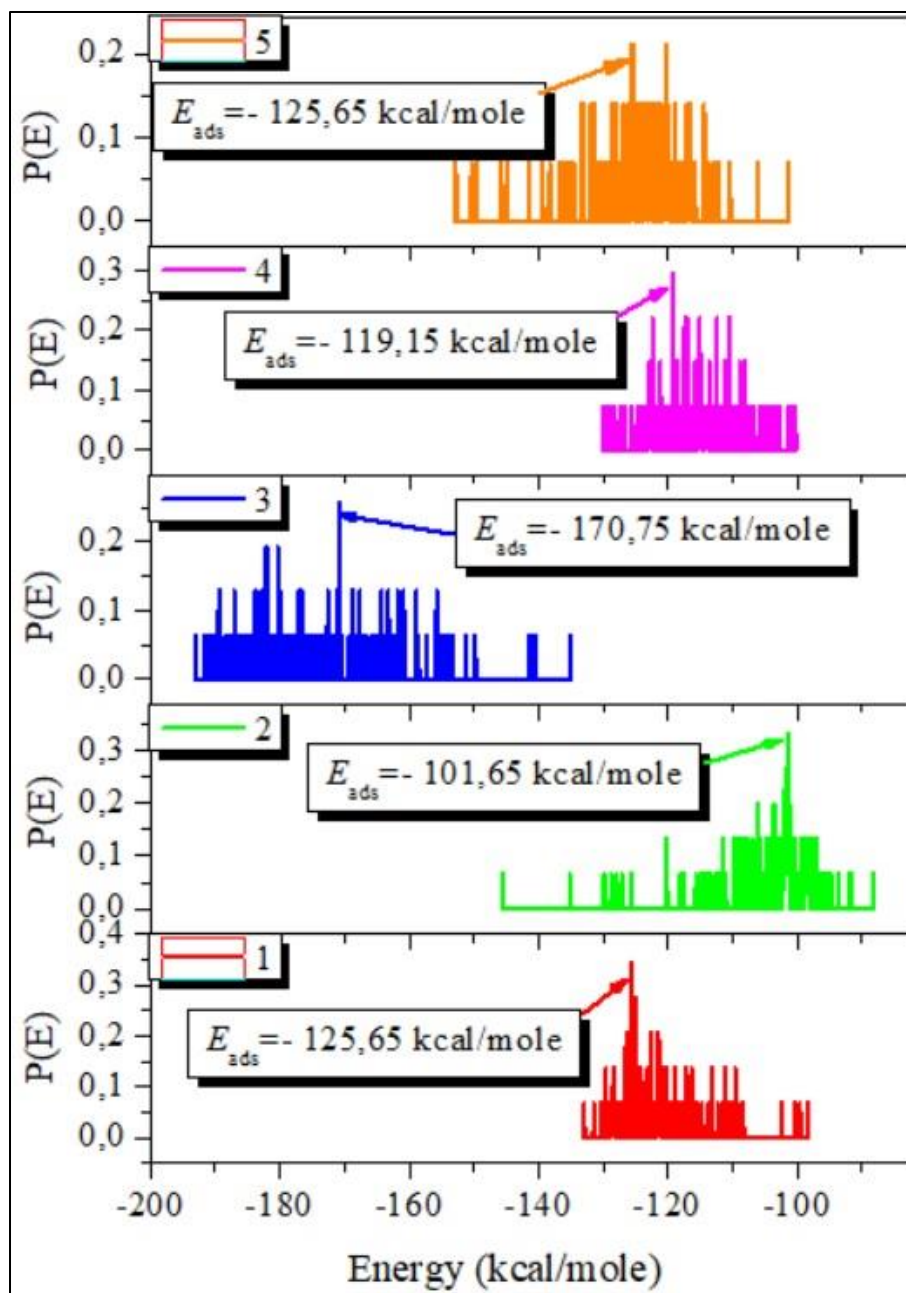


**Figure 4.87.** Distribution of the  $E_{ads}$  of the (1) Piceid, (2) Resveratrol, (3) Emodin, (4) Emodin-1-O-glucoside and (5) 1-O-Methylemodin inhibitors on the Fe(1 1 0) surface via MC simulation.

#### 4.5.9.3. RDF (Radial Distribution Function) analysis

RDF is a computational technique used to study the atomic structure of materials. In the context of the given statement, the RDF approach was applied to evaluate the bond length between Fe atoms and atoms of inhibitors (1) Piceid, (2) Resveratrol, (3) Emodin, (4) Emodin-1-O-glucoside

and (5) 1-O-Methylemodin. By estimating bond length values, various kinds of bonds formed between these atoms were evaluated. The RDF analysis produced a graph that showed peaks at certain distances from the Fe(1 1 0) substrate, which provided crucial insights into the type of adsorption activity taking place on the metallic surface. Chemisorption is a type of adsorption that involves the emergence of a chemical bond between the adsorbate (inhibitor molecule) and the substrate (Fe(1 1 0) substrate). When the peak in the RDF graph was indulged between 1 and 3.5 Å, it was considered a chemisorption pathway. On the other hand, physisorption is a type of adsorption that comprises weak Van der Waals forces between the adsorbate and substrate. The RDF spikes were predicted to be evident at distances larger than 3.5 Å for physisorption.

The results of the RDF analysis showed that the inhibitor molecules were located very close to the metallic surface, as shown in **Figure 4.88**. As a result, the derived inhibitor molecules had a relatively significant interaction with the substrate, which endorses their inhibitory functionality. This strong interaction between the inhibitor and metallic surface is likely to be owing to chemisorption, which involves the emergence of a covalent bond between the inhibitor and metallic surface, leading to a stronger bond compared to physisorption. Overall, the RDF analysis provided valuable insights into the atomic structure of the inhibitory molecules and their interaction with the Fe(1 1 0) substrate, which is essential for understanding their inhibitory performance.

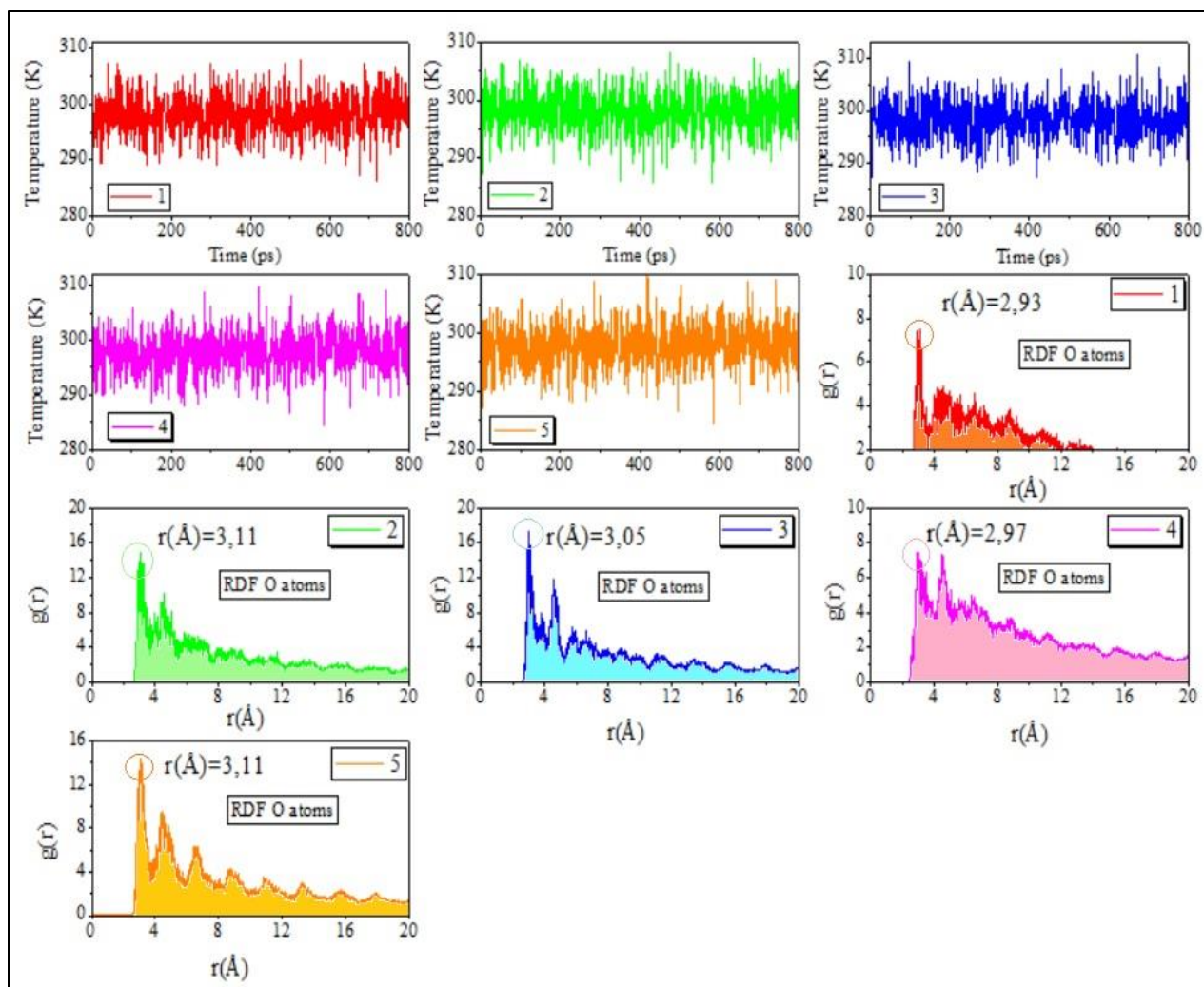


**Figure 4.88.** Temperature fluctuation ( $T=298$  K) and RDF of the Si and O atoms for major constituents of the extract (1) Piceid, (2) Resveratrol, (3) Emodin, (4) Emodin-1-O-glucoside and (5) 1-O-Methylemodin, obtained via MD.

#### 4.5.10. Biodegradability of PCRE

The biodegradation of PCRE refers to the breakdown of the chemical structure of PCRE by microorganisms in the environment. Biodegradation is an important factor in determining the environmental fate of chemicals and their potential impact on the ecosystem. **Figure 4.89** shows the rate of biodegradation of PCRE after 28 days. The rate of biodegradation is represented by the percentage of PCRE that has degraded over time. At 28 days, the rate of CBE degradation accelerated and reached 88.93% computed using equation (19). This means that after 28 days, almost 90% of the PCRE had been degraded by microorganisms.

According to the North-East Atlantic Accords for Ecological Prevention, anything that degrades more than 60% in 28 days is considered rapidly biodegradable<sup>224</sup>. Since PCRE degraded more than 60% within 28 days, it can be classified as a rapidly biodegradable corrosion inhibitor. This information is important because it indicates that PCRE is likely to have a lower impact on the environment compared to non-biodegradable corrosion inhibitors. Rapid biodegradation means that PCRE is broken down into harmless substances more quickly, reducing the potential for environmental harm.

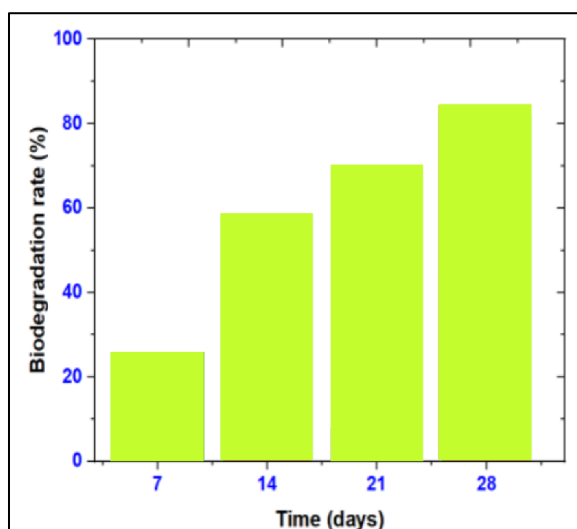


**Figure 4.89.** Biodegradability rate of PCRE.

#### 4.6. *Asphodelus Tenuifolius*

*Asphodelus Tenuifolius* (AT) commonly known as fine-leaved asphodel or narrow-leaved asphodel, is a perennial herbaceous plant that belongs to the family Asphodelaceae. It is native to the Mediterranean region and is commonly found in countries such as Greece, Italy, Spain, India and Turkey. The plant has a tall, erect stem that grows up to 1 meter in height, with narrow leaves that are 5-15 mm wide and 15-40 cm long. The leaves are arranged in a rosette at the base of the stem and are linear in shape. The plant produces clusters of white, trumpet-shaped flowers that bloom in the spring and summer months. AT is often used in traditional medicine to treat various ailments, including stomach disorders, fever, and inflammation. The plant contains several bioactive compounds such as phenolics, flavonoids, and alkaloids that have been shown to have antioxidant and anti-inflammatory properties. According to the previous investigation<sup>228</sup>, ATAE contains several key phytochemical components such as Trans-2-decen-1-ol, trimethylsilyl ether, 1,4-anhydro-d-glactitol and 5-hydroxymethylfurfural, as illustrated in **Figure 4.90**. This investigation was crucial because there is currently no comprehensive evidence on the effectiveness of ATAE as a corrosion inhibitor for mild steel in corrosive media. Herein, we have used gravimetric techniques, electrochemical investigations (including EIS and PDP), and morphological evaluation utilizing SEM to extract and evaluate ATAE's ability to reduce the intensity of mild steel corrosion in 0.5M HCl media. The utilization of ATAE as a green corrosion inhibitor for mild steel is expected to have significant benefits, including reduced inhibitor costs, promotion of weed cultivation, and minimal impact on humans and the environment. ATAE offers advantages such as low toxicity, biodegradability, eco-friendliness, cost-effectiveness, and ease of availability, making it a sustainable alternative to traditional chemical inhibitors. Its usage has the potential to replace hazardous chemical inhibitors and provide a green solution to corrosion prevention.

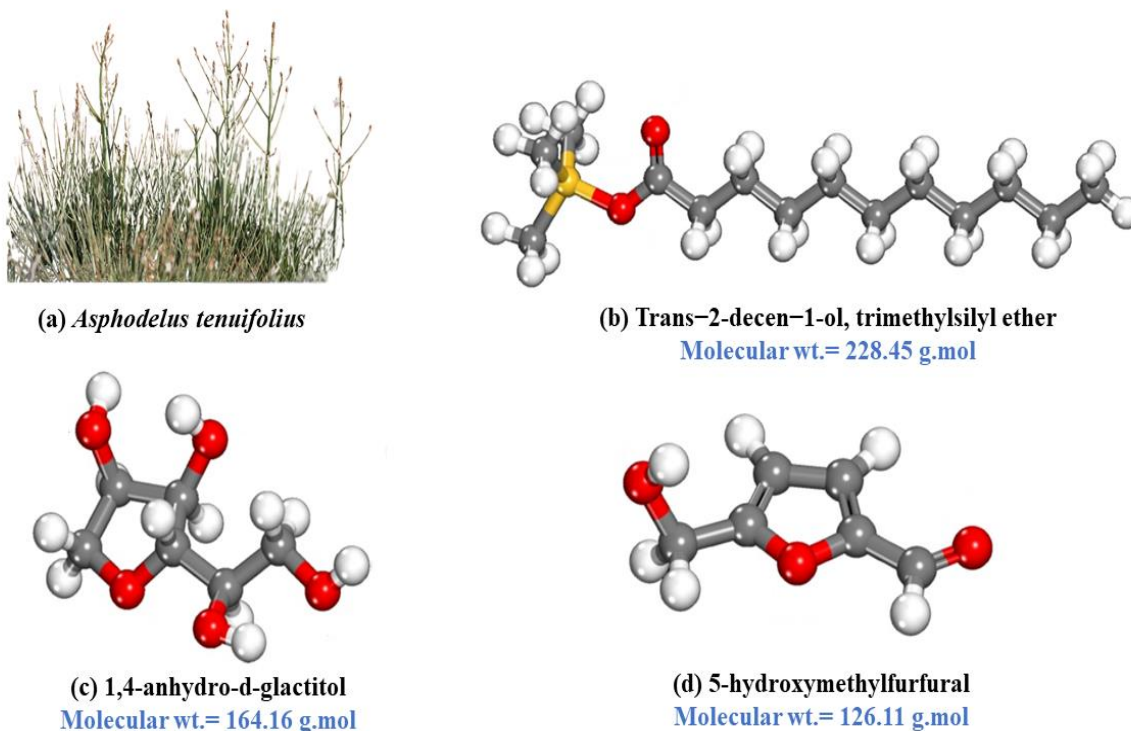


**Figure 4.90.** Molecular structures of the major phytoconstituents present in the ATAE.

#### 4.6.1. Preparation of *Asphodelus Tenuifolius* extract

The aerial parts of *Asphodelus Tenuifolius* (AT) were gathered from a nearby farm in Kapurthala during the summer season and later affirmed by Prof. Neera, Botany Department, HPU, India. The aerial parts were first air-dried in the sun for 8-10 days to remove any moisture. After being dried, the aerial parts were pounded into a minute powder and sieved to remove any large particles. The resultant powder was then combined at a proportion of 30:70 (v/v) with 80% methanol and further subjected to the cold maceration process<sup>228</sup>. After 24 hrs, the mixture was filtered through a Millipore filter with a 0.45  $\mu\text{m}$  nylon membrane to remove any solid particles. The filtrate was concentrated at 40 °C using a rotary evaporator and stored in a cool place(4–6°C) until use. This was to prevent any degradation or degradation of the active compounds. In 0.5 M HCl, the obtained ATAE was most soluble up to 250 mg/L.



#### 4.6.2. FT-IR evaluation

The adsorption of ATAE molecules onto mild steel surfaces for corrosion reduction might be facilitated by the inclusion of aromatic ring geometries and heteroatoms (O). **Figure 4.91** illustrates the ATAE's FTIR spectrum. The FTIR spectra of the ATAE illustrate  $\text{-C-H}$  stretch at  $2925\text{ cm}^{-1}$  as indicative of the presence of aliphatic hydrocarbon groups in the sample.  $\text{-O-H}$  stretch at  $3366\text{ cm}^{-1}$  as indicative of the existence of hydroxyl groups in the sample.  $\text{-C-O}$  stretch at  $1023\text{ cm}^{-1}$  as an indicative of the existence of carbonyl groups in the sample.  $\text{-CH}_3$  bend at  $1379\text{ cm}^{-1}$  is indicative of the existence of methyl group in the sample.  $\text{-C=O}$  stretch at  $1722\text{ cm}^{-1}$  as indicative of the presence of carbonyl groups in the sample.  $\text{=C-H}$  stretch at  $904\text{ cm}^{-1}$  is indicative of the existence of aliphatic hydrocarbon groups in the sample. The  $\text{-CH}_2$  bend at  $1459\text{ cm}^{-1}$  is a characteristic vibration of the methylene group in a molecule. The  $\text{-CHO}$  stretch at  $2854\text{ cm}^{-1}$  is a characteristic vibration of the carbonyl group in a molecule. Based on the FTIR outcomes, it can be documented that the sample contains aliphatic hydrocarbon groups, hydroxyl groups, carbonyl groups, and methyl groups. Additionally, these outcomes showed that ATAE included heteroatom (oxygen) in  $\text{-C-O}$ ,  $\text{-C=O}$  moieties, aromatic ring structures and linear molecules, which illustrates that ATAE has significant corrosion inhibition efficacy in  $0.5\text{M HCl}$  and the attained results are in accordant with the geometries of conventional corrosion inhibitors.

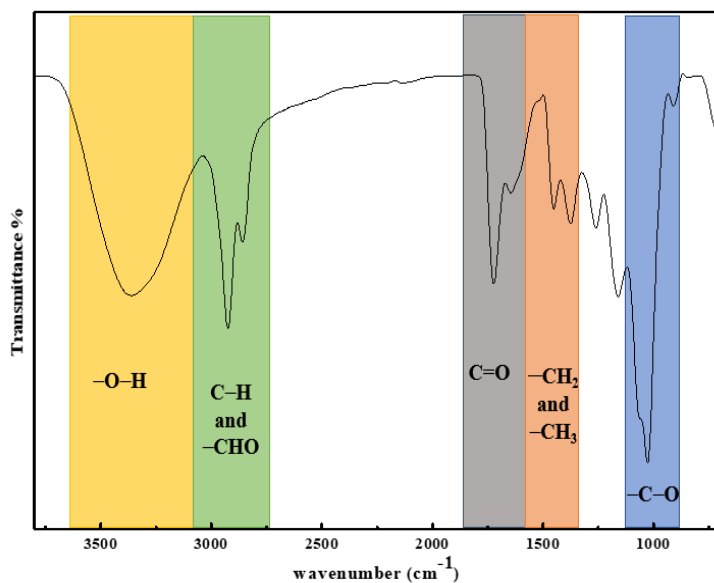


**Figure 4.91.** FT-IR analysis of the ATAE.

### 4.6.3. UV-Vis spectrometry

The UV-Vis spectrum of ATAE was examined before and after corrosion testing, as demonstrated in **Figure 4.92**. The inhibitor configuration displays absorption peaks at 481 nm and 684 nm, indicating the  $n-\pi^*$  and  $\pi-\pi^*$  transitions, respectively, following corrosion predictions. The initial peak is attributed to the  $\pi-\pi^*$  transition, which is associated with the  $-C=C$  conjugation present in the inhibitor molecules. The absorption spectrum of ATAE exhibits an absorption peak in the wavelength region of 600-700 nm, corresponding to the  $n-\pi^*$  transition, which is attributed to the various functional groups present in inhibitor molecules, such as  $-C=O$ ,  $-C-O$ , and so on. The results show a hypsochromic shift in the optimal adsorption after the corrosion study<sup>348</sup>. This suggests the possibility of a complex formation between Fe and phytochemicals, as demonstrated in **Figure 4.92**, and that these peaks were redistributed after the corrosion analysis. It clearly illustrates that when the metallic sample was immersed in 0.5M HCl+250ppm of ATAE, numerous molecules from the media (inhibitor) were adsorbed onto the metallic substrate.

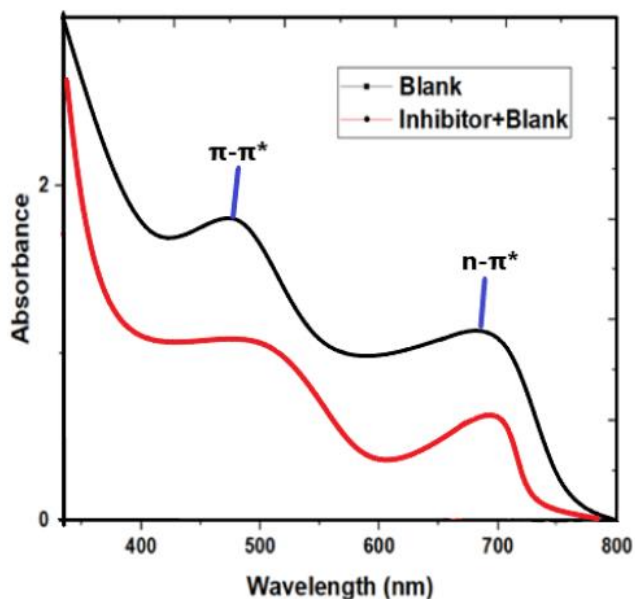


**Figure 4.92.** UV Spectra of pre- and post-metal dipping in 0.5M HCl and with the inclusion of ATAE.

#### 4.6.4. Weight loss measurement

Weight loss measurement is a commonly used method to evaluate corrosion and corrosion inhibition in materials. This method provides valuable insights into the corrosion rate and the effectiveness of corrosion inhibitors by measuring the decrease in mass of a sample due to the corrosion process. In this study, a weight loss assessment was conducted after immersing the samples in a 0.5M HCl solution for 24 hours. The results summarized in **Table 4.42** indicated that ATAE exhibited outstanding inhibition efficiency against MS corrosion in this medium. The blank column represents the mild steel samples that were not treated with ATAE, and the  $C_R$  was found to be  $2.68 \text{ mg.cm}^{-2}.\text{h}^{-1}$ . On the other hand, the ATAE-treated samples at different concentrations (50-250 ppm) show a significant decrease in the  $C_R$ , with the lowest  $C_R$  recorded at 250 ppm ( $0.15 \text{ mg.cm}^{-2}.\text{h}^{-1}$ ). As the concentration of the ATAE inhibitor increased, the inhibition efficiency ( $\eta_{WL}$ ) increased from 43.28% at 50 ppm to 94.40% at 250 ppm. This result shows that the ATAE inhibitor is effective in reducing the corrosion of mild steel in 0.5M HCl medium. The surface coverage ( $\theta$ ) also increased as the concentration of the inhibitor increased, suggesting that ATAE molecules adsorb on the metal surface to form a protective barrier that retards corrosion. This behavior indicates the strong adsorption capabilities of ATAE in establishing a protective barrier on the metallic substrate and contributing to its excellent corrosion inhibition efficacy<sup>341</sup>.

**Table 4.42**

Gravimetric outcomes for mild steel in 0.5M HCl without and with ATAE.

Inhibitor	Conc. (ppm)	$C_R$ ( $\text{mg.cm}^{-2}.\text{h}^{-1}$ )	$\eta_{WL}$ (%)	$\theta$
Blank	0	2.68	-	-
ATAE	50	1.52	43.28	0.433
	100	1.19	55.59	0.556
	150	0.58	78.35	0.786
	200	0.29	89.17	0.892
	250	0.15	94.40	0.944

#### 4.6.4.1. Concentration's effect on inhibition performance

The impact of concentration on the efficiency of a corrosion inhibitor depends on various factors such as the inhibitor type, the metal being protected, the corrosive environment, and the evaluation method used. Generally, increasing the concentration of the inhibitor enhances its inhibitory efficiency up to a certain point. This is because a higher concentration provides more active sites for the inhibitor to adsorb onto the metal surface, resulting in a greater reduction in corrosion rate. In this experiment, the effect of ATAE concentration on the corrosion inhibition of mild steel in 0.5M HCl was investigated by measuring weight loss at different concentrations ranging from 50ppm to 250ppm over a 24-hour immersion period at a temperature range of 298-313K (as shown in **Figures 4.93** and **4.94**). The results indicate that as the concentration of ATAE increased, the corrosion rate decreased and the inhibition efficiency increased (as shown in **Figures 4.93** and **4.94**). This is due to the strong adsorption of the inhibitor on the mild steel surface, which reduces the rate of metal dissolution. The highest inhibition efficiency achieved in this study was 94.40% with a corrosion rate of  $0.15 \text{ (mg.cm}^{-2}.\text{h}^{-1}\text{)}$  at a concentration of 250ppm.

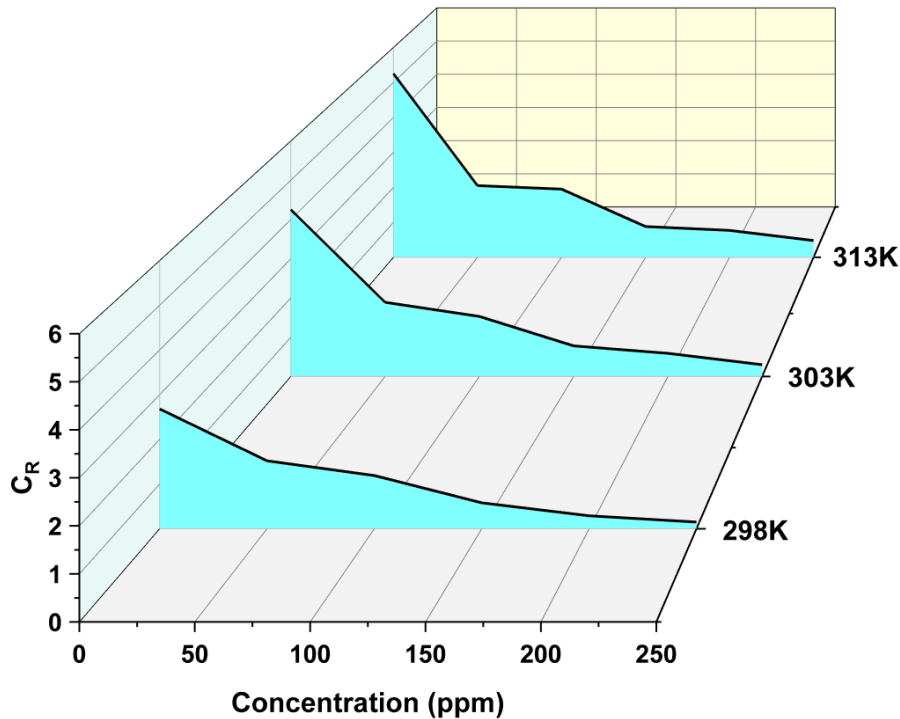


**Figure 4.93.** Corrosion rate variation at different ATAE concentrations at various temperatures.

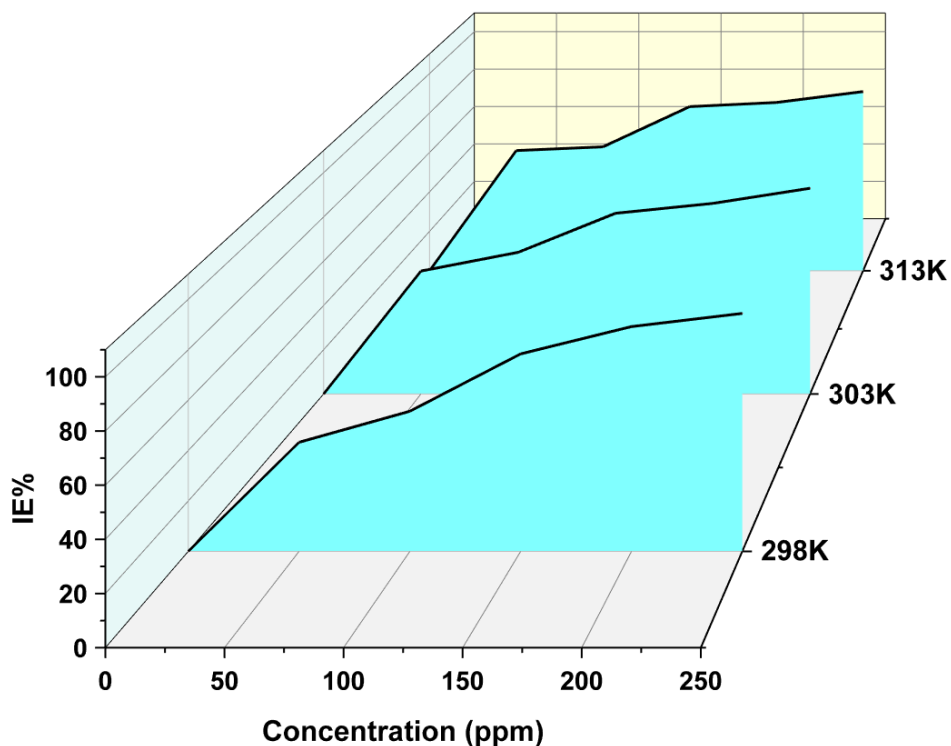


**Figure 4.94.** Effect of inhibition efficiency at different concentrations of ATA E at various temperatures.

#### 4.6.5. Temperature impact and activation parameters

Temperature is the next significant factor that influences the activity of inhibitors and substrates in hostile media. At higher temperatures, the ATA E molecules become more soluble and desorb from the metallic substrate, as a result, mild steel's corrosion resistance declines as the temperature rises. In this experiment, three different temperatures (298K, 303K, and 313K) were taken to conduct gravimetric analysis with varying concentrations of ATA E (50-250ppm) to ascertain the impact of temperature on the IE% of the ATA E. **Table 4.43** illustrates the impact of various inhibitor concentrations on corrosion rates under different temperatures. At 298K, the blank (0ppm) had a  $C_R$  of  $2.68 \text{ mg.cm}^{-2}.\text{h}^{-1}$ , while the addition of ATA E at concentrations ranging from 50ppm to 250ppm led to a decrease in the  $C_R$ , with the highest inhibition efficiency (94.40%) observed at 250ppm. The surface coverage also increased with an increase in inhibitor concentration, reaching a maximum of 0.944 at 250 ppm. At 303K, the blank had a higher  $C_R$  of  $4.25 \text{ mg.cm}^{-2}.\text{h}^{-1}$ , and the addition of ATA E again led to a decrease in the  $C_R$ . The highest inhibition efficiency (92.94%) was observed at 250ppm, and the surface coverage reached a maximum of

0.921 at the same concentration. At 313K, the blank had the highest  $C_R$  of  $5.25 \text{ mg.cm}^{-2}.\text{h}^{-1}$ , and the addition of ATAE resulted in a decrease in the  $C_R$  as well. The highest inhibition efficiency (90.85%) was observed at 250 ppm, and the surface coverage reached a maximum of 0.901 at the same concentration. These findings significantly suggested that with an increase in temperature from 298K to 313K, the  $C_R$  increased with a reduction in the IE% and  $\Theta$  as compared to the findings in 298K and 303K revealing the desorption of adhered molecules of ATAE on the mild steel surface and increase in the active spots for the attack of corrosive ions which ultimately led to the corrosion of mild steel.

**Table 4.43**

Corrosion rate, Inhibition performance (%) and surface coverage of mild steel in 0.5M HCl solution of ATAE.

Temperature (K)	Concentration (ppm)	$C_R$ ( $\text{mg.cm}^{-2}.\text{h}^{-1}$ )	$\eta_{WL}$ (%)	$\Theta$
298	0	2.68	-	-
	50	1.52	43.28	0.433
	100	1.19	55.59	0.556
	150	0.58	78.35	0.786
	200	0.29	89.17	0.892
	250	0.15	94.40	0.944
303	0	4.25	-	-
	50	1.89	55.53	0.555
	100	1.53	64.01	0.640
	150	0.78	81.64	0.816
	200	0.59	86.11	0.861
	250	0.3	92.94	0.921
313	0	5.25	-	-
	50	2.05	60.95	0.609
	100	1.95	62.85	0.628
	150	0.88	83.23	0.832
	200	0.77	85.33	0.853
	250	0.48	90.85	0.901

It is clear that the  $C_R$  increased as the temperature rose from 298K to 313K, which illustrates that the protective inhibitors' ability to reduce corrosion at various concentrations decreased, suggesting that the protective layer was eroding as the temperature rose. Additionally, to deliberate more, an Arrhenius-type behavior has been exhibited between temperature and  $C_R$ . By using equation (20) the activation energy ( $E_a$ ) of the corrosion mechanism at different temperature ranges was evaluated in both the presence and absence of ATAE. Following transition state theory, the thermodynamic parameters enthalpy ( $\Delta H_a$ ) and entropy ( $\Delta S$ ) for the corrosion process were computed. The slope of the equation ( $-E_a/RT$ ) in the inclusion and exclusion of the investigated inhibitor was used to compute the activation energy of the metal-dissolving process (**Figure 4.95**). **Table 4.44** shows the several activation parameters in the existence and non-existence of ATAE.

**Table 4.44**

Mild steel activation parameters ( $E_a$ ,  $\Delta H_a$ ,  $\Delta S$ ) in the existence and non-existence of ATAE.

Medium	Conc. (ppm)	$E_a$ (KJ/mol)	$\Delta H_a$ (KJ/mol)	$\Delta S$ (J mol <sup>-1</sup> K <sup>-1</sup> )	$E_a - \Delta H_a$ (KJ/mol)
Blank	0	13.385	15.963	-143.082	2.6
	50	14.134	16.711	-130.944	2.6
	100	24.360	26.937	-115.313	2.6
	150	25.690	28.268	-100.431	2.6
	200	48.055	50.549	-46.889	2.6
	250	55.205	57.699	-28.266	2.6

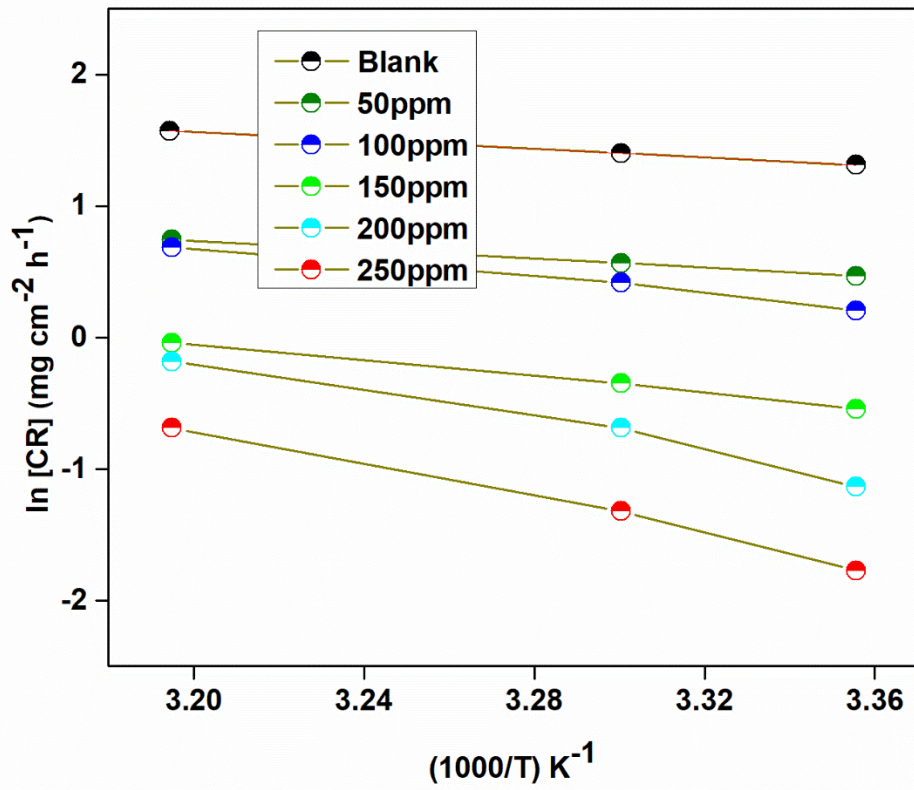


**Figure 4.95.**  $\ln [CR]$  vs.  $1000/T$  for mild steel corrosion in 0.5 M HCl solution in the exclusion and inclusion of various dosages of ATAE.



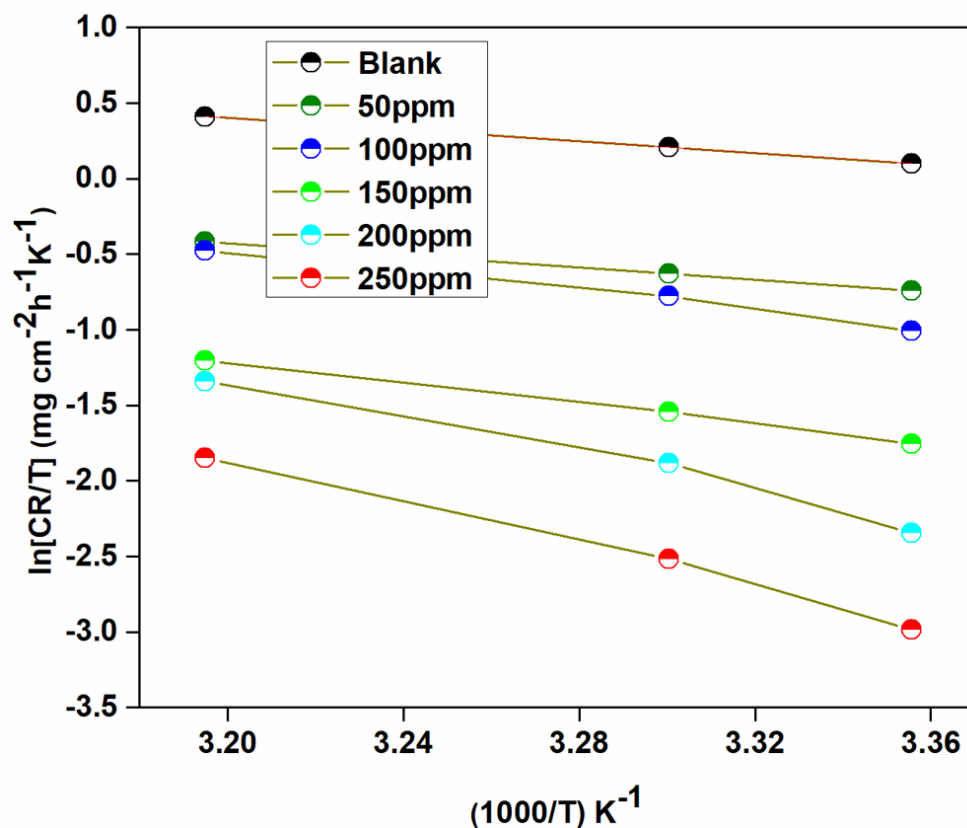


**Figure 4.96.**  $\ln [CR/T]$  vs.  $1000/T$  for mild steel corrosion in 0.5 M HCl solution in the exclusion and inclusion of various dosages of ATAE.

The values of  $\Delta H_a$  and  $\Delta S$  are shown in **Table 4.44** and were computed from the plot of  $\ln(C_R/T)$  v/s  $1/T$  (**Figure 4.96**). This table provides information on the activation energy ( $E_a$ ), enthalpy of adsorption ( $\Delta H_a$ ), the entropy of adsorption ( $\Delta S$ ), and the difference between  $E_a$  and  $\Delta H_a$  for ATAE adsorbed onto a medium at different concentrations (50-250 ppm). The  $E_a$  represents the energy need for a chemical reaction to occur. In the context of adsorption,  $E_a$  indicates the energy required for the adsorbate (ATAE) to overcome the barrier to adsorption and become adsorbed onto the adsorbent surface. The enthalpy of adsorption ( $\Delta H_a$ ) represents the variation in enthalpy interlinked with the adsorption mechanism, and the entropy of adsorption ( $\Delta S$ ) represents the variation in entropy interlinked with the adsorption mechanism.

The results show that in the absence of ATAE (blank), the activation energy of mild steel was 13.385 KJ/mol, and the enthalpy of activation was 15.963 KJ/mol, while the entropy of activation was  $-143.082 \text{ J mol}^{-1}\text{K}^{-1}$ . When ATAE was added, the activation energy increased to 14.134 KJ/mol

at 50 ppm, and then increased significantly to 55.205 KJ/mol at 250 ppm. The enthalpy of activation also increased from 16.711 KJ/mol at 50 ppm to 57.699 KJ/mol at 250 ppm suggesting physisorption. Meanwhile, the entropy of activation decreased from  $-130.944 \text{ J mol}^{-1}\text{K}^{-1}$  at 50 ppm to  $-28.266 \text{ J mol}^{-1}\text{K}^{-1}$  at 250 ppm. The difference between  $E_a$  and  $\Delta H_a$  can provide insight into the nature of the adsorption process. If  $E_a - \Delta H_a$  is positive, it suggests that the adsorption process is primarily driven by enthalpy changes (e.g. attractive forces between the adsorbate and the adsorbent surface). If  $E_a - \Delta H_a$  is negative, it suggests that the adsorption process is primarily driven by entropy changes (e.g. an elevation in the disorder of the system). The average difference in  $E_a - \Delta H$  ( $\sim 2.6 \text{ kJ/mol}$ ) resembles the average  $RT$  ( $2.64 \text{ kJ/mol}$ ), inferring the corrosion mechanism via a unimolecular gaseous reaction<sup>342</sup>. It is evident that as the dosage of ATAE increased from 50 to 250 ppm, both the  $E_a$  and  $\Delta H_a$  increased, while the  $\Delta S$  decreased. It revealed that the adsorption of ATAE onto the medium is primarily driven by enthalpy changes (as  $E_a - \Delta H_a$  is positive) and that the adsorption process becomes stronger at higher concentrations of ATAE. These results suggest that the addition of ATAE to the mild steel solution increased the activation energy and enthalpy of activation, indicating that more energy was required for the corrosion reaction to occur. The increase in activation energy was attributed to the adsorption of ATAE on the mild steel surface, which created a barrier that hindered the attack of corrosive ions on the metal surface. The decrease in entropy of activation with an increase in ATAE concentration suggested that the adsorption of the inhibitor on the metal surface reduced the degree of disorder of the reactants and products. Overall, these findings indicate that ATAE is an effective inhibitor for mild steel corrosion, and its inhibitive action is due to its ability to adsorb on the metal surface and create a barrier against corrosive ions.

#### **4.6.6. Adsorption studies**

The study of corrosion inhibition heavily relies on adsorption isotherms and kinetics, which provide valuable information on the adsorption behavior and rate of corrosion inhibitors on the surface of corroded materials. Adsorption isotherms illustrate the relationship between the amount of a corrosion inhibitor adsorbed on the surface of corroded material and its concentration in solution, with different isotherms such as Langmuir, Freundlich, and Temkin used to describe the behavior of different inhibitors. The shape of an adsorption isotherm can reveal the type of adsorption and the nature of the interaction between the inhibitor and the corroded material. On

the other hand, adsorption kinetics variables describe the rate at which corrosion inhibitors are adsorbed on the corroded material's surface. In this study, the Langmuir adsorption isotherm equation (4) and **Figure 4.97**, were used to examine the adsorption behavior and correlate the surface coverage ( $\Theta$ ) with the concentration of inhibitors ( $C_{inh}$ ). The collected  $\Theta$  values from **Table 4.47** were analyzed to gain a better understanding of the adsorption behavior of the inhibitors. After data evaluation, it is determined that the linear curve fitting produced by the Langmuir adsorption isotherm has a regression coefficient of 0.99591, near the unity. The Langmuir adsorption isotherm is a model utilized to describe the behavior of the adsorption of molecules onto a solid surface. It assumes that adsorption occurs at specific sites over the surface and that each site can only adsorb one molecule. The experimental results revealed that the experimental results obtained with the ATAE are highly reliable and compatible with the Langmuir adsorption isotherm. It indicates that the Langmuir model is a good fit for exploring the adsorption behavior of the ATAE onto the adsorbent surface and that the assumptions made by the Langmuir model are likely valid for this system. Equation (4), which is the reciprocal of the intercept of a linear line, was used to compute  $K_{ads}$ , and equation (7), which correlates  $K_{ads}$  to  $\Delta G^{\circ}_{ads}$  (standard free energy of the adsorption isotherm), was also used.

**Table 4.45**

Various adsorption variables for ATAE in 0.5M HCl solution.

<b>Isotherm</b>	<b>Inhibitor</b>	<b><math>R^2</math></b>	<b>Parameter</b>		<b><math>K_{ads}</math></b>	<b><math>\Delta G^{\circ}_{ads}</math>(kJ/mol)</b>
<b>Langmuir</b>	ATAE	0.99591	Slope	1.067	5.615	-27.68

**Table 4.45** presents significant information regarding the Langmuir adsorption isotherm used to describe the adsorption of the inhibitor compound (ATAE) onto an adsorbent surface. The table provides Langmuir model parameters  $K_{ads}$  and  $\Delta G^{\circ}_{ads}$ , as well as the regression coefficient ( $R^2$ ) obtained from data evaluation. The high  $R^2$  value of 0.99591 indicates that the experimental data has a strong correlation with the Langmuir model, demonstrating the model's effectiveness in describing the adsorption behavior of the ATAE inhibitor. The Langmuir parameter  $K_{ads}$  of 5.615 indicates a strong affinity between the adsorbent surface and the ATAE inhibitor. Moreover, the negative value of  $\Delta G^{\circ}_{ads}$  (-27.68 kJ/mol) implies that the adsorption process is spontaneous and exothermic, indicating that the adsorbate's adsorption on the adsorbent surface is energetically

favorable resembling. Additionally, it is known that if the  $\Delta G^{\circ}_{\text{ads}}$  are higher than -20 kJ/mol and lower than -40 kJ/mol, it suggests physisorption and chemisorption<sup>50,349</sup>. In this case, the value of  $\Delta G^{\circ}_{\text{ads}}$  range between -20 kJ/mol and -40 kJ/mol, which indicates that investigated inhibitors have been adsorbed by the combination of both physical and chemical. These findings suggest that the Langmuir adsorption isotherm is a suitable model for characterizing the adsorption behavior of the ATAE inhibitor on the adsorbent surface, which is energetically favorable and driven by the strong affinity between the adsorbate and the adsorbent surface.

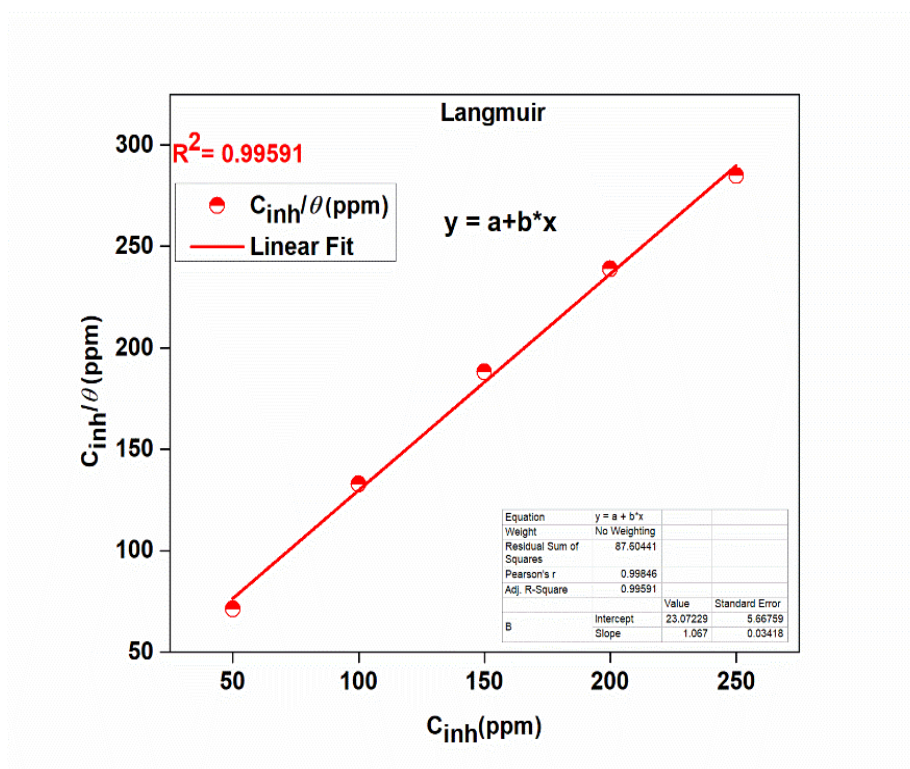


**Figure 4.97.** Different isotherm for adsorption of ATAE on mild steel in 0.5 M HCl.

#### 4.6.7. Electrochemical analysis

##### 4.6.7.1. Open circuit potential (OCP)

Open-circuit potential (OCP) is a crucial parameter that plays a significant role in studying corrosion and corrosion inhibition of metals using electrochemical impedance spectroscopy (EIS). OCP refers to the potential of a metal when it is not connected to an external electrical circuit, and it reflects the balance between charge-transfer and mass-transport processes at the metal-solution interface<sup>238</sup>. In EIS measurements of corrosion, the OCP serves as a reference potential for the measurement. In this investigation, the mild steel rod, used as the working electrode, was

submerged in the test media for 1 hour throughout each investigation involving the variation in concentration from 50ppm to 250ppm. It is crucial to establish a consistent OCP before conducting the potentiodynamic polarization (PDP) and EIS assessments. **Figure 4.98** shows the trends of OCP versus time (seconds) in the presence and absence of various dosages of ATAE. From the analysis of **Figure 4.98**, it can be observed that after immersion, the potential of the mild steel specimens dipped in the media containing all the desired concentrations of ATAE stabilized. The potential measurements for the inhibited and uninhibited specimens both significantly shifted toward the negative value, indicating that ATAE acts as a cathodic inhibitor in the aggressive medium of 0.5 M HCl. The negative shift in the OCP of the pristine specimen could be attributed to the production/dissolution of iron oxide on the metallic substrate.

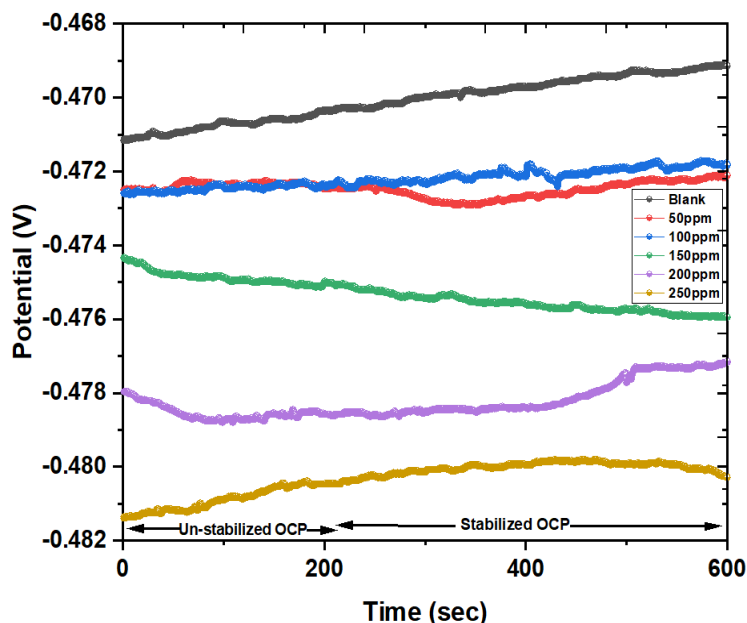


**Figure 4.98.** OCP vs. time graph for corrosion inhibition of mild steel after exposure to various ATAE concentrations (50-250ppm) in 0.5M HCl.

#### 4.6.7.2. Potentiodynamic polarization (PDP)

PDP measurement is a commonly used approach in the study of corrosion and corrosion inhibition of metals. PDP is used to evaluate the  $C_R$  and the corrosion potential of metal in a corrosive solution. The corrosion potential is the potential at which the metal begins to corrode, and it is an important parameter for the evaluation of corrosion inhibitors. In PDP measurement, a metal is subjected to a series of increasing potentials in a corrosive solution, and the current density at each

potential is measured<sup>346</sup>. The data is then plotted as a function of the potential, and the attained plot is called a Tafel plot. The Tafel plot provides information about the  $C_R$  and the corrosion potential of the metal. The Tafel plot is characterized by two linear regions, the anodic region and the cathodic region. The anodic region is characterized by a positive slope and corresponds to the oxidation of the metal. The cathodic region is characterized by a negative slope and denotes the reduction of the corroding species. The point at which the anodic and cathodic regions intersect is the corrosion potential. The Tafel plot can be used to evaluate the impact of corrosion inhibitors on the corrosion rate and corrosion potential. For example, an inhibitor that decreases the  $C_R$  will result in a shift of the Tafel plot to more negative potentials, while an inhibitor that increases the  $C_R$  will result in a shift of the Tafel plot to more positive potentials. In this investigation, by using the PDP technique, the impact of ATAE over the cathodic hydrogen ions reduction and anodic dissolving of mild steel was determined. Additionally, the kinetics of cathodic and anodic reactions was evaluated using PDP analysis. The polarization plots are depicted in **Figure 4.99**. The corrosion potential ( $E_{\text{corr}}$ ), corrosion current densities ( $i_{\text{corr}}$ ), anodic ( $\beta_a$ ) and cathodic ( $\beta_c$ ) Tafel slope values were attained through the analysis of associated polarization parameters, as reported in **Table 4.46**. The IE% of ATAE was attained by equation (9).

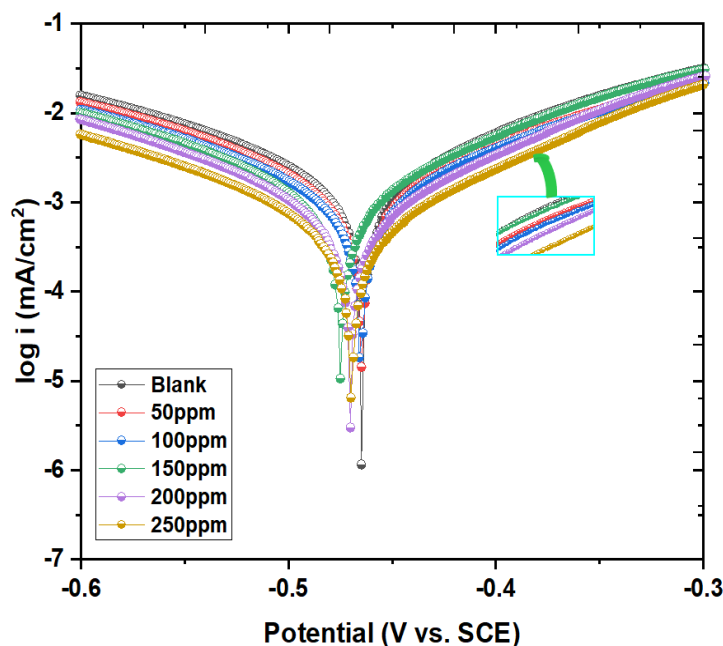


**Figure 4.99.** Tafel graph for the corrosion inhibition of mild steel in blank media subjected to 50-250ppm amounts of ATAE at 298 K.

**Table 4.46**

Tafel variables for the corrosion mitigation of mild steel in blank solution subjected to 50-250ppm amounts of ATAE at 298 K.

Conc. (ppm)	$-E_{\text{corr}}$ (mV vs. SCE)	$i_{\text{corr}}$ ( $\mu\text{A}$ )	$\beta_a$ (mV/dec)	$-\beta_c$ (mV/dec)	$C_R$ (mm/yr)	IE%	$\chi^2$
Blank	465.44	1157.9	135.13	157.75	34.42	-	2.274E-07
50	466.53	189.07	147.89	154.05	21.97	83.67	5.5345E-08
100	466.33	165.49	141.86	161.44	19.23	85.71	2.5094E-07
150	472.12	155.47	125.34	151.19	18.066	86.57	5.7231E-07
200	466.95	132.77	110.73	127.43	10.246	88.53	1.1889E-06
250	463.3	114.24	108.89	129.33	7.091	90.13	1.0074E-06

Through the investigation of **Figure 4.99** and **Table 4.46**, it could be noted that the value of  $i_{\text{corr}}$  and  $C_R$  declined dramatically from 1157.9 to 114.24 and 94.42 to 7.091 with increasing ATAE concentrations (50-250 ppm). The preventative impact of the ATAE on mild steel was continuously enhanced as the inhibitor amount was elevated from 50 to 250 ppm. These results demonstrated that ATAE delayed the mechanism of hydrogen generation as well as the dissolution of metal. Furthermore, the anodic Tafel slope remains relatively constant across all concentrations, while the cathodic Tafel slope becomes more negative with increasing concentration, indicating that ATAE may be more effective at reducing cathodic reduction than anodic dissolution as shown by the polarization slope affirming the mixed-type nature of the ATAE inhibitor action, as the displacement in the  $E_{\text{corr}}$  is <85mV. **Table 4.46** further depicts that when the inhibitor was added, the  $\beta_c$  and  $\beta_a$  values often altered, illustrating that the utilization of the ATAE inhibitor does not alter the corrosion process nature. The inhibition efficiency increased up to 90.13% with increasing concentrations of ATAE, suggesting that the inhibitor is becoming more effective at higher concentrations. Additionally, the values for both the  $\beta_c$  and  $\beta_a$  Tafel slopes seem to decrease as the concentration of the ATAE increased, which suggests that the existence of the ATAE reduced the rate at which the current density changes with potential, resulting in lower corrosion rates. This

may be own to the inhibitor molecule's adsorption upon the mild steel surface, obscuring it and restricting the extent of active spots for the interaction despite retaining the charge transmission pathway of hydrogen evolution.

#### **4.6.7.3. Electrochemical impedance spectroscopy (EIS)**

EIS measurement is a frequently utilized approach in the study of corrosion and corrosion inhibition of metals<sup>95</sup>. Nyquist plots attained from this study are used to obtain information about the impedance and conductivity of a metal in a corrosive solution, and they provide valuable information about the  $C_R$  and the resistance of the metal to corrosion. In EIS measurements of corrosion, a metal is subjected to an alternating current in a corrosive solution, and the resulting potential and current responses are measured. The data is then plotted as a Nyquist plot, with the imaginary component of the impedance on the y-axis and the real component of the impedance on the x-axis. The Nyquist plot is characterized by a semi-circle in the low-frequency region and a straight line in the high-frequency region. The semi-circle represents the impedance of the metal and its corroded surface, while the linear line represents the impedance of the metal. The shape and position of the semi-circle provide crucial insights into the  $C_R$  and the resistance of the metal to corrosion, while the shape and position of the straight line provide information about the resistance of the metal. In this investigation, in order to attain relevant information regarding the corrosion mitigation process, the EIS evaluation of mild steel dipped in several amounts of ATAE in 0.5 M HCl was conducted to corroborate the findings of the PDP and WL examinations. The critical outcomes are summarized in **Table 4.47**. The Nyquist plot is depicted in **Figure 4.100**. A substantial capacitive curve could be observed at a higher frequency on the Nyquist graph, whereas an inductive curve is visible at a lower frequency. The adsorption of  $Hads^+$ ,  $Cl^-$ , and ATAE molecules over the surface of mild steel expedited the relaxation phase that formed the lower-frequency inductive loop. In contrast, the surface distortion and charge transfer mechanism generated the high-frequency capacitive curve. The re-disintegration of the passivated substrate at a lesser frequency may be a probability. The pattern of all slopes in the Nyquist graph remained unchanged whether an inhibitor was used or not, showing that the metallic corrosion mechanism was unaffected. Furthermore, their geometries weren't ideal due to frequency dispersal, roughness, and non-uniformity of the working electrode substrate. The radii of the curves were demonstrated to increase as ATAE levels increased from 50 to 250 ppm, indicating that ATAE dispersion over



the electrode substrate improved and a protective covering formed, thereby preventing corrosion on the electrode surface.

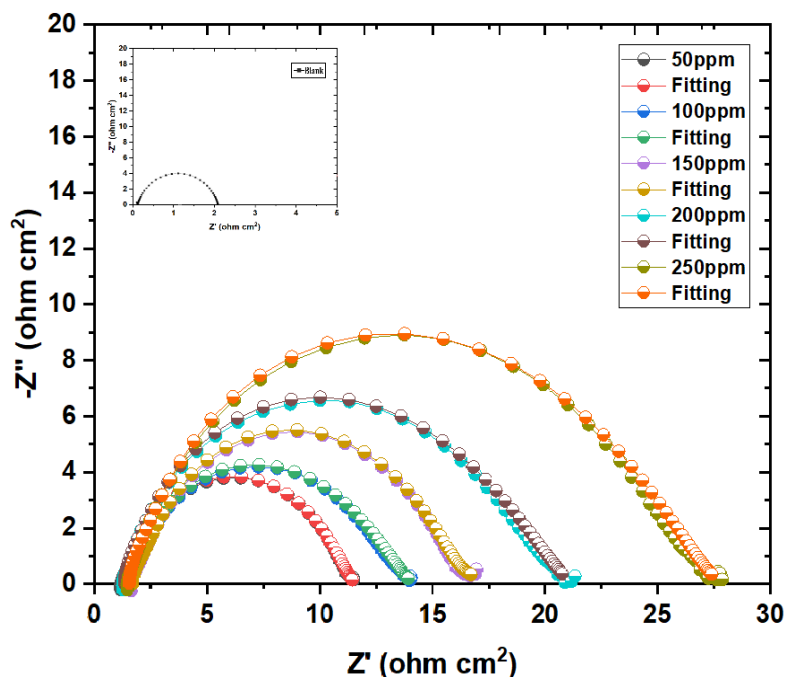


**Figure 4.100.** Nyquist graph for mild steel corrosion inhibition in 0.5M HCl with 50–250 ppm ATAE at ambient temperature.

Similarly, Bode plot measurement is a commonly used methodology in the study of corrosion and corrosion inhibition of metals using electrochemical impedance spectroscopy (EIS). Bode plots are used to obtain information about the impedance and phase angle of a metal in a corrosive solution, and they provide valuable information about the  $C_R$  and the resistance of the metal to corrosion<sup>97,239</sup>. The Bode plot provides information about the impedance and phase angle of the metal in a corrosive solution as a function of frequency. The impedance magnitude is proportional to the corrosion rate, while the phase angle is proportional to the resistance of the metal to corrosion. The Bode graphs for the metal in the addition and lack of diverse quantities of ATAE (50-250ppm) in the acidic solution at 298K are depicted in **Figure 4.101**. The impedance modulus improved with the increased quantity of ATAE across the frequency range investigated in this research. The frequency spectra also expanded at the highest phase angles. As per the previous reports, the optimum capacitance at an intermediary frequency can be accepted, if the curve of the  $\log |Z|$  versus  $\log f$  with a maximum phase angle of  $90^\circ$  tends to be  $1$ <sup>229,240,241</sup>. This demonstrated

that in the 0.5 M HCl, ATAE has a significant inhibition efficacy toward the corrosion of mild steel.

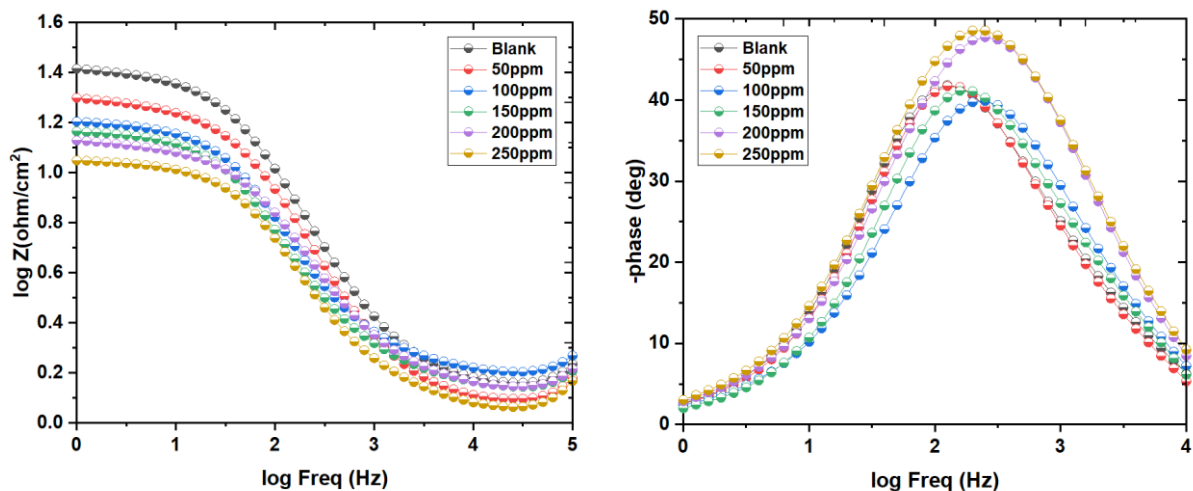


**Figure 4.101.** Bodes graph for the corrosion mitigation of mild steel in blank media subjected to 50-250ppm conc. of ATAE at 298 K.

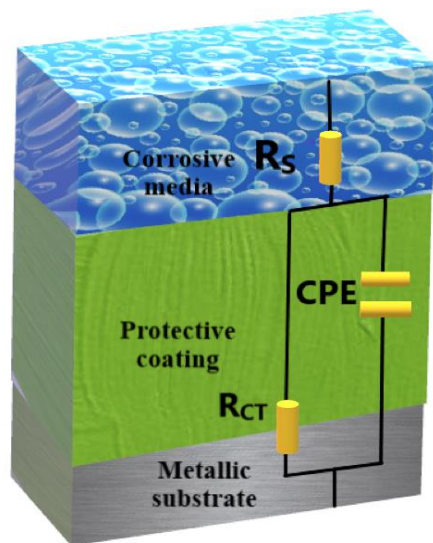


**Figure 4.102.** An equivalent circuit model utilized for the data fitting.

**Table 4.47** reports the EIS metrics, wherein  $R_s$  represents solution resistance,  $R_{ct}$  denotes charge transfer resistance,  $n$  represents phase shift, CPE denotes constant phase element and the

discrepancy scale of the eqv. circuit fitting denoted by  $\chi^2$ . The datasets of  $\chi^2$  within  $10^{-3}$  and  $10^{-5}$  suggest that the depicted equivalent circuit layout is reliable and stable, confirming to be consistent with the ideal fitting. It could be observed that at increasing concentrations of the inhibitor, there is a decrease in CPE.Yo and n values, indicating a decrease in the double-layer capacitance and a change in the surface characteristics of the metal. There is also an increase in  $R_s$ ,  $R_p$ , and  $R_{ct}$  in, indicating a decrease in the ion conductivity and an elevation in the charge transit resistance at the metal-inhibitor interface. At 250 ppm, the inhibitor has the lowest CPE.Yo and n values, the highest  $R_p$  and  $R_{ct}$  in values, and the lowest Cdl value (677.973), indicating the highest inhibition efficiency (92.17%). **Table 4.47** illustrates that as the quantity of ATAE was expanded, the  $R_{ct}$  and IE% increased, reaching an optimum IE% of 92.17% at 250ppm, revealing to be remarkably consistent with the analyses of the PDP and WL experimentations. When several amounts of ATAE were introduced, the  $R_s$  value did not alter drastically. Moreover, the  $n$  values (0.965-0.790) did not impact considerably, demonstrating that charge transfer regulated the mild steel dissolution in a corrosive medium. The values of  $\theta$  obtained from the experiment were used to determine the degree of surface coverage of the inhibitor on the metal surface. The results showed that the degree of surface coverage increased with increasing concentration of ATAE, with the highest value of 0.877 obtained for the 250 ppm concentration of ATAE. Finally, the goodness of fit ( $\chi^2$ ) values were calculated to assess the accuracy of the model used to fit the experimental data. The values of  $\chi^2$  obtained were low, indicating a good fit of the model to the experimental data. Overall, the results suggest that the inhibitor has a valuable impact on the impedance parameters of the metal-inhibitor system, with higher concentrations providing greater protection against corrosion<sup>350</sup>.

**Table 4.47**

IE% values for the corrosion mitigation of mild steel in 0.5M HCl subjected to 50-250ppm conc. of ATAE at 298 K.

Conc. (ppm)	CPE.Yo (μF)	<i>n</i>	$R_s$ (Ω)	$R_p$ (Ω)	$R_{ct}$ in (Ωcm <sup>2</sup> )	$R_{ct}$ bl (Ωcm <sup>2</sup> )	Cdl (μF/cm <sup>2</sup> )	IE (%)	$\theta$	$\chi^2$
<b>Blank</b>	422.78	0.965	0.984	3.814	-	2.12	-	-		0.579
<b>50</b>	290.32	0.818	1.189	10.147	12.16	2.12	3375.01	82.56	0.702	0.612
<b>100</b>	221.11	0.757	1.394	12.405	14.24	2.12	2529.928	85.11	0.754	0.302
<b>150</b>	266.03	0.820	1.605	14.485	17.12	2.12	1669.865	87.62	0.798	0.336
<b>200</b>	187.92	0.767	1.207	19.001	21.38	2.12	1158.302	90.08	0.837	0.425
<b>250</b>	162.94	0.790	1.426	24.916	27.09	2.12	677.973	92.17	0.877	0.380

#### 4.6.8. Surface morphology analysis

##### 4.6.8.1. SEM

In this research, SEM was employed to evaluate the topographical state of metallic samples after the 6hrs of dipping in a solution of 0.5M HCl at 298K in the exclusion and inclusion of ATAE, and the outcomes have been shown in **Figure 4.103**. The flat view of the SEM micrograph of the unprocessed plain steel sample has been depicted in **Figure 4.103 (a)**. While **Figure 4.103 (b)** represents the flat view of the sample immersed in 0.5 M HCl which is characterized by an extremely coarse surface having several pits and an incredibly high degree of roughness on it resembling corrosion products over the metallic surface<sup>351–353</sup>. It means that there is obvious degradation and substantial degradation on the blank steel substrate. With the introduction of ATAE (250 ppm concentration), the surface's roughness was substantially reduced compared to the uninhibited environment by creating a defensive film on the mild steel specimen's surfaces, preventing corrosive ions from attacking the surface and leaving fewer pits and corrosion products shown in the corresponding **Figure 4.103 (c)** which consequently leads to corrosion reduction which is the goal of this research. These findings imply that the ATAE molecules were adsorbed onto the mild steel surface, creating a defensive covering composed of CI mono-layers leading to a smoother outer layer.

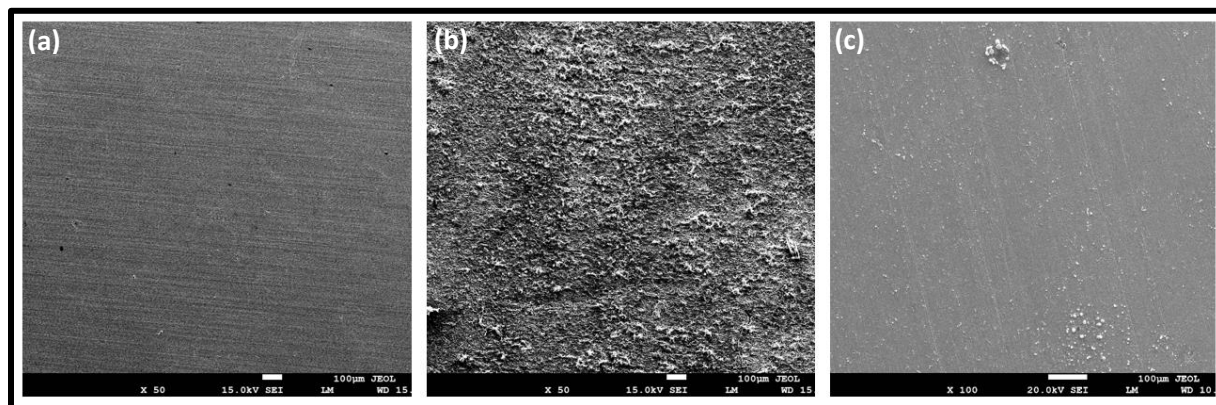


**Figure 4.103.** SEM visuals of (a) plain metal, (b) metal submerged in 0.5 M HCl (c) metal submerged in 0.5 M HCl + ATAIE (250ppm) at 298K for 6hrs.

#### 4.6.8.2. Contact angle (CA) assessment

The study provides additional insights into adhesion, wetting, and absorption irregularities on mild steel surfaces. The researchers utilized contact angle (CA) analysis to evaluate the hydrophobicity/hydrophilicity of both untreated and treated mild steel substrates. **Figure 4.104 (a, b)** displays the CA images obtained from the metal substrate with and without the inclusion of 250ppm of ATAIE. The figure indicates that the metallic sample treated with the inhibitor had a higher CA value ( $73.65^\circ$ ) in comparison to the sample treated only with 0.5M HCl ( $55.43^\circ$ ). This suggests that the surface of mild steel had lower hydrophobicity prior to ATAIE treatment (**Figure 4.104 (a)**), but the hydrophobicity increased post-treatment (**Figure 4.104 (b)**). In an acidic environment, aggressive ions can adhere to mild steel surfaces due to their minimal hydrophobicity, promoting corrosion. However, the adhesion of inhibitor molecules can alter the surface tension, resulting in the creation of a protective layer over the metal substrate, ultimately reducing corrosion.

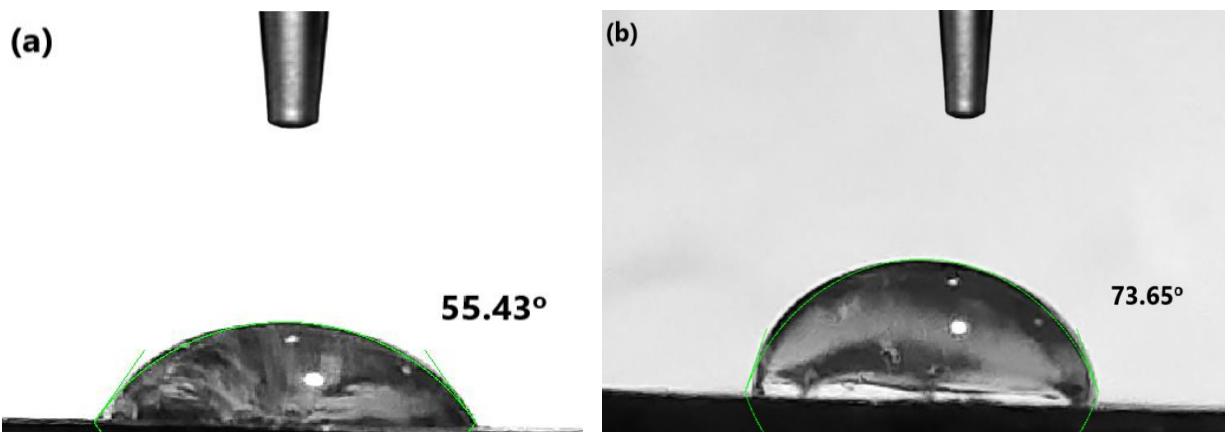


**Figure 4.104.** CA assessment performed on the metallic sample in (a) 0.5M HCl media and (b) metallic specimen+250ppm of ATA E.

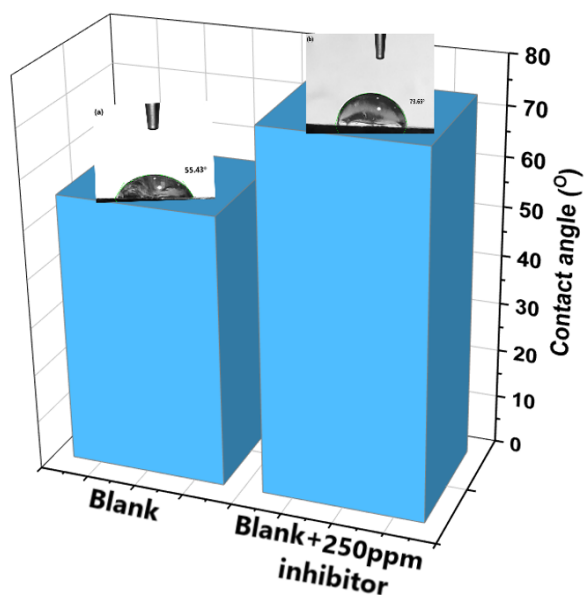


**Figure 4.105.** Graph showing the progress in the hydrophobic nature of mild steel surface after treatment with 250ppm of ATA E.

#### 4.6.9. Computational studies

##### 4.6.9.1. DFT

Quantum chemical methods, and more specifically density functional theory (DFT), are increasingly used to describe molecular properties, understand the mechanism of action and predict

the effectiveness of corrosion inhibitors. DFT is a widely used theoretical approach in the field of materials science, including corrosion inhibition. DFT calculations can provide valuable insights into the electronic structure and reactivity of materials, which can be used to predict their efficacy as corrosion inhibitors<sup>24,332</sup>. In the context of corrosion inhibition, DFT can be utilized to explore the interaction between a potential inhibitor and a metallic surface. By calculating the electronic properties of the inhibitor and the metallic surface, DFT can predict the strength of the adsorption of the inhibitor onto the surface, as well as the IE%. In this analysis, the geometric structures of the studied molecules were obtained by global optimizations characterized by a calculation of the vibration frequencies using the DFT method (utilizing Dmol<sup>3</sup>, which comprised the B3LYP/ DND / COSMO (water) model). We have used the Materials Studio 8.0 software to perform MC and MD simulations. For the simulations of the adsorption modes of the molecules investigated on the Fe surface in this study, we choose the Fe(1 1 0) surface. The simulation box employed to carry out the MD simulations had the dimensions (24.823 × 24.823 × 18.241 Å). The iron slice and the number of water molecules comprising the studied compound are associated with the simulation box. Before starting the simulation, the surface of Fe(1 1 0) and the molecular geometry of the compounds studied were simulated by minimizing the energies. Using the COMPASS III (Edition 1.0) force field, MD simulations were carried out at 298 K using the NVT setup, a phase stride of 1 fs, and a simulation duration of 800 ps. This model included a Fe layer, 10 hydronium ions, 10 chloride ions, 800 H<sub>2</sub>O molecules and 1 inhibitor molecule and a 35-vacuum layer included in the simulation box.

The charge density profiles indicate how electrons are dispersed on a surface and elaborate on the solubility of the inhibitor molecules. Employing the COSMO model's computations enables the production of a charge density curve accompanied using a  $\sigma$ -profile. Partial atomic charges represent the electrostatic potential. As shown in **Figure 4.106**, the major phytoconstituents of ATAE i.e., Trans-2-decen-1-ol, trimethylsilyl ether, 1,4-anhydro-d-glactitol and 5-hydroxymethylfurfural are proficient in functioning the dual role of H-bond donors and acceptors. The formation of H-bond acceptor/donor interactions between water molecules during inhibitor dissolution determines the inhibitors' solubility, which is governed by their ability to create H-bonds. The geometry optimizations were performed on all molecules. The stable structures of the molecules are presented in **Figure 4.106**.

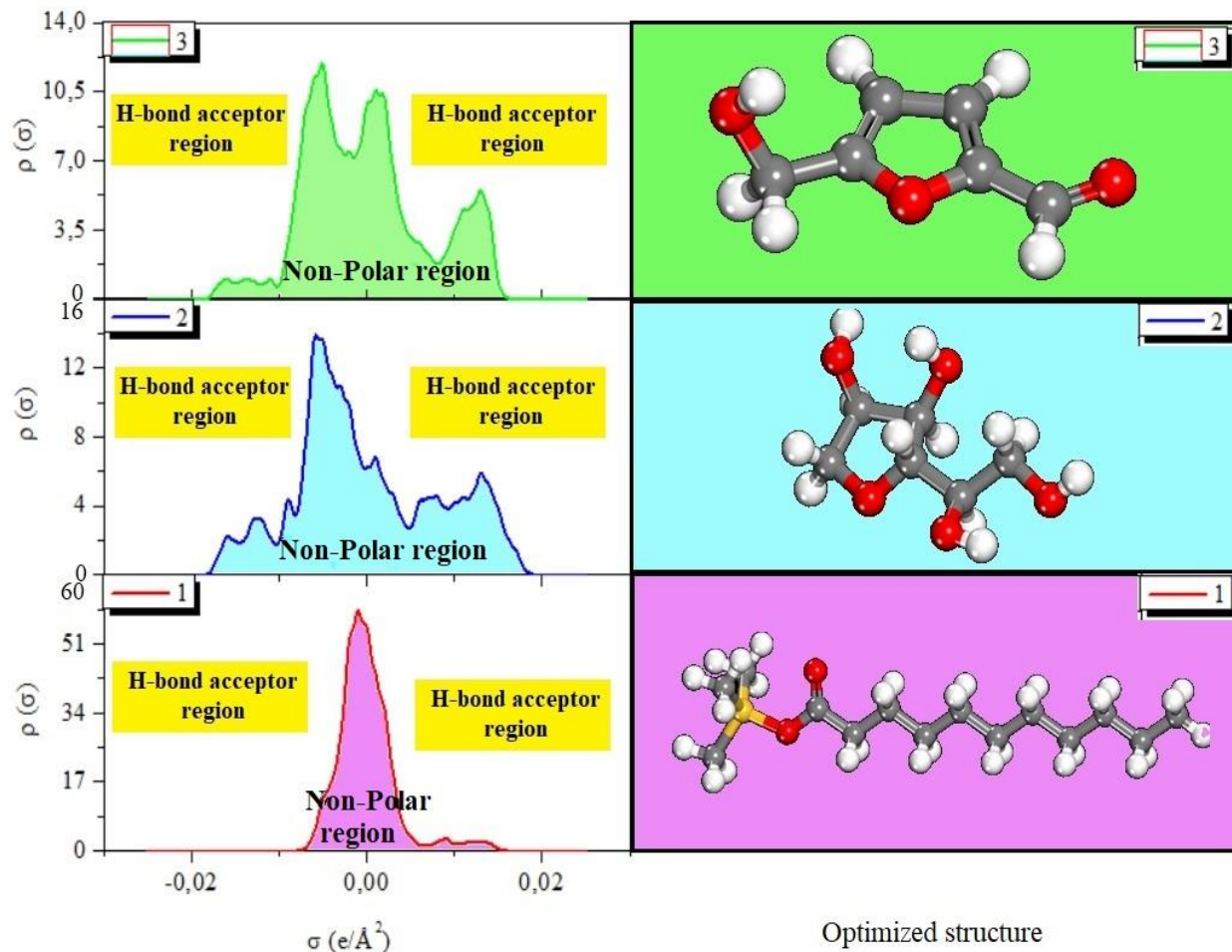


**Figure 4.106.** Charge density profiles ( $\sigma$ ) and optimized structure of the (1) Trans-2-decen-1-ol, trimethylsilyl ether, (2) 1,4-anhydro-d-glactitol and (3) 5-hydroxymethylfurfural molecules.

**Figure 4.107** illustrates the optimized geometric configurations of the investigated molecules, procured by global optimization of the vibration frequencies. The electronic charge dispersion on each atom in a molecule or other molecule is quantified by the Mulliken Atomic Charges (MAC). They offer a reliable and compelling marker of the atoms that are engaged in the mechanism of metal adsorption, in which metal ions bond to the surface of a substance. In the case of inhibitors, these are molecules that are added to the surface of a metal to prevent or reduce the rate of corrosion. The MAC values are calculated using quantum mechanical methods that take into account the electron density and the molecular configuration of the atoms. In the context of metal adsorption, the MAC values of the metal atoms over the surface and the inhibitor molecules can be compared to identify which atoms are most likely to interact.



The results of the analysis of the population of MAC presented in **Figure 4.107**, indeed show that the most negative oxygen atoms, have the highest values of the charge and can be preferential sites for the protonation (active centers). From **Figure 4.107**, it can be seen that the negative charges are located in the following volumes: O(-0.529) and the most negative atom is O in red O(-0.730) for the compound: (1) Trans-2-decen-1-ol, trimethylsilyl ether; O(-0.575), O(-0.731), O(-0.735), O(-0.752) and the most negative atom O(-0.756) for the compound: (2) 1,4-anhydro-d-glactitol and O(-0.486), O(-0.527) and the most negative atom O(-0.730) for compound (3) 5-hydroxymethylfurfural.

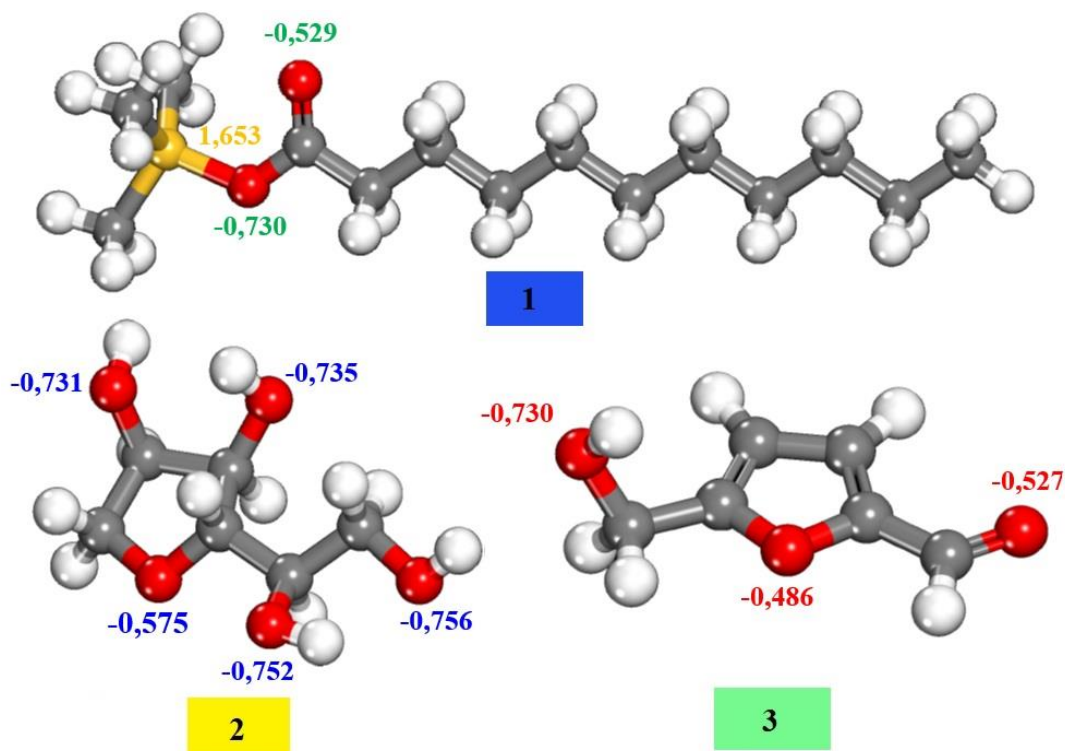


**Figure 4.107.** Distribution of the Mulliken Atomic Charges (MAC) values O and Si atoms of (1) Trans-2-decen-1-ol, trimethylsilyl ether, (2) 1,4-anhydro-d-glactitol and (3) 5-hydroxymethylfurfural molecules.

The optimized molecular structures as well as the HOMO, LUMO density distribution and ESP of the studied inhibitors are graphically depicted in **Figure 4.108**. It can be seen that the HOMO and LUMO density distribution has been distributed almost over all of the two molecules (2) 1,4-anhydro-d-glactitol and (3) 5-hydroxymethylfurfural molecules and in the molecule (1) Trans-2-decen-1-ol, trimethylsilyl ether has been distributed over the carboxyl group, owing to the presence

of the atoms of oxygen and carbon comprising several  $\pi$  and n electrons in chemical structures. Thus, the unoccupied orbital (d) of the iron atom can accept electrons from the molecules of the inhibitors to form a coordination jump. This implies that the iron atom can coordinate with the inhibitor molecules, leading to the formation of a stable complex.

The quantum parameters results obtained for the three major molecules of the plant extract, namely (1) Trans-2-decen-1-ol, trimethylsilyl ether, (2) 1,4-anhydro-d-glactitol and (3) 5-hydroxymethylfurfural, are collated in **Table 4.48**. The first works carried out mainly focused on the study of the properties of isolated molecules such as the level of the HOMO level, the level of the LUMO level and the energy difference ( $\Delta E$ ) between these two orbitals. These different data are determined owing to quantum calculations and a correlation with the inhibitory properties of the molecules is carried out. Different electronic properties have thus been linked to the inhibitory properties of molecules. By definition  $E_{\text{HOMO}}$  energy is often associated with the electron-donating capacity of the inhibitor. The effectiveness of inhibition increases with increasing  $E_{\text{HOMO}}$  values. The literature shows that the high  $E_{\text{HOMO}}$  energy values indicate that the inhibitor tends to donate electrons to appropriate acceptor molecules.  $E_{\text{LUMO}}$  indicates the ability of the molecule to accept electrons. The lowest  $E_{\text{LUMO}}$  value, suggests that the molecule readily accepts electrons from donor molecules. Trans-2-decen-1-ol, trimethylsilyl ether has the highest  $E_{\text{HOMO}}$ . This shows that Trans-2-decen-1-ol, trimethylsilyl ether's electron donating ability is strong. The  $\Delta N$  from the inhibitor to the metal surface from the inhibitor molecule to the metal atom was calculated using equation (17). If  $\Delta N < 3.6$ , the IE (%) increases with the molecule tends to donate electrons to the metal substrate. In this study, the three molecules studied presented values of  $\Delta N < 3.6$  (**Table 4.48**) and consequently, the targeted molecules are electron donors and the metal surface is an acceptor.

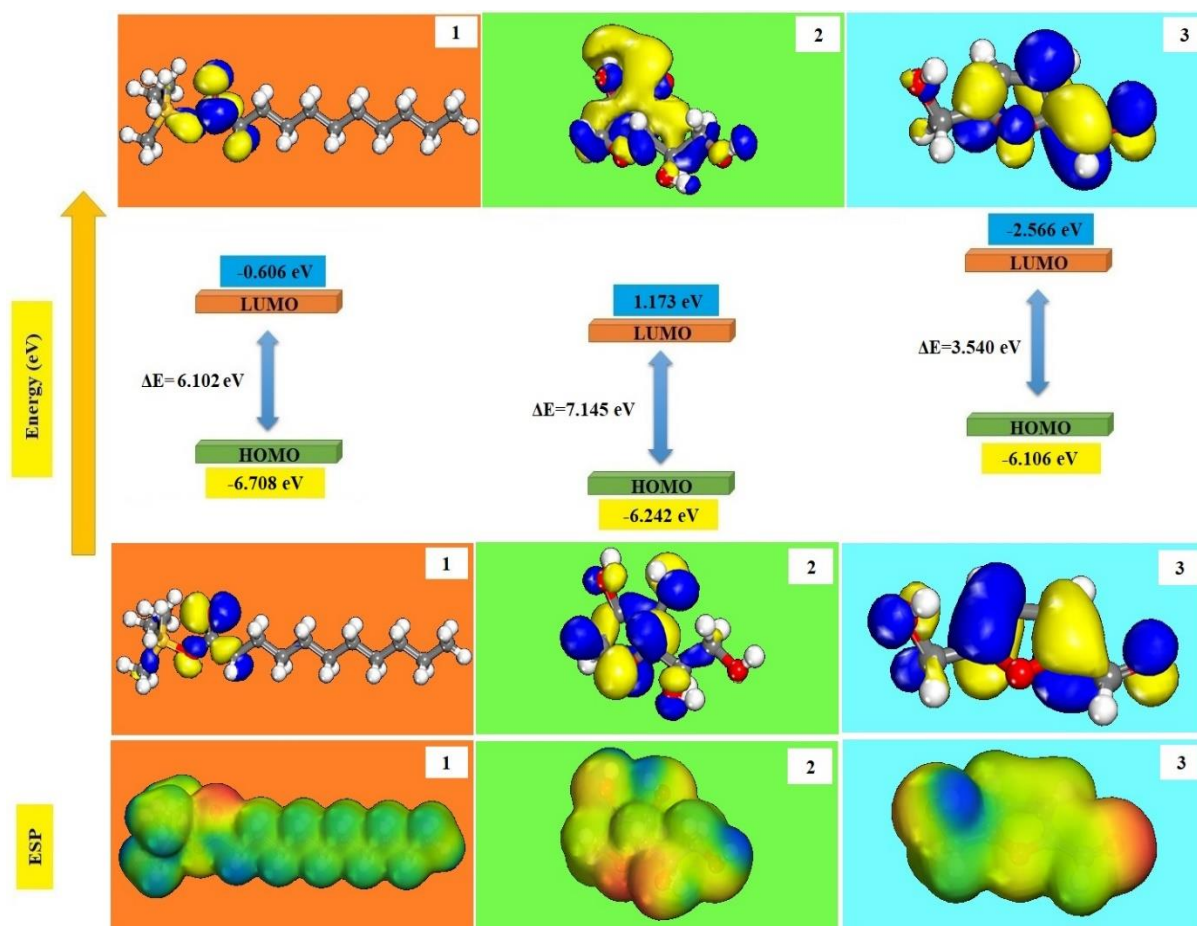


**Figure 4.108.** LUMO, HOMO and ESP pictures of (1) Trans-2-decen-1-ol, trimethylsilyl ether, (2) 1,4-anhydro-d-glactitol and (3) 5-hydroxymethylfurfural molecules

**Table 4.48**

Calculated theoretical parameters of the Trans-2-decen-1-ol, trimethylsilyl ether, 1,4-anhydro-d-glactitol and 5-hydroxymethylfurfural inhibitors.

Theoretical parameters	Trans-2-decen-1-ol, trimethylsilyl ether	1,4-anhydro-d-glactitol	5-hydroxymethylfurfural inhibitors
$E_{\text{HOMO}}$ (eV)	-6.708	-6.242	-6.106
$E_{\text{LUMO}}$ (eV)	-0.606	1.173	-2.566
$\Delta E$ (eV)	6.102	7.145	3.540
<b>I</b> (eV)	6.708	6.242	6.106
<b>A</b> (eV)	0.606	-1.173	2.566

$\chi$ (eV)	3.657	2.534	4.336
$\eta$ (eV)	3.051	3.707	1.770
$\sigma$ (eV <sup>-1</sup> )	0.327	0.269	0.564
$\Delta N$	0.547	0.602	0.752
$\Delta E_{\text{back-donation}}$	-0.762	-0.926	-0.442

In order to evaluate the active zones of the inhibitor molecule, the Molecular electrostatic potential (ESP) was determined and shown in **Figure 4.108**. ESP maps indicate the active electrophilic and nucleophilic zones are depicted by different colors. The potential values can be classified according to the following increasing sequence: red (negative electrostatic potential) \ yellow \ orange \ green (region of zero potential) \ blue (positive electrostatic potential). In all cases, the most electron-rich regions are generally presented around heteroatoms and conjugated double bonds.

#### 4.6.9.2. MC and MD simulations

The last few years have seen a rapid increase in the use of MC and MD simulations to understand the interaction across the corrosion inhibitor and the metal surface. MC and MD simulations are powerful computational techniques used to explore the function of molecules and materials at the atomic level. These simulations are increasingly being used in the field of corrosion inhibition to comprehend the mechanisms of corrosion inhibition and design new corrosion inhibitors. MD simulations involve the integration of the equations of motion for a system of atoms or molecules to simulate the behavior of the system over time. This allows researchers to investigate the behavior of corrosion inhibitors at the molecular level, such as their interactions with metal surfaces and the formation of protective films. MD simulations can also be used to study the impact of different environmental factors, including temperature and pH, on the potency of corrosion inhibitors. MC simulations, on the other hand, use random sampling to simulate the behavior of a system. In the context of corrosion inhibition, MC simulations can be used to explore the adsorption of corrosion inhibitors onto metal surfaces. This involves randomly placing inhibitor molecules over the substrate and calculating the free energy of adsorption. MC simulations can also be used to study the impact of various factors, including inhibitor concentration and temperature, on the adsorption behavior. The adsorption energy ( $E_{\text{ads}}$ ) may be deduced from

equation (18) to offer a quantifiable estimate of the incidence of this phenomenon. The adsorption equilibrium configurations of the studied inhibitory molecules (1) Trans-2-decen-1-ol, trimethylsilyl ether, (2) 1,4-anhydro-d-glactitol and (3) 5-hydroxymethylfurfural inhibitors on the Fe(1 1 0) substrate are presented in **Figure 4.109**. It is observed in **Figure 4.109**, that the inhibitor molecules are adsorbed with a position almost parallel to the plane of the metal surface. From these configurations, it can be concluded that the most significant interactions (chemisorption) are the interactions involving the Fe atoms with the oxygen atoms of the inhibitors with a maximum distance of less than 3.5 Å for the (1) Trans-2-decen-1-ol, trimethylsilyl ether, (2) 1,4-anhydro-d-glactitol and (3) 5-hydroxymethylfurfural inhibitors whereas the physical interactions between the inhibitory molecules and the iron atoms driven by Van Der Waals dispersion forces, may be contributed to the attraction of the net molecule surface.

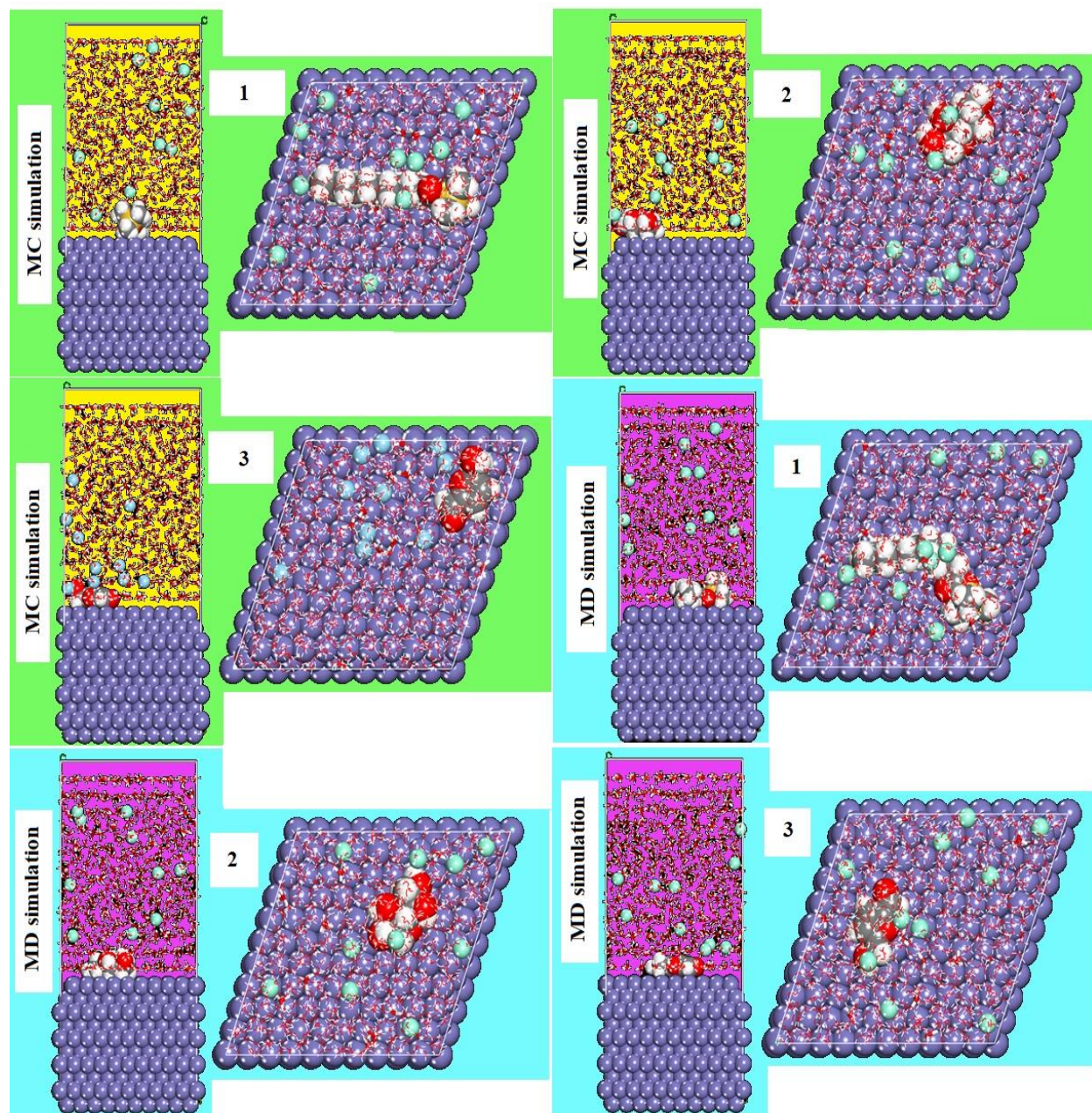


**Figure 4.109.** MC and MD simulation results in adsorption configurations and positions of the (1) Trans-2-decen-1-ol, trimethylsilyl ether, (2) 1,4-anhydro-d-glactitol and (3) 5-hydroxymethylfurfural inhibitors forms.

**Figure 4.110** indicated the distribution of the  $E_{\text{ads}}$  for the (1) Trans-2-decen-1-ol, trimethylsilyl ether, (2) 1,4-anhydro-d-glactitol and (3) 5-hydroxymethylfurfural inhibitors forms onto the Fe(110) substrate by MC simulations. According to these results, the values of  $E_{\text{ads}}$  can be classified according to the following order: Trans-2-decen-1-ol, trimethylsilyl ether (-147,75

kcal/mole) > 1,4-anhydro-d-glactitol (-126,95 kcal/mole) > 5-hydroxymethylfurfural (-102,75 kcal/mole) (Figure 4.110). The high values of binding energies are related to the stiffness of the interaction of molecules. It is found that the compound Trans-2-decen-1-ol, trimethylsilyl ether is the most effective inhibitor due to its molecular structure. The oxygen and Si atoms present in the compound Trans-2-decen-1-ol, trimethylsilyl ether is mainly responsible for the adsorption of corrosion inhibitor.

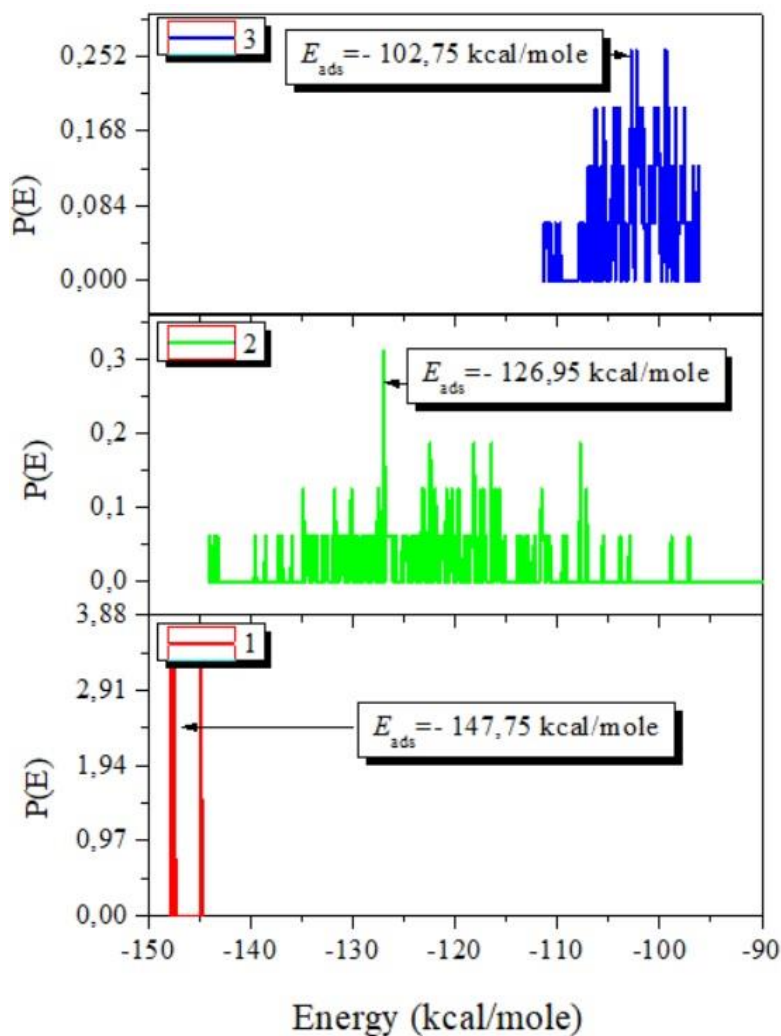


**Figure 4.110.** Distribution of the  $E_{ads}$  of the (1) Trans-2-decen-1-ol, trimethylsilyl ether, (2) 1,4-anhydro-d-glactitol and (3) 5-hydroxymethylfurfural on the Fe(1 1 0) surface via MC simulation.

The adsorption processes of corrosion inhibitors in dynamic condition was investigated by MD simulations. In addition to this, the adsorption positions of (1) Trans-2-decen-1-ol, trimethylsilyl ether, (2) 1,4-anhydro-d-glactitol and (3) 5-hydroxymethylfurfural inhibitors on the metal surface were also studied in dynamic conditions. The most energetic stable positions of inhibitors are found by studying the T (K) variations in MD simulation analyses. As seen in **Figure 4.111**, the T(K) drift is minimal, suggesting that the MD of our system was effective. The findings of this study are important for understanding the mechanisms of corrosion inhibition and for designing effective inhibitors that can protect metal surfaces from corrosion under dynamic conditions.

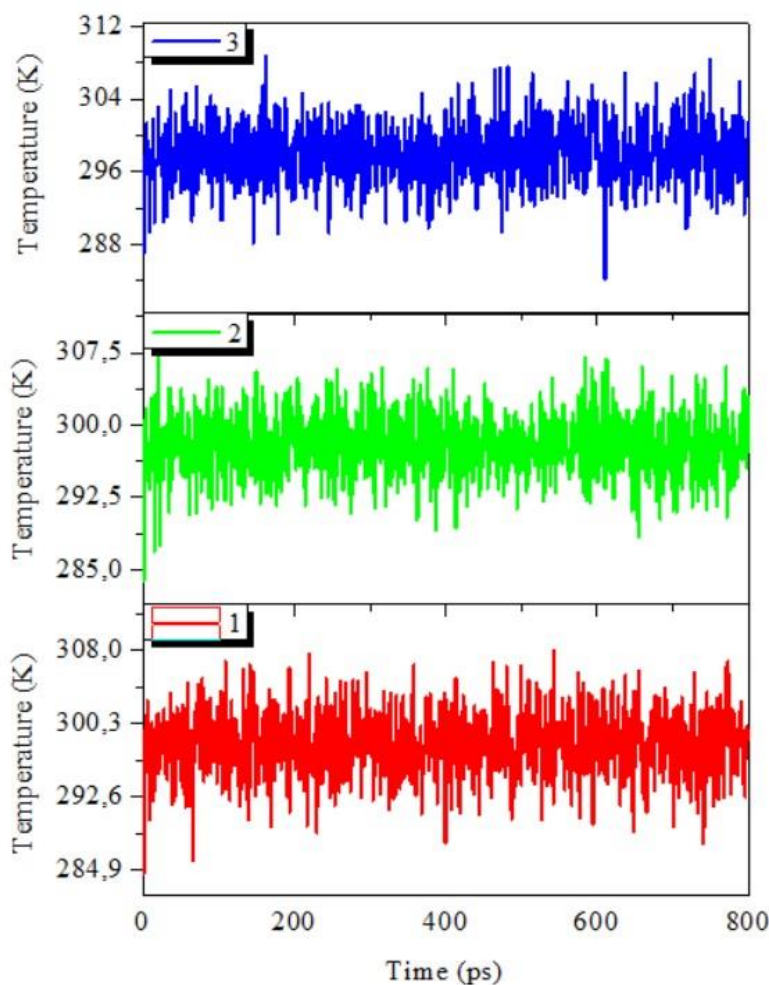


**Figure 4.111.** Temperature fluctuation during the MD run for the (1) Trans-2-decen-1-ol, trimethylsilyl ether, (2) 1,4-anhydro-d-glactitol and (3) 5-hydroxymethylfurfural inhibitors.



#### 4.6.9.3. Radial Distribution Function (RDF) analysis

RDF is a computational technique used to study the atomic structure of materials. In the context of the given statement, the RDF approach was applied to evaluate the bond length between Fe atoms and atoms of inhibitors (1) Trans-2-decen-1-ol, trimethylsilyl ether, (2) 1,4-anhydro-d-glactitol and (3) 5-hydroxymethylfurfural. By estimating bond length values, various kinds of bonds formed between these atoms were evaluated. The RDF analysis produced a graph that showed peaks at certain distances from the Fe(1 1 0) substrate, which provided crucial insights into the type of adsorption activity taking place on the metallic surface. Chemisorption is a type of adsorption that involves the emergence of a chemical bond between the adsorbate (inhibitor molecule) and the substrate (Fe(1 1 0) substrate). When the peak in the RDF graph was indulged between 1 and 3.5 Å, it was considered a chemisorption pathway. On the other hand, physisorption is a type of adsorption that comprises weak Van der Waals forces between the adsorbate and substrate. The RDF spikes were predicted to be evident at distances larger than 3.5 Å for physisorption.

The results of the RDF analysis showed that the inhibitor molecules were located very close to the metallic surface, as shown in **Figure 4.112**. As a result, the derived inhibitor molecules had a relatively significant interaction with the substrate, which endorses their inhibitory functionality. According to the findings of the RDF experiment, some of the molecules in the plant extract contact with the material surface by chemisorption, whilst the other molecules interact with the metal surface via physisorption. Overall, the RDF analysis provided valuable insights into the atomic structure of the inhibitory molecules and their interaction with the Fe(1 1 0) substrate, which is essential for understanding their inhibitory performance.

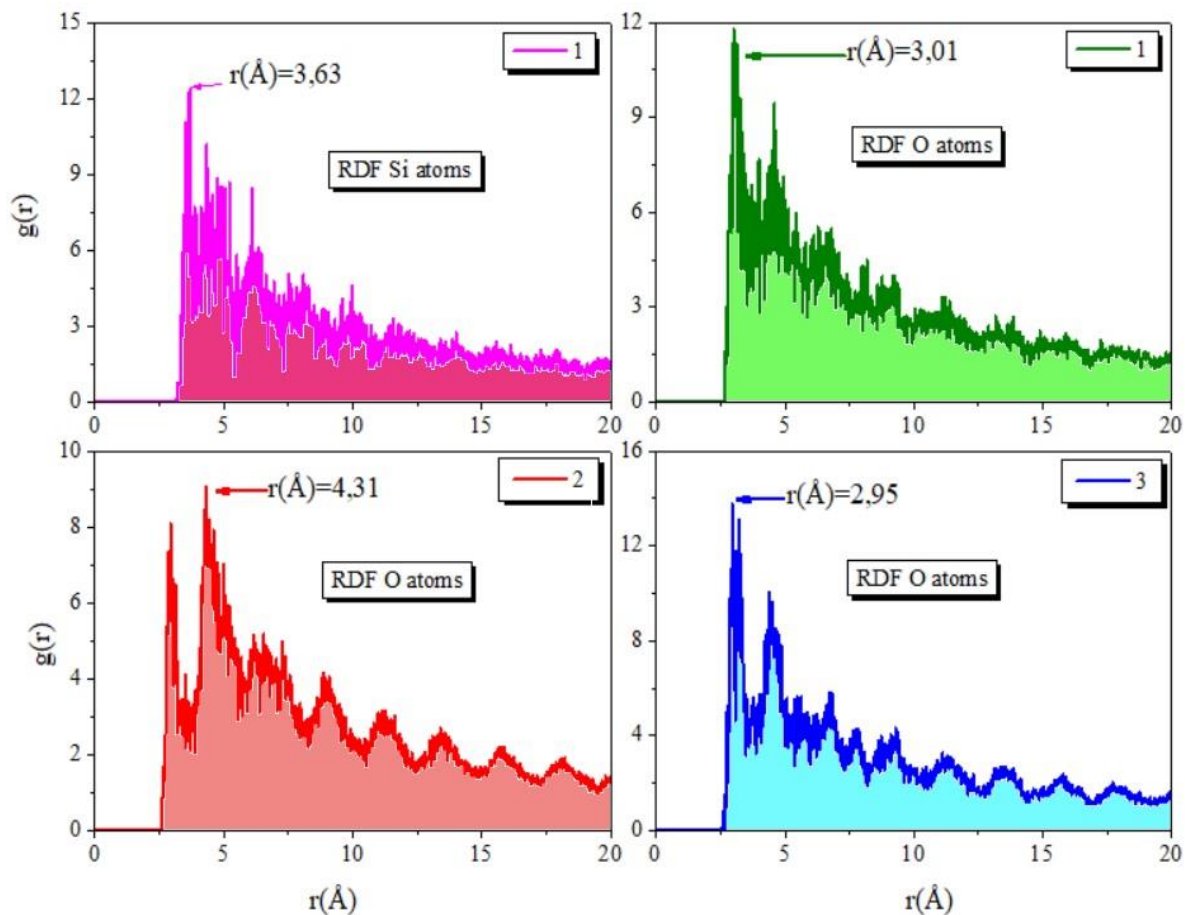


**Figure 4.112.** RDF of the Si and O atoms for (1) Trans-2-decen-1-ol, trimethylsilyl ether, (2) 1,4-anhydro-d-glactitol and (3) 5-hydroxymethylfurfural obtained via MD.

#### 4.6.10. Biodegradability of ATAE

The biodegradation of ATAE refers to the breakdown of the chemical structure of ATAE by microorganisms in the environment. Biodegradation is an important factor in determining the environmental fate of chemicals and their potential impact on the ecosystem. **Figure 4.113** shows the rate of biodegradation of ATAE after 28 days. The rate of biodegradation is represented by the percentage of ATAE that has degraded over time. At 28 days, the rate of CBE degradation accelerated and reached 89.15% computed using equation (19). This means that after 28 days, almost 90% of the ATAE had been degraded by microorganisms.

According to the North-East Atlantic Accords for Ecological Prevention, anything that degrades more than 60% in 28 days is considered rapidly biodegradable<sup>224</sup>. Since ATAE degraded more than

60% within 28 days, it can be classified as a rapidly biodegradable corrosion inhibitor. This information is important because it indicates that ATAE is likely to have a lower impact on the environment compared to non-biodegradable corrosion inhibitors. Rapid biodegradation means that ATAE is broken down into harmless substances more quickly, reducing the potential for environmental harm.

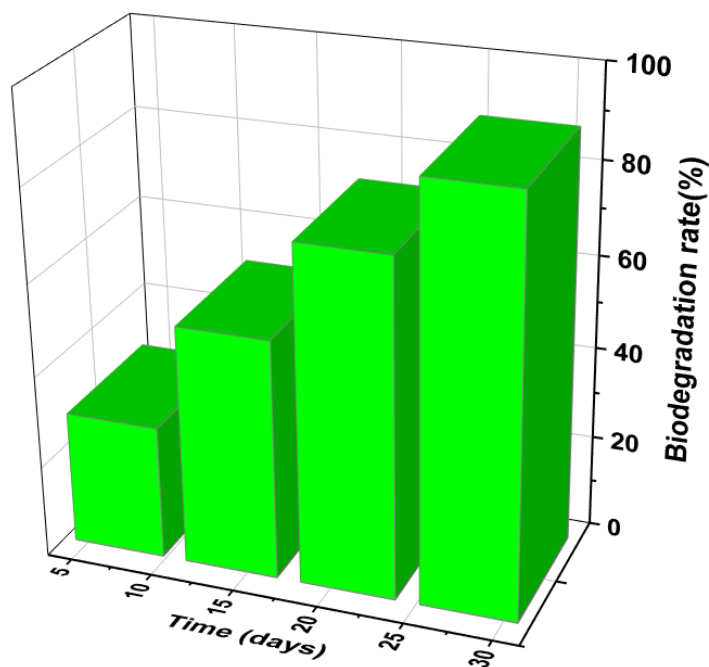


**Figure 4.113.** Biodegradability rate of ATAE.

---

---

***Chapter 5***

***Summary and Conclusion***

---

---

## **5.1. Summary**

The thesis titled “STUDY ON THE CORROSION INHIBITION EFFICIENCY OF SOME COMMON WEEDS ON MILD STEEL” involves the investigation of the corrosion inhibition potential of weeds such as *Cnicus Benedictus*, *Vicia Sativa*, *Asphodelus Tenuifolius*, *Polygonum cuspidatum*, *Thysanolaena latifolia* and *Trianthema Portulacstrum* for mild steel protection in a 0.5 M HCl solution. The study involved several experimental investigations, including UV-vis spectroscopy, FTIR, weight loss measurements, adsorption isotherms, and thermodynamic variables, EIS, PDP, surface morphology such as SEM, and contact angle measurement. Computational analysis such as DFT, Monte Carlo, and molecular dynamics simulations were also carried out. Beneath, the outcomes of each investigation have been summarized.

### **5.1.1. Experimental Investigations:**

#### **5.1.1.1. UV-vis spectroscopy:**

UV-vis spectroscopy was employed to study the electronic properties of the weed extract and its interaction with mild steel. The results showed a significant shift in the absorption peak towards the lower wavelength region, indicating the formation of a complex between the extract and mild steel. The shift in the absorption peak indicates that there is a change in the energy levels of the molecules involved in the reaction. The formation of a complex between the weed extract and mild steel suggests that there is an interaction between the two species. The shift towards the lower wavelength region could be attributed to the charge transfer between the weed extract and mild steel. The shift in the absorption peak can also be used to determine the binding constant of the inhibitor to the metal surface.

#### **5.1.1.2. FT-IR analysis:**

FT-IR was used to examine the functional groups present in the weed extract. The results revealed the presence of hydroxyl, carbonyl, and aromatic groups, which could be responsible for the extract's inhibition properties. Hydroxyl groups are known to have a high affinity for metals and can form strong bonds with the metal surface. Carbonyl groups can also form strong bonds with metals and are known to be effective in inhibiting the corrosion of metals. Aromatic groups, on the other hand, are known to form stable complexes with metals. The presence of such functional groups may be accountable for the significant corrosion inhibition efficacy of the selected weeds.

#### **5.1.1.3. Weight loss measurements:**

Weight loss measurements were carried out to determine the corrosion rate of mild steel in the presence and absence of the weed extract. The results showed a reduction in the corrosion rate with increasing concentration of the extract, indicating its potential as an inhibitor. The reduction in the corrosion rate can be attributed to the ability of the inhibitor to form a protective layer on the metal surface, which prevents the corrosive species from reaching the metal surface.

#### **5.1.1.4. Adsorption Isotherms and Thermodynamic Variables:**

Adsorption isotherms were used to investigate the adsorption behavior of the weed extracts on the mild steel surface. The Langmuir isotherm was used to model the adsorption process, and the maximum adsorption capacity was calculated. The Langmuir isotherm assumes monolayer adsorption and homogeneous surface adsorption. The adsorption data fit well with the Langmuir model, indicating that the adsorption process was monolayer and that the surface was homogeneous. The thermodynamic parameters such as Gibbs free energy, enthalpy, and entropy were calculated to evaluate the adsorption process's spontaneity, exothermic or endothermic nature, and randomness. The negative value of the Gibbs free energy indicated the spontaneity of the adsorption process, while the negative value of the enthalpy indicated the exothermic nature of the adsorption process. The positive value of the entropy indicated the randomness of the system. The thermodynamic parameters indicated that the adsorption process was spontaneous, exothermic, and random.

#### **5.1.1.5. Electrochemical Impedance Spectroscopy (EIS):**

Electrochemical impedance spectroscopy (EIS) was used to investigate the effect of the weed extracts on the corrosion behavior of the mild steel. The Nyquist and Bode plots were analyzed to obtain information about the corrosion process, such as the corrosion rate, charge transfer resistance, and double-layer capacitance. The Nyquist plot of the mild steel in the absence of the weed extracts showed a semicircle that represented the charge transfer resistance and a linear part that represented the Warburg impedance. The addition of the weed extracts decreased the charge transfer resistance and increased the double-layer capacitance, indicating the formation of a protective layer on the mild steel surface. Additionally, the Bode plot showed that the phase angle increased with frequency, indicating that the corrosion process was controlled by the charge

transfer mechanism. The addition of the weed extracts increased the phase angle, indicating a decrease in the corrosion rate of the mild steel.

#### **5.1.1.6. Potentiodynamic Polarization (PDP):**

Potentiodynamic polarization (PDP) measurements were used to evaluate the corrosion rate of the mild steel in the absence and presence of the weeds extracts. The PDP curves showed the anodic and cathodic branches of the polarization curve and the corrosion potential, which is the potential at which the anodic and cathodic currents are equal. The corrosion rate was calculated from the Tafel slopes. The results showed that the addition of the weed extracts to the 0.5 M HCl solution led to a significant decrease in the corrosion current density of the mild steel. The polarization curves of the mild steel in the presence of the weeds extracts showed a shift in the corrosion potential to more positive values and a decrease in the corrosion current density, indicating a decrease in the corrosion rate.

#### **5.1.1.7. Surface Morphology:**

##### **5.1.1.7.1. SEM:**

In this study, SEM was used to investigate the surface morphology of mild steel before and after exposure to 0.5 M HCl solution with and without weed extract inhibitors. The SEM images showed that the surface of mild steel without inhibitors was severely corroded, with extensive pitting and cracking evident on the surface. In contrast, the surface of mild steel with weed extract inhibitors was significantly smoother and less corroded. The inhibitors appeared to form a protective layer on the surface of the metal, which prevented the corrosive solution from reaching the metal surface. The SEM images also revealed that the surface of mild steel with inhibitors had a more uniform texture compared to the surface of mild steel without inhibitors. This suggests that the weed extract inhibitors can not only protect the metal from corrosion but also improve its surface morphology.

##### **5.1.1.7.2. Contact Angle Measurement:**

The contact angle of the mild steel surface with and without weed extract inhibitors was measured using a contact angle goniometer. The contact angle of the mild steel surface without inhibitors was found to be lower than that of the mild steel surface with inhibitors. This indicates that the surface of mild steel with weed extract inhibitors has a higher hydrophobicity, which reduces the contact between the metal surface and the corrosive solution. The higher hydrophobicity of the

mild steel surface in the presence of weed extract inhibitors can be attributed to the adsorption of the inhibitors onto the metal surface. The adsorption of the inhibitors can modify the surface properties of the metal, making it more hydrophobic and reducing the contact between the metal surface and the corrosive solution.

#### **5.1.1.8. Computational Analysis:**

##### **5.1.1.8.1. Density Functional Theory (DFT):**

Density functional theory (DFT) is a computational method used to study the electronic structure and properties of materials. In this study, DFT calculations were performed to investigate the electronic properties of the weed extract inhibitors. The DFT calculations showed that the weed extract inhibitors had a high electron density on the oxygen atom, which indicates that the oxygen atom is responsible for the adsorption of the inhibitors onto the mild steel surface. This is consistent with previous studies that have shown that several such heteroatoms such as oxygen and nitrogen atoms in organic inhibitors are responsible for their adsorption onto metal surfaces. Additionally, the calculated adsorption energy was found to be high, which suggests that the inhibitors can form strong bonds with the metal surface, leading to efficient corrosion inhibition. This is also consistent with experimental findings that showed that the weed extract inhibitors can form a protective layer on the mild steel surface, which prevents the corrosive solution from reaching the metal surface.

##### **5.1.1.8.2. Monte Carlo Simulation:**

Monte Carlo simulation is a computational method used to study the behavior of complex systems. In this study, Monte Carlo simulations were used to investigate the adsorption behavior of the weed extract inhibitors on the mild steel surface. The Monte Carlo simulations showed that the inhibitors can adsorb onto the mild steel surface through hydrogen bonding and van der Waals forces. Additionally, the simulation results indicated that the inhibitors can form a protective layer on the mild steel surface, which prevents the corrosive solution from reaching the metal surface. The Monte Carlo simulations also revealed that the inhibitors can self-assemble on the mild steel surface, forming a highly ordered adsorption layer. This is consistent with previous studies that have shown that organic inhibitors can form self-assembled monolayers (SAMs) on metal surfaces, which provide effective corrosion protection.

##### **5.1.1.8.3. Molecular Dynamics Simulation:**



The molecular dynamics simulations were used to investigate the interaction between the weed extract inhibitors and the mild steel surface. The results showed that the inhibitors can form strong bonds with the metal surface, leading to the formation of a stable adsorption layer. Additionally, the simulation results indicated that the inhibitors can reduce the mobility of the corrosive species near the metal surface, which leads to a reduction in the corrosion rate. The molecular dynamics simulations also indicated that the inhibitors can reduce the mobility of the corrosive species near the metal surface, which leads to a reduction in the corrosion rate. The inhibitors were observed to reduce the diffusion rate of the corrosive species towards the metal surface, leading to a decrease in the corrosion rate. This reduction in the corrosion rate was attributed to the formation of a stable adsorption layer that prevented the corrosive species from reaching the metal surface. Overall, molecular dynamics simulations were an important tool in the investigation of the corrosion inhibition potential of weed extracts for mild steel protection in 0.5 M HCl solution. The simulations provided valuable insights into the adsorption behavior of the inhibitors on the metal surface and their ability to form a protective layer. The results of the simulations were consistent with the experimental observations, providing further support for the effectiveness of weed extracts as corrosion inhibitors for mild steel in acidic environments. In addition, **Table 5.1** compares the efficacy of several sustainable inhibitors for mild steel corrosion in a corrosive solution, demonstrating the current investigated weed extracts i.e. *Cnicus Benedictus*, *Vicia Sativa*, *Asphodelus tenuifolius*, *Polygonum Cuspidatum*, *Thysanolaena Latifolia*, and *Trianthema Portulacastrum* significant potential as an effective inhibitor for mild steel corrosion in an acidic solution attained as >90% at an optimized concentration of 250 and 1000 ppm, which could be considered as an exemplary and reliable corrosion inhibitor for mild steel and other metals as well.

**Table 5.1**

Evaluation of inhibitory efficiency of numerous sustainable inhibitors for mild steel corrosion in the corrosive solution.

S. No.	Sustainable CI	Corrosive solution	Conc.	Maximal IE%	Ref's
1.	<i>Vernonia amygdalina</i>	1M HCl	500 ppm	80.85%	354
2.	<i>Inula viscosa</i>	1M HCl	700 ppm	92%	355
3.	<i>Citrullus lanatus</i>	1M HCl	800 ppm	91%	222

4.	<i>Gongronema latifolium</i>	0.5M HCl	1000 ppm	81.69%	356
5.	<i>Laurus nobilis</i>	1M HCl	400 ppm	92%	357
6.	<i>Artemisia herba alba</i>	1M HCl	1000 ppm	89%	358
7.	<i>Senecio anteuphorbium</i>	1M HCl	1000 ppm	91.10%	359
8.	<i>Ammi visnaga umbels</i>	1M HCl	700 ppm	84%	50
9.	<i>Oxalis stricta</i>	1N H <sub>2</sub> SO <sub>4</sub>	750 ppm	92.6%	360
10.	<i>Clinopodium acinos</i>	1M HCl	300 ppm	87.9%	361
11.	<i>Spilanthes uliginosa</i>	2M HCl	500 ppm	90%	133
12.	<i>Cnicus benedictus</i>	0.5M HCl	1000 ppm	92.45%	Currently investigated inhibitor
13.	<i>Vicia Sativa</i>	0.5M HCl	1000 ppm	91.24%	Currently investigated inhibitor
14.	<i>Asphodelus Tenuifolius</i>	0.5M HCl	250ppm	94.40%	Currently investigated inhibitor
15.	<i>Polygonum cuspidatum</i>	0.5M HCl	1000 ppm	96.71%	Currently investigated inhibitor
16.	<i>Thysanolaena latifolia</i>	0.5M HCl	1000 ppm	93.90%	Currently investigated inhibitor
17.	<i>Trianthema Portulacstrum</i>	0.5M HCl	1000 ppm	94.33%	Currently investigated inhibitor

## 5.2. Conclusion

In conclusion, the research conducted on the corrosion inhibition potential of weeds extracts for mild steel protection in 0.5 M HCl solution using a range of experimental techniques and computational analysis showed promising results. The attained corrosion inhibitors such as *Cnicus benedictus* and *Vicia Sativa* showed promising inhibition efficiencies of 92.45% and 91.24%, respectively. *Asphodelus Tenuifolius* stood out with an impressive 94.40% efficiency even at a lower concentration of 250ppm. *Polygonum cuspidatum* revealed to be the maximum at 96.71% efficiency, making it a strong eco-benign corrosion inhibitor. Furthermore, *Thysanolaena latifolia* demonstrated a notable 93.90% efficiency, and *Trianthema Portulacstrum* showed promising efficiency of 94.33%. These results highlight the potential of these inhibitors for mild steel corrosion protection. Additionally, the adsorption isotherms and thermodynamic variables indicated that the adsorption of the weed extracts on the mild steel surface was a physisorption

process driven mainly by van der Waals forces and hydrogen bonding. The EIS and PDP results demonstrated that the weed extracts significantly reduced the corrosion rate and formed a protective film on the mild steel surface. The surface morphology analysis using SEM and contact angle measurement showed that the weed extracts prevented severe corrosion damage such as pitting and cracking, indicating their potential as effective corrosion inhibitors. Moreover, computational analyses involving Density Functional Theory (DFT), Monte Carlo simulations, and molecular dynamics simulations complemented the experimental findings by offering deeper insights into the adsorption behavior and corrosion inhibition mechanism of the weed extracts. In conclusion, these findings provide invaluable insights into the potential of natural inhibitors, specifically weed extracts, as sustainable and cost-effective alternatives to traditional chemical inhibitors for corrosion protection.

### **5.3. Future scope of the work**

The research conducted on the corrosion inhibition potential of weed extracts for mild steel protection in 0.5 M HCl solution using a range of experimental techniques and computational analysis has provided valuable insights into the development of sustainable corrosion protection strategies. However, there is still scope for further research in this area to explore the potential of natural inhibitors in industrial applications and address the limitations of the current study. One possible future direction of research is to investigate the effectiveness of weed extracts as corrosion inhibitors under different environmental conditions. For example, the study could be extended to investigate the performance of the weed extracts in other corrosive environments such as acidic solutions of different concentrations or in the presence of other aggressive ions such as chloride, sulfate, and nitrate. This would provide a more comprehensive understanding of the practicality and effectiveness of using weed extracts as corrosion inhibitors in various industrial applications. Another potential area of research could be to explore the potential of weed extracts as a sustainable alternative to traditional chemical inhibitors in other applications such as the protection of concrete structures, pipelines, and storage tanks. The use of weed extracts as corrosion inhibitors could potentially offer several advantages over traditional chemical inhibitors, including lower environmental impact, cost-effectiveness, and ease of application.

Additionally, the molecular dynamics simulations could be extended to investigate the effect of different structural parameters of the weed extracts, such as functional groups and molecular

weight, on their adsorption behavior and corrosion inhibition potential. This would provide a better understanding of the structure-property relationship of the weed extracts and could aid in the development of more effective and efficient natural inhibitors. Furthermore, the weed extracts could be combined with other corrosion inhibitors or corrosion protection strategies to enhance their performance. For example, the weed extracts could be used in conjunction with inhibitors that function through different mechanisms or applied in combination with other protective coatings to create a more robust and durable corrosion protection system. Finally, the scale-up of the production of weed extracts for industrial applications could be investigated. The large-scale production of weed extracts for corrosion inhibition could have significant implications for the development of sustainable corrosion protection strategies and could potentially offer a more cost-effective and environmentally friendly alternative to traditional chemical inhibitors.

## References

- (1) Bashir, S.; Sharma, V.; Lgaz, H.; Chung, I.-M.; Singh, A.; Kumar, A. The Inhibition Action of Analgin on the Corrosion of Mild Steel in Acidic Medium: A Combined Theoretical and Experimental Approach. *J. Mol. Liq.* **2018**, *263*, 454–462. <https://doi.org/10.1016/j.molliq.2018.04.143>.
- (2) Fares, M. M.; Maayta, A. K.; Al-Qudah, M. M. Pectin as Promising Green Corrosion Inhibitor of Aluminum in Hydrochloric Acid Solution. *Corros. Sci.* **2012**, *60*, 112–117. <https://doi.org/10.1016/j.corsci.2012.04.002>.
- (3) Grassino, A. N.; Halambek, J.; Djaković, S.; Rimac Brnčić, S.; Dent, M.; Grabarić, Z. Utilization of Tomato Peel Waste from Canning Factory as a Potential Source for Pectin Production and Application as Tin Corrosion Inhibitor. *Food Hydrocoll.* **2016**, *52*, 265–274. <https://doi.org/10.1016/j.foodhyd.2015.06.020>.
- (4) Gudic, S.; Vrsalovic, L.; Kliškic, M.; Jerkovic, I.; Radonic, A.; Zekic, M. Corrosion Inhibition of Aa 5052 Aluminium Alloy in Nacl Solution by Different Types of Honey. *Int. J. Electrochem. Sci.* **2016**, *11* (2), 998–1011.
- (5) Finšgar, M.; Jackson, J. Application of Corrosion Inhibitors for Steels in Acidic Media for the Oil and Gas Industry: A Review. *Corros. Sci.* **2014**, *86*, 17–41. <https://doi.org/10.1016/j.corsci.2014.04.044>.
- (6) Bashir, S.; Thakur, A.; Lgaz, H.; Chung, I.-M.; Kumar, A. Computational and Experimental Studies on Phenylephrine as Anti-Corrosion Substance of Mild Steel in Acidic Medium. *J. Mol. Liq.* **2019**, *293*, 111539. <https://doi.org/10.1016/j.molliq.2019.111539>.
- (7) Bashir, S.; Lgaz, H.; Chung, I. I. I. M.; Kumar, A. Potential of Venlafaxine in the Inhibition of Mild Steel Corrosion in HCl: Insights from Experimental and Computational Studies. *Chem. Pap.* **2019**, *73* (9), 2255–2264. <https://doi.org/10.1007/s11696-019-00775-0>.
- (8) Bashir, S.; Sharma, V.; Singh, G.; Lgaz, H.; Salghi, R.; Singh, A.; Kumar, A. Electrochemical Behavior and Computational Analysis of Phenylephrine for Corrosion

- Inhibition of Aluminum in Acidic Medium. *Metall. Mater. Trans. A* **2019**, *50* (1), 468–479. <https://doi.org/10.1007/s11661-018-4957-9>.
- (9) Nawafleh, E.; Irshadat, M.; Bataineh, T.; Muhaidat, R.; Alomary, A. The Effects of Inula Viscosa Extract on Corrosion of Copper in NaOH Solution. *Res. J. Chem. Sci.* **2012**, *2* (9), 37–41.
- (10) Osarolube, E.; James, A. Corrosion Inhibition of Copper Using African Black Velvet Tamarind (*Dialium Indium*) Extract in Sulphuric Acid Environment. *J. Sci. Res. Reports* **2014**, *3* (18), 2450–2458. <https://doi.org/10.9734/jsrr/2014/9434>.
- (11) S-Fouda, A.-E.-A.; El-Dossoki, F.; El-Nadr, H.-A.; El-Hussein, A. Moringa Oleifera Plant Extract as a Copper Corrosion Inhibitor in Binary Acid Mixture (HNO<sub>3</sub> + H<sub>3</sub>PO<sub>4</sub>). *Zast. Mater.* **2018**, *59* (3), 422–435. <https://doi.org/10.5937/zasmat1803422f>.
- (12) Sangeetha, T. V.; Fredimoses, M. Inhibition of Mild Copper Metal Corrosion in HNO<sub>3</sub> Medium by Acid Extract of Azadirachta Indica Seed. *E-Journal Chem.* **2011**, *8* (SUPPL. 1), 1–7. <https://doi.org/10.1155/2011/135952>.
- (13) Raghavendra, N.; Bhat, J. I. Chemical Components of Mature Areca Nut Husk Extract as a Potential Corrosion Inhibitor for Mild Steel and Copper in Both Acid and Alkali Media. *Chem. Eng. Commun.* **2018**, *205* (2), 145–160. <https://doi.org/10.1080/00986445.2017.1370709>.
- (14) Bashir, S.; Lgaz, H.; Chung, I. M.; Kumar, A. Effective Green Corrosion Inhibition of Aluminium Using Analgin in Acidic Medium: An Experimental and Theoretical Study. *Chem. Eng. Commun.* **2020**, *1* (0), 1–10. <https://doi.org/10.1080/00986445.2020.1752680>.
- (15) Bashir, S.; Singh, G.; Kumar, A. Shatavari (*Asparagus Racemosus*) as Green Corrosion Inhibitor of Aluminium in Acidic Medium. *J. Mater. Environ. Sci.* **2017**, *8* (12), 4284–4291.
- (16) Bashir, S.; Singh, G.; Kumar, A. An Investigation on Mitigation of Corrosion of Aluminium by *Origanum Vulgare* in Acidic Medium. *Prot. Met. Phys. Chem. Surfaces* **2018**, *54* (1), 148–152. <https://doi.org/10.1134/S2070205118010185>.
- (17) Ongun Yüce, A.; Doğru Mert, B.; Kardaş, G.; Yazıcı, B. Electrochemical and Quantum

- Chemical Studies of 2-Amino-4-Methyl-Thiazole as Corrosion Inhibitor for Mild Steel in HCl Solution. *Corros. Sci.* **2014**, *83*, 310–316.  
<https://doi.org/10.1016/j.corsci.2014.02.029>.
- (18) Qiang, Y.; Zhang, S.; Xu, S.; Guo, L.; Chen, N.; Obot, I. B. Effective Protection for Copper Corrosion by Two Thiazole Derivatives in Neutral Chloride Media: Experimental and Computational Study. *Int. J. Electrochem. Sci.* **2016**, *11* (4), 3147–3163.  
<https://doi.org/10.20964/110403147>.
- (19) Zaki, A. Types of Corrosion : Materials and Environments. *Princ. Corros. Eng. Corros. Control* **2006**, 120–270.
- (20) Miralrio, A.; Vázquez, A. E. Plant Extracts as Green Corrosion Inhibitors for Different Metal Surfaces and Corrosive Media: A Review. *Processes* **2020**, *8* (8), 942.  
<https://doi.org/10.3390/PR8080942>.
- (21) Berrissoul, A.; Loukili, E.; Mechbal, N.; Benhiba, F.; Guenbour, A.; Dikici, B.; Zarrouk, A.; Dafali, A. Anticorrosion Effect of a Green Sustainable Inhibitor on Mild Steel in Hydrochloric Acid. *J. Colloid Interface Sci.* **2020**, *580*, 740–752.  
<https://doi.org/10.1016/j.jcis.2020.07.073>.
- (22) Chauhan, D. S.; Mouaden, K. EL; Quraishi, M. A.; Bazzi, L. Aminotriazolethiol-Functionalized Chitosan as a Macromolecule-Based Bioinspired Corrosion Inhibitor for Surface Protection of Stainless Steel in 3.5% NaCl. *Int. J. Biol. Macromol.* **2020**, *152*, 234–241. <https://doi.org/10.1016/j.ijbiomac.2020.02.283>.
- (23) Umoren, S. A.; Solomon, M. M.; Obot, I. B.; Suleiman, R. K. A Critical Review on the Recent Studies on Plant Biomaterials as Corrosion Inhibitors for Industrial Metals. *J. Ind. Eng. Chem.* **2019**, *76*, 91–115. <https://doi.org/10.1016/j.jiec.2019.03.057>.
- (24) Koumya, Y.; Idouhli, R.; Oukhrib, A.; Khadiri, M.; Abouelfida, A.; Benyaich, A. Synthesis, Electrochemical, Thermodynamic, and Quantum Chemical Investigations of Amino Cadalene as a Corrosion Inhibitor for Stainless Steel Type 321 in Sulfuric Acid 1M. *Int. J. Electrochem.* **2020**, *2020*, 1–10. <https://doi.org/10.1155/2020/5620530>.
- (25) Emembolu, L. N.; Onukwuli, O. D.; Okafor, V. N. Characterization and Optimization

- Study of Epiphyllum Oxypetalum Extract as Corrosion Inhibitor for Mild Steel in 3 M H<sub>2</sub>SO<sub>4</sub> Solutions. **2020**, *145* (April), 256–273.
- (26) Khaled, R. H.; Abdel-Gaber, A. M.; Rahal, H. T.; Awad, R. A Potential Green Anti-Scaling and Corrosion Inhibitor for Mild Steel in Brine Solution. *Int. J. Electrochem. Sci.* **2020**, *15*, 6790–6801. <https://doi.org/10.20964/2020.07.54>.
- (27) Fekkar, G.; Yousfi, F.; Elmsellem, H.; Aiboudi, M.; Ramdani, M.; Abdel-Rahman; Hammouti, B.; Bouyazza, L. Eco-Friendly Chamaerops Humilis L. Fruit Extract Corrosion Inhibitor for Mild Steel in 1 M HCL. *Int. J. Corros. Scale Inhib.* **2020**, *9* (2), 446–459. <https://doi.org/10.17675/2305-6894-2020-9-2-4>.
- (28) Verma, C.; Chauhan, D. S.; Quraishi, M. A. Drugs as Environmentally Benign Corrosion Inhibitors for Ferrous and Nonferrous Materials in Acid Environment: An Overview. *J. Mater. Environ. Sci.* **2017**, *8* (11), 4040–4051.
- (29) Fayomi, O. S. I.; Akande, I. G.; Odigie, S. Economic Impact of Corrosion in Oil Sectors and Prevention: An Overview. *J. Phys. Conf. Ser.* **2019**, *1378* (2). <https://doi.org/10.1088/1742-6596/1378/2/022037>.
- (30) Al-Qudah, M. A.; Al-Keifi, H. G.; Al-Momani, I. F.; Abu-Orabi, S. T. Capparis Aegyptia as a Green Inhibitor for Aluminum Corrosion in Alkaline Media. *Int. J. Corros. Scale Inhib.* **2020**, *9* (1), 201–218. <https://doi.org/10.17675/2305-6894-2020-9-1-12>.
- (31) Aourabi, S.; Driouch, M.; Sfaira, M.; Mahjoubi, F.; Hammouti, B.; Verma, C.; Ebenso, E. E.; Guo, L. Phenolic Fraction of Ammi Visnaga Extract as Environmentally Friendly Antioxidant and Corrosion Inhibitor for Mild Steel in Acidic Medium. *J. Mol. Liq.* **2021**, *323* (December), 114950. <https://doi.org/10.1016/j.molliq.2020.114950>.
- (32) Prabhu, P. R.; Prabhu, D.; Rao, P. Analysis of Garcinia Indica Choisy Extract as Eco-Friendly Corrosion Inhibitor for Aluminum in Phosphoric Acid Using the Design of Experiment. *J. Mater. Res. Technol.* **2020**, *9* (3), 3622–3631. <https://doi.org/10.1016/j.jmrt.2020.01.100>.
- (33) Verma, C.; Ebenso, E. E.; Quraishi, M. A. Molecular Structural Aspects of Organic Corrosion Inhibitors: Influence of –CN and –NO<sub>2</sub> Substituents on Designing of Potential



- Corrosion Inhibitors for Aqueous Media. *J. Mol. Liq.* **2020**, *316*, 113874.  
<https://doi.org/10.1016/j.molliq.2020.113874>.
- (34) Basik, M.; Mobin, M. Chondroitin Sulfate as Potent Green Corrosion Inhibitor for Mild Steel in 1 M HCl. *J. Mol. Struct.* **2020**, *1214*, 128231.  
<https://doi.org/10.1016/j.molstruc.2020.128231>.
- (35) Vasyliiev, G.; Vorobyova, V.; Zhuk, T. Raphanus Sativus L. Extract as a Scale and Corrosion Inhibitor for Mild Steel in Tap Water. *J. Chem.* **2020**, *2020*, 1–9.  
<https://doi.org/10.1155/2020/5089758>.
- (36) Bhawsar, J.; Jain, P. K.; Jain, P. Experimental and Computational Studies of Nicotiana Tabacum Leaves Extract as Green Corrosion Inhibitor for Mild Steel in Acidic Medium. *Alexandria Eng. J.* **2015**, *54* (3), 769–775. <https://doi.org/10.1016/j.aej.2015.03.022>.
- (37) Cordeiro, R. F. B.; Belati, A. J. S.; Perrone, D.; D’Elia, E. Coffee Husk as Corrosion Inhibitor for Mild Steel in HCl Media. *Int. J. Electrochem. Sci.* **2018**, *13* (12), 12188–12207. <https://doi.org/10.20964/2018.12.29>.
- (38) Boumhara, K.; Harhar, H.; Tabyaoui, M.; Bellaouchou, A.; Guenbour, A.; Zarrouk, A. Corrosion Inhibition of Mild Steel in 0.5 M H<sub>2</sub>SO<sub>4</sub> Solution by Artemisia Herba-Alba Oil. *J. Bio- Tribo-Corrosion* **2019**, *5* (1), 1–9. <https://doi.org/10.1007/s40735-018-0202-8>.
- (39) Ejikeme, P. M.; Umana, S. G.; Menkiti, M. C.; Onukwuli, O. D. Inhibition of Mild Steel and Aluminium Corrosion in 1M H<sub>2</sub>SO<sub>4</sub> by Leaves Extract of African Breadfruit. *Int. J. Mater. Chem.* **2015**, *5* (1), 14–23. <https://doi.org/10.5923/j.ijmc.20150501.03>.
- (40) Ramdani, M.; Elmsellem, H.; Elkhiaati, N.; Haloui, B.; Aouniti, A.; Ramdani, M.; Ghazi, Z.; Chetouani, A.; Hammouti, B. Caulerpa Prolifera Green Algae Using as Eco-Friendly Corrosion Inhibitor for Mild Steel in 1 M HCl Media. *Der Pharma Chem.* **2015**, *7* (2), 67–76.
- (41) Bashir, S.; Thakur, A.; Lgaz, H.; Chung, I. M.; Kumar, A. Corrosion Inhibition Efficiency of Bronopol on Aluminium in 0.5 M HCl Solution: Insights from Experimental and Quantum Chemical Studies. *Surfaces and Interfaces* **2020**, *20* (April), 100542.  
<https://doi.org/10.1016/j.surfin.2020.100542>.

- (42) Bashir, S.; Thakur, A.; Lgaz, H.; Chung, I.-M.; Kumar, A. Corrosion Inhibition Performance of Acarbose on Mild Steel Corrosion in Acidic Medium: An Experimental and Computational Study. *Arab. J. Sci. Eng.* **2020**, *45* (6), 4773–4783.  
<https://doi.org/https://doi.org/10.1007/s13369-020-04514-6>.
- (43) Kumar, A.; Bashir, S. Ethambutol: A New and Effective Corrosion Inhibitor of Mildsteel in Acidic Medium. *Russ. J. Appl. Chem.* **2016**, *89* (7), 1158–1163.  
<https://doi.org/10.1134/S1070427216070168>.
- (44) Parveen, G.; Bashir, S.; Thakur, A.; Saha, S. K.; Banerjee, P.; Kumar, A. Experimental and Computational Studies of Imidazolium Based Ionic Liquid 1-Methyl- 3-Propylimidazolium Iodide on Mild Steel Corrosion in Acidic Solution Experimental and Computational Studies of Imidazolium Based Ionic Liquid 1-Methyl- 3-Propylimidazolium. *Mater. Res. Express* **2020**, *7* (1), 016510.  
<https://doi.org/https://doi.org/10.1088/2053-1591/ab5c6a>.
- (45) Rajeev, P.; Surendranathan, A. O.; Murthy, C. S. N. Corrosion Mitigation of the Oil Well Steels Using Organic Inhibitors-A Review. *J. Mater. Environ. Sci.* **2012**, *3* (5), 856–869.
- (46) Prabha, S. S.; Rathish, R. J.; Dorothy, R.; Brindha, G.; Pandiarajan, M.; Al-Hashem, A.; Rajendran, S. Corrosion Problems in Petroleum Industry and Their Solution. *Eur. Chem. Bull.* **2014**, *3* (3), 300–307. <https://doi.org/10.17628/ECB.2014.3.300>.
- (47) Muthukumar, N.; Ilangovan, A.; Maruthamuthu, S.; Palaniswamy, N.; Kimura, A. 1-Aminoanthraquinone Derivatives as a Novel Corrosion Inhibitor for Carbon Steel API 5L-X60 in White Petrol-Water Mixtures. *Mater. Chem. Phys.* **2009**, *115* (1), 444–452.  
<https://doi.org/10.1016/j.matchemphys.2008.12.027>.
- (48) Marzorati, S.; Verotta, L.; Trasatti, S. P. Green Corrosion Inhibitors from Natural Sources and Biomass Wastes. *Molecules* **2019**, *24* (1), 48.  
<https://doi.org/10.3390/molecules24010048>.
- (49) Abeng, F. E.; Idim, V. D. Green Corrosion Inhibitor for Mild Steel in 2 M HCl Solution : Flavonoid Extract of Erigeron Floribundus. **2018**, *98* (April), 89–99.
- (50) Zaher, A.; Aslam, R.; Lee, H. S.; Khafouri, A.; Boufellous, M.; Alrashdi, A. A.; El aoufir,

- Y.; Lgaz, H.; Ouhssine, M. A Combined Computational & Electrochemical Exploration of the Ammi Visnaga L. Extract as a Green Corrosion Inhibitor for Carbon Steel in HCl Solution. *Arab. J. Chem.* **2022**, *15* (2), 103573.  
<https://doi.org/10.1016/j.arabjc.2021.103573>.
- (51) Mahfoud, H.; Rouag, N.; Boudiba, S.; Benahmed, M.; Morakchi, K.; Akkal, S. Mathematical and Electrochemical Investigation of Lamium Flexuosum Extract as Effective Corrosion Inhibitor for CS in Acidic Solution Using Multidimensional Minimization Program System. *Arab. J. Sci. Eng.* **2022**, *47* (5), 6605–6616.  
<https://doi.org/10.1007/s13369-021-06546-y>.
- (52) Idouhli, R.; Oukhrib, A.; Khadiri, M.; Zakir, O.; Aityoub, A.; Abouelfida, A.; Benharref, A.; Benyaich, A. Understanding the Corrosion Inhibition Effectiveness Using Senecio Anteuphorbium L. Fraction for Steel in Acidic Media. *J. Mol. Struct.* **2021**, *1228* (October), 129478. <https://doi.org/10.1016/j.molstruc.2020.129478>.
- (53) Fayomi, O. M.; Chahul, H. F.; Ike, D. C.; Ndukwe, G. I.; Phoebe, I. M. Thermodynamic and Adsorption Study of the Corrosion Inhibition of Mild Steel by Aframomum Chrysanthum Extract in 0.1 M Hydrochloric Acid Solution. *Asian J. Appl. Chem. Res.* **2021**, *8* (4), 64–73. <https://doi.org/10.9734/ajacr/2021/v8i430200>.
- (54) Bu, U.; Me, O.; To, M. Phytochemical Constituents of Taraxacum Officinale Leaves as Eco-Friendly and Nontoxic Organic Inhibitors for Stainless Steel Corrosion in 0.2 M HCl Acid Medium. *Int. J. Chem. Sci. www.chemicaljournals.com* **2018**, *2* (November), 35–43.
- (55) Guedes, L. A. L.; Bacca, K. G.; Lopes, N. F.; da Costa, E. M. Tannin of Acacia Mearnsii as Green Corrosion Inhibitor for AA7075-T6 Alluminum Alloy in Acidic Medium. *Mater. Corros.* **2019**, *70* (7), 1288–1297. <https://doi.org/10.1002/maco.201810667>.
- (56) Raghavendra, N. Latest Exploration on Natural Corrosion Inhibitors for Industrial Important Metals in Hostile Fluid Environments: A Comprehensive Overview. *J. Bio-Tribo-Corrosion* **2019**, *5* (3). <https://doi.org/10.1007/s40735-019-0240-x>.
- (57) Ioto, R. T.; Loto, C. A.; Akinyele, M. Effect of Ginger, Pomegranate and Celery Extracts on Zinc Electrodeposition, Surface Morphology and Corrosion Inhibition of Mild Steel.

- Alexandria Eng. J.* **2020**, *59* (2), 933–941. <https://doi.org/10.1016/j.aej.2020.03.014>.
- (58) Faiz, M.; Zahari, A.; Awang, K.; Hussin, H. Corrosion Inhibition on Mild Steel in 1 M HCl Solution by: *Cryptocarya Nigra* Extracts and Three of Its Constituents (Alkaloids). *RSC Adv.* **2020**, *10* (11), 6547–6562. <https://doi.org/10.1039/c9ra05654h>.
- (59) Bui, H. T. T.; Dang, T. D.; Le, H. T. T.; Hoang, T. T. B. Comparative Study on Corrosion Inhibition of Vietnam Orange Peel Essential Oil with Urotropine and Insight of Corrosion Inhibition Mechanism for Mild Steel in Hydrochloric Solution. *J. Electrochem. Sci. Technol.* **2019**, *10* (1), 69–81. <https://doi.org/10.5229/JECST.2019.10.1.69>.
- (60) Deyab, M. A. Corrosion Inhibition of Aluminum in Biodiesel by Ethanol Extracts of Rosemary Leaves. *J. Taiwan Inst. Chem. Eng.* **2016**, *58*, 536–541. <https://doi.org/10.1016/j.jtice.2015.06.021>.
- (61) Picco, S.; Villegas, L.; Tonelli, F.; Merlo, M.; Rigau, J.; Diaz, D.; Masuelli, M. We Are IntechOpen , the World ' s Leading Publisher of Open Access Books Built by Scientists , for Scientists TOP 1 %. *Intech* **2016**, No. tourism, 13.
- (62) Honarvar Nazari, M.; Shihab, M. S.; Havens, E. A.; Shi, X. Mechanism of Corrosion Protection in Chloride Solution by an Apple-Based Green Inhibitor: Experimental and Theoretical Studies. *J. Infrastruct. Preserv. Resil.* **2020**, *1* (1), 1–19. <https://doi.org/10.1186/s43065-020-00007-w>.
- (63) Thanh, L. T.; Vu, N. S. H.; Binh, P. M. Q.; Dao, V. A.; Thu, V. T. H.; Van Hien, P.; Panaitescu, C.; Nam, N. D. Combined Experimental and Computational Studies on Corrosion Inhibition of *Houttuynia Cordata* Leaf Extract for Steel in HCl Medium. *J. Mol. Liq.* **2020**, *315*, 113787. <https://doi.org/10.1016/j.molliq.2020.113787>.
- (64) Ghazouani, T.; Ben Hmamou, D.; Meddeb, E.; Salghi, R.; Benali, O.; Bouya, H.; Hammouti, B.; Fattouch, S. Antioxidant Activity and Effect of Quince Pulp Extract on the Corrosion of C-Steel in 1M HCl. *Res. Chem. Intermed.* **2015**, *41* (10), 7463–7480. <https://doi.org/10.1007/s11164-014-1837-9>.
- (65) A. Moore, O. The Extraction, Anticancer Effect, Bioavailability, and Nanotechnology of Baicalin. *J. Nutr. Med. Diet Care* **2016**, *2* (1), 1–12. <https://doi.org/10.23937/2572->

3278.1510011.

- (66) Obot, I. B.; Obi-Egbedi, N. O.; Umoren, S. A. Antifungal Drugs as Corrosion Inhibitors for Aluminium in 0.1 M HCl. *Corros. Sci.* **2009**, *51* (8), 1868–1875. <https://doi.org/10.1016/j.corsci.2009.05.017>.
- (67) Perumal, S.; Muthumanickam, S.; Elangovan, A.; Karthik, R.; Kannan, R. S.; Mothilal, K. Bauhinia Tomentosa Leaves Extract as Green Corrosion Inhibitor for Mild Steel in 1M HCl Medium. *J. Bio- Tribo-Corrosion* **2017**, *3* (2), 13. <https://doi.org/10.1007/s40735-017-0072-5>.
- (68) Paul, O. A. Inhibitory Action of Albizia Zygia Gum on Mild Steel Corrosion in Acid Medium. *African J. Pure Appl. Chem.* **2014**, *8* (2), 37–46. <https://doi.org/10.5897/ajpac2014.0549>.
- (69) Ibrahim, T.; Gomes, E.; Obot, I. B.; Khamis, M.; Abou Zour, M. Corrosion Inhibition of Mild Steel by Calotropis Procera Leaves Extract in a CO<sub>2</sub> Saturated Sodium Chloride Solution. *J. Adhes. Sci. Technol.* **2016**, *30* (23), 2523–2543. <https://doi.org/10.1080/01694243.2016.1185229>.
- (70) Gupta, N. K.; Quraishi, M. A.; Singh, P.; Srivastava, V.; Srivastava, K.; Verma, C. Analytical & Curcumine Longa : Green and Sustainable Corrosion. *Anal. Bioanal. Electrochem.* **2017**, *9* (2), 245–265.
- (71) Hart, K.; James, A. O. The Inhibitive Effect of Aloe Vera Barbadensis Gel on Copper in Hydrochloric Acid Medium. *J. Emerg. Trends Eng. Appl. Sci.* **2014**, *5* (1), 24–29.
- (72) Haruna, K.; Obot, I. B.; Ankah, N. K.; Sorour, A. A.; Saleh, T. A. Gelatin: A Green Corrosion Inhibitor for Carbon Steel in Oil Well Acidizing Environment. *J. Mol. Liq.* **2018**, *264* (2017), 515–525. <https://doi.org/10.1016/j.molliq.2018.05.058>.
- (73) Hassan, K. H.; Khadom, A. A.; Kurshed, N. H. Citrus Aurantium Leaves Extracts as a Sustainable Corrosion Inhibitor of Mild Steel in Sulfuric Acid. *South African J. Chem. Eng.* **2016**, *22*, 1–5. <https://doi.org/10.1016/j.sajce.2016.07.002>.
- (74) Khadraoui, A.; Khelifa, A.; Hachama, K.; Mehdaoui, R. Thymus Algeriensis Extract as a New Eco-Friendly Corrosion Inhibitor for 2024 Aluminium Alloy in 1 M HCl Medium. *J.*

- Mol. Liq.* **2016**, *214*, 293–297. <https://doi.org/10.1016/j.molliq.2015.12.064>.
- (75) Kayed, A. M.; Elghaly, E.-S. M.; El-hela, A. A. New Epoxy Megastigmane Glucoside from *Dactyloctenium Aegyptium* L . P . Beauv Wild. **2016**, *4* (6), 237–244.
- (76) Singh, A.; Kumar, A.; Pramanik, T. A Theoretical Approach to the Study of Some Plant Extracts as Green Corrosion Inhibitor for Mild Steel in HCl Solution. *Orient. J. Chem.* **2013**, *29* (1), 1–7.
- (77) Njoku, D. I.; Ukaga, I.; Ikenna, O. B.; Oguzie, E. E.; Oguzie, K. L.; Ibisi, N. Natural Products for Materials Protection: Corrosion Protection of Aluminium in Hydrochloric Acid by *Kola Nitida* Extract. *J. Mol. Liq.* **2016**, *219* (July), 417–424. <https://doi.org/10.1016/j.molliq.2016.03.049>.
- (78) Ndukwe, A. I.; Anyakwo, C. N. Modelling of Corrosion Inhibition of Mild Steel in Hydrochloric Acid by Crushed Leaves of *Sida Acuta* (Malvaceae). *Int. J. Eng. Sci.* **2017**, *06* (01), 22–33. <https://doi.org/10.9790/1813-0601032233>.
- (79) Nazeer, A. A.; Shalabi, K.; Fouda, A. S. Corrosion Inhibition of Carbon Steel by Roselle Extract in Hydrochloric Acid Solution: Electrochemical and Surface Study. *Res. Chem. Intermed.* **2015**, *41* (7), 4833–4850. <https://doi.org/10.1007/s11164-014-1570-4>.
- (80) Ekezie, F. G. C.; Sun, D. W.; Cheng, J. H. Acceleration of Microwave-Assisted Extraction Processes of Food Components by Integrating Technologies and Applying Emerging Solvents: A Review of Latest Developments. *Trends Food Sci. Technol.* **2017**, *67*, 160–172. <https://doi.org/10.1016/j.tifs.2017.06.006>.
- (81) Maria, M. F. F.; Ikhmal, W. M. K. W. M.; Amirah, M. N. N. S.; Manja, S. M.; Syaizwadi, S. M.; Chan, K. S.; Sabri, M. G. M.; Adnan, A. Green Approach in Anti-Corrosion Coating by Using *Andrographis Paniculata* Leaves Extract as Additives of Stainless Steel 316L in Seawater. *Int. J. Corros. Scale Inhib.* **2019**, *8* (3), 644–658. <https://doi.org/10.17675/2305-6894-2019-8-3-13>.
- (82) Aralu, C. C.; Chukwuemeka-Okorie, H. O.; Akpomie, K. G. Inhibition and Adsorption Potentials of Mild Steel Corrosion Using Methanol Extract of *Gongronema Latifolium*. *Appl. Water Sci.* **2021**, *11* (2), 1–7. <https://doi.org/10.1007/s13201-020-01351-8>.

- (83) Jessima, S. J. H. M.; Subhashini, S.; Arulraj, J. Sunova Spirulina Powder as an Effective Environmentally Friendly Corrosion Inhibitor for Mild Steel in Acid Medium. *J. Bio-Tribo-Corrosion* **2020**, *6* (3), 1–13. <https://doi.org/10.1007/s40735-020-00370-x>.
- (84) Gapsari, F.; Soenoko, R.; Suprpto, A.; Suprpto, W. Bee Wax Propolis Extract as Eco-Friendly Corrosion Inhibitors for 304SS in Sulfuric Acid. *Int. J. Corros.* **2015**, *2015*, 1–10. <https://doi.org/10.1155/2015/567202>.
- (85) Fouda, E.-A.; El-Hossiany, A.; Ramadan, H. Calotropis Procera Plant Extract as Green Corrosion Inhibitor for 304 Stainless Steel in Hydrochloric Acid Solution. *Zast. Mater.* **2017**, *58* (4), 541–555. <https://doi.org/10.5937/zasmat1704541f>.
- (86) Fouda, A. S.; Rashwan, S. M.; Abo-Mosallam, H. A. Fennel Seed Extract as Green Corrosion Inhibitor for 304 Stainless Steel in Hydrochloric Acid Solutions. *Desalin. Water Treat.* **2014**, *52* (28–30), 5175–5186. <https://doi.org/10.1080/19443994.2013.806223>.
- (87) Ehsani, A.; Mahjani, M. G.; Hosseini, M.; Safari, R.; Moshrefi, R.; Mohammad Shiri, H. Evaluation of Thymus Vulgaris Plant Extract as an Eco-Friendly Corrosion Inhibitor for Stainless Steel 304 in Acidic Solution by Means of Electrochemical Impedance Spectroscopy, Electrochemical Noise Analysis and Density Functional Theory. *J. Colloid Interface Sci.* **2017**, *490*, 444–451. <https://doi.org/10.1016/j.jcis.2016.11.048>.
- (88) De Faria Neto, A. D. R.; De Souza, A. P. N.; Passos, R. R.; Pereira, M. D. S.; Pocrifka, L. A.; De Souza, R. F. B.; Rios, E. D. C. Evaluation of Paullinia Cupana as a Green Corrosion Inhibitor for Carbon Steel Utilizing Gravimetric and Electrochemical Noise Techniques. *Mater. Res. Express* **2019**, *6* (7), 076522. <https://doi.org/10.1088/2053-1591/ab13c0>.
- (89) Nadi, I.; Belattmania, Z.; Sabour, B.; Reani, A.; Sahibed-dine, A.; Jama, C.; Bentiss, F. Sargassum Muticum Extract Based on Alginate Biopolymer as a New Efficient Biological Corrosion Inhibitor for Carbon Steel in Hydrochloric Acid Pickling Environment: Gravimetric, Electrochemical and Surface Studies. *Int. J. Biol. Macromol.* **2019**, *141*, 137–149. <https://doi.org/10.1016/j.ijbiomac.2019.08.253>.
- (90) Ayoola, A. A.; Fayomi, O. S. I.; Akande, I. G.; Ayeni, O. A.; Agboola, O.; Obanla, O. R.;

- Abatan, O. G.; Chukwuka, C. J. Inhibitive Corrosion Performance of the Eco-Friendly Aloe Vera in Acidic Media of Mild and Stainless Steels. *J. Bio- Tribo-Corrosion* **2020**, *6* (3), 1–13. <https://doi.org/10.1007/s40735-020-00361-y>.
- (91) Mohammed, A. R. I.; Solomon, M. M.; Haruna, K.; Umoren, S. A.; Saleh, T. A. Evaluation of the Corrosion Inhibition Efficacy of Cola Acuminata Extract for Low Carbon Steel in Simulated Acid Pickling Environment. *Environ. Sci. Pollut. Res.* **2020**, *27* (27), 34270–34288. <https://doi.org/10.1007/s11356-020-09636-w>.
- (92) Haque, J.; Verma, C.; Srivastava, V.; Nik, W. B. W. Corrosion Inhibition of Mild Steel in 1M HCl Using Environmentally Benign Thevetia Peruviana Flower Extracts. *Sustain. Chem. Pharm.* **2021**, *19* (December 2020), 100354. <https://doi.org/10.1016/j.scp.2020.100354>.
- (93) Boumezzourh, A.; Ouknin, M.; Chibane, E.; Costa, J.; Bouyanzer, A.; Hammouti, B.; Majidi, L. Inhibition of Tinplate Corrosion in 0.5 M H<sub>2</sub>C<sub>2</sub>O<sub>4</sub> Medium by Mentha Pulegium Essential Oil. *Int. J. Corros. Scale Inhib.* **2020**, *9* (1), 152–170. <https://doi.org/10.17675/2305-6894-2020-9-1-9>.
- (94) Sedik, A.; Lerari, D.; Salci, A.; Athmani, S.; Bachari, K.; Gecibesler, H.; Solmaz, R. Dardagan Fruit Extract as Eco-Friendly Corrosion Inhibitor for Mild Steel in 1 M HCl: Electrochemical and Surface Morphological Studies. *J. Taiwan Inst. Chem. Eng.* **2020**, *107*, 189–200. <https://doi.org/10.1016/j.jtice.2019.12.006>.
- (95) Anadebe, V. C.; Okafor, C. S.; Onukwuli, O. D. Electrochemical, Molecular Dynamics, Adsorption Studies and Anti-Corrosion Activities of Moringa Leaf Biomolecules on Carbon Steel Surface in Alkaline and Acid Environment. *Chem. Data Collect.* **2020**, *28*, 100437. <https://doi.org/10.1016/j.cdc.2020.100437>.
- (96) Akbarzadeh, S.; Ramezanzadeh, M.; Ramezanzadeh, B.; Bahlakeh, G. Detailed Atomic/Molecular-Level/Electronic-Scale Computer Modeling and Electrochemical Explorations of the Adsorption and Anti-Corrosion Effectiveness of the Green Nitrogen-Based Phytochemicals on the Mild Steel Surface in the Saline Solution. *J. Mol. Liq.* **2020**, *319*, 114312. <https://doi.org/10.1016/j.molliq.2020.114312>.



- (97) Berrissoul, A.; Ouarhach, A.; Benhiba, F.; Romane, A.; Zarrouk, A.; Guenbour, A.; Dikici, B.; Dafali, A. Evaluation of Lavandula Mairei Extract as Green Inhibitor for Mild Steel Corrosion in 1 M HCl Solution. Experimental and Theoretical Approach. *J. Mol. Liq.* **2020**, *313*, 113493. <https://doi.org/10.1016/j.molliq.2020.113493>.
- (98) Ameh, P. O. Electrochemical and Computational Study of Gum Exudates from Canarium Schweinfurthii as Green Corrosion Inhibitor for Mild Steel in HCl Solution . *J. Taibah Univ. Sci.* **2018**, *12* (6), 783–795. <https://doi.org/10.1080/16583655.2018.1514147>.
- (99) Berdimurodov, E.; Kholikov, A.; Akbarov, K.; Obot, I. B.; Guo, L. Thioglycoluril Derivative as a New and Effective Corrosion Inhibitor for Low Carbon Steel in a 1 M HCl Medium: Experimental and Theoretical Investigation. *J. Mol. Struct.* **2021**, *1234*, 130165. <https://doi.org/10.1016/j.molstruc.2021.130165>.
- (100) Akin, M.; Nalbantoglu, S.; Cuhadar, O.; Uzun, D.; Saki, N. Juglans Regia L. Extract as Green Inhibitor for Stainless Steel and Aluminium in Acidic Media. *Res. Chem. Intermed.* **2015**, *41* (2), 899–912. <https://doi.org/10.1007/s11164-013-1241-x>.
- (101) Bammou, L.; Belkhaouda, M.; Salghi, R.; Benali, O.; Zarrouk, A.; Zarrok, H.; Hammouti, B. Corrosion Inhibition of Steel in Sulfuric Acidic Solution by the Chenopodium Ambrosioides Extracts. *J. Assoc. Arab Univ. Basic Appl. Sci.* **2014**, *16*, 83–90. <https://doi.org/10.1016/j.jaubas.2013.11.001>.
- (102) Behpour, M.; Ghoreishi, S. M.; Khayat Kashani, M.; Soltan, N. Inhibition of 304 Stainless Steel Corrosion in Acidic Solution by Ferula Gumosa (Galbanum) Extract. *Mater. Corros.* **2009**, *60* (11), 895–898. <https://doi.org/10.1002/maco.200905182>.
- (103) Bentrach, H.; Rahali, Y.; Chala, A. Gum Arabic as an Eco-Friendly Inhibitor for API 5L X42 Pipeline Steel in HCl Medium. *Corros. Sci.* **2014**, *82*, 426–431. <https://doi.org/10.1016/j.corsci.2013.12.018>.
- (104) Boudalia, M.; Guenbour, A.; Bellaouchou, A.; Laqhaili, A.; Mousaddak, M.; Hakiki, A.; Hammouti, B.; Ebenso, E. E. Corrosion Inhibition of Organic Oil Extract of Leaves of Lavandula Stoeckas on Stainless Steel in Concentrated Phosphoric Acid Solution. *Int. J. Electrochem. Sci.* **2013**, *8* (5), 7414–7424.

- (105) Fouda, A. E. A. S.; Rashwan, S. M.; Abo-Mosallam, H. A. Aqueous Extract of Coriander Seeds as Green Corrosion Inhibitor for 304 Stainless Steel in Hydrochloric Acid Solutions. *J. Korean Chem. Soc.* **2014**, *58* (1), 25–32.  
<https://doi.org/10.5012/jkcs.2014.58.1.25>.
- (106) Garai, S.; Garai, S.; Jaisankar, P.; Singh, J. K.; Elango, A. A Comprehensive Study on Crude Methanolic Extract of Artemisia Pallens (Asteraceae) and Its Active Component as Effective Corrosion Inhibitors of Mild Steel in Acid Solution. *Corros. Sci.* **2012**, *60*, 193–204. <https://doi.org/10.1016/j.corsci.2012.03.036>.
- (107) Jokar, M.; Farahani, T. S.; Ramezanzadeh, B. Electrochemical and Surface Characterizations of Morus Alba Pendula Leaves Extract (MAPLE) as a Green Corrosion Inhibitor for Steel in 1M HCl. *J. Taiwan Inst. Chem. Eng.* **2016**, *63*, 436–452.  
<https://doi.org/10.1016/j.jtice.2016.02.027>.
- (108) Kadapparambil, S.; Yadav, K.; Ramachandran, M.; Victoria Selvam, N. Electrochemical Investigation of the Corrosion Inhibition Mechanism of Tectona Grandis Leaf Extract for SS304 Stainless Steel in Hydrochloric Acid. *Corros. Rev.* **2017**, *35* (2), 111–121.  
<https://doi.org/10.1515/corrrev-2016-0074>.
- (109) Li, X.; Deng, S.; Fu, H. Inhibition of the Corrosion of Steel in HCl, H<sub>2</sub>SO<sub>4</sub> Solutions by Bamboo Leaf Extract. *Corros. Sci.* **2012**, *62*, 163–175.  
<https://doi.org/10.1016/j.corsci.2012.05.008>.
- (110) Abiola, O. K.; Otaigbe, J. O. E. The Effects of Phyllanthus Amarus Extract on Corrosion and Kinetics of Corrosion Process of Aluminum in Alkaline Solution. *Corros. Sci.* **2009**, *51* (11), 2790–2793. <https://doi.org/10.1016/j.corsci.2009.07.006>.
- (111) Abiola, O. K.; Otaigbe, J. O. E.; Kio, O. J. Gossipium Hirsutum L. Extracts as Green Corrosion Inhibitor for Aluminum in NaOH Solution. *Corros. Sci.* **2009**, *51* (8), 1879–1881. <https://doi.org/10.1016/j.corsci.2009.04.016>.
- (112) Sharma V, Kumar S, Bashir S, Ghelichkhah Z, Obot IB, K. A. Use of Sapindus (Reetha) as Corrosion Inhibitor of Aluminium in Acidic Medium. *Mater. Res. Express* **2018**, *5* (7), 076510.

- (113) Ambrish, S. Azwain (Trachyspermum Copticum) Seed Extract as an Efficient Corrosion Inhibitor for Aluminium in NaOH Solution. *Res. J. Recent Sci.* **2012**, *1*, 57–61.
- (114) Soltani, N.; Tavakkoli, N.; Khayatkashani, M.; Jalali, M. R.; Mosavizade, A. Green Approach to Corrosion Inhibition of 304 Stainless Steel in Hydrochloric Acid Solution by the Extract of Salvia Officinalis Leaves. *Corros. Sci.* **2012**, *62*, 122–135.  
<https://doi.org/10.1016/j.corsci.2012.05.003>.
- (115) Arora, P.; Kumar, S.; Sharma, M. K.; Mathur, S. P. Corrosion Inhibition of Aluminium by Capparis Decidua in Acidic Media. *E-Journal Chem.* **2007**, *4* (4), 450–456.  
<https://doi.org/10.1155/2007/487820>.
- (116) Ating, E. I.; Umoren, S. A.; Udousoro, I. I.; Ebenso, E. E.; Udoh, A. P. Leaves Extract of Ananas Sativum as Green Corrosion Inhibitor for Aluminium in Hydrochloric Acid Solutions. *Green Chem. Lett. Rev.* **2010**, *3* (2), 61–68.  
<https://doi.org/10.1080/17518250903505253>.
- (117) Ayeni, F. A.; Alawode, S.; Joseph, D.; Sukop, P.; Olawuyi, V.; Alonge, T. E.; Alabi, O. O.; Oluwabunmi, O.; Alo, F. I. Investigation of &lt;I&gt;Sida Acuta&lt;/I&gt; (Wire Weed) Plant Extract as Corrosion Inhibitor for Aluminium-Copper-Magnesium Alloy in Acidic Medium. *J. Miner. Mater. Charact. Eng.* **2014**, *02* (04), 286–291.  
<https://doi.org/10.4236/jmmce.2014.24033>.
- (118) Chauhan, R.; Garg, U.; Tak, R. K. Corrosion Inhibition of Aluminium in Acid Media by Citrullus Colocynthis Extract. *E-Journal Chem.* **2011**, *8* (1), 85–90.  
<https://doi.org/10.1155/2011/340639>.
- (119) Deng, S.; Li, X. Inhibition by Jasminum Nudiflorum Lindl. Leaves Extract of the Corrosion of Aluminium in HCl Solution. *Corros. Sci.* **2012**, *64*, 253–262.  
<https://doi.org/10.1016/j.corsci.2012.07.017>.
- (120) El-Etre, A. Y. Inhibition of Aluminum Corrosion Using Opuntia Extract. *Corros. Sci.* **2003**, *45* (11), 2485–2495. [https://doi.org/10.1016/S0010-938X\(03\)00066-0](https://doi.org/10.1016/S0010-938X(03)00066-0).
- (121) Li, X.; Deng, S. Inhibition Effect of Dendrocalamus Brandisii Leaves Extract on Aluminum in HCl, H<sub>3</sub>PO<sub>4</sub> Solutions. *Corros. Sci.* **2012**, *65*, 299–308.

<https://doi.org/10.1016/j.corsci.2012.08.033>.

- (122) Mejeha, I. M.; Nwandu, M. C.; Okeoma, K. B.; Nnanna, L. A.; Chidiebere, M. A.; Eze, F. C.; Oguzie, E. E. Experimental and Theoretical Assessment of the Inhibiting Action of *Aspilia Africana* Extract on Corrosion Aluminium Alloy AA3003 in Hydrochloric Acid. *J. Mater. Sci.* **2012**, *47* (6), 2559–2572. <https://doi.org/10.1007/s10853-011-6079-2>.
- (123) Nathiya, R. S.; Raj, V. Evaluation of *Dryopteris Cochleata* Leaf Extracts as Green Inhibitor for Corrosion of Aluminium in 1 M H<sub>2</sub>SO<sub>4</sub>. *Egypt. J. Pet.* **2017**, *26* (2), 313–323. <https://doi.org/10.1016/j.ejpe.2016.05.002>.
- (124) Nnanna, L. a; Obasi, V. U.; Nwadiuko, O. C.; Mejehe, K. I.; Ekekwe, N. D.; Udensi, S. C. Inhibition by *Newbouldia Leavis* Leaf Extract of the Corrosion of Aluminium in HCl and H<sub>2</sub>SO<sub>4</sub> Solutions. *Arch. Appl. Sci. Res.* **2012**, *4* (1), 207–217.
- (125) Nnanna, L. A.; C. Nwadiuko, O.; D. Ekekwe, N.; F. Ukpabi, C.; C. Udensi, S.; B. Okeoma, K.; N. Onwuagba, B.; M. Mejeha, I. Adsorption and Inhibitive Properties of Leaf Extract of *Newbouldia Leavis* as a Green Inhibitor for Aluminium Alloy in H<sub>2</sub>SO<sub>4</sub>. *Am. J. Mater. Sci.* **2012**, *1* (2), 143–148. <https://doi.org/10.5923/j.materials.20110102.24>.
- (126) O, A. K.; O, A.; C.O, A.; E.A, A. Adsorption Properties of *Azadirachta Indicia* Extract on Corrosion of Aluminium in 1.85 M Hydrochloric Acid. *J. Int. Assoc. Adv. Technol. Sci.* **2015**, *16* (04), 1–11.
- (127) Fouda, A. S.; Abdallah, Y. M.; Elawady, G. Y.; Ahmed, R. M. *Zygophyllum Coccineum* L. Extract as Green Corrosion Inhibitor for Copper in 1 M HNO<sub>3</sub> Solutions. *Int. J. Adv. Res.* **2014**, *2* (11), 517–531.
- (128) Fouda, A. S.; Elmorsi, M. A.; Abou-Elmagd, B. S. Adsorption and Inhibitive Properties of Methanol Extract of *Euphorbia Heterophylla* for the Corrosion of Copper in 0.5 M Nitric Acid Solutions. *Polish J. Chem. Technol.* **2017**, *19* (1), 95–103. <https://doi.org/10.1515/pjct-2017-0014>.
- (129) Fouda, A. S.; Shalabi, K.; Idress, A. A. *Ceratonia Siliqua* Extract as a Green Corrosion Inhibitor for Copper and Brass in Nitric Acid Solutions. *Green Chem. Lett. Rev.* **2015**, *8* (3–4), 17–29. <https://doi.org/10.1080/17518253.2015.1073797>.

- (130) Fouda, A. S.; Shalabi, K.; Idress, A. A. Thymus Vulgarise Extract as Nontoxic Corrosion Inhibitor for Copper and  $\alpha$ -Brass in 1 M HNO<sub>3</sub> Solutions. *Int. J. Electrochem. Sci.* **2014**, *9* (9), 5126–5154.
- (131) Hart, K.; James, A. Corrosion Inhibition of Copper in Hydrochloric and Tetraoxosulphate (Vi) Acid Solutions Using Aloe Vera Barbadensis Gel. *Br. J. Appl. Sci. Technol.* **2014**, *4* (28), 4052–4065. <https://doi.org/10.9734/bjast/2014/9658>.
- (132) Krishnaveni, K.; Ravichandran, J. Influence of Aqueous Extract of Leaves of Morinda Tinctoria on Copper Corrosion in HCl Medium. *J. Electroanal. Chem.* **2014**, *735*, 24–31. <https://doi.org/10.1016/j.jelechem.2014.09.032>.
- (133) Durodola, S. S.; Adekunle, A. S.; Olasunkanmi, L. O.; Oyekunle, J. A. O. Inhibition of Mild Steel Corrosion in Acidic Medium by Extract of Spilanthes Uliginosa Leaves. *Electroanalysis* **2020**, *32* (12), 2693–2702. <https://doi.org/10.1002/elan.202060227>.
- (134) Fouda, A. S.; Megahed, H. E.; Fouad, N.; Elbahrawi, N. M. Corrosion Inhibition of Carbon Steel in 1 M Hydrochloric Acid Solution by Aqueous Extract of Thevetia Peruviana. *J. Bio- Tribo-Corrosion* **2016**, *2* (3), 1–13. <https://doi.org/10.1007/s40735-016-0046-z>.
- (135) Ituen, E. B.; James, A. O.; Akaranta, O. Elephant Grass Biomass Extract as Corrosion Inhibitor for Mild Steel in Acidic Medium. *J. Mater. Environ. Sci.* **2017**, *8* (4), 1498–1507.
- (136) Akalezi, C. O.; Ogukwe, C. E.; Ejele, E. A.; Oguzie, E. E. Corrosion Inhibition Properties of Gongronema Latifolium Extract in Acidic Media. *Int. J. Corros. Scale Inhib.* **2016**, *5* (3), 232–247. <https://doi.org/10.17675/2305-6894-2016-5-3-4>.
- (137) Nwosu, F. O.; Muzakir, M. M. Thermodynamic and Adsorption Studies of Corrosion Inhibition of Mild Steel Using Lignin from Siam Weed (Chromolaena Odorata) in Acid Medium. *J. Mater. Environ. Sci.* **2016**, *7* (5), 1663–1673.
- (138) Li, D.; Zhao, X.; Liu, Z.; Liu, H.; Fan, B.; Yang, B.; Zheng, X.; Li, W.; Zou, H. Synergetic Anticorrosion Mechanism of Main Constituents in Chinese Yam Peel for Copper in Artificial Seawater. *ACS Omega* **2021**, *6* (44), 29965–29981. <https://doi.org/10.1021/acsomega.1c04500>.

- (139) Meng, S.; Liu, Z.; Zhao, X.; Fan, B.; Liu, H.; Guo, M.; Hao, H. Efficient Corrosion Inhibition by Sugarcane Purple Rind Extract for Carbon Steel in HCl Solution: Mechanism Analyses by Experimental and: In Silico Insights. *RSC Adv.* **2021**, *11* (50), 31693–31711. <https://doi.org/10.1039/d1ra04976c>.
- (140) Alrefaee, S. H.; Rhee, K. Y.; Verma, C.; Quraishi, M. A.; Ebenso, E. E. Challenges and Advantages of Using Plant Extract as Inhibitors in Modern Corrosion Inhibition Systems: Recent Advancements. *J. Mol. Liq.* **2021**, *321* (October), 114666. <https://doi.org/10.1016/j.molliq.2020.114666>.
- (141) Abdallah, M.; Altass, H. M.; Al-Gorair, A. S.; Al-Fahemi, J. H.; Jahdaly, B. A. A. L.; Soliman, K. A. Natural Nutmeg Oil as a Green Corrosion Inhibitor for Carbon Steel in 1.0 M HCl Solution: Chemical, Electrochemical, and Computational Methods. *J. Mol. Liq.* **2021**, *323*, 115036. <https://doi.org/10.1016/j.molliq.2020.115036>.
- (142) Galo, G. T.; Morandim-Giannetti, A. de A.; Cotting, F.; Aoki, I. V.; Aquino, I. P. Evaluation of Purple Onion (*Allium Cepa* L.) Extract as a Natural Corrosion Inhibitor for Carbon Steel in Acidic Media. *Met. Mater. Int.* **2021**, *27* (9), 3238–3249. <https://doi.org/10.1007/s12540-020-00679-9>.
- (143) Chaubey, N.; Savita; Qurashi, A.; Chauhan, D. S.; Quraishi, M. A. Frontiers and Advances in Green and Sustainable Inhibitors for Corrosion Applications: A Critical Review. *J. Mol. Liq.* **2021**, *321*, 114385. <https://doi.org/10.1016/j.molliq.2020.114385>.
- (144) Haldhar, R.; Prasad, D.; Bahadur, I.; Dagdag, O.; Kaya, S.; Verma, D. K.; Kim, S. C. Investigation of Plant Waste as a Renewable Biomass Source to Develop Efficient, Economical and Eco-Friendly Corrosion Inhibitor. *J. Mol. Liq.* **2021**, *335*, 116184. <https://doi.org/10.1016/j.molliq.2021.116184>.
- (145) Karthik, R.; Muthukrishnan, P.; Chen, S. M.; Jeyaprabha, B.; Prakash, P. Anti-Corrosion Inhibition of Mild Steel in 1M Hydrochloric Acid Solution by Using *Tiliacora Accuminata* Leaves Extract. *Int. J. Electrochem. Sci.* **2014**, *10* (5), 3707–3725.
- (146) Chung, I. M.; Malathy, R.; Priyadharshini, R.; Hemapriya, V.; Kim, S. H.; Prabakaran, M. Inhibition of Mild Steel Corrosion Using *Magnolia Kobus* Extract in Sulphuric Acid

- Medium. *Mater. Today Commun.* **2020**, *25* (September), 101687.  
<https://doi.org/10.1016/j.mtcomm.2020.101687>.
- (147) Dehghani, A.; Bahlakeh, G.; Ramezanzadeh, B. Green Eucalyptus Leaf Extract: A Potent Source of Bio-Active Corrosion Inhibitors for Mild Steel. *Bioelectrochemistry* **2019**, *130*, 107339. <https://doi.org/10.1016/j.bioelechem.2019.107339>.
- (148) Thirumangalam Karunanithi, B.; Chellappa, J. Adsorption and Inhibition Properties of Tephrosia Purpurea as Corrosion Inhibitor for Mild Steel in Sulphuric Acid Solution. *J. Dispers. Sci. Technol.* **2019**, *40* (10), 1441–1450.  
<https://doi.org/10.1080/01932691.2018.1516150>.
- (149) Haldhar, R.; Prasad, D.; Saxena, A.; Kumar, R. Experimental and Theoretical Studies of Ficus Religiosa as Green Corrosion Inhibitor for Mild Steel in 0.5 M H<sub>2</sub>SO<sub>4</sub> Solution. *Sustain. Chem. Pharm.* **2018**, *9* (July), 95–105. <https://doi.org/10.1016/j.scp.2018.07.002>.
- (150) Khadom, A. A.; Abd, A. N.; Ahmed, N. A. Xanthium Strumarium Leaves Extracts as a Friendly Corrosion Inhibitor of Low Carbon Steel in Hydrochloric Acid: Kinetics and Mathematical Studies. *South African J. Chem. Eng.* **2018**, *25*, 13–21.  
<https://doi.org/10.1016/j.sajce.2017.11.002>.
- (151) S.J. Olusegun, T. S. Joshua, M.O. Bodunrin, and S. A. Inhibition of Mild Steel Corrosion in HCl Solution by Plant Extract of Bidden Pilosa. *Nat. Sci.* **2018**, *16* (1), 1–8.  
<https://doi.org/10.7537/marsnsj160118.01.Keywords>.
- (152) Vidhya Thomas, K.; Thomas Kakkassery, J.; Raphael, V. P.; Ragi, K.; Johnson, R. Ixora Coccinea Extract as an Efficient Eco-Friendly Corrosion Inhibitor in Acidic Media: Experimental and Theoretical Approach. *Curr. Chem. Lett.* **2021**, *10* (3), 139–150.  
<https://doi.org/10.5267/J.CCL.2020.12.001>.
- (153) Baran, E.; Cakir, A.; Yazici, B. Inhibitory Effect of Gentiana Olivieri Extracts on the Corrosion of Mild Steel in 0.5 M HCl: Electrochemical and Phytochemical Evaluation. *Arab. J. Chem.* **2019**, *12* (8), 4303–4319. <https://doi.org/10.1016/j.arabjc.2016.06.008>.
- (154) Moukhles, A.; Belcadi, H.; Raissouni, I.; Ben driss, A.; Mansour, A. I. Chemical Composition, in Vitro Antibacterial Activity and Corrosion Inhibition of Essential Oil and

- Hydrolat Extract from Aerial Parts of *Thymbra Capitata* (L.) Cav Harvested at Northern Morocco. *J. Essent. Oil-Bearing Plants* **2020**, *23* (2), 375–389.  
<https://doi.org/10.1080/0972060X.2020.1760147>.
- (155) Shamsuzzaman, M.; Kalaiselvi, K.; Prabakaran, M. Evaluation of Antioxidant and Anticorrosive Activities of *Cerriops Tagal* Plant Extract. *Appl. Sci.* **2021**, *11* (21), 10150.  
<https://doi.org/10.3390/app112110150>.
- (156) Ragul, R.; Kathiravan, S.; Muruges, A.; Ravichandran, J. Anticorrosion Performance of *Mitracarpus Hirtus* Extract on Mild Steel in 1 M HCl. *J. Bio- Tribo-Corrosion* **2018**, *4* (4), 1–11. <https://doi.org/10.1007/s40735-018-0180-x>.
- (157) Sin, H. L. Y.; Abdul Rahim, A.; Gan, C. Y.; Saad, B.; Salleh, M. I.; Umeda, M. *Aquilaria Subintergra* Leaves Extracts as Sustainable Mild Steel Corrosion Inhibitors in HCl. *Meas. J. Int. Meas. Confed.* **2017**, *109*, 334–345.  
<https://doi.org/10.1016/j.measurement.2017.05.045>.
- (158) Trindade, R. da S.; Dos Santos, M. R.; Cordeiro, R. F. B.; D’Elia, E. A Study of the Gorse Aqueous Extract as a Green Corrosion Inhibitor for Mild Steel in HCl Aqueous Solution. *Green Chem. Lett. Rev.* **2017**, *10* (4), 444–454.  
<https://doi.org/10.1080/17518253.2017.1398354>.
- (159) Shanmuga Priya, K.; Prathibha, B. S.; Vasudha, V. G.; Nagaswarupa, H. P. *Spathodea Campanulata* as a Corrosion Inhibitor for Mild Steel in 1N H<sub>2</sub>SO<sub>4</sub> Media. *Mater. Today Proc.* **2018**, *5* (10), 22595–22604. <https://doi.org/10.1016/j.matpr.2018.06.633>.
- (160) Ibrahim, T. H.; Gomes, E. E.; Obot, I. B.; Khamis, M.; Sabri, M. A. Mild Steel Green Inhibition by *Ficus Carica* Leaves Extract under Practical Field Conditions. *J. Adhes. Sci. Technol.* **2017**, *31* (24), 2697–2718. <https://doi.org/10.1080/01694243.2017.1317458>.
- (161) Salmasifar, A.; Edraki, M.; Alibakhshi, E.; Ramezanzadeh, B.; Bahlakeh, G. Combined Electrochemical/Surface Investigations and Computer Modeling of the Aquatic Artichoke Extract Molecules Corrosion Inhibition Properties on the Mild Steel Surface Immersed in the Acidic Medium. *J. Mol. Liq.* **2021**, *327*, 114856.  
<https://doi.org/10.1016/j.molliq.2020.114856>.



- (162) Karki, N.; Neupane, S.; Gupta, D. K.; Das, A. K.; Singh, S.; Koju, G. M.; Chaudhary, Y.; Yadav, A. P. Berberine Isolated from Mahonia Nepalensis as an Eco-Friendly and Thermally Stable Corrosion Inhibitor for Mild Steel in Acid Medium. *Arab. J. Chem.* **2021**, *14* (12), 103423. <https://doi.org/10.1016/j.arabjc.2021.103423>.
- (163) Khiya, Z.; Hayani, M.; Gamar, A.; Kharchouf, S.; Amine, S.; Berrekhis, F.; Bouzoubae, A.; Zair, T.; El Hilali, F. Valorization of the Salvia Officinalis L. of the Morocco Bioactive Extracts: Phytochemistry, Antioxidant Activity and Corrosion Inhibition. *J. King Saud Univ. - Sci.* **2019**, *31* (3), 322–335. <https://doi.org/10.1016/j.jksus.2018.11.008>.
- (164) Thirupathi, P.; Venkatraman, B. R. Corrosion Inhibition Behaviour on Carbon Steel in Well-Water by Ethanolic Extract of Portulaca Quadrifida (Chicken Weed) Leaves. *Indian J. Sci. Technol.* **2021**, *14* (18), 1488–1504. <https://doi.org/10.17485/ijst/v14i18.630>.
- (165) Anh, H. T.; Vu, N. S. H.; Huyen, L. T.; Tran, N. Q.; Thu, H. T.; Bach, L. X.; Trinh, Q. T.; Prabhakar Vattikuti, S. V.; Nam, N. D. Ficus Racemosa Leaf Extract for Inhibiting Steel Corrosion in a Hydrochloric Acid Medium. *Alexandria Eng. J.* **2020**, *59* (6), 4449–4462. <https://doi.org/10.1016/j.aej.2020.07.051>.
- (166) El Ouariachi, E.; Bouyanzer, A.; Salghi, R.; Hammouti, B.; Desjobert, J. M.; Costa, J.; Paolini, J.; Majidi, L. Inhibition of Corrosion of Mild Steel in 1 M HCl by the Essential Oil or Solvent Extracts of Ptychotis Verticillata. *Res. Chem. Intermed.* **2015**, *41* (2), 935–946. <https://doi.org/10.1007/s11164-013-1246-5>.
- (167) Wahiba Ebdelly; Ben Hassen, S.; Nóvoa, X. R.; Ben Amor, Y. Inhibition of Carbon Steel Corrosion in Neutral Calcareous Synthetic Water by Eruca Sativa Extract. *Physicochem. Probl. Mater. Prot.* **2019**, *55* (3), 591–602. <https://doi.org/10.1134/S2070205119030110>.
- (168) Okewale, A.; Omoruwuo, F. Neem Leaf Extract as a Corrosion Inhibitor on Mild Steel in Acidic Solution. *Int. J. Eng. Res. Africa* **2018**, *35*, 208–220. <https://doi.org/10.4028/www.scientific.net/JERA.35.208>.
- (169) Sathiyapriya, T.; Rathika, G.; Dhandapani, M. In Depth Analysis of Anti Corrosion Behaviour of Eco Friendly Gum Exudate for Mild Steel in Sulphuric Acid Medium. *J. Adhes. Sci. Technol.* **2019**, *33* (22), 2443–2461.

<https://doi.org/10.1080/01694243.2019.1645261>.

- (170) Olusegun, S. J. Corrosion Inhibition of Pulverized Jatropha Curcas Leaves on Medium Carbon Steel in 0 . 5 M H<sub>2</sub>SO<sub>4</sub> and NaCl Environ ... *Int. J. Sci. Technol.* **2013**, 2 (7), 510–515.
- (171) Olanrewaju, A.; Oluseyi, A. K.; Ayomide, B. V.; Theresa, A. O.; Oluwakayode, A. S. Corrosion Inhibitive Properties of Epimedium Grandiflorum on Mild Steel in HCl Acidic Media. *IOP Conf. Ser. Mater. Sci. Eng.* **2019**, 509 (1), 012008.  
<https://doi.org/10.1088/1757-899X/509/1/012008>.
- (172) Omran, M. A.; Fawzy, M.; Mahmoud, A. E. D.; Abdullatef, O. A. Optimization of Mild Steel Corrosion Inhibition by Water Hyacinth and Common Reed Extracts in Acid Media Using Factorial Experimental Design. *Green Chem. Lett. Rev.* **2022**, 15 (1), 214–230.  
<https://doi.org/10.1080/17518253.2022.2032844>.
- (173) Divya, P.; Saratha, R.; Priya, S. V. Chemical Science Review and Letters Impediment Effect of Galinsoga Parviflora (Quick Weed) on Mild Steel Corrosion in 1 M HCl. *Chem Sci Rev Lett* **2016**, 5 (18), 115–126.
- (174) Kathiravan, S.; Ragul, R.; Raja, G.; Ravichandran, J. Theoretical and Experimental Studies About the Inhibitive Action of Ruellia Tuberosa L on Mild Steel in HCl Medium. *J. Bio- Tribo-Corrosion* **2018**, 4 (3), 1–14. <https://doi.org/10.1007/s40735-018-0162-z>.
- (175) Jeslina, V. D. A. M.; Kirubavathy, S. J.; Al-Hashem, A.; Rajendran, S. S.; Joany, R. M.; Lacnjevac, C. Inhibition of Corrosion of Mild Steel by an Alcoholic Extract of a Seaweed Sargassum Muticum. *Mater. Prot.* **2021**, 62 (4), 304–315.  
<https://doi.org/10.5937/zasmat2104304J>.
- (176) Okafor, P. C.; Ikpi, M. E.; Uwah, I. E.; Ebenso, E. E.; Ekpe, U. J.; Umoren, S. A. Inhibitory Action of Phyllanthus Amarus Extracts on the Corrosion of Mild Steel in Acidic Media. *Corros. Sci.* **2008**, 50 (8), 2310–2317. <https://doi.org/10.1016/j.corsci.2008.05.009>.
- (177) Nnenna, W.; Adeola, S.; Msenhamba, M.; Akanimo, N. Synsepalum Dulcificum Leaves Extract as Green Inhibitor for Mild Steel Corrosion in Hydrochloric Acid. *ChemSearch J.* **2021**, 12 (1), 47–54.

- (178) Iloamaeke, I. M.; Umeobika, C. U.; Egwuatu, C. I.; Ekwe, N. S.; Oguwa, C. J. CORROSION INHIBITION AND ADSORPTION BEHAVIOUR OF ALUMINIUM IN 1M H<sub>2</sub>SO<sub>4</sub> MEDIUM USING PERSEA AMERICANA (AVOCADO PEAR) LEAVES EXTRACT. *J. Basic Phys. Res.* **2017**, 7 (2), 47–57.
- (179) Singh, A.; Ahamad, I.; Singh, V. K.; Quraishi, M. A. Inhibition Effect of Environmentally Benign Karanj (Pongamia Pinnata) Seed Extract on Corrosion of Mild Steel in Hydrochloric Acid Solution. *J. Solid State Electrochem.* **2011**, 15 (6), 1087–1097. <https://doi.org/10.1007/s10008-010-1172-z>.
- (180) Nasibi, M.; Mohammady, M.; Ghasemi, E.; Ashrafi, A.; Zaarei, D.; Rashed, G. Corrosion Inhibition of Mild Steel by Nettle (*Urtica Dioica* L.) Extract: Polarization, EIS, AFM, SEM and EDS Studies. *J. Adhes. Sci. Technol.* **2013**, 27 (17), 1873–1885. <https://doi.org/10.1080/01694243.2013.764144>.
- (181) Orubite, K. O.; Oforka, N. C. Inhibition of the Corrosion of Mild Steel in Hydrochloric Acid Solutions by the Extracts of Leaves of *Nypa Fruticans* Wurmb. *Mater. Lett.* **2004**, 58 (11), 1768–1772. <https://doi.org/10.1016/j.matlet.2003.11.030>.
- (182) Lebrini, M.; Robert, F.; Lecante, A.; Roos, C. Corrosion Inhibition of C38 Steel in 1M Hydrochloric Acid Medium by Alkaloids Extract from *Oxandra Asbeckii* Plant. *Corros. Sci.* **2011**, 53 (2), 687–695. <https://doi.org/10.1016/j.corsci.2010.10.006>.
- (183) Oguzie, E. E. Inhibition of Acid Corrosion of Mild Steel by *Telfaria Occidentalis* Extract. *Pigment Resin Technol.* **2005**, 34 (6), 321–326. <https://doi.org/10.1108/03699420510630336>.
- (184) Quraishi, M. A.; Singh, A.; Singh, V. K.; Yadav, D. K.; Singh, A. K. Green Approach to Corrosion Inhibition of Mild Steel in Hydrochloric Acid and Sulphuric Acid Solutions by the Extract of *Murraya Koenigii* Leaves. *Mater. Chem. Phys.* **2010**, 122 (1), 114–122. <https://doi.org/10.1016/j.matchemphys.2010.02.066>.
- (185) Singh, A.; Singh, V. K.; Quraishi, M. A. Aqueous Extract of *Kalmegh* (*Andrographis Paniculata*) Leaves as Green Inhibitor for Mild Steel in Hydrochloric Acid Solution. *Int. J. Corros.* **2010**, 2010, 1–10. <https://doi.org/10.1155/2010/275983>.

- (186) Verma, D. K.; Khan, F. Corrosion Inhibition of Mild Steel in Hydrochloric Acid Using Extract of Glycine Max Leaves. *Res. Chem. Intermed.* **2016**, *42* (4), 3489–3506. <https://doi.org/10.1007/s11164-015-2227-7>.
- (187) Arockiasamy, P.; Sheela, X. Q. R.; Thenmozhi, G.; Franco, M.; Sahayaraj, J. W.; Santhi, R. J. Evaluation of Corrosion Inhibition of Mild Steel in 1 M Hydrochloric Acid Solution by Mollugo Cerviana. *Int. J. Corros.* **2014**, *2014*, 1–7. <https://doi.org/10.1155/2014/679192>.
- (188) Sharma, M. K.; Arora, P.; Kumar, S.; Mathur, S. P.; Ratnani, R. Inhibitive Effect of Prosopis Cineraria on Mild Steel in Acidic Media. *Corros. Eng. Sci. Technol.* **2008**, *43* (3), 213–218. <https://doi.org/10.1179/174327807X196816>.
- (189) El Bribri, A.; Tabyaoui, M.; Tabyaoui, B.; El Attari, H.; Bentiss, F. The Use of Euphorbia Falcata Extract as Eco-Friendly Corrosion Inhibitor of Carbon Steel in Hydrochloric Acid Solution. *Mater. Chem. Phys.* **2013**, *141* (1), 240–247. <https://doi.org/10.1016/j.matchemphys.2013.05.006>.
- (190) James, O. A.; Akaranta, O. Inhibition of Corrosion of Zinc in Hydrochloric Acid Solution by Red Onion Skin Acetone Extract. *Res. J. Chem. Sci.* **2011**, *1* (1), 31–37.
- (191) Satapathy, A. K.; Gunasekaran, G.; Sahoo, S. C.; Amit, K.; Rodrigues, P. V. Corrosion Inhibition by Justicia Gendarussa Plant Extract in Hydrochloric Acid Solution. *Corros. Sci.* **2009**, *51* (12), 2848–2856. <https://doi.org/10.1016/j.corsci.2009.08.016>.
- (192) Shyamala, M.; Kasthuri, P. K. The Inhibitory Action of the Extracts of Adathoda Vasica, Eclipta Alba, and Centella Asiatica on the Corrosion of Mild Steel in Hydrochloric Acid Medium: A Comparative Study. *Int. J. Corros.* **2012**, *2012*. <https://doi.org/10.1155/2012/852827>.
- (193) Lebrini, M.; Robert, F.; Roos, C. Alkaloids Extract from Palicourea Guianensis Plant as Corrosion Inhibitor for C38 Steel in 1 M Hydrochloric Acid Medium. *Int. J. Electrochem. Sci.* **2011**, *6* (3), 847–859.
- (194) Alibakhshi, E.; Ramezanzadeh, M.; Bahlakeh, G.; Ramezanzadeh, B.; Mahdavian, M.; Motamedi, M. Glycyrrhiza Glabra Leaves Extract as a Green Corrosion Inhibitor for Mild

- Steel in 1 M Hydrochloric Acid Solution: Experimental, Molecular Dynamics, Monte Carlo and Quantum Mechanics Study. *J. Mol. Liq.* **2018**, *255*, 185–198.  
<https://doi.org/10.1016/j.molliq.2018.01.144>.
- (195) Krishnegowda, P. M.; Venkatesha, V. T.; Krishnegowda, P. K. M.; Shivayogiraju, S. B. Acalypha Torta Leaf Extract as Green Corrosion Inhibitor for Mild Steel in Hydrochloric Acid Solution. *Ind. Eng. Chem. Res.* **2013**, *52* (2), 722–728.  
<https://doi.org/10.1021/ie3018862>.
- (196) V. G., V. Mild Steel Corrosion Inhibition by Cucurbitamaxima Plant Extract in Hydrochloric Acid Solution. *J. Environ. Nanotechnol.* **2014**, *3* (1), 16–22.  
<https://doi.org/10.13074/jent.2014.01.132047>.
- (197) Singh, A.; Singh, V. K.; Quraishi, M. A. Inhibition Effect of Environmentally Benign Kuchla (*Strychnos Nuxvomica*) Seed Extract on Corrosion of Mild Steel in Hydrochloric Acid Solution. *Rasayan J. Chem.* **2010**, *3* (4), 811–824.
- (198) Lebrini, M.; Robert, F.; Blandinières, P. A.; Roos, C. Corrosion Inhibition by Isertia Coccinea Plant Extract in Hydrochloric Acid Solution. *Int. J. Electrochem. Sci.* **2011**, *6* (7), 2443–2460.
- (199) Ibrahim, T. H.; Zour, M. A. Corrosion Inhibition of Mild Steel Using Fig Leaves Extract in Hydrochloric Acid Solution. *Int. J. Electrochem. Sci.* **2011**, *6* (12), 6442–6455.
- (200) Chevalier, M.; Robert, F.; Amusant, N.; Traisnel, M.; Roos, C.; Lebrini, M. Enhanced Corrosion Resistance of Mild Steel in 1 M Hydrochloric Acid Solution by Alkaloids Extract from Aniba Rosaeodora Plant: Electrochemical, Phytochemical and XPS Studies. *Electrochim. Acta* **2014**, *131*, 96–105. <https://doi.org/10.1016/j.electacta.2013.12.023>.
- (201) Chauhan, L. R.; Gunasekaran, G. Corrosion Inhibition of Mild Steel by Plant Extract in Dilute HCl Medium. *Corros. Sci.* **2007**, *49* (3), 1143–1161.  
<https://doi.org/10.1016/j.corsci.2006.08.012>.
- (202) Anupama, K. K.; Ramya, K.; Shainy, K. M.; Joseph, A. Adsorption and Electrochemical Studies of Pimenta Dioica Leaf Extracts as Corrosion Inhibitor for Mild Steel in Hydrochloric Acid. *Mater. Chem. Phys.* **2015**, *167*, 28–41.

<https://doi.org/10.1016/j.matchemphys.2015.09.013>.

- (203) Anupama, K. K.; Ramya, K.; Joseph, A. Electrochemical Measurements and Theoretical Calculations on the Inhibitive Interaction of *Plectranthus Amboinicus* Leaf Extract with Mild Steel in Hydrochloric Acid. *Meas. J. Int. Meas. Confed.* **2017**, *95*, 297–305. <https://doi.org/10.1016/j.measurement.2016.10.030>.
- (204) Bahrami, M. J.; Hosseini, S. M. A.; Pilvar, P. Experimental and Theoretical Investigation of Organic Compounds as Inhibitors for Mild Steel Corrosion in Sulfuric Acid Medium. *Corros. Sci.* **2010**, *52* (9), 2793–2803. <https://doi.org/10.1016/j.corsci.2010.04.024>.
- (205) Benali, O.; Benmehdi, H.; Hasnaoui, O.; Selles, C.; Salghi, R. Green Corrosion Inhibitor: Inhibitive Action of Tannin Extract of *Chamaerops Humilis* Plant for the Corrosion of Mild Steel in 0.5M H<sub>2</sub>SO<sub>4</sub>. *J. Mater. Environ. Sci.* **2013**, *4* (1), 127–138.
- (206) Benali, O.; Selles, C.; Salghi, R. Inhibition of Acid Corrosion of Mild Steel by *Anacyclus Pyrethrum* L. Extracts. *Res. Chem. Intermed.* **2014**, *40* (1), 259–268. <https://doi.org/10.1007/s11164-012-0960-8>.
- (207) Bhuvaneswari, T. K.; Vasantha, V. S.; Jeyaprabha, C. *Pongamia Pinnata* as a Green Corrosion Inhibitor for Mild Steel in 1N Sulfuric Acid Medium. *Silicon* **2018**, *10* (5), 1793–1807. <https://doi.org/10.1007/s12633-017-9673-3>.
- (208) Bothi Raja, P.; Sethuraman, M. G. *Strychnos Nux-Vomica* an Eco-Friendly Corrosion Inhibitor for Mild Steel in 1 M Sulfuric Acid Medium. *Mater. Corros.* **2009**, *60* (1), 22–28. <https://doi.org/10.1002/maco.200805027>.
- (209) Gobara, M.; Zaghoul, B.; Baraka, A.; Elsayed, M.; Zorainy, M.; Kotb, M. M.; Elnabarawy, H. Green Corrosion Inhibition of Mild Steel to Aqueous Sulfuric Acid by the Extract of *Corchorus Olitorius* Stems. *Mater. Res. Express* **2017**, *4* (4), 046504. <https://doi.org/10.1088/2053-1591/aa664a>.
- (210) Ji, G.; Shukla, S. K.; Dwivedi, P.; Sundaram, S.; Prakash, R. Inhibitive Effect of *Argemone Mexicana* Plant Extract on Acid Corrosion of Mild Steel. *Ind. Eng. Chem. Res.* **2011**, *50* (21), 11954–11959. <https://doi.org/10.1021/ie201450d>.
- (211) Ji, G.; Shukla, S. K.; Ebenso, E. E.; Prakash, R. *Argemone Mexicana* Leaf Extract for

- Inhibition of Mild Steel Corrosion in Sulfuric Acid Solutions. *Int. J. Electrochem. Sci.* **2013**, *8* (8), 10878–10889.
- (212) Mourya, P.; Banerjee, S.; Singh, M. M. Corrosion Inhibition of Mild Steel in Acidic Solution by Tagetes Erecta (Marigold Flower) Extract as a Green Inhibitor. *Corros. Sci.* **2014**, *85*, 352–363. <https://doi.org/10.1016/j.corsci.2014.04.036>.
- (213) Muthukrishnan, P.; Jeyaprabha, B.; Prakash, P. Adsorption and Corrosion Inhibiting Behavior of Lannea Coromandelica Leaf Extract on Mild Steel Corrosion. *Arab. J. Chem.* **2017**, *10*, S2343–S2354. <https://doi.org/10.1016/j.arabjc.2013.08.011>.
- (214) Okafor, P. C.; Osabor, V. I.; Ebenso, E. E. Eco-Friendly Corrosion Inhibitors: Inhibitive Action of Ethanol Extracts of Garcinia Kola for the Corrosion of Mild Steel in H<sub>2</sub>SO<sub>4</sub> Solutions. *Pigment Resin Technol.* **2007**, *36* (5), 299–305. <https://doi.org/10.1108/03699420710820414>.
- (215) Patel, N. L.; Jauhariand, S.; Mehta, G. N.; Al-Deyab, S. S.; Warad, I.; Hammouti, B. Mild Steel Corrosion Inhibition by Various Plant Extracts in 0.5 M Sulphuric Acid. *Int. J. Electrochem. Sci.* **2013**, *8* (2), 2635–2655.
- (216) Pitchaipillai, M.; Raj, K.; Balasubramanian, J.; Periakaruppan, P. Benevolent Behavior of Kleinia Grandiflora Leaf Extract as a Green Corrosion Inhibitor for Mild Steel in Sulfuric Acid Solution. *Int. J. Miner. Metall. Mater.* **2014**, *21* (11), 1083–1095. <https://doi.org/10.1007/s12613-014-1013-7>.
- (217) Prabakaran, M.; Kim, S. H.; Mugila, N.; Hemapriya, V.; Parameswari, K.; Chitra, S.; Chung, I. M. Aster Koraiensis as Nontoxic Corrosion Inhibitor for Mild Steel in Sulfuric Acid. *J. Ind. Eng. Chem.* **2017**, *52*, 235–242. <https://doi.org/10.1016/j.jiec.2017.03.052>.
- (218) Sethuraman, M. G.; Raja, P. B. Corrosion Inhibition of Mild Steel by Datura Metel in Acidic Medium. *Pigment Resin Technol.* **2005**, *34* (6), 327–331. <https://doi.org/10.1108/03699420510630345>.
- (219) Singh, A.; Quraishi, M. A. The Extract of Jamun (Syzygium Cumini) Seed as Green Corrosion Inhibitor for Acid Media. *Res. Chem. Intermed.* **2015**, *41* (5), 2901–2914. <https://doi.org/10.1007/s11164-013-1398-3>.

- (220) Umoren, S. A.; Obot, I. B.; Obi-Egbedi, N. O. Raphia Hookeri Gum as a Potential Eco-Friendly Inhibitor for Mild Steel in Sulfuric Acid. *J. Mater. Sci.* **2009**, *44* (1), 274–279. <https://doi.org/10.1007/s10853-008-3045-8>.
- (221) Dehghani, A.; Bahlakeh, G.; Ramezanzadeh, B.; Ramezanzadeh, M. Potential of Borage Flower Aqueous Extract as an Environmentally Sustainable Corrosion Inhibitor for Acid Corrosion of Mild Steel: Electrochemical and Theoretical Studies. *J. Mol. Liq.* **2019**, *277*, 895–911. <https://doi.org/10.1016/j.molliq.2019.01.008>.
- (222) Dehghani, A.; Bahlakeh, G.; Ramezanzadeh, B.; Ramezanzadeh, M. A Combined Experimental and Theoretical Study of Green Corrosion Inhibition of Mild Steel in HCl Solution by Aqueous Citrullus Lanatus Fruit (CLF) Extract. *J. Mol. Liq.* **2019**, *279*, 603–624. <https://doi.org/10.1016/j.molliq.2019.02.010>.
- (223) Thakur, A.; Kaya, S.; Abousalem, A. S.; Kumar, A. Experimental , DFT and MC Simulation Analysis of Vicia Sativa Weed Aerial Extract as Sustainable and Eco-Benign Corrosion Inhibitor for Mild Steel in Acidic Environment. *Sustain. Chem. Pharm.* **2022**, *29* (July), 100785. <https://doi.org/10.1016/j.scp.2022.100785>.
- (224) Thakur, A.; Kaya, S.; Abousalem, A. S.; Sharma, S.; Ganjoo, R.; Assad, H.; Kumar, A. Computational and Experimental Studies on the Corrosion Inhibition Performance of an Aerial Extract of Cnicus Benedictus Weed on the Acidic Corrosion of Mild Steel. *Process Saf. Environ. Prot.* **2022**, *161*, 801–818. <https://doi.org/10.1016/j.psep.2022.03.082>.
- (225) Thakur, A.; Kumar, A.; Sharma, S.; Ganjoo, R.; Assad, H. Materials Today : Proceedings Computational and Experimental Studies on the Efficiency of Sonchus Arvensis as Green Corrosion Inhibitor for Mild Steel in 0 . 5 M HCl Solution. *Mater. Today Proc.* **2022**, *66*, 609–621. <https://doi.org/10.1016/j.matpr.2022.06.479>.
- (226) Thakur, A.; Kumar, A.; Kaya, S.; Marzouki, R.; Zhang, F.; Guo, L. Recent Advancements in Surface Modification , Characterization and Functionalization for Enhancing the Biocompatibility and Corrosion Resistance of Biomedical Implants. *Coatings* **2022**, *12*, 1459. <https://doi.org/https://doi.org/10.3390/coatings12101459>.
- (227) Thakur, A.; SAVAŞ, K.; Kumar, A. Recent Trends in the Characterization and Application



- Progress of Nano-Modified Coatings in Corrosion Mitigation of Metals and Alloys. *Appl. Sci.* **2023**, *13*, 730. <https://doi.org/10.3390/app13020730>.
- (228) Younis, W.; Alamgeer; Schini-Kerth, V. B.; Junior, A. G.; Majid, M. Cardioprotective Effect of *Asphodelus Tenuifolius* Cav. on Blood Pressure and Metabolic Alterations in Glucose-Induced Metabolic Syndrome Rats—An Ethnopharmacological Approach. *J. Ethnopharmacol.* **2018**, *214* (May), 168–178. <https://doi.org/10.1016/j.jep.2017.12.005>.
- (229) Benahmed, M.; Selatnia, I.; Djeddi, N.; Akkal, S.; Laouer, H. Adsorption and Corrosion Inhibition Properties of Butanolic Extract of *Elaeoselinum Thapsioides* and Its Synergistic Effect with *Reutera Lutea* (Desf.) Maires (Apiaceae) on A283 Carbon Steel in Hydrochloric Acid Solution. *Chem. Africa* **2020**, *3* (1), 251–261. <https://doi.org/10.1007/s42250-019-00093-8>.
- (230) Nwanonyeni, S. C.; Obasi, H. C.; Eze, I. O. Hydroxypropyl Cellulose as an Efficient Corrosion Inhibitor for Aluminium in Acidic Environments: Experimental and Theoretical Approach. *Chem. Africa* **2019**, *2* (3), 471–482. <https://doi.org/10.1007/s42250-019-00062-1>.
- (231) Thakur, A.; Kumar, A. Sustainable Inhibitors for Corrosion Mitigation in Aggressive Corrosive Media: A Comprehensive Study. *J. Bio- Tribo-Corrosion* **2021**, *7* (2), 1–48. <https://doi.org/10.1007/s40735-021-00501-y>.
- (232) Hynes, N. R. J.; Selvaraj, R. M.; Mohamed, T.; Mukesh, A. M.; Olfa, K.; Nikolova, M. P. *Aerva Lanata* Flowers Extract as Green Corrosion Inhibitor of Low-Carbon Steel in HCl Solution: An in Vitro Study. *Chem. Pap.* **2021**, *75* (3), 1165–1174. <https://doi.org/10.1007/s11696-020-01361-5>.
- (233) Ouakki, M.; Galai, M.; Rbaa, M.; Abousalem, A. S.; Lakhrissi, B.; Touhami, M. E.; Cherkaoui, M. Electrochemical, Thermodynamic and Theoretical Studies of Some Imidazole Derivatives Compounds as Acid Corrosion Inhibitors for Mild Steel. *J. Mol. Liq.* **2020**, *319*, 114063. <https://doi.org/10.1016/j.molliq.2020.114063>.
- (234) Rehioui, M.; About, S.; Benzidia, B.; Hammouch, H.; Erramli, H.; Daoud, N. A.; Badrane, N.; Hajjaji, N. Corrosion Inhibiting Effect of a Green Formulation Based on

- Opuntia Dillenii Seed Oil for Iron in Acid Rain Solution. *Heliyon* **2021**, 7 (4), e06674. <https://doi.org/10.1016/j.heliyon.2021.e06674>.
- (235) Das, M.; Biswas, A.; Kumar Kundu, B.; Adilia Januário Charmier, M.; Mukherjee, A.; Mobin, S. M.; Udayabhanu, G.; Mukhopadhyay, S. Enhanced Pseudo-Halide Promoted Corrosion Inhibition by Biologically Active Zinc(II) Schiff Base Complexes. *Chem. Eng. J.* **2019**, 357 (October), 447–457. <https://doi.org/10.1016/j.cej.2018.09.150>.
- (236) Bao, J.; Zhang, H.; Zhao, X.; Deng, J. Biomass Polymeric Microspheres Containing Aldehyde Groups: Immobilizing and Controlled-Releasing Amino Acids as Green Metal Corrosion Inhibitor. *Chem. Eng. J.* **2018**, 341 (October 2017), 146–156. <https://doi.org/10.1016/j.cej.2018.02.047>.
- (237) Zhou, X.; Wang, Y.; Gong, C.; Liu, B.; Wei, G. Production, Structural Design, Functional Control, and Broad Applications of Carbon Nanofiber-Based Nanomaterials: A Comprehensive Review. *Chem. Eng. J.* **2020**, 402 (March), 126189. <https://doi.org/10.1016/j.cej.2020.126189>.
- (238) Hashim, N. Z. N.; Anouar, E. H.; Kassim, K.; Zaki, H. M.; Alharthi, A. I.; Embong, Z. XPS and DFT Investigations of Corrosion Inhibition of Substituted Benzylidene Schiff Bases on Mild Steel in Hydrochloric Acid. *Appl. Surf. Sci.* **2019**, 476 (July 2018), 861–877. <https://doi.org/10.1016/j.apsusc.2019.01.149>.
- (239) Palaniappan, N.; Cole, I.; Caballero-Briones, F.; Manickam, S.; Justin Thomas, K. R.; Santos, D. Experimental and DFT Studies on the Ultrasonic Energy-Assisted Extraction of the Phytochemicals of: *Catharanthus Roseus* as Green Corrosion Inhibitors for Mild Steel in NaCl Medium. *RSC Adv.* **2020**, 10 (9), 5399–5411. <https://doi.org/10.1039/c9ra08971c>.
- (240) Haldhar, R.; Prasad, D.; Bhardwaj, N. Surface Adsorption and Corrosion Resistance Performance of Acacia Concinna Pod Extract: An Efficient Inhibitor for Mild Steel in Acidic Environment. *Arab. J. Sci. Eng.* **2020**, 45 (1), 131–141. <https://doi.org/10.1007/s13369-019-04270-2>.
- (241) Benabbouha, T.; Nmila, R.; Siniti, M.; Chefira, K.; El Attari, H.; Rchid, H. The Brown Algae *Cystoseira Baccata* Extract as a Friendly Corrosion Inhibitor on Carbon Steel in

- Acidic Media. *SN Appl. Sci.* **2020**, 2 (4), 1–11. <https://doi.org/10.1007/s42452-020-2492-y>.
- (242) El Basiony, N. M.; Badr, E. E.; Baker, S. A.; El-Tabei, A. S. Experimental and Theoretical (DFT&MC) Studies for the Adsorption of the Synthesized Gemini Cationic Surfactant Based on Hydrazide Moiety as X-65 Steel Acid Corrosion Inhibitor. *Appl. Surf. Sci.* **2021**, 539, 148246. <https://doi.org/10.1016/j.apsusc.2020.148246>.
- (243) Lin, B. lan; Shao, J. jie; Xu, Y. ye; Lai, Y. ming; Zhao, Z. ning. Adsorption and Corrosion of Renewable Inhibitor of Pomelo Peel Extract for Mild Steel in Phosphoric Acid Solution. *Arab. J. Chem.* **2021**, 14 (5). <https://doi.org/10.1016/j.arabjc.2021.103114>.
- (244) Kirichenko, E. O.; Gatapova, E. Y. Studying of the Contact Angle Hysteresis on Various Surfaces. *MATEC Web Conf.* **2016**, 72 (14), 2014–2016. <https://doi.org/10.1051/mateconf/20167201045>.
- (245) Kumar, H.; Yadav, V. Musa Acuminata (Green Corrosion Inhibitor) as Anti-Pit and Anti-Cracking Agent for Mild Steel in 5M Hydrochloric Acid Solution. *Chem. Data Collect.* **2020**, 29, 100500. <https://doi.org/10.1016/j.cdc.2020.100500>.
- (246) Izionworu, V.; Ukpaka, C.; Oguzie, E. Green and Eco-Benign Corrosion Inhibition Agents: Alternatives and Options to Chemical Based Toxic Corrosion Inhibitors. *Chem. Int.* **2020**, 6 (4), 232–259.
- (247) Singh, A.; Ansari, K. R.; Chauhan, D. S.; Quraishi, M. A.; Kaya, S. Anti-Corrosion Investigation of Pyrimidine Derivatives as Green and Sustainable Corrosion Inhibitor for N80 Steel in Highly Corrosive Environment: Experimental and AFM/XPS Study. *Sustain. Chem. Pharm.* **2020**, 16 (March), 100257. <https://doi.org/10.1016/j.scp.2020.100257>.
- (248) Vorobyova, V.; Skiba, M. Apricot Pomace Extract as a Natural Corrosion Inhibitor of Mild Steel Corrosion in 0.5 M NaCl Solution: A Combined Experimental and Theoretical Approach. *J. Chem. Technol. Metall.* **2020**, 55 (1), 210–222.
- (249) Zhang, W.; Ma, Y.; Chen, L.; Wang, L. J.; Wu, Y. C.; Li, H. J. Aloe Polysaccharide as an Eco-Friendly Corrosion Inhibitor for Mild Steel in Simulated Acidic Oilfield Water: Experimental and Theoretical Approaches. *J. Mol. Liq.* **2020**, 307, 112950.

<https://doi.org/10.1016/j.molliq.2020.112950>.

- (250) Tariq Saeed, M.; Saleem, M.; Niyazi, A. H.; Al-Shamrani, F. A.; Jazzar, N. A.; Ali, M. Carrot (*Daucus Carota* L.) Peels Extract as an Herbal Corrosion Inhibitor for Mild Steel in 1M HCl Solution. *Mod. Appl. Sci.* **2020**, *14* (2), 97. <https://doi.org/10.5539/mas.v14n2p97>.
- (251) Paun, G.; Neagu, E.; Moroeanu, V.; Albu, C.; Savin, S.; Lucian Radu, G. Chemical and Bioactivity Evaluation of *Eryngium Planum* and *Cnicus Benedictus* Polyphenolic-Rich Extracts. *Biomed Res. Int.* **2019**, *2019*, 1–10. <https://doi.org/10.1155/2019/3692605>.
- (252) Chkirate, K.; Azgaou, K.; Elmsellem, H.; El Ibrahim, B.; Sebbar, N. K.; Anouar, E. H.; Benmessaoud, M.; El Hajjaji, S.; Essassi, E. M. Corrosion Inhibition Potential of 2-[(5-Methylpyrazol-3-yl)methyl]benzimidazole against Carbon Steel Corrosion in 1 M HCl Solution: Combining Experimental and Theoretical Studies. *J. Mol. Liq.* **2021**, *321*, 114750. <https://doi.org/10.1016/j.molliq.2020.114750>.
- (253) El Aoufir, Y.; Sebhaoui, J.; Lgaz, H.; El Bakri, Y.; Guenbour, A.; Bentiss, F.; Zarrouk, A.; Essassi, E. M.; Oudda, H. Theoretical Prediction and Experimental Study of Benzimidazole Derivate as a Novel Corrosion Inhibitor for Carbon Steel in 1.0 M HCl. *Prot. Met. Phys. Chem. Surfaces* **2020**, *56* (5), 1027–1038. <https://doi.org/10.1134/S2070205120050056>.
- (254) Verma, C.; Haque, J.; Ebenso, E. E.; Quraishi, M. A. Melamine Derivatives as Effective Corrosion Inhibitors for Mild Steel in Acidic Solution: Chemical, Electrochemical, Surface and DFT Studies. *Results Phys.* **2018**, *9*, 100–112. <https://doi.org/10.1016/j.rinp.2018.02.018>.
- (255) Verma, C.; Haque, J.; Quraishi, M. A.; Ebenso, E. E. Aqueous Phase Environmental Friendly Organic Corrosion Inhibitors Derived from One Step Multicomponent Reactions: A Review. *J. Mol. Liq.* **2019**, *275*, 18–40. <https://doi.org/10.1016/j.molliq.2018.11.040>.
- (256) Verma, C.; Verma, D. K.; Ebenso, E. E.; Quraishi, M. A. Sulfur and Phosphorus Heteroatom-Containing Compounds as Corrosion Inhibitors: An Overview. *Heteroat. Chem.* **2018**, *29* (4), e21437. <https://doi.org/10.1002/hc.21437>.
- (257) Tan, B.; He, J.; Zhang, S.; Xu, C.; Chen, S.; Liu, H.; Li, W. Insight into Anti-Corrosion

- Nature of Betel Leaves Water Extracts as the Novel and Eco-Friendly Inhibitors. *J. Colloid Interface Sci.* **2021**, *585* (December), 287–301.  
<https://doi.org/10.1016/j.jcis.2020.11.059>.
- (258) Singh, A.; Pramanik, T.; Kumar, A.; Gupta, M. Phenobarbital: A New and Effective Corrosion Inhibitor for Mild Steel in 1 M HCl Solution. *Asian J. Chem.* **2013**, *25* (17), 9808–9812. <https://doi.org/10.14233/ajchem.2013.15414>.
- (259) Mallakpour, S.; Hatami, M.; Hussain, C. M. Recent Innovations in Functionalized Layered Double Hydroxides: Fabrication, Characterization, and Industrial Applications. *Adv. Colloid Interface Sci.* **2020**, *283*, 102216. <https://doi.org/10.1016/j.cis.2020.102216>.
- (260) Mishra, A.; Verma, C.; Srivastava, V.; Lgaz, H.; Quraishi, M. A.; Ebenso, E. E.; Chung, I. M. Chemical, Electrochemical and Computational Studies of Newly Synthesized Novel and Environmental Friendly Heterocyclic Compounds as Corrosion Inhibitors for Mild Steel in Acidic Medium. *J. Bio-Tribo-Corrosion* **2018**, *4* (3), 1–20.  
<https://doi.org/10.1007/s40735-018-0147-y>.
- (261) Verma, C.; Ebenso, E. E. Ionic Liquid-Mediated Functionalization of Graphene-Based Materials for Versatile Applications: A Review. *Graphene Technol.* **2019**, *4* (1–2), 1–15.  
<https://doi.org/10.1007/s41127-018-0023-z>.
- (262) Olasunkanmi, L. O.; Obot, I. B.; Kabanda, M. M.; Ebenso, E. E. Some Quinoxalin-6-Yl Derivatives as Corrosion Inhibitors for Mild Steel in Hydrochloric Acid: Experimental and Theoretical Studies. *J. Phys. Chem. C* **2015**, *119* (28), 16004–16019.  
<https://doi.org/10.1021/acs.jpcc.5b03285>.
- (263) Raghavendra, N. Green Compounds to Attenuate Aluminum Corrosion in HCl Activation: A Necessity Review. *Chem. Africa* **2020**, *3* (1), 21–34. <https://doi.org/10.1007/s42250-019-00114-6>.
- (264) Venkatesh, C.; Mohiddin, S. K.; Ruben, N. Corrosion Inhibitors Behaviour on Reinforced Concrete—A Review. *Lect. Notes Civ. Eng.* **2019**, *25* (March 2020), 127–134.  
[https://doi.org/10.1007/978-981-13-3317-0\\_11](https://doi.org/10.1007/978-981-13-3317-0_11).
- (265) Jyothi, S.; Rao, Y. V. S.; Ratnakumar, P. S. S. Natural Product as Corrosion Inhibitors in

- Various Corrosive Media: A Review. *Rasayan J. Chem.* **2019**, *12* (2), 537–544.  
<https://doi.org/10.31788/RJC.2019.1225000>.
- (266) Douche, D.; Elmsellem, H.; Anouar, E. H.; Guo, L.; Hafez, B.; Tüzün, B.; El Louzi, A.; Bougrin, K.; Karrouchi, K.; Himmi, B. Anti-Corrosion Performance of 8-Hydroxyquinoline Derivatives for Mild Steel in Acidic Medium: Gravimetric, Electrochemical, DFT and Molecular Dynamics Simulation Investigations. *J. Mol. Liq.* **2020**, *308*, 113042. <https://doi.org/10.1016/j.molliq.2020.113042>.
- (267) Elmsellem, H.; Nacer, H.; Halaimia, F.; Aouniti, A.; Lakehal, I.; Chetouani, A.; Al-Deyab, S. S.; Warad, I.; Touzani, R.; Hammouti, B. Anti-Corrosive Properties and Quantum Chemical Study of (E)-4-Methoxy-N-(Methoxybenzylidene)Aniline and (E)-N-(4-Methoxybenzylidene)-4-Nitroaniline Coating on Mild Steel in Molar Hydrochloric. *Int. J. Electrochem. Sci.* **2014**, *9* (9), 5328–5351.
- (268) Guruprasad, A. M.; Sachin, H. P. Novel Cost-Effective Aqueous Amorphophallus Paeoniifolius Leaves Extract as a Green Corrosion Inhibitor for Mild Steel Corrosion in Hydrochloric Acid Medium: A Detailed Experimental and Surface Characterization Studies. *Chem. Data Collect.* **2021**, *34*, 100734.  
<https://doi.org/10.1016/j.cdc.2021.100734>.
- (269) Kaya, S.; Kaya, C. A New Method for Calculation of Molecular Hardness: A Theoretical Study. *Comput. Theor. Chem.* **2015**, *1060*, 66–70.  
<https://doi.org/10.1016/j.comptc.2015.03.004>.
- (270) Kaya, S.; Kaya, C. A Simple Method for the Calculation of Lattice Energies of Inorganic Ionic Crystals Based on the Chemical Hardness. *Inorg. Chem.* **2015**, *54* (17), 8207–8213.  
<https://doi.org/10.1021/acs.inorgchem.5b00383>.
- (271) Gazquez, J. L. Electrodonating and Electroaccepting Related Papers. *J. Phys. Chem. A* **2007**, *111* (10), 1966–1970.
- (272) Mobin, M.; Aslam, R. Experimental and Theoretical Study on Corrosion Inhibition Performance of Environmentally Benign Non-Ionic Surfactants for Mild Steel in 3.5% NaCl Solution. *Process Saf. Environ. Prot.* **2018**, *114* (February), 279–295.

<https://doi.org/10.1016/j.psep.2018.01.001>.

- (273) States, U.; Protection, E. Environmentally Acceptable Lubricants. *Encycl. Lubr. Lubr.* **2014**, No. November, 526–526. [https://doi.org/10.1007/978-3-642-22647-2\\_100214](https://doi.org/10.1007/978-3-642-22647-2_100214).
- (274) Romeo, V.; Verzera, A.; Ziino, M.; Concurso, C.; Tripodi, G. Headspace Volatiles of *Vicia Sativa* l. (Leguminosae) by Solid-Phase Microextraction and Gas Chromatography/Mass Spectrometry. *J. Essent. Oil Res.* **2009**, *21* (1), 33–35. <https://doi.org/10.1080/10412905.2009.9700101>.
- (275) Salehi, B.; Abu-Reidah, I. M.; Sharopov, F.; Karazhan, N.; Sharifi-Rad, J.; Akram, M.; Daniyal, M.; Khan, F. S.; Abbaass, W.; Zainab, R.; Carbone, K.; Fahmy, N. M.; Al-Sayed, E.; El-Shazly, M.; Lucarini, M.; Durazzo, A.; Santini, A.; Martorell, M.; Pezzani, R. *Vicia* Plants—A Comprehensive Review on Chemical Composition and Phytopharmacology. *Phyther. Res.* **2021**, *35* (2), 790–809. <https://doi.org/10.1002/ptr.6863>.
- (276) Belghiti, M. E.; Echihi, S.; Dafali, A.; Karzazi, Y.; Bakasse, M.; Elalaoui-Elabdallaoui, H.; Olasunkanmi, L. O.; Ebenso, E. E.; Tabyaoui, M. Computational Simulation and Statistical Analysis on the Relationship between Corrosion Inhibition Efficiency and Molecular Structure of Some Hydrazine Derivatives in Phosphoric Acid on Mild Steel Surface. *Appl. Surf. Sci.* **2019**, *491* (April), 707–722. <https://doi.org/10.1016/j.apsusc.2019.04.125>.
- (277) Manssouri, M.; Znini, M.; Lakbaibi, Z.; Ansari, A.; El Ouadi, Y. Experimental and Computational Studies of Perillaldehyde Isolated from *Ammodaucus Leucotrichus* Essential Oil as a Green Corrosion Inhibitor for Mild Steel in 1.0 M HCl. *Chem. Pap.* **2021**, *75* (3), 1103–1114. <https://doi.org/10.1007/s11696-020-01353-5>.
- (278) Lv, B.; Wu, K.; Zhou, Z.; Jing, G. How Did the Corrosion Inhibitor Work in Amino-Functionalized Ionic Liquids for CO<sub>2</sub> Capture: Quantum Chemical Calculation and Experimental. *Int. J. Greenh. Gas Control* **2019**, *91* (July), 102846. <https://doi.org/10.1016/j.ijggc.2019.102846>.
- (279) Olivares-Xometl, O.; Lijanova, I. V.; Likhanova, N. V.; Arellanes-Lozada, P.; Hernández-Cocoletzi, H.; Arriola-Morales, J. Theoretical and Experimental Study of the Anion

- Carboxylate in Quaternary-Ammonium-Derived Ionic Liquids for Inhibiting the Corrosion of API X60 Steel in 1 M H<sub>2</sub>SO<sub>4</sub>. *J. Mol. Liq.* **2020**, *318*, 114075.  
<https://doi.org/10.1016/j.molliq.2020.114075>.
- (280) Quadri, T. W.; Olasunkanmi, L. O.; Akpan, E. D.; Alfantazi, A.; Obot, I. B.; Verma, C.; Al-Mohaimed, A. M.; Ebenso, E. E.; Quraishi, M. A. Chromeno-Carbonitriles as Corrosion Inhibitors for Mild Steel in Acidic Solution: Electrochemical, Surface and Computational Studies. *RSC Adv.* **2021**, *11* (4), 2462–2475. <https://doi.org/10.1039/d0ra07595g>.
- (281) Ikpeseni, S. C.; Owamah, H. I.; Owebor, K.; Ameh, E. S.; Sada, S. O.; Otuaro, E. Corrosion Inhibition Efficiency, Adsorption and Thermodynamic Studies of Ocimum Gratissimum on Carbon Steel in 2 M Sodium Chloride Solution. *J. Bio- Tribo-Corrosion* **2021**, *7* (3), 1–14. <https://doi.org/10.1007/s40735-021-00505-8>.
- (282) Kumar, A.; Thakur, A. *Encapsulated Nanoparticles in Organic Polymers for Corrosion Inhibition*; Elsevier Inc., 2020. <https://doi.org/10.1016/b978-0-12-819359-4.00018-0>.
- (283) Thakur, A.; Kumar, A. Nanotechnology and Its Significance in Food Industries : An Overview. *J. Emerg. Technol. Innov. Res.* **2019**, *6* (1), 344–348.
- (284) Thakur, A.; Kumar, A. Potential of Weeds Extract As A Green Corrosion Inhibitor on Mild Steel: A Review. *Think India J.* **2019**, *22* (16), 3226–3240.
- (285) Thakur, A.; Kumar, A. A Review on Ammonia Derivatives as Corrosion Inhibitors for Metals and Alloys. *Eur. J. Mol. Clin. Med.* **2020**, *07* (07), 49–67.  
[https://doi.org/10.1007/978-3-030-35106-9\\_3](https://doi.org/10.1007/978-3-030-35106-9_3).
- (286) Thakur, A.; Kumar, A. Potential of Natural Product Extract as Green Corrosion Inhibitors for Steel- A Review. *J. Gujarat Res. Soc.* **2019**, *21* (8), 200–212.
- (287) Thakur, A.; Kumar, A.; Kaya, S.; Vo, D. V. N.; Sharma, A. Suppressing Inhibitory Compounds by Nanomaterials for Highly Efficient Biofuel Production: A Review. *Fuel* **2022**, *312* (September 2021), 122934. <https://doi.org/10.1016/j.fuel.2021.122934>.
- (288) Umoren, S. A.; Solomon, M. M.; Obot, I. B.; Suleiman, R. K. Date Palm Leaves Extract as a Green and Sustainable Corrosion Inhibitor for Low Carbon Steel in 15 Wt.% HCl Solution: The Role of Extraction Solvent on Inhibition Effect. *Environ. Sci. Pollut. Res.*



- 2021**, 28 (30), 40879–40894. <https://doi.org/10.1007/s11356-021-13567-5>.
- (289) El Hajjaji, F.; Salim, R.; Taleb, M.; Benhiba, F.; Rezki, N.; Chauhan, D. S.; Quraishi, M. A. Pyridinium-Based Ionic Liquids as Novel Eco-Friendly Corrosion Inhibitors for Mild Steel in Molar Hydrochloric Acid: Experimental & Computational Approach. *Surfaces and Interfaces* **2021**, 22 (September 2020), 100881. <https://doi.org/10.1016/j.surfin.2020.100881>.
- (290) Odunlami, O. A.; Loto, R. T.; Fajobi, M. A.; Olomukoro, O. T.; Akande, I. G.; Oke, M. A.; Oladimeji, T. E. Data on the Corrosion Inhibition Property of Rosemary on High Carbon Steel in Dilute Sulphuric Acid, Citric Acid and Sodium Chloride Solution. *Chem. Data Collect.* **2021**, 32, 100660. <https://doi.org/10.1016/j.cdc.2021.100660>.
- (291) Odusote, J. K.; Asafa, T. B.; Oseni, J. G.; Adeleke, A. A.; Adediran, A. A.; Yahya, R. A.; Abdul, J. M.; Adedayo, S. A. Inhibition Efficiency of Gold Nanoparticles on Corrosion of Mild Steel, Stainless Steel and Aluminium in 1M HCl Solution. *Mater. Today Proc.* **2021**, 38 (February), 578–583. <https://doi.org/10.1016/j.matpr.2020.02.984>.
- (292) Oshomogho, F. O.; Akhihero, T. E.; Edokpayi, O.; Ossai, J. E. Green Corrosion Inhibition of Mild Steel Using Prunus Dulcis Seeds Extract in an Acidic Medium. *Glob. J. Pure Appl. Sci.* **2020**, 26 (2), 171–178. <https://doi.org/10.4314/gjpas.v26i2.9>.
- (293) Fouda, A. S.; Gadow, H. S.; Abd Elal, E. G.; El-Tantawy, M. I. Corrosion Inhibition of Aluminium by Rice Straw Extract in 2 M Hydrochloric Acid Solution. *J. Bio- Tribo- Corrosion* **2021**, 7 (3), 1–17. <https://doi.org/10.1007/s40735-021-00527-2>.
- (294) Kumar, D.; Jain, V.; Rai, B. Imidazole Derivatives as Corrosion Inhibitors for Copper: A DFT and Reactive Force Field Study. *Corros. Sci.* **2020**, 171 (April), 108724. <https://doi.org/10.1016/j.corsci.2020.108724>.
- (295) Zuo, X.; Li, W.; Luo, W.; Zhang, X.; Qiang, Y.; Zhang, J.; Li, H.; Tan, B. Research of Liliun Brownii Leaves Extract as a Commendable and Green Inhibitor for X70 Steel Corrosion in Hydrochloric Acid. *J. Mol. Liq.* **2021**, 321, 114914. <https://doi.org/10.1016/j.molliq.2020.114914>.
- (296) Vasanthajothi, R.; Saratha, R.; Krishnaveni, K. Mild Steel Green Inhibition by Hardwickia

- Binata Roxb. Leaves Extract in Acid Medium. *J. Adhes. Sci. Technol.* **2021**, *35* (3), 296–312. <https://doi.org/10.1080/01694243.2020.1801248>.
- (297) Li, R.; Hu, H.; Li, X.; Zhang, P.; Xu, Y.; Yang, J.; Wang, Y. Essential Oils Composition and Bioactivities of Two Species Leaves Used as Packaging Materials in Xishuangbanna, China. *Food Control* **2015**, *51*, 9–14. <https://doi.org/10.1016/j.foodcont.2014.11.009>.
- (298) Bathily, M.; Ngom, B.; Gassama, D.; Tamba, S. Review on Essential Oils and Their Corrosion-Inhibiting Properties Review on Essential Oils and Their Corrosion-Inhibiting Properties. *J. Appl. Chem.* **2021**, *9* (June), 65--73. <https://doi.org/10.11648/j.ajac.20210903.12>.
- (299) Lekbach, Y.; Bennouna, F.; El Abed, S.; Balouiri, M.; El Azzouzi, M.; Aouniti, A.; Ibsouda Koraichi, S. Green Corrosion Inhibition and Adsorption Behaviour of Cistus Ladanifer Extract on 304L Stainless Steel in Hydrochloric Acid Solution. *Arab. J. Sci. Eng.* **2021**, *46* (1), 103–113. <https://doi.org/10.1007/s13369-020-04791-1>.
- (300) Zhao, A.; Sun, H.; Chen, L.; Huang, Y.; Lu, X.; Mu, B.; Gao, H.; Wang, S.; Singh, A. Electrochemical Studies of Bitter Gourd (*Momordica Charantia*) Fruits as Ecofriendly Corrosion Inhibitor for Mild Steel in 1 M HCl Solution. *Int. J. Electrochem. Sci.* **2019**, *14* (7), 6814–6825. <https://doi.org/10.20964/2019.07.75>.
- (301) Benabbouha, T.; Siniti, M.; El Attari, H.; Chefira, K.; Chibi, F.; Nmila, R.; Rchid, H. Red Algae *Halopitys Incurvus* Extract as a Green Corrosion Inhibitor of Carbon Steel in Hydrochloric Acid. *J. Bio- Tribo-Corrosion* **2018**, *4* (3), 0. <https://doi.org/10.1007/s40735-018-0161-0>.
- (302) Lebrini, M.; Suedile, F.; Salvin, P.; Roos, C.; Zarrouk, A.; Jama, C.; Bentiss, F. Bagassa Guianensis Ethanol Extract Used as Sustainable Eco-Friendly Inhibitor for Zinc Corrosion in 3% NaCl: Electrochemical and XPS Studies. *Surfaces and Interfaces* **2020**, *20*, 1–31. <https://doi.org/10.1016/j.surfin.2020.100588>.
- (303) Begum, A. A. S.; Vahith, R. M. A.; Kotra, V.; Shaik, M. R.; Abdelgawad, A.; Awwad, E. M.; Khan, M. *Spilanthes Acmella* Leaves Extract for Corrosion Inhibition in Acid Medium. *Coatings* **2021**, *11* (1), 1–24. <https://doi.org/10.3390/coatings11010106>.

- (304) Kasprzhitskii, A.; Lazorenko, G. Corrosion Inhibition Properties of Small Peptides: DFT and Monte Carlo Simulation Studies. *J. Mol. Liq.* **2021**, *331*, 115782. <https://doi.org/10.1016/j.molliq.2021.115782>.
- (305) Hossain, N.; Asaduzzaman Chowdhury, M.; Kchaou, M. An Overview of Green Corrosion Inhibitors for Sustainable and Environment Friendly Industrial Development. *J. Adhes. Sci. Technol.* **2021**, *35* (7), 673–690. <https://doi.org/10.1080/01694243.2020.1816793>.
- (306) Anupama, K. K.; Joseph, A. Experimental and Theoretical Studies on Cinnamomum Verum Leaf Extract and One of Its Major Components, Eugenol as Environmentally Benign Corrosion Inhibitors for Mild Steel in Acid Media. *J. Bio- Tribo-Corrosion* **2018**, *4* (2), 1–14. <https://doi.org/10.1007/s40735-018-0146-z>.
- (307) Mohammadi, Z.; Rahsepar, M. The Use of Green Bistorta Officinalis Extract for Effective Inhibition of Corrosion and Scale Formation Problems in Cooling Water System. *J. Alloys Compd.* **2019**, *770*, 669–678. <https://doi.org/10.1016/j.jallcom.2018.08.198>.
- (308) Zhao, X.; Liu, X.; Fan, B.; Zheng, X. Optimized Anticorrosion of Polypyrrole Coating by Inverted-Electrode Strategy: Experimental and Molecular Dynamics Investigations. *Polymers (Basel)*. **2022**, *14* (7), 1356. <https://doi.org/10.3390/polym14071356>.
- (309) Fan, B.; Wei, G.; Hao, H.; Guo, A.; Li, J. Preparation of a Ceramic Membrane from Prevalent Natural Clay for the Purification of Phosphate Wastewater. *Desalin. Water Treat.* **2016**, *57* (37), 17308–17321. <https://doi.org/10.1080/19443994.2015.1084598>.
- (310) Ogunleye, O. O.; Eletta, O. A.; Arinkoola, A. O.; Agbede, O. O. Gravimetric and Quantitative Surface Morphological Studies of Mangifera Indica Peel Extract as a Corrosion Inhibitor for Mild Steel in 1 M HCl Solution. *Asia-Pacific J. Chem. Eng.* **2018**, *13* (6), e2257. <https://doi.org/10.1002/apj.2257>.
- (311) Asaad, M. A.; Ismail, M.; Tahir, M. M.; Huseien, G. F.; Raja, P. B.; Asmara, Y. P. Enhanced Corrosion Resistance of Reinforced Concrete: Role of Emerging Eco-Friendly Elaeis Guineensis/Silver Nanoparticles Inhibitor. *Constr. Build. Mater.* **2018**, *188*, 555–568. <https://doi.org/10.1016/j.conbuildmat.2018.08.140>.
- (312) Tan, B.; Xiang, B.; Zhang, S.; Qiang, Y.; Xu, L.; Chen, S.; He, J. Papaya Leaves Extract as

- a Novel Eco-Friendly Corrosion Inhibitor for Cu in H<sub>2</sub>SO<sub>4</sub> Medium. *J. Colloid Interface Sci.* **2021**, *582* (December), 918–931. <https://doi.org/10.1016/j.jcis.2020.08.093>.
- (313) Salleh, S. Z.; Yusoff, A. H.; Zakaria, S. K.; Taib, M. A. A.; Abu Seman, A.; Masri, M. N.; Mohamad, M.; Mamat, S.; Ahmad Sobri, S.; Ali, A.; Teo, P. Ter. Plant Extracts as Green Corrosion Inhibitor for Ferrous Metal Alloys: A Review. *J. Clean. Prod.* **2021**, *304*, 127030. <https://doi.org/10.1016/j.jclepro.2021.127030>.
- (314) Jmiai, A.; Tara, A.; El Issami, S.; Hilali, M.; Jbara, O.; Bazzi, L. A New Trend in Corrosion Protection of Copper in Acidic Medium by Using Jujube Shell Extract as an Effective Green and Environmentally Safe Corrosion Inhibitor: Experimental, Quantum Chemistry Approach and Monte Carlo Simulation Study. *J. Mol. Liq.* **2021**, *322* (October 2020). <https://doi.org/10.1016/j.molliq.2020.114509>.
- (315) Abd-Elaal, A. A.; Elbasiony, N. M.; Shaban, S. M.; Zaki, E. G. Studying the Corrosion Inhibition of Some Prepared Nonionic Surfactants Based on 3-(4-Hydroxyphenyl) Propanoic Acid and Estimating the Influence of Silver Nanoparticles on the Surface Parameters. *J. Mol. Liq.* **2018**, *249*, 304–317. <https://doi.org/10.1016/j.molliq.2017.11.052>.
- (316) Santos, A. M.; Aquino, I. P.; Cotting, F.; Aoki, I. V.; de Melo, H. G.; Capelossi, V. R. Evaluation of Palm Kernel Cake Powder (*Elaeis Guineensis* Jacq.) as Corrosion Inhibitor for Carbon Steel in Acidic Media. *Met. Mater. Int.* **2021**, *27* (6), 1519–1530. <https://doi.org/10.1007/s12540-019-00559-x>.
- (317) Olivares-xometl, O.; Álvarez-álvarez, E.; Victorovna, N. Synthesis and Corrosion Inhibition Mechanism of Ammonium-Based Ionic Liquids on API 5L X60 Steel in Sulfuric Acid Solution. *J. Adhes. Sci. Technol.* **2017**, No. November, 1–22. <https://doi.org/10.1080/01694243.2017.1397422>.
- (318) Lahbib, H.; Ben Hassen, S.; Gerengi, H.; Rizvi, M.; Ben Amor, Y. Corrosion Inhibition Performance of Dwarf Palm and *Cynara Cardunculus* Leaves Extract for St37 Steel in 15% H<sub>2</sub>SO<sub>4</sub>: A Comparative Study. *J. Adhes. Sci. Technol.* **2021**, *35* (7), 691–722. <https://doi.org/10.1080/01694243.2020.1819701>.

- (319) Zhu, L.; Fan, J.; Huang, H.; Guo, L.; Zhu, M.; Zheng, X.; Obot, I. B. Inhibitive Effect of Different Solvent Fractions of Bamboo Shoots Extract on the Corrosion of Mild Steel in 0.5 Mol/L H<sub>2</sub>SO<sub>4</sub> Solution. *J. Mol. Struct.* **2021**, *1243*, 130852. <https://doi.org/10.1016/j.molstruc.2021.130852>.
- (320) Berdimurodov, E.; Kholikov, A.; Akbarov, K.; Guo, L.; Abdullah, A. M.; Elik, M. A Gossypol Derivative as an Efficient Corrosion Inhibitor for St2 Steel in 1 M HCl + 1 M KCl: An Experimental and Theoretical Investigation. *J. Mol. Liq.* **2021**, *328* (January), 115475. <https://doi.org/10.1016/j.molliq.2021.115475>.
- (321) Deyab, M. A.; Mohsen, Q.; Guo, L. Theoretical, Chemical, and Electrochemical Studies of Equisetum Arvense Extract as an Impactful Inhibitor of Steel Corrosion in 2 M HCl Electrolyte. *Sci. Rep.* **2022**, *12* (1), 1–14. <https://doi.org/10.1038/s41598-022-06215-6>.
- (322) Fernandes, C. M.; Ferreira Fagundes, T. da S.; Escarpini dos Santos, N.; Shewry de M. Rocha, T.; Garrett, R.; Borges, R. M.; Muricy, G.; Valverde, A. L.; Ponzio, E. A. Ircinia Strobilina Crude Extract as Corrosion Inhibitor for Mild Steel in Acid Medium. *Electrochim. Acta* **2019**, *312*, 137–148. <https://doi.org/10.1016/j.electacta.2019.04.148>.
- (323) karima, H.; Sameh, B.; Baya, B.; Louiza, B.; Soraya, H.; Hatem, B.; Merzoug, B. Corrosion Inhibition Impact of Pyracantha Coccinea M. Roem Extracts and Their Use as Additives in Zinc Electroplating: Coating Morphology, Electrochemical and Weight Loss Investigations. *J. Taiwan Inst. Chem. Eng.* **2021**, *121*, 337–348. <https://doi.org/10.1016/j.jtice.2021.04.007>.
- (324) Lavanya, M. A Brief Insight into Microbial Corrosion and Its Mitigation with Eco-Friendly Inhibitors. *J. Bio- Tribo-Corrosion* **2021**, *7* (3), 1–9. <https://doi.org/10.1007/s40735-021-00563-y>.
- (325) Ramírez-Peralta, G. I.; León-Silva, U.; Nicho Díaz, M. E.; Valladares-Cisneros, M. G. Effect of Equisetum Arvense Extract as Corrosion Inhibitor of A36 Steel in Sulfuric Acid Solution. *Mater. Corros.* **2018**, *69* (11), 1631–1637. <https://doi.org/10.1002/maco.201810119>.
- (326) Abd El-Gawad, A. M.; El Gendy, A. G.; Elshamy, A. I.; Omer, E. A. Chemical

- Composition of the Essential Oil of *Trianthema Portulacastrum* L. Aerial Parts and Potential Antimicrobial and Phytotoxic Activities of Its Extract. *J. Essent. Oil-Bearing Plants* **2016**, *19* (7), 1684–1692. <https://doi.org/10.1080/0972060X.2016.1205523>.
- (327) Li, Q.; Wang, D.; Zhao, M.; Yang, M.; Tang, J.; Zhou, K. Modeling the Corrosion Rate of Carbon Steel in Carbonated Mixtures of MDEA-Based Solutions Using Artificial Neural Network. *Process Saf. Environ. Prot.* **2021**, *147*, 300–310. <https://doi.org/10.1016/j.psep.2020.08.035>.
- (328) Dawuda, A. W.; Taleb-berrouane, M.; Khan, F. A Probabilistic Model to Estimate Microbiologically Influenced Corrosion Rate. *Process Saf. Environ. Prot.* **2021**, *148*, 908–926. <https://doi.org/10.1016/j.psep.2021.02.006>.
- (329) Foorginezhad, S.; Mohseni-Dargah, M.; Firoozirad, K.; Aryai, V.; Razmjou, A.; Abbassi, R.; Garaniya, V.; Beheshti, A.; Asadnia, M. Recent Advances in Sensing and Assessment of Corrosion in Sewage Pipelines. *Process Saf. Environ. Prot.* **2021**, *147* (September), 192–213. <https://doi.org/10.1016/j.psep.2020.09.009>.
- (330) Fouda, A. S.; Killa, H. M.; Farouk, A.; Salem, A. M. Calicotome Extract as a Friendly Corrosion Inhibitor of Carbon Steel in Polluted NaCl (3.5% NaCl + 16 Ppm NA2S): Chemical and Electrochemical Studies. *Egypt. J. Chem.* **2019**, *62* (10), 1879–1894. <https://doi.org/10.21608/EJCHEM.2019.7656.1649>.
- (331) Fouda, A. S.; Ibrahim, A. R. Aqueous Extract of *Juniperus* as a Green Corrosion Inhibitor for Mild Steel (MS) in Sulfamic Acid (NH<sub>2</sub>SO<sub>3</sub>H) Solutions. *Prot. Met. Phys. Chem. Surfaces* **2018**, *54* (6), 1194–1203. <https://doi.org/10.1134/S2070205118060102>.
- (332) Ojha, L. K.; Tüzün, B.; Bhawsar, J. Experimental and Theoretical Study of Effect of *Allium Sativum* Extracts as Corrosion Inhibitor on Mild Steel in 1 M HCl Medium. *J. Bio-Tribo-Corrosion* **2020**, *6* (2), 1–10. <https://doi.org/10.1007/s40735-020-00336-z>.
- (333) Kumar, H.; Yadav, V.; Anu, Kr. Saha, S.; Kang, N. Adsorption and Inhibition Mechanism of Efficient and Environment Friendly Corrosion Inhibitor for Mild Steel: Experimental and Theoretical Study. *J. Mol. Liq.* **2021**, *338*, 116634. <https://doi.org/10.1016/j.molliq.2021.116634>.

- (334) Rani, A. T. J.; Thomas, A.; Joseph, A. Inhibition of Mild Steel Corrosion in HCl Using Aqueous and Alcoholic Extracts of *Crotalaria Pallida* – A Combination of Experimental, Simulation and Theoretical Studies. *J. Mol. Liq.* **2021**, *334*, 116515. <https://doi.org/10.1016/j.molliq.2021.116515>.
- (335) Nwankwo, H. U.; Akpan, E. D.; Olasunkanmi, L. O.; Verma, C.; Al-Mohaimed, A. M.; Farraj, D. A. A.; Ebenso, E. E. N-Substituted Carbazoles as Corrosion Inhibitors in Microbiologically Influenced and Acidic Corrosion of Mild Steel: Gravimetric, Electrochemical, Surface and Computational Studies. *J. Mol. Struct.* **2021**, *1223*, 129328. <https://doi.org/10.1016/j.molstruc.2020.129328>.
- (336) Fathima, H.; Pais, M.; Rao, P. Anticorrosion Performance of Biopolymer Pectin on 6061 Aluminium Alloy: Electrochemical, Spectral and Theoretical Approach. *J. Mol. Struct.* **2021**, *1243* (July), 130775. <https://doi.org/10.1016/j.molstruc.2021.130775>.
- (337) Chauhan, D. S.; Verma, C.; Quraishi, M. A. Molecular Structural Aspects of Organic Corrosion Inhibitors: Experimental and Computational Insights. *J. Mol. Struct.* **2021**, *1227* (xxxx), 129374. <https://doi.org/10.1016/j.molstruc.2020.129374>.
- (338) Khadraoui, A.; Khelifa, A.; Boutoumi, H.; Karzazi, Y.; Hammouti, B.; Al-Deyab, S. S. The Oil from *Mentha Rotundifolia* as Green Inhibitor of Carbon Steel Corrosion in Hydrochloric Acid. *Chem. Eng. Commun.* **2016**, *203* (2), 270–277. <https://doi.org/10.1080/00986445.2014.993469>.
- (339) M'hiri, N.; Veys-Renaux, D.; Rocca, E.; Ioannou, I.; Boudhrioua, N. M.; Ghoul, M. Corrosion Inhibition of Carbon Steel in Acidic Medium by Orange Peel Extract and Its Main Antioxidant Compounds. *Corros. Sci.* **2016**, *102*, 55–62. <https://doi.org/10.1016/j.corsci.2015.09.017>.
- (340) Shan, B.; Cai, Y. Z.; Brooks, J. D.; Corke, H. Antibacterial Properties of *Polygonum Cuspidatum* Roots and Their Major Bioactive Constituents. *Food Chem.* **2008**, *109* (3), 530–537. <https://doi.org/10.1016/j.foodchem.2007.12.064>.
- (341) Hossain, S. M. Z.; Razzak, S. A.; Hossain, M. M. Application of Essential Oils as Green Corrosion Inhibitors. *Arab. J. Sci. Eng.* **2020**, *45* (9), 7137–7159.

<https://doi.org/10.1007/s13369-019-04305-8>.

- (342) Noor, E. A. Temperature Effects on the Corrosion Inhibition of Mild Steel in Acidic Solutions by Aqueous Extract of Fenugreek Leaves. *Int. J. Electrochem. Sci.* **2007**, *2* (12), 996–1017.
- (343) Ocheje Ameh, P.; Okon Eddy, N.; Ameh, P. O.; Eddy, N. O. Theoretical and Experimental Investigations of the Corrosion Inhibition Action of Piliostigma Thonningii Extract on Mild Steel in Acidic Medium. *Commun. Phys. Sci.* **2020**, *2018* (1), 27–42.
- (344) Onyeachu, I. B.; Solomon, M. M. Benzotriazole Derivative as an Effective Corrosion Inhibitor for Low Carbon Steel in 1 M HCl and 1 M HCl + 3.5 Wt% NaCl Solutions. *J. Mol. Liq.* **2020**, *313*, 113536. <https://doi.org/10.1016/j.molliq.2020.113536>.
- (345) Ahanotu, C. C.; Onyeachu, I. B.; Solomon, M. M.; Chikwe, I. S.; Chikwe, O. B.; Eziukwu, C. A. Pterocarpus Santalinoides Leaves Extract as a Sustainable and Potent Inhibitor for Low Carbon Steel in a Simulated Pickling Medium. *Sustain. Chem. Pharm.* **2020**, *15* (October 2019), 100196. <https://doi.org/10.1016/j.scp.2019.100196>.
- (346) Ma, X.; Dang, R.; Kang, Y.; Gong, Y.; Luo, J.; Zhang, Y.; Fu, J.; Li, C.; Ma, Y. Electrochemical Studies of Expired Drug (Formoterol) as Oilfield Corrosion Inhibitor for Mild Steel in H<sub>2</sub>SO<sub>4</sub> Media. *Int. J. Electrochem. Sci.* **2020**, *15* (3), 1964–1981. <https://doi.org/10.20964/2020.03.65>.
- (347) Emori, W.; Zhang, R. H.; Okafor, P. C.; Zheng, X. W.; He, T.; Wei, K.; Lin, X. Z.; Cheng, C. R. Adsorption and Corrosion Inhibition Performance of Multi-Phytoconstituents from Dioscorea Septemloba on Carbon Steel in Acidic Media: Characterization, Experimental and Theoretical Studies. *Colloids Surfaces A Physicochem. Eng. Asp.* **2020**, *590* (January), 124534. <https://doi.org/10.1016/j.colsurfa.2020.124534>.
- (348) Huang, H.; Fu, Y.; Wang, X.; Gao, Y.; Wang, Z.; Zhang, S.; Li, H.; Gao, F.; Chen, L. Nano- to Micro-Self-Aggregates of New Bisimidazole-Based Copoly(Ionic Liquid)s for Protecting Copper in Aqueous Sulfuric Acid Solution. *ACS Appl. Mater. Interfaces* **2019**, *11* (10), 10135–10145. <https://doi.org/10.1021/acsami.8b19993>.
- (349) Dhouibi, I.; Masmoudi, F.; Bouaziz, M.; Masmoudi, M. A Study of the Anti-Corrosive



- Effects of Essential Oils of Rosemary and Myrtle for Copper Corrosion in Chloride Media. *Arab. J. Chem.* **2021**, *14* (2), 102961.  
<https://doi.org/10.1016/j.arabjc.2020.102961>.
- (350) Thakur, A.; Sharma, S.; Ganjoo, R.; Assad, H.; Kumar, A. Anti-Corrosive Potential of the Sustainable Corrosion Inhibitors Based on Biomass Waste: A Review on Preceding and Perspective Research. *J. Phys. Conf. Ser.* **2022**, *2267* (1), 012079.  
<https://doi.org/10.1088/1742-6596/2267/1/012079>.
- (351) Mohammadinejad, F.; Hosseini, S. M. A.; Zandi, M. S.; Bahrami, M. J.; Golshani, Z. Metoprolol: New and Efficient Corrosion Inhibitor for Mild Steel in Hydrochloric and Sulfuric Acid Solutions. *Acta Chim. Slov.* **2020**, *67* (3), 710–719.  
<https://doi.org/10.17344/acsi.2019.5301>.
- (352) Si, N.; Vu, H.; Hien, P. Van; Mathesh, M.; Thi, V.; Thu, H.; Nam, N. D. Improved Corrosion Resistance of Steel in Ethanol Fuel Blend by Titania Nanoparticles and Aganonerion Polymorphum Leaf Extract. *ACS Omega* **2019**, *4*, 146–158.  
<https://doi.org/10.1021/acsomega.8b02084>.
- (353) El Nagy, H. A.; H. El Tamany, E.; Ashour, H.; El-Azabawy, O. E.; Zaki, E. G.; Elsaeed, S. M. Polymeric Ionic Liquids Based on Benzimidazole Derivatives as Corrosion Inhibitors for X-65 Carbon Steel Deterioration in Acidic Aqueous Medium: Hydrogen Evolution and Adsorption Studies. *ACS Omega* **2020**, *5* (47), 30577–30586.  
<https://doi.org/10.1021/acsomega.0c04505>.
- (354) Oyedeko, K. F. O.; Lasisi, M. K.; Akinyanju, A. S. Study of Blend of Extracts from Bitter Leaf (*Vernonia Amygdalina*) Leaves and Banana (*Musa Acuminata*) Stem as Corrosion Inhibitor of Mild Steel in Acidic Medium. *Eur. J. Eng. Technol. Res.* **2022**, *7* (1), 48–56.  
<https://doi.org/10.24018/ejeng.2022.7.1.2708>.
- (355) Kouache, A.; Khelifa, A.; Boutoumi, H.; Moulay, S.; Feghoul, A.; Idir, B.; Aoudj, S. Experimental and Theoretical Studies of Inula Viscosa Extract as a Novel Eco-Friendly Corrosion Inhibitor for Carbon Steel in 1 M HCl. *J. Adhes. Sci. Technol.* **2021**, *36* (9), 1–29. <https://doi.org/10.1080/01694243.2021.1956215>.

- (356) Eddy, N. O.; Ebenso, E. E. Corrosion Inhibition and Adsorption Properties of Ethanol Extract of Gongronema Latifolium on Mild Steel in H<sub>2</sub>SO<sub>4</sub>. *Pigment Resin Technol.* **2010**, *39* (2), 77–83. <https://doi.org/10.1108/03699421011028653>.
- (357) Dehghani, A.; Bahlakeh, G.; Ramezanzadeh, B.; Ramezanzadeh, M. Experimental Complemented with Microscopic (Electronic/Atomic)-Level Modeling Explorations of Laurus Nobilis Extract as Green Inhibitor for Carbon Steel in Acidic Solution. *J. Ind. Eng. Chem.* **2020**, *84*, 52–71. <https://doi.org/10.1016/j.jiec.2019.12.019>.
- (358) Boudalia, M.; Fernández-Domene, R. M.; Tabyaoui, M.; Bellaouchou, A.; Guenbour, A.; García-Antón, J. Green Approach to Corrosion Inhibition of Stainless Steel in Phosphoric Acid of Artemesia Herba Albamedium Using Plant Extract. *J. Mater. Res. Technol.* **2019**, *8* (6), 5763–5773. <https://doi.org/10.1016/j.jmrt.2019.09.045>.
- (359) Idouhli, R.; Oukhrib, A.; Khadiri, M.; Zakir, O.; Aityoub, A.; Abouelfida, A.; Benharref, A.; Benyaich, A. Understanding the Corrosion Inhibition Effectiveness Using Senecio Anteuphorbium L. Fraction for Steel in Acidic Media. *J. Mol. Struct.* **2021**, *1228* (January 2021), 129478. <https://doi.org/10.1016/j.molstruc.2020.129478>.
- (360) Sannaiah, P. N.; Alva, V. D. P.; Bangera, S. An Experimental, Theoretical, and Spectral Approach to Evaluating the Effect of Eco-Friendly Oxalis Stricta Leaf Extract on the Corrosion Inhibition of Mild Steel in 1 N H<sub>2</sub>SO<sub>4</sub> Medium. *J. Iran. Chem. Soc.* **2022**, *19* (5), 1817–1835. <https://doi.org/10.1007/s13738-021-02422-6>.
- (361) Fouda, A. E. A. S.; El-Gharkawy, E. S.; Ramadan, H.; El-Hossiany, A. Corrosion Resistance of Mild Steel in Hydrochloric Acid Solutions by Clinopodium Acinos as a Green Inhibitor. *Biointerface Res. Appl. Chem.* **2021**, *11* (2), 9786–9803. <https://doi.org/10.33263/BRIAC112.97869803>.

## List of Publications

(Citations: 742, h-index: 15, i10-index: 17 as per the google scholar on September, 2023)

### A. Published corrosion articles as the first author

1. **Abhinay Thakur**, Savas Kaya, A. S. Abousalem, Shveta Sharma, Richika Ganjoo, Humira Assad, and Ashish Kumar. "Computational and experimental studies on the corrosion inhibition performance of an aerial extract of Cnicus Benedictus weed on the acidic corrosion of mild steel." *Process Safety and Environmental Protection* 161 (2022): 801-818.
2. **Abhinay Thakur**, Savas Kaya, Ashraf S. Abousalem, and Ashish Kumar. "Experimental, DFT and MC simulation analysis of Vicia sativa weed aerial extract as sustainable and eco-benign corrosion inhibitor for mild steel in acidic environment." *Sustainable Chemistry and Pharmacy* 29 (2022): 100785.
3. **Abhinay Thakur**, Ashish Kumar, Shveta Sharma, Richika Ganjoo, and Humira Assad. "Computational and experimental studies on the efficiency of Sonchus arvensis as green corrosion inhibitor for mild steel in 0.5 M HCl solution." *Materials Today: Proceedings* 66 (2022): 609-621.
4. **Abhinay Thakur**, and Ashish Kumar. "Sustainable inhibitors for corrosion mitigation in aggressive corrosive media: a comprehensive study." *Journal of Bio-and Tribo-Corrosion* 7 (2021): 1-48.
5. **Abhinay Thakur**, Ashish Kumar, Savaş Kaya, Riadh Marzouki, Fan Zhang, and Lei Guo. "Recent advancements in surface modification, characterization and functionalization for enhancing the biocompatibility and corrosion resistance of biomedical implants." *Coatings* 12, no. 10 (2022): 1459.
6. **Abhinay Thakur**, Savas Kaya, and Ashish Kumar. "Recent Innovations in Nano Container-Based Self-Healing Coatings in the Construction Industry." *Current Nanoscience* 18, no. 2 (2022): 203-216.
7. **Abhinay Thakur**, Shveta Sharma, Richika Ganjoo, Humira Assad, and Ashish Kumar. "Anti-Corrosive Potential of the Sustainable Corrosion Inhibitors Based on Biomass

Waste: A Review on Preceding and Perspective Research." In *Journal of Physics: Conference Series*, vol. 2267, no. 1, p. 012079. IOP Publishing, 2022.

8. **Abhinay Thakur**, Savaş Kaya, and Ashish Kumar. "Recent Trends in the Characterization and Application Progress of Nano-Modified Coatings in Corrosion Mitigation of Metals and Alloys." *Applied Sciences* 13, no. 2 (2023): 730.
9. **Abhinay Thakur**, and Ashish Kumar. "A Review On Thiazole Derivatives As Corrosion Inhibitors For Metals And Their Alloys." *European Journal of Molecular & Clinical Medicine* 7, no. 07 (2020): 2020.

## **B. Published corrosion articles as co-author**

1. Sumayah Bashir, **Abhinay Thakur**, Hassane Lgaz, Ill-Min Chung, and Ashish Kumar. "Computational and experimental studies on Phenylephrine as anti-corrosion substance of mild steel in acidic medium." *Journal of Molecular Liquids* 293 (2019): 111539.
2. Sumayah Bashir, **Abhinay Thakur**, Hassane Lgaz, Ill-Min Chung, and Ashish Kumar. "Corrosion inhibition performance of acarbose on mild steel corrosion in acidic medium: an experimental and computational study." *Arabian Journal for Science and Engineering* 45 (2020): 4773-4783.
3. Sumayah Bashir, **Abhinay Thakur**, Hassane Lgaz, Ill-Min Chung, and Ashish Kumar. "Corrosion inhibition efficiency of bronopol on aluminium in 0.5 M HCl solution: Insights from experimental and quantum chemical studies." *Surfaces and Interfaces* 20 (2020): 100542.
4. Gulista Parveen, Sumayah Bashir, **Abhinay Thakur**, Sourav Kr Saha, Priyabrata Banerjee, and Ashish Kumar. "Experimental and computational studies of imidazolium based ionic liquid 1-methyl-3-propylimidazolium iodide on mild steel corrosion in acidic solution." *Materials Research Express* 7, no. 1 (2019): 016510.
5. Shveta Sharma, Richika Ganjoo, Sourav Kr Saha, Namhyun Kang, **Abhinay Thakur**, Humira Assad, and Ashish Kumar. "Investigation of inhibitive performance of Betahistine dihydrochloride on mild steel in 1 M HCl solution." *Journal of Molecular Liquids* 347 (2022): 118383.

6. Shveta Sharma, Sourav Kr Saha, Namhyun Kang, Richika Ganjoo, **Abhinay Thakur**, Humira Assad, and Ashish Kumar. "Multidimensional analysis for corrosion inhibition by Isoxsuprine on mild steel in acidic environment: Experimental and computational approach." *Journal of Molecular Liquids* 357 (2022): 119129.
7. Richika Ganjoo, Shveta Sharma, **Abhinay Thakur**, Humira Assad, Praveen Kumar Sharma, Omar Dagdag, Avni Berisha, Mahamadou Seydou, Eno E. Ebenso, and Ashish Kumar. "Experimental and theoretical study of Sodium Cocoyl Glycinate as corrosion inhibitor for mild steel in hydrochloric acid medium." *Journal of Molecular Liquids* 364 (2022): 119988.
8. Shveta Sharma, Richika Ganjoo, Sourav Kr. Saha, Namhyun Kang, **Abhinay Thakur**, Humira Assad, Vivek Sharma, and Ashish Kumar. "Experimental and theoretical analysis of baclofen as a potential corrosion inhibitor for mild steel surface in HCl medium." *Journal of Adhesion Science and Technology* 36, no. 19 (2022): 2067-2092.
9. Richika Ganjoo, Aayan Bharmal, Shveta Sharma, **Abhinay Thakur**, Humira Assad, and Ashish Kumar. "Imidazolium based ionic liquids as green corrosion inhibitors against corrosion of mild steel in acidic media." In *Journal of Physics: Conference Series*, vol. 2267, no. 1, p. 012023. IOP Publishing, 2022.
10. Shveta Sharma, Richika Ganjoo, **Abhinay Thakur**, and Ashish Kumar. "Electrochemical characterization and surface morphology techniques for corrosion inhibition—a review." *Chemical Engineering Communications* (2022): 1-36.
11. Shveta Sharma, Richika Ganjoo, **Abhinay Thakur**, and Ashish Kumar. "Investigation of corrosion performance of expired Irnocam on the mild steel in acidic medium." *Materials Today: Proceedings* 66 (2022): 540-543.
12. Richika Ganjoo, Shveta Sharma, **Abhinay Thakur**, and Ashish Kumar. "Thermodynamic study of corrosion inhibition of Dioctylsulfosuccinate Sodium Salt as corrosion inhibitor against mild steel in 1 M HCl." *Materials Today: Proceedings* 66 (2022): 529-533.

### **C. Published Book (Edited) related to corrosion**

1. Ashish Kumar, and **Abhinay Thakur**, eds. *Corrosion Mitigation: Biomass and Other Natural Products*. Walter de Gruyter GmbH & Co KG, 2022.

### **D. Published book chapters related to corrosion**

1. **Abhinay Thakur**, Ashish Kumar, Praveen Kumar Sharma, Shveta Sharma, Richika Ganjoo, and Humira Assad. "Carbon Allotropes as Corrosion Inhibitors." In *Functionalized Nanomaterials for Corrosion Mitigation: Synthesis, Characterization, and Applications*, pp. 115-140. American Chemical Society, 2022.
2. **Abhinay Thakur**, Humira Assad, Shveta Sharma, Richika Ganjoo, Savas Kaya, and Ashish Kumar. "Coordination Polymers as Corrosion Inhibitors." In *Functionalized Nanomaterials for Corrosion Mitigation: Synthesis, Characterization, and Applications*, pp. 231-254. American Chemical Society, 2022.
3. **Abhinay Thakur**, Richika Ganjoo, and Ashish Kumar. "Surface Modified Carbon Nanotubes in Corrosion Protection." In *Surface Modified Carbon Nanotubes Volume 1: Fundamentals, Synthesis and Recent Trends*, pp. 235-255. American Chemical Society, 2022.
4. Kumar, Ashish, and **Abhinay Thakur**. "Encapsulated nanoparticles in organic polymers for corrosion inhibition." In *Corrosion Protection at the Nanoscale*, pp. 345-362. Elsevier, 2020.
5. **Abhinay Thakur**, and Ashish Kumar. "Self-healing nanocoatings for automotive application." In *Nanotechnology in the Automotive Industry*, pp. 403-427. Elsevier, 2022.
6. **Abhinay Thakur**, Humira Assad, Savaş Kaya, and Ashish Kumar. "Plant extracts as environmentally sustainable corrosion inhibitors II." In *Eco-Friendly Corrosion Inhibitors*, pp. 283-310. Elsevier, 2022.
7. **Abhinay Thakur**, Praveen Kumar Sharma, and Ashish Kumar. "Economics and commercialization of carbon allotropes nanostructured corrosion inhibitors." *Carbon Allotropes: Nanostructured Anti-Corrosive Materials* (2022): 383.

8. **Abhinay Thakur**, and Ashish Kumar. "Advance 16 Surface Treatments for Enhancing the Biocompatibility of Biomaterials." *Materials Development and Processing for Biomedical Applications* (2022): 227.

## List of Conferences/ Webinars/ Short term courses attended

### A. Conferences attended

- 1. Oral presentation** on *Spergula arvensis* extract as sustainable corrosion inhibitor for mild steel in 0.5 M HCl: Electrochemical and surface morphological studies in Recent Developments on Materials, Reliability, Safety and Environmental issues – 2021 at NIT, Jalandhar, Punjab on 25-27 June, 2021.
- 2. Oral presentation** on Experimental, DFT and morphological assessments of aerial extract of *Woodfordia fruticosa* as sustainable eco-friendly inhibitor for mild steel corrosion in 1M HCl corrosive media in International Symposium on Sustainable Urban Environment (ISSUE-2022) at UPES on 11-14 October, 2022.
- 3. Oral presentation** on Computational and Experimental studies on the efficiency of *Sonchus Arvensis* as green corrosion inhibitor for mild steel in 0.5M HCl solution in International Conference on Advances in Materials Processing (ICAMP-2022) at NIT Raipur on 8-9 January, 2022.
- 4. Poster presentation** on Anti-corrosive potential of the sustainable corrosion inhibitors based on biomass waste: A review on preceding and perspective research in the International Conference on Recent Advances in Fundamentals and Applied Sciences (RAFAS-21) organized by School of Chemical Engineering and Physical Sciences, Lovely Professional University, Punjab on 25-26 June, 2021.
- 5. Poster presentation** on Potential of weeds extract as a green corrosion inhibitor on mild steel: A review in the National Conference on Innovations in Applied Science and Engineering at NIT, Jalandhar, Punjab on 27-28 April, 2019.
- 6. Paper presentation** on Insight into the corrosion inhibition behavior of Ionic liquids for metals and their alloys in corrosive media: A comprehensive review in the International Conference on Materials for Emerging Technologies (ICMET-21) organized by Department of Research Impact and Outcome, Division of Research and Development, Lovely Professional University, Punjab on 18-19 February, 2022.



## **B. Workshops attended**

1. National Workshop on Advanced instrumentation organized by Central Instrumentation Facility, Division of Research and Development at Lovely Professional University, Punjab on 20 April, 2019.
2. IP Awareness/Training program under National Intellectual Property Awareness Mission organized by Intellectual Property Office, India on 17 February, 2023.

## **C. Short term courses attended**

1. Awareness Program to Introduce *Giloy* in Routine Life for The Promotion of Health organized under the funded project entitled National Campaign on Amrita for Life (*Tinospora cordifolia*) at Lovely Professional University, Punjab on 26 March 2022.
2. Part-I of Nano E-Talks at Maharaja Agrasen University, Himachal Pradesh on 11 December, 2021.
3. Coating Characterization for faster product development and production organized by Formulation-Smart scientific analysis on 14 December, 2021.
4. ChemSci2021: Leaders in the Field Symposium organized by Royal Society of Chemistry (RSC) on 15 December, 2021.
5. National Science Day organized by School of Chemical Engineering & Physical Sciences (SCEPS), Lovely Professional University, Punjab, India on 28 February, 2022.